THE JOURNAL
OF
CHEMICAL PHYSICS

VOLUME 32, NUMBER 2 FEBRUARY, 1960

Raman Intensities of the A_1 Lines of Oxyanions*

GEORGE W. CHANTRY AND ROBERT A. PLANE

Department of Chemistry, Cornell University, Ithaca, New York

(Received August 14, 1959)

The trace of the derived polarizability tensor has been measured on an absolute scale for the ions $CO_3^{=}$, NO_3^{-}, PO_4^{-3}, $SO_4^{=}$, and ClO_4^{-} in aqueous solution. From these and the known normal coordinate matrix elements, the values of the derivative with respect to bond length have been calculated. Results are interpreted in terms of bond order, and indicate appreciable π bonding in the ions NO_3^{-}, $SO_4^{=}$, and ClO_4^{-}. In these cases, as opposed to hydrocarbons, a π electron makes a larger contribution to the derived bond polarizability than does a σ electron.

THE observed intensity of a Raman line is given by

$$I_p=\frac{KM(\nu_0-\nu_p)^4}{\nu_p[1-\exp(-h\nu_p/kT)]}\cdot 45(\partial\bar{\alpha}/\partial Q_p)^2\cdot[6/(6-7\rho)].$$

In this equation K is a constant, M the molar concentration of the scattering species, ν_0 the frequency of the exciting line, ν_p the vibrational frequency of the pth normal mode Q_p, $\bar{\alpha}$ the mean molecular polarizability, and ρ the degree of depolarization. When the transformation from internal coordinates to normal coordinates is known, it is possible to express $\partial\bar{\alpha}/\partial Q_p$ in terms of derivatives with respect to bond lengths, changes of interbond angle, etc. For a tetrahedral XY_4 molecule, there is but one normal mode of the class A_1—the only class for which $\partial\bar{\alpha}/\partial Q_p$ can be anything but zero—and consequently the single normal coordinate matrix element is found immediately from the corresponding G matrix element: similar remarks apply to planar XY_3 molecules. Hence the derivative of the mean polarizability with respect to normal coordinate Q_1 can be written:

$$XY_4(\partial\bar{\alpha}/\partial Q_1)=2M_Y^{-1}\bar{\alpha}_{XY}',$$

$$XY_3(\partial\bar{\alpha}/\partial Q_1)=\sqrt{3}M_Y^{-1}\bar{\alpha}_{XY}',$$

where $\bar{\alpha}_{XY}'$ is the derivative of mean polarizability with respect to the extension of the X—Y bond.

The importance of the derived bond polarizability is that it has been suggested[1] that when a bond stretches, the only change in the molecular polarizability is localized in that bond, so $\bar{\alpha}_{XY}'$ is a bond property and an important one for it gives immediate information on the electrons actually forming the bond. However, this simple picture can be expected only to be approximately correct, and such effects as changes in lone pair hybridization, bond-bond interaction, and nonbonded atom perturbations may be sufficient to obscure the meaning of small changes in $\bar{\alpha}_{XY}'$ in going from one molecule to another. Meaningful results can be obtained only when the environment of a changing bond does not change—an excellent example being an isoelectronic series.

It has been known for some time[2] that the value of $\bar{\alpha}_{XY}'$ depends on the bond type; it is exceedingly small for a pure ionic bond, and very much larger for a pure covalent bond. Woodward and Long[3] showed that their experimental results for the Group IV tetrahalides could be explained by assuming $\bar{\alpha}_{XY}'$ to be proportional to the percentage covalency and to the sum of the atomic numbers of X and Y. The work of Bernstein and Yoshino[4] with hydrocarbon gases led to the remarkable conclusion that in these cases $\bar{\alpha}_{XY}'$ is directly proportional to bond order. Thus both previous studies seem to reveal the potential power of Raman

* This research was supported by the U. S. Air Force through the Air Force Office of Scientific Research of the Air Research and Development Command, under Contract No. AF 49(638)-279. Reproduction in whole or in part is permitted for any purpose of the U. S. Government.

[1] M. Wolkenstein, Compt. rend. acad. sci. U.R.S.S. **32**, 185 (1941).
[2] Cf. D. A. Long, Proc. Roy. Soc. (London) **A217**, 203 (1953).
[3] L. A. Woodward and D. A. Long, Trans. Faraday Soc. **45**, 1131 (1949).
[4] Paper read at the Institute of Petroleum Hydrocarbon Research Group Conference on Molecular Spectroscopy, London, February 1958.

Copyright © 1960 by the American Institute of Physics

TABLE I. Raman intensities.

Species	A_1 Frequency	Relative intensity (I_p)[a]	$\bar{\alpha}_{XY}'$
CCl_4	459 cm^{-1}	1.00	2.00 A^2
CO_3^{-2}	1065	0.178 (ρ=0.106)	1.04
NO_3^-	1040	0.500 (ρ=0.170)	1.64
PO_4^{-3}	935	0.188	0.91
SO_4^{-2}	981	0.396	1.37
ClO_4^-	935	0.675	1.73

[a] Average integrated intensity observed with 4358 A excitation. Included in average are values obtained from 4047 A, and corrected for the fourth-power dependence.

intensity studies for the investigation of chemical bonding. The present work has been undertaken to extend the techniques to different species. Because of the apparent dependence of $\bar{\alpha}_{XY}'$ on atomic number, two sets of isoelectronic species: CO_3^{-2}, NO_3^-, and PO_4^{-3}; SO_4^{-2} and ClO_4^-, have been chosen for study.

EXPERIMENTAL

Measurements were made on *ca* 1 *M* aqueous solutions of the sodium salts (Reagent Grade), and the spectra were recorded using the Cary Model 81 Raman spectrophotometer. For the two planar ions, the spectra were recorded with a polarizing screen surrounding the Raman tube and oriented so that the electric vector of the incident light was perpendicular to the tube axis. From known depolarization ratios, a calibration was found to relate ρ-observed with ρ. All intensities were measured relative to ν_1 of ClO_4^- with the exception of ν_1 for PO_4^{-3}, which coincides with that line and so was measured relative to ν_1 of NO_3^-. This comparison technique was adopted in order to minimize errors due to differences of refractive indices of the various solutions.

Two corrections were applied to the measured integrated intensities in order that the derived bond polarizabilities be comparable with values given by previous workers. The first was to allow for the differing response of the instrument at differing wavelengths, and the second was the adoption of a common factor (the value of $\bar{\alpha}_{ClO}'$) to place the results on an agreed scale. A calibration curve for the instrument was obtained from a comparison of observed intensities for methylene chloride with the theoretical intensities calculated from the data given by Long, Milner, and Thomas.[5] The filter solution used to isolate Hg 4358 A was removed for this experiment as for all other measurements also, and lines excited by both Hg 4358 A and Hg 4047 A were obtained. The calibration curve extended from 4150 A to 5000 A, and the sensitivity was found to increase throughout this interval. The increase within the range covered by the present experiment, however, was found to be less than 5%. The second correction was obtained from experiments in which the integrated intensities of ν_1 ClO_4^- and ν_1 CCl_4 were measured from spectra obtained with a solution of $HClO_4 \cdot 2\frac{1}{2}$ H_2O and CCl_4 in absolute ethanol. The absolute scale employed is to refer all derived bond polarizabilities to that of the C—H bond, for which most of the complicating factors mentioned above are absent. $\bar{\alpha}_{CH}'$ is given the value 1.00×10^{-16} cm^2 which is close to the experimentally determined value given by Bernstein and Yoshino.[4] On this scale $\bar{\alpha}_{C-Cl}'$ for CCl_4 is 2.00×10^{-16} cm^2, this value being obtained from the data for CCl_4, CCl_3H, and CCl_2H_2 given by Long, Milner, and Thomas,[5] and the inverse L matrices listed by Long and Thomas.[6]

RESULTS AND DISCUSSION

Table I lists values of the integrated Raman intensities for the A_1 lines of the species studied as well as the values of $\bar{\alpha}_{XY}'$.

To interpret the derived bond polarizabilities an assessment should be made of the various contributing factors: the changing distribution of shared electrons; the changed distribution of unshared especially "lone pair" electrons; interactions between nonbonded atoms, or groups of atoms. The very fact that electrostatically bound atoms show no detectable Raman intensity seems to suggest that of the three factors, the last is of little importance. In many covalently bound molecules, the first two terms are inseparable; however some indication of the importance of the third can be gained. Data exist for the compounds CCl_4, CCl_3H, and CCl_2H_2.[5] The values of $\bar{\alpha}_{C-Cl}'$ are 2.00, 1.86, and 1.55 A^2, respectively. Thus the magnitude of the interaction between a C—Cl bond and a similar bond is roughly 10% of the total $\bar{\alpha}_{C-Cl}'$. This is about the same as the effect of nonbonded interactions on force constants.

Woodward and Long list values for derived bond polarizabilities for the series CCl_4, $SiCl_4$, $GeCl_4$, $SnCl_4$, CBr_4, and $SnBr_4$.[3] The observation that the values for the tetrabromides are about twice the values of the corresponding tetrachlorides can be attributed, at least in part, to the increased contribution from lone pairs and nonbonding interactions. However the trend observed within the tetrahalides (CCl_4=$SiCl_4$<$GeCl_4$<$SnCl_4$) is not thus interpretable. It seems likely that the trend is due to changes in bond hybridization, i.e., increasing *d* character giving rise to larger values. (Such an explanation would account also for the quite large value obtained for $TiCl_4$.[3]) Hence it would be expected that the convenient relationship noted by Yoshino and Bernstein for hydrocarbons[4] is not applicable in more general cases.

There has been controversy in the interpretation of the bonding in the oxyanions studied in the present work.[7] Since the ions divide into two isoelectronic sequences it seems that the values of $\bar{\alpha}_{XY}'$ within each

[5] Long, Milner, and Thomas, Proc. Roy. Soc. (London) **A237**, 197 (1956).

[6] D. A. Long and A. G. Thomas, Proc. Roy. Soc. (London) **A223**, 130 (1954).

[7] A. F. Wells, J. Chem. Soc. **1949**, 55.

sequence, should be affected similarly by "lone pair" and adjacent bond interactions, and hence should provide information concerning the bonding involved.

If only nonpolarized σ bonds are used for the construction of the molecules in the sequence PO_4^{-3}, SO_4^{-2}, ClO_4^{-1} it follows that the central atom has a formal charge $+1$, $+2$, and $+3$, respectively. That such a situation is unlikely is indicated by the arguments of Pauling[8] for essential electrical neutrality, as well as by noting the change in base strength within the sequence. The dissociation constants for HPO_4^{-2}, HSO_4^{-}, and $HClO_4$ increase markedly, indicating a decrease in the negative charge of the oxygen atoms through the sequence. Thus the oxygen atoms in PO_4^{-3} might be assumed to carry -1 charges, those of SO_4^{-2} less, and those of ClO_4^{-} less still. Two mechanisms can be postulated for removing negative charge from the oxygen atoms and positive charge from the central atom. The first is by polarization of the σ bonds, and the second by formation of $p_\pi - d_\pi$ bonds in addition to the σ bonds. The first mechanism would cause a decrease in $\bar{\alpha}_{XY}'$ in going through the sequence, whereas increasing π bonding would cause an increase. The present results indicate that it is the second mechanism which is operative.

From a comparison of the symmetry of the d and p atomic orbitals involved, it follows that at most two of the $3d$ orbitals of the tetrahedrally surrounded atoms can be combined with the $p\pi$ orbital of the oxygens to form effective π bonds.[9] The relative magnitudes of $\bar{\alpha}_{XO}'$ for ClO_4^{-} and PO_4^{-3} suggest that these cases represent the extremes in the extent of $p\pi - d\pi$ bonding. Thus for ClO_4^{-} the number of π bonds approaches the maximum of 2, while for PO_4^{-3} there is little, if any, π bonding. Sulfate ion can be interpreted as showing an intermediate degree of π bonding. That such a trend should exist is consistent with the postulated contraction of d orbitals with increasing formal charge and the subsequent increased contribution to bonding.[10] Comparison of the values of $\bar{\alpha}_{XO}'$ for CO_3^{-} and NO_3^{-} in Table I, and the respective dissociation constants of HCO_3^{-} and HNO_3 similarly leads to the conclusion that the extent of π bonding is considerably greater in NO_3^{-} than in CO_3^{-2}. If it is assumed that there is one π bond in NO_3^{-}, CO_3^{-2} probably contains only σ bonds.

From the interpretation given above and the numerical values listed in Table I, it is clear that there is an important difference between these and the results given by Yoshino and Bernstein.[4] Whereas the contributions of a σ and a π electron to $\bar{\alpha}_{CC}'$ apparently are equal in the case of hydrocarbon molecules, this cannot be true in the species observed in the present study. The most plausible explanations of the difference are either that the presence of the formal charges affects σ and π electrons differently, or else that the equality reported by Yoshino and Bernstein is illusory. The formal charges would indeed polarize the σ bonds, but the dative π bonding would reduce the formal charges and consequently relieve the polarization. However, the remaining small formal charge might be expected to reduce the σ contribution more than the π contribution. The second explanation would seem the more reasonable, for introduction of π bonding in a hydrocarbon molecule invariably is accompanied by a change in hybridization at the carbon atoms involved. Such changes lead to bond shortening and consequently to a reduction in the σ contribution to $\bar{\alpha}_{CC}'$ (cf. Bell[11] and the discussion of these ideas by Yoshino and Bernstein[4]). If the π contribution is inherently larger than the σ, the observed $\bar{\alpha}_{CC}'$, which is the sum of the two, fortuitously might be twice that for $sp^3 - sp^3$ carbon-carbon bonds.

[8] L. Pauling, J. Chem. Soc. **1948**, 1461.

[9] Eyring, Walter, and Kimball, *Quantum Chemistry* (John Wiley and Sons, Inc., New York, 1944), p. 231.

[10] Craig, Maccoll, Nyholm, Orgel, and Sutton, J. Chem. Soc. **1954**, 332.

[11] R. P. Bell, Trans. Faraday Soc. **38**, 422 (1942).

THE JOURNAL OF CHEMICAL PHYSICS VOLUME 32, NUMBER 2 FEBRUARY, 1960

Growth and Crystal Symmetry of Metal Chelate Salt Crystals

L. G. VAN UITERT AND R. G. TREUTING

Bell Telephone Laboratories, Incorporated, Murray Hill, New Jersey

(Received June 8, 1959)

A method for growing large single crystals of metal chelate salts such as NaNi triacetylacetonate·*p*-dioxane and NaNi triacetylacetonate·benzene has been devised. The growth habits of these crystals are described. X-ray studies of three of the NaNi and NaMg salts indicate a diffraction symmetry consistent with space group $P\bar{3}1c$, with two molecules per unit cell. Paramagnetic resonance measurements by M. Peter indicate that the benzene compounds are truly trigonal, while the dioxane compounds are macroscopically trigonal as a result of disordering among unit cells that are individually monoclinic.

THERE is a growing interest in the properties of paramagnetic salts, particularly in understanding and controlling the electron transitions which can occur in them. In some paramagnetic resonance studies it may be desirable to maintain a relatively large separation between the paramagnetic ions in order to minimize line broadening effects from spin-spin interactions. This can be accomplished in two ways, by dilution with a diamagnetic material or by employing crystals whose structure confers a wide separation. Of these two, the former confers a statistical distribution with a given fraction of overly close-spaced ions, while the latter ensures a uniform interionic spacing. Advantage can be taken of both conditions by employing isomorphous metal chelate salts which have large unit cells. To this end compounds related to sodium-nickel triacetylacetonate *p*-dioxane, NaNi $(CH_3\cdot CO\cdot CH\cdot CO\cdot CH_3)_3\cdot O\cdot CH_2\cdot CH_2\cdot O\cdot CH_2\cdot CH_2$, have been studied.

SAMPLE PREPARATION

A number of the divalent metal ions which can enter into octahedral coordination take part in the formation of metal chelate salts. A series of such salts[1] having the general formula $M^{I}M^{II}\ Acac_3\cdot p$-dioxane, where Acac represents acetylacetonate ion, is formed when $M^{I}=Na^+$ or K^+ and $M^{II}=Mg^{2+}$, Mn^{2+}, Fe^{2+}, Co^{2+}, Ni^{2+}, or Zn^{2+}. Similar series of salts form when *p*-dioxane is replaced by benzene, fluorobenzene, ethanol, methanol, acetone, glycerine, or phenol.

It has been found that single crystals of these salts can be readily prepared by a vapor diffusion process. A typical procedure is as follows: To 100 ml H_2O add 15 ml 1*N* NaOH, followed by 2 ml (20 milli-equivalents) of acetylacetone, and stir until the solution of the acetylacetone is completed. Then add 5 ml of 1 molar divalent metal salt solution. The resulting mixture will be a clear solution tinted by the color characteristic of the metal chelate group present. If the metal ion is added before the NaOH, small amounts of the neutral chelate species may separate from solutions and act as nuclei for crystallization. An uncovered beaker containing the solution is then placed under a bell jar with a second uncovered beaker containing dioxane, benzene, or other members of the foregoing series. With the passage of time, dioxane vapor diffuses into the prepared solution, nuclei of the metal chelate salt form, and crystal growth proceeds. The diffusion of dioxane is sufficiently slow so that, quite often, only one or two crystals are formed. These have been grown up to a centimeter on a side.

SINGLE CRYSTAL CHARACTERISTICS

The dioxane-containing crystals grow in the form of hexagonal prisms and related forms. Their densities approximate 1.4 g/cc, and from the x-ray data the structure accommodates one divalent metal ion per 550 A^3. They are clear crystals with colorations characteristic of the divalent metal chelate; blue-green for nickel, yellow for manganese, and deep red for cobalt. The magnesium and zinc crystals are clear to slightly tinged with yellow. The crystals appear to be quite stable when exposed to air at room temperature. However, in a matter of months they may turn opaque through decomposition of the surface unless kept in a tight container.

The sodium-manganese salt grows in the form of numerous parallel hexagonal columns and is quite opaque. This is related to the larger size of the manganese ion. The condition is somewhat alleviated by diluting with magnesium. When the sodium ion in the sodium-manganese salt is replaced by potassium, which has a greater ionic radius, a stable crystal is again formed. However, the growth habit is markedly changed. The sodium salts form hexagonal plates of considerable thickness, while the potassium-manganese salt forms thin, rectangular sheets that grow approximately one centimeter to a side and 10^{-3} centimeters thick under the conditions employed. The potassium-nickel salts show greater planar growth than do those of sodium, resulting in relatively thin plates in this case also. However, this tendency in the nickel salts is not so marked as in those of manganese.

CRYSTALLOGRAPHIC STUDIES

X-ray studies have been made of the crystal symmetry and cell size of three of the salts described,

[1] Van Uitert, Fernelius, and Douglas, J. Am. Chem. Soc. **75**, 457 (1953); J. Am. Chem. Soc. **75**, 2736 (1953).

NaNi $Acac_3 \cdot p$-dioxane, $NaNi_{0.04}Mg_{0.96}$ $Acac_3 \cdot p$-dioxane, and NaNi $Acac_3 \cdot$benzene. In each case a suitable crystal, characteristically blue-green and transparent and in the form of a well-developed hexagonal prism, was selected.

Weissenberg and precession photographs show diffraction symmetry consistent with trigonal space groups $P\bar{3}1c$ and $P31c$ in each case. Values for the cell constants of NaNi $Acac_3 \cdot p$-dioxane taken from calibrated layer line and zero level Weissenberg patterns are $a=10.23$ A, $c=12.20\pm0.02$ A, giving a unit cell volume of approximately 1100 A^3. Since the density is about 1.4 g/cc, there are two molecules to the trigonal unit cell. The $NaNi_{0.04}Mg_{0.96}$ $Acac_3 \cdot p$-dioxane and NaNi $Acac_3 \cdot$benzene salts do not differ significantly.

The NaNi $Acac_3 \cdot p$-dioxane crystals were tested for both pyroelectric and piezoelectric effects, the former in a most sensitive manner.[2] Since no effect was found, there is a very high probability that the structure has a center of symmetry. On the basis of the diffraction patterns and these tests, $P\bar{3}1c$ is indicated as the most probable space group.

In this type of compound, when it is desired to minimize spin-spin interactions the paramagnetic divalent ion spacing is of primary interest. In $P\bar{3}1c$ there are four pairs of special positions available to accommodate the two pairs of metal ions in the trigonal unit cell. Two sets of these, the (a) and (b), lead to an interionic spacing of $c/2=6.10$ A and would contribute to the intensities of only those *hkil* reflections for which $l=2n$. Qualitatively, odd n-level reflections are systematically much weaker than the even save for a few low-index reflections. There is a tendency for the cell to be halved. The (a) and (b) sites seem more likely.

In the Ni chelate groups, Ni $Acac_3^-$, it is to be expected that the metal ion is bonded to the 6 oxygen atoms in octahedral configuration, with planar acetylacetonate groups supplying the neighboring oxygen atoms. This has been found in Fe $Acac_3$,[3] as proposed earlier by Morgan.[4] Such an arrangement has a threefold axis normal to the octahedral planes defined by three unlinked oxygen atoms, but does not have a center of symmetry. It does have twofold axes normal to the threefold and in the planes of the chelate rings. The point symmetry is therefore 32 rather than $\bar{3}$. Of the more likely sites, the Ni^{++} ions would then be in the 2(a) positions at $0,0,\frac{1}{4}$; $0,0,\frac{3}{4}$. The glide plane is effected by a relative rotation of 180° between the two Ni chelate groups (compare reference 3). The Na^+ ions may very tentatively be assigned to the 2(c) or 2(d) positions.

With the indicated layering of the structure, the most probable disposition of the benzene or dioxane rings is parallel to the basal plane. This poses no problem for the benzene ring, but a dioxane ring does not have a threefold axis; it has twofold symmetry at most. Hence, in the dioxane compounds these rings are either disordered from cell to cell, or they are ordered with the O and CH_2 radicals hexagonally disposed and of sufficiently equivalent scattering power to afford the observed diffraction symmetry. In the former case the unit cells are individually monoclinic but the structure is statistically trigonal; in the latter case the structure in toto would be truly monoclinic.

This question has been resolved by an investigation of the paramagnetic resonance spectra of NaNi $Acac_3 \cdot p$-dioxane and of NaNi $Acac_3 \cdot$benzene conducted by M. Peter of these Laboratories and to be reported in detail elsewhere.[5] Peter observed the angular dependence of the paramagnetic resonance arising from the spin levels of Ni^{++} ion. He found cylindrical symmetry about the threefold axis of the NaNi $Acac_3 \cdot$benzene, while in the crystals which contain p-dioxane, a pattern having the symmetry C_{2v} was observed. This pattern was repeated three times, i.e., every 60° around the trigonal axis. From crystal field calculations he has shown that while the NaNi $Acac_3 \cdot p$-dioxane is macroscopically trigonal, the dioxane molecules are stacked along the c axis, with their planes normal thereto, and with the O—O bonds paralleling each other and one of the twofold symmetry axes within each stack. Each such vertically aligned group is then most probably oriented at random with respect to its neighbors.

The paramagnetic resonance measurements were made at 4°K, and hence the conclusions apply strictly only to this temperature. However, a transition to an ordered monoclinic state at higher temperature does not appear likely. The possibility that at higher temperature the dioxane rings start to rotate around the trigonal axis cannot be ruled out. At 4° they stay in each equivalent position for at least a millimicrosecond, as was determined by measuring the line width of the paramagnetic absorption.

These findings are consistent with the x-ray analysis. The cylindrical pattern shows that the benzene rings are preserving the D_3 symmetry of the Ni^{++} ion. The oxygens of the dioxane reduce the symmetry. The threefold appearance of the pattern shows that the dioxane rings are indeed disordered.

SUMMARY

Single crystals of M^I M^{II} $Acac_3 \cdot p$-dioxane, where $M^{II}=Mg^{2+}$, Mn^{2+}, Fe^{2+}, Co^{2+}, Ni^{2+}, Zn^{2+}, and mixtures of these, and $M^I=Na^+$ and K^+, can be readily grown by a vapor diffusion process. In this process p-dioxane can be replaced by benzene, fluorobenzene, methanol, ethanol, acetone, glycerine, or phenol. There are four classes of adjustable parameters available to influence the paramagnetic behavior of the divalent

[2] A. G. Chynoweth, J. Appl. Phys. **27**, 78 (1956).
[3] R. B. Roof, Jr., Acta Cryst. **9**, 781 (1956).
[4] G. T. Morgan, Proc. Roy. Soc. (London) **A112**, 465 (1925).
[5] M. Peter (submitted to Phys. Rev.).

metal ions. These are substitutions of the Na^+ ion, substitutions of M^{++} ions, substitutions of groups on the acetylacetone ions, and substitutions of solvate molecules.

X-ray studies of the NaNi and NaMg $Acac_3 \cdot p$-dioxane and of NaNi $Acac_3 \cdot$benzene indicate that these have a diffraction symmetry consistent with space group $P\bar{3}1c$, with two molecules per unit cell. Paramagnetic resonance measurements support the view that the dioxane compounds are macroscopically trigonal, but that this symmetry results from disorder among monoclinic unit cells. Invoking the positions available in the idealized space group $P\bar{3}1c$, the most probable positions of the paramagnetic divalent ions in NaNi acetylacetonate$_3 \cdot p$-dioxane are the 2(a), giving an interionic distance of $c/2=6.10$ A.

ACKNOWLEDGMENTS

The authors gratefully acknowledge the invaluable contributions of M. Peter's paramagnetic resonance measurements and permission to cite his results, the aid rendered by S. Geller and R. D. Burbank in discussions of the structural aspects of this problem, and by T. H. Geballe in performing the pyroelectric and piezoelectric tests. We wish to thank K. D. Bowers and W. B. Mims for important contributions to the resonance data, and F. J. Schnettler and J. H. Scaff for their helpful comments.

THE JOURNAL OF CHEMICAL PHYSICS VOLUME 32, NUMBER 2 FEBRUARY, 1960

Electrical Properties of Poly-Copper Phthalocyanine

A. Epstein and Bernard S. Wildi

Research and Engineering Division, Monsanto Chemical Company, Dayton, Ohio

(Received July 20, 1959)

Hall effect and electrical resistivity measurements as a function of temperature to ~450°C have been carried out on a polymer of copper phthalocyanine. From the Hall effect data it is concluded that intrinsically the polymer of copper phthalocyanine is *P* type. Two states of this polymer have been determined, one has an activation energy of 0.26 ev and a carrier density $\sim 10^{16}/cm^3$ (the carrier concentration varying with temperature), a second, a heat-treated polymer, also shows *P* type conductivity but the carrier density is $\sim 10^{18}/cm^3$ and is constant in the range of temperature measured. The mobility in the heat-treated polymer is found to increase with increasing temperature. *N* type conductivity observed on the first structure is believed to be a consequence of impurities.

INTRODUCTION

ALTHOUGH evidence of "semiconductor" behavior has been noted or predicted in some of the organic materials notably the aromatic ring compounds, such as the phthalocyanines, isobenzanthrone, dibenzanthrone, pyranthrone, anthracene, naphthalene, and others by earlier workers[1–8] there has been no comprehensive study made of the electrical properties of these compounds. In order to provide a basis for an understanding of the conduction mechanism in organic compounds, further information on the conductivity type and number of carriers is required. To provide such information the most convenient tool is the Hall effect measurement. Since the resistivity in the foregoing compounds is too high for straightforward and satisfactory measurements of the Hall coefficient emphasis has been placed on preparing and studying compounds having resistivities of suitable magnitude for Hall effect measurements. A satisfactory compound for this purpose and chosen because of chemical stability and ease of physical preparation is a polymeric form of copper phthalocyanine prepared by heating

[1] D. D. Eley, Nature **162**, 819 (1948); Eley *et al.*, Trans. Faraday Soc. **49**, 79 (1953); Trans. Faraday Soc. **51**, 152 (1955).
[2] Inokuchi *et al.*, Bull. Chem. Soc. Japan **24**, 222 (1951); **25**, 281 (1952); **27**, 22 (1954); J. Chem. Phys. **18**, 8101 (1950).
[3] H. Mette and H. Pick, Z. Physik **134**, 566 (1953).
[4] A. G. Chynoweth and W. G. Schneider, J. Chem. Phys. **22**, 1021 (1954).
[5] A. T. Vartanyan, J. Phys. Chem. (U.S.S.R.) **22**, 769 (1949); Act. Physicochim. U.R.S.S. **22**, 201 (1947).
[6] D. Kleitman, "Electrical properties of phthalocyanine," PB 111419 (August 1953).
[7] Winslow *et al.*, J. Am. Chem. Soc. **77**, 4751 (1951).
[8] C. A. Coulson, *Determination of Organic Structures by Physical Methods*, E. R. Braude and F. C. Nachod, Editors (Academic Press, Inc., New York, 1955), pp. 727–756.

pyromellitonitrile with cuprous chloride and urea:

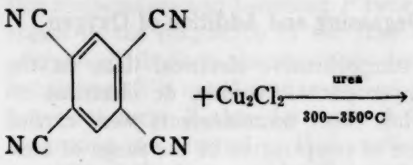

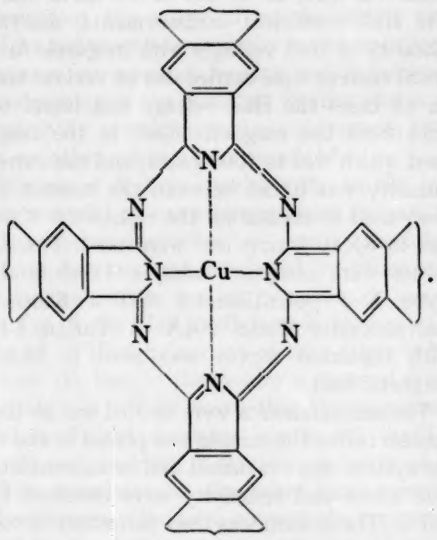

While Winslow *et al.*[7] have studied the pyrolysis effects of polyvinylidene chloride and pre-oxidized polydivinylbenzene as related to paramagnetic resonance absorption and from this have postulated that *P* type conductivity should result in the aromatic compounds, there are a scarcity of quantitative measurements to corroborate their hypothesis.

CHEMICAL PREPARATION OF MATERIAL (SYNTHESIS)

Monomeric phthalocyanines can be prepared by heating phthalonitrile with the appropriate metal and a trace of urea serving as a source of hydrogen.[9] Poly-copper phthalocyanine was prepared by heating pyromellitonitrile (1,2,4,5-tetracyanobenzene) with cuprous chloride. A purplish black material was obtained which was purified by exhaustive extraction and sublimation procedures. The material was difficult to analyze, giving consistently low values for carbon. (Pyrolysis of the polymer at 410°C showed a marked change in the nitrogen content. The nature of the change is being investigated in more detail.)

Pyromellitamide

A mixture consisting of 109 g (0.5 mole) of pyromellitic dianhydride (mp 285–7°C), 100 g (1.65 mole) of urea, and 740 g of trichlorobenzene was heated at 130°C for several hours, then at 150–60°C for two hours. The crude, pink colored pyromellitamide did not melt below 310°C. Treatment of the crude amide with 750 ml aqueous ammonia at room temperature gave 83 g of nearly colorless pyromellitamide. The amide decomposed at 285°C.

Pyromellitonitrile

A suspension of 50.0 g of crude pyromellitamide in 750 ml of dimethyl formamide was treated with phosgene for four hours, during which the temperature rose from 10 to 30°C. After the addition was completed, the mixture was stirred at 30°C for 18.5 hr, then centrifuged to remove 3.6 g of the starting amide. The supernatant liquid was poured into 2 liters of ice and water, and filtered to yield 29 g of tan solid. Recrystallization of the product from a solution of 400 ml of dioxane and 150 ml of water yielded 23.4 g (66% yield; 71% conversion) of pyromellitonitrile, mp 264–7°C. A sample was prepared for analysis by a recrystallization from dioxane and sublimation at 0.05 mm.

Analysis of the nitrile give the following results: *Anal.* Calculated for $C_{10}H_2N_4$: C, 67.41; H, 1.13; N, 31.45. Found: C, 67.36, 67.36; H, 1.33, 1.44; N, 31.33.

Poly-Copper Phthalocyanine

A mixture of 16 g of pyromellitonitrile, 5.3 g Cu_2Cl_2, and 1.0 g urea was ground in a mortar then heated at 300°C under 1000 psi of nitrogen in a glass lined bomb for 18 hr. The temperature was raised to 350°C and the mixture heated for two additional hours. The solid was ground in a mortar then triturated with boiling pyridine until the triturates were colorless. The product was dried and heated at 350°C/0.05 mm for 72 hr. During the sublimation a trace of white material was removed. The residue was again extracted for 48 hr with boiling pyridine in a Soxhlet to remove traces of copper salts. The material was dried and again heated at 340°C/0.05 mm for six hours.

Analysis of the polymer gave the following results: *Anal.* Calculated for $C_{20}H_4N_8Cu$: C, 57.20; H, 0.960; N, 26.68; Cu, 15.14. Found: C, 52.91, 52.93; H, 1.25, 1.21; N, 27.06, 27.24; Cu, 15.93, 15.90.

The polymer was a black-purple solid, only slightly soluble in cold sulfuric acid. No data have been obtained on the molecular weight of the polymer.

PREPARATION OF SAMPLES FOR PHYSICAL MEASUREMENTS

The polymer of copper phthalocyanine as made is in the form of a powder. (No crystalline material has as yet been successfully made.) To prepare samples for Hall effect and electrical measurements the material was pressed in the shape of rectangular parallelopipeds. Samples having dimensions 0.9×0.3×0.8 cm were used.

[9] K. Venkataraman, *The Chemistry of Synthetic Dyes* (Academic Press, Inc., New York, 1952), pp. 1118–1142.

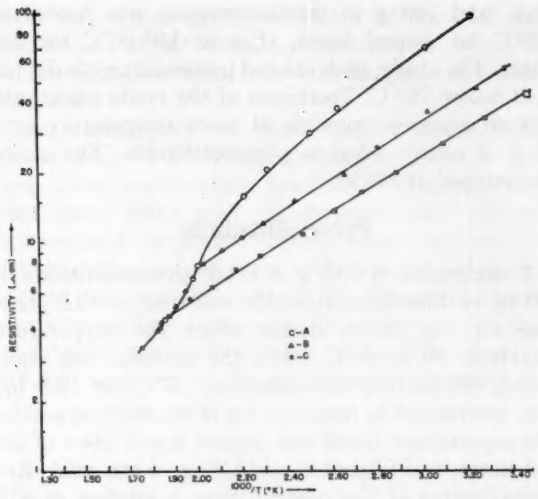

FIG. 1. Electrical resistivity *vs* inverse absolute temperature [1000/T(°K)] of poly-copper phthalocyanine sample No. 30 as function of outgassing.

Samples were compacted using pressures from 20 000 to 200 000 psi. Sample resistances were of the order of 5000 Ω or less.

For electrical contacts pressure type contacts, evaporated silver, or silver paint were used. Reproducible results were obtained with each type of contact and linearity of the current and voltage was found in the range of currents used. Current densities to 8×10^{-2} amp/cm² were used. Temperature was measured by means of an iron-constantan thermocouple (B and S Gauge No. 30). The sample was placed on a lavite sample holder and electrical connections to external circuits were arranged through glass-metal seals. The sample holder was placed in a Vycor tube and so arranged that it was possible to either evacuate the system or expose the sample to any desired atmosphere. In this way experiments were carried out in vacuo at pressures of from 10^{-2} to 10^{-5} mm Hg. A heater was placed around the Vycor tube to provide the desired temperature.

EFFECT OF GRAIN BOUNDARIES AND CONTACT RESISTANCE

To investigate the effect of grain boundary contributions, contact resistance, and pressure on the results obtained in the following, both dc and ac measurements of resistivity were carried out. The ac measurements were carried out on a Q-meter Type 260-A (Boonton Radio Corp.) to 5 Mc; dc measurements were made using the Kelvin method. Within the accuracy of our experiment (20%), both dc and ac measurements were found to give the same results within the range of pressures used (20 000–200 000 psi) and within the range of frequencies from dc to 5 Mc.

It was therefore possible to conclude that the measurements reported in the following were not primarily due to contact effects or grain boundary contributions.

ELECTRICAL MEASUREMENTS

Effect of Degassing and Addition of Oxygen

To provide comprehensive electrical data on the polymer of copper phthalocyanine, dc electrical resistivity and Hall effect measurements were carried out as a function of temperature in the range of temperatures from 25 to 450°C. To check the validity of the Hall coefficient measurements, determination of linearity of Hall voltages with magnetic field and electrical current were carried out at various temperatures. In all cases the Hall voltage was found to be linear with both the magnetic field, in the range of fields used which was to 4000 gauss, and the current. Similar linearity was found between the current and voltage drop used in measuring the resistivity. Current densities to 8×10^{-2} amp/cm² were used. The dc measurements were obtained using a Leeds and Northrup Type K-3 potentiometer and a Kintel electronic Galvanometer Model 204A. A Varian 4-in. magnet with regulated supply was used to obtain the dc magnetic field.

The measurements were carried out in the following manner: after the sample was placed in the vycor tube, the system was evacuated and measurements of the dc Hall effect and resistivity were obtained from 25 to 250°C. The system was then permitted to cool down to room temperature (25°C) and the procedure was repeated twice. The results are shown in Figs. 1 and 2 where the successive measurements are denoted by symbols A, B, and C. Following this the sample was sufficiently outgassed so that reproducibility was noted and the runs believed characteristic of the materials are shown in Figs. 3 and 4, curves D, E, and F.

In Figs. 1 and 2 there are several effects to be noted. The Hall coefficient is negative for curves A and B at

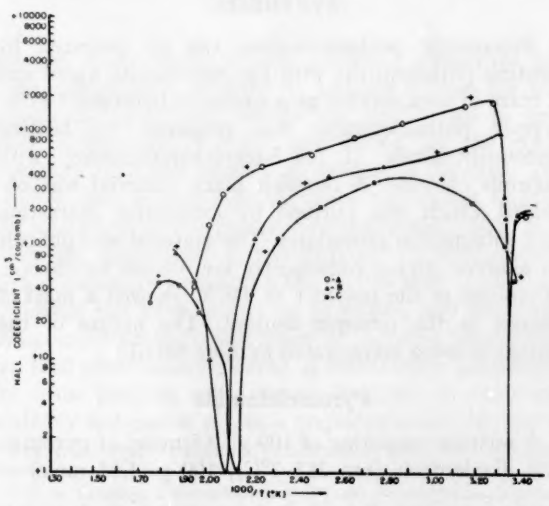

FIG. 2. Hall coefficient *vs* inverse absolute temperature [1000/T(°K)] of poly-copper phthalocyanine sample No. 30 as function of outgassing.

room temperature, undergoing a reversal just above this temperature and becoming P type. There is a decrease in the magnitude of the Hall coefficient with outgassing. Similarly the resistivity decreases with the outgassing. It is noted that in general the R/δ ratio is lower for curve B than for curve A. With increased outgassing the reversal in Hall coefficient can be removed and the type remains P type (curve C, Figs. 1 and 2) throughout the range of measurements and thereafter. The apparent irreversibility in the resistivity curve disappears on repeated heating and is believed related to outgassing of the material. Similar effects as noted by resistivity *vs* temperature measurements have been found on other organic compounds.[5,6]

The indication of N type conductivity in the low temperature material at room temperature appears to be related to gaseous impurities or vapors associated with the atmosphere and can be altered by either outgassing, high temperature cycling in vacuo, or use of oxygen. In Fig. 5 the Hall coefficient is plotted at a temperature of 25°C as a function of time (time being measured from the instant the system is pumped down to 10^{-2} mm Hg). It will be noted that the magnitude of the Hall coefficient decreases continually until a value of -20 cm³/coulomb is attained, a factor of 10 decrease. The resistivity on the other hand remains unchanged with time. One may convert the type from N to P type by the following two methods: (1) use of oxygen at room temperature; (2) temperature cycling. In Table I the Hall coefficient is shown as a function of oxygen pressure.

The sign of the Hall coefficient is observed to change with an oxygen pressure greater than 490 mm Hg. Evidence for the effect of temperature cycling affecting the Hall coefficient can be seen in Fig. 1 where on heating to ~250°C in vacuo of 10^{-2} mm or better one

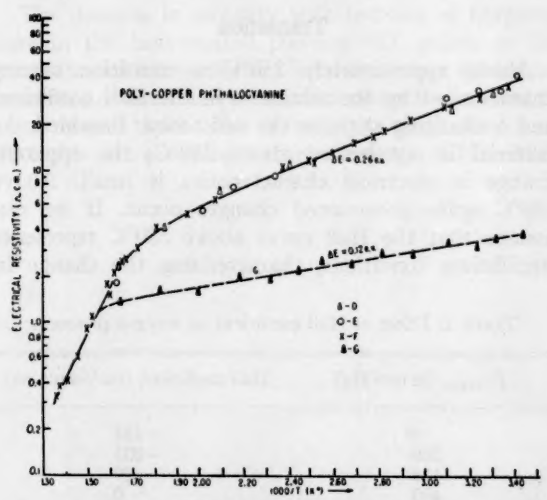

FIG. 3. Characteristic curve of electrical resistivity *vs* inverse absolute temperature $[1000/T(°K)]$ of poly-copper phthalocyanine sample No. 30 and heat treated poly-copper phthalocyanine.

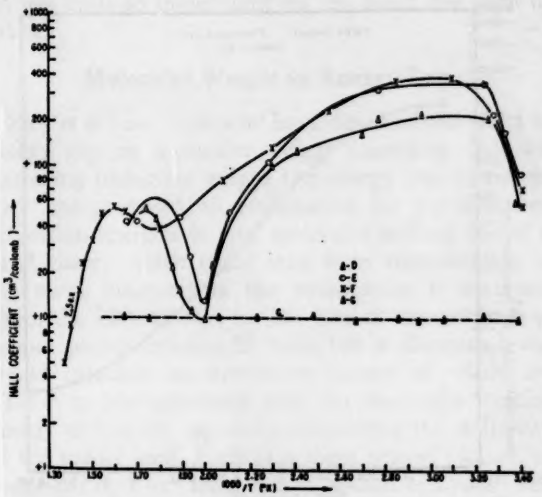

FIG. 4. Characteristic curves of Hall coefficient *vs* inverse absolute temperature $[1000/T(°K)]$ of poly-copper phthalocyanine sample No. 30 and heat treated poly-copper phthalocyanine.

can convert from N type to P type at $T=25$°C. Qualitative adsorption studies made on the material at room temperature reveal the possibility of water vapor adsorption. It is therefore conceivable that the low-temperature Hall reversal observed in Fig. 1 may be related to a physical (adsorption) desorption process and would fit in a very *general* way with impurity concepts normally associated with inorganic semiconductors.

Effect of Temperature Cycling

Heating to 350°C

Characteristic resistivity and Hall effect *vs* temperature runs are shown in Figs. 3 and 4 (curves D, E, F) for poly-copper phthalocyanine. The resistivity curve is reproducible with a room temperature resistivity for the material of 40 ohm cm. This is a decrease by a factor of 3 in the material over that which has not been outgassed. The Hall coefficient is similarly decreased which suggests that the number density of effective carriers may be increasing. With increasing temperature, to a temperature of 250°C one can associate an activation energy with the resistivity *vs* temperature curve of 0.26 ev *assuming* an expression for the resistivity of $\rho=\rho_0 \exp(-\Delta E/2kT)$.* No such

* While this expression can be written down to represent the experimental data, an interpretation of the relationship is not so simple. Evidence presented in the text points to a great dependence of the electrical resistivity on both the molecule and the intermolecular barriers, hence ΔE may be a composite of both effects. The number of electrons available for conduction in the ring compound may actually not be as temperature dependent (or temperature sensitive) as the transport phenomena leading to conduction. Such a picture is quite different from that found in elementary structures of the inorganic type such as germanium or silicon where the dependence on neighboring atoms and lattice interactions may account for the availability of electrons and holes and a greater dependence of carrier density on temperature than is found for the mobility.

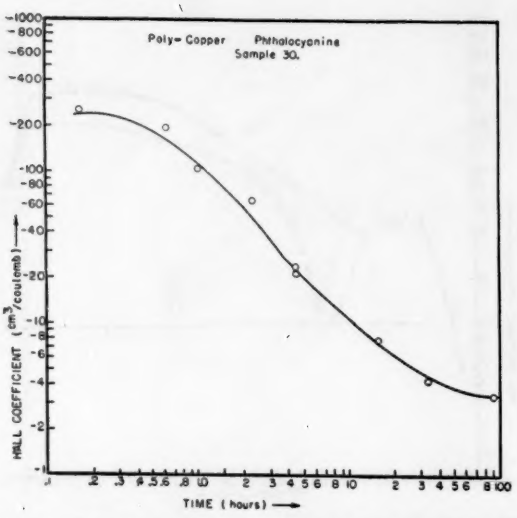

FIG. 5. Variation of Hall coefficient of poly-copper phthalocyanine with time at a temperature of 25°C.

slope is evident on the Hall curve but it will be noted that the Hall curve though remaining P type shows a minimum at 250°C and a steep decrease before that; the minimum shifts in temperature and changes in magnitude depending on the highest temperature to which the sample is heated. Following the minimum, the Hall coefficient increases with increasing temperature until a value of $\sim+60$ cm³/coulomb is reached, whereupon it declines steeply up to 450°C. This behavior is also reflected in the resistivity *vs* temperature curve which indicates a much more rapid decrease in resistivity. Provided one does not heat the material above 350°C it is possible to reproduce the resistivity curve and the general shape of the Hall curve.

Heating to 450°C

On heating above 350°C and especially above 400°C there is a pronounced irreversibility in both the Hall effect and the electrical resistivity. The effects of this irreversibility are shown in Figs. 3 and 4, curve G, where a sample previously heated to 450°C, on reheating exhibits entirely new Hall effect and electrical resistivity characteristics. It will be noted that the Hall coefficient while still positive (P type) has dropped by almost an order of magnitude in value and becomes constant with a value of $+10$ cm³/coulomb. The resistivity also shows a tenfold decrease from $\sim$40 to $\sim$4 ohm cm at room temperature (25°C) with an activation energy of 0.12 ev*. If we assume intrinsic conditions and with the hole mobility $\mu_h \gg \mu_e$ then we find, providing one can use the simple expression for the Hall effect, that $n \approx 1/Re \approx 10^{18}$/cm³ and $\mu_h \approx 2.5$ cm²/v sec at room temperature increasing to a value of $\sim$10 cm²/v sec at 350°C. It is noteworthy that the activation energy reported for the resistivity *vs* temperature curve may be associated more closely with a mobility variation than with a change in the number density of carriers. The new characteristics are believed associated with a new structure resulting from a breaking of the C—N bonds and a possible rearrangement within the molecules with an overall loss of nitrogen.

A 0.65-g sample of the polymer was heated for eighteen hours at 410°C/0.25 mm. During this treatment the weight loss of the sample was 10.8%. No material collected at room temperature on the walls of the sublimation apparatus. The material had the following analysis:

Anal. Found: C, 52.65, 52.78; H, 1.42, 1.22; N, 24.30, 24.18.

DISCUSSION

The measurement of P type conductivity observed at the higher temperatures fits in well with the observations of Kleitman of P type conductivity in phthalocyanine,[6] the predictions of Winslow *et al.*,[7] the results of Chynoweth *et al.* on anthracene,[4] and the observations on polymer carbons.[7] Our observations on the polymer of copper phthalocyanine would further tend to support the hypothesis of P type conductivity in condensed aromatic ring compounds.

Polymer, SI

The results of our measurements on this "low temperature polymer" of copper phthalocyanine reveals that "intrinsically" the material is P type and has an "activation energy" of 0.26 ev. R/ρ roughly corresponds to $\sim$10 cm²/v sec with a number density of carriers of $\sim 10^{16}$/cm³ at $T=25$°C. The carrier density is temperature dependent. In a very general way this characterizes the "low temperature polymer" which we call SI.

Transition

Above approximately 250°C a transition occurs, characterized by the minimum in the Hall coefficient and a changing slope in the resistivity. Provided the material is not heated above 250°C, the apparent change in electrical characteristics is small. Above 350°C quite pronounced changes occur. If we can assume that the Hall curve above 350°C represents equilibrium conditions, characterizing the change in

TABLE I. Effect of Hall coefficient on oxygen pressure.

P_{Oxygen} (in mm Hg)	Hall coefficient (cm³/coulomb)
0[a]	−252
209	−103
414	−39
490	0
775	+105

[a] ±Sample was initially evacuated to a pressure 10^{-5} mm Hg for a period of 42 hr at $T=23$°C, constant temperature was maintained.

state, then the slope of the Hall curve may provide information on the energy characterizing the change. The activation energy calculated from the Hall curve is 2.5 ev. It is interesting that the energy required to break a C—N bond is ~3 ev or within range of the experimental activation energy. It is possible that the pyrolyzing action leads to a breaking of bonds giving rise to a new chemical composition. The chemical analysis of the "heat-treated polymer" showed a marked decrease in the percentage of nitrogen when compared to the analysis of the starting polymer thus providing some chemical evidence for such a change.

Heat-Treated Polymer, SII

The heat-treated material in contrast to the original polymer showed a large increase in the carrier density to $\sim 10^{18}/cm^3$, a decrease in the mobility, and a very small activation energy of 0.12 ev which with a constant Hall coefficient could be associated with the mobility. The conductivity type still remains *P* type.

P Type Conduction

The increase in carrier density noted on going from the original polymer SI to the heat-treated polymer SII, could be associated with an increase in unsaturation and of unpaired electrons. Such an action could then lead, as Winslow *et al.*[7] have postulated to *P* type conduction by a mechanism of the type $Me^{n+} + Me^{(n+1)+} \rightarrow Me^{(n+1)+} + Me^{n+}$ where Me^{n+}, $Me^{(n+1)+}$ represents an atom (or molecule) in two stages of ionization. These radical sites are able to drift through the conjugated network in successive steps resembling holes.

Mobility

The increase in mobility with increase of temperature in the heat-treated polymer SII points to the possibility of intermolecular barriers or to a strong dependence of the transport coefficient on the number of unsaturated bonds. For a mobility of the order of 10 cm^2/v sec, assuming a thermal energy of $kT \sim 0.025$ ev, one finds an upper limit for the mean free path of ~1 A.

Molecular Weight *vs* Energy Gap

Eley *et al.*[1] and Inokuchi[2] have discussed the effect of energy gap on molecular weight remarking that for increasing molecular weight the energy gap decreases. Eley has proposed an explanation for the observed activation energies in ring molecules making use of a band theory which could arise from consideration of the wave functions of the overlapping π electrons. From the Eley theory, for the case of this polymer of copper phthalocyanine SI with 140 π electrons,† one would calculate an activation energy of ~0.20 ev. This is in fair agreement with the observed activation energy of 0.26 ev, especially considering the simplicity of the model used. Perhaps a more refined picture, as suggested by Fox[10] using a modification of Lyons[11] and accounting for the observed *P* type conduction and the low R/ρ ratio by the introduction of a second conduction band (narrow in width) to simulate a jump process (as suggested in the foregoing), may lead to closer agreement and perhaps a somewhat better interpretation of the conduction process.

CONCLUSIONS

We have been able to determine, on a polymer of copper phthalocyanine, by Hall effect measurements, the existence of *P* type conduction and a carrier mobility in the polymer of ~10 cm^2/v sec. Two states of this polymer have been studied: one (SI) has an activation energy of 0.26 ev and a carrier density $\sim 10^{16}/cm^3$ (the density varying with temperature); a second state SII (heat-treated polymer), is also found to give *P* type conduction but the carrier density is $\sim 10^{18}/cm^3$ and constant and the mobility increases with increasing temperature. *N* type conductivity observed in SI is believed to be a consequence of impurities.

† This value was calculated on the basis of five phthalocyanine units.

[10] D. Fox, J. Phys. Chem. Solids **8**, 439 (1959).

[11] L. E. Lyons, J. Chem. Soc. **1957**, 5001.

"Improved" Free-Volume Theory of Liquids. II*

JOHN S. DAHLER,† *Aeronautical Research Laboratory, Wright-Patterson Air Force Base, Ohio*

AND

JOSEPH O. HIRSCHFELDER, *University of Wisconsin Theoretical Chemistry Laboratory, Madison, Wisconsin*

(Received August 10, 1959)

The Kirkwood nonlinear integral equation for determining the optimum free volume of a liquid is integrated by an iterative procedure with the approximation that the cell distribution function is spherically symmetrical. The potential of the system is assumed to be pairwise additive and the interaction between two molecules obeys the Lennard-Jones 12–6 potential. To simplify the computations, the contributions to the cell potential by molecules beyond the first shell of nearest neighbors are calculated as though the molecules were located at their lattice points. The method of Levine, Mayer, and Aroeste was used to optimize the lattice dimensions and take into account the existence of holes. Extensive tables are given for the configurational internal energy, compressibility factor, and configurational entropy. Comparison of the configurational internal energy and compressibility factor with the Monte Carlo calculations indicates that our isotherms correspond to extensions of the crystalline phase into a metastable low density region. Comparison of our configurational entropy with experimental data indicates that we are lacking the entropy of fusion. Our values of the configurational internal energy agree rather well and our values of the compressibility factor agree very poorly with the experimental data. Comparisons are also made with the results of other theoretical treatments.

I. INTRODUCTION

KIRKWOOD[1] has developed a nonlinear integral equation which determines the optimum free volume of a liquid. In the present paper, approximations are introduced which spherically symmetrize the free volume and make the Kirkwood equations suitable for solving by high speed digital calculating machines. These solutions, and the resulting equation of state of a liquid, are obtained and compared with experiments. The agreement is very poor, suggesting that there is something intrinsically wrong with the free-volume concept of a liquid. The agreement is not improved appreciably when the equation of state is corrected to take into account the existence of holes in the liquid using the method of Levine, Mayer, and Aroeste.[2] Thus, it appears that correlations between the motions of neighboring molecules play an important role in the structure of a liquid. This conclusion was reached in a previous article[3] outlining the problems involved in determining the optimum free-volume equation of state of a liquid.

The cell model for liquids is based upon the physically appealing notion that the average arrangement of molecules in a liquid should rather closely resemble that in a crystalline solid. To defend this assumption one can argue that the tightly packed structure of a liquid will severely restrict the translational motions of the molecules. Thus, to progress from one point in the liquid to another, a molecule must first penetrate the confining energy barrier which arises from its interactions with neighbor molecules. Its gross progress through the liquid can, therefore, be described as a sequence of short jumps or random flights each of which involves its escape from one group of neighbors and its subsequent entrapment by another. At high densities, the frequency of occurrence for these jumps[4] should be much less than that associated with the oscillatory motion which the molecule performs while confined by the force fields of its neighbors. Therefore, on the average, we expect that a given molecule will lie within a cagelike structure or cell whose boundaries are formed by other molecules.

On the basis of these considerations it seems likely that a satisfactory estimate for the average potential energy of a molecule could be obtained by assuming that the arrangement of its neighbors is much like that in a crystalline solid. If this viewpoint is adopted, then the problem of theoretically determining the thermodynamical properties of the liquid reduces to that of constructing the effective or mean potential energy field within a cell. Once this potential function is known, it is possible to compute the corresponding Boltzmann factor and so determine the probability with which a molecule occupies different points within its cell. From a knowledge of this cell distribution function, one can then proceed directly to the calculation of the thermodynamical properties and equation of state for the liquid.

Of the many theories which have been based upon this model, the best known and most thoroughly

* This work was supported in part by United States Air Force Contract AF33(616)-3414 with The University of Wisconsin.

† Present address, Department of Chemical Engineering, University of Minnesota, Minneapolis 14, Minnesota.

[1] J. G. Kirkwood, J. Chem. Phys. **18**, 380 (1950).

[2] Levine, Mayer, and Aroeste, J. Chem. Phys. **26**, 201 (1957).

[3] Dahler, Hirschfelder, and Thacher, J. Chem. Phys. **25**, 249 (1956). This article was entitled, "The Improved Free-Volume Theory of Liquids. I."

[4] The diffusion process requires an accumulation of excess translational energy by the particular molecule in question, the simultaneous occurrence of a void space in its vicinity, and a fluctuation of its molecular environment which will permit passage to this void. For a more detailed description of this mechanism see S. A. Rice, Phys. Rev. **112**, 804 (1958).

tested is that due to Lennard-Jones and Devonshire.[5,6] According to this method, one constructs the cell potential by fixing the neighbors of each molecule directly upon their respective lattice sites. The equation of state and thermodynamical properties obtained from this theory agree surprisingly well with experiments. However, the high cost which one pays for this success is a physically unpalatable microscopic characterization of the liquid wherein each molecule plays the curious double role of (1) a rigidly constrained portion of the lattice environment about each of its neighbors and (2) a quasi-free wanderer in the potential field derived by fixing all of the others directly upon their lattice sites. Therefore, it must be concluded that the success of the Lennard-Jones and Devonshire theory is somewhat fortuitous and not indicative of the validity of the assumptions upon which it is based.

The present study is concerned with the more rigorous and mathematically complicated theory developed by Kirkwood.[1] We find that the isotherms derived from this theory resemble continuations of the crystalline isotherms and agree neither with the Monte Carlo nor with the experimental isotherms for liquids. Furthermore, the results of our calculations are not in accord with those obtained by the method of Lennard-Jones and Devonshire. A major factor contributing to this failure of the cell theory is the artificially high degree of order built into the model. Although it has often been supposed that this order could be disrupted by introducing holes or empty cells into the theory, we find that the slight increase of entropy which accompanies the introduction of such a hole is more than offset by the enormous amount of energy required for its production. Therefore, the criterion of thermodynamical stability based upon the free energy function does not favor a large number of holes. As a consequence of this the introduction of holes will not significantly alter the theoretical estimates for the thermodynamical properties.

As in the Lennard-Jones and Devonshire treatment, we assume that the forces between the molecules in a liquid are pairwise additive and the interaction between each pair of molecules corresponds to a Lennard-Jones 6–12 intermolecular potential. The validity of these assumptions is open to question. The quantum mechanical calculations of Jansen[7] would lead us to suppose that the deviations from pairwise additivity of the intermolecular forces might account for rather large deviations in the internal energy of a liquid. Then, too, when the equation of state of the liquid noble gases is expressed in terms of reduced variables there are considerable differences between the corresponding states relationships as determined from the different noble gases. These deviations provide experimental evidence for either deviations from the Lennard-Jones 6–12 potential or a lack of pairwise additivity. Such errors in our basic assumptions could readily account for our lack of agreement with the experimental equations of state of liquids. However, the same assumptions as to pairwise additivity and potential energy function are made in the Monte Carlo calculations and therefore these assumptions cannot explain the rather large differences between our results and those obtained by Monte Carlo.

In addition to these shortcomings of the theory itself, approximations involved in our calculations may also have contributed to the observed disparity between theory and experiment. Studies are presently being conducted to assess the quantitative effects of these approximations.

II. KIRKWOOD'S THEORY

The partition function for a system composed of N identical and structureless molecules is equal to $(2\pi mkT/h^2)^{3N/2}Q_N(V, T)$. Here m represents the mass of an individual molecule, T the absolute temperature, and V the total volume of the system. The configuration integral

$$Q_N(V, T)=(1/N!)\int_V\int_V\cdots\int_V W_N d\tau_1 d\tau_2\cdots d\tau_N \quad (1)$$

is defined in terms of $W_N=\exp(-\Phi_N/kT)$, the Boltzmann factor associated with the total interaction energy of the N molecules ($d\tau_i=dx_i dy_i dz_i$ is the differential element of volume for the ith molecule).

Following Kirkwood, we now imagine the volume of the system to be spanned by N identical cells, $\Delta_1, \Delta_2, \Delta_3, \cdots, \Delta_N$, the centers of which form a regular quasi-lattice. Each integration appearing in Eq. (1) then becomes a sum of integrals over the various cells, i.e.,

$$\int_V d\tau_i=\sum_{h_i=1}^{N}\int_{\Delta_{h_i}} d\tau_i.$$

From this it follows that the configuration integral may be written as the sum of N^N terms corresponding to the N^N different ways of placing N molecules in N cells:

$$Q_N(V, T)=\frac{1}{N!}\sum_{h_1=1}^{N}\sum_{h_2=1}^{N}\cdots\sum_{h_N=1}^{N}\int_{\Delta_{h_1}}\int_{\Delta_{h_2}}\cdots \int_{\Delta_{h_N}} W_N d\tau_1 d\tau_2\cdots d\tau_N$$

$$=\sum_{\{m\}} Q_N(m_1, m_2, \cdots, m_N)/\prod_{i=1}^{N} m_i!. \quad (2)$$

Here $Q_N(m_1, m_2, \cdots, m_N)$ denotes that contribution to

[5] Hirschfelder, Curtiss, and Bird, *Molecular Theory of Gases and Liquids* (John Wiley & Sons, Inc., New York, 1954), p. 293.
[6] Wentorf, Buehler, Hirschfelder, and Curtiss, J. Chem. Phys. **18**, 1484 (1950).
[7] L. Jansen and Z. I. Slawski, J. Chem. Phys. **22**, 1701 (1954); L. Jansen and R. T. McGinnies, Phys. Rev. **104**, 961 (1956); R. T. McGinnies and L. Jansen, Phys. Rev. **104**, 1301 (1956).

TABLE I. The lattice parameters for the face-centered cubic (F.C.C.), the hexagonal close-packed (H.C.P.), the simple cubic (S.C.), and the body-centered cubic (B.C.C.) lattices.[a]

Lattice	b	Z_1	A_{12}	A_6
F.C.C.	$(2)^{\frac{1}{2}}$	12	0.131 88	2.453 92
H.C.P.	$(2)^{\frac{1}{2}}$	12	0.132 29	2.454 89
S.C.	1	6	0.202 10	2.401 92
B.C.C.	$(27/16)^{\frac{1}{2}}$	8	1.114 18	4.253 30

[a] See reference 9.

the configuration integral which arises from arrangement of m_1 molecules in the first cell, m_2 in the second cell, etc. Since the most probable arrangement should be that for which each cell is singly occupied, we rewrite Eq. (2) in the form

$$Q_N(V, T)=Q_N^{(1)}\beta^N, \tag{3}$$

where

$$Q_N^{(1)}=Q_N(1, 1, \cdots, 1), \tag{4}$$

and

$$\beta^N=\sum_{\{m\}}\left(\prod_{i=1}^{N} m_i!\right)^{-1}Q_N(m_1, m_2, \cdots, m_N)/Q_N^{(1)}. \tag{5}$$

This procedure of Kirkwood's factors from the configuration integral that portion which we intuitively believe to be the most important. The term β^N represents those contributions which arise from the less favored distributions of the molecules over the cells. At very low densities β approaches a limiting value of e; at high densities it tends to a limit of unity. There is also some reason to believe that the value of β will lie very near unity throughout the range of liquid densities.[8] Consequently, for liquids it seems justified to neglect the dependence of β upon temperature and density and focus attention upon $Q_N^{(1)}$.

To evaluate $Q_N^{(1)}$ Kirkwood proposed that the probability distribution be chosen in the same way for each cell and that it be dependent only upon the vector displacement of a molecule from the center of its cell. This approximation amounts to replacing the actual distribution given by the Boltzmann factor W_N with a product of functions each of which refers to only a single one of the N molecules. A close analog to this procedure is the use of Hartree wave functions in the quantum mechanics of many-electron systems. The assumption in both instances is that a system of strongly interacting particles can be represented as a collection of quasi-independent particles, each acted upon by some sort of average force field. In atomic and molecular problems this field arises from the Coulombic interactions of the electrons with one another and with the nuclei; in the cell theory it is due to the interactions of a molecule with its neighbors in the quasi-lattice.

[8] J. Pople, Phil. Mag. **42**, 459 (1951).

From thermodynamics we are assured that the optimum choice for the cell distribution function will be that for which the Helmholtz free energy is a minimum. In Kirkwood's theory this criterion serves to uniquely characterize the cell distribution function as the solution of a particular integral equation. However, to actually solve this equation it seems necessary to suppress the angular dependence of the cell distribution function. Thus, we have introduced the function $s(R)$ such that $s(R)4\pi R^2dR$ is the probability that a particular molecule will lie at a distance between R and $R+dR$ from the center of its cell. Here R is measured in units of d_0, the separation between neighboring sites of the lattice. The value of d_0 can be expressed by the relation, $d_0^3=b(V/N)$, where b is a geometrical factor depending upon the lattice type. Values of b are given in Table I[9] for a number of different types of lattice. Each spherical cell is bounded by the radius a (expressed in units of d_0). In general, the "sphericalized" distribution function $s(R)$ depends not only upon the value of R but also upon the locations of the molecules which lie in neighboring cells. In Kirkwood's theory, these correlations are neglected. The justification for neglecting the correlations between the instantaneous configurations and motions of the neighboring molecules must ultimately rest upon the success of the resulting theory.

By minimization of the free energy it is found that the optimum function $s(R)$ satisfies the Kirkwood integral equation

$$s(R; T^*, V^*)=V_f'(T^*, V^*)^{-1}\cdot\exp\{-(1/T^*)[\phi(R; T^*, V^*)-\phi(0; T^*, V^*)]\}, \tag{6}$$

where

$$V_f'(T^*, V^*)=4\pi\int_0^a\cdot\exp\{-(1/T^*)[\phi(R; T^*, V^*)-\phi(0; T^*, V^*)]\}R^2dR. \tag{7}$$

Here R, the distance that a molecule lies from the center of its cell, is measured in units of d_0, the separation between the neighboring sites of the lattice. The function $\phi(R; T, V)$ is the cell potential function and the function $V_f'(T^*, V^*)$ is simply related to the free volume. The cell potential is the potential energy of a molecule at a distance R from the center of its cell, due to interactions with all of the other molecules in the liquid.

In the present investigation, it is assumed that the molecular interactions are pairwise additive and the energy of interaction of each pair of molecules is repre-

[9] The information needed for the construction of this table is found in Hirschfelder, Curtiss, and Bird, *Molecular Theory of Gases and Liquids* (John Wiley & Sons, Inc., New York, 1954), p. 1036.

sented by the Lennard-Jones 12–6 potential

$$u=4\epsilon[(\sigma/\rho)^{12}-(\sigma/\rho)^{6}]. \quad (8)$$

Here ρ is the distance between the two molecules, ϵ is the maximum energy of attraction of the pair, and σ is the low velocity collision diameter. The two parameters involved in this energy function can be used to define the reduced temperature, $T^*=kT/\epsilon$, and the reduced molecular volume, $V^*=V/N\sigma^3$. It is convenient to measure all distances in units of d_0. If now, R_{12} is the distance between the two molecules expressed in units of d_0, then the pair potential energy function becomes

$$u(R_{12}, V^*)=4\epsilon[(bV^*)^{-4}R_{12}^{-12}-(bV^*)^{-2}R_{12}^{-6}]. \quad (9)$$

Since the energies of interaction of the molecules are pairwise additive, each shell of molecules provides a contribution to the cell potential. Thus,

$$\phi(R; T^*, V^*)=\sum_{r=1}\phi_r(R; T^*, V^*). \quad (10)$$

Here $\phi_r(R; T^*, V^*)$ is the contribution of the rth removed shell of neighbors which contains Z_r molecules and lies at a distance $l_r d_0$ from the lattice point in question. If we hold molecule 1 fixed at a distance R from its lattice point and let molecule 2 lie at a distance R' from a lattice point in the rth shell, then $\phi_r(R; T^*, V^*)$ is equal to the product of Z_r times $u(R_{12}, V^*)$ averaged over all orientations of both molecules and over all values of R':

$$\phi_r(R; T^*, V^*)$$

$$=Z_r 4\pi\int_0^a K(l_r, R, R'; V^*)s(R'; T^*, V^*)R'^2dR', \quad (11)$$

where

$$K(l_r, R, R'; V^*)=(4\pi)^{-2}\iint u(R_{12}, V^*)d\omega_1 d\omega_2. \quad (12)$$

The integration in Eq. (12) is easy to carry out since we have previously[3] obtained the general result that if a function $Y(l_r, R, R', R_{12})$ does not depend upon the orientations of either of the two molecules, then

$$4RR'l_r(4\pi)^{-2}\iint Y d\omega_1 d\omega_2$$

$$=\int_{l_r-R-R'}^{l_r+R-R'}(R_{12}-l_r+R+R')\,Y R_{12}dR_{12}$$

$$+\int_{l_r+R-R'}^{l_r-R+R'}2RY R_{12}dR_{12}$$

$$+\int_{l_r-R+R'}^{l_r+R+R'}(-R_{12}+l_r+R+R')\,Y R_{12}dR_{12}. \quad (13)$$

With the aid of Eq. (13), it follows that the angle-averaged values of R_{12}^{-12} and R_{12}^{-6} are given by

$$(4\pi)^{-2}\iint R_{12}^{-12}d\omega_1 d\omega_2=(360RR'l_r)^{-1}G_r(9; l_r, R, R'), \quad (14)$$

and

$$(4\pi)^{-2}\iint R_{12}^{-6}d\omega_1 d\omega_2=(48RR'l_r)^{-1}G_r(3; l_r, R, R'), \quad (15)$$

where

$$G_r(n; l_r, R, R')=(l_r+R+R')^{-n}+(l_r-R-R')^{-n}$$
$$-(l_r+R-R')^{-n}-(l_r-R+R')^{-n}. \quad (16)$$

Thus, by making use of Eqs. (9), (14), and (15), Eq. (11) becomes

$$\phi_r(R; T^*, V^*)=(Z_r\epsilon/3Rl_r)$$
$$[(\tfrac{1}{15})(bV^*)^{-4}\Gamma_r(9, T^*, V^*; R)$$
$$-(\tfrac{1}{2})(bV^*)^{-2}\Gamma_r(3, T^*, V^*; R)], \quad (17)$$

where

$$\Gamma_r(n, T^*, V^*; R)$$

$$=2\pi\int_0^a s(R'; T^*, V^*)G_r(n; l_r, R, R')R'dR'. \quad (18)$$

The calculation of $\phi_r(0; T^*, V^*)$ requires special consideration since $G_r(n; l_r, 0, R')$ is zero. However,

$$\lim_{R\to 0}[G_r(n; l_r, R, R')/R]$$
$$=2n[(l_r-R')^{-(n+1)}-(l_r+R')^{-(n+1)}]. \quad (16')$$

Thus,

$$\phi_r(0; T^*, V^*)=(Z_r\epsilon/3l_r)[(\tfrac{1}{15})(bV^*)^{-4}\gamma_r(9, T^*, V^*; 0)$$
$$-(\tfrac{1}{2})(bV^*)^{-2}\gamma_r(3, T^*, V^*; 0)], \quad (17')$$

where

$$\gamma_r(n, T^*, V^*; 0)$$

$$=4\pi n\int_0^a[(l_r-R')^{-(n+1)}-(l_r+R')^{-(n+1)}]s(R')R'dR'. \quad (18')$$

The configurational internal energy U_c can be expressed in the form

$$U_c=(N/2)4\pi\int_0^\infty \phi(R; T^*, V^*)s(R; T^*, V^*)R^2dR. \quad (19)$$

With the help of Eqs. (10) and (19),

$$U_c/NkT=\sum_{r=1}(Z_r/3l_rT^*)[(\tfrac{1}{15})(bV^*)^{-4}\gamma_r(9; T^*, V^*)$$
$$-(\tfrac{1}{2})(bV^*)^{-2}\gamma_r(3; T^*, V^*)], \quad (20)$$

where

$$\gamma_r(n; T^*, V^*) = 2\pi\int_0^a \Gamma_r(n, T^*, V^*; R)s(R; T^*, V^*)RdR. \quad (21)$$

The free volume of a molecule in the liquid is

$$V_f(T^*, V^*) = V_f'(bV/N)\exp\{(2U_c/NkT) - \phi(0; T^*, V^*)/T^*\}. \quad (22)$$

Here the factor bV/N occurs because V_f' is expressed in units of d_0^3 [as is apparent from Eq. (7)]. The exponential factor results from the fact that the zero of energy in V_f' was taken to be the potential in the center of the cell. It is easy to show that

$$\log_e V_f = \log_e(bV/N) - 4\pi\int_0^a s(R)\log_e[s(R)]R^2dR. \quad (23)$$

The partition function for the cell model liquid can be expressed in terms of the free volume

$$Q_N(V, T) = [\beta\lambda^{-3}V_f\exp(-U_c/NkT)]^N. \quad (24)$$

Here $\lambda^2 = h^2/(2\pi mkT)$ where h is Planck's constant and m is the mass of a molecule.

The entropy of the liquid is given by

$$S/Nk = (\tfrac{3}{2}) + \log_e\beta - 3\log_e\lambda + \log_e V_f. \quad (25)$$

The entropy of an ideal gas at the same volume and temperature is given by

$$S_{\text{ideal}}/Nk = (\tfrac{5}{2}) - 3\log_e\lambda + \log_e(V/N). \quad (26)$$

The configurational entropy S_c is defined as the difference between the entropy of the liquid and the entropy of an ideal gas at the same volume and temperature. Thus,

$$S_c/Nk = -1 + \log_e\beta + \log_e V_f - \log_e(V/N). \quad (27)$$

Or making use of Eq. (22),

$$S_c/Nk = -1 + \log_e\beta + \log_e(bV_f') + (2U_c/NkT) - \phi(0; T^*, V^*)/T^*. \quad (28)$$

In the numerical tables of configurational entropy, we have assumed that the molecules in the liquid do not possess communal entropy so that $\log_e\beta = 0$.

The statistical mechanical equation of state of the liquid is

$$p/kT = \partial\log_e(Q_N(V, T))/\partial V. \quad (29)$$

where p is the pressure. Assuming that β is independent of volume in the density range under consideration and making use of Eqs. (23) and (24), the equation of state becomes

$$pV/NkT = 1 - V^*(\partial/\partial V^*)\cdot\left\{(U_c/NkT) + 4\pi\int_0^a s(R)\log_e[s(R)]R^2dR\right\}. \quad (30)$$

For present purposes, it is convenient to express (U_c/NkT) in the form

$$(U_c/NkT) = \sum_{r=1}\frac{Z_r(2\pi)^2}{3T^*}\int_0^a\int_0^a\left[\frac{G_r(9; t_r, R, R')}{15(bV^*)^4} - \frac{G_r(3; t_r, R, R')}{2(bV^*)^2}\right]s(R)s(R')R^2R'^2dRdR'. \quad (31)$$

Since a is independent of V^*, the order of performing the integrations and differentiations in Eq. (30) may be reversed. All the terms involving $[\partial s(R)/\partial V^*]$ may be grouped together to give

$$-V^*4\pi\int_0^a[\partial s(R)/\partial V^*]\{1 + \log_e[s(R)] + \phi(R; T^*, V^*)/T^*\}R^2dR. \quad (32)$$

However, inasmuch as the distribution function satisfies the integral relation of Eq. (6), we see that

$$\{1 + \log_e[s(R)] + \phi(R; T^*, V^*)/T^*\} = [1 - \log_e V_f' + \phi(0; T^*, V^*)/T^*]. \quad (33)$$

Clearly the terms on the right-hand side of Eq. (33) are independent of R. The terms in the bracket of (32) can therefore be moved outside of the integration sign. The remaining integral is zero because of the normalization of $s(R)$,

$$4\pi\int_0^a[\partial s(R)/\partial V^*]R^2dR = \frac{\partial}{\partial V^*}\left[4\pi\int_0^a s(R)R^2dR\right] = 0. \quad (34)$$

Thus the integral given in (32) is zero. The remaining terms in the equation of state arise from taking the derivative of the bracket in Eq. (31) with respect to V^*. In this manner we obtain the following relation for the compressibility factor:

$$pV/NkT = 1 + \sum_{r=1}(4Z_r/3T^*)\cdot[(\tfrac{1}{15})(bV^*)^{-4}\gamma_r(9; T^*, V^*) - (\tfrac{1}{4})(bV^*)^{-2}\gamma_r(3; T^*, V^*)]. \quad (35)$$

At high densities, where the cell theory should apply, the value of the cell radius is unimportant since $s(R)$ becomes effectively zero for large values of R. Thus, it is only at low densities, where the cell theory is a poor approximation, that the value selected for the cell radius affects the calculated physical properties of the system. In principle, the value of the cell radius a should be determined by the condition that the volume

of the cell equals the specific volume of a molecule in the liquid, $a=(3V/4\pi Nd_0^3)^{1/3}$. This would lead to overlapping of the cells since the value of a would be greater than 0.5 (for a face-centered cubic or hexagonal close-packed lattice, a would equal 0.55267; for a simple cubic lattice, a would equal 0.62035; for a body-centered cubic lattice, a would equal 0.56854). However, as has been previously shown,[3] some mathematical difficulties are encountered if the cells overlap so that molecules in neighboring cells are permitted to collide and have their centers occupy the same position in space. These difficulties are eliminated by setting $a=0.5$ (or slightly smaller). For none of the cases considered in the present calculations did $s(R)$ have an appreciable value for values of R greater than $R=0.375$. Thus, for our purposes, it makes no difference what value is taken for a (provided it is greater than 0.375). To specify the calculations precisely, let us set $a=0.5$.

In order to simplify the numerical solution of the integral equation to determine $s(R)$, we change our assumption as to the energy of interaction of a molecule with its neighbors beyond the first shell. Instead of supposing that the pair potential for these distant neighbors is $u(R_{12}, V^*)$, we take it to be $u(l_r, V^*)$. Thus, the distant neighbors contribute to the potential energy of a molecule in its cell but do not exert any resultant force on the molecule. Since the long-range intermolecular forces are predominantly attractive, only the nearest neighbor interactions exert a confining influence upon a molecule. The twice and further removed neighbors all tend to delocalize the distribution and draw the enclosed molecule towards the boundaries of its cell. Neglecting the forces produced by distant neighbors should lead to cell distribution functions which are excessively localized. Thus our estimates of the entropy, pressure, and internal energy should be too small. The magnitude of these errors is now being calculated and will be communicated at a later time.

Approximating the potential due to neighbors beyond the first shell leads to the new integral equation

$$s(R; T^*, V^*)=V_f' \exp\{-(1/T^*)[\phi_1(R; T^*, V^*) -\phi_1(0; T^*, V^*)]\}, \quad (36)$$

where

$$V_f'(T^*, V^*)=4\pi\int_0^a \exp\{-(1/T^*)[\phi_1(R; T^*, V^*) -\phi_1(0; T^*, V^*)]\}R^2dR. \quad (37)$$

This approximation also leads to the following expressions for the properties of the liquid:

(1) Configurational internal energy

$$U_c/NkT=(U_c/NkT)_1+(U_c/NkT)_{2,3,\ldots}. \quad (38)$$

Here $(U_c/NkT)_1$ is the contribution due to the first shell. It is equal to the term in Eq. (20) with $r=1$. The $(U_c/NkT)_{2,3,\ldots}$ is the contribution due to the second and more distant shells. It is given by

$$(U_c/NkT)_{2,3,\ldots}=(2/T^*)(A_{12}(bV^*)^{-4}-A_6(bV^*)^{-2}). \quad (39)$$

Here the constants A_{12} and A_6 are the sums

$$A_n=\sum_{r=2} Z_r l_r^{-n}. \quad (40)$$

The values of the A_{12} and A_6 are given in Table I for a number of different lattice types.

(2) Configurational entropy

$$S_c/Nk=-1+\log_e\beta+\log_e(bV_f')+2(U_c/NkT)_1 -\phi_1(0; T^*, V^*)/T^*. \quad (41)$$

Here V_f' is given by Eq. (37) and not Eq. (7).

(3) Compressibility factor

$$pV/NkT=(pV/NkT)_1+(pV/NkT)_{2,3,\ldots}. \quad (42)$$

Here $(pV/NkT)_1$ is the contribution due to the first shell. It is equal to unity plus the term in Eq. (35) with $r=1$. The $(pV/NkT)_{2,3,\ldots}$ is the contribution due to

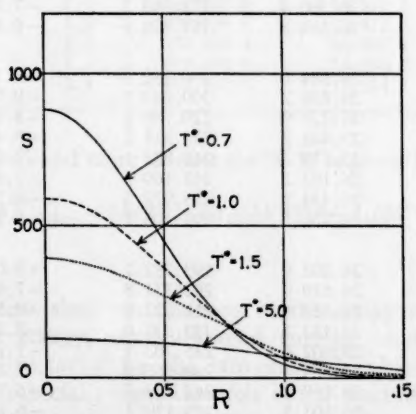

FIG. 1. Dependence on the reduced temperature of the cell distribution function for the reduced volume $V^*=1.0$.

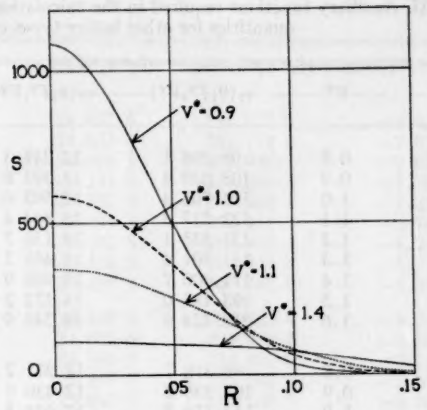

FIG. 2. Dependence on the reduced volume of the cell distribution function for the reduced temperature $T^*=1.0$.

TABLE II. Auxiliary functions required in the calculation of the properties of a face-centered cubic cell model lattice. Corresponding quantities for other lattice types can be obtained by suitable interpolations in this table.

T^*	V^*	$\gamma_1(9;T^*,V^*)$	$\gamma_1(3;T^*,V^*)$	$V_f'(T^*,V^*)$	$\gamma_1(3,T^*,V^*;0)$	$\gamma_1(9,T^*,V^*;0)$	$\phi_1(0;T^*,V^*)/T^*$
0.7	0.8	98.298 1	12.241 3	0.000 380	24.239 9	188.052 1	−10.382 0
	0.9	103.839 4	12.391 8	0.000 593	24.386 1	193.157 2	−14.970 8
	1.0	111.706 4	12.593 6	0.001 137	24.580 2	200.087 0	−16.058 7
	1.1	122.217 3	12.844 4	0.001 999	24.817 4	208.817 6	−15.717 0
	1.2	135.555 1	13.136 7	0.003 255	25.088 4	219.140 3	−14.824 4
	1.3	151.801 4	13.461 2	0.004 960	25.382 3	230.748 8	−13.761 4
	1.4	171.000 7	13.988 9	0.007 144	25.689 6	243.332 6	−12.691 6
	1.5	193.188 0	14.172 2	0.009 817	26.002 6	256.620 6	−11.681 9
	1.6	218.424 8	14.545 9	0.012 971	26.316 2	270.404 8	−10.755 8
0.8	0.8	99.378 7	12.271 2	0.000 335	24.269 0	189.062 2	−8.935 5
	0.9	105.538 2	12.436 6	0.000 700	24.429 3	194.684 2	−12.972 1
	1.0	114.176 2	12.654 3	0.001 323	24.638 0	202.189 9	−13.948 4
	1.1	125.583 7	12.920 5	0.002 288	24.888 5	211.496 4	−13.673 3
	1.2	139.916 4	13.226 6	0.003 665	25.170 5	222.351 9	−12.913 6
	1.3	157.249 2	13.562 8	0.005 499	25.472 9	234.431 0	−12.000 8
	1.4	177.628 8	13.920 3	0.007 812	25.786 3	247.423 7	−11.078 2
	1.5	201.106 3	14.291 9	0.010 602	26.103 9	261.071 0	−10.204 7
	1.6	227.741 6	14.672 5	0.013 850	26.420 6	275.166 1	−9.401 7
0.9	0.8	100.439 0	12.300 3	0.000 392	24.297 2	190.046 1	−7.813 8
	0.9	107.189 5	12.479 4	0.000 809	24.470 6	196.152 2	−11.421 7
	1,0	116.556 7	12.711 7	0.001 507	24.692 5	204.186 1	−12.311 2
	1.1	128.804 3	12.991 7	0.002 570	24.954 7	214.012 2	−12.087 6
	1.2	144.072 6	13.310 0	0.004 060	25.246 2	225.343 8	−11.430 3
	1.3	162.430 3	13.656 6	0.006 013	25.555 9	237.844 5	−10.633 5
	1.4	183.929 2	14.022 8	0.008 441	25.874 8	251.205 8	−9.824 4
	1.5	208.631 2	14.401 9	0.011 336	26.196 2	265.176 3	−9.056 3
	1.6	236.624 8	14.789 1	0.014 674	26.515 8	279.566 2	−8.348 7
1.0	0.8	101.480 0	12.328 6	0.000 450	24.324 7	191.006 1	−6.919 2
	0.9	108.798 0	12.520 5	0.000 918	24.510 2	197.566 6	−10.184 6
	1.0	118.857 2	12.766 2	0.001 691	24.743 9	206.087 2	−11.004 7
	1.1	131.902 1	13.058 7	0.002 847	25.016 6	216.387 7	−10.821 8
	1.2	148.058 3	13.388 1	0.004 442	25.316 6	228.152 9	−10.245 8
	1.3	167.392 1	13.744 0	0.006 505	25.632 8	241.037 2	−9.541 1
	1.4	189.963 8	14.118 2	0.009 040	25.956 5	254.736 5	−8.822 4
	1.5	215.846 4	14.504 2	0.012 032	26.281 4	269.006 0	−8.138 1
	1.6	245.122 4	14.897 1	0.015 448	26.603 4	283.655 8	−7.506 4
1.1	0.8	102.503 2	12.356 2	0.000 509	24.351 5	191.942 9	−6.18 95
	0.9	110.366 8	12.560 1	0.001 028	24.548 1	198.931 5	−9.17 53
	1.0	121.087 9	12.818 1	0.001 872	24.792 7	207.905 1	−9.93 85
	1.1	134.891 5	13.122 0	0.003 117	25.074 9	218.641 4	−9.78 85
	1.2	151.891 8	13.461 4	0.004 811	25.382 4	230.801 8	−9.27 85
	1.3	172.156 1	13.825 8	0.006 976	25.704 3	244.035 6	−8.64 85
	1.4	195.755 4	14.207 3	0.009 610	26.032 2	258.044 4	−8.00 33
	1.5	222.778 8	14.599 7	0.012 691	26.360 4	272.593 2	−7.38 73
	1.6	253.319 6	14.998 3	0.016 184	26.684 8	287.496 5	−6.81 74
1.2	0.9	111.899 8	12.598 3	0.001 139	24.584 6	200.252 3	−8.336 4
	1.0	123.255 3	12.867 7	0.002 052	24.839 2	209.648 1	−9.052 2
	1.1	137.783 1	13.182 1	0.003 381	25.129 9	220.786 4	−8.929 3
	1.2	155.593 4	13.530 6	0.005 168	25.444 2	233.312 2	−8.473 8
	1.3	176.757 5	13.903 0	0.007 429	25.771 3	246.872 1	−7.905 7
	1.4	201.350 7	14.291 2	0.010 155	26.103 2	261.169 5	−7.321 3
	1.5	229.467 3	14.689 4	0.013 319	26.434 1	275.972 5	−6.761 9
	1.6	261.222 6	15.093 2	0.016 881	26.760 5	291.106 7	−6.243 3
1.3	0.8	104.499 7	12.409 3	0.000 630	24.402 9	193.752 1	−5.072 6
	0.9	113.399 5	12.635 2	0.001 250	24.619 9	201.531 8	−7.628 6
	1.0	125.364 5	12.915 2	0.002 230	24.883 6	211.322 9	−8.304 1
	1.1	140.591 3	13.239 4	0.003 640	25.182 1	222.837 6	−8.203 8
	1.2	159.182 0	13.596 4	0.005 516	25.502 6	235.703 1	−7.794 0
	1.3	181.213 6	13.976 1	0.007 867	25.834 4	249.565 8	−7.277 9
	1.4	206.770 8	14.370 6	0.010 679	26.169 8	264.133 3	−6.744 8
	1.5	235.958 5	14.774 3	0.013 920	26.503 5	279.179 3	−6.233 0
	1.6	268.903 5	15.183 1	0.017 549	26.832 1	294.536 0	−5.757 7

TABLE II.—*Continued.*

T^*	V^*	$\gamma_1(9;T^*,V^*)$	$\gamma_1(3;T^*,V^*)$	$V_f'(T^*,V^*)$	$\gamma_1(3,T^*,V^*;0)$	$\gamma_1(9,T^*,V^*;0)$	$\phi_1(0;T^*,V^*)/T^*$
1.4	0.8	105.474 9	12.434 8	0.000 691	24.427 6	194.627 0	−4.636 1
	0.9	114.868 3	12.671 0	0.001 360	24.653 8	202.772 8	−7.023 5
	1.0	127.421 9	12.960 9	0.002 406	24.926 1	212.936 7	−7.664 5
	1.1	143.319 8	13.294 1	0.003 893	25.231 8	224.801 5	−7.583 2
	1.2	162.665 3	13.659 0	0.005 853	25.557 9	237.985 4	−7.212 3
	1.3	185.536 7	14.045 4	0.008 289	25.894 1	252.131 2	−6.740 5
	1.4	212.028 6	14.445 9	0.011 182	26.232 8	266.951 3	−6.251 0
	1.5	242.256 8	14.854 8	0.014 497	26.568 9	282.225 4	−5.779 8
	1.6	276.358 6	15.268 2	0.018 187	26.899 3	297.789 9	−5.341 6
1.5	0.8	106.435 6	12.459 8	0.000 753	24.451 8	195.483 4	−4.259 3
	0.9	116.308 1	12.705 6	0.001 471	24.686 6	203.978 2	−6.500 6
	1.0	129.432 1	13.004 9	0.002 580	24.966 9	214.495 0	−7.111 5
	1.1	145.980 3	13.346 5	0.004 142	25.279 2	226.689 9	−7.046 5
	1.2	166.052 0	13.718 7	0.006 181	25.610 5	240.169 1	−6.709 0
	1.3	189.737 7	14.111 5	0.008 698	25.950 6	254.580 4	−6.275 3
	1.4	217.137 8	14.517 5	0.011 667	26.292 3	269.638 1	−5.823 4
	1.5	248.377 8	14.931 3	0.015 050	26.630 7	285.126 7	−5.387 4
	1.6	283.606 9	15.349 1	0.018 799	26.962 8	300.887 6	−4.981 0
2.0	0.8	111.047 5	12.577 0	0.001 069	24.564 3	199.519 4	−2.953 9
	0.9	123.138 9	12.864 8	0.002 017	24.836 5	209.554 1	−4.684 7
	1.0	138.879 3	13.203 9	0.003 419	25.149 8	221.587 4	−5.188 6
	1.1	158.415 8	13.581 1	0.005 315	25.489 0	235.187 8	−5.178 1
	1.2	181.863 5	13.984 2	0.007 708	25.841 4	249.936 6	−4.954 9
	1.3	209.342 0	14.404 0	0.010 575	26.197 7	265.486 5	−4.652 3
	1.4	240.999 1	14.833 8	0.013 873	26.551 6	281.570 3	−4.330 2
	1.5	277.009 5	15.268 8	0.017 552	26.899 4	297.994 2	−4.015 5
	1.6	317.570 6	15.706 0	0.021 556	27.238 8	314.615 6	−3.719 8
3.0	0.8	119.509 3	12.781 0	0.001 707	24.757 9	206.619 8	−1.684 9
	0.9	135.413 3	13.131 9	0.003 066	25.083 9	219.026 0	−2.904 1
	1.0	155.622 7	13.528 8	0.004 960	25.442 6	233.317 8	−3.296 0
	1.1	180.295 1	13.957 0	0.007 392	25.817 8	248.983 5	−3.333 2
	1.2	209.591 6	14.404 6	0.010 332	26.198 1	265.593 1	−3.218 0
	1.3	243.720 0	14.863 8	0.013 728	26.575 8	282.827 3	−3.041 2
	1.4	282.911 0	15.328 9	0.017 518	26.946 4	300.448 3	−2.844 7
	1.5	327.428 7	15.796 1	0.021 638	27.307 2	318.287 7	−2.648 3
	1.6	377.560 5	16.263 1	0.026 024	27.656 9	336.224 9	−2.461 0
5.0	0.8	134.386 6	13.110 0	0.002 945	25.063 8	218.257 1	−0.727 7
	0.9	156.535 8	13.544 8	0.004 974	25.456 7	233.924 3	−1.531 7
	1.0	184.084 2	14.016 4	0.007 617	25.868 9	251.228 4	−1.824.0
	1.1	217.288 5	14.510 2	0.010 825	26.285 9	269.628 5	−1.889 3
	1.2	256.441 6	15.016 1	0.014 528	26.698 2	288.718 2	−1.851 6
	1.3	301.897 9	15.527 6	0.018 645	27.100 9	308.215 8	−1.768 3
	1.4	354.048 1	16.040 6	0.023 095	27.491 1	327.923 5	−1.667 0
	1.5	413.312 9	16.552 3	0.027 802	27.867 5	347.703 0	−1.561 3
	1.6	480.136 1	17.061 0	0.032 698	28.229 7	367.457 2	−1.457 8
10.0	0.8	165.137 4	13.698 1	0.005 701	25.592 3	239.552 2	−0.099 8
	0.9	199.441 9	14.251 0	0.008 912	26.068 8	260.010 3	−0.576 4
	1.0	241.467 9	14.826 5	0.012 781	26.545 3	281.658 9	−0.776 8
	1.1	291.759 4	15.412 6	0.017 195	27.011 3	303.994 7	−0.848 1
	1.2	350.960 4	16.002 1	0.022 038	27.461 8	326.688 6	−0.856 7
	1.3	419.690 4	16.590 2	0.027 199	27.894 2	349.494 2	−0.834 7
	1.4	498.736 8	17.174 7	0.032 586	28.308 2	372.282 8	−0.798 2

the second and more distant shells. It is given by

$$(pV/NkT)_{2,3,\ldots} = (4/T^*)\,(2A_{12}(bV^*)^{-4} - A_6(bV^*)^{-2}). \tag{43}$$

The first shell contributions to the configurational internal energy, configurational entropy, and compressibility factor for the face-centered cubic lattice play an especially significant role in our treatment. On this amount, we give them special designations: $f_U(T^*, V^*)$, $f_S(T^*, V^*)$, and $f_p(T^*, V^*)$, respectively. Here

$$f_U(T^*, V^*) = (U_c/NkT)_{1;\,\text{F·C·C·}}$$
$$= (1/T^*)\left[\left(\tfrac{1}{18}\right)(V^*)^{-4}\gamma_1(9; T^*, V^*) - \left(\tfrac{1}{2}\right)(V^*)^{-2}\gamma_1(3; T^*, V^*)\right] \tag{44}$$

$$f_S(T^*, V^*) = (S_c/Nk)_{\text{F·C·C·}} = 2f_U(T^*, V^*) + \log_e V_f'(T^*, V^*) - \phi_1(0; T^*, V^*)/T^* - 1 + \left(\tfrac{1}{2}\right)\log_e 2 \tag{45}$$

TABLE III. The compressibility factor, the configurational internal energy, and the configurational entropy for a face-centered cubic cell model lattice. The configurational entropy S_c is the difference between the entropy of the liquid and the entropy that a perfect gas would have at the same temperature and volume. No corrections have been made for holes in the liquid structure. The quantities f_p, f_U, and f_S are the contributions of the first shell to pV/NkT, U_c/NkT, and S_c/Nk, respectively. Our approximate treatment of distant neighbor interactions is responsible for the relationship, $f_S = S_c/Nk$. The tabulated values for S_c/Nk are based upon the assumption that $\beta=1$ and so include no communal entropy. In the case of full communal entropy, $\beta=e$, the values for S_c/Nk are larger by unity than those given here.

T^*	V^*	f_p	pV/NkT	$-f_U$	$-U_c/NkT$	$-S_c/Nk=-f_S$
0.7	0.8	37.774 3	27.739 2	4.468 6	9.716 1	7.387 8
	0.9	17.582 2	9.500 7	6.782 0	10.966 3	6.677 3
	1.0	7.573 0	0.938 6	7.352 2	10.763 6	6.078 3
	1.1	2.471 3	−3.065 7	7.214 4	10.047 2	5.580 1
	1.2	−0.161 3	−4.848 6	6.806 5	9.195 5	5.169 6
	1.3	−1.510 2	−5.526 9	6.316 9	8.358 2	4.832 3
	1.4	−2.172 2	−5.651 1	5.825 4	7.589 4	4.554 1
	1.5	−2.459 1	−5.500 8	5.363 9	6.903 3	4.322 8
	1.6	−2.537 5	−5.218 8	4.942 9	6.297 9	4.128 5
0.8	0.8	33.940 0	25.159 3	3.748 6	8.340 2	7.215 5
	0.9	16.234 6	9.163 3	5.787 4	9.448 7	6.520 5
	1.0	7.422 9	1.617 8	6.303 2	9.288 2	5.939 4
	1.1	2.896 4	−1.948 5	6.199 7	8.678 4	5.459 4
	1.2	0.528 8	−3.572 5	5.858 5	7.948 9	5.065 7
	1.3	−0.710 9	−4.225 5	5.443 5	7.229 7	4.742 8
	1.4	−1.342 7	−4.386 8	5.024 5	6.568 0	4.476 4
	1.5	−1.638 4	−4.299 8	4.629 5	5.976 5	4.254 5
	1.6	−1.745 1	−4.091 2	4.268 2	5.454 0	4.067 9
0.9	0.8	30.946 0	23.140 9	3.190 8	7.272 2	7.065 8
	0.9	15.170 1	8.884 5	5.016 7	8.271 2	6.385 2
	1.0	7.287 1	2.127 0	5.490 2	8.143 5	5.820 0
	1.1	3.206 8	−1.099 8	5.413 2	7.616 5	5.356 0
	1.2	1.046 3	−2.599 3	5.123 4	6.981 5	4.976 5
	1.3	−0.106 7	−3.230 8	4.766 0	6.353 7	4.665 7
	1.4	−0.712 7	−3.418 6	4.402 9	5.774 9	4.409 3
	1.5	−1.013 4	−3.379 1	4.059 3	5.256 6	4.195 5
	1.6	−1.139 7	−3.225 1	3.744 3	4.798 2	4.015 0
1.0	0.8	28.540 7	21.516 1	2.746 5	6.419 8	6.933 9
	0.9	14.305 2	8.648 2	4.402 4	7.331 4	6.266 5
	1.0	7.162 9	2.518 8	4.842 3	7.230 3	5.715 8
	1.1	3.439 6	−0.436 3	4.786 2	6.769 2	5.265 6
	1.2	1.445 9	−1.835 1	4.537 1	6.209 4	4.898 5
	1.3	0.363 8	−2.447 9	4.225 3	5.654 2	4.598 1
	1.4	−0.219 9	−2.655 2	3.906 5	5.141 3	4.350 1
	1.5	−0.522 9	−2.652 1	3.603 8	4.681 4	4.143 1
	1.6	−0.664 3	−2.541 2	3.325 6	4.274 1	3.968 5
1.1	0.8	26.564 3	20.178 3	2.384 6	5.723 9	6.816 2
	0.9	13.586 4	8.443 6	3.901 7	6.564 4	6.161 1
	1.0	7.049 1	2.827 2	4.314 1	6.485 0	5.623 5
	1.1	3.617 6	0.094 0	4.274 9	6.077 6	5.185 8
	1.2	1.761 0	−1.221 7	4.058 9	5.579 2	4.829 6
	1.3	0.738 0	−1.818 1	3.784 1	5.083 1	4.538 3
	1.4	0.173 8	−2.040 0	3.501 3	4.623 8	4.297 8
	1.5	−0.129 7	−2.065 3	3.231 8	4.211 4	4.096 6
	1.6	−0.281 7	−1.987 9	2.983 4	3.845 7	3.926 6
1.2	0.9	12.978 2	8.264 0	3.486 0	5.926 9	6.066 6
	1.0	6.943 9	3.073 8	3.875 5	5.865 5	5.541 0
	1.1	3.755 6	0.525 7	3.850 3	5.502 8	5.114 4
	1.2	2.014 1	−0.720 1	3.661 5	5.055 1	4.767 9
	1.3	1.041 8	−1.301 3	3.417 3	4.608 1	4.484 6
	1.4	0.495 0	−1.534 4	3.164 3	4.193 3	4.250 5
	1.5	0.191 6	−1.582 7	2.922 3	3.820 3	4.054 7
	1.6	0.031 3	−1.532 7	2.698 7	3.489 1	3.889 0
1.3	0.8	23.503 6	18.100 1	1.831 5	4.657 1	7.614 0
	0.9	12.455 6	8.104 0	3.135 7	5.388 8	5.981 1
	1.0	6.846 2	3.273 8	3.505 8	5.342 7	5.466 5
	1.1	3.864 3	0.882 8	3.492 2	5.017 6	5.049 9
	1.2	2.220 8	−0.303 1	3.326 3	4.612 7	4.712 1
	1.3	1.292 1	−0.870 7	3.107 6	4.206 8	4.435 9
	1.4	0.760 9	−1.112 3	2.879 7	3.829 5	4.207 5
	1.5	0.458 8	−1.179 1	2.660 8	3.489 7	4.016 4
	1.6	0.292 3	−1.151 5	2.458 0	3.187 6	3.854 4

TABLE III.—*Continued.*

T^*	V^*	f_p	pV/NkT	$-f_U$	$-U_c/NkT$	$-S_c/Nk=-f_S$
1.4	0.8	22.292 6	17.275 1	1.615 9	4.239 7	6.526 0
	0.9	12.000 7	7.960 0	2.836 6	4.928 8	5.903 2
	1.0	6.755 2	3.438 0	3.190 0	4.895 7	5.398 7
	1.1	3.950 1	1.181 6	3.186 3	4.602 7	4.991 4
	1.2	2.391 5	0.047 9	3.039 7	4.234 2	4.661 3
	1.3	1.500 9	−0.507 5	2.842 9	3.863 6	4.391 5
	1.4	0.983 8	−0.755 6	2.636 3	3.518 3	4.168 4
	1.5	0.683 3	−0.837 5	2.437 0	3.206 7	3.981 5
	1.6	0.512 0	−0.828 6	2.252 0	2.929 5	3.822 9
1.5	0.8	21.238 0	16.555 0	1.430 1	3.878 9	6.445 1
	0.9	11.600 5	7.829 1	2.578 5	4.531 2	5.831 8
	1.0	6.670 2	3.574 2	2.917 4	4.509 4	5.336 6
	1.1	4.018 6	1.434 7	2.922 0	4.244 0	4.937 7
	1.2	2.533 8	0.346 4	2.792 1	3.907 0	4.614 8
	1.3	1.676 8	−0.197 6	2.614 1	3.566 7	4.350 9
	1.4	1.172 6	−0.450 8	2.425 8	3.249 0	4.132 5
	1.5	0.874 0	−0.545 4	2.243 5	2.961 9	3.949 4
	1.6	0.699 0	−0.552 2	2.073 8	2.706 1	3.793 9
2.0	0.8	17.496 6	13.984 3	0.788 8	2.625 4	6.118 1
	0.9	10.142 0	7.313 5	1.685 1	3.149 6	5.545 0
	1.0	6.313 3	3.991 3	1.972 6	3.166 6	5.088 3
	1.1	4.202 6	2.264 6	2.005 3	2.996 8	4.723 1
	1.2	2.982 6	1.342 1	1.932 1	2.768 3	4.428 2
	1.3	2.249 8	0.843 9	1.818 3	2.532 8	4.187 0
	1.4	1.796 3	0.578 6	1.692 9	2.310 3	3.986 9
	1.5	1.509 6	0.445 0	1.569 1	2.107 9	3.818 6
	1.6	1.325 8	0.387 3	1.452 4	1.926 6	3.675 2
3.0	0.8	13.621 6	11.280 1	0.173 0	1.397 4	5.687 7
	0.9	8.537 8	6.652 1	0.817 6	1.795 9	5.171 8
	1.0	5.813 9	4.265 9	1.051 4	1.847 4	4.766 3
	1.1	4.256 4	2.964 4	1.107 4	1.769 4	4.444 1
	1.2	3.315 7	2.222 0	1.088 3	1.645 7	4.184 4
	1.3	2.721 7	1.784 5	1.035 5	1.511 8	3.971 3
	1.4	2.332 2	1.520 4	0.970 5	1.382 1	3.793 9
	1.5	2.068 8	1.359 1	0.902 9	1.262 1	3.644 0
	1.6	1.885 8	1.260 2	0.837 4	1.153 6	3.515 7
5.0	0.8	10.304 5	8.899 6	−0.277 6	0.457 0	5.198 6
	0.9	7.035 8	5.904 4	0.163 3	0.749 1	4.752 1
	1.0	5.211 3	4.282 5	0.348 9	0.826 5	4.404 8
	1.1	4.118 5	3.343 3	0.416 9	0.816 2	4.129 5
	1.2	3.424 6	2.768 4	0.436 7	0.771 2	3.907 2
	1.3	2.962 3	2.400 0	0.428 3	0.714 1	3.724 1
	1.4	2.641 7	2.154 6	0.408 0	0.655 0	3.570 9
	1.5	2.411 6	1.985 8	0.382 8	0.598 3	3.440 7
	1.6	2.241 6	1.866 2	0.356 1	0.545 8	3.328 6
10.0	0.8	7.470 5	6.768 0	−0.547 4	−0.180 1	4.626 2
	0.9	5.587 4	5.021 7	−0.267 1	0.025 8	4.263 5
	1.0	4.473 8	4.009 4	−0.127 1	0.111 7	3.982 6
	1.1	3.766 5	3.378 9	−0.054 7	0.255 3	3.759 4
	1.2	3.290 9	2.962 8	−0.017 0	0.150 2	3.577 9
	1.3	2.955 2	2.674 0	0.002 1	0.145 0	3.427 8
	1.4	2.709 5	2.466 0	0.010 8	0.134 3	3.301 0

[here $f_S(T^*, V^*)$ has been calculated on the basis of $\beta=1$ so that there is no communal entropy]

$$f_p(T^*, V^*)=(pV/NkT)_{1;\text{F.C.C.}}$$
$$=1+(1/T^*)[(\tfrac{4}{15})(V^*)^{-4}\gamma_1(9; T^*, V^*)$$
$$-2(V^*)^{-2}\gamma_1(3; T^*, V^*)]. \quad (46)$$

One interesting result occurs as a consequence of approximating the potential due to neighbors beyond the first shell. The first shell contributions to the configurational internal energy, configurational entropy, and compressibility factors for an arbitrary type of lattice depend upon only two variables: $12T^*/Z_1$ and $bV^*/(2)^{\frac{1}{2}}$. This may be seen by a close scrutiny of the previous equations. Thus, for an arbitrary lattice at the reduced temperature T^* and the reduced volume V^*,

$$(U_c/NkT)_1=f_U(12T^*/Z_1, bV^*/(2)^{\frac{1}{2}}), \quad (47)$$

$$S_c/Nk=f_S(12T^*/Z_1, bV^*/(2)^{\frac{1}{2}})+\log_e b-(\tfrac{1}{2})\log_e 2, \quad (48)$$

$$(pV/NkT)_1=f_p(12T^*/Z_1, bV^*/(2)^{\frac{1}{2}}). \quad (49)$$

TABLE IV. The compressibility factor, the configurational internal energy, and the configurational entropy for a face-centered cubic cell model lattice corrected for the presence of holes. Here the values given for $(S_c/Nk)'$ have been calculated on the basis of no communal entropy or $\beta=1$. For full communal entropy, or $\beta=e$, each tabulated value for $(S_c/Nk)'$ is increased by unity. The function $\rho(T^*, V^*)=N/L$ is the fraction of occupied cells in the lattice while the values in parentheses are those of ζ where ζ_{21} is the average number of molecules lying in cells adjacent to an occupied cell.

T^*	V^*	$(pV/NkT)'$	$-(U_c/NkT)'$	$-(S_c/Nk)'$	$\rho(T^*, V^*)$
0.7	0.8	27.739 2	9.716 1	7.387 8	1.000 0
	0.9	9.500 7	10.966 3	6.677 3	1.000 0
	1.0	0.938 6	10.763 6	6.078 3	1.000 0
	1.1	−3.065 7	10.047 2	5.579 5	1.000 0
	1.2	−4.812 9	9.193 0	5.165 8	0.998 7
	1.3	−5.386 1	8.355 8	4.820 0	0.991 5(0.991 6)
	1.4	−5.342 7	7.585 8	4.526 9	0.958 8(0.961 2)
0.8	0.8	25.159 3	8.340 2	7.215 5	1.000 0
	0.9	9.163 3	9.448 7	6.520 5	1.000 0
	1.0	1.617 8	9.288 2	5.939 4	1.000 0
	1.1	−1.948 5	8.678 4	5.458 4	1.000 0
	1.2	−3.517 0	7.944 7	5.061 1	0.998 3
	1.3	−4.079 6	7.225 8	4.728 1	0.990 2(0.990 3)
	1.4	−4.087 4	6.570 2	4.450 8	0.965 3(0.966 8)
0.9	0.8	23.140 9	7.272 2	7.065 8	1.000 0
	0.9	8.884 5	8.271 2	6.385 2	1.000 0
	1.0	2.127 0	8.143 5	5.820 0	1.000 0
	1.1	−1.093 8	7.615 9	5.355 2	0.999 8
	1.2	−2.536 9	6.976 8	4.970 9	0.997 9
	1.3	−3.095 9	6.352 4	4.647 5	0.989 6(0.990 6)
	1.4	−3.160 1	5.776 7	4.352 1	0.968 0(0.969 0)
	1.5	−2.999 9	5.212	4.157 1	0.919 4(0.925 7)
1.0	0.8	21.516 1	6.419 8	6.933 9	1.000 0
	0.9	8.648 2	7.331 4	6.266 5	1.000 0
	1.0	2.518 8	7.230 3	5.715 8	1.000 0
	1.1	−0.427 6	6.768 3	5.264 4	0.999 7
	1.2	−1.782 4	6.205 4	4.891 7	0.997 4
	1.3	−2.272 2	5.644 1	4.580 0	0.988 9
	1.4	−2.408 0	5.139 5	4.318 9	0.969 9
	1.5	−2.311 7	4.694 4	4.079 6	0.932 1(0.935 9)
	1.6	−2.135 5	4.309 2	3.917 1	0.863 0(0.877 7)
1.1	0.8	20.178 3	5.723 9	6.816 2	1.000 0
	0.9	8.443 6	6.564 4	6.161 1	1.000 0
	1.0	2.827 2	6.485 0	5.623 5	1.000 0
	1.1	0.104 8	6.076 4	5.184 2	0.999 6
	1.2	−1.165 9	5.574 3	4.821 6	0.997 0
	1.3	−1.678 9	5.076 0	4.519 3	0.988 1(0.988 3)
	1.4	−1.818 2	4.621 9	4.264 2	0.969 4(0.970 1)
	1.5	−1.749 2	4.219 3	4.050 2	0.937 8(0.940 6)
	1.6	−1.616 7	3.870 9	3.870 3	0.892 1(0.899 3)
1.2	0.9	8.264 0	5.926 9	6.066 6	1.000 0
	1.0	3.073 8	5.865 5	5.541 0	1.000 0
	1.1	0.539 1	5.501 3	5.112 3	0.999 5
	1.2	−0.659 2	5.049 7	4.758 9	0.996 5
	1.3	−1.159 9	4.599 9	4.465 2	0.987 4(0.988 5)
	1.4	−1.306 8	4.187 6	4.215 8	0.969 1(0.969 8)
	1.5	−1.283 5	3.824 3	4.006 3	0.941 1(0.943 3)
	1.6	−1.185 2	3.506 9	3.828 6	0.901 9(0.907 6)
1.3	0.8	18.100 1	4.657 1	6.614 0	1.000 0
	0.9	8.104 0	5.388 8	5.981 1	1.000 0
	1.0	3.273 8	5.342 7	5.466 5	1.000 0
	1.1	0.898 7	5.015 7	5.047 4	0.999 4
	1.2	−0.238 6	4.606 7	4.702 0	0.996 0
	1.3	−0.728 5	4.197 9	4.413 5	0.986 6(0.986 8)
	1.4	−0.891 0	3.822 6	4.171 1	0.969 1(0.969 7)
	1.5	−0.893 2	3.490 6	3.966 0	0.942 9(0.944 7)
	1.6	−0.822 4	3.200 1	3.791 1	0.908 5(0.913 0)
1.4	0.8	17.275 1	4.239 7	6.526 0	1.000 0
	0.9	7.960 0	4.928 8	5.903 2	1.000 0
	1.0	3.438 0	4.895 7	5.398 2	1.000 0
	1.1	1.200 4	4.600 6	4.988 3	0.999 2
	1.2	0.116 9	4.227 7	4.650 1	0.995 5
	1.3	−0.364 4	3.854 0	4.367 8	0.985 9(0.986 0)
	1.4	−0.539 2	3.510 2	4.130 3	0.968 7(0.969 2)
	1.5	−0.562 1	3.205 9	3.929 0	0.943 9(0.945 6)
	1.6	−0.513 9	2.937 8	3.756 9	0.912 7(0.916 3)

TABLE IV.—*Continued.*

T^*	V^*	$(pV/NkT)'$	$-(U_c/NkT)'$	$-(S_c/Nk)'$	$\rho(T^*, V^*)$
1.5	0.8	16.555 0	3.878 9	6.445 1	1.000 0
	0.9	7.829 1	4.531 2	5.831 8	1.000 0
	1.0	3.574 2	4.509 4	5.336 0	1.000 0
	1.1	1.456 4	4.241 4	4.934 1	0.999 0
	1.2	0.419 0	3.899 9	4.602 6	0.995 0
	1.3	−0.053 7	3.556 5	4.325 7	0.985 1(0.985 2)
	1.4	−0.238 2	3.239 8	4.092 7	0.968 2(0.968 7)
	1.5	−0.278 1	2.958 4	3.894 7	0.944 5(0.945 9)
	1.6	−0.248 6	2.711 2	3.725 2	0.915 4(0.918 5)
2.0	0.8	13.984 3	2.625 4	6.118 1	1.000 0
	0.9	7.313 5	3.149 6	5.544 9	1.000 0
	1.0	3.998 2	3.165 6	5.087 1	0.999 7
	1.1	2.299 8	2.992 3	4.716 5	0.998 0
	1.2	1.431 0	2.758 8	4.410 5	0.992 3
	1.3	0.994 6	1.520 0	4.154 9	0.981 3(0.981 4)
	1.4	−0.782 5	2.295 7	3.939 1	0.964 9(0.965 3)
	1.5	−0.689 1	2.095 9	3.754 3	0.943 9(0.944 9)
	1.6	−0.662 5	1.917 4	3.594 6	0.920 0(0.921 8)
3.0	0.8	11.280 1	1.397 4	5.687 7	1.000 0
	0.9	6.654 7	1.795 4	5.171 3	0.999 9
	1.0	4.285 7	1.843 9	4.762 1	0.998 9
	1.1	3.024 8	1.759 0	4.430 5	0.995 2
	1.2	2.336 3	1.627 0	4.156 7	0.987 0
	1.3	1.951 3	1.488 9	3.927 3	0.974 2(0.974 3)
	1.4	1.733 0	1.352 3	3.732 0	0.957 4(0.957 7)
	1.5	1.591 9	1.242 2	3.567 9	0.937 8(0.938 5)
	1.6	1.480 6	1.167 3	3.434 8	0.916 8(0.917 9)
5.0	0.8	8.915 2	0.454 2	5.199 7	0.999 9
	0.9	5.918 1	0.746 8	4.748 9	0.999 2
	1.0	4.330 0	0.820 3	4.393 0	0.996 1
	1.1	3.439 2	0.806 5	4.104 2	0.988 7
	1.2	2.907 3	0.760 5	3.865 7	0.977 0
	1.3	2.572 5	0.705 1	3.665 7	0.961 6(0.961 7)
	1.4	2.346 0	0.653 1	3.498 3	0.943 7(0.943 9)
	1.5	2.197 0	0.593 6	3.341 3	0.924 3(0.924 7)
	1.6	2.134 6	0.483 2	3.122 9	0.904 4(0.904 9)
10.0	0.8	6.789 5	−0.183 7	4.620 5	0.999 0
	0.9	5.069 2	0.131 0	4.241 9	0.995 0
	1.0	4.101 6	0.866 0	3.934 4	0.986 2
	1.1	3.516 1	0.105 5	3.677 8	0.973 0
	1.2	3.137 0	0.100 4	3.458 3	0.956 3
	1.3	2.878 0	0.085 1	3.266 9	0.937 5
	1.4	2.693 0	0.065 8	3.211 5	0.917 6

In addition, the following results were obtained by interpolation and are not nearly as reliable as the rest of this table.

2.75	0.8	11.850	1.584 8	5.795 3	
	0.9	6.759	2.054 0	5.264 7	
	1.0	4.250	2.099 3	4.843 3	
	1.1	2.896	2.019 2	4.502 0	
	1.2	2.170	1.848 2	4.220 1	
	1.3	1.808	1.690 9	3.984 2	
	1.4	1.586	1.538 2	3.783 8	
	1.5	1.454	1.413 8	3.614 5	
	1.6	1.298	1.263 6	3.474 7	

Since the functions f_v, f_s, and f_p are tabulated for a wide range of reduced temperatures and volumes, the generalization of our results from face-centered cubic to any other lattice type is accomplished by simple interpolations in our tables.

III. NUMERICAL PROCEDURE

To solve the Kirkwood integral equation, Eqs. (36) and (37), for given T^* and V^* we first chose a trial function, $s_0(R;\ T^*,\ V^*)$, which was normalized to unity on the interval $(0,\ a)$. Next this trial solution was used to construct initial estimates of the cell potential, $\phi_1\ (R;\ T^*,\ V^*)$, and of the normalization factor, V_f'. Substitution of these estimates into the right-hand side of Eq. (36) then resulted in a "first improved" cell distribution function, $s_1(R;\ T^*,\ V^*)$. With this new function in place of s_0, construction of the cell potential and the normalization factor was repeated and a "second improved" solution obtained. This cycling was continued until the difference between the

functions, s_m and s_{m+1}, fell within a preassigned tolerance. Actually, we have used as a measure of equality, not the functions themselves, but their normalization factors, V_f'. The iteration was said to have converged when the normalization factors for successive cycles agreed to within about 0.5%.

The numerical integrations were performed using Simpson's rule with an interval size of 0.005 (for the variable R). Although the cell radius, a, was taken equal to 0.45 at the high densities which we considered, a significantly smaller value would have been equally as satisfactory. The solution of the integral equation for one choice of T^* and V^* was used as the initial trial function in the next calculation.

The representative curves of Figs. 1 and 2 illustrate the dependence of the cell distribution functions upon temperature and density.[10] From these figures we conclude that for small V^* and T^* the molecules lie very near the centers of their cells. However, as either or both of these variables increases, the extent of localization tends to diminish. These qualitative features are of course just what one would intuitively expect. At very high densities the cell distributions are practically Gaussian. However, the general behavior of these functions is much more complicated and conforms to no simple analytical representation.

The results of our calculations are presented in Tables II and III. In Table II are collected the γ_1 integrals together with the normalization factor $V_f'(T^*, V^*)=1/s(0; T^*, V^*)$ and the first shell contribution to the cell potential at the center of the cell. In Table III, the configurational internal energy, the configurational entropy, and the compressibility factor are given for the face-centered cubic lattice together with their first shell contributions, f_U, f_S, and f_p. As a result of approximating the potential energy due to neighbors beyond the first shell, $S_c/Nk=f_S$. The calculations in Table III were made using Eqs. (38) through (46).

In Sec. V, our calculated values for the cell model lattice properties are compared with experimental data, the results of Monte Carlo calculations,[11] and other theoretical calculations. However, first we should improve our results by allowing holes in our lattice.

IV. CORRECTIONS DUE TO EMPTY CELLS (THE HOLE THEORY OF LIQUIDS)

Experimentally[12] it is observed that in liquids the number of nearest neighbors to a molecule steadily decreases with rising temperature and/or with decreasing density. However, according to the cell theory described in the previous sections the number of neighbors is a constant, Z_1, which depends only upon the nature of the quasi-lattice. To remedy this deficiency of the theory Eyring and Cernuschi[13] suggested that holes or unoccupied cells be incorporated into the model for liquids.[14] According to this extension of the model we must now imagine the volume of the system to be spanned by an array of $L \geq N$ identical cells. The reduced volume of an individual cell will therefore be equal to $V'=V^*\rho$ where $V^*=V/N\sigma^3$ and $\rho=N/L$ is the average number of molecules per cell. It is then assumed that each of these cells can be occupied by no more than one molecule. This approximation is certainly justified since at high densities there should be little chance that two or more molecules will share the same cell.

The Helmholtz free energy calculated from this cell model will, or course, always exceed the true equilibrium value. We may therefore conclude that the best choices for L and for the cell distribution function are those for which this free energy is a minimum. These thermodynamical criteria are essential to the theory since they provide the means for uniquely defining the cell distribution function and L, the number of cells. Also these conditions are sufficient to insure the internal consistency of the theory. Thus, as Mayer and Careri[15] have illustrated, the entropy calculated from this theory will be the same as that obtained by temperature derivation of the free energy and, furthermore, the pressure obtained by volume derivation of the free energy will equal that given by the virial theorem of mechanics.

To determine the optimum number of cells we must first characterize the relative probabilities for the various arrangements of the occupied and unoccupied cells. Unfortunately, the only solutions to this order-disorder problem which are presently known involve the neglect of interactions (and hence correlations in position) between molecules in twice or further removed cells. For this "nearest neighbor" approximation we shall employ the methods of Levine, Mayer, and Aroeste.[2]

By minimization of the free energy it is found that the optimum choice for the cell distribution function satisfies an equation precisely analogous to Eq. (37). However, the reduced temperature and volume which appear in Eq. (37) are now replaced by T' and V'. Here $T'=T^*/\zeta$ is an "effective" reduced temperature defined in terms of $Z_1\zeta$, the average number of molecules lying in cells adjacent to an occupied cell. The equation of state and thermodynamical properties of the system are

[10] Complete tables of $s(R; T^*, V^*)$ are given in the Air Force Wright Air Development Center Report WADC TN 59-234 by J. S. Dahler and J. O. Hirschfelder. Copies of these tables are available at the University of Wisconsin Theoretical Chemistry Laboratory.

[11] W. W. Wood and F. R. Parker, J. Chem. Phys. **27**, 720 (1957).

[12] A. Eisenstein and N. S. Gingrich, Phys. Rev. **62**, 261 (1942); see also G. H. Vineyard, *Liquid Metals and Solidification* (Am. Soc. for Metals, Cleveland, Ohio, 1958).

[13] F. Cernuschi and H. Eyring, J. Chem. Phys. **7**, 547 (1939).

[14] In Kirkwood's theory an empty cell can occur only if some other cell is multiply occupied.

[15] J. E. Mayer and G. Careri, J. Chem. Phys. **20**, 1001 (1952); G. Careri, J. Chem. Phys. **20**, 1114 (1952).

related to T' and V' in the manner

$$(pV/NkT)_1=f_p(T', V')=F_p(\rho, q), \quad (50)$$

$$(U_c/NkT)_1=f_U(T', V')=F_U(\rho, q), \quad (51)$$

and

$$S_c/Nk=f_S(T', V')+F_S(\rho, q). \quad (52)$$

The variable q is[16] equal to $(-12\rho f_U(T', V')/\zeta Z_1)$ and the expressions for the F functions obtained by Levine, Mayer, and Aroeste are (for the face-centered cubic lattice)

$$F_U(\rho, q)=-q\left[1+\frac{(1-\rho)^2}{6\rho}q+\frac{(1-\rho)^2(1+4\rho-4\rho)^2}{72\rho^2}q^2 + \cdots\right], \quad (53)$$

$$F_p(\rho, q)=F_U(\rho, q)-(1/\rho)\log_e(1-\rho) + \frac{1-\rho^2}{12\rho}q^2+\frac{(1-\rho)(1+2\rho+2\rho^2-4\rho^3)}{108\rho^2}q^3+\cdots, \quad (54)$$

and

$$F_S(\rho, q)=-(1/\rho)\left[(1-\rho)\log_e(1-\rho)+\tfrac{1}{12}(1-\rho)^2q^2 + \frac{(1-\rho)^2(1+4\rho-4\rho^2)}{108\rho}q^3+\cdots\right]. \quad (55)$$

These double series representations for the thermodynamical properties were derived from a complicated and very elegent mathematical approach to the order-disorder problem. For a detailed description of this method the reader is referred to the original publication by Levine, Mayer, and Aroeste.[2]

To use this theory we begin by solving the Kirkwood integral equation, Eq. (37), for a variety of values of T' and V'. The cell distribution functions so obtained are then used to construct f_p, f_U, and f_S. Next, the equations $f_p=F_p$ and $f_U=F_U$ are solved for $\rho(T', V')$ and $q(T', V')$ and the results used to calculate

$$F_S[\rho(T', V'), q(T', V')]$$

and

$$\zeta(T', V')=-\rho(T', V')f_U(T', V')/q(T', V'). \quad (56)$$

For each choice of T' and V' we can then determine the corresponding values of $T^*=T'\zeta(T', V')$ and $V^*=V'/\rho(T', V')$. Finally, by interpolation of these values, tabular representations of the functions $T^*=T^*(T', V')$ and $V^*=V^*(T', V')$ are constructed. At this stage of the calculation we possess: (1) tabulations of the thermodynamical properties for given values of T' and V', and (2) tabulations of T^* and V^* in terms of T' and V'. A final interpolation is then performed to construct tables of the thermodynamical properties for given values of the reduced temperature and volume.

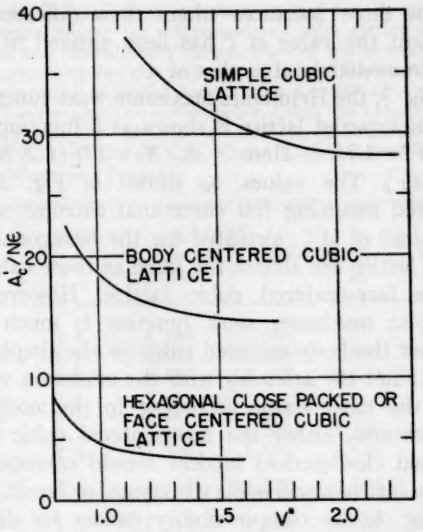

FIG. 3. Dependence of the configurational Helmholtz free energy upon lattice type for $T^*=2.75$. This shows that either the hexagonal close-packed or the face-centered cubic structures are much more stable than either the body-centered or simple cubic lattices. Here $A_c'/Ne=T^*[(U_c'/NkT)-(S_c'/Nk)]$ and the values were computed assuming full communal entropy or $\beta=e$.

The solutions of the Kirkwood integral equation which we have already obtained can, of course, be used in these new calculations. The equations $f_p=F_p$ and $f_U=F_U$ are then solved by a straightforward iteration procedure. As trial solutions[2] we chose $q_0=-f_U(T', V')$ and

$$-\rho_0^{-1}\log_e(1-\rho_0)=f_p(T', V')-f_U(T', V'). \quad (57)$$

For the ranges of temperature and density considered in this investigation the convergence of the iterative process was extremely rapid. Our calculations reveal that the difference between $\rho(T', V')$ and $\zeta(T', V')$ is at most 1% and so the arrangement of occupied and unoccupied cells is essentially random throughout the region of high densities. Consequently, our final results would have been about the same if we had used the Bragg-Williams approximation to the order-disorder problem in place of the more rigorous method of Levine, Mayer, and Aroeste. To perform the several interpolations mentioned above we employed Aitken's method.[17]

The results of these calculations for a face-centered cubic lattice are summarized in Table IV. The primes indicate that the quantities have been corrected for the presence of holes. The entries labeled $\rho(T^*, V^*)$ are the computed values of N/L, the fraction of occupied cells. In most cases ρ and ζ differed by so little that their separate tabulation seemed unnecessary. How-

[16] According to the notation of reference 2, $q=6\rho\lambda$.

[17] F. B. Hildebrand, *Methods of Applied Mathematics* (Prentice-Hall, Inc., Englewood Cliffs, New Jersey, 1952), p. 49.

ever, in those instances where their difference was significant the value of ζ has been entered in parentheses immediately after that of ρ.

In Fig. 3, the Helmholtz maximum work function for different types of lattice is shown as a function of V^* for $T^*=2.75$. Here $A_c'/N\epsilon=T^*[(U_c'/NkT)-(S_c'/Nk)]$. The values, as shown in Fig. 3, were calculated assuming full communal entropy or $\beta=e$. The values of A_c' calculated for the hexagonal close-packed lattice are almost the same as those calculated for the face-centered cubic lattice. However, the Helmholtz maximum work function is much larger for either the body-centered cubic or the simple cubic lattice. Since the assembly with the minimum value of A_c' is the most stable according to thermodynamic considerations, either the face-centered cubic or the hexagonal close-packed lattices should correspond to the structure of a real noble gas crystal or liquid.

In Fig. 4, the compressibility factors for different types of lattice are shown for the $T^*=2.74$ isotherm. These are compared with the results of Monte Carlo calculations.[11] The face-centered cubic or hexagonal close-packed lattice gives slightly smaller values for the compressibility factor than does the body-centered cubic structure. Note how the compressibility factor for the body-centered lattice merges into the Monte Carlo crystalline isotherm at very high densities.

V. DISCUSSION OF RESULTS

It appears from our results that the free-volume or lattice treatments are "intrinsically" wrong for liquids and the partial success of the Lennard-Jones and Devonshire form of the free-volume theory is fortuitous. Such theoretical developments seem appropriate for the crystalline solid state but not for the liquid or dense gas.‡

The inaccuracies in the present treatment result from:

(1) The assumption that each pair of molecules interacts according to the Lennard-Jones 12–6 potential. An Exp-6 potential would be slightly more realistic. For every substance there is a special form for the pair potential which must be determined, either from quantum mechanical calculations or from experiment.

(2) The assumption that the potential energy of the system is pairwise additive. There is mounting evidence indicating that three and four body forces may be very important. Such many body forces would tend to reduce the contributions from shells of distant neighbors.

(3) The assumption that the cell potential can be approximated by replacing the contributions of the second and more distant shells of neighbors by terms calculated on the basis of all of the molecules being located at their lattice points. This assumption was made to simplify the calculations. However, with the availability of improved high-speed computing machines, this assumption is no longer required. We do not know the magnitude of the errors which result from this cause.

(4) The errors inherent in any cell treatment of a dense system. No cell theory can introduce the degree of order-disorder which is present in a real substance.

The over-all accuracy of theoretical calculations can be ascertained by comparison with experimental data. The precise measurements of the equation of state of argon by Michels[18] and his co-workers provides a test of our results for volumes equal to or greater than $V^*=1.4$. For smaller volumes or higher densities, the only available data are Bridgman's measurements[19] of the isotherm for argon corresponding to $T^*=2.74$ and extending to volumes as low as $V^*=0.96$. Because of the great experimental difficulties of working at such high pressure (over 10 000 atmos), Bridgman's values are probably not very accurate. Since 1935, when these measurements were made, experimental techniques have improved tremendously. Thus it should be possible for our experimental colleagues to reduce a rather big gap in our knowledge of the structure of matter by making a thorough study of the isotherms of argon up to very high pressures and densities.

Even when good experimental equation of state data are available, their unambiguous interpretation is difficult to accomplish. One must assign to the molecules appropriate values of the Lennard-Jones parameters ϵ/k and σ. These are usually selected so as to make the calculated second virial coefficient or viscosity of the dilute gas agree with experimental data over a wide range of temperature. Because of errors in the experimental second virial coefficient and viscosity, there is a considerable lattitude for the choice of the Lennard-Jones parameters. Thus, Miss Levelt[20] obtained two

‡ The authors wish to thank Charles E. Hecht for pointing out that Terrill Hill [*Statistical Mechanics* (McGraw-Hill Book Company, Inc., New York, 1956), p. 366] agrees that when β is taken independent of temperature and density in our Eq. (3) and therefore omitted from the minimization of the free energy, one obtains a Kirkwood type integral equation [such as our Eq. (6)] for $s(R)$. However, Hill argues that since there can be no significance to any set of fixed lattice points in a liquid, the singlet density or $s(R)$ cannot depend upon the distance from such a lattice point. Thus $s(R)$ must be a constant independent of R. However, from the Kirkwood integral equation it follows that $s(R)$ cannot be a constant except in the limit of zero density. It is then perfectly consistent that we find from our Figs. 5 and 6 that the isotherms calculated by the Kirkwood cell theory correspond to a metastable extension of the crystalline isotherms rather than to the liquid isotherm.

[18] (Isotherms from 0 to 150°C) Michels, Wijker, and Wijker, Physica **15**, 627 (1949); (thermodynamic properties from 0 to 150°C) Michels, Lunbeck, and Wolkers, Physica **15**, 689 (1949); (isotherms from −150 to 0°C) Michels, Levelt, and de Graaff, Physica **24**, 659 (1958); (thermodynamic properties from −150 to 0°C) Michels, Levelt, and Wolkers, Physica **24**, 769 (1958).

[19] P. W. Bridgman, Proc. Am. Acad. Arts Sci. **70**, 1 (1935).

[20] J. M. H. Levelt, "Reduced experimental compressibility factor, energy, and entropy of argon and xenon" (to be published); and University of Wisconsin Theoretical Chemistry Laboratory Report WIS-OOR-24 (1959).

sets of reduced properties of argon from the experimental measurements of Michels and co-workers[18] by taking two reasonable sets of Lennard-Jones parameters: set I corresponds to $\epsilon/k=119.3°K$ and $\sigma=3.43$ A; set II corresponds to $\epsilon/k=119.8°K$ and $\sigma=3.405$ A. Thus for a particular T and V, the value of T^* and V^* is different for the two sets of reduced parameters. The difference between the properties of the substance reduced in the two ways gives an indication of the range of accuracy of the experimental values.

Until additional experimental data become available, the Monte Carlo calculations of Wood and Parker[11] provide the only test of the accuracy of our results at high densities or small volumes. In the Monte Carlo treatment, a small number of "molecules" are placed in a cell which is repeated periodically so as to serve as a unit cell in a space-filling lattice. Wood and Parker made our assumptions (1) and (2) that the potential of the system is pairwise additive and each pair of molecules obeys the Lennard-Jones 12–6 potential. Then their high-speed computing machine played a rather complicated game in which it is proposed that a particular molecule make a move in accordance with numbers selected in a random fashion. The resulting change in the potential energy of the system was computed. If the potential decreased, the move was accepted; if the potential energy increased, the move was either accepted or rejected in accordance with an *a priori* probability based upon the Boltzmann distribution of energies. The computing machine then proposed a move for another molecule and the process was repeated until the fluctuations in the over-all properties of the system became small. In principle, the Monte Carlo method should give exact solutions to the equation of state in the limit that a large number of molecules are introduced into the unit cell. With only a small number of molecules in the unit cell the radial distribution function cannot be reliable, and there are rather large corrections to the properties of the system which must be made to take into account the interactions with molecules in neighboring cells. In order to estimate such errors, Wood and Parker have carried out their calculations with both 108 and 32 molecules in the unit cell. By a comparison of their results for the two cases one can estimate the probable accuracy to be of the order of one or two percent in either U_c/NkT or pV/NkT. The Monte Carlo calculations have only been made for the isotherm $T^*=2.74$. No values of S_c/Nk have been reported.

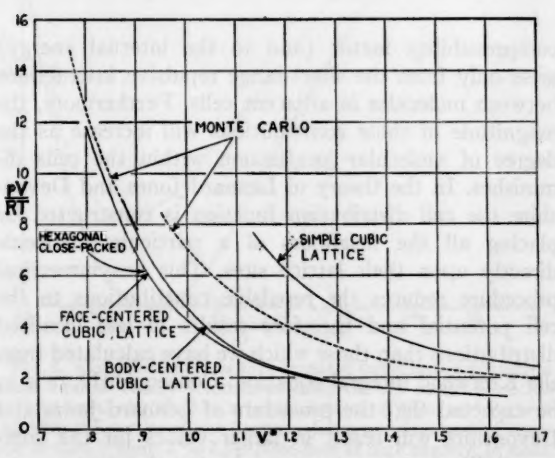

FIG. 4. Comparison of the compressibility factor calculated for different lattice types (using the cell model corrected for holes) with the results of Monte Carlo calculations.[11] Here $T^*=2.74$.

TABLE V. Comparison of calculated values for the configurational internal energy for a face-centered cubic lattice with experimental and Monte Carlo values. The cell model calculations include corrections for the presence of holes. The experimental values correspond to liquid Argon. Miss Levelt[20] obtained two limits: (I) corresponds to assuming for Argon the Lennard-Jones 12–6 parameters $\epsilon/k=119.3°K$, $\sigma=3.43$ A; (II) corresponds to $\epsilon/k=119.8°K$, $\sigma=3.405$ A. The Monte Carlo calculations were made by Wood and Parker.[11]

		$-U_c/NkT$			
		Calculated	Experimental		Monte
T^*	V^*	cell model	I	II	Carlo
1.2	1.4	4.188	3.848		
	1.5	3.824	3.606	3.665	
	1.6	3.507	3.395	3.450	
1.3	1.4	3.823	3.507		
	1.5	3.491	3.288	3.340	
	1.6	3.200	3.095	3.144	
1.4	1.6	2.938	2.832	2.876	
1.5	1.6	2.711	2.609	2.650	
2.0	1.6	1.917	1.838	1.865	
2.74	0.8	1.59			1.54
	0.9	2.06			1.86
	1.0	2.11			1.59
	1.2	1.86			1.59
	1.4	1.55	1.368		1.46
	1.8		1.107	1.122	1.16
2.75	1.4	1.538	1.362		
	1.5	1.414	1.292	1.307	
	1.6	1.264	1.225	1.241	
3.0	1.4	1.352	1.208		
	1.5	1.242	1.149	1.162	
	1.6	1.167	1.092	1.105	

In Tables V–VII our values of U_c/NkT, pV/NkT, and S_c/Nk computed for the face-centered cubic lattice (and corrected for holes) are compared with experimental[20] and Monte Carlo[11] results. In Fig. 5, our comcompressibility factor for the $T^*=2.74$ isotherm is compared with experimental, Monte Carlo, and Lennard-Jones and Devonshire results. In Fig. 6, our internal energy for the $T^*=2.74$ isotherm is compared with the Monte Carlo and Lennard-Jones and Devonshire calculations.

From Fig. 5 we see that at very high pressures the theoretical curve tends to approach the Monte Carlo isotherm. However, at low and intermediate pressures

TABLE VI. Comparison of calculated values for the compressibility factor for a face-centered cubic lattice with experimental[20] and Monte Carlo[11] values. The significance of the Experimental I and II columns is explained in the heading of Table V. The calculated values are corrected for the presence of holes.

		pV/NkT			
T^*	V^*	Calculated cell model	Experimental I	Experimental II	Monte Carlo
1.2	1.4	−1.307	0.805 1		
	1.5	−1.284	0.490 9	0.590 0	
	1.6	−1.185	0.308 0	0.373 8	
1.3	1.4	−0.891	1.078 9		
	1.5	−0.893	0.750 3	0.853 1	
	1.6	−0.822	0.549 6	0.620 7	
1.4	1.6	−0.514	0.755 5	0.830 3	
1.5	1.6	−0.249	0.931 9	1.009 5	
2.0	1.6	−0.663	1.521 3	1.604 2	
2.74	0.8	11.9			12.3
	0.9	6.8			7.8
	1.0	4.3			7.1
	1.2	2.16			4.0
	1.4	1.58	2.536 8	2.671 4	2.66
	1.8		1.617 8	1.672 4	1.76
2.75	1.4	1.586	2.539 9	2.674 4	
	1.5	1.454	2.195 6	2.299 5	
	1.6	1.298	1.946 4	2.028 8	
3.0	1.4	1.586	2.617 5	2.749 1	
	1.5	1.454	2.277 9	2.380 0	
	1.6	1.298	2.030 3	2.111 7	

TABLE VII. Comparison of calculated and experimental[20] values for the configurational entropy of a face-centered cubic lattice. The significance of the Experimental I and II columns is explained in the heading of Table V. The configurational entropy S_c is the difference between the entropy of the liquid and the entropy of a perfect gas at the same temperature and volume. The calculated values are corrected for the presence of holes. The calculated values are given both with full communal entropy ($\beta=e$) and without communal entropy ($\beta=1$).

		$-S_c/Nk$			
		Calculated cell model			
T^*	V^*	No communal entropy	Full communal entropy	Experimental I	Experimental II
1.2	1.4	4.216	3.216	2.202	
	1.5	4.006	3.006	1.987	2.051
	1.6	3.829	2.829	1.815	1.869
1.3	1.4	4.171	3.171	2.159	
	1.5	3.966	2.966	1.945	2.007
	1.6	3.791	2.791	1.772	1.828
1.4	1.6	3.757	2.757	1.731	1.783
1.5	1.6	3.725	2.725	1.696	1.747
2.0	1.6	3.595	2.595	1.558	1.605
2.75	1.4	3.784	2.784	1.727	
	1.5	3.615	2.615	1.564	1.611
	1.6	3.475	2.475	1.428	1.470
3.0	1.4	3.732	2.732	1.686	
	1.5	3.568	2.568	1.527	1.574
	1.6	3.435	2.435	1.396	1.437

the agreement is much less satisfactory. Had we not neglected the more distant neighbors in our calculation of the cell potential, the theoretical estimates of the pressure would undoubtedly have been greater. However, the magnitude of the error incurred by this neglect has not yet been determined. A comparison of the entries in Tables II and III reveals just how minor the corrections due to holes really are.

Throughout the entire range of densities the crude theory of Lennard-Jones and Devonshire provides larger (and hence better) estimates of the compressibility factor than does the more rigorous theory we have employed. To see why this is so we must first recognize that significant *positive* contributions to the

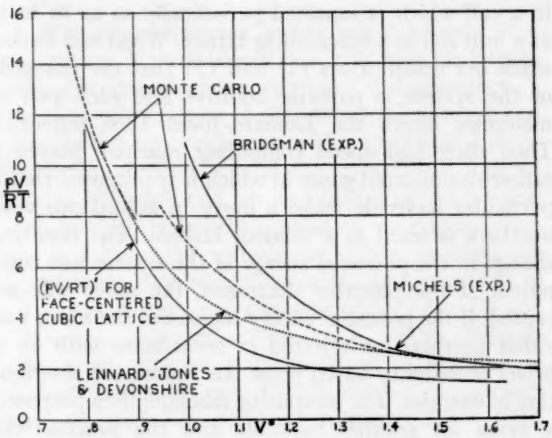

FIG. 5. Comparison of our face-centered cubic lattice compressibility factor (calculated using the cell model corrected for holes) with the experimental data of Michels and his co-workers,[18,20] with the experimental data of Bridgman,[19] with the Monte Carlo calculations of Wood and Parker,[11] and with the results of the Lennard-Jones and Devonshire equation of state.[11] Here $T^*=2.74$. Note how our cell model isotherm merges into the solid branch of the Monte Carlo curve at very high density, or small values of V^*.

compressibility factor (and to the internal energy) arise only from the short-range repulsive interactions between molecules in adjacent cells. Furthermore, the magnitude of these contributions will increase as the degree of molecular localization within the cells diminishes. In the theory of Lennard-Jones and Devonshire the cell distribution function is constructed by placing all the neighbors of a particular molecule directly upon their lattice sites. This unsymmetrical procedure reduces the repulsive contributions to the cell potential and therefore results in less localized distributions than those which we have calculated from the Kirkwood integral equation. Consequently, it is to be expected that the procedure of Lennard-Jones and Devonshire will result in larger values for the compressibility factor, entropy, and internal energy.

From both Figs. 5 and 6, it would seem that the isotherms calculated by our cell treatment correspond

to a metastable extension of the crystalline isotherms rather than to an approximation to the liquid isotherms. This viewpoint is consistent with the fact, as may be seen from Table VII, that the experimental values for the configurational entropy are larger by $2Nk$ than our values assuming no communal entropy, or larger by Nk than our values assuming full communal entropy. Joseph Mayer has pointed out to us that, since the entropy of an Einstein crystal is smaller than that of a Debye crystal by an amount of the order of Nk, it is not unreasonable to obtain a low value for the entropy of a cell model liquid. However, the values of the entropy computed on the basis of the cell model seem to be lacking the entropy of fusion.

It has been mentioned previously that our own estimates of the compressibility factor would have been greater if we had not neglected the distant neighbor contributions to the cell potential. Although the precise magnitude of the error incurred by this neglect is unknown, it most certainly will not be great enough to explain the considerable difference between the theoretical and Monte Carlo isotherms. The most that it would seem reasonable to expect is that the inclusion of these distant neighbor contributions might bring the predictions of the Kirkwood theory into close agreement with those derived from the theory of Lennard-Jones and Devonshire. If this analysis of the situation

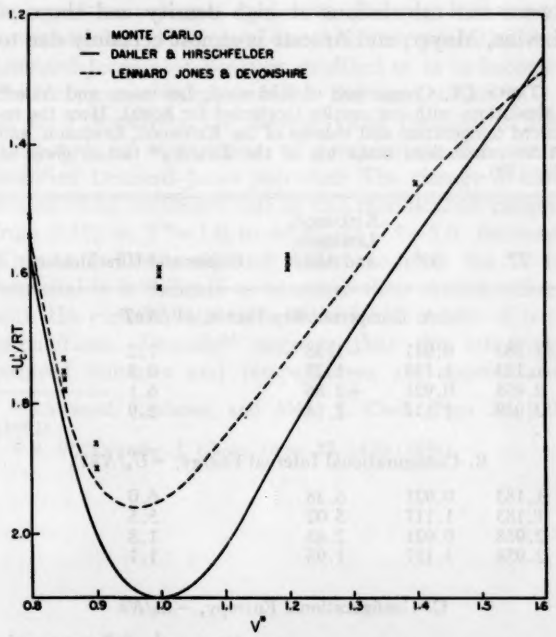

FIG. 6. Comparison of our face-centered cubic lattice configurational internal energy (calculated using the cell model corrected for holes) with the Monte Carlo calculations of Wood and Parker[11] and with the results of the Lennard-Jones and Devonshire equation of state.[11] Here $T^*=2.74$. Note how at high density, or small values of V^*, our configurational internal energy agrees with the Monte Carlo calculation for a solid, but at large volumes our configurational internal energy does not agree with the Monte Carlo calculations for the liquid.

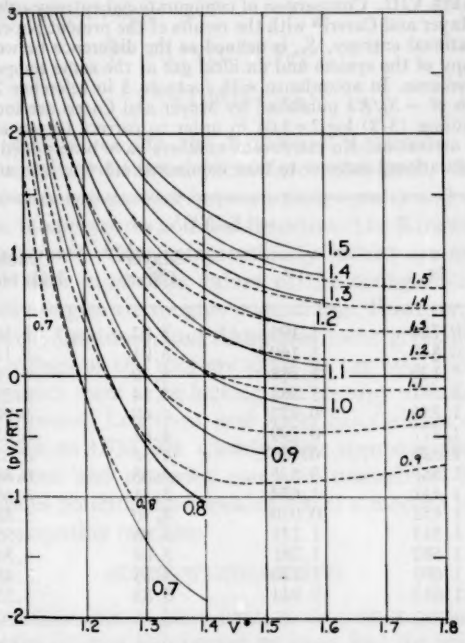

FIG. 7. The first shell contributions to the compressibility factor (corrected for holes), $(pV/RT)_1'$. The solid curves refer to our calculations. The dotted curves refer to the calculations of Levine, Mayer, and Aroeste.[24] The numbers given on the figure are the values of T^*. This figure shows the sensitivity of the cell theory to the choice of the pair potential energy function and the exact shape of the cell distribution function. A very small shift in the scale of the reduced volume, V^*, brings our results into almost perfect agreement with those of Levine, Mayer, and Aroeste.

is correct, then it would appear that some rather drastic modification of the cell model is necessary before it can be transformed into a quantitative theory of liquids. In this connection it should be emphasized that even if our predictions of the equation of state had agreed with the Monte Carlo isotherm, the theory itself could not have been deemed correct. For the high degree of spatial ordering which is an intrinsic part of the cell model does not exist in real liquids. Thus, the radial distribution functions calculated on the basis of the cell model differ markedly from those obtained by x-ray diffraction methods.[21] To diminish this high degree of ordering one could simply ignore the thermodynamical criterion of minimum free energy and introduce whatever number of holes is necessary to produce agreement between theory and experiment. The extent to which this procedure is successful will be discussed in a future communication.

A more sophisticated and theoretically sound approach requires the invention of alternate mechanisms for producing disorder. For example, one might attempt to represent the liquid as a collection of very small crystallites belonging to several lattice types and

[21] J. S. Dahler, J. Chem. Phys. **29**, 1082 (1958); see also J. Corner and J. E. Lennard-Jones, Proc. Roy. Soc. (London) **A178**, 401 (1941).

TABLE VIII. Comparison of configurational entropy calculated by Mayer and Careri[15] with the results of the present paper. Configurational entropy, S_c, is defined as the difference between the entropy of the system and an ideal gas at the same temperature and volume. In accordance with footnote 3 in reference 24, the values of $-S_c/Nk$ published by Mayer and Careri are increased by adding $(3/2)\log_e 2=1.04$ in order to correct for an error in their derivation. No extraneous numbers have been added to the configurational entropy to take communal entropy into account.

		$-(S_c/Nk)'$	
T^*	V^*	Mayer-Careri	Dahler-Hirschfelder
0.734	1.195	5.02	5.16
0.848	1.160	5.01	5.17
1.100	1.281	4.39	4.58
1.141	1.383	4.14	4.29
1.236	0.927	4.68	5.90
1.277	0.799	4.67	6.63
1.328	0.968	4.38	5.61
1.387	0.825	4.35	6.38
1.441	1.654	3.51	3.65
1.452	0.970	4.10	5.52
1.513	1.125	3.88	4.85
1.582	1.281	3.69	4.34
1.605	1.730	3.35	3.48
1.610	0.944	3.83	5.55

separated from one another by cracks.[22] The success of this approach would presumably depend upon the relative magnitude of the energy required for the formation of a crack and the attendant increase in entropy. Another possibility is that of describing the disorder in terms of density fluctuations whereby some small portions of the liquid are momentarily compressed and others dilated. These and several other mechanisms are presently being studied. It is our hope that from investigations of this sort a more satisfactory statistical theory and molecular scale characterization of the liquid will finally emerge.

Our results for the contributions from the first shell of neighbors should be compared with the calculations of Mayer and Careri[15] and Levine, Mayer, and Aroeste[23] who considered only nearest neighbors, approximated the cell distribution by Gaussian error functions, corrected their results for the presence of holes, and used for the pair potential energy the Morse function

$$u(r)=\epsilon[\exp\{-12[(r/r_e)-1]\}-2\exp\{-6[(r/r_e)-1]\}]. \quad (58)$$

This Morse function has the same curvature around the potential minimum at $r=r_e$ as does the Lennard-Jones 12–6 potential. The Morse potential is zero when the intermolecular separation is $\sigma'=[1-(\frac{1}{6})\log_e 2]r_e=0.884475\,r_e$, as contrasted to the Lennard-Jones 12–6 potential which is zero when the separation is $\sigma=2^{-(1/6)}r_e=0.890899r_e$. At the separation $2r_e$, the Morse potential has the value -0.00495ϵ while the Lennard-Jones 12–6 potential is -0.03101ϵ. The second virial coefficient for this Morse function has not been tabulated. Thus it is difficult to compare the results of Mayer and his co-workers with either experimental data or with our results. However, to establish trends and gross differences, we take Mayer's reduced volume as $V^*=2^{\frac{1}{2}}V/Nr_e^3$ and the reduced temperature as $T^*=kT/\epsilon$.

In Fig. 7, the first shell (with holes) contributions and the compressibility factor of Levine, Mayer, and Aroeste are compared with ours. For a given T^* and V^* their compressibility factor is always less than ours. This result can be explained by the more strongly repulsive nature of the 12–6 potential at small separations. The comparison between the two sets of computations is interesting, since it gives some indication of how sensitive the cell theory is to (1) the choice of the pair potential energy function and/or (2) the approximation to the solution of Kirkwood's integral equation by a Gaussian distribution function. At high densities, the Gaussian approximation becomes virtually correct. Therefore, the principle cause of difference between our calculations at high density and those of Levine, Mayer, and Aroeste is almost certainly due to

TABLE IX. Comparison of Kirkwood, Lewinson, and Alder[25] calculations with our results (corrected for holes). Here the reduced temperature and volume of the Kirkwood, Lewinson, and Alder calculations make use of the Zwanzig[26] factors given in Eq. (59).

T^*	V^*	Kirkwood, Lewinson, and Alder	Dahler and Hirschfelder	
		A. Compressibility Factor, pV/NkT		
1.183	0.921	−1.38	7.2	
1.183	1.117	−1.27	0.3	
2.958	0.921	+2.86	6.1	
2.958	1.117	2.14	2.9	
		B. Configurational Internal Energy, $-U_c/NkT$		
1.183	0.921	6.28	6.0	
1.183	1.117	5.02	5.5	
2.958	0.921	2.45	1.8	
2.958	1.117	1.95	1.7	
		C. Configurational Entropy, $-S_c/Nk$		
			no communal entropy	full communal entropy
1.183	0.921	3.29	6.0	5.0
1.183	1.117	2.48	5.0	4.0
2.958	0.921	3.44	5.0	4.0
2.958	1.117	2.66	4.4	3.4

[22] Eyring, Ree, and Hirai, Proc. Natl. Acad. Sci. U.S. **44**, 683 (1958).

[23] Levine, Mayer, and Aroeste, J. Chem. Phys. **26**, 207 (1957). Their results for large values of V going up to the critical volume are probably not very accurate since their calculational procedure is essentially a perturbation method valid only if the number of holes is small.

the difference between the 12–6 and the Morse potentials.

In Table VIII the configurational entropy calculated by Mayer and Careri[15] is compared with our values (assuming no communal entropy and correcting for holes). For half the cases, the agreement is excellent; for the remaining cases, the agreement is very poor with our values of $-S_c/Nk$ larger than those of Mayer and Careri. The bad agreement occurs for small values of V^* where the Morse potential should be very nearly the same as the Lennard-Jones 12–6. Thus, computational errors in either the Mayer-Careri or our paper would seem to be the most logical explanation. Of course, both sets of calculated entropies would have been improved if the contributions of distant neighbors to the cell potential had been taken into account. It is unfortunate that Levine, Mayer, and Aroeste did not publish their calculated values of entropy and provide us with an additional check.

An entirely different type of theoretical equation of state calculation has been made by Kirkwood, Lewinson, and Alder[24] who used the superposition approximation to obtain an integral equation for the radial distribution function. Such a treatment is free from the objections of the cell theory. However, for rigid spheres at high densities, the superposition principle does not give isotherms which agree well with the Monte Carlo calculations. Thus, the inherent accuracy of the superposition principle is open to question. Kirkwood, Lewinson, and Alder used for their pair potential the Lennard-Jones 12–6 function modified so as to become discontinuously infinite when the separation is σ. In their Appendix III, second virial coefficients are computed as a function of temperature for their modified Lennard-Jones potential. The change in the second virial coefficient due to this modification ranges from 3.3% at $T^*=1.0$ to 44.8% at $T^*=5.0$. Because Kirkwood, Lewinson, and Alder modified the 12–6 potential it is difficult to compare their results either with the experimental data or with the results of our calculations. Zwanzig[25] suggests that the following reduced volumes and temperatures are appropriate for such comparisons:

$$V^*=0.7533V/(N\sigma_K^3),$$
$$T^*=1.183kT/\epsilon_K, \qquad (59)$$

where σ_K and ϵ_K are the Kirkwood, Lewinson, and Alder modified Lennard-Jones force constants. Table IX shows a comparison between their results and ours for two temperatures and two densities. The Kirkwood, Lewinson, and Alder compressibility factors are much smaller than ours. The values of the configurational internal energies are roughly comparable. However, the Kirkwood, Lewinson, and Alder treatment gives much better values of the entropy than do the cell calculations (which seem to be lacking the entropy of fusion). The Kirkwood, Lewinson, and Alder calculations were made with an IBM 604. Clearly their approach should be repeated and extended using an unmodified Lennard-Jones potential and making use of a modern high-speed computing machine.

[24] Kirkwood, Lewinson, and Alder, J. Chem. Phys. **20**, 929 (1952).
[25] R. W. Zwanzig, J. Chem. Phys. **22**, 1420 (1954).

ACKNOWLEDGMENTS

These calculations have been made over a period of five years. During this period we have had the help of many able mathematicians. First of all, we would like to thank Frank Parker for programming and carrying out part of the calculations on the MURA IBM 704 computing machine. Then we would like to thank Gertrude Blanch for help in carrying out calculations on the Air Force Wright Air Development Center E-101 computing machine; Dale Rudd, for calculations on the University of Minnesota Remington-Rand 1103; Audrey Schlafke, for calculations on the University of Wisconsin Numerical Analysis Laboratory IBM 650; Marion Taylor, for calculations on the University of Wisconsin Theoretical Chemistry Laboratory's Bendix G-15D computing machine. Of course we wish to thank each of the institutions named above for the use of their equipment and the help of their staff.

The authors are especially grateful to Henry Thacher, Lars Onsager, John Kirkwood, and Charles Curtiss for many helpful discussions. Elizabeth Hirschfelder assisted in the preparation and proof reading of the manuscript. Beatrice Belda and Florence Daul performed the typing.

Energy Requirements of Mechanical Shear Degradation in Concentrated Polymer Solutions*†‡

A. B. BESTUL

National Bureau of Standards, Washington, D. C.

(Received March 9, 1959)

Molecular weight decrease by mechanical shearing results when solutions of around 10% of polyisobutene having average molecular weights above 500 000 are forced through a capillary at nominal rates of shear above 10 000 sec^{-1}. Comparison of observed plots of shear load *vs* duration of shearing at fixed rates of shear during this degradation process with the corresponding estimated plots which would be expected to obtain if degradation did not occur provide a means of evaluating the amount of applied shearing energy which is dissipated by the degradation process. The result is several hundred thousand kilocalories per mole of broken bonds, which is several thousand times the bond energy of carbon-carbon bonds. This finding is consistent with the hypothesis that whenever a bond breaks the system loses much of the free energy temporarily stored in bonds and macromolecular chains located in a comparatively large volume surrounding the broken bond, these bonds and chains having been involved in concentrating the required activation energy into the ruptured bond.

I. INTRODUCTION

UNDER certain conditions the molecular weights of polymers are reduced by mechanical shearing in the flow of their concentrated solutions through capillary tubes.[1,2] The energy of reaction for such a polymer degradation process is probably a small positive value if estimated either from the energy of polymerization[3] or from the energies of the chemical bonds broken and made in hypothetical reaction schemes for the process.[4] The energy of activation for such a degradation process must be limited by the bond energy of aliphatic carbon-carbon bonds (about 80 kcal per mole) as the upper limit. This value is in the neighborhood of values around 50 kcal per mole of broken bonds reported by various authors[5-8] for the activation energy of thermal degradation in several different polymers. This paper reports and compares with the foregoing estimates the experimentally observed energy consumption of the mechanical shear degradation process as a function of the following experimental variables: nominal rate of shear, shearing temperature, polymer concentration in solution, and polymer molecular weight.

II. EXPERIMENTAL PROCEDURES, MATERIALS, AND RESULTS

The solutions of polyisobutenes in *n*-hexadecane investigated and the experimental techniques used here have been described in detail in a previous publication[9] to which the reader is referred. The θ temperature for these solutions has been evaluated as 175°K,[10] but the solvent freezes at 18°C. Column five of Table I gives the final viscosity average molecular weights after degradation for the polymers, concentrations, temperatures, and nominal rates of shear listed in the first four columns, respectively, of that table. The shear loads as functions of the number of shearing passes under these conditions have been reported elsewhere.[1,4] Figure 1 shows the shear loads as functions of viscosity average molecular weight at several values of nominal rate of shear (D) under conditions where no shear degradation occurs.

III. TREATMENT OF DATA

In order to convert the change in viscosity average molecular weight into the number of bonds ruptured, the somewhat drastic approximation is made of using the relation

$$B/AW=(1/\bar{M}_n-1/\bar{M}_{n_0}), \qquad (1)$$

where B is the number of bonds ruptured, A is Avogadro's number, W is the weight of polymer sample, and $\bar{M}_{n_0}$ and $\bar{M}_n$ are the initial and final *number* average molecular weights, respectively. Viscosity average molecular weights M_v calculated in this investigation are substituted for the number average molecular weights in Eq. (1). This procedure introduces an uncertainty which is dependent on the molecular weight distribution of the undegraded and the degraded polymers. For a polydisperse polymer $\bar{M}_v$ is always greater than $\bar{M}_n$. Therefore if the form of the molecular

* Extracted partly from a thesis submitted to the Graduate School of the University of Maryland in partial fulfillment of the requirements for the degree of Doctor of Philosophy.

† This work was performed as part of a research project last sponsored by the National Science Foundation in connection with the Government Synthetic Rubber Program.

‡ Some of the results reported herein were presented orally before the sessions of the Division of High Polymer Physics at the American Physical Society meeting in Detroit and Ann Arbor, Michigan, on March 18–20, 1954.

[1] A. B. Bestul, J. Chem. Phys. **24**, 1196 (1956).

[2] A. B. Bestul, J. Phys. Chem. **61**, 418 (1957).

[3] C. E. Schildknecht, *Vinyl and Related Polymers* (John Wiley & Sons, Inc., New York, 1952), pp. 14, 245, 368, 372, 496, 562, and 703.

[4] A. B. Bestul (Ph.D. Thesis, University of Maryland, 1953), p. 41.

[5] Vatinov, Kobeko, and Marei, J. Phys. Chem. (USSR) **16**, 106 (1942).

[6] A. Atherton, J. Polymer Sci. **5**, 378 (1950).

[7] D. S. Montgomery and C. A. Winkler, Can. J. Research **B28**, 429 (1950).

[8] S. L. Madorsky, J. Polymer Sci. **9**, 133 (1952).

[9] A. B. Bestul, J. Appl. Phys. **25**, 1069 (1954).

[10] T. G. Fox, Jr., and P. J. Flory, J. Am. Chem. Soc. **73**, 1090 (1951).

TABLE I. Energy requirement data for shear degradation of polyisobutene in *n*-hexadecane under various conditions.

Vistanex No.	Concentration, wt%	Temperature, °C	Nominal rate of shear, D, sec^{-1}	Final molecular weight, $\bar{M}_v \times 10^{-6}$	Bonds ruptured per cm^3 solution, moles, $\times 10^8$	H, degradation energy area, lb×pass	Degradation energy per mole bonds ruptured, kcal
B—60 ($\bar{M}_{v0}$=910 000)	10	40	66 000	0.79	1.27	454.9	291 000
B—80 ($\bar{M}_{v0}$=1 020 000)		40	65 600	0.83	1.71	485.2	230 000
			33 000	0.94	0.639	142.8	182 000
			18 900	1.02	0	...	...
	15	40	66 000	0.74	4.23	907.9	175 000
B—100 ($\bar{M}_{v0}$=1 750 000)	5	40	65 600	1.34	0.667	360.0	448 000
			33 000	1.59	0.221	130.5	478 000
			18 900	1.75	0	...	...
	10	30	65 600	0.90	4.11	1339.0	265 000
			33 000	1.28	1.60	607.2	308 000
			18 900	1.49	0.802	321.5	326 000
		40	65 600	1.13	2.39	966.4	329 000
			33 000	1.41	1.05	393.6	305 000
			18 900	1.55	0.563	239.8	348 000
			9 500	1.75	0	...	...
		50	65 600	1.28	1.60	628.6	319 000
			33 000	1.42	1.01	334.7	269 000
			26 000	1.57	0.502	252.2	408 000
			18 900	1.60	0.414	50.6	99 000
	15	40	65 600	1.00	5.12	1616.0	256 000
				1.02	4.90	1576.3	260 000
				1.02	4.90	1566.6	261 000
			33 000	1.27	2.46	780.1	257 000
			18 900	1.51	1.04	377.3	295 000
	20	40	66 000	0.87	8.79	2653.0	245 000
B—120 ($\bar{M}_{v0}$=1 900 000)	10	40	66 000	1.20	2.34	970.0	337 000
B—140 ($\bar{M}_{v0}$=2 520 000)		20	66 000	0.76	6.99	3315.0	385 000
		30	66 000	0.94	5.07	2125.1	340 000
		40	65 600	1.40	2.34	1384.0	481 000
			33 000	1.83	1.13	512.6	368 000
			18 900	2.16	0.502	262.0	424 000
		50	66 000	1.49	2.08	785.7	307 000
		60	66 000	1.58	1.80	616.9	278 000
		70	66 000	1.75	1.32	515.1	316 000
		80	66 000	2.09	0.616	395.3	521 000
	15	40	66 000	1.06	6.23	2647.9	345 000

weight distribution remained unchanged during degradation so that the ratio of $\bar{M}_v$ to $\bar{M}_n$ remained constant, the foregoing procedure would overestimate the number of bonds ruptured and therefore underestimate the energy consumed per rupture. However this conclusion may be affected by a change in the form of the molecular weight distribution during degradation, the possibility of which we now explore.

The form of the molecular weight distribution of polyisobutene samples similar to the undegraded polymers investigated here is given by Van Holde and Williams.[11] They are wide and highly skewed. Substantial low molecular weight material is present and a long narrow tail extends to relatively high molecular

[11] K. E. Van Holde and J. W. Williams, J. Polymer Sci. 11, 243 (1953).

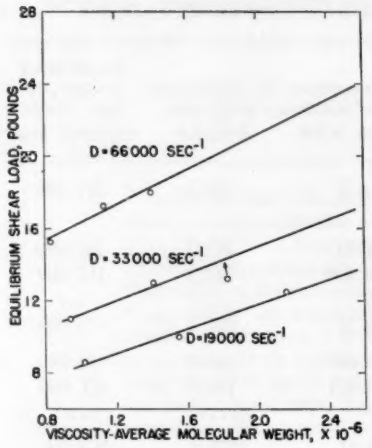

FIG. 1. Equilibrium shear load in absence of shear degradation as a function of viscosity average molecular weight for 10 wt% B–100 polyisobutene in *n*-hexadecane at 40° and several nominal rates of shear (D) indicated.

weights. The effect of shear degradation on this distribution is believed to be to cut off most of the high molecular weight end relatively sharply above a critical molecular weight value. The material which disappears from the high molecular weight end of course reappears at lower molecular weights below this critical value. This interpretation is supported by the incidental fractionation data given in reference 2. The effect of a high molecular weight tail is to increase the ratio of viscosity average to number average molecular weight. Therefore, the effect of eliminating such a tail in the degradation process is to decrease the ratio of $\bar{M}_v$ to $\bar{M}_n$. This further increases the overestimate of the number of ruptured bonds as obtained by the foregoing procedure. Therefore the values finally obtained for energy consumed per bond rupture are certainly lower than the true values. However, sample calculations for extreme situations consistent with the extent of degradation observed show that this discrepancy is certainly no greater than a factor of 2 or so. Column six of Table I gives the ultimate number of bonds ruptured per cm³ of solution for all the conditions listed there.

If the plots in Fig. 1 are extrapolated to molecular weights higher than those for which data are shown there, estimates are obtained for the equilibrium shear loads which would be obtained for the higher molecular weights if degradation did not occur for them. It is of course impossible to directly observe these equilibrium shear loads for the higher molecular weights since degradation does in fact occur for them. The linear plots shown in Fig. 1 are used for these extrapolations because they provide as sensitive a functionality between ordinate and abscissa as can be supported by the experimental data in the figure. These data do not determine any of the more sophisticated functionalities which have been discussed between molecular weight and viscosity (to which equilibrium shear load should be proportional at a given rate of shear). Representative plots for the observed actual shear load and the estimated equilibrium shear load determined as above are shown in Fig. 2, which applies specifically to the shear degradation of a solution of 10 wt % Vistanex B-100 at 40° and 66 000 sec^{-1}.

A large and abrupt increase in observed shear load is seen when a shearing condition where shear degradation occurs is compared with a condition where degradation does not occur (cf. Figs. 1, 5, and 7 of reference 9). This fact suggests[9] the identification of the equilibrium shear load with energy used in the shearing process in actually overcoming viscoelastic resistance to flow as distinct from energy used in the rupture of polymer molecular bonds. This latter energy is accordingly identified with the difference between the observed and the equilibrium shear loads.

A set of curves such as those shown in Fig. 2 applies to a fixed nominal rate of shear. The product of this rate and the shearing stress (proportional to the shear load on the ordinate) gives the rate of energy dissipation. Since pass number is in effect a time coordinate, the area between the observed and the equilibrium shear load curves, shaded in Fig. 2, is directly proportional to the energy used in the degradation process and can be converted thereto simply by multiplying by the appropriate proportionality factor.

For a number of conditions represented in Table I data are not available to make the extrapolations, as in Fig. 1, necessary to construct an estimated equilibrium shear load plot. To handle these cases, the horizontal line through the final observed shear load (see Fig. 2) has been used as an approximate equilibrium shear load curve and a correction applied by comparison

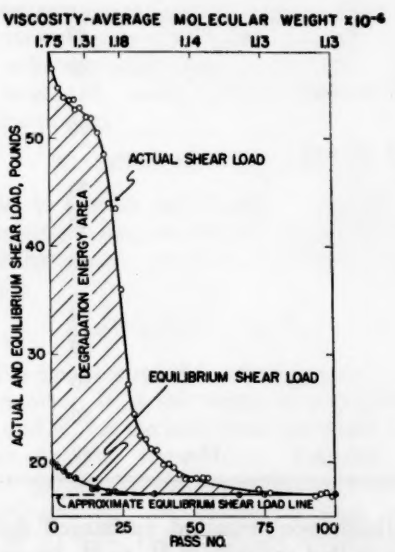

FIG. 2. Actual and equilibrium shear load as a function of amount of shearing for 10 wt% Vistanex B-100 polyisobutene in *n*-hexadecane at 40° and 66 000 sec^{-1} nominal rate of shear (D). Shaded area represents degradation energy. Dashed horizontal line represents approximate equilibrium shear load. The top scale represents the molecular weights existing at the various stages of degradation corresponding to the pass numbers on the bottom scale. (It is in fact a cross plot of the ordinate of Fig. 7 in reference 9).

TABLE II. Degradation energy (kcal/mole bonds ruptured) $\times 10^{-3}$.

Concentration wt%		5			10				15	20
Temperature °C		40	20	30	40	50	60	70	80	40	40
Viscosity average molecular wt—$\bar{M}_v \times 10^{-3}$	Nominal rate shear D sec$^{-1} \times 10^{-2}$										
0.91	66				291						
1.02	66				230					175	
	33				182						
1.75	66	448		265	329	319				260	245
	33	478		308	305	269				257	
	26					408					
	19			326	348	99				295	
1.90	66				337						
2.52	66		385	340	481	307	278	316	521	345	
	33				368						
	19				424						

of results from the approximate and from the extrapolated equilibrium shear load curves for those conditions for which the latter is available. The average ratio of approximate to actual degradation energy area is 0.97 and the variation from that value is small. Therefore in the cases where actual degradation energy areas are not obtainable, an area is obtained by correcting the approximate area by the factor of 0.97. For all the conditions listed in Table I, column seven gives either the actual degradation energy area or the corrected approximate area if the actual area is not obtainable.

The part of the observed shear load which corresponds to energy used in bond rupture does not have the nature of a force overcoming resistance to viscous flow. Therefore the observed shear load data cannot be treated by rheological techniques such as the differentiation method to reduce them to flow curves relating the fundamental rheological quantities of shearing stress and actual rate of shear. Accordingly these quantities cannot be used for any direct estimation of degradation energies or for the conversion of degradation energy area to degradation energy itself. This conversion can, however, be accomplished with completely equivalent results directly from the shear load and the geometry of the instrument. The result gives the average value throughout the capillary which is the same average as obtained for the number of bonds ruptured. However, since the shearing stress and rate of shear change with radial position in the capillary, the energy consumption at any particular position in the capillary may differ correspondingly from this average.

The cross-sectional area of the piston to which the shear load is applied is 1.307 cm^2. Therefore in each pass, the energy corresponding to 1 cm of piston travel is supplied to 1.307 cm^3 of polymer solution. Since a pound of force is equal to 444 822 dynes, each pound of shear load applied to the piston corresponds in each pass to (444 822 dyne cm cm^{-1})/(1.307 cm^3 cm^{-1}) (4.184×10^{10} erg kcal^{-1}) $= 8.12 \times 10^{-6}$ kcal per cm^3 of solution. For all the conditions represented in Table I, column eight gives the degradation energy per mole of bonds ruptured.

IV. DISCUSSION

The result for 10% B-100 Vistanex at 50° and 18 900 sec^{-1} is out of line with the other degradation energies. The result at this condition in the kinetic analysis of the degradation process[1] is also discordant. Apparently an undetected error has entered the results at this condition.

An indication of the reproducibility of the results is given by the three values listed for 15% B-100 Vistanex at 40° and 65 600 sec^{-1}. These are results for independent repeated degradations for these conditions.

Table II suggests the amount of shear energy used in degradation to be nearly independent of nominal rate of shear and of temperature, to decrease with increasing concentration, and to increase with increasing original molecular weight. More extensive measurements[12] at 80° where the degradation is becoming less severe than at lower temperatures, suggest that the degradation energy increases as temperature rises into the range of less severe degradation. These variations probably represent variations in the respective amounts of the stored free energy in the bonds or macromolecular chains surrounding a ruptured bond which are dissipated with and without contributing to overcoming viscoelastic resistance to flow when the bond ruptures.

The immediately outstanding feature of the results is that the energy dissipated in rupturing a bond is several thousand times the bond energy. No explanation of this behavior has been found in terms of the energy of reaction. A sensible explanation can be proposed, however, in terms of the energy of activation for the degradation process.

As discussed previously[1] the bond rupture in mechanical shear degradation is considered to be activated by energy supplied from the mechanical shearing forces

[12] P. Goodman and A. B. Bestul, J. Polymer Sci. 18, 235 (1955).

and temporarily stored in the bonds during the small but finite times required for the occurrence of the individual inter- and intramolecular motions which collectively constitute the viscoelastic shearing process. The increased potential energy of the bonds associated with this storage is conceived to be more than just the barriers to internal rotation of bonds within macromolecules. The configurational changes of the macromolecular chains can be accounted for entirely by internal rotation. However, it is considered unlikely that the actual process of deformation proceeds exclusively by internal rotation at all stages. The end result may be energetically equivalent to pure internal rotation. However, during the actual occurrence of the deformation it is likely that bond length stretchings and bond angle distortions occur as well as internal rotations. The stretchings and distortions raise the potential energy while they exist and provide a means of activating mechanical bond rupture. As time elapses for internal rotation to occur sufficiently to completely accomodate the deformation, the high energy bond conditions relax and the net effects are those of internal rotation.

Upon the completion of an individual inter- or intramolecular movement the free energy temporarily stored during the movement as potential energy in the interatomic bonds involved in the movement becomes stored as reduced entropy of deformation of the polymer chain molecules. In the equilibrium static deformation of polymers the major part (say 85%[13]) of the stored free energy is in the form of reduced entropy of deformation. It is clear, however, that the only part of the stored free energy which can activate bond rupture is that in the form of potential energy in the bond-to-be-ruptured. No mechanism is conceivable by which reduced entropy of deformation of the molecular chains can raise the energy of an individual interatomic bond as would be necessary to activate rupture.

In order to accumulate sufficient energy in a bond to activate its rupture, however, it is considered that free energy introduced by the shear field into many bonds or macromolecular chains is concentrated into the bond-to-be-ruptured through any of several types of interatomic connections in crude analogy with the combination of tensions in entangled strings. In this process the only function of the stored free energy is to produce tension in the macromolecular chains so both potential energy stored in individual bonds and reduced entropy of deformation stored in the chains can be effective.

Consider that free energy which is temporarily stored in those unruptured bonds and macromolecular chains involved in concentration energy into the ruptured bond. It may be dissipated upon rupture without contributing to overcoming viscoelastic resistance to flow. If so, all the energy so dissipated would be included in the energy consumed in the rupture process. This quantity would then be in no way limited by the energy actually required to activate the rupture of the ruptured bond. In this case the energy consumed can give some rough information about the number of bonds or macromolecular chains involved in concentration energy into the ruptured bond.

Such information cannot be very definite since it is impossible to know reliably the amount of energy temporarily stored in the individual bonds or macromolecular chains involved in concentrating energy into the ruptured bond. It is also impossible to know what portion, if any, of the energy so stored is used after rupture to help overcome viscoelastic resistance to flow. However, some limits may be set.

Since a flow process involves continuous shearing, polymer molecules present find no static equilibrium deformed condition and continuously perform inter- and intramolecular movements in reaction to the continuous shearing. It is during the occurrence of these movements that free energy is stored as potential energy in individual bonds. Therefore in a flow process the stored free energy should include a greater proportion of potential energy than it does for equilibrium static deformation mentioned earlier. For a flow process no means of analysis has been devised to evaluate the relative division of the stored free energy between potential energy in bonds and reduced configurational entropy of deformation. However, it appears that both possibilities probably make substantial contributions.

A reasonable procedure seems to be first to consider the two extreme cases where (1) all the stored free energy is reduced configurational entropy of deformation and (2) all the stored free energy is potential energy in bonds. Subsequently the existing balance of the two cases can be considered. Let us assume that all the stored free energy involved in concentrating the required energy of activation into a bond-to-be-ruptured is dissipated at the time of rupture without contributing to overcoming viscoelastic resistance to flow. This assumption will promote a minimum estimate for the number of bonds or macromolecular chains involved in concentrating energy of activation into a bond-to-be-ruptured.

4.1. Storage Completely as Configurational Entropy of Deformation

The kinetic theory of rubber elasticity provides a means of calculating the free energy associated with the reduction of configurational entropy by deformation of a section of a macromolecule between two adjacent entanglements with other macromolecular chains. For large deformations the force f on a chain macromolecular section containing n links each of length l, and whose ends are held a distance r apart is given in the Langevin approximation[14] as

$$f = (kT/l)\mathcal{L}^{-1}(r/nl), \tag{2}$$

[13] Cf. L. R. G. Treloar, *The Physics of Rubber Elasticity* (Oxford University Press, New York, 1949), p. 26.

[14] Reference 13, p. 98.

where T is absolute temperature, k is the Boltzmann constant, and $\mathcal{L}^{-1}(r/nl)$ is the inverse Langevin function defined by

$$(r/nl) = \coth\mathcal{L}^{-1}(r/nl) - 1/\mathcal{L}^{-1}(r/nl). \quad (3)$$

For each section the corresponding energy stored E in going from the undeformed to a deformed condition is

$$E = \int_{r_0}^{r} (kT/l)\mathcal{L}^{-1}(r/nl)\,dr$$

$$= \int_{(r/nl)_0}^{(r/nl)} (kT/l)\mathcal{L}^{-1}(r/nl)\,d(r/nl)\,nl$$

$$= \int_{(r/nl)_0}^{(r/nl)} (kTn\mathcal{L}^{-1}(r/nl)\,d(r/nl). \quad (4)$$

The quantity r_0 is the most probable distance between ends for the undeformed macromolecular section and[15] from reference 13,

$$(r/nl)_0 = (r_0/nl) = (l/nl)(2n/3)^{\frac{1}{2}} = (2/3n)^{\frac{1}{2}}. \quad (5)$$

For polyisobutene, measurements of viscosity as a function of molecular weight indicate that the molecular weight between chain entanglements is about 17 000 for the undiluted polymer.[16-17] If the polymer is diluted with solvent the molecular weight between entanglements varies inversely with the volume fraction of polymer.[17] For the present 10 wt % solutions the value is then about 150 000. For the purposes of calculation we assume that each monomer unit of base molecular weight 56 constitutes a chain link. The number n of links between entanglements for the present case then becomes about 2700. Inserting $n=2700$ into Eq. (5) gives $(r/nl)_0 = 0.016$.
For

$$\mathcal{L}^{-1}(r/nl) > 5,$$

$$\coth\mathcal{L}^{-1}(r/nl) = 1.0000$$

and

$$(r/nl) = 1 - 1/\mathcal{L}^{-1}(r/nl). \quad (6)$$

In terms of (r/nl) the range of validity for this approximation is $(r/nl) > 0.8$. In this range

$$\mathcal{L}^{-1}(r/nl) = 1/[1-(r/nl)]. \quad (7)$$

Then

$$E = \int_{0.016}^{(r/nl)>0.8} kTn\{1/[1-(r/nl)]\}d(r/nl) \quad (8)$$

$$= \{-kTn\ln[1-(r/nl)]\}_{0.016}^{(r/nl)>0.8}. \quad (9)$$

In comparison with the value of the intergral at the upper limit of $(r/nl) > 0.8$ its value at the lower limit of 0.016 can be neglected. Therefore

$$E = -2.303RTn\log[1-(r/nl)],\ (r/nl) > 0.8 \quad (10)$$

per mole of macromolecular sections between entanglements, R being the gas constant. For $n=2700$ at 313°K

$$E = -3900\log[1-(r/nl)]\text{kcal/mole}$$

macromolecular sections. (11)

A value of $(r/nl)=0.9$ intuitively seems unreasonably high. Yet even for this value, E as calculated above is only about one one-hundredth of the observed degradation energy. In order for E to be equal to the observed degradation energy, values of $\log[1-(r/nl)]$ around -100 would be required.

For purposes of discussion let us take 0.9 as the upper limit for the maximum acceptable value for (r/nl). Then about 100 macromolecular sections between entanglements would be required to store the observed degradation energy. Since the molecular weight of a macromolecular section between entanglements is about 150 000 there would be about 10 of these sections per molecule at the lowest molecular weight (1 500 000) for which degradation occurs for polyisobutene fractions.[2]

It is improbable that these fractions contain any individual macromolecules ten times as big as the average. This is especially true for fractions precipitated from previously degraded polymer. Accordingly we must eliminate the activation of shear degradation by intramolecular energy concentration. Intermolecular concentration must be involved.

4.2. Storage Completely as Potential Energy in Bonds

The maximum amount of energy that can be stored as potential energy in a bond is the activation energy for rupture (say 80 kcal/mole), since more than this would rupture the bond. If it is assumed that all this energy is dissipated upon rupture without contributing to overcoming viscoelastic resistance to flow, there can be calculated the minimum number of bonds that were involved in concentrating energy into the ruptured bond. The present results give a value in the neighborhood of 4000 for this limit. A polyisobutene molecule of molecular weight 112 000 would have 4000 chain bonds, so *at this limit* the possibility of intramolecular as distinct from intermolecular energy concentration is admitted. This lower limit, however, is probably much smaller than that corresponding to the true situation.

A higher estimate, though still not an upper limit, of the number of bonds involved in concentrating energy into the ruptured bond is obtained by considering the volume in the capillary shear field in which the energy used up per rupture is dissipated on a uniform basis. A representative figure for this energy, from Table I, is $320\,000/6.2\times10^{23} = 5.31\times10^{-19}$ kcal per ruptured bond. Forty pounds may be taken as a

[15] Reference 13, p. 51.
[16] T. G. Fox, Jr., and P. J. Flory, J. Phys. Colloid Chem. **55**, 221 (1951).
[17] F. Bueche, J. Appl. Phys. **26**, 728 (1955).

representative part of the shear load corresponding to degradation energy. Following the calculation in the last paragraph of Sec. III, in one shearing pass 5.31×10^{-19} kcal of degradation energy will be dissipated in a volume of $(5.31\times10^{-19}\times1.307)/(40\times8.12\times10^{-6})=2.14\times10^{-15}$ cm³. In a 10 wt % solution of polyisobutene (density about 0.9 g/cm³) in *n*-hexadecane (density=0.77 g/cm³) this volume corresponds to 3.6×10^{6} chain atoms. A single polymer molecule incorporating all these atoms would have a molecular weight of 9.36×10^{7}, which is about 100 times higher than the values around 10^{6} with which we are dealing here. Also a single molecule incorporating this many chain atoms would undoubtedly extend into a much larger volume than that stated above, sharing it with atoms from other individual molecules. Therefore by this estimate it seems necessary to rule out intramolecular energy concentration in favor of intermolecular energy concentration.

4.3. Combined Effect of Storage as Deformation Entropy and as Potential Energy

The observed degradation energy is probably divided between reduced configurational entropy of deformation of molecular chains and potential energy in strained bonds. This division should not affect the conclusion of the two preceding subsections. They indicated that intermolecular concentration of energy is necessary to activate a macromolecular chain bond for rupture in mechanical shear degradation. This conclusion remains intact because the storage of free energy in a sequence of bonds forming a macromolecular chain or portion thereof as reduced configurational entropy and that as potential energy are not independent.

Consider a macromolecular chain changing from a configuration of greater probability to one of lower probability. The potential energy in the bonds involved will be greatest during the time the change is actually in progress. At this time there will be less than the final reduction of configurational entropy. However, when the change of configuration is completed the potential energy in the bonds will be at a minimum. The reduction of configurational entropy will also then be fully developed. Thus a given sequence of bonds cannot be involved at one time in both the maximum increase of potential energy and the maximum reduction of configurational entropy. When the increase of potential energy is large the reduction of configurational entropy is small and vice versa. If the two are mixed in substantial proportions of both it is not likely that the stored free energy associated with their sum will be appreciably greater than the maximum stored free energy associated with either one if it were present to the exclusion of the other.

V. CONCLUSION

The very large amount of energy consumed by the mechanical shear degradation process per mole of ruptured bonds can be readily explained within the framework of the mechanism proposed for this degradation process. This mechanism involves the activation of rupture in an individual bond by concentrating into it free energy introduced by the shear field into many other bonds or macromolecular chains and stored there. This concentrating of energy may be accomplished through any of several types of interatomic connections.

The observed values of the degradation energy indicate that intermolecular concentration of energy is necessary to accumulate sufficient energy into a macromolecular chain bond to activate its rupture. This conclusion is arrived at by quantitative estimates for two extreme cases of free energy storage during flow exclusively by: (1) reduced configurational entropy of deformation of macromolecular chains and (2) potential energy of strained bonds in the macromolecular chains. In the second case one poor method of approximation permits intramolecular concentration of energy. This method is rejected in favor of a more realistic one requiring intermolecular concentration. The division of the observed degradation energy between the above two storage mechanisms is not likely to alter the conclusion requiring intermolecular concentration of energy for activation of rupture in mechanical shear degradation.

The variations of degradation energy with experimental variables apparently represent variations in the respective amounts of the stored free energy which does and does not contribute to overcoming viscoelastic resistance to flow after a bond ruptures.

VI. ACKNOWLEDGMENTS

The assistance of Miss H. V. Belcher and of Maria Bestul in the experimental work reported is gratefully acknowledged. The author expresses his appreciation to Dr. George M. Brown of the Department of Chemistry of the University of Maryland, who was in charge of the thesis from which part of the results reported herein were extracted. Thanks are offered to the Enjay Company, Inc. who supplied gratis the polyisobutene samples investigated.

THE JOURNAL OF CHEMICAL PHYSICS VOLUME 32, NUMBER 2 FEBRUARY, 1960

Energy Transfer in Molecular Complexes. II. The Anthracene-*sym*-Trinitrobenzene Complex*

S. P. McGlynn, J. D. Boggus, and E. Elder

Coates Chemical Laboratories, Louisiana State University, Baton Rouge, Louisiana,

AND

Department of Chemistry, The Florida State University, Tallahassee, Florida

(Received August 13, 1959)

The emission spectrum of the anthracene-*sym*-trinitrobenzene complex has been investigated in a solid solution in a diethylether-isopentane (EP) glass at 77°K. The observed luminescence consists of two distinct electronic transitions: one transition is the reverse of the charge-transfer $E \leftarrow N$ absorption of the complex; the other transition is a phosphorescence very similar to the $T \rightarrow S$ emission of anthracene in EP, but blurred somewhat in vibrational structure, blue shifted by 113 cm^{-1}, decreased in lifetime by a factor of about 2 and showing decreases in the ground state vibrational frequencies of a few percent. These results, as opposed to previous conclusions (vide infra), would suggest that the phosphorescence is truly a $T \rightarrow S$ process of the complex which is largely localized on the anthracene component.

Vibrational analyses of $T \rightarrow S$ spectra of anthracene in EPA and in EP and of the $T \rightarrow S$ and $E \rightarrow N$ spectra of the complex in EP at 77°K are given.

INTRODUCTION

THE emission spectra of π complexes of *sym*-trinitrobenzene (TNB) with polyacenes have recently been discussed[1] from the viewpoint of the energy levels of the complex. It was expected that excitation in the charge-transfer $E \leftarrow N$ absorption band of a complex in which the triplet level of the donor component lay energetically below the E state of the complex, would result, after an intersystem crossing and a dissociation process, in a population of the lowest triplet level of the polyacene. The polyacene, subject to considerations of internal and external quenching, might then be expected to phosphoresce, and this phosphorescence would compete with the $E \rightarrow N$ emission.

A complex in which such behavior is expected is that of anthracene with TNB. This complex is also of interest for another reason: it was one of the complexes studied by Reid[2] in his initial observation of sensitized phosphorescence in π complexes of TNB; however a misunderstanding of the spectrum of the complex and a consequent misassignment of the lowest triplet state of anthracene led to some confusion regarding the species and behavior of the lowest triplet states of the polyacenes. This latter controversy has since been resolved[3]; on the other hand much debate and suggestion[4–6] concerning the origins of the luminescence of the complex has not resulted in any better understanding of the electronic processes involved.[7] It is for these reasons that this note considers the anthracene-TNB complex only,[8] and in considerable experimental detail.

Complexes of tetrachlorophthalic anhydride with naphthalene, phenanthrene, durene, and benzanthracene have recently been studied by Czekalla, Briegleb, and collaborators[9,10]; their results for the most part are comparable to those obtained here and should be consulted in conjunction with this work.

EXPERIMENTAL

The anthracene used was Eastman blue-violet fluorescence grade. Chromatography in an inert atmosphere on a column of Wöelm alumina produced no change in either the fluorescence or phosphorescence; further purification by this method was discontinued and the material was used directly from the bottle. The TNB was an Eastman "white label" grade, and was purified by several recrystallizations from ether in the dark. In the initial absorption and emission experiments the solvents used were alcohol and EPA,[11] respectively. It was noted that absorption spectra of TNB in alcohol differed from those in ether. The freshly prepared alcoholic solutions exhibited a weak but definite absorption band at 20 500 cm^{-1}. Upon standing in the dark at 72°F the color deepened considerably with production of two new bands, one at 18 000 cm^{-1}, the other at 21 700 cm^{-1}. The growth of

* This research was carried out under Contract 11–863 between the National Science Foundation and Louisiana State University, but was initiated under Contract AF–18(600)–678 between the Office of Scientific Research, U. S. Air Force and Florida State University.

[1] Paper I in this series: S. P. McGlynn and J. D. Boggus, J. Am. Chem. Soc. **80**, 5096 (1958).

[2] C. Reid, J. Chem. Phys. **20**, 1212, 1214 (1952).

[3] McGlynn, Padhye, and Kasha, J. Chem. Phys. **23**, 593 (1955); Padhye, McGlynn, and Kasha, *ibid.* **24**, 588 (1956).

[4] L. E. Orgel, Quart. Rev. (London) **8**, 442 (1954).

[5] H. Sponer, Ann. Rev. Phys. Chem. **6**, 193 (1955).

[6] A. Bier and J. A. A. Ketelaar, Rec. trav. chim. **73**, 264 (1954). A. Bier, *ibid.* **75**, 866 (1956).

[7] A review may be found in S. P. McGlynn, Chem. Revs. **58**, 1113 (1958).

[8] The other complexes studied will be considered in No. III of this series, in preparation for publication.

[9] Czekalla, Briegleb, Herre, and Glier, Z. Electrochem. **61**, 537 (1957); Czekalla, Schmillen, and Mager, Z. Electrochem. **61**, 1053 (1957).

[10] Czekalla, Briegleb, Herre, and Vahlensieck, Z. Electrochem. (to be submitted for publication).

[11] EPA is diethylether: isopentane: alcohol mixed in a 5:5:2 volume ratio; EP is diethylether: isopentane mixed in a 1:1 volume ratio.

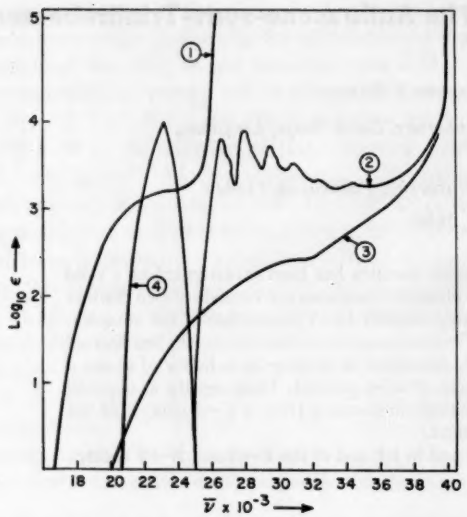

FIG. 1. The Hg–4358 excitation band pass (curve 4) compared to the absorption spectra of the various components which are present in a solution of complex in EP. Curve 1 is the absorption spectrum of the complex, curve 2 is the absorption spectrum of anthracene, and curve 3 is the absorption spectrum of TNB, all in EP at 25°C. The log ε scale does not apply to curve 4.

these two new bands was accelerated tremendously by exposure to sunlight. It would seem that the band present at zero time has a different origin to the two new bands whose growth is time dependent, and it is attributed to a weak complex of TNB and alcohol, presumably stabilized by either hydrogen bonding or charge-transfer. The latter alternative has been suggested[12] as the origin of the color produced in the "fast" reaction of sodium ethoxide and 2,4,6-trinitroanisole, and is the more attractive. The two bands which arise with time are similar in intensity and band split to those observed by Foster[13] for Meisenheimer type compounds[14] in which the $OC_2H_5^-$ is covalently bonded through the oxygen to a carbon of the benzene nucleus. Because of these complications usage of alcohol as a solvent was discontinued and all absorption work was done in EP at room temperature and all emission work in the same solvent at 77°K.

The spectrograph used for emission work was a Steinheil Model GH Universal Spectrograph with three glass prisms. Excitation was effected using a 1 kw GE A-*H*6 lamp of special design. Since excitation only in the *E*←*N* absorption band was desired the Hg-4358 line was isolated with a filter train consisting of Corning glass filters 5113 and 3389 and 5 cm of a 100g/l solution of $CuSO_4 \cdot 5H_2O$ in water. The band pass of this train compared to the absorption spectra of the various components present in a solution of complex is illustrated by curve 4 of Fig. 1. Total emission experiments in which anthracene alone in EP at 77°K was irradiated with light of this band pass produced no detectable luminescence even at wide slit (1 mm) and photography for 24 hr. This accords of course with the fact that anthracene (curve 2 of Fig. 1) absorbs no radiation of this wavelength. Similar excitation of TNB and photography for 20 hr also gave no emission. Since TNB does absorb (curve 3 of Fig. 1) light of this band pass, the lack of luminescence is to be attributed to a very effective self-quenching of the excited TNB due to disruption of the aryl-NO_2 bonds.[15] The photographic plates used were Eastman-Kodak I—N plates, hypersensitized in ammonia before use. Excitation of the anthracene phosphorescence by Hg-3650 in solutions of anthracene in EPA and EP was done using a filter train of Corning glass filter 5680, 5 cm of a 100g/l solution of $CuSO_4 \cdot 5H_2O$ and 1 cm of a 20 mg/100 ml of CN dye[16] in water. The phosphoroscope used had a resolution time of 10^{-4} sec. Plates were traced on a Leeds and Northrup densitometer.

All absorption spectra were measured on a Beckman DK recording spectrophotometer. The extinction coefficient of the *E*←*N* band of the complex (curve 1 of Fig. 1) was determined by first deriving the equilibrium constant of the complex using a Benesi-Hildebrand procedure[17] at 25°C, and $\epsilon_{max} = 1600$ was found.

RESULTS AND DISCUSSION

The phosphorescence of the complex in EP excited by Hg-4358 is depicted in Fig. 2(c). The phosphorescences of anthracene in EPA and in EP excited by Hg-

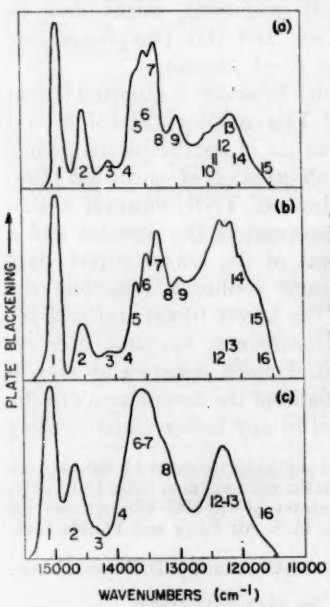

FIG. 2. The phosphorescence of anthracene excited by Hg–3650 in EPA is given in (a), and that in EP is given in (b). Phosphorescence of anthracene-TNB excited by Hg–4358 in EP is given in (c). This last phosphorescence is to be compared intensity-wise with (a) and wave number-wise with (b).

[12] J. B. Ainscough and E. F. Caldin, J. Chem. Soc. **1956**, 2528.
[13] R. Foster, Nature **176**, 746 (1955); **180**, 1042 (1959).
[14] J. Meisenheimer, Ann. Chemie. **323**, 205 (1902).
[15] E. Lippert, Z. physik. Chem. (N.F.) **2**, **5**, 328 (1954); J. phys. radium **15**, 627 (1954).
[16] M. Kasha, J. Opt. Soc. Am. **38**, 21 (1948).
[17] H. A. Benesi and J. H. Hildebrand, J. Am. Chem. Soc. **71**, 2703 (1949).

TABLE I. Vibrational analysis of the phosphorescence of anthracene in EPA at 77°K excited by Hg-3650.

Band No.[a]	$\bar{\nu}$, cm^{-1}	14 928$-\bar{\nu}$	Assignment[b]	Intensity[c]
1	14 928±2	0	$^3B_{2u}\rightarrow{}^1A_{1g}$	S
2	14 519±1	409±3	410±3, a_g	M
3	14 106±17	822±19	2(410)=820±6	W
4	13 788±38	1140±40	1137±30, a_g	W
5	13 654±5	1274±7	1266±7, a_g	M
6	13 523±7	1405±9	1414±9, a_g	S
7	13 361±11	1567±13	1573±12, a_g	S
8	13 142±30	1786±32	1414+410=1824±12	W
9	13 002±2	1926±4	1573+410=1983±15(?)	M
10	12 513±14	2415±16	1266+1137=2403±37	W
11	12 397±7	2531±9	1266+1266=2532±14	M
12	12 288±30	2640±32	1266+1414=2680±16	S
13	12 160±20	2768±22	1266+1573=2839±19	S
14	12 068±25	2860±27	2(1414)=2828±18	W
15	11 705±45	3223±47	2(1414)+410=3238±21	W
16	not present	...	...	...

[a] Number as given in Fig. 2(a).
[b] For comparison of these frequencies with those of the ground state as observed in fluorescence of solutions, crystals and mixed crystals, and in the Raman of anthracene, see J. W. Sidman, Phys. Rev. **102**, 96 (1956). The frequencies quoted here are the mean of those found on five different plates by three observers.
[c] S=Strong; M=Medium, and W=Weak.

TABLE II. Vibrational analysis of the phosphorescence of anthracene in EP at 77°K excited by Hg-3650.

Band No.[a]	$\bar{\nu}$, cm^{-1}	14 944$-\bar{\nu}$	Assignment	Intensity
1	14 944±3	0	$^3B_{2u}\rightarrow{}^1A_{1g}$	S
2	14 534±4	410±7	410±3	M
3	14 120	824	(410)2=820	W
4	13 810	1134	1137	W
5	13 685	1259	1266	M
6	13 520	1424	1414	S
7	13 360	1584	1573	S
8	13 180	1764	1414+410=1824	W
9	12 990	1954	1573+410=1983	M
10	undetected	...	...	...
11	undetected	...	...	...
12	12 330	2614	1266+1414=2680	S
13	12 160	2784	1266+1573=2839	S
14	12 010	2934	2(1414)=2832	W
15	11 740	3204	2(1414)+410=3238	W
16	11 550	3394	1414+1573+410=3397	W

[a] Number as given in Fig. 2(b).

TABLE III. Vibrational analysis of the phosphorescence of the anthracene-TNB complex in EP at 77°K excited by Hg-4358.

Band No.[a]	$\bar{\nu}$, cm^{-1}	15 059$-\bar{\nu}$	Assignment	Intensity
1	15 059±3	0	$^3A''\rightarrow{}^1A'$[b]	S
2	14 660±5	399±8	394±8	M
3	14 280	779	2(394)=788±16	W
4	13 920	1139	1139	W
6–7	13 600	1459	(1414+1573)/2=1493[c]	S
8	13 250	1809	1414[d]+394=1808	M
12–13	12 310	2749	(2680+2839)/2=2759[c]	M
16	11 750	3309	1414[d]+1573[d]+394=3381	W

[a] Number as given in Fig. 2(c).
[b] Symmetry species of the transition $^3B_{2u}\rightarrow{}^1A_{1g}$ in point group C_{2h}' defined in reference 1 of text.
[c] Mean positions of bands 6–7 and 12–13 relative to 0,0 transition as determined from Table I.
[d] Frequencies found in Tables I and II.

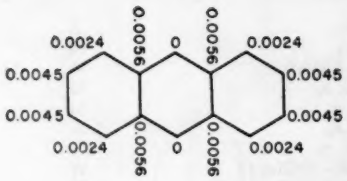

FIG. 3. The decrease in electron density at the carbon atoms of anthracene consequent to formation of the $^1A'$ state of an anthracene-TNB complex which has C'_{1h} symmetry. The numbers given are 4% of the electron density in a b_{2g} (D_{2h}) MO of anthracene as evaluated in reference 1 of text. The value of 4% is derived from considerations relative to change in dipole moment occasioned by complexing (see reference 7 of text).

3650 are given in Fig. 2(a) and (b), respectively. These latter two emissions are not excited by Hg-4358. Phosphorescence (b) is a short time exposure (max. plate blackening 35%) made in an effort to resolve the longer wavelength end of the spectrum. Phosphorescences (a) and (c) both have 64% plate blackening; as a result (c) should be compared intensity-wise with (a) and wave number-wise with (b).

In the course of this work some five photographs of the spectrum of anthracene in EPA were made. It was consequently possible to study the emission in some detail, and to get estimates of errors involved in locating band maxima. These errors are primarily caused by the uncertainty in marking the maximum of a rather broad band. Furthermore, some vibrational peaks observable in low intensity work were not observable in high intensity work, and vice versa. For these reasons a vibrational analysis of the anthracene phosphorescence is given in Table I, the 0, 0 transition being interpreted[3] as $^3B_{2u}\rightarrow{}^1A_{1g}$.

Vibrational analyses of the $T\rightarrow S$ luminescences of anthracene and of the complex both in EP are given in Tables II and III, respectively. The most striking

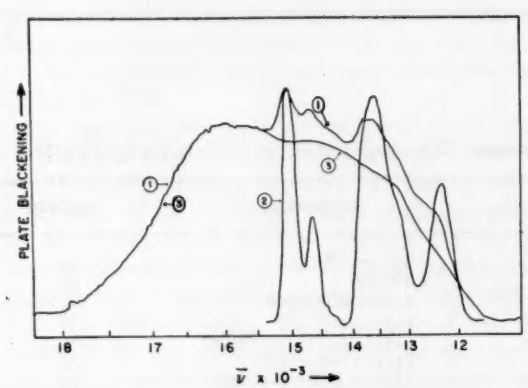

FIG. 4. The total emission of the complex excited by Hg-4358 in EP at 77°K is shown in curve 1, and the phosphorescence excited under similar circumstances is shown in curve 2. Subtraction of 17.2% of the plate blackening of curve 2 from curve 1 yields curve 3, the presumed $E\rightarrow N$ fluorescence of complex.

TABLE IV. The $E\rightarrow N$ fluorescence of the complex in EP at 77°K excited by Hg-4358.

$\bar{\nu}$, cm^{-1}	15 750$-\bar{\nu}$	Assignment
15 750	0	$^1A'\rightarrow{}^1A'$[a]
14 500	1250	1250
13 250	2500	2(1250) = 2500
12 000	3750	3(1250) = 3750

[a] Symmetry species of $E\rightarrow N$ fluorescence in point group C'_{1h} defined in reference 1 of text.

change in the luminescence of the complex, apart from considerable broadening of the individual bands, is that the a_g skeletal bending vibration (ν_1 of naphthalene[18]) at 410 cm^{-1} has decreased in frequency by 16 cm^{-1}, a 4% change, and that the sum of the 1414 cm^{-1} symmetric breathing vibration (ν_4 of naphthalene) and the 1573-cm^{-1} C—C stretching vibration (ν_3 of naphthalene) has decreased in frequency by some 50 cm^{-1}, a 2.5% change. No definite statement may be made about the 1137 and 1266 vibrational quanta, except that they appear to be unchanged in frequency. Both these latter two a_g vibrations involve C—H bending, and in this respect are qualitatively different from the former three vibrations. If emission occurred from the uncomplexed anthracene, it is difficult to see why the vibrational frequencies should be so decreased. It must then be concluded, contrary to previous assertions,[1] that the excess energy of the dissociative triplet state is dissipated, and that reformation of the complex occurs in its excited triplet state in a time short compared to the 0.09 = sec lifetime[3] of the $^3B_{2u}$ state of free anthracene. This seems reasonable enough. The terminal state of the phosphorescence emission of the complex is its $^1A'$ state. Anthracene complexed with TNB in the $^1A'$ (or no-bond) state differs from free anthracene in that the π electron densities on the carbon atoms of the complexed variety are lower by the amounts depicted in Fig. 3. These electron density changes are rather small but would certainly accord with decreases in the frequencies of the skeletal bending and C—C stretching vibrations, as observed experimentally, and would predict little effect on C—H bending vibra-

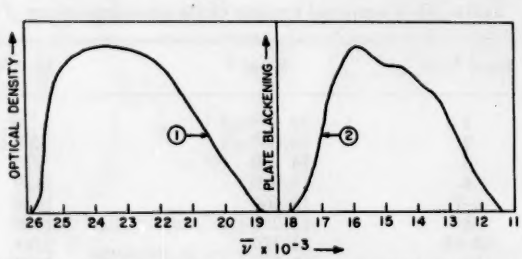

FIG. 5. Illustrating the mirror-image relationship of the $E\leftarrow N$ absorption (curve 1) as determined from Fig. 6 and the presumed $E\rightarrow N$ emission (curve 2) as determined from Fig. 4.

[18] E. R. Lippincott and E. J. O'Reilly, Jr., J. Chem. Phys. **23**, 238 (1955).

tions. Such small decreases in vibrational frequencies of the ground states of molecules caused by charge-transfer complexing are well known in the Raman and infrared spectra and have a similar basis.[7]

The blue shift of 113 cm^{-1} in the $T \rightarrow S$ spectrum of the complex is somewhat more difficult to interpret. Assuming that the phosphorescing state is $^3A''$ of the complex, one would expect a red shift primarily because the stabilization energy of the $^3A''$ state would be greater than that of the $^1A'$ state because of the higher polarizability of the former. This small blue shift is coupled with a small but significant decrease in lifetime from 0.09[3] to 0.04 sec.[19]

The total emission spectrum of the complex excited by Hg-4358 is given in Fig. 4, curve 1. The fine structure of this band is undoubtedly the phosphorescence of the complex (curve 2), and when subtracted out in a manner such as to yield a minimum amount of fine structure in the remainder yields curve 3. Curve 3 exhibits four bands which are tabulated in Table IV. The structure seems real and is not entirely unexpected because the $E \rightarrow N$ transition is accompanied by a large redistribution of electronic charge in both the anthracene and TNB components, which might excite vibrations of either one or both of them.

The mirror-image relationship of the presumed $E \rightarrow N$ emission and the $E \leftarrow N$ absorption is illustrated in Fig. 5 and differs quite markedly from that of Bier and Ketelaar.[6] The $E \leftarrow N$ absorption was obtained as illustrated in Fig. 6, by drawing in the exponential tail (Fig. 6, curve 3) of the $^1B_{2u} \leftarrow {}^1A_{1g}$ transition of anthracene as evaluated from values of the optical density at shorter wavelengths where the intensity of the $E \leftarrow N$ transition was considered to be zero. This was then subtracted from the absorption spectrum of the complex in the $E \leftarrow N$ wavelength region to yield the pure $E \leftarrow N$ transition of the complex (Fig. 6, curve 2; Fig. 5, curve 1). The maximum extinction coefficient of this transition is 1600.

A mirror-image relationship does exist, but it is not an overly good one. The Franck-Condon gap of about 7000 cm^{-1} is large but rather to be expected because of the lack of parallelism of the potential energy curves of the ground state of the complex (N) and its charge-transfer state (E). Thus, for example, the minimum of potential energy in the E state has an intermolecular distance 0.35 A shorter than that of the N state. The

[19] As measured by a photographic method at different sector speeds and different disposition of phosphoroscope blades.

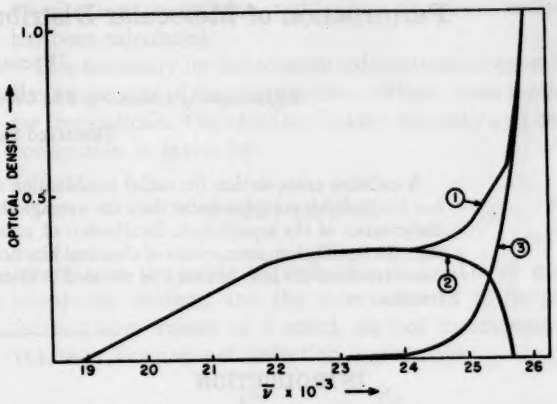

FIG. 6. Curve 1 is the absorption spectrum of the complex in the charge transfer region. Curve 3 is the exponential tail of the $^1B_{2u} \leftarrow {}^1A_{1g}$ transition of anthracene in the same solution drawn in from readings of the optical density at shorter wavelengths where the $E \leftarrow N$ absorption is negligible. The difference (curve 2) gives the pure $E \leftarrow N$ transition of the complex.

Franck-Condon gap expected[20] is of the order of 4000 cm^{-1}, in not too bad disagreement with experiment.

In conclusion we wish to comment on the use of the term "sensitized phosphorescence." This term has been used to describe phosphorescence resulting from a presumed transfer of energy between the triplet state of one molecule (the sensitizer) and the lowest triplet level level of the phosphorescer.[21] Since this presumed process is quite different to that invoked here to account for the emission spectra of aromatic molecular complexes, it would seen best to reserve the term "sensitized" for the former process, if indeed such a process exist. However, the phosphorescence described by us is "sensitized" in the sense that it can be excited by Hg-4358, which will not excite phosphoresence of anthracene, and that the ratio of quantum yields $Q(T \rightarrow S)/Q(N \rightarrow E) = 1/12$ for the complex, whereas $Q(T \rightarrow S)/Q(S' \rightarrow S)$ is certainly less than 1/100 for uncomplexed anthracene.

ACKNOWLEDGMENT

The authors are indebted to Ethyl Corporation of Baton Rouge for the drawing and reproduction of their diagrams. We wish also to thank Mr. R. Sunseri for the absorption data, and Professor M. Kasha for extensive discussion.

[20] See Fig. 2 of reference 1, for example.

[21] A. N. Terenin and V. L. Ermolaev, Doklady Akad. Naak S.S.S.R. 85, 547 (1952); Trans. Faraday Soc. 52, 1042 (1956).

THE JOURNAL OF CHEMICAL PHYSICS VOLUME 32, NUMBER 2 FEBRUARY, 1960

Perturbation of Molecular Distribution Functions by Chemical Reaction

BRUCE H. MAHAN

Department of Chemistry, The University of California, Berkeley, California

(Received September 28, 1959)

A collision cross section for radial combination reactions is derived which indicates that translationally hot free radicals combine faster than the average thermal radicals. The cross section is used to calculate the disturbance of the equilibrium distribution of velocities by radical combination reactions. It is concluded that the equilibrium assumption of chemical kinetics is justified for photochemical systems where the radical concentrations are low, but may be violated in systems where free radical concentrations approach 0.1 mole fraction.

INTRODUCTION

A CHEMICAL reaction is bound to result in a disturbance of the Maxwell-Boltzmann energy distribution of the reaction system. Nevertheless, in the conventional forms of both the absolute reaction rate theory and collisional theory, the perturbation of the equilibrium distribution function by the chemical reaction is ignored. This equilibrium assumption has been justified for bimolecular reactions where translational energy is primarily involved by the reasoning that, as a result of the existence of high activation energies and low steric factors, there are generally more unreactive or thermalizing collisions than reactive collisions, and thus the departure from a Maxwell-Boltzmann distribution of energies is bound to be negligible. Prigogine and coworkers[1,2] and Curtiss[3] examined the conditions under which the equilibrium assumption is valid by using a generalized form of the Boltzmann transport equation to calculate the distribution function of a reacting gas. Prigogine and Xhrouet showed that nonequilibrium effects become important only for reactions of low activation energy at high temperature. In addition, the size of the nonequilibrium effect was found to be quite sensitive to the form of the reaction cross section. The most serious deviations from the equilibrium reaction rate may be expected to occur in free radical combination reactions, since these reactions involve little or no activation energy. Since the cross sections used by Prigogine are not appropriate for free radical combination reactions, it is the purpose of this paper to formulate a collision cross section for radical combination, and to calculate the effect of such reactions on the translational distribution function.

THE CROSS SECTION FOR RADICAL COMBINATION

In the treatment of radical combination by the absolute rate theory,[4] it is assumed that two free radicals are attracted to each other at all distances by a London polarizability force, and that this force is opposed by a centrifugal force arising from the rotation of the two radicals about a common center of mass. The activated complex is located at the maximum of the resulting pseudo-potential energy curve, and an evaluation of the appropriate partition functions leads to an expression for the rate constant. We make here the same assumptions concerning the interaction potential, but proceed by obtaining first a reaction cross section which does not involve assumptions concerning the distribution of velocities.

If the collision of two free radicals is treated as an equivalent one-body problem involving a particle of reduced mass μ approaching a fixed center with relative speed g, and impact parameter b, the trajectory may be obtained by integrating the equation[5]

$$\theta=-\int_{\infty}^{r}\frac{b\,dr}{r^2[1-V(r)/\frac{1}{2}\mu g^2-b^2/r^2]^{1/2}}. \tag{1}$$

Here θ and r locate the moving particle relative to the scattering center at the origin and a line through the origin parallel to the initial direction of the particle. In order to calculate the maximum value of the reaction cross section, it is not necessary to perform the integration. Elementary considerations[6] show that for potentials of the form $V=-a/r^n$, where $n>2$, all particles which pass over the repulsive centrifugal barrier inevitably pass through the origin. The critical initial conditions which make it possible for a particle to just reach the top of the barrier may be found by realizing that for such a particle at the top of the barrier, both the radial velocity and its time derivative are zero. If we let $V=-a/r^6$, these conditions are expressed by the equivalent set of relations

$$(dr/dt)^2=0=g^2-g^2b^2/r^2+2a/\mu r^6 \tag{2a}$$

$$0=\mu g^2b^2r^4-6a. \tag{2b}$$

It is most convenient to solve these equations for the square of the critical impact parameter b_c in terms of the initial relative speed. The result is

$$b_c^2=\tfrac{3}{2}(4a/\mu g^2)^{1/3}. \tag{3}$$

[1] I. Prigogine and E. Xhrouet, Physica **15**, 913 (1949).
[2] I. Prigogine and M. Mahieu, Physica **16**, 51 (1950).
[3] C. F. Curtiss, University of Wisconsin, Report CM-476, (June, 1948).
[4] E. Gorin, Acta Physicochim. U.R.S.S. **9**, 691 (1938).
[5] Hirschfelder, Curtiss, and Bird. *Molecular Theory of Gases and Liquids* (John Wiley & Sons, Inc., New York, 1954).
[6] H. Goldstein, *Classical Mechanics* (Addison-Wesley Press, Inc., Cambridge, Massachusetts, 1951).

This quantity, when multiplied by π, becomes the reaction cross section, since for $b<b_c$, the colliding particle passes over the centrifugal barrier and through the origin. In the absolute rate theory treatment only Eq. (2b) is used to calculate the dimensions of the activated complex as a function of its angular momentum. The use of Eqs. (2a) and (2b) to determine the reaction cross section shows the close relation between the collision theory and the conventional absolute rate theory.

The condition for a reactive collision may be derived by an alternate procedure. If we substitute $\rho=r^2/b^2$ in Eq. (1), we obtain

$$\theta=\tfrac{1}{2}\int_{\rho}^{\infty}[d\rho/(\rho^3-\rho^2+\eta)^{1/2}], \tag{4}$$

where

$$\eta=2a/\mu g^2b^6.$$

The roots of the polynomial within the square root determine the turning points of the orbit. When η is small enough, the polynomial has three real roots, with the largest positive root equal to the distance of closest approach. A particle starting from infinity can never reach the origin under this condition. For η very large there are no positive roots, and the orbit passes through the origin. The critical condition occurs when η is such that the polynomial has a double set of roots. The condition for this is that $\eta=4/27$, which leads directly to Eq. (3).

The product of πb_c^2 and the relative speed g is the reactive volume swept out per unit time by a free radical. This reactive volume increases as $(g)^{1/3}$, and thus we may note that free radicals which are produced with excessive translational energy will combine faster than free radicals with an equilibrium distribution of energies, if deactivation of the resulting combination product is not rate determining. The rate constant corresponding to the reaction cross section can be obtained by averaging the reaction volume over the Maxwell-Boltzmann distribution of speeds. The integral

$$k_0=4\pi(\mu/2\pi kT)^{3/2}\tfrac{3}{2}\pi(4a/\mu)^{1/3}\int_0^{\infty}g^{7/3}\cdot\exp[-\tfrac{1}{2}(\mu g^2/kT)]dg \tag{5}$$

can be evaluated in terms of the gamma function to give

$$k_0=2^{11/6}(\pi)^{-1/2}\Gamma(\tfrac{3}{2})(a)^{1/3}(\mu)^{-1/2}(kT)^{1/6}. \tag{6}$$

This expression for the rate constant, aside from a factor of $\frac{1}{4}$ which should be added as an electronic degeneracy factor, is identical with that derived by the absolute rate theory.[4] This identity again emphasizes the equivalence of the absolute rate and collision theories, but the collisional formulation does offer an advantage in that one may delay making the equilibrium distribution assumption until after the cross section has been calculated.

It is necessary for subsequent calculations to examine the magnitude of the nonreactive collision cross section for free radicals. The cross section for viscosity and heat conduction is given by[7]

$$\sigma=2\pi\int\sin^2\chi b db, \tag{7}$$

where χ is the angle of deflection in center of mass coordinate system, and the integration is to be performed over values of b which do not correspond to reaction. The angle of deflection is given by[8]

$$\chi=\pi-2\theta_m=\pi-\int_{\rho_m}^{\infty}\frac{d\rho}{[\rho^3-\rho^2+4/27\,(b_c/b)^6]^{1/2}}, \tag{8}$$

where we have made the substitution $\eta=4/27\ (b_c/b)^6$, and ρ_m corresponds to the square of the distance of closest approach.

If we ignore electronic degeneracy effects momentarily, only those collisions with $b>b_c$ will contribute to the transport processes, and the polynomial will have 3 real roots $\alpha>\beta>\gamma$. The substitution

$$(\rho-\alpha)/(\rho-\beta)=x^2$$

leads, after some straightforward manipulation,[8] to

$$\chi=\pi-[2/(\alpha-\gamma)^{1/2}]\int_0^1\{dx/[(1-x^2)(1-k^2x^2)]^{1/2}\} \tag{9}$$

where $k^2=(\beta-\gamma)/(\alpha-\gamma)$. The value of this complete elliptic integral of the first kind has been tabulated as a function of k^2, and the roots α, β, γ are easily computed as functions of b/b_c. The cross section (7) then can be evaluated graphically or numerically. The result can be expressed in terms of the critical impact parameter as

$$\sigma=0.092\pi b_c^2. \tag{10}$$

Thus, insofar as a collision can be defined in terms of cross sections for reaction and heat conductivity, nonpolar free radicals with favorable electron spin orientation recombine on nine out of ten collisions.

PERTURBATION OF THE DISTRIBUTION FUNCTION AND THE REACTION RATE

For the purposes of calculating an approximate translational distribution function in a reacting system, we assume the presence of only free radicals and an inert gas of the same molecular weight. The collisions involving one or two inert molecules are described by a hard sphere collision diameter d. We include two free radicals with unfavorable spin orientation as inert molecules. Collisions between free radicals where $b>b_c$ can be

[7] R. D. Present, *Kinetic Theory of Gases* (McGraw-Hill Book Company, Inc., New York, 1958).

[8] An expression closely related to this was first derived by J. F. Stader, J. reine angewandte Math. **46**, 262 (1853). Readers of Latin are referred to this paper for details.

ignored, since Eq. (10) indicates the cross section for such collisions is quite small. It is further supposed that the vibrationally excited combination product is always deactivated to a stable molecule, and that this deactivation takes place through many collisions, each of which involves only a small transfer of energy to the translational degrees of freedom.[9] Under these conditions the heat of the reaction will have a negligible effect on the velocity distribution function, since no one molecule is ever suddenly endowed with translational energy amounting to the heat of reaction. Finally, we assume that the reaction is in its initial stages, so that the concentration of the product may be entirely ignored.

In all other respects, the calculation is similar to those of Prigogine.[1,2] A Boltzmann equation is written for each component, neglecting thermal and pressure gradients. These Boltzmann equations are solved by assuming a distribution function of the form

$$f=f^0(1+\Phi),$$

where f^0 is the Maxwellian distribution function, and Φ is a correction factor to be determined. As a first approximation, Φ is expressed in terms of a Sonine polynomial involving the reduced velocity of a molecule $C\equiv(m/2kT)^{1/2}v$. Thus,

$$\Phi=a_2(\tfrac{15}{8}-\tfrac{5}{2}C^2+\tfrac{1}{2}C^4).$$

The factor a_2 is shown by Prigogine[1,2] to be the ratio of an integral involving the concentration of reactants and the reaction cross section to a sum of integrals giving the total nonreactive collision rate. The integration involving the reaction cross section (3) is quite lengthy but straightforward. The result is

$$a_2=-\tfrac{2}{6}\tfrac{6}{4}\tfrac{5}{}\Gamma(\tfrac{1}{2})\Gamma(\tfrac{2}{3})\cdot[a^{1/3}\mu^{-1/2}(kT)^{1/6}/d^2(\pi kT/\mu)^{1/2}](X_R)^2,$$

where X_R is the mole fraction of free radicals. The negative sign of a_2 and the form of the Sonine polynomial show that the higher velocities are the ones most seriously affected by the chemical reaction.

The reaction rate constant may be calculated by

$$k(n_R)^2=\pi\iiint f^0f_1^0(1+\Phi)(1+\Phi_1)gb_c^2dv_1dv,$$

where v, v_1 are the individual velocities of the reactants, and n_R is their concentration. If one transforms to relative velocity and retains only corrections which are first order in Φ, the result is

$$k=k_0[1-(31.5/d^2)(a/kT)^{1/3}X_R^2].$$

Here k_0 is the rate constant calculated by assuming an equilibrium distribution of velocities. The correction term for the rate constant is related to the quantity a_2 by a numerical factor, and thus involves the ratio of the rate of reactive collisions to the rate of reactive collisions to the rate of thermalizing collisions. If one choses the values of $d=4\times10^{-8}$ cm, $a=8\times10^{-60}$ erg cm^6, and $T=300°$K, the value of the coefficient of $(X_R)^2$ is 11.5. Corrections to the equilibrium rate only become important when the free radical concentration approaches 0.1 mole fraction. This unsensitivity of the rate to the distribution function perturbation is a consequence of the feeble dependence of the reaction cross section on velocity. We may conclude that the equilibrium assumption of chemical kinetics is valid for free radical combination reaction in photochemical systems where the mole fraction of free radicals does not exceed 0.01, but may not be valid in flames and detonations where radical concentrations may exceed 0.1 mole fraction.

ACKNOWLEDGMENT

The author would like to express grateful appreciation of support by the U. S. Air Force through AFOSR of the Air Research and Development Command, under Contract No. 49(638)-1.

[9] B. H. Mahan, J. Phys. Chem. **62**, 100 (1958).

THE JOURNAL OF CHEMICAL PHYSICS VOLUME 32, NUMBER 2 FEBRUARY, 1960

Trapped Free Radical Concentrations*

CHARLES E. HECHT

The Enrico Fermi Institute for Nuclear Studies, University of Chicago, Chicago, Illinois

(Received June 15, 1959)

Average concentrations of trapped free radicals condensed from a gaseous mixture are calculated on the basis of a statistical model that assumes these concentrations to be those obtaining in the solid for which the free radicals and diluents are distributed in such a way that the entropy of the system is a maximum. This entropy is calculated in an independent pair, Bethe approximation. All kinetic and energetic considerations are neglected. The results are given as a function of diluent concentration and of the number of nearest neighbors in the solid. When condensed from a completely dissociated gas without diluents the free radical fraction ranges from 0.12 for a simple cubic lattice to 0.08 for a face-centered cubic lattice.

1. INTRODUCTION

IN this paper we treat the problem of estimating the concentration of free radicals to be found trapped in a solid matrix which has been condensed on a surface at very low temperature from a gaseous mixture of dissociated molecules and inert diluents, or from a mixture of both dissociated and undissociated molecules of the same species. This problem has been studied previously by Jackson and Montroll[1] to which reference should be made for citation of papers on the experimental background. In concordance with I we assume that the condensed matrix has a fairly regular lattice structure characterized by an average number c of nearest neighbors. A free radical is assumed trapped if all of its nearest neighbors are (a) parts of undissociated molecules, (b) inert diluent atoms, (c) free radicals already recombined with a further neighbor free radical, or (d) combinations thereof. If any two free radicals end up on the matrix as nearest neighbor pairs they are assumed to recombine into a molecule. This molecule is assumed to occupy the two adjacent sites and to remain inert (no free radical can be bound to more than one other).

As in I all energetic and kinetic processes (such as diffusion) are neglected in arriving at our free radical concentration estimates. We consider only what concentrations will result from the most likely distribution of free radicals and diluents over the lattice as a function of coordination number and of diluent concentration. In the case of condensing a beam of both dissociated and undissociated molecules the latter serve formally as diluents which can occupy two adjacent sites. To find the most likely configuration we maximize an expression for the entropy of the system. In doing so we reproduce the exact results for one-dimensional chains which were obtained in another manner in I. For the higher dimensional systems our method gives only approximate results but these are an improvement over those given in I. This is because in that work it is assumed that the state of occupation of a single site is independent of the occupation state of all other single sites while here we go one step further and need only assume that a pair configuration is independent of the configurations of all other pairs. This results in free radical concentrations lower than those given in I by from 10–20% depending on the coordination number or by a nearly constant 2% absolute decrease of predicted radical concentration for all higher dimensional lattices. The major results in the case of condensation from a completely dissociated gas are given in Fig. 1 and range from a free radical fraction x_1 of 0.177 for coordination number 2 to 0.061 for coordination number 18. We have extended the figure to such a fairly high coordination number since, as pointed out by Jackson and Montroll, if next nearest neighbor pairs of free radicals also recombine the effective coordination number of the matrix is increased. For a body-centered cubic lattice it would then be 14 and for simple cubic and face-centered cubic lattices it would be 18.

At the time of completing this work it was learned that Dr. R. Kikuchi, whose general methods we use in Sec. 2, has also formulated similar equations in the same way. The work, however, has not been published nor any numerical calculations made.

2. FRACTION OF FREE RADICALS WITH SINGLE SITE DILUENT

We consider first the case of condensing a gas of free radicals and inert diluents, the latter making up a fraction α of the total number of gas particles. The diluents are assumed to occupy a single site on the lattice. There are no undissociated molecules in the gas. The entropy of the lattice is written as,

$$S=k\ln G, \tag{1}$$

where G is the total number of ways of constructing our lattice system subject to the required probability parameters of various configurations of individual lattice points and of pairs of points as given in Tables I and II, respectively.

In these Tables c denotes the coordination number of the lattice. The x's and y's are the probabilities of

* Research supported by the Atomic Energy Commission and in part presented at the Fourth International Symposium on Free Radical Stabilization, Washington, D. C. (September, 1959).

[1] J. L. Jackson and E. W. Montroll, J. Chem. Phys. **28**, 1101 (1958) to be referred to as I.

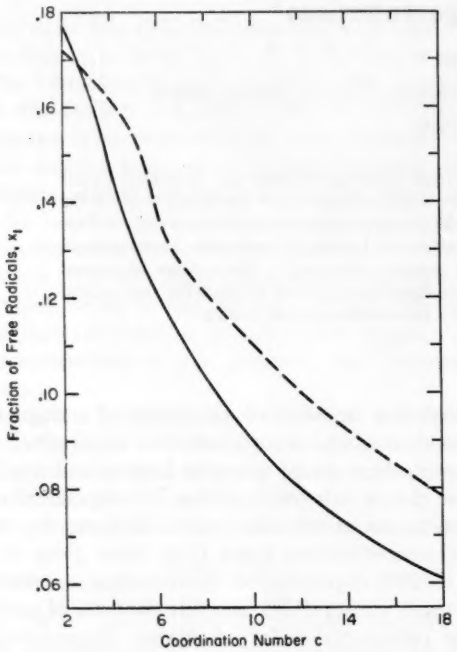

FIG. 1. Variation of free radical fraction with coordination number c of condensed solid matrix; solid line, this research; dashed line, results of reference 1.

finding one of the respective configurations and the weights are the number of different configurations having the same probability due to the symmetry of the lattice. For example α_2 is c because there are c different sites to which the free radical can be bound. β_2 is two since the free radical and the diluent can be interchanged. For the pair with probability y_4 the radical can be bound only to one of $(c-1)$ neighbors and not to D but there is a further factor two because of possible interchange and so on. We of course do not permit a pair of nearest neighbor free radicals to exist.

The quantity we seek is x_1, the free radical fraction on the lattice.

The combinatorial factor G in Eq. (1) will be used in the Bethe[2] approximation but as given in a particularly useful way as a special case of Kikuchi's treatment[3] of the entropy of lattice arrangements. This form is

$$\ln G = N[(c-1)\sum_{i=1}^{3}\alpha_i x_i \ln x_i - (c/2)\sum_{i=1}^{6}\beta_i y_i \ln y_i], \quad (2)$$

in which N is the total number of lattice sites. A useful discussion of this approximation has also been given by Brush.[4]

The equivalence of this Bethe approximation to the so-called quasi-chemical method has been discussed by Fowler and Guggenheim.[5] Temperley[6] and Rushbrooke and Ursell[7] have shown that the quasi-chemical method is exact in one dimension and thus we will be able to reproduce the exact results of I for free radical concentrations on a chain.

The probability parameters are related by one independent normalization condition

$$x_1+cx_2+x_3=1, \quad (3.1)$$

and four consistency equations,

$$x_1=(c-1)y_1+y_2, \quad (3.2)$$

$$x_2=y_1+(c-1)y_3+y_4, \quad (3.3)$$

$$x_2=y_6 \quad (3.4)$$

$$x_3=y_2+(c-1)y_4+y_5. \quad (3.5)$$

Equation (3.3), for example, is derived by equating the number of lattice points of probability type x_2 with the total number of such points involved in the pairs, thus:

$$Ncx_2=(Nc/2)[2(c-1)y_1+2(c-1)^2y_3+2(c-1)y_4] \cdot(1/(c-1)).$$

The normalization of the pair probabilities follows from Eqs. (3) and is not an independent relation.

In this calculation x_3 is a known, disposable parameter equal to α, the fraction of diluent particles:

$$x_3=\alpha. \quad (4)$$

This leaves us with eight unknowns of which three are independent. We choose these to be x_2, y_3, and y_4. The dependent variables are, with use of Eq. (4),

$$x_1=1-\alpha-cx_2, \quad (5.1)$$

$$y_1=x_2-(c-1)y_3-y_4. \quad (5.2)$$

$$y_2=(1-\alpha)-(2c-1)x_2+(c-1)^2y_3+(c-1)y^4, \quad (5.3)$$

$$y_5=(2\alpha-1)+(2c-1)x_2-(c-1)^2y_3-2(c-1)y_4, \quad (5.4)$$

$$y_6=x_2. \quad (5.5)$$

TABLE I. Point configurations.

Configuration		Probability	Weight (α_i)
Free Radical	R	x_1	1
Recombined Free Radical	R—	x_2	c
Diluent	D	x_3	1

[2] H. A. Bethe, Proc. Roy. Soc. (London) **A150**, 552 (1935).
[3] R. Kikuchi, Phys. Rev. **81**, 988 (1951), Sec. B; Kurata, Kikuchi, and Watari, J. Chem. Phys. **21**, 434 (1953).
[4] S. G. Brush, Proc. Roy. Soc. (London) **A242**, 544 (1957).
[5] R. Fowler and E. A. Guggenheim, *Statistical Thermodynamics* (Cambridge University Press, New York, 1949), p. 595.
[6] H. N. V. Temperley, Proc. Cambridge Phil. Soc. **40**, 239 (1944).
[7] G. S. Rushbrooke and H. D. Ursell, Proc. Cambridge Phil. Soc. **44**, 263 (1948).

When we neglect all consideration of internal energy, the most probable distribution is given by the maximum entropy. Hence we maximize the S of Eq. (1) with respect to the three independent variables. This yields the following three relations

$$(x_2/x_1)^{2(c-1)}=[y_1^{2(c-1)}y_5^{(2c-1)}y_6]/y_2^{2(2c-1)}, \quad (6.1)$$

$$y_2^2y_3=y_1^2y_5, \quad (6.2)$$

$$y_2y_4=y_1y_5. \quad (6.3)$$

Equations (3) and (6) may then be solved:

$$y_2=\{y_1[\alpha-(c-1)y_4]/(y_1+y_4)\}, \quad (7.1)$$

$$y_3=\{y_4(y_1+y_4)/[\alpha-(c-1)y_4]\}, \quad (7.2)$$

$$y_5=\{y_4[\alpha-(c-1)y_4]/(y_1+y_4)\}, \quad (7.3)$$

$$y_6=x_2=\{\alpha(y_1+y_4)/[\alpha-(c-1)y_4]\}, \quad (7.4)$$

$$x_1=\{\alpha[1-\alpha-y_4-cy_1]-(c-1)y_4\}/[\alpha-(c-1)y_4]. \quad (7.5)$$

To obtain y_1 and y_4 we must solve the following two equations numerically:

$$\alpha^{2c-3}y_1^{2c}[\alpha-(c-1)y_4]^{2c} = y_4^{2c-1}(y_1+y_4)^2\{\alpha[1-\alpha-y_4-cy_1]-(c-1)y_4\}^{2(c-1)}, \quad (8.1)$$

$$2[\alpha+(c-1)]y_4 = (c-1)^2y_1^2-[2\alpha+(c-1)]y_1-\alpha(\alpha-1)\pm Q^{\frac{1}{2}}, \quad (8.2)$$

in which

$$Q=(c-1)^4y_1^4-2(c-1)^2y_1^3[2\alpha+(c-1)]-y_1^2 \cdot[2\alpha^2(c-1)(c+3)+(c-1)^2(6\alpha-1)] -2\alpha y_1[2\alpha^2+(c-1)(3\alpha-1)]+\alpha^2(\alpha-1)^2. \quad (9)$$

With y_1 and y_4 determined the free radical fraction is found from Eq. (7.5). Except for α nearly unity the $Q^{\frac{1}{2}}$ of Eq. (8.2) must be taken with the plus sign and usually obviously so. At one of our calculated points, namely $c=2$, $\alpha=0.8$, it was necessary to take $Q^{\frac{1}{2}}$ with the minus sign.

TABLE II. Pair configurations.

Configuration	Probability	Weight (β_i)
R R	y_1	2(c-1)
R D	y_2	2
R R	y_3	$(c-1)^2$
R D	y_4	2(c-1)
D D	y_5	1
R R	y_6	1

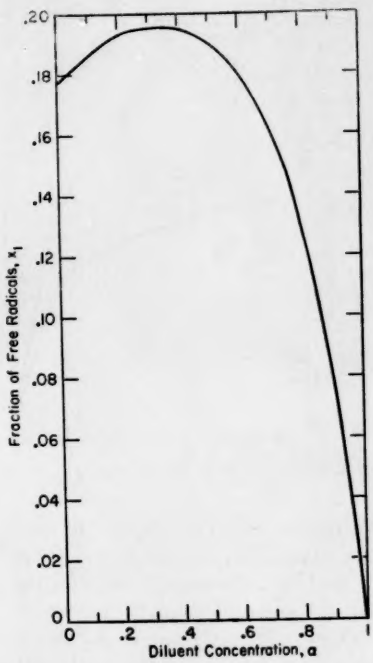

FIG. 2. The exact variation of free radical fraction in the one-dimensional case with inert diluent concentration.

For the case of no diluent present ($\alpha=0$) $y_2=y_4=y_5=0$ and we can solve Eq. (3) with Eq. (6.1) in the form

$$(x_2/x_1)^{2(c-1)}=(x_2y_3/y_1^2)\,(y_3/y_1)^{2(c-1)}, \quad (10)$$

and find

$$y_1=x_1/(c-1),$$
$$y_3=\{[(c-1)-x_1(2c-1)]/c(c-1)^2\},$$
$$y_6=x_2=(1-x_1)/c, \quad (11)$$

where x_1 is to be numerically found from

$$c^2(c-1)^{2(c-1)}x_1^2(1-x_1)^{(2c-3)} = \{(c-1)-x_1(2c-1)\}^{(2c-1)}. \quad (12)$$

The numerical work proceeded as follows. First x_1 was found from Eq. (12) for the case of the pure free radical gas at given coordination number. With diluent present in small amount a trial y_1 value was selected, somewhat less than that found for $\alpha=0$ and like c value, and a trial y_4 computed from (8.2). These two trial values were then put into Eq. (8.1) and the left and right sides of that equation compared. This was repeated for a series of original y_1 trial values until the two sides of (8.1) were substantially the same to a number of significant figures to obtain x_1 to two or three figures.

The results in the case of a pure gas of free radicals are presented in Fig. 1 as a function of coordination number. The second (dashed) curve is that found by the independent single site approximation of Jackson and Montroll. Particular free radical fractions ap-

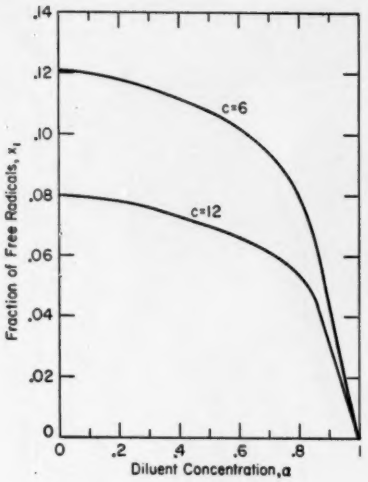

FIG. 3. Variation of free radical fraction for higher dimensional lattices with inert diluent concentration; c= coordination number.

propriate to cubic lattices of $c=6$, 8, and 12 are, respectively, 0.121, 0.103, and 0.0803.

In Fig. 2 the exact results for the free radical fraction in the one dimensional case are given as a function of diluent concentration, α. As mentioned previously, this is a reproduction of the work in I which was however the result of a different method.

In Fig. 3 the variation of free radical fraction with diluent concentration is shown for $c=6$ and $c=12$.

In general when diluent particles are present they act to keep free radicals apart but at the same time they take up space otherwise available to free radicals. We may conclude from Figs. 2 and 3 that only in the one-dimensional case is there a net increase in the free radical fraction with moderate diluent concentration. In the higher dimensional lattices the free radical fraction begins to fall off at once. Jackson and Montroll found a slight peak in their curves for low diluent admixture for all coordination numbers with their less careful counting. We note that the free radical fraction is rather insensitive to diluent concentration until α increases beyond 0.2 and that there is a very sharp decrease only after α reaches 0.7–0.8. The reasons for this behavior are graphically illustrated for the simple cubic lattice ($c=6$) in Fig. 4 where we have plotted the fraction of free radical-bound free radical pairs ($10y_1$) and the fraction of free radical-diluent pairs ($2y_2$) as function of α. The decrease of the former and increase of the latter conspire to maintain their sum at a nearly constant 24% of all pairs until α is greater than 0.2. Until α increases beyond 0.7 the fraction of free radical-diluent pairs is increasing so that there is still a 'mechanism' retarding a rapid decrease in the single site free radical fraction. This is no longer true when α is greater than 0.7.

3. FRACTION OF FREE RADICALS WITH INCOMPLETE DISSOCIATION

We now treat the case of an incompletely dissociated gas without other diluent particles. Each dissociated molecule is assumed to have provided two identical free radicals to the gas and each undissociated molecule will be considered as a diluent that can occupy two adjacent lattice sites upon condensation onto a lattice. The point and pair configurations are tabulated in Tables III and IV, respectively.

Since $Ncx_3/2$ is the number of undissociated molecules in the original gas and $[N-Ncx_3]/2$ is the number of dissociated molecules, x_3 is related to the known, disposable quantity β, the fraction of molecules undissociated, by the following equation:

$$cx_3=\beta. \tag{13}$$

Following Sec. 2 we have for the entropy of the system

$$S=k\ \ln G=Nk[(c-1)\sum_{i=1}^{3}\alpha_i x_i\ \ln x_i-(c/2)\sum_{i=1}^{7}\beta_i y_i\ \ln y_i]. \tag{14}$$

The normalization and consistency equations are

$$x_1+cx_2+cx_3=1, \tag{15.1}$$

$$x_1=(c-1)y_1+(c-1)y_2, \tag{15.2}$$

$$x_2=y_1+(c-1)y_3+(c-1)y_4, \tag{15.3}$$

$$x_2=y_6 \tag{15.4}$$

$$x_3=y_2+(c-1)y_4+(c-1)y_5, \tag{15.5}$$

$$x_3=y_7. \tag{15.6}$$

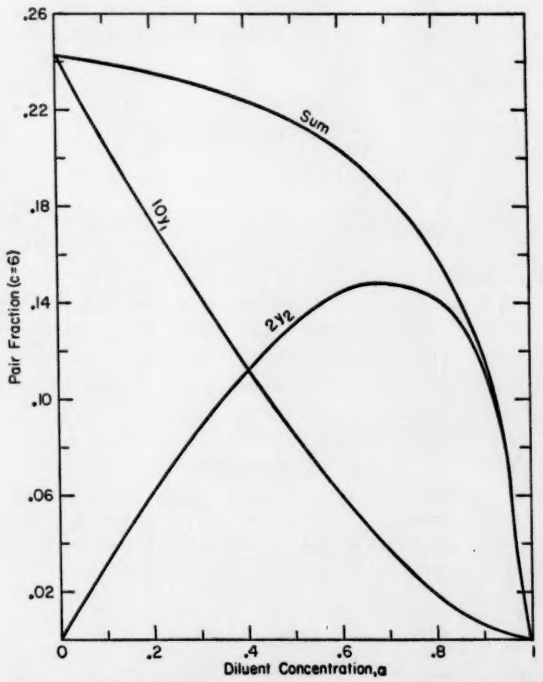

FIG. 4. Effect of diluent concentration on fraction of free radical-bound free radical pairs ($10y_1$) and on fraction of free radical-diluent pairs ($2y_2$) and on their sum for coordination number 6. Note that the sum is precisely twice the fraction of free radical sites.

The fraction undissociated determines x_3 and also y_7. We are left with eight unknowns of which, again, only three are independent. We choose these to be x_2, y_3, and y_4. The dependent variables are expressed as

$$x_1=1-cx_2-cx_3, \tag{16.1}$$

$$y_1=x_2-(c-1)y_3-(c-1)y_4, \tag{16.2}$$

$$(c-1)y_2=1-cx_3-(2c-1)x_2 + (c-1)^2y_3+(c-1)^2y_4, \tag{16.3}$$

$$(c-1)^2y_5=(2c-1)x_3 + (2c-1)x_2-1-(c-1)^2y_3-2(c-1)^2y_4, \tag{16.4}$$

$$y_6=x_2. \tag{16.5}$$

Maximizing the entropy of Eq. (14) with respect to the three independent variables we find

$$(x_2/x_1)^{2(c-1)}=y_1^{2(c-1)}y_5^{(2c-1)}y_6/y_2^{2(2c-1)}, \tag{17.1}$$

$$y_2^2y_3=y_1^2y_5, \tag{17.2}$$

$$y_2y_4=y_1y_5. \tag{17.3}$$

Solving Eqs. (15) and (17) we have

$$y_2=\{y_1[x_3-(c-1)y_4]/[y_1+(c-1)y_4]\}, \tag{18.1}$$

$$y_3=\{y_4[y_1+(c-1)y_4]/[x_3-(c-1)y_4]\}, \tag{18.2}$$

$$y_5=\{y_4[x_3-(c-1)y_4]/[y_1+(c-1)y_4]\}, \tag{18.3}$$

$$y_6=x_2=\{x_3[y_1+(c-1)y_4]/[x_3-(c-1)y_4]\}, \tag{18.4}$$

$$x_1=\{x_3[1-cx_3-cy_1]-(c-1)y_4\}/[x_3-(c-1)y_4]. \tag{18.5}$$

To obtain y_1 and y_4 we must solve the following two equations numerically:

$$x_3^{2c-3}y_1^{2c}[x_3-(c-1)y_4]^{2c} = y_4^{2c-1}[y_1+(c-1)y_4]^2\{x_3[1-cx_3-cy_1] -(c-1)y_4\}^{2(c-1)}, \tag{19.1}$$

$$2(c-1)y_4=y_1^2(c-1)-y_1(1+x_3)-x_3(cx_3-1)\pm Q_\beta^{\frac{1}{2}}, \tag{19.2}$$

in which

$$Q_\beta=(c-1)^2y_1^4-2(c-1)(1+x_3)y_1^3 -y_1^2[x_3^2(2c^2-2c-1)+2x_3(3c-2)-1] +2y_1x_3[cx_3^2-x_3(3c-1)+1]+x_3^2(cx_3-1)^2. \tag{20}$$

TABLE III. Point configurations.

Configuration		Probability	Weight (α_i)
Free Radical	R	x_1	1
Recombined Free Radical	R	x_2	c
Diluent	D	x_3	c

TABLE IV. Pair configurations.

Configuration	Probability	Weight (β_i)
R R	y_1	2(c-1)
R D	y_2	2(c-1)
R R	y_3	$(c-1)^2$
R D	y_4	$2(c-1)^2$
D D	y_5	$(c-1)^2$
R R	y_6	1
D D	y_7	1

These equations are all quite similar to those of Sec. 2. The free radical fraction that we seek is given by x_1 as found from Eq. (18.5) after determination of y_1 and y_4 through use of Eq. (19).

No extensive calculations using these equations have been carried out. For the one-dimensional case the exact results of I (their Fig. 4) should be obtainable and this was checked at only one point, $\beta=0.4$, for which the result was $x_1=0.155$. Note that the free radical concentration falls off at once if the gas which is condensed is not completely dissociated. This is a qualitative difference between the one-dimensional case with single site diluent and with fractional dissociation. There are no qualitative differences when we consider the higher dimensional lattices, only a slightly more rapid decrease of free radical concentration with β than was the case with α. To illustrate this, the free radical concentration for coordination number 12 at $\beta=0.2$ was calculated and found to be 0.076. This is to be compared with the corresponding free radical fraction at coordination number 12 and $\alpha=0.2$ which was found to be 0.078.

4. FRACTION OF FREE RADICALS WITH DILUENT AND INCOMPLETE DISSOCIATION

The case for which the gas is only partially dissociated and also contains single site diluent particles can be easily treated using four point configurations and eleven pair configurations. However, a solution of the equations leads to a set of three simultaneous equations in three unknowns which must be solved numerically. In view of the oversimplified nature of our model there would be little point in such an elaboration and it will not be presented here.

5. DISCUSSION

Empirical data on the concentrations of frozen free radical species are still rather meager but two references may be cited. Broida and Lutes[8] were able to deduce that the minimum fraction of trapped nitrogen atoms was 0.002. Recently this work has been followed up by

[8] H. P. Broida and O. S. Lutes, J. Chem. Phys. **24**, 484 (1956).

Minkoff, Scherber, and Gallagher.[9] However their paper is ambiguous for our purposes since they nowhere give an estimate of the extent of dissociation in the original gas from which they trap radicals on a cold surface. They refer only to a "discharged" original gas and find a value of 0.04 for the fraction of nitrogen atoms trapped. Similarly they find values of 0.04–0.05 for the fraction of oxygen atoms trapped from a "discharged" gas of oxygen assuming that all the heat liberated on warmup of the condensed solid comes from the recombination $O+O=O_2$ ($\Delta H=-117$ kcal/mole). If however all the heat liberated should come from the addition reaction $O+O_2=O_3$ ($\Delta H=-25$ kcal/mole) then the atomic fraction would be two to three times 0.04 and 0.04 is thus only a lower limit in their experiments.

If the results for nitrogen have been obtained from a completely or nearly completely dissociated gas then they are lower than any that can be obtained from our model which, even assuming that second neighbor free atoms bind in a close-packed cubic structure gives a value 0.06 for the free atom fraction. In such a case the neglected kinetic effects, most probably free radical diffusion during formation of the solid matrix, must be held accountable for the discrepancy. However, if there has been less than 50% dissociation achieved in the original gas then such low results could be obtained from the equations given here with $c=18$ and $\beta=0.5$ or with $c=12$ and $\beta=0.8$. In any case the oxygen data do not exclude our model even with complete dissociation since the result 0.04 is only a lower limit.

In general the model here presented provides us with a qualitative picture of what to expect upon condensing gases containing active species. It can furthermore serve as a useful reference with which to compare new experimental data. If such experimental results are low, say 0.04 or less for the free radical fraction condensed from a completely dissociated gas then the importance of free radical diffusion in the solid is indicated. If the results are high, say greater than 0.12, then this would indicate the action of some mechanism retarding the recombination of active species.

Finally, we must append, in view of very recent experimental data and discussion,[10,11] that the calorimetric work of reference 9 is in doubt and that observed free radical concentrations are quite less than that predicted by this paper. Therefore, diffusion effects impose a severe limitation on the applicability of our model to actual systems of small free radicals.

[9] Minkoff, Scherber, and Gallagher, J. Chem. Phys. **30**, 753 (1959).

[10] B. J. Fontana, J. Chem. Phys. **31**, 148 (1959).

[11] "Program of the Fourth International Symposium on Free Radical Stabilization, August 31–September 2, 1959, sponsored by National Bureau of Standards, Washington, D. C." (unpublished).

THE JOURNAL OF CHEMICAL PHYSICS VOLUME 32, NUMBER 2 FEBRUARY, 1960

Effects of Gases on Irradiated Polyvinyl Chloride as Studied by Electron Spin Resonance

ZENICHIRO KURI, HISASHI UEDA,* AND SHOJI SHIDA

Tokyo Laboratories, Japanese Association for Radiation Research on Polymers, Kamifujimae, Bunkyo-ku, Tokyo, Japan

(Received July 9, 1959)

The radicals produced by gamma irradiation of polyvinyl chloride powder in various gases and in vacuum are observed by electron spin resonance. Different patterns are observed for the irradiation in vacuum, air, and sulfur dioxide. No electron spin resonance absorption is obtained by the irradiation in nitrogen oxide, halogens, and hydrogen sulfide. The recombination reaction velocity of the radical produced in vacuum is measured at different temperatures to get the activation energy 38 kcal/mole.

INTRODUCTION

A FEW studies have been done on the effect of various gases on gamma-ray irradiated polymers. Rexroad and Gordy[1] reported the effects of absorbed nitric oxide, hydrogen, carbon monoxide, oxygen, and ionized air on irradiated Teflon. We have studied the effect of gaseous reagents on irradiated polyvinyl chloride (PVC) from the standpoint of the radical reaction by the method of electron spin resonance (ESR), and found several phenomena specific to PVC.

EXPERIMENTAL

Measurements were made at a frequency of 9410 Mc/sec with an automatic recording spectrometer which can display the first derivative of the true resonance curve. In order to obtain the absorption curve, the derivative was graphically integrated.

Line width of the absorption curve was measured by the proton-resonance meter. The calibration of sweep fields was accomplished by observing signals with 14-Mc frequency field having side bands spaced at intervals of 100 kc from the center frequency.[2] DPPH was used as a standard of spectroscopic position.

The irradiation was done by a kilocurie cobalt-60 gamma-ray source. The sample PVC in fine particles was set in a capillary for ESR measurement in a high vacuum or with the coexistence of various gases and was irradiated at the dosage of 10^7r.

Nitric oxide (NO), nitrogen dioxide (NO_2), hydrogen sulfide (H_2S), sulfur dioxide (SO_2), ammonia (NH_3), and hydrogen (H_2) were prepared by standard methods.

RESULTS

I. Radicals Formed in Gamma-Ray Irradiated PVC in Vacuum

The ESR pattern of PVC irradiated in vacuum has a spread of 120 gauss as shown in Fig. 1, which coincides with that obtained by Abraham *et al.*[3] An arrow in the figure shows the spectroscopic position in the magnetic field of DPPH selected as a standard. The absence of hyperfine structure may be caused by inhomogeneous line broadening, anisotropic g factor, or dipolar interactions.

Since the decay of this radical in vacuum at room temperature was found to be negligibly small, it was possible to find the relation between spin concentration c (spin/cc) and the dose, given in Fig. 2. From this data the G value for radical production was obtained as 17 at the primary stage of irradiation.

This radical, however, disappears at higher temperatures according to a second-order reaction $dc/dt=kc^2$ as shown in Fig. 3 and 38 kcal/mole is obtained for the activation energy of recombination in the range of 70° to 100° C. The velocity constant k is thus determined as follows:

$$k=0.7\times \exp(-38\,000/RT)\ \text{cc spin}^{-1}\ \text{sec}^{-1}.$$

By measuring the remaining radicals after treatment for 20 min at several temperatures, the glass transition point can be found at 80°C as shown in Fig. 4. The long life of the radical is naturally ascribed to this high glass transition point and the large activation energy.

Most reagents known as radical scavengers such as H_2S, NO, NO_2, I_2, and O_2 (air) quench the radical. The former four reagents scavenge the radical immediately after their introduction, while air changes the ESR pattern more slowly, taking a few minutes as shown in

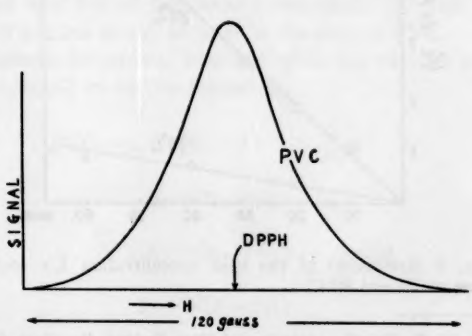

FIG. 1. Electron spin resonance of gamma-ray irradiated polyvinyl chloride in vacuum. The arrow in the figure shows the spectroscopic position in magnetic field of DPPH selected as a standard.

* On leave from Toyo Spinning Company Ltd., Osaka, Japan.

[1] H. N. Rexroad and W. Gordy, J. Chem. Phys. **30**, 399 (1959).

[2] J. T. Arnold and M. E. Packard, J. Chem. Phys. **19**, 1608 (1951).

[3] R. J. Abraham and D. H. Whiffen, Trans. Faraday Soc. **54**, 1291 (1958).

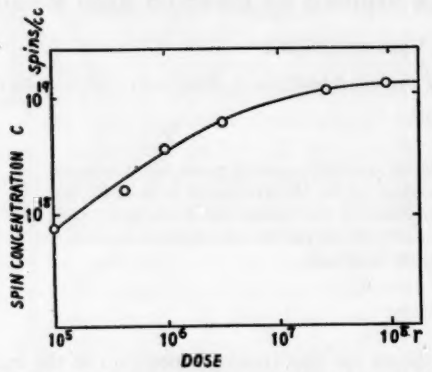

FIG. 2. Relation between spin concentration c (spin/cc) in polyvinyl chloride irradiated in vacuum and the dose given.

Fig. 5. The resulting pattern decays even more gradually taking a time measured in hours. Contrary to the result for Teflon reported by Rexroad *et al.*,[1] hydrogen molecules do not react with the radical, which may indicate a difference in reactivity between Teflon and PVC polymer radicals.

SO_2, which had been expected to react with the radical,[4,5] does not change the pattern. These results are summarized in Table I.

II. Radicals Formed in Gamma-Ray Irradiated PVC in Open Air

When the sample is irradiated in open air, an asymmetric pattern is observed in differential form. Its integrated curve can be separated into two components appearing at smaller magnetic fields than that of DPPH as shown in Fig. 6. This radical does not decay in vacuum, but does in air in a time measured in months. It is to be noted that the pattern obtained in open air differs from that obtained when air is introduced into PVC previously irradiated in vacuum,

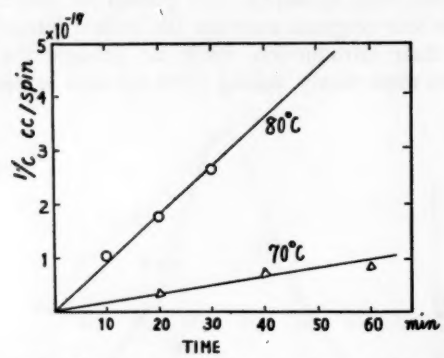

FIG. 3. Reciprocal of the spin concentration $1/c$ (cc/spin) *vs* time at 70 and 80°C.

[4] E. W. R. Steacie, *Atomic and Free Radical Reactions* (Reinhold Publishing Corporation, New York, 1954), p. 787.
[5] J. I. Black and E. F. Baxter Jr., "Second United Nations International Conference on the Peaceful Uses of Atomic Energy," P/797 (1958).

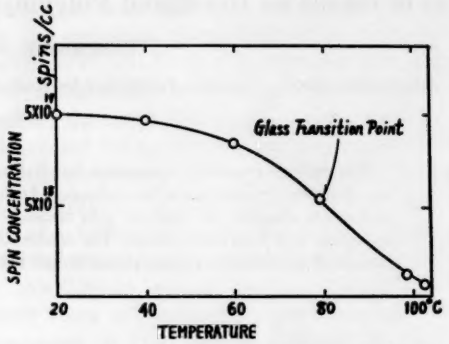

FIG. 4. Concentration of the remaining radicals after treatment for 20 min at several temperatures. The glass transition point can be found at 80°C.

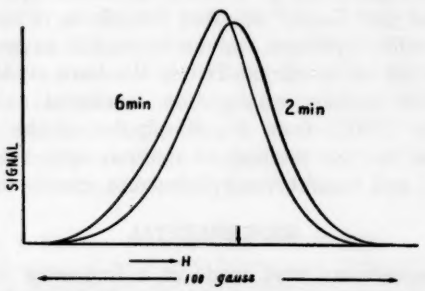

FIG. 5. Change of the pattern of resonance after introduction of air into the irradiated polyvinyl chloride in vacuum.

TABLE I. Effects of gases on PVC irradiated in vacuum.

Gases	Change in ESR
Air	Rapid change followed by slow decay
NO and NO_2	Immediate decay
SO_2, H_2 and NH_3	No change
I_2 and H_2S	Rapid decay

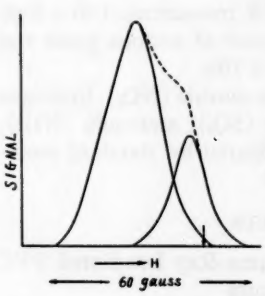

FIG. 6. Electron spin resonance gamma-ray irradiated polyvinyl chloride in open air. The dotted line indicates the original form.

TABLE II. Effects of gases on PVC irradiated in open air.

Gases	Change in ESR
Air	Very slow decay
NO and NO_2	Immediate decay
SO_2, H_2, NH_3, Cl_2, and I_2	No change

whereas both patterns coincide in the case of polypropylene.[6]

NO and NO_2 gases quench the radicals, although the other gases, even chlorine and iodine, do not. Reactivity of the radicals against various gases is summarized in Table II.

III. Radicals Formed in Gamma-Ray Irradiated PVC in Various Gases

1. H_2 and NH_3. The effect of these gases is negative and the same patterns are obtained as in the case of vacuum.

2. SO_2. A rather symmetric differential pattern is obtained by the irradiation in SO_2 gas. The integral form shows that it has two components as shown in Fig. 7. It is to be noted that it has a considerably narrower line width than that of PVC in vacuum. We can not determine this radical to be of the type $RSO_2\cdot$ from this new pattern, because the pattern of the radical produced in vacuum was not changed when SO_2 gas was introduced. However, when SO_2 gas is introduced onto polypropylene or polyethylene powder irradiated in vacuum, the same ESR pattern as that shown in Fig. 7 appears. Furthermore, the same pattern is obtained in these polymers when irradiated in SO_2 gas. Consequently the radical of PVC produced under irradiation in SO_2 gas can be supposed to be of the type $RSO_2\cdot$.

3. NO, NO_2, Br_2, and H_2S. No ESR absorption is observed when PVC is irradiated in NO, NO_2, Br_2, and H_2S.

The reactivity of the radicals discussed in the foregoing is summarized in Table III.

TABLE III. Effects of gases on PVC irradiated in various gases.

Irradiated in	Reacted with	Change in ESR
H_2 and NH_3	Air	Rapid change followed by slow decay
SO_2	NO and NO_2	Immediate decay
	Air	No change but slow decay
Br_2, NO, NO_2, and H_2S	No ESR is observed	

DISCUSSION

As stated previously, the ESR pattern of polypropylene irradiated in O_2 or SO_2 coincides with that obtained when O_2 or SO_2 is introduced onto the polypropylene irradiated in vacuum. In the case of PVC, however, introduction of O_2 or SO_2 does not change the radical formed in vacuum into the one which is produced by the irradiation in O_2 or SO_2 gas. From these results, the following scheme may be considered:

$$\text{PVC}\text{—}\vee\vee\vee\rightarrow \text{R}\cdot + \text{H or Cl} \qquad (1)$$

$$\text{R}\cdot \longrightarrow \text{r}\cdot \qquad (2)$$

$$\text{r}\cdot + \text{O}_2 \rightarrow \text{quench} \qquad (3)$$

$$\text{r}\cdot + \text{SO}_2 \rightarrow \text{not react} \qquad (4)$$

$$\text{R}\cdot + \text{O}_2(\text{or } \text{SO}_2) \rightarrow \text{RO}_2\cdot(\text{or } \text{RSO}_2\cdot) \qquad (5)$$

$$\text{RO}_2\cdot(\text{or } \text{RSO}_2\cdot) + \text{O}_2 \rightarrow \text{slow decay.} \qquad (6)$$

When PVC is irradiated in vacuum, a radical R· is produced [Eq. (1)] which is then modified into another one r·[Eq. (2)], which is quenched by O_2[Eq. (3)], but does not react with SO_2 gas [Eq. (4)]; when PVC is irradiated in a gas, the radical R· obtained in Eq. (1) reacts with O_2 or SO_2 before being transformed into the radical r· to become $RO_2\cdot$ or $RSO_2\cdot$ radical (5). Both of the radicals $RO_2\cdot$ and $RSO_2\cdot$ are very stable, for they do not react even with halogens except NO and NO_2. The reaction with O_2 in Eq. (6) is also extremely slow. The following reaction is generally considered to occur:

$$\text{RSO}_2\cdot + \text{Cl}_2 \rightarrow \text{RSO}_2\text{Cl} + \text{Cl} \qquad (7)$$

$$\text{RO}_2\cdot + \text{H}_2 \rightarrow \text{RO}_2\text{H} + \text{H}, \qquad (8)$$

but as was stated previously, reactions (7) and (8) cannot always occur, at least in the case of PVC.

Schemes for radical reaction with the various gases are expected to be the following:

$$\text{PVC}\text{—}\vee\vee\vee\rightarrow \text{R}\cdot \longrightarrow \text{r}\cdot$$

$$\text{r}\cdot + \text{O}_2 \rightarrow \text{rO}_2\cdot$$

$$\text{rO}_2\cdot + \text{O}_2 \rightarrow \text{r=O} \qquad \text{rapid}$$

$$\text{r}\cdot + \text{NO} \rightarrow \text{rNO}$$

$$+\text{I}_2 \rightarrow \text{rI}$$

$$+\text{H}_2\text{S} \rightarrow \text{rH}.$$

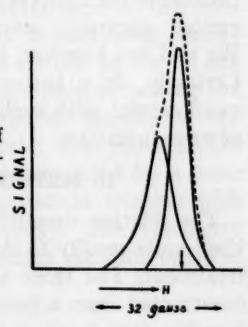

FIG. 7. Electron spin resonance of gamma-ray irradiated polyvinyl chloride in SO_2 gas. The dotted line indicates the original form.

[6] Ohnishi, Kashiwagi, Ikeda, and Nitta, Isotopes and Radiation (Japan) 1, 210 (1958).

In open air

$$R\cdot+O_2\rightarrow RO_2\cdot$$
$$RO_2\cdot+O_2\rightarrow R{=}O \quad \text{very slow}$$
$$+NO\rightarrow RO_2NO.$$

In H_2 and NH_3

$$PVC\text{—}\vee\vee\vee\rightarrow R\rightarrow r.$$

In SO_2

$$R\cdot+SO_2\rightarrow RSO_2\cdot$$
$$RSO_2\cdot+O_2\rightarrow ?. \quad \text{very slow}$$

In Br_2, NO, and H_2S

$$R\cdot+Br_2\rightarrow RBr$$
$$+NO\rightarrow RNO$$
$$+H_2S\rightarrow RH.$$

ACKNOWLEDGMENT

The authors wish to thank Mr. Tamura for his helpful advice in the resonance measurement. They also wish to express their gratitude to Dr. K. Shinohara for his helpful advice and encouragement.

THE JOURNAL OF CHEMICAL PHYSICS VOLUME 32, NUMBER 2 FEBRUARY, 1960

Short-Range Interaction between a Hydrogen Molecule and a Hydrogen Atom. II

WILLIAM J. JAMESON, JR.,* AND HENRY AROESTE

Lockheed Missiles and Space Division Research Laboratory, Palo Alto, California

(Received August 10, 1959)

Computations of the interaction between a hydrogen atom and a hydrogen molecule, where one of the three atoms is in a two-quantum electronic state, have been made using a modified Heitler-London procedure. The calculated interaction energies of the system including a degenerate state for which the magnetic quantum number is $m=0$ are about 5 ev lower than the previous Heitler-London results in which no excited state were considered. The results are compared with experimentally determined energies, and a possible explanation of the discrepancy between theoretical and experimental values is presented. Calculations are also presented for cases where $m=1$.

I. INTRODUCTION

IN a previous paper,[1] henceforth referred to as I, we considered the H_2—H interaction using both Heitler-London (HL) and LCAO techniques. In I we attempted to close the gap between the experimental results of Amdur and Pearlman[2] and the theoretical results.[3] Although the LCAO treatment lowered the theoretical H_2—H interaction energies appreciably, these energies are still considerably higher than the experimental values.

One of the main reasons for this paper is to examine theoretically what effect on experimental results would be expected if one of the three H atoms is in an excited electronic state. One source of excited H atoms in the experiment would be in the incident beam. The only states from this source which could affect the results, however, would be s states; the others would most probably decay in the beam before collision. Perhaps the primary source of excited states arises from the inelastic collisions in the chamber. As Amdur and Pearlman suggest, it is possible that there was a certain amount of inelastic scattering present in their experiments. Applying a modified "adiabatic" criterion[4] for inelastic collisions, one can estimate the energy E' of the incident H atom for the maximum excitation cross section for transition from the $1s$ to a two-quantum state. By this method E' has been approximated as 470 ev which is within the 200–800-ev energy range of the experiment.

We have been reconciled to a modified HL treatment because of the complexity induced by the presence of an excited electronic state in the three-body problem. We still feel however, that our results are meaningful. Certainly, in a better approximation one would be more careful with such problems as nonorthogonality of wave functions.

II. METHODS AND RESULTS

The relative simplifity of the H_2—H system lends itself quite readily to the Heitler-London valence bond treatment. The three atom eigenfunctions have been constructed from a linear combination of Slater deter-

* Present address: Department of Mathematics, Iowa State University, Ames, Iowa.

[1] H. Aroeste and W. Jameson, J. Chem. Phys. **30**, 372 (1959).

[2] I. Amdur and H. Pearlman, J. Chem. Phys. **8**, 7 (1940). For additional or revised comments on interpretation of results see also I. Amdur, J. Chem. Phys. **17**, 844 (1949), and Amdur, Kells, and Davenport, J. Chem. Phys. **18**, 1676 (1950).

[3] H. Margenau, J. Chem. Phys. **66**, 303 (1944).

[4] B. H. Armstrong (private communication). See also, N. Massey and E. Burhop, *Electronic and Ionic Impact Phenomena* (Clarendon Press, Oxford, 1952), p. 479.

minants; for example,

$$\psi_{A_\rho}=\begin{pmatrix} a & b & c_\rho \\ \beta & \alpha & \alpha \end{pmatrix}+\begin{pmatrix} a & b_\rho & c \\ \beta & \alpha & \alpha \end{pmatrix}+\begin{pmatrix} a_\rho & b & c \\ \beta & \alpha & \alpha \end{pmatrix}, \quad (1)$$

$$\psi_{B_\rho}=\begin{pmatrix} a & b & c_\rho \\ \alpha & \beta & \alpha \end{pmatrix}+\begin{pmatrix} a & b_\rho & c \\ \alpha & \beta & \alpha \end{pmatrix}+\begin{pmatrix} a_\rho & b & c \\ \alpha & \beta & \alpha \end{pmatrix}, \quad (2)$$

$$\psi_{C_\rho}=\begin{pmatrix} \alpha & \alpha & c_\rho \\ \alpha & \alpha & \beta \end{pmatrix}+\begin{pmatrix} a & b_\rho & c \\ \alpha & \alpha & \beta \end{pmatrix}+\begin{pmatrix} a_\rho & b & c \\ \alpha & \alpha & \beta \end{pmatrix}, \quad (3)$$

are three such eigenfunctions. The letters a, b, and c denote the hydrogenic orbitals associated with the nuclei a, b, and c (Fig. 1). The subscript ρ indicates that the orbital refers to a specific two-quantum state.[5] In notation similar to Kotani's,[6] ρ signifies either s', σ, π, or π', where s' indicates a hydrogenic $2s$ orbital; σ, a $2p\sigma$ orbital; π, a $2p\pi$ orbital; and π', a $2p\pi'$ orbital. Lower case letters without subscripts refer to $1s$ orbitals; the symbols α and β denote spin functions. Each particular Slater determinant, therefore, represents the given two-quantum state associated with a different atom. The wave function subscripts A, B, and C are useful primarily as notations to construct eigenfunctions which assign H_2 bonds between pairs of the atoms a, b, and c.

In applying a Heitler-London approximation to the system of three hydrogen atoms, one of which is in a two-quantum state, one obtains an eighth-order secular determinant for the energy. From the orthogonality properties of the $2p\pi$ states, however, certain off-diagonal elements vanish. These vanishing elements refer to interactions of $1s$, $2s$, or $2p\sigma$ states with $2p\pi$ states. As a result, the eighth-order determinant separates into one fourth-order determinant, which represents $2s$ and $2p\sigma$ interaction, and two second-order determinants, which have identical roots and represent the energy of the H_2—H system with one atom in a $2p\pi$ state.

In general, we have restricted our calculations to an isosceles triangle configuration, wherein the nuclei a and b are at the endpoints of the base of the triangle, and the nucleus c is at the opposite vertex (see Fig. 1). In addition to the symmetry advantages of this configuration, it is the condition of impact most readily compared with the experimental results. In Fig. 1, one can consider the incoming atom c as approaching the molecule ab along the perpendicular bisector of the internuclear axis of the molecule. The roots of the $2s-2p\sigma$ determinant have been calculated for a more restricted configuration, an equilateral triangle with sides of length $1.4a_0$ (Bohr radii). The symmetry involved in this calculation results in the elimination of many terms.

[5] A two-quantum state is defined as one for which the principal quantum number is $n=2$.

[6] Kotani, Anemiya, Ishiguro, and Kimura, *Table of Molecular Integrals* (Maruzen Company, Ltd., Tokyo, 1955).

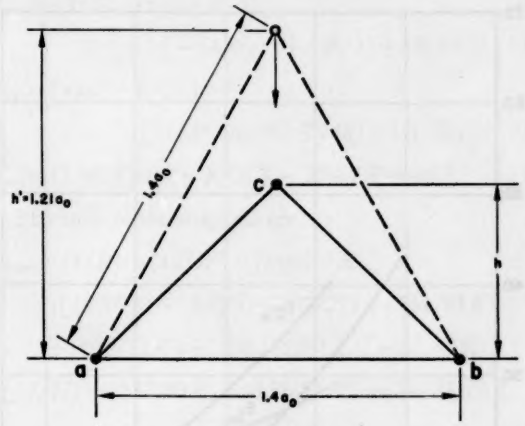

FIG. 1. Configurations of atoms.

Using the same procedure that was adopted in I, the wave functions which have been constructed are of the form

$$\Psi_{I_\rho}=\psi_{A_\rho}-\psi_{B_\rho} \quad (4)$$

$$\Psi_{II_\rho}=2\psi_{C_\rho}-\psi_{A_\rho}-\psi_{B_\rho}. \quad (5)$$

Here Ψ_{I_ρ} denotes an H_2 bond between atoms a and b, and Ψ_{II_ρ} refers to an H_2 bond alternating between c and a or b. For the system involving one $2p\pi$ and two $1s$ states[7] in which the altitude h of the isosceles triangle is greater than the altitude h' of the equilateral triangle, Ψ_{I_π} relates to the lower root of the second-order secular determinant for the energy. When h is less than h', Ψ_{II_π} provides the lower root. When $h=h'$ (equilateral triangle), $\Psi_{I_\pi}=\Psi_{II_\pi}$. In solving the fourth-order determinant which arises from terms describing the system of one $2s$ or $2p\sigma$ and two $1s$ states, the basis set we have chosen consists of wave functions of the type given in Eq. (4) since the symmetry degeneracy of the equilateral triangle configuration produces the same results for either type of wave function. The approximate wave functions Ψ_{III} and Ψ_{IV} which correspond to the energy roots of the fourth-order determinant, can be constructed from the basis set as linear combinations of the form $C_1\Psi_{I_{s'}}+C_2\Psi_{I_\sigma}$. The coefficients C_1 and C_2 are functions of the particular root.

Calculations have been made for the three distinct roots of the eighth-order secular determinant for the equilateral triangle configuration.[8] For the two roots of the second-order determinants representing one atom in a $2p\pi$ state we have also made computations for several isosceles triangle configurations. The base of the triangle is always $1.4a_0$, and a screening constant of unity has been assumed. All of the one and two

[7] The two roots of the $2p\pi$ determinant are identically equal to the two roots of the $2p\pi'$ determinant.

[8] For the equilateral triangle configuration, the four roots of the fourth-order sub-determinant representing the $2s-2p\sigma$ terms exhibit a symmetry degeneracy leading to only two distinct roots; the $2p\pi$ (or $2p\pi'$) roots are also symmetry degenerate, providing only one additional distinct root.

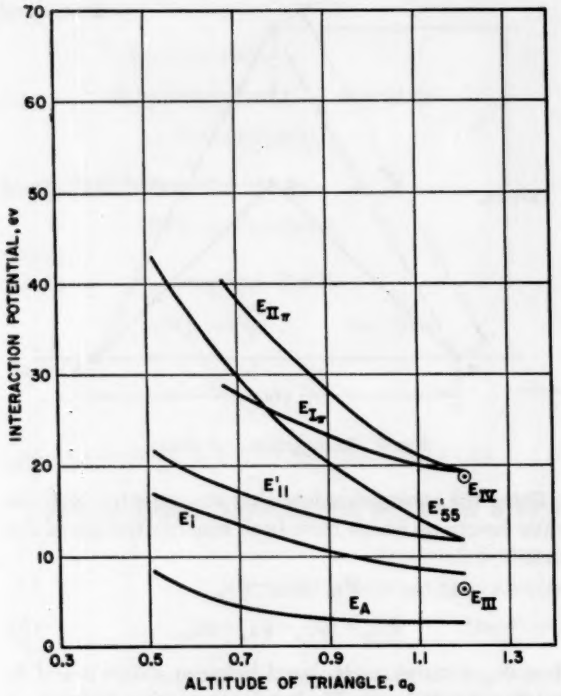

FIG. 2. Interaction potentials as a function of the altitude of the triangle.

center integrals involved were taken from various existing tables,[9] determined in closed form, or computed numerically on the Univac 1103A computer. The appendix lists the integrals which have been evaluated in closed form. The three-center integrals were approximated by the Rudenberg-Mulliken method.[10]

A composite of results from the present and previous papers is given in Fig. 2, where all the energy values are interaction energies between an H_2 molecule and an H atom. In Fig. 2 the curves E_{II}' and E_{55}' refer to an HL calculation for a system of three 1s H atoms; E_i, to an LCAO treatment of the same system; and E_{I_π} and E_{II_π}, to the system of two 1s and one $2p\pi$ atoms. The two points E_{III} and E_{IV} denote the two roots of the $2s-2p\sigma$ determinant for the equilateral triangle configuration. E_A is a plot of the experimental results.

From Fig. 2 one may obtain the energies necessary to approximate the wave functions corresponding to the roots E_{III} and E_{IV}. These are

$$\Psi_{III}=N_1(\Psi_{I_\sigma}-0.38\Psi_{1_{s'}}) \quad (6)$$

$$\Psi_{IV}=N_2(\Psi_{I_\sigma}+11.8\Psi_{1_{s'}}), \quad (7)$$

where the coefficients N_1 and N_2 are the necessary normalization constants.

[9] See, for example, H. Preuss, *Integraltafeln Zur Quantenchemie* (Springer-Verlag, Berlin, 1956), or Miller, Gerhauser, and Matsen, *Quantum Chemistry Integrals and Tables* (University of Texas Press, Austin, 1959).

[10] K. Rudenberg, J. Chem. Phys. **19**, 1433 (1951).

III. DISCUSSION

The foregoing results indicate that the system consisting of a ground-state H_2 molecule and one two-quantum H atom with magnetic quantum number $m=0$ exhibits a lower interaction energy than the H_2—H system of three 1s atoms. The calculated interaction energy of the system with one atom in a two-quantum state for which $m=1$ is somewhat higher. For the two cases $m=0$ and $m=1$ the difference in shape or angular orientation of the electronic charge distribution of the excited H atoms presumably accounts for the difference between the energies E_{III} and E_{I_π} or E_{II_π}. If a better approximation were to be used, it would be interesting to note whether or not there is any improvement of results as occurred in I, where the LCAO approach appreciably lowered the calculated energy of the three 1s H atom complex.

As the level of excitation of one of the H atoms is increased, the excited atom is closer to ionization, and in this respect the system more closely approximates the H_3^+ molecule which is stable under certain circumstances. Hence, one might suspect that as the principal quantum number n of the excited H atom increases to higher values, the interaction energy decreases. For large n one would then predict that the interaction energy of a three H atom complex would be lower than for three 1s H atoms, but that any degenerate states for which $m=0$ would, in general, yield lower energies than those for which $m\neq 0$.

Thus, referring again to the experiment, if a significant proportion of H atoms are in excited electronic states, the present results might narrow the discrepancy between experiment and theory.

ACKNOWLEDGMENT

We are indebted to Gladys R. Garabedian for the evaluation of the integrals in closed form, for the Univac 1103A programs, and for some numerical computations.

APPENDIX

The molecular integrals presented here are essentially in Kotani's notation. The differences from his notation are that the subscript h refers to a hydrogenic 1s orbital, and s' denotes a hydrogenic 2s orbital.

The one center integrals are:

$$S_{h\sigma}=(2^{9/2}/27)[\exp(-R/2)][3R-16+(32/R)+(64/R^2)]-(256/27)[\exp(-R)]\cdot[1+(8/R)+(8/R^2)], \quad (1)$$

$$S_{s\sigma}=-[\exp(-R/2)]\cdot[(R^4/240)+(R^3/60)-(R^2/20)-(R/2)+1]. \quad (2)$$

$$S_{hs'}=-(2^{9/2}/9)[\exp(-R/2)]\cdot[1-(32/3R)+(64/3R^2)]+(2^{11/2}/27)[\exp(-R)][5+(32/R)], \quad (3)$$

$$S_{s's'}=[\exp(-R/2)[(R^4/240)+(R^2/12)+(R/2)+1], \quad (4)$$

$$S_{\sigma s'}=-[\exp(-R/2)](R^4/240)[1+(2/R)], \quad (5)$$

$$K_{hs}=(2^{15/2}/243R^2)-2^{-1}[\exp(-3R/2)] \cdot[(4R/9)+(32/27)+(128/81R)+(256/243R^2)], \quad (6)$$

$$K_{\sigma\sigma}=(1/R)+(12/R^3)-(R^2/8)[\exp(-R)] \cdot[1+(6/R)+(22/R^2)+(56/R^3)+(96/R^4)+(96/R^5)], \quad (7)$$

$$K_{hs'}=(2^{3/2}/9)R[\exp(-3R/2)][1+(2/3R)], \quad (8)$$

$$K_{s's'}=(1/R)-(R^2/8)[\exp(-R)] \cdot[1+(2/R)+(6/R^2)+(8/R^3)], \quad (9)$$

$$K_{\sigma s'}=-(3/R^2)+(R^2/8)[\exp(-R)] [1+(4/R)+(12/R^2)+(24/R^3)+(24/R^4)], \quad (10)$$

$$J_{hs}=2^{-1}\{[\exp(-R/2)][(4R/3)-(32/9) +(128/27R)+(256/27R^2)]-[\exp(-R)] \cdot[(256/27R)+(256/27R^2)]\}, \quad (11)$$

$$J_{sh}=2^{-1}\{[\exp(-R/2)][(32/9)-(256/27R) -(512/27R^2)]+[\exp(-R)] \cdot[(32/9)+(512/27R)+(512/27R^2)]\}, \quad (12)$$

$$J_{\sigma\sigma}=[\exp(-R/2)][(R^3/96)-(R/8)-(1/4)], \quad (13)$$

$$J_{hs'}=(2^{3/2}/3)[\exp(-R/2)][-R+(14/3)-(80/9R)] +5(2^{11/2}/27R)[\exp(-R)], \quad (14)$$

$$J_{s'h}(2^{9/2}/9)[\exp(-R/2)][-1+(14/3R)] -(2^{5/2}/9)[\exp(-R)][5+(56/3R)], \quad (15)$$

$$J_{s's'}=(1/32)[\exp(-R/2)] \cdot[-(4R^2/3)+(R^3/3)+4R+8], \quad (16)$$

$$J_{\sigma s'}=[\exp(-R/2)] \cdot[-(R^3/96)+(R^2/48)+(R/24)], \quad (17)$$

$$J_{s'\sigma}=(1/96)[\exp(-R/2)][-R^3+2R^2+4R], \quad (18)$$

The two center integrals are:

$$C_{hshs}=(1/R)+(12/R^3)-[\exp(-R)] \cdot[(2R^2/9)+(4R/9)+(92/27)+(544/81R) +(896/81R^2)+(896/81R^3)]-[\exp(-2R)] \cdot[(7/27)+(137/81R)+(152/81R^2)+(76/81R^3)], \quad (19)$$

$$C_{hs'hs'}=(1/R)+[\exp(-R)] \cdot[-(2R^2/9)+(4R/9)-(76/27)+(128/81R)] -[\exp(-2R)][(5/9)+(209/81R)], \quad (20)$$

$$C_{hhhs}=(2^{15/2}/243R^2)+2^{-1}\{[\exp(-3R/2)] \cdot[-(2^{10}R/21^2)+11(2^{13}/21^3)-83(2^{16}/21^4R) -83(2^{17}/3\cdot 21^4R^2)]+[\exp(-2R)] \cdot[3(2^9/7^3)+165(2^9/7^4R)+165(2^8/7^4R^2)]\}, \quad (21)$$

$$C_{hhhs'}=2^{-1}\{[\exp(-3R/2)] \cdot[(2^{10}R/21^2)-65(2^{11}/21^3)+3(2^{15}/7^4R)] -[\exp(-2R)][(2^{11}/7^3)+3(2^{15}/7^4R)]\}, \quad (22)$$

$$C_{hshs'}=-(3/R^2)+(2R^2/9)[\exp(-R)] \cdot[1+(12/R^2)+(80/9R^3)+(80/9R^4)] -(1/27)[\exp(-2R)][10+(166/3R)+(83/3R^2)]. \quad (23)$$

THE JOURNAL OF CHEMICAL PHYSICS VOLUME 32, NUMBER 2 FEBRUARY, 1960

Threshold Law for the Probability of Excitation by Electron Impact

F. H. DORMAN, J. D. MORRISON, AND A. J. C. NICHOLSON

Division of Chemical Physics, Chemical Research Laboratories, Commonwealth Scientific and Industrial Research Organization, Melbourne, Australia

(Received August 27, 1959)

The threshold law for processes of excitation is difficult to measure directly and lack of experimental evidence has prevented a choice being made between different theoretical treatments. The ionization efficiency curves for the ion-pair processes, I^+ from I_2, O^+ from O_2, and C^+ from CO, and for what is here claimed to be auto-ionization in N_2^+ and O_2^+ have been measured. It is shown that these curves measure excitation probabilities and that the threshold law is in all cases a step function of the energy. The implications of this with regard to the assignment of dissociation products and the measurement of appearance potentials are discussed.

THIS paper deals with the class of reactions in which an atom or a molecule absorbs energy from an electron beam and is excited to a higher neutral electronic state. Its aim is to establish the threshold law for the probability of excitation, i.e., the variation of $p(E)$, the probability of excitation by an electron of energy E, with $(E-E_c)$, where E_c is the relevant excitation potential. For reactions leading to direct ionization, the experimental evidence is clear-cut and theory is in good agreement with experiment. For excitations the situation is still very confusing. Experimentally this arises because the presence of excitation can be detected only by relatively indirect means. Several theoretical treatments of the problem have been published but experimental data to test these theories have been lacking.

Excitation processes have been studied by Massey and his collaborators.[1] They point out that the probability of excitation will be different for different transitions depending on whether angular momentum is transferred from the bombarding electron during impact or not. Considerations such as this are undoubtedly important in determining the over-all shape of the probability curves over a range of hundreds of electron volts, but the assumptions made in these calculations are not considered to be valid in the nieghborhood of the threshold, which is the region of immediate interest.

The most fruitful suggestions have been those of Wigner[2] and Wannier.[3] Wigner discussing two-particle collision reactions generally, considered that the probability of a given reaction near threshold depends solely on the ability of the collision complex to dissociate, this depending on the long range interaction of the dissociating particles and not on the nature of the transition. Wannier extended this concept specifically to the case of direct ionization by electron impact, where the dissociating particles separate in a coulomb field. He postulated that the way in which the excess energy was carried off after the reaction determines the threshold law. Conservation of momentum requires that almost all the excess energy be carried away by the electrons. With two electrons leaving the collision complex (single ionization) the total energy of the electrons is determined, and one degree of freedom remains. Thus $p(E)$ is a linear function of $(E-E_c)$. With three electrons (double ionization) there are two degrees of freedom, hence $p(E) \propto (E-E_c)^2$ and so on. It is generally accepted that single ionization follows a linear law, and it has been shown by the present authors that this hypothesis is valid for n-fold ionization where $n=2$, 3, and 4.[4,5]

Extension of this hypothesis to single ionization by photon impact would predict a step-function dependence on the energy as do the calculations of Geltman[6] and this seems to be borne out by the data.[7,8] It has been proposed by Morrison[9] that the hypothesis is of more general applicability and that the threshold law is determined only by the number of independent electrons leaving the collision complex. The force field operating, be it simple coulomb, or induced electron-dipole, is of secondary importance. If this is correct, the three kinds of process, exemplified by

$$NO+h\nu \rightarrow NO^+ + e. \quad (1)$$

$$O_2+e \rightarrow O_2^* + e, \quad (2)$$

$$O^- + h\nu \rightarrow O + e, \quad (3)$$

in which one electron leaves the collision complex will all have the same threshold law, namely a step-function.

On the other hand, recent calculations by Geltman[10,11] give $p(E)$ for excitation proportional to $E(E-E_c)^{\frac{1}{2}}$

[1] H. S. W. Massey and E. H. S. Burhop, *Electronic and Ionic Impact Phenomena* (Clarendon Press, Oxford, 1952), pp. 30–186.
[2] E. P. Wigner, Phys. Rev. **73**, 1002 (1948).
[3] G. H. Wannier, Phys. Rev. **100**, 1180 (1956).
[4] J. D. Morrison and A. J. C. Nicholson, J. Chem. Phys. **31**, 1321 (1959).
[5] Dorman, Morrison, and Nicholson, J. Chem. Phys. **31**, 1335 (1959).
[6] S. Geltman, Phys. Rev. **102**, 171 (1956).
[7] K. Watanabe, J. Chem. Phys. **22**, 1564 (1954).
[8] Hurzeler, Inghram, and Morrison, J. Chem. Phys. **28**, 76 (1958).
[9] J. D. Morrison, J. Appl. Phys. **28**, 1409 (1957).
[10] Branscomb, Burch, Smith, and Geltman, Phys. Rev. **111**, 504 (1958).
[11] S. Geltman, Phys. Rev. **112**, 176 (1958).

where $x=1$ for atoms and heteronuclear molecules and 3 and 1 for homonuclear molecules according to whether they have gerade or ungerade symmetry. In its simplest form this expression is similar to the result obtained by Wigner for the separation of two particles with no forces between them for which he predicted $p(E) \propto (E-E_c)^{\frac{1}{2}}$.

Experimental evidence for discriminating between these hypotheses is scanty and conflicting. Measurements of the intensity of spectral lines excited by electron impact[1] cover a wide range of energies but there are few data for the region close to threshold. Brode,[12] reviewing this work, considers that the probability rises to a maximum at or very close to threshold and then decreases. Photodetachment measurements by Branscomb and his collaborators[10,13] on reactions of type (3) give results which it is claimed fit the threshold laws postulated by Geltman. The experiments of Schulz and Fox[14] and of Schulz[15] on the formation of metastable atoms in helium, produced apparently by a process of type (2) give a $p(E)$—$(E-E_c)$ curve that is linear for the first 0.2 ev above threshold but which then curves over and falls (to zero?) after about 1 ev. An ingenious attempt[16] has been made to account for the fact that these results seem to disagree with all theoretical predictions by suggesting that this reaction is not of type (2) but proceeds through an initial step of resonance capture which is later followed by dissociation into a metastable atom and an electron.

The experimental difficulty lies in the detection of small numbers of excited atoms. It does not seem to be generally realized that there are excitation processes which can be studied by the usual methods of positive-ion analysis, namely those in which the excited product decomposes spontaneously to give a positive ion. Two such processes are ion-pair production, I, and autoionization, II. These must proceed by the intermediate reactions:

$$\text{(I)} \qquad e+\text{AB}\rightarrow\text{AB}^*+e; \qquad \text{AB}^*\rightarrow\text{A}^+\text{+B}^-,$$

$$\text{(II)} \qquad e+\text{X}\rightarrow\text{X}^*+e; \qquad \text{X}^*\rightarrow\text{X}^+\text{+}e.$$

In each case the first reaction is a Franck-Condon transition taking about 10^{-16} sec and is dependent on the energy of the incident electron. In case I the second step is much slower, of the order of a vibration time, and in case II it is at least slower than the first reaction. In either case it will be independent of the electron energy. (The criterion for distinguishing an autoionization is that the spectral line corresponding to the transition is diffuse.[17] Since, therefore, the products of the first reaction will have separated well before the second reaction occurs, the ionization efficiency (I.E.) curve for the production of the ion should provide a measure of the probability law for the excitation process.

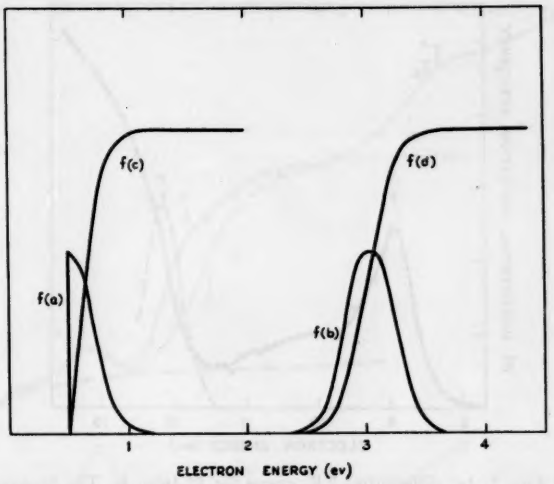

FIG. 1. Diagram showing the effect on a step-function threshold law of two kinds of electronic transition probability functions, f(a), f(b), for molecules. Here f(c) and f(d) are the contour integrals of a step function with f(a) and f(b).

The least energetic processes leading to ion-pair production will occur at an energy lower than that for production of the same positive ion by direct ionization ($\text{AB}+e\rightarrow\text{A}^+\text{+B}+2e$) by the electron affinity of B, usually >1 ev, so the two processes will not overlap. The discussion will be presented in terms of 1st differential I.E. curves since this brings out most clearly the differences between the various threshold laws. There are four possibilities: (i) If the threshold law for a given process of excitation involving sharply defined energy levels is a step function, the 1st differential I.E. curve will be a peak which is the reversed energy spread of the exciting electrons. (ii) If it is $p(E) \propto (E-E_c)^{\frac{1}{2}}$ [the variation of E in Geltman's expression can be neglected compared with that of $(E-E_c)$], then the 1st differential I.E. curve is still a peak but of a different shape. (iii) If it is $p(E) \propto (E-E_c)$, the 1st differential I.E. curve is a step. (iv) If $p(E)$ varies as a power of $(E-E_c)$ greater than 1, then the 1st differential I.E. curve rises continuously. In comparing threshold laws it may be difficult to distinguish between cases (i) and (ii) but the distinction between either of them and cases (iii) and (iv) should be unequivocal.

For molecules a complication arises but the argument outlined below shows that it does not seriously affect the interpretation of the results. For ion-pair production the exciting transition occurs from the ground state of the molecule to a part of the potential curve of the excited state which lies above a dissociation limit. Transitions are therefore possible over a range of energies with a probability given approximately by the reflection of the square of the ground state eigenfunction in the upper-state curve. Two cases can be distinguished with transition probabilities given by curves

[12] W. Brode, Revs. Modern Phys. **5**, 257 (1933).
[13] Burch, Smith, and Branscomb, Phys. Rev. **112**, 171 (1958).
[14] G. J. Schulz and R. E. Fox, Phys. Rev. **106**, 1179 (1957).
[15] G. J. Schulz, Phys. Rev. **112**, 150 (1958).
[16] E. Baranger and E. Gerjuoy, Phys. Rev. **106**, 1182 (1957).
[17] H. Beutler, Z. Physik **93**, 177 (1935).

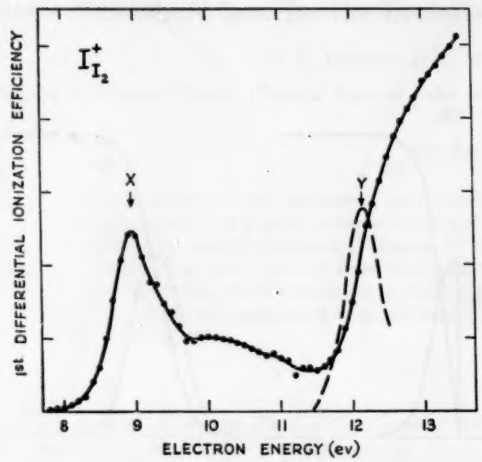

FIG. 2. 1st differential I.E. curve for I^+ from I_2. The broken curve is the 2nd differential I.E. curve.

f(a) and f(b) in Fig. 1; f(a) when the Franck-Condon region cuts the upper state curve both above and below a dissociation limit. f(b) when it cuts it only above the limit. For a mono-energetic electron beam the observed I.E. curves are the contour integrals of f(a) and f(b) with the appropriate threshold law. Taking $p(E)$ as a step function gives f(c) and f(d), respectively. For an electron beam with energy spread $m(U)$, the observed I.E. curves will be given by the contour integrals of f(c) and f(d) with $m(U)$. The result of these corrections will be that in cases (i) and (ii) the width of the peaks in the 1st differential I.E. curves will be greater for molecules than for atoms. For cases (iii) and (iv) the curves will not be greatly altered.

For auto-ionization essentially the same relationships hold. Interpretation is more difficult in that auto-ionization processes are necessarily superposed on direct ionization curves.

So far the I.E. curve has been discussed as if it resulted from one isolated process. In general it represents the sum of several processes which are assumed to be independent of each other. For a molecular ion, as the electron energy increases, auto-ionization can occur at energies corresponding to suitable excited states of the molecule and additional ionization processes can occur which lead to the formation of excited states of the molecular ion. For a fragment ion, the process of lowest energy is the production of an ion-pair, the next is of a ground state ion and a ground state neutral fragment and thereafter further processes occur in which either the ion or the neutral fragment are excited. Other ion-pair processes can occur in which the positive ion is formed in an excited state. In favorable cases these different processes can be completely resolved and it will be shown that even when resolution is not complete the shape of the I.E. curve can reveal that more than one process is occurring and give some indication of their type and appearance potential.

EXPERIMENTAL METHODS AND RESULTS

A study has been made of what is indisputably ion-pair production from I_2, O_2, and CO and of what is believed to be auto-ionization in N_2^+ and O_2^+. The experimental methods have been described previously.[5] The ion-repeller electrodes were held at +1.5v with respect to the ion chamber, this giving a reasonable compromise between loss of sensitivity and the broadening of the electron energy spread caused by the repeller field. The 1st differential I.E. curve, $\Delta I/\Delta V$ *vs* V, was measured directly at intervals of 0.1v, ΔV being 0.1v. In all figures the I.E. ordinates are in arbitrary units. An I.E. curve for Ne^+ was measured under standard conditions at various times during the experiments and the 2nd differential of this, reversed on the energy scale, was taken as representing the energy spread of the ionizing electron beam. In fact the energy spread measured in this way is about 0.15 ev broader than the true spread. 0.1 ev of this is contributed by the finite differential (this applies to all peaks measured). The rest is due to the fact that the Ne^+ peak is the sum of two processes.

ION-PAIR PROCESSES

I^+ *from* I_2.—It is known from photo-ionization measurements[18] that the first appearance of I^+ ions from I_2 is due to the process

$$e+I_2 \rightarrow I_2^* + e; \qquad I_2^* \rightarrow I^+ + I^-, \tag{4}$$

and that the ions carry little kinetic energy. Figure 2 shows that this process gives a peak while a second process gives the 1st differential I.E. curve characteristic of direct single ionization. The second process is

$$e+I_2 \rightarrow I^+ + I + 2e. \tag{5}$$

The energy difference between these processes is $EA(\mathrm{I})$, the electron affinity of the iodine atom. If the hypothesis that the threshold law for excitation is a step-function is correct, this difference will be the distance between the peak maximum X and the steepest part Y of the curve for the direct ionization process (i.e., the peak in the 2nd differential of this part of the I.E. curve).* The average for 3 curves like those in Fig. 2 gave $EA(\mathrm{I}) = 3.0_5$ ev. With repeller voltages of 0.5 and 8.0 v values of 3.2 and 2.9 ev, respectively, were obtained indicating that the repeller field introduces a small error. This value for $EA(\mathrm{I})$ may be compared with Pritchard's "best" value of 3.27 ± 0.07 ev.[19] The difference may be due to the experimental scatter of our results or to the ion carrying off a small amount of kinetic energy. There is some indication of

[18] Hurzeler, Inghram, and Morrison (to be published).

* All results in this paper are treated in this manner and the agreement found with independently obtained data constitutes the test of the hypothesis.

[19] H. O. Pritchard, Chem. Revs. **52**, 529 (1953).

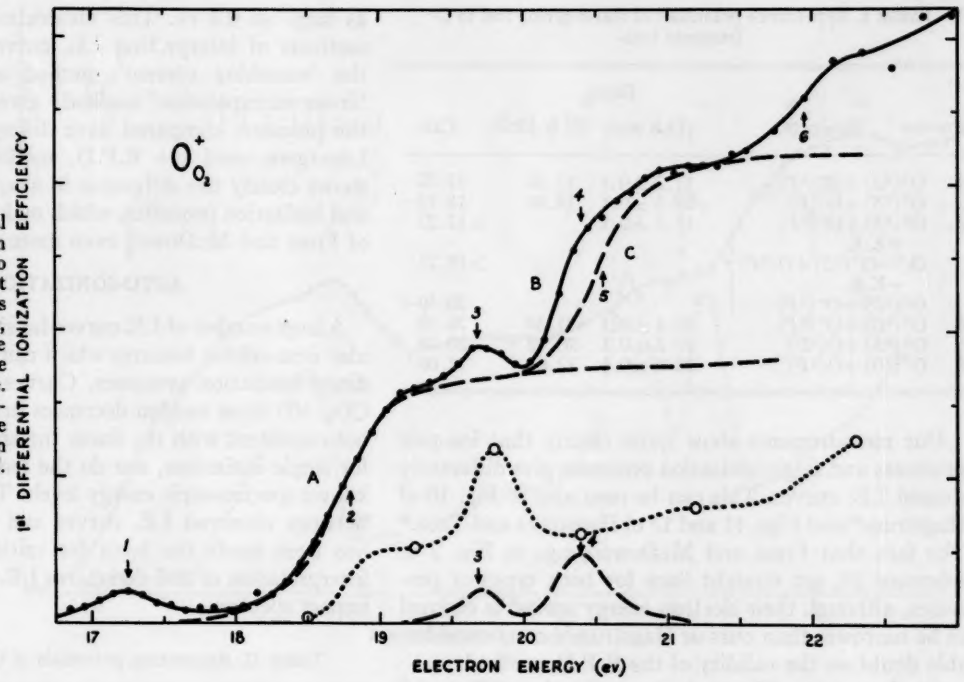

FIG. 3. 1st differential I.E. curve for O^+ from O_2. The contribution to the curve of direct single ionization is shown as a broken line, the residual of the curve is shown similarly at the bottom of the figure. The open circles connected by a dotted line are the photo-ionization results of Weissler *et al.*

fine structure in the energy region between the two processes (this was also observed in the photoionization experiments).[18] This is probably due to additional ion-pair processes, since the lowest state of I^+ is a triplet with the two higher components about 0.8 ev above the ground level.

O^+ *from* O_2.—Figure 3 shows the 1st differential I.E. curve for O^+ from O_2; the energy scale is calibrated by taking the vertical I.P. of O_2 as 12.2 ev. The curve consists of an initial peak followed by rounded steps and another peak. The first step at A, closely resembles the 1st differential curve for Ne^+ (shown dashed on the figure) indicating that it is due to a direct ionization process with the ions formed having little kinetic energy. The rise at the onset of the second step at B is much steeper than can possibly be accounted for in terms of a direct ionization process alone. The dashed curve at C represents the contribution of a direct ionization process and when this is subtracted from the full curve two peaks remain (shown dashed at the bottom of the figure). A third step is also shown and the steepest points of these ionization processes are marked with arrows 2, 5, and 6 at 18.8, 20.5$_5$, and 21.9$_5$ ev.

It is known from the work of Hagstrum[20] and Thorburn[21] that there are ion-pair processes at ~17 and 20.5 ev, some ions being formed without kinetic energy and these correspond to our peaks 1 and 4. The peak 3 at 19.7 ev remains unassigned. Confirmation of its reality is given by the photo-ionization data of Weissler, Samson, Ogawa, and Cook[22] which have been inserted in our Fig. 3 (open circles and dotted line). Its shape suggests that it is an excitation process. If it is an ion-pair process it might correspond to the formation of O^+ and O^- from a repulsive state in which excess kinetic energy would be present. Alternatively, it could be due to auto-ionization to a state which later dissociates into O^+ and O. A third alternative is that an excited state of O^- exists, cf. Laidler and Gill[23] who tentatively suggest O^- (^4P) of excitation energy slightly less than 1.45 ev.

The energy values obtained (averages from 3 curves like Fig. 3) are assembled in Table I and compared with the energies calculated from the data $D(O_2)=5.115$ ev,[24] $I(O)=13.62$ ev,[25] $EA(O)=1.465$ ev,[10] $E[O(^1D)-O(^3P)]=1.97$ ev,[25] and $E[O^+(^2D)-O^+(^4S)]=3.32$[25] with the assignments shown. The results of Frost and McDowell,[26] who used the Retarding Potential Difference (R.P.D.) method of Fox, Hickam, Grove and Kjeldaas[27] are also quoted. Agreement is excellent for processes 1, 2, and 6 but Frost's and McDowell's assignments for processes 4 and 5 seem forced.

[20] H. D. Hagstrum, Revs. Modern Phys. **23**, 185 (1951); energy scale corrected J. Chem. Phys. **23**, 1178 (1955).
[21] R. Thorburn, Report of Conference on Applied Mass Spectroscopy, Institute of Petroleum, London (1955), p. 185.
[22] Weissler, Samson, Ogawa, and Cook, J. Opt. Soc. Am. **29**, 339 (1959).
[23] K. J. Laidler and E. K. Gill, Trans. Faraday Soc. **54**, 633 (1958).
[24] P. Brix and G. Herzberg, J. Chem. Phys. **21**, 2240 (1953).
[25] C. E. Moore, J. Natl. Bur. Standards Circ. 467 (1949).
[26] D. C. Frost and C. A. McDowell, J. Am. Chem. Soc. **80**, 6183 (1958).
[27] Fox, Hickam, Grove, and Kjeldaas, Jr., Rev. Sci. Instr. **26**, 1101 (1955).

TABLE I. Appearance potentials of states giving rise to O^+ fragment ions.

Process	Products	Exptl. This work	Exptl. F. & McD.	Calc.
1	$O^+(^4S)+O^-(^2P)$	17.2$_5$±0.1	17.30	17.27
2	$O^+(^4S)+O(^3P)$	18.8 ±0.1	18.99	18.73
3	$O^+(^4S)+O^-(^2P)$ +K.E.	19.7 ±0.1		>17.27
	$O_2^+ \rightarrow O^+(^4S)+O(^3P)$ +K.E.			>18.73
	$O^+(^2D)+O^-(^4P)$			20.59–?
4	$O^+(^2D)+O^-(^2P)$	20.4 ±0.1	21.30	20.59
5	$O^+(^4S)+O(^1D)$	20.5$_5$±0.1	20.42	20.70
6	$O^+(^2D)+O(^3P)$	22.0 ±0.1	22.03	22.06

Our measurements show quite clearly that ion-pair processes and single ionization processes give differently shaped I.E. curves. This can be seen also in Fig. 10 of Hagstrum[20] and Figs. 11 and 15 of Hagstrum and Tate.[28] The fact that Frost and McDowell, e.g., in Fig. 2 of reference 26, get straight lines for both types of processes, although their electron energy spread is claimed to be narrower than ours or Hagstrum's casts considerable doubt on the validity of the R.P.D. method.

C^+ *from* CO.—Figure 4 shows the 1st differential I.E. curve from C^+ from CO; the energy scale is calibrated by taking $I(\text{Ne})=21.6$ ev. Again it is known that the first process involves formation of an ion-pair without kinetic energy. Table II gives a comparison between the experimental appearance potentials (average from 5 curves like Fig. 4) with the values calculated using $D(\text{CO})=11.11$ ev,[29] $I(\text{C})=11.27$ ev[25] and $EA(\text{O})=1.465$.[10] It is noteworthy that our experimental value for process 2 fits nicely with $D(\text{CO})=11.11$ ev whereas Hagstrum[20] and Lagergren[30] both obtained 22.8 ev and considered that their experimental error could not be as large as 0.4 ev. This illustrates that conventional methods of interpreting I.E. curves (Hagstrum used the 'vanishing current' method and Lagergren the 'linear extrapolation' method) give false results when the processes compared have different threshold laws. Lagergren used the R.P.D. method and his Fig. 8 shows clearly the difference in shape between ion-pair and ionization processes, which makes the straight lines of Frost and McDowell even more surprising.

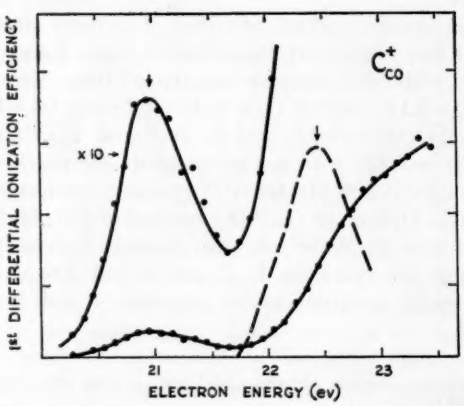

FIG. 4. 1st differential I.E. curve for C^+ from CO. The broken curve is the 2nd differential I.E. curve.

AUTO-IONIZATION

A large number of I.E. curves for singly charged molecular ions exhibit features which cannot be explained as direct ionization processes. Curves for Hg, N_2, C_2H_6, CO_2, NO show sudden decreases in gradient which are not consistent with the linear threshold law established for single ionization, nor do the features coincide with known spectroscopic energy levels. This poor agreement between observed I.E. curves and spectroscopic data has been made the basis for criticism of Morrison's interpretation of 2nd derivative I.E. curves as electron-impact spectra.

TABLE II. Appearance potentials of C^+ ions from CO.

Process	Products	Exptl.	Calc.
1	$C^+(^2P)+O^-(^2P)$	21.0±0.1	20.91
2	$C^+(^2P)+O(^3P)$	22.4±0.1	22.38

Hickam, Fox, and Kjeldaas[31] showed that when the linear parts of the I.E. curve for Kr^+ (due to direct ionization to the $^2P_{\frac{1}{2}}$ and $^2P_{\frac{3}{2}}$ states) are subtracted from the observed curve a residue remains which they attributed to auto-ionization of neutral levels lying between the ionic states cf. Beutler.[17] Similar phenomena were observed by Hickam[32] in the I.E. curves for Cd, Hg, and Sn. In this case, the residuals appeared to be fairly sharp peaks in the direct I.E. curves. Auto-ionization is believed to occur in molecules (O_2—Price and Collins,[33] N_2—Tanaka and Takamine[34]) where lines in the spectra in regions above the lowest ionization limit are found to be diffuse.

The observed 1st differential I.E. curves for O_2 and N_2 are shown in Figs. 5 and 6. In neither case can the curves be synthesised by any linear combination of direct ionization processes with curves of the type observed for Ne. At the top of the figures are marked the most prominent lines in the far UV spectra of these molecules, the diffuse lines being starred. If the threshold law for auto-ionization is a step function, peaks in the 1st differential I.E. curve should occur with their maxima at the positions of the starred lines. Our

[28] H. D. Hagstrum and J. T. Tate, Phys. Rev. **59**, 354 (1941).
[29] A. E. Douglas and C. K. Møller, Can. J. Phys. **33**, 125 (1955).
[30] C. R. Lagergren, Ph.D. thesis, University of Minnesota (1955).
[31] Fox, Hickam, and Kjeldaas, Phys. Rev. **89**, 555 (1953).
[32] W. M. Hickam, Phys. Rev. **95**, 703 (1954).
[33] W. C. Price and G. Collins, Phys. Rev. **48**, 714 (1935).
[34] Y. Tanaka and T. Takamine, Sci. Papers Inst. Phys. Chem. Research. (Tokyo) **39**, 427 (1941–2).

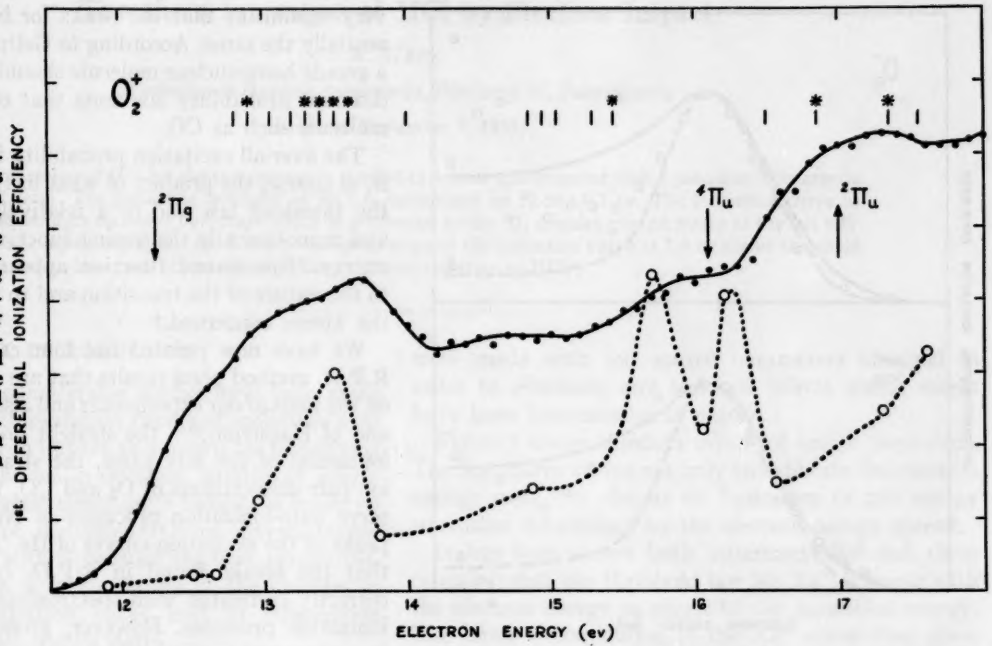

FIG. 5. 1st differential I.E. curves for O_2^+. The open circles connected by a dotted line are the photo-ionization results of Weissler *et al.* and the most intense lines in the far UV absorption spectrum are superposed on the figure. Diffuse lines are marked with an asterisk. Known ionization limits are shown with arrows.

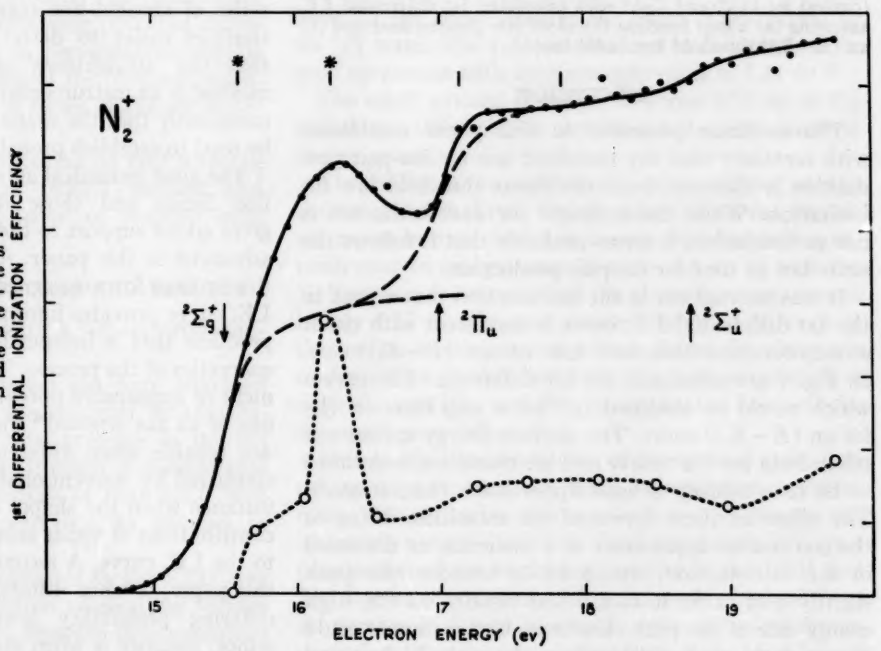

FIG. 6. 1st differential I.E. curve for N_2^+. The open circles connected by a dotted line are the photo-ionization results of Weissler *et al.* and the most intense lines in the far uv absorption spectrum are superposed on the figure. Diffuse lines are marked with an asterisk. Known ionization limits are shown with arrows.

data are not inconsistent with this interpretation. It also follows that there should be a 1:1 correspondence between the 1st differential I.E. curve for electron impact and the direct I.E. curve for photon impact. The photo-ionization results of Weissler *et al.*[22] have been inserted at the foot of Figs. 5 and 6. Unfortunately the intervals between their experimental points are wide but good agreement is found for the pronounced first peak in each curve. Agreement is not good for the two O_2^+ peaks at about 16 ev. The I.E. curve for N_2^+ obtained by Clarke[35] who used an electron-energy filter, shows a decrease in gradient which exactly corresponds to the feature in our data. On the other hand two R.P.D. studies[36,37] of N_2 did not detect this feature.

[35] E. M. Clarke, Can. J. Phys. **32**, 764 (1954).
[36] R. E. Fox and W. M. Hickam, J. Chem. Phys. **22**, 2059 (1954).
[37] D. C. Frost and C. A. McDowell, Proc. Roy. Soc. (London) **A232**, 227 (1955).

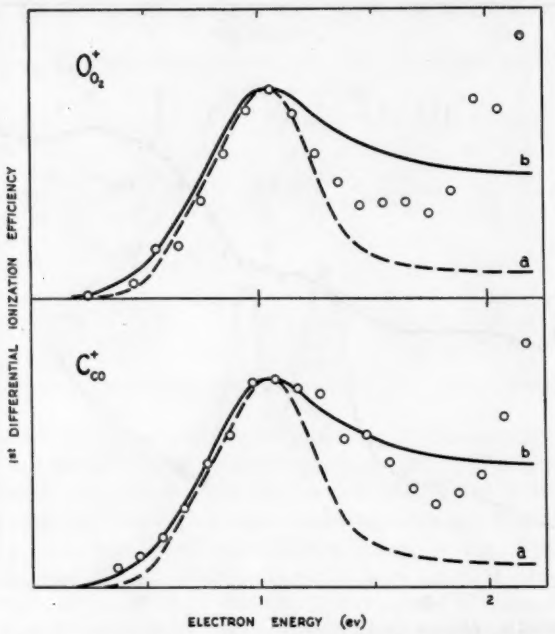

FIG. 7. Comparison of the experimental 1st differential I.E. (circles) for $O_{O_2}^+$ and C_{CO}^+ with calculated 1st differential I.E. assuming (a) a step function threshold law (broken line) and (b) an $(E-E_c)^{\frac{1}{2}}$ threshold law (solid line).

DISCUSSION

The evidence presented in this paper establishes with certainty that the threshold law for ion-pair production is different from the linear threshold law for ionization. While the evidence for auto-ionization is not so conclusive, it seems probable that it follows the same law as that for ion-pair production.

It was pointed out in the introduction that a peak in the 1st differential I.E. curve is consistent with either a step-function threshold law or an $(E-E_c)^{\frac{1}{2}}$ law. In Fig. 7 are calculated the 1st differential I.E. curves which would be obtained (a) for a step-function (b) for an $(E-E_c)^{\frac{1}{2}}$ curve. The electron energy spread was taken from our Ne^+ curve and the transition is assumed to be to a sharply defined upper state (i.e., atomic). The effect on these curves of the transitions being to the continuous upper state of a molecule, as discussed in the introduction, would be to broaden the peak slightly and cause it to fall less rapidly on the high energy side of the peak. Under no circumstances could it narrow the peak width or lower it on the high energy side. The figure shows the experimental points for $O^+_{O_2}$ and C^+_{CO} and it is seen that the experimental points on the high energy side of the peak lie above the curve for a step-function law as would be expected from the considerations outlined above. On the other hand, no obvious interpretation can be advanced which would raise these points to fit the $(E-E_c)^{\frac{1}{2}}$ curve. It is very significant that the peaks for both gases are essentially the same. According to Geltman's calculations a gerade homonuclear molecule should have a markedly different probability law from that of a heteronuclear molecule such as CO.

The over-all excitation probability for a given process is, of course, the product of what has here been termed the threshold law and of a relatively slowly varying and monotonically decreasing function of the electron energy. This second function appears to be sensitive to the nature of the transition and to the complexity of the atoms concerned.†

We have now pointed out four cases in which the R.P.D. method gives results that are quite inexplicable on the basis of our experiments and also those of Clarke[35] and of Hagstrum;[20,27] the straight lines for the double ionization of the rare gases, the straight lines for the ion-pair dissociations of O_2 and CO, the failure to observe auto-ionization processes in N_2 and O_2 and the peaks in the excitation curves of He. There is no doubt that the breaks found in R.P.D. curves have been correctly correlated with spectroscopically determined ionization processes. However, given a discontinuity in a curve any method which makes the curve into a series of straight-line segments will make the discontinuities easier to detect. A tentative suggestion is that the 'straightness' of the lines in the R.P.D. method is an instrumental effect. It can be stated more confidently that the shape of R.P.D. curves should not be used to establish probability laws.‡

The good numerical agreement between our dissociation limits and those determined spectroscopically gives added support to the method of treating the data advanced in this paper. An important consequence of this is that for unassigned processes the shape of the I.E. curve provides information about the dissociation products that is independent of that provided by the energetics of the process. The implications for measurement of appearance potentials are obvious. Previously, one of us has stressed[38] that appearance potentials are not reliable when differently shaped I.E. curves are compared by conventional methods; in that particular instance when the shapes differed because of different contributions of upper energy levels of the positive ion to the I.E. curve. A second instance, that discussed in this paper, is when differences in shape are caused by differing probability laws. A third, comparatively minor, instance is when different shapes are caused by differences in the eigenfunction products as shown in Fig. 1.

† Similar considerations apply to ionization probabilities; c.f. J. D. Morrison, Revs. Pure Appl. Chem. (Australia) **5**, 22 (1955).

‡ Except for the linear first ionization of He where the line extends over 8 ev. In most other cases the "lines" are very short.

[38] A. J. C. Nicholson, J. Chem. Phys. **29**, 1312 (1958).

Threshold Ionization of HCl by Electron Impact

R. E. Fox

Westinghouse Research Laboratories, Pittsburgh 35, Pennsylvania

(Received September 9, 1959)

The ionization of HCl by electron impact is studied in a mass spectrometer with a pseudomonoenergetic electron beam. The ionization potential of HCl is determined as 12.56±0.1 ev. The ionization curve at threshold exhibits excessive curvature which is attributed to the $^2\Pi_i$ doublet ground states of the ion estimated to be separated by 0.3 ev. A sharp change in slope of the ionization curve at 1.6 ev above threshold is attributed to the onset of ionization of the $A\ ^2\Sigma^+$ excited state of HCl^+.

I. INTRODUCTION

In recent years considerable studies have been made of the shapes of ionization curves of molecules near threshold by electron impact as a means for identifying energy states of the ion in question. Studies of ionization by monoenergetic electrons[1–3] have been made on a large number of molecules.[4] Other investigations[5] have been made with a broader electron energy distribution in which a careful study of the changes in shape of the ionization curve lead to information concerning the ionic energy states.

Frost and McDowell[6] have recently reported studies of HF^+ and HI^+, using the retarding potential difference method[7] for obtaining a pseudomonoenergetic electron beam with a discussion of the observed structure in the ionization curves in terms of the electronic energy states of these ions.

This paper reports an investigation on HCl with the retarding potential difference (RPD) method and discussion of these data in terms of possible ionic energy states.

II. EXPERIMENTAL PROCEDURES AND RESULTS

The results were obtained with a 90° sectored magnetic field mass spectrometer.

Anhydrous HCl gas and xenon gas were admitted simultaneously to the mass spectrometer in approximately equal amounts to a total pressure in the ion source of about 10^{-5} mm Hg. Initially a considerable shift in the appearance potentials of both HCl^+ and Xe^+ was observed, due presumably, to changes in surface potentials.

The difference ion current obtained by the RPD[7] was measured as a function of electron accelerating voltage for both HCl^+ and Xe^+. Five separate determinations were made with ion source parameters changed in order to eliminate any spurious effects which might have been instrumental in nature.

Figure 1 shows the data taken for one of these runs. The Xe^+ curve serves not only to calibrate the electron energy scale but also as an indication of the energy resolution determined by the electron energy spread.

It has been shown both experimentally[8] and theoretically[9] that the threshold law for Xe^+ is linear with the electron energy in excess of the ionization energy. The linear extrapolation of the Xe^+ curve then gives the onset of ionization to the $^2P_{\frac{1}{2}}$ state while the first break in the curve denotes the onset of ionization to the $^2P_{\frac{3}{2}}$ state. The 1.33 ev obtained in this curve is in good agreement with spectroscopic value of 1.31 ev.[10]

The small amount of tailing of about 0.15 ev at the ionization threshold is attributed to the electron energy spread.

The HCl^+ shows considerably more tailing at the ionization onset. From Fig. 2, which shows the threshold region in more detail, it is seen that this tailing extends over an energy range of about 0.6 ev. If from the Xe^+ curve one assumes that the electron energy spread is only 0.15 ev one must assume two energy levels in this region which are unresolved. From the electronic configuration of this molecule, the ground state is a doublet with $^2\Pi_{\frac{1}{2}}$ and $^2\Pi_{\frac{3}{2}}$ components. This will be discussed more fully below.

Due to the doublet nature of the ground state it is not appropriate to use a linear extrapolation to determine the ionization potential. For this reason the ionization potential of HCl^+ has been determined by a comparison of the vanishing currents of the HCl^+ and Xe^+ curves. A value of 12.56±0.1 ev is obtained from an average of 5 runs where the error is the maximum deviation. This is in good agreement with the values of 12.53±0.09 ev and 12.78±0.03 ev obtained by Morrison,[11] using the linear extrapolation and critical slope methods, respectively. This does not agree, however, with the value of 12.90 ev obtained spectroscopically.[12]

[1] R. E. Fox and W. M. Hickam, J. Chem. Phys. **22**, 2059 (1954).
[2] E. M. Clarke, Can. J. Phys. **32**, 764 (1954).
[3] D. C. Frost and C. A. McDowell, Proc. Roy. Soc. **A202**, 155 (1955).
[4] The use of the pseudomonoenergetic electron beam obtained by the retarding potential difference method has been extended to the study of some 30 different molecules by 11 different investigators.
[5] J. D. Morrison, J. Chem. Phys. **21**, 1767 (1953).
[6] D. C. Frost and C. A. McDowell, Can. J. Chem. **36**, 39 (1958).
[7] Fox, Hickam, Grove, and Kjeldaas, Rev. Sci. Instr. **26**, 1101 (1955).
[8] Fox, Hickam, and Kjeldaas, Phys. Rev. **89**, 555 (1953).
[9] S. Geltman, Phys. Rev. **102**, 171 (1956).
[10] C. E. Moore, "Atomic energy levels," National Bureau of Standards Circular 467, U. S. Government Printing Office, Washington, D. C. (1952).
[11] J. D. Morrison, J. Chem. Phys. **19**, 1305 (1951).
[12] W. C. Price, Chem. Revs. **41**, 257 (1947).

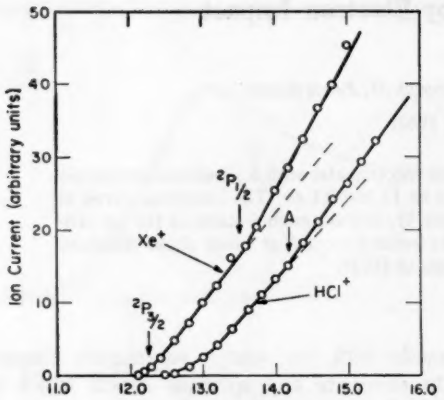

FIG. 1. The formation of Xe^+ and HCl^+ as a function of electron energy (uncorrected). The Xe^+ curve is used to establish the energy scale by the vanishing current as well as to ascertain the electron energy spread.

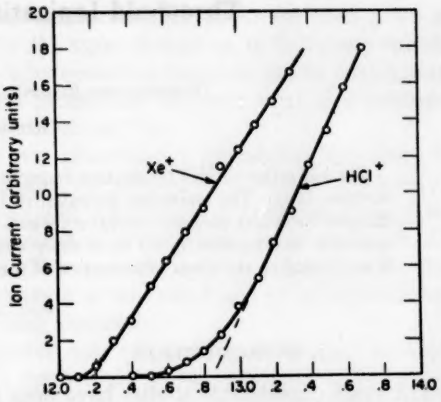

FIG. 2. The formation of Xe^+ and HCl^+ by electron impact near the threshold.

There is a pronounced break in the HCl^+ curve at A (Fig. 1) which is attributed to the onset of ionization to the $A\ ^2\Sigma^+$ state. An average of three determinations yields a value of 1.6±0.2 ev.

III. DISCUSSION

The electronic configurations for the halogen hydrides lead to a $X\ ^2\Pi_{\frac{3}{2},\frac{1}{2}}$ ground state for the molecular ions. Frost and McDowell[6] were not able to observe any unusually large amount of tailing of the HF^+ curve which could be attributed to the presence of this doublet state. From an estimate of their electron energy spread based on their data, one concludes that the doublet separation is less than 0.2 ev. For HI^+, however, they were able to resolve these two states obtaining a value of 0.7 ev for the energy separation.

From the curves of Fig. 2 the total tailing of the HCl^+ is about 0.6 ev. If we assume that 0.3 ev can be accounted for by a 0.15-ev electron energy spread then we obtain a value of about 0.3 ev for the $^2\Pi_{\frac{1}{2}}-{}^2\Pi_{\frac{3}{2}}$ separation in HCl^+.

HCl as well as the other halogen hydrides is an atomic molecule[13] and hence we might expect a correlation of these molecules with the corresponding rare gases. We note that in two respects the correlation is quite remarkable: (1) The ionization potentials[10] of the rare gases decrease progressively from a value of 21.56 for Ne^+ to 12.13 for Xe^+, while the ionization potentials of the halogen halides decrease progressively from a value of 15.77 ev[6] for HF^+ to 10.44 ev for HI^+; (2) The energy separation of the two $^2\Pi_i$ components increases progressively for the rare gases from 0.10 ev for Ne^+ to 1.3 ev for Xe^+.

A calculation of the relative transition probabilities was made for transitions from the ground state of the molecule to the ground state ($X\ ^2\Pi_{\frac{3}{2}}$) of HCl^+ and to the first vibrational state of the $X\ ^2\Pi_{\frac{3}{2}}$ state of HCl^+. The calculations were made using a simple harmonic oscillator as a model and the values of the overlap integrals for the two cases indicated that the 0→0 transition was about 15 times more probable than the 0→1 transition. It therefore appears that the excessive tailing is due to the $^2\Pi_i$ doublet rather than to excitation of vibrational states of the HCl^+ ion.

The break at 1.6 ev above the $X\ ^2\Pi_{\frac{3}{2}}$ threshold is, therefore, attributed to the onset of ionization to the $A\ ^2\Sigma^+$ excited state of HCl^+. This value is consistent with the values of 1.14 ev and 2.83 ev for the similar states[6] in HF^+ and HI^+, respectively, if one assumes that the energy separation of the $X\ ^2\Pi_{\frac{3}{2}}-A\ ^2\Sigma^+$ states should increase progressively. It is not in agreement with the spectroscopic value of 3.48 ev obtained by Norling.[14]

An examination of the data presented by Morrison for HCl indicates structure which suggests a second process about 1.5 ev above the threshold.[15]

The $A\ ^2\Sigma^+$ state for the halogen hydrides results from the removal of an electron from a $2p\ \sigma$ type orbital and thus one might expect the binding energy of the σ electron to vary as the dissociation energy of the H—X bond. Since the dissociation energy decreases progressively for these molecules (5.83 ev for HF,[16] 4.43 for HCl,[13] 3.75 for HBr,[13] and 3.06 for HI[13]) one might expect the value of the $X\ ^2\Pi_{\frac{3}{2}}\rightarrow A\ ^2\Sigma$ energy separation to vary in a progressive manner. If this is so then the 1.6 value for the $X\ ^2\Pi\rightarrow A\ ^2\Sigma$ separation is consistent whereas the 3.48-ev value is not.

[13] G. Herzberg, *Spectra of Diatomic Molecules* (D. Van Nostrand Company, Inc., New York, 1950).

[14] F. Norling, Z. Physik **104**, 638 (1936).

[15] A private communication from Morrison confirms that his data indicate a second ionization process at about 1.5 ev above threshold.

[16] A. Hurley, Proc. Phys. Soc. (London) **A69**, 301 (1956).

THE JOURNAL OF CHEMICAL PHYSICS VOLUME 32, NUMBER 2 FEBRUARY, 1960

NMR Study in Rochelle Salt

R. Blinc and A. Prelesnik

J. Stefan Institute, Ljubljana, Yugoslavia

(Received August 11, 1959)

The angular dependence of the proton magnetic resonance absorption of a Rochelle salt single crystal has been measured. The experimental second moments are compared with the theoretical curves, as calculated for the structures proposed so far. Lösche's model was found to reproduce the qualitative form of the angular dependence, whereas the other structures gave no agreement at all.

The occurrence of transitions in the proton magnetic absorption line widths at +24°C and below −20°C demonstrates that the assumption of protonic motion, upon which the dynamic theories of ferroelectricity in Rochelle salt are based, is essentially correct.

ALTHOUGH the structure of Rochelle salt has been the subject of several investigations, there is relatively little known about the positions of the water molecule hydrogens, which were claimed[1] to be responsible for the occurrence of the ferroelectric transitions. Several structures have been proposed by various authors, who used different methods of investigation, but their results are in poor agreement. The single crystal neutron diffraction study,[2] which has been undertaken by Pepinsky *et al.* is not yet completed. The preliminary results, published by this group so far, differ from the second set of the results obtained by Baker and Webber,[3] who used polarized IR technique, only in the location of one H atom. However, the results of a recently published proton resonance experiment, made by Lösche,[4] are in disagreement with either of the aforementioned studies. In this experiment, Pake's method[5] of deriving the proton-proton separation and the orientation of the interprotonic vector of the water molecules from the doublet structure of the absorption line was used. But in the case of Rochelle salt there are 16 water molecules per unit cell, and the question arises whether the fine structure is resolved well enough to allow a unique separation of the absorption line into doublets. Therefore it seemed worth while to undertake a new NMR single crystal study, using Van Vleck's[6] second moments method, which is known to be better suited for the study of complicated systems.

The direct "trial and error" calculation of the protonic coordinates from the second moment data is not yet completed. Here we wish to report some results which should check the structures proposed so far and elucidate the particularly interesting question about the motion of the protons in the nonferroelectric and ferroelectric phases.

In Fig. 1 the measured second moments are plotted as a function of the orientation of the crystal in the magnetic field, and are compared with the theoretical curves. The experimental data, given in Fig. 1, were obtained at room temperature. The liquid nitrogen temperature data, which are given in Fig. 2, disclosed no significant difference in the angular dependence, but are larger by the amount of ≈ 5 gauss^2.

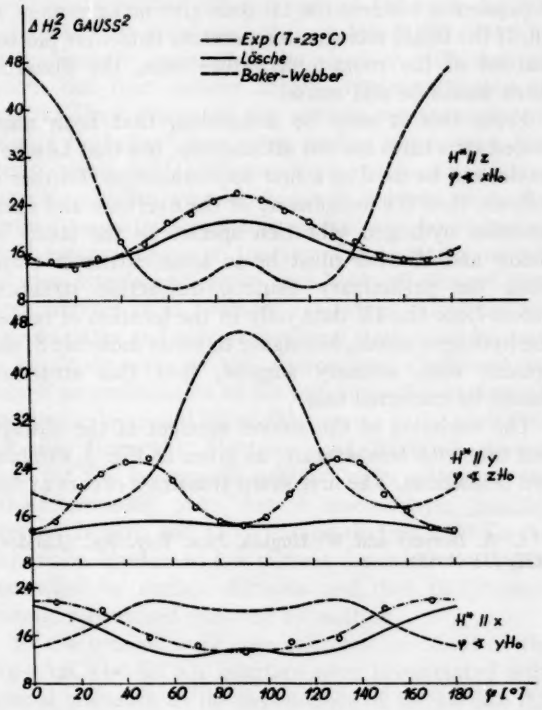

FIG. 1. Comparison of the experimental and theoretical second moment's angular dependences as calculated for the structures proposed by Lösche, and Baker and Webber (H_0=steady field, H^x=rf field).

Theoretical values of the second moments have been calculated for the structures proposed by Lösche, and Baker and Webber. In the latter case two possible structures were proposed, but only set 2 is considered in Fig. 1. Set 1 could be definitely excluded since the interprotonic distance of water molecule 10—following

[1] W. P. Mason, Phys. Rev. **72**, 1 (1947).
[2] Shirane, Jona, and Pepinsky, Proc. Inst. Radio Engrs. **43**, 1738 (1955).
[3] A. N. Baker and D. S. Webber, J. Chem. Phys. **27**, 689 (1957).
[4] A. Lösche, Izv. Akad. Nauk SSSR **21**, 1064 (1957).
[5] G. E. Pake, J. Chem. Phys. **16**, 327 (1948).
[6] J. H. Van Vleck, Phys. Rev. **74**, 1168 (1948).

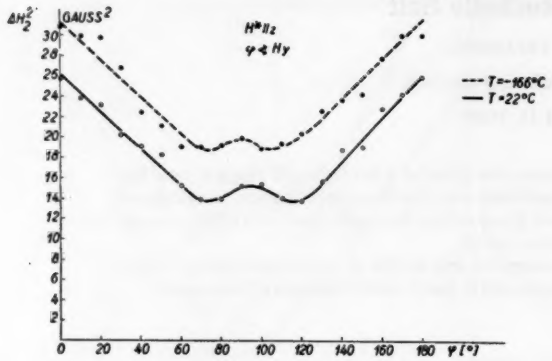

FIG. 2. Comparison of the angular dependence of the second moments, measured at room and at liquid nitrogen temperatures.

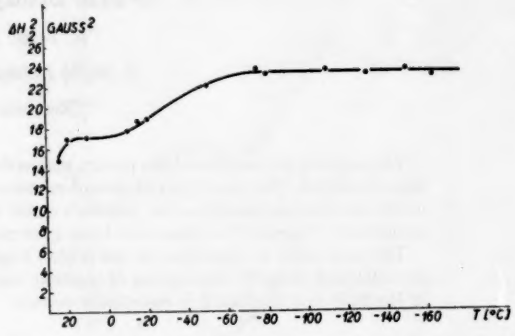

FIG. 3. The second moment of the proton magnetic resonance absorption for a particular crystal orientation plotted against temperature.

the nomenclature of Beevers and Hughes[7]—should be 1.13 A, which would result in a second moment many times as large as observed.

As can be seen from Fig. 1, Lösche's model reproduces at least the qualitative form of the angular dependence, whereas the IR data give no agreement at all. If the liquid nitrogen temperature data were plotted instead of the room-temperature ones, the disagreement would be still worse.

From this it may be concluded, that both mentioned structures are not satisfactory, but that Lösche's model can be used as a first approximation. Further it follows, that the assignment of the overtone and combination hydrogen vibration spectra in the study of Baker and Webber must be to some extent in error. Since the preliminary neutron diffraction structure differs from the IR data only in the location of one of the hydrogen atoms, belonging to water molecule 8, the present data strongly suggest, that this structure should be corrected too.

The variation of the second moment of the absorption line with temperature, as given in Fig. 3, exhibits two transitions. The first sharp transition occurs at the upper Curie point. On going to the polarized phase, the second moment increases from ~15 to ~17 gauss², demonstrating the beginning of "freezing in" of the protonic motion. Below the lower Curie point, in the region between −20 and −60°C, a second transition occurs, after which the line width becomes constant indicating the complete "freezing in" of the protons. In this connection it is interesting to note that below −60°C the absorption signal becomes unobservably small due to saturation. In order to make the investigation possible also in this region, the spin lattice relaxation time has been artificially shortened by irradiating the samples with a Co^{60} source. The dose was $3–5.10^6$ r.

From the preceding data we may conclude that the assumption of the occurrence of protonic motion in Rochelle salt, upon which the dynamic theories of ferroelectricity are based, is essentially correct. Moreover, the present data prove that the protons are moving to some extent also in the ferroelectric phase.

ACKNOWLEDGMENTS

The authors are grateful to Dr. S. Detoni for the gift of the Rochelle salt single crystal, to Mr. Hribar for the irradiation of the samples, and to Professor I. Kuscer, who read the manuscript critically.

[7] C. A. Beevers and W. Hughes, Proc. Roy. Soc. (London) **A177**, 251 (1941).

THE JOURNAL OF CHEMICAL PHYSICS VOLUME 32, NUMBER 2 FEBRUARY, 1960

Kinetics of the Deposition and Dissolution of Silver

A. R. DESPIC* AND J. O'M. BOCKRIS

John Harrison Laboratory of Chemistry, University of Pennsylvania, Philadelphia 4, Pennsylvania

(Received April 27, 1959)

Galvanostatic measurements, made on spherical silver electrodes in highly purified aqueous acid solutions of silver perchlorate at current densities up to 10 amp cm^{-2}, gave overpotential as a function of time and Faradaic current density at constant total current. Variables were total current density, concentration of silver ions and state of the electrode surface.

The theory of the surface diffusion kinetics was developed to encompass high current density regions and the surface adion concentration ($c_{ad}{}^{0}$) evaluated.

A theoretical analysis of the steady state of surface diffusion control of the metal-ion exchange reaction shows that the current is distributed nonuniformly between growing sites, with constant potential over the electrode surface.

An equation previously developed by Rojter, Juza, and Polujan has been modified and shown to be applicable to galvanostatic transients when the transfer reaction is rate controlling. The symmetry factor β, of electrode kinetics, is shown to be potential dependent, and, in systems of sufficiently high i_0 values, to tend to zero at high overpotential. This results in a limiting current density for a transfer controlled process. The tendency towards such a current was observed and shown to be quantitatively consistent with the discussion of β.

I. INTRODUCTION

THE mechanism of metal disposition has often, and that of metal dissolution hardly ever, been discussed.[1-6] Until recently, specific conclusions concerning the path- and rate-determining step in these reactions had not been drawn. This was largely due to difficulties in technique.

During the last few years, progress in elucidating the mechanism of the deposition and dissolution of monolayers has been significant. Gerischer and Vielstich[7] reported evidence that, near to equilibrium, the exchange between metal and solution for Ag in aqueous $AgClO_4$—$HClO_4$ was controlled by "Gitteraufbau" (i.e., lattice formation), while Lorenz[8,9] discussed the theory of the steady-state kinetics of these processes with reference to surface diffusion. He showed that the concept[5] of resistance overpotential at the growth sites (which gives rise to a linear current density (i)-overpotential (η) relation over large η ranges), is untenable. He concluded that in cadmium deposition the rate-determining reaction is $Cd^{++}+2e_0^- \rightarrow Cd$. Mehl and Bockris[10] showed how analysis of galvanostatic transients could give information on mechanism, and formulated a kinetic theory of the $i-\eta$ relation for transfer and surface diffusion control. On Ag in $AgClO_4$—$HClO_4$, they concluded that at low i the rate was predominantly controlled by surface diffusion of adions but that transfer became rate-determining at high i. They evaluated the surface concentration of adions. Gerischer[11] later drew similar conclusions, but found significantly different parameters for an apparently similar system. Lorenz[12] showed that the surface concentration of adions could also be evaluated from measurements of the impedance of the metal-solution interface. Conway and Bockris[13] showed how large differences in heats of activation calculated for various paths and rate-determining steps could be used to eliminate some of the alternatives. Christov[14] reported an examination of the tunneling of *ions* through the double layer and found this process to be negligible (cf. also Gurney[15]). Mattsson and Bockris[16] showed that for Cu in aqueous acidic $CuSO_4$ solutions, the rate-determining step was a one-electron transfer process. Bockris and Enyo[17] found that on solid Ga the deposition kinetics at low current densities was largely controlled by surface diffusion and that this characteristic was indeed removed by melting.

In the present work, the electrode processes at the Ag—$AgClO_4$—$HClO_4$ interface were investigated with special reference to the dependence of the surface diffusion of adions upon conditions of the electrode surface and the singular characteristic of the rate-determining transfer mechanism at very high rates.

* On leave of absence from the University of Belgrade, Belgrade, Yugoslavia.

[1] M. Le Blanc, Abhandl. Bunsenges. Halle (1910).
[2] N. Kohlschutter, Trans. Electrochem. Soc. **45**, 229 (1924).
[3] H. Brandes, Z. physik. Chem. (Leipzig) **A142**, 97, 103 (1929).
[4] M. Volmer, *Das Elektrolytishe Kristallwachstum* (Herrman et Cie., Paris, 1934).
[5] T. Erdey-Gruz and M. Volmer, Z. physik. Chem. (Leipzig) **A157**, 165 (1931).
[6] Rojter, Polujan, and Juza, Zhur. Fiz. Khim. **13**, 605, 805 (1939); Acta Physicochim. U.R.S.S. **10**, 389 (1939).
[7] H. Gerischer and W. Vielstich, Compt. rend. réunion 4th Meeting Comité intern. thermodynam. de cinét. electrochim. (1952); Z. Elektrochem. **56**, 380 (1952); H. Gerischer, Z. physik. Chem. (Leipzig) **201**, 55 (1952).
[8] W. Lorenz, Z. Naturforsch. **7a**, 750 (1952); Z. physik Chem. (Leipzig) **202**, 275 (1953); Z. Elektrochem. **57**, 382 (1953); Z. Naturforsch. **9a**, 716 (1954).
[9] W. Lorenz, Naturwissenschaften **22**, 578 (1953); Z. Elektrochem. **58**, 912 (1954).
[10] W. Mehl and J. O'M. Bockris, J. Chem. Phys. **27**, 818 (1957).
[11] H. Gerischer, Z. Elektrochem. **62**, 256 (1958).
[12] W. Lorenz, Z. physik. Chem. (Leipzig) **17**, 136 (1958).
[13] B. E. Conway and J. O'M. Bockris, Proc. Roy. Soc. (London) **A248**, 394 (1958).
[14] St. G. Christov, Z. Elektrochem. **62**, 567 (1958).
[15] R. Gurney, Proc. Roy. Soc. (London) **A134**, 137 (1931).
[16] E. Mattsson and J. O'M. Bockris, Trans. Faraday Soc. **55**, 1586 (1959).
[17] J. O'M. Bockris and M. Enyo, unpublished (cf. M. Enyo's thesis, University of Pennsylvania, 1960).

II. EXPERIMENTAL

1. Preparation of the Electrodes

This was effected by a method similar to that of Conway, Bockris, and Mehl.[18] The spectroscopically pure silver wire (0.2 mm diameter) was heated in a quartz tube lined with a Pt cylinder (to reduce direct contact of Ag and SiO_2 vapors) in purified He (cf. Azzam *et al.*[19]). Bright Ag spheres were obtained by careful melting of the wire from the top towards the Pyrex sleeve. To obtain good geometry, and avoid contamination from heated glass, the melting was discontinued before the sphere had reached the sleeve so that 0.2 to 0.5 mm of the original silver wire remained connecting the sphere with the contact inside the sleeve. Without contact with air, the sphere and sleeve were sealed inside a thoroughly cleaned glass bulb, filled with He. Microscopic examination sometimes revealed a negligible quantity of silver silicate adhering in patches.

2. Preparation of Solutions

Anhydrous $AgClO_4$ was dissolved in conductivity water, the AgCl residue filtered off, and the solution introduced into a crystallization vessel, through which He was passed. All experimental work was performed in semidarkness. $AgClO_4$ was recrystallized twice in conductivity water saturated with He. The $AgClO_4$ solution was pre-electrolyzed at a Pt cathode in He for twenty-four hours at an initial current density of 0.7 amp cm^{-2}.

Pure $HClO_4$ was obtained by three recrystallizations of concentrated $HClO_4$ in a closed vessel in contact with He at -30 to $-40°C$. The concentrated ($\simeq 11N$) $HClO_4$ was diluted in the cell to about $1N$ and then pre-electrolyzed at a Pt cathode in contact with He for twenty-four hours ($i=0.6$ amp cm^{-2}).

The pertinent solution was made up by transferring under He pressure $AgClO_4$ in solution to the pre-electrolyzed $1N$ solution of $HClO_4$ in the cell immediately before the measurements.

3. The Electrolytic Cell

This was similar to that described elsewhere,[16,20] and was enclosed in an air-thermostat lined with metal sheets which were earthed. All connecting cables were screened.

The Pt counter-electrode was plated with silver from the solution in the cell, prior to the measurements. Spectroscopically pure Ag wire in the same solution was used as a reference electrode.

4. Method

Potentiostatic and galvanostatic methods were both tested in preliminary investigations. The electronic potentiostat (rise time: 2 μsec) used is described elsewhere.[21] The potentiostatic method was found to be inapplicable for systems with i_0 values sufficiently high to make the ohmic resistance of the same order as the Faradaic one. (Compensating devices to eliminate the effect of the IR drop were used but these involve preliminary galvanostatic measurements and therefore detract from the advantages of the potentiostatic method.) Hence, the galvanostatic method was used throughout the work.

The arrangement was similar to that of Mattsson and Bockris.[16] Both current and overpotential were measured oscilloscopically (Tektronix, 531), using time scales between 10^{-6} and 10^{-3} sec cm^{-1}.

The accuracy in overpotential readings varied with the scale used (due to the increase of pseudo-ohmic overpotential, η_Ω, with i) from 0.5 to 5%, the mean accuracy being 1%.

An uncertainty of $\pm 3\%$ in the absolute value of i arose from the electrode area measurement. For any given electrode, the error in i was $\pm 0.5\%$.

5. Measuring Procedure

After lowering a given electrode into the solution, and the shattering of its glass bulb, the electrode was subjected to a cathodic pulse with a given i value and the associated overpotential-time ($\eta-t$) relation photographed on a given time scale. The electrode was thereafter subjected to a corresponding anodic pulse of equal duration, during which no record of the $\eta-t$ behavior was made in order to avoid readjustment of the triggering circuit. The procedure was repeated at i, for three further time scales. The i value was increased and the procedure repeated for about 20 i values.

After the highest desired i value was reached, recordings at a few of the lowest i values were repeated. The entire procedure was then again carried out while recording the anodic pulses.

In some instances the electrodes were submitted to a few cathodic and anodic pulses at higher i prior to the regular set. Such electrodes will be referred to as "activated."

III. RESULTS

Experiments were carried out in $1N$ $HClO_4$ solution at $AgClO_4$ concentrations varying from 0.4 to $0.001N$. The i range was between 0.005 and 10 amp cm^{-2}. A typical recorded potential-time dependence is shown in Fig. 1.

[18] Conway, Bockris, and Mehl, J. Sci. Instr. **33**, 400 (1956).
[19] Azzam, Bockris, Conway, and Rosenberg, Trans. Faraday Soc. **46**, 918 (1950).
[20] Pentland, Bockris, and Sheldon, J. Electrochem. Soc. **104**, 182 (1957).
[21] Blomgren, Despic, and Bockris (to be published).

1. Pseudo-Ohmic Overpotentital (η_Ω)

The η_Ω is established[22] in about 10^{-11} sec. It should therefore be observed on an oscilloscope as a gap in the trace between the zero point and the beginning of the $\eta-t$ transient. However, a much longer time than 10^{-11} sec is required for the *current* to reach a constant value because of the significant reactance of the electric circuit external to the cell. Since η_Ω is proportional to current, its rise time is that of the external electric circuit. The rise time of the measuring electric circuit (oscilloscope, reference electrode ensemble) may also prevent a separation of η_Ω, particularly when narrow Luggin capillaries are employed.[23] In this work the final η_Ω values were attained after 1–2 μsec, whilst the lowest rise time of the electrode reaction in the concentration range investigated, was of the order of 5 μsec. A typical value of the ohmic resistance was $1.9\pm0.4\ \Omega$.

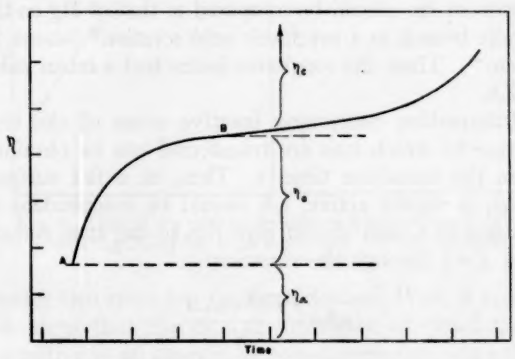

FIG. 1. Typical recorded $\eta-t$ relation.

2. Nonsteady-State Overpotential

The overpotential-time relations ($\eta-t$) for a given electrode at a given current density in various time regions (microseconds to milliseconds) were plotted on an $\eta-\log t$ graph. (Cf., e.g., Fig. 2.)

(a) *Double Layer Capacitance*, C_{DL}

At sufficiently short times,

$$i=C_{DL}(d\eta/dt)_{t\to 0}. \qquad (1)$$

Mean values of C_{DL} are presented in Table II, Column 6. When application of (1) at $t\to 0$ was not possible, C_{DL} was evaluated from $d\eta/dt$ at the transition time since the $\eta-t$ behavior at this time also essentially reflects the charging of the double layer. (Method 2, cf. Table II, Column 6.*)

[22] G. Falk and E. Lange, Z. Elektrochem. **54**, 132 (1950); Falk, Krieg, and Lange, *ibid.* **55**, 396 (1951).

[23] M. Seipt, Compt. rend. réunion 7th Meeting Comité intern. thermodynam. de cinét. electrochim. (1957).

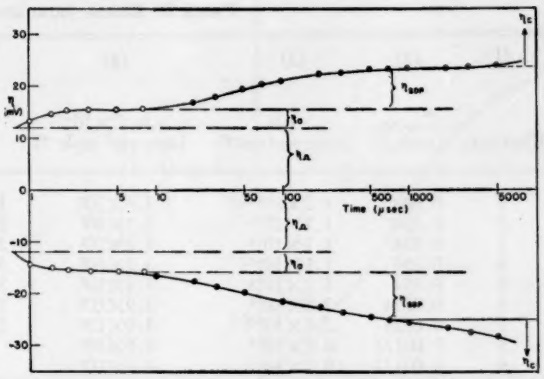

FIG. 2. $\eta-\log t$ relation in case of anodic (a) and cathodic (c) polarization of Ag in $0.35N$ $AgClO_4+1N$ $HClO_4$ solution. $i=79.5$ ma cm^{-2}.

(b) *Concentration Overpotential*, (η_c)

Experimental transition times, $\tau_{c\,obs}$, were measured.[24] They are given in Tables I and II.

(c) *Activation Overpotential*, (η_a)

The η_a-t transients were evaluated, e.g., from the section A–B of Fig. 1. Under certain conditions, they exhibited two sections, (cf. Fig. 2). Parameters based upon these transients are evaluated in Sec. IV.

(d) *Effect of Experimental Conditions*

(*i*) *State of the electrode surface.*—$\eta-t$ relations taken before and directly after activation of the surfaces are shown in Fig. 3.

(*ii*) *Purity of Solution.*—The rise time of $\eta_a(=4\tau_{DL}$, where τ_{DL} is the time constant for double layer charging) and C_{DL} increased markedly if an $AgClO_4$ solution stored for days was used. For this reason, only results obtained in freshly prepared solutions are quoted.

TABLE I. Typical solution concentration polarization ($0.0724N$ $AgClO_4+1N$ $HClO_4$ solution).

Electrode	i (amp cm^{-1})	$\tau_{c\,obs}$ (sec)	$\tau_{c\,calc}$ (sec)	A_{τ_c}	$A\,c_{DL}$
1	0.416	4.7×10^{-3}	3.8×10^{-3}	1.11	
	0.554	2.6×10^{-3}	2.1×10^{-3}	1.11	
	1.47	4.0×10^{-4}	3.0×10^{-4}	1.15	
	2.17	1.9×10^{-4}	1.4×10^{-4}	1.17	
	4.16	5.2×10^{-5}	3.7×10^{-5}	1.18	3.6
2	0.51	1.9×10^{-3}	2.5×10^{-3}	0.88	
	0.98	5.4×10^{-4}	6.7×10^{-4}	0.90	
	3.45	7.9×10^{-5}	5.5×10^{-5}	1.21	
	4.13	6.0×10^{-5}	3.8×10^{-5}	1.26	
	5.11	3.7×10^{-5}	2.5×10^{-5}	1.23	4.4

$\tau_{c\,calc}=6.5\times10^{-4}(1/i^2)$

[24] P. Delahay, *New Instrumental Methods in Electrochemistry* (Interscience Publishers, Inc., New York, 1954), p. 208.

TABLE II. Kinetic parameters of Ag—Ag^+ exchange reaction.

(1)	(2)	(3)	(4)	(5)	(6)	(7)	(8)		(9)
Electrode	C_{AgClO_4} (mole/l)	$\tau_c^{\frac{1}{2}}i$ (amp sec$^{\frac{1}{2}}$ cm^{-2})	$\tau_c^{\frac{1}{2}}i/C\times10^{-3}$ (amp sec$^{\frac{1}{2}}$ mole^{-1})	C_{DL}/i_0 (f/a)	C_{DL} (μf cm^{-2})	$4\tau_{DL}^{\circ}$ (sec)	i_0 (amp cm^{-2}) 1	2	β
1	0.364	1.2×10^{-1}	3.4×10^{2}	$1.35(\pm0.02)\times10^{-4}$	49 ± 4	1.4×10^{-5}	0.36	0.29	0.52
2	0.364	1.1×10^{-1}	3.1×10^{2}	$1.2(\pm0.1)\times10^{-4}$	48 ± 7	1.2×10^{-5}	0.40	0.26	0.53
3	0.354	1.1×10^{-1}	3.2×10^{2}	$3.1(\pm0.6)\times10^{-5}$	55 ± 20	3.2×10^{-6}	1.8	0.62	0.50
4	0.354	1.1×10^{-1}	3.2×10^{2}	$3.2(\pm0.6)\times10^{-5}$	35 ± 10	3.3×10^{-6}	1.1	0.47	0.33
5	0.354	1.2×10^{-1}	3.4×10^{2}	$3.0(\pm1.5)\times10^{-5}$	42 ± 10	3.1×10^{-6}	1.4	0.57	0.42
6	0.0724	2.8×10^{-2}	3.9×10^{2}	$3.8(\pm0.2)\times10^{-4}$	93 ± 2	3.9×10^{-5}	0.24	0.26	0.49
7	0.0724	2.2×10^{-2}	3.0×10^{2}	$3.6(\pm0.1)\times10^{-4}$	114×4	3.7×10^{-5}	0.32	0.27	0.48
8	0.00121	6.8×10^{-4}	5.6×10^{2}	...	153*	3.9×10^{-4}	...	0.04	$0.5(\pm0.1)$
9	0.00121	9.7×10^{-4}	8.0×10^{2}	...	74*	1.9×10^{-4}	...	0.04	$0.5(\pm0.2)$

Addition of Hg to the solution resulted in a 2.5-fold increase in η_a, giving rise to an $\eta-t$ relation similar to that for inactivated electrodes (cf. Fig. 3).

3. Steady-State i-η Relations

The steady state was defined as that corresponding to $t>4\tau_{DL}$ and $<\tau_c$. Typical $i-\eta$ relations for inactivated (a) and activated (b) electrodes are given in Fig. 4.

IV. DISCUSSION

1. Electrode Surface

The mean value for the double layer capacity is 76 μf per geometric sq cm (Table II). Values for individual electrodes were constant over many sweeps to $\pm5\%$. The scatter among electrodes of $\pm40\%$ hence represents a fluctuation of real electrode area per sq cm. A cause for this may lay in different rates of quenching during preparation.

The potential of zero charge for Ag is slightly negative to the potential of the standard H electrode[25] and therefore all measurements were made in a region positive with respect to the zero charge potential. Hence, the double layer capacity of the Hg-solution interface with which the above value of 76 μf per geometric sq cm should be compared is that of Hg on the anodic branch in a perchloric acid solution[26] (about 26 μf cm^{-2}). Thus, the roughness factor had a mean value of 2.8.

Information concerning inactive areas of the true surface to which ions are transferred can be obtained from the transition time, τ_c. Thus, at a flat surface, which is wholly active, $\tau_c^{\frac{1}{2}}i$ should be independent of changes in i, and should give rise to the true surface area $A=1$ through the equation:

$$\tau_c^{\frac{1}{2}}=\frac{\pi^{\frac{1}{2}}D^{\frac{1}{2}}Fc_{Ag^+}A}{2i}. \qquad (2)$$

Theoretical values of τ_c were calculated from (2), assuming $A=1$, and the diffusion coefficient of Ag^+ ions $D=1.7\times10^{-5}$ cm^2 sec^{-1}.[27]

A rough agreement was found with experimental τ_c (cf. Table I) and also a constancy of $\tau_c^{\frac{1}{2}}i$ at a given concentration or of $\tau_c^{\frac{1}{2}}i/c_{Ag^+}$ in the whole investigated concentration range. However, A ($=\tau_{c\ obs}^{\frac{1}{2}}/\tau_{c\ calc}^{\frac{1}{2}}$) revealed a small variation with i (cf. Table I), which may be interpreted along lines similar to those suggested by Lorenz.[28]

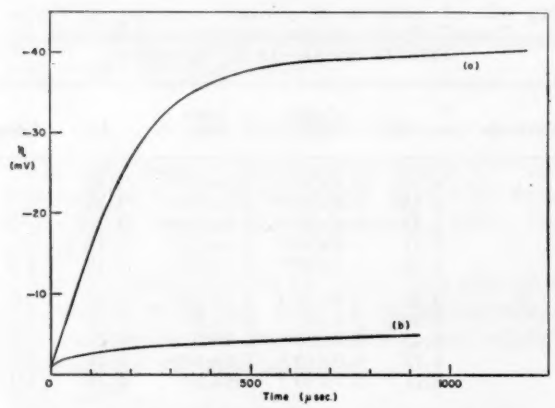

FIG. 3. $\eta-t$ relation (a) before and (b) after the electrode was activated by one high i ($=10$ amp cm^{-2}) pulse in both direction. 0.0724N $AgClO_4$+1N $HClO_4$ solution. $i=10.6$ ma cm^{-2}.

2. Surface Diffusion Polarization

(a) *Rate-Determining Steps in Metal Deposition and Dissolution*

It appears that the *path* during the deposition of simple cations consists of the following consecutive steps: transfer; surface diffusion; lattice growth.

Experimental distinction between transfer and surface and surface diffusion was first recorded by Mehl and Bockris[6]; a method for distinguishing between the

[25] R. Parsons in J. O'M. Bockris, *Modern Aspects of Electrochemistry* (Butterworths Scientific Publishers, London, 1954).

[26] D. C. Grahame, Office of Naval Research Report No. NR-051-150 (1951).

[27] I. M. Kolthoff and J. J. Lingane, *Polarography* (Interscience Publishers, Inc., New York, 1952), p. 50.

[28] W. Lorenz, Z. Elektrochem. **59**, 730 (1955).

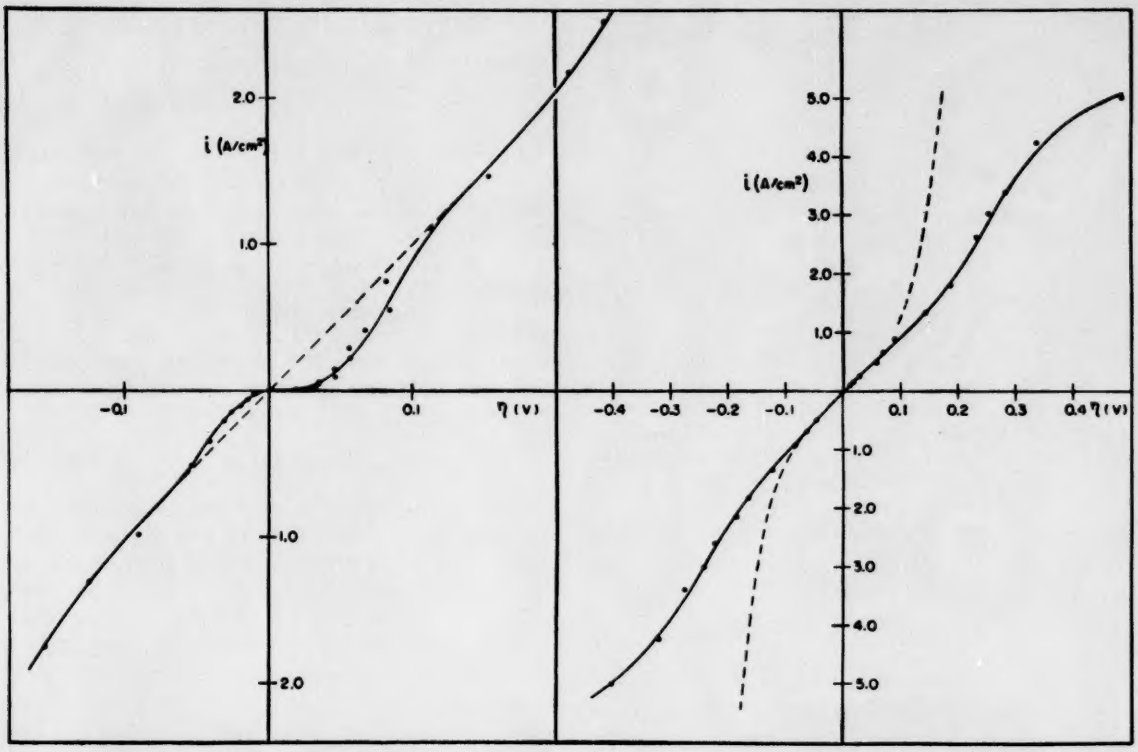

FIG. 4. Typical i–η relation in case of a nonactivated (a) and an activated electrode (b). (a) 0.0724N $AgClO_4$+1N $HClO_4$ solution. (b) 0.364N $AgClO_4$+1N $HClO_4$ solution. – – – – Butler-Volmer curve with β=const.

latter two steps has not been devised. Were it possible to show that the rate of deposition or dissolution is sensitive to an amount of poison corresponding only to the surface concentration of dislocations, the rate-determining character of the third step could be established.

The distinction between rate controlling transfer and surface diffusion will be considered below. η_a–t transients are controlled by the time constants of the transfer and surface diffusion processes. Consequently clear information about either process can be obtained when (a) the time constants are such that the two transients are clearly separated (cf. Fig. 2) or (b) when the contribution of one of the processes to is negligible.

(*b*) *Transient Potential-Time Relation under Surface Diffusion Control*

When appreciable surface diffusion effects are present for times at which the charging of the double layer can be neglected ($t>10\tau_{DL}$), the anodic current density is given by[29]

$$i=i_0\{(c_{ad}/c_{ad}^0)_t \exp[[(1-\beta)zF/RT]\eta_{a,t}] - \exp[-(\beta zF/RT)\eta_{a,t}]\} \quad (2)$$

where c_{ad} and c_{ad}^0 are the adion concentrations at a time t (corresponding to $\eta_{a,t}$) and at equilibrium, respectively. Also

$$-(dc_{ad}/dt)=(i/zF)-(v_0/c_{ad}^0)(c_{ad}^0-c_{ad}) \quad (3)\dagger$$

or

$$c_{ad}/c_{ad}^0=1-(i/zFv_0)[1-\exp(-t/\tau_{SD})] \quad (4)$$

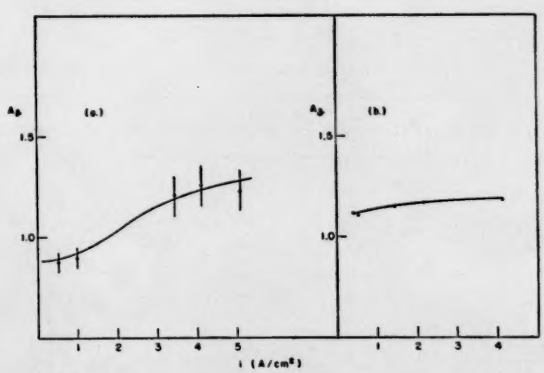

FIG. 5. The change of the true surface area with increasing current density at two different electrodes. 0.0724N $AgClO_4$+1N $HClO_4$ solution.

[29] W. Mehl and J. O'M. Bockris, Can. J. Chem. **37**, 190 (1959).

† Equation (3) is equivalent to that derived by Mehl and Bockris for cathodic polarization (cf. reference 29, Eq. (8)).

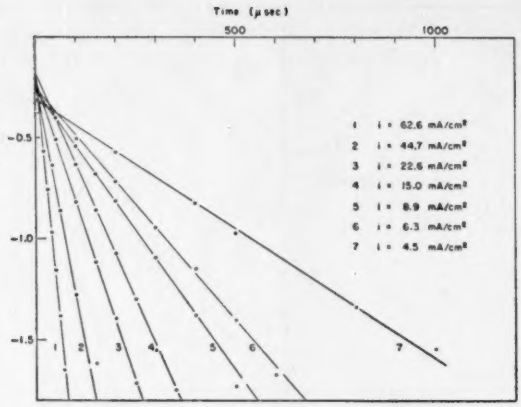

FIG. 6. Surface diffusion polarization at various current densities. Ag electrode of 0.052 cm² surface area in 0.0724N $AgClO_4$+ 1N $HClO_4$ solution.

where $\tau_{SD}=c_{ad}^0/v_0$. Substituting (4) into (2), introducing the fact that as $t\to\infty$, $\eta_{a,t}\to\eta_{a,\infty}$, and rearranging, one obtains

$$\log(\exp[-(zF/RT)\eta_{a,t}]-\exp[-(zF/RT)\eta_{a,\infty}] +(i/i_0)\{\exp[[-(1-\beta)zF/RT]\eta_{a,t}] -\exp[[-(1-\beta)zF/RT]\eta_{a,\infty}]\}) =-(t/2.3\tau_{SD})+\log(i/zFv_0). \quad (5)$$

From (5) at $i<0.1i_0$,

$$p=\log\{\exp[-(zF/RT)\eta_{a,t}]-\exp[-(zF/RT)\eta_{a,\infty}]\} =-(t/2.3\tau_{SD})+\log(i/zFv_0). \quad (6)$$

Equation (6) was applied to the experimental η_a-t relations for nonactivated electrodes (Fig. 6). Parameters such as τ_{SD}, v_0, and c_{ad}^0 were evaluated (Table III) from Eq. (6) (method 1).

Values of c_{ad}^0 were also obtained from the equation

$$(d\eta/dt)=(RT/z^2F^2)(i/c_{ad}^0) \quad (7)$$

where $d\eta/dt$ refers to the lowest time region in which the overpotential is growing under diffusion control (cf. references 11, 10) (method 2).

(c) *Adion Concentration at the Reversible Potential*

On a given electrode in the same solution, reproducibility of c_{ad}^0 with i, at low i, was good (±10%, see Table III). For different electrodes in the same solution, reproducibility was ±100%; there is no systematic variation with concentration; electrodes which were polarized for the first time after preparation by quenching in He gave c_{ad}^0 values which were in the order of $0.5-1\times10^{-10}$ mole cm^{-2}, while the activated ones gave c_{ad}^0 values about ten times greater (cf. also Mattsson and Bockris[16]).

TABLE III. Kinetic parameters of surface diffusion for the Ag—Ag^+ system.

(a) Typical variation with increasing current density in the low-current density region.

$i\times10^{-3}$ (amp cm^{-2})	$\tau_{SD}\times10^{-6}$ (sec)	$v_0\times10^{-7}$ (mole/cm² sec^{-1})	$C_{ad}^0\times10^{-10}$ (mole cm^{-2})
4.5	342	0.95	0.33
6.3	187	1.14	0.21
8.9	156	1.68	0.26
15.0	96	2.36	0.23
22.6	75	4.11	0.32
44.7	53	7.36	0.58
62.6	22	9.70	0.11

Method 1: Ag electrode of 0.092 cm² in 0.0724N $AgClO_4$+1N $HClO_4$ solution (cf. also Fig. 6).

(b) Typical variation with increasing current density in high-current density region at three electrodes in one and the same solution.

Electrode 1		Electrode 2		Electrode 3		Electrode 3[a]	
$i\times10^{-3}$ (amp cm^{-2})	$C_{ad}^0\times10^{-10}$ (mole cm^{-2})	$i\times10^{-3}$ (amp cm^{-2})	$C_{ad}^0\times10^{-10}$ (mole cm^{-2})	$i\times10^{-3}$ (amp cm^{-2})	$C_{ad}^0\times10^{-10}$ (mole cm^{-2})	$i\times10^{-3}$ (amp cm^{-2})	$C_{ad}^0\times10^{-10}$ (mole cm^{-2})
−40.7	2.4	82.0	1.7	−65.5	0.50	−65.5	17.0
40.7	2.0	105	2.4	−84.5	0.53	−84.5	11.7
−79.5	1.7	160	2.5	−128	0.68	−128	13.6
79.5	1.9	240	2.7	−192	1.22	−192	14.6
−192	2.1			−308	0.83	−308	16.4
192	1.5						
Average:	1.9±0.2 (±10%)	Average:	2.3±0.3 (±14%)	Average:	0.75±0.2 (±29%)	Average:	14.5±1.6 (±11%)

[a] Activated by high-current pulses (up to 3.2 amp cm^{-2}). Methol 2; solution 0.354N $AgClO_4$ + 1N $HClO_4$.

Values of c_{ad}^0 obtained hitherto for Ag are given in Table IV. According to simple thermodynamic considerations, the range implies a difference of only about 2 kcal mole^{-1} in the values of F_{ad}^0 on various surfaces.

TABLE IV. Values of surface adion concentration on Ag electrodes from various workers.

	C_{ad}^0 (moles cm^{-2})
Mehl and Bockris	90×10^{-11}
Gerischer	15×10^{-11}
Lorenz	3×10^{-11}
Despic and Bockris	
(a) Nonactivated:	3×10^{-11}
(b) Activated:	160×10^{-11}

(d) *Steady-State Current Density*

(*i*) *Distribution of current on surface.*—The model given by Mehl and Bockris[29] for surface diffusion control involved the assumption of a linear concentration gradient between a growth line and a point in the middle of a crystal plane, bounded by "edges" in the Kossel-Stranski sense. Lorenz[8] considered in more detail the distribution of adions as a function of position with respect to a growth line. However, he assumed a thermodynamic relation between the changing adion concentration and the potential, an assumption tantamount to that of a p.d. along a surface normally considered equipotential. In the present work this has been amended and it has been shown that there is a dependence of current density upon position on the electrode. This arises from the fact that the delivery of cations to a planar surface of an electrode occurs homogeneously at a constant potential, while the corresponding transfer of adions back into the solution must be a function of position, since it depends on the local adion concentration, which itself depends on position.

Consider an infinitesimal area on the electrode surface (Fig. 7). Then:

$$(i_{a,x}/zF)\,dxdy=(i_{c,x}/zF)\,dxdy+D(\partial^2 c_{ad,x}/\partial x^2)\,dxdy \quad (8)$$

where i_{ax} is the anodic current density at the surface at x from the growth line and $i_{c,x}$ is the corresponding cathodic current density. Since

$$i_{a,x}/zF=(i_0/zFc_{ad}^0)\,c_{ad,x}\exp\{[(1-\beta)zF/RT]\eta_a\}$$
$$=K_{a,\eta}c_{ad,x} \quad (9)$$

and

$$i_{c,x}/zF=(i_0/zF)\,\exp[-(\beta zF/RT)\eta_a] \quad (10)$$

Equation (8) becomes

$$c_{ad,x}-(D/K_{a,\eta})\,(\partial^2 c_{ad,x}/\partial x^2)=c_{ad}^{\infty}, \quad (11)$$

where

$$c_{ad}^{\infty}=(i_c/zFK_{a,\eta})=c_{ad}^0\exp[-(zF/RT)\eta_a] \quad (12)$$

and c_{ad}^{∞} is the adion concentration at a point so distant from the growth line that $D(\partial^2 c_{ad,x}/\partial x^2)\to 0$.

To solve (11) one uses the boundary conditions,

$$c_{ad,x=0}=c_{ad}^0, \quad (13)$$

corresponding to the assumption that virtual equilibrium remains undisturbed at the growth line, and also

$$(dc_{ad,x}/dx)_{x=x_0}=0. \quad (14)$$

Solving (11), with (13) and (14):

$$c_{ad,x}/c_{ad}^0=\exp[-(zF/RT)\eta_a]+\frac{1-\exp[-(zF/RT)\eta_a]}{1+\exp[-2(i_0/zFv_0)^{\frac{1}{2}}p]}$$
$$\cdot\{\exp[-2(i_0/zFv_0)^{\frac{1}{2}}p]\exp[(i_0/zFv_0)^{\frac{1}{2}}p(x/x_0)]$$
$$+\exp[-(i_0/zFv_0)^{\frac{1}{2}}p(x/x_0)]\}, \quad (15)$$

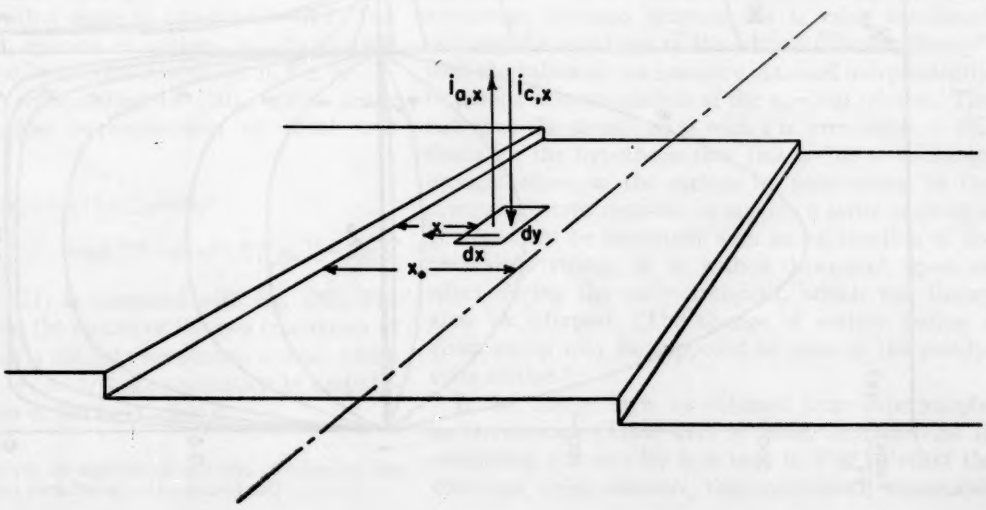

FIG. 7. The model of the electrode surface.

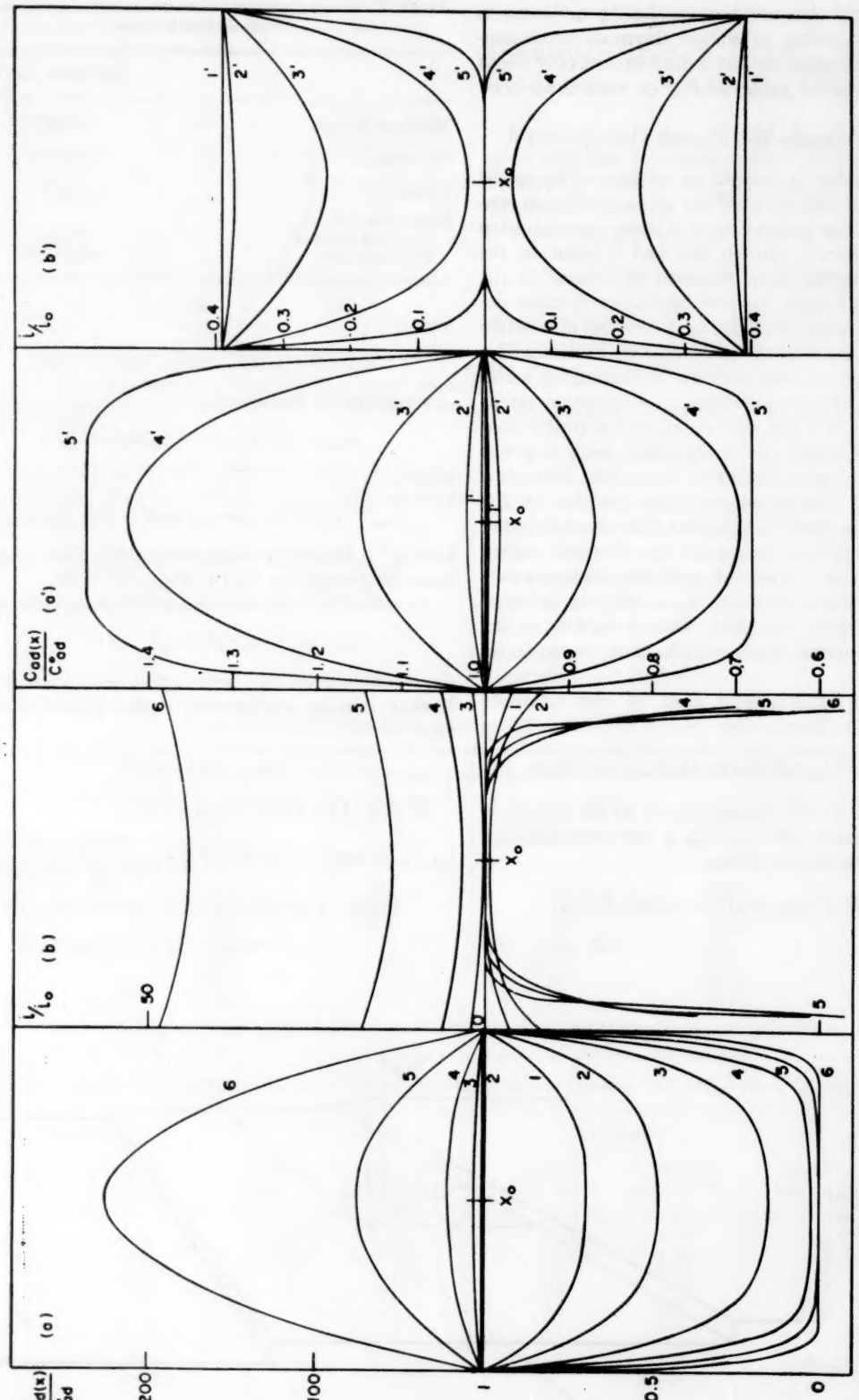

FIG. 8. Concentration profiles (*a* and *a'*) and current density distributions (*b* and *b'*) between two growth lines. (*a*), (*b*): constant $i_0/FV_0 = 10$ and varying η: 1, $\eta = -10$ mv; 2, $\eta = -20$ mv; 3, $\eta = -50$ mv; 4, $\eta = -100$ mv; 5, $\eta = -150$ mv; 6, $\eta = -200$ mv; (*a'*), (*b'*): constant $\eta = 10$ mv and varying $i_0/FV_0 = 0.01$ (1); 0.1 (2); 1.0 (3); 10 (4); 100 (5).

where

$$p=\exp\{[(1-\beta)zF/RT]\eta_a\} \qquad (16)$$

and

$$v_0=(Dc_{ad}{}^0/x_0{}^2). \qquad (17)$$

Now

$$i_x=i_0\{(c_{ad,x}/c_{ad}{}^0)\exp[[(1-\beta)zF/RT]\eta_a] - \exp[-(\beta zF/RT)\eta_a]\}. \qquad (18)$$

By introducing (15) into (18) the distributions of adion concentration and current density can be calculated as a function of position, x/x_0, on the electrode surface (Fig. 8).

The average i for the whole electrode surface follows by integrating i_x from $x=0$ to $x=x_0$ and dividing by x_0. It is

$$i=i_0{}^{\frac{1}{2}}(zFv_0)^{\frac{1}{2}}\exp[[-(1+\beta)zF/2RT]\eta_a] \cdot\{\exp[(zF/RT)\eta_a]-1\}\frac{\{1-\exp[-2(i_0/zFv_0)^{\frac{1}{2}}p]\}}{\{1+\exp[-2(i_0/zFv_0)^{\frac{1}{2}}p]\}}. \qquad (19)$$

Equation (19) can be rewritten as

$$y=[(1+\beta)zF/4.6RT]\eta_a +\log\frac{\{1+\exp[-2(i_0/zFv_0)^{\frac{1}{2}}p]\}}{\{1-\exp[-2(i_0/zFv_0)^{\frac{1}{2}}p]\}}-\tfrac{1}{2}\log(i_0zFv_0) \quad (20)\ddagger$$

where

$$y=\exp\{[(zF/RT)\eta_a]-1/i\}.$$

When $(zFv_0/i_0)\to\infty$, i.e., when the specific rate of the surface diffusion is much faster than that of the transfer reaction, (20) tends to become identical with the Butler-Volmer equation, i.e., the current density becomes uniform. With increasing y values the second term of (20) tends towards zero and the $y-\eta_a$ relation becomes linear with a slope of $(1+\beta)zF/4.6RT$. The trend of the $y-\eta_a$ relation at various (i_0/zFv_0) ratios, assuming i_0 to be 0.26 amp cm^{-2}, is shown in Fig. 9.

The relation corresponding to (20), which arises from the first-order approximation of Mehl and Bockris,[29] is

$$y=(\beta zF/2.3RT)\eta_a+\log\{1+(i_0/zFv_0) \cdot\exp[[(1+\beta)zF/RT]\eta_a]\}-\log i_0.$$

In Fig. 9 Eq. (21) is compared with Eq. (20). The difference between the results of the two treatments at low overpotentials is not very significant, a result which justifies the use of the first approximation in simplifying the derivation of the η_a-t relation.

‡ Similar relation can be derived for cathodic polarization, the coefficient in the first term being $-(1-\beta)zF/4.6RT$.

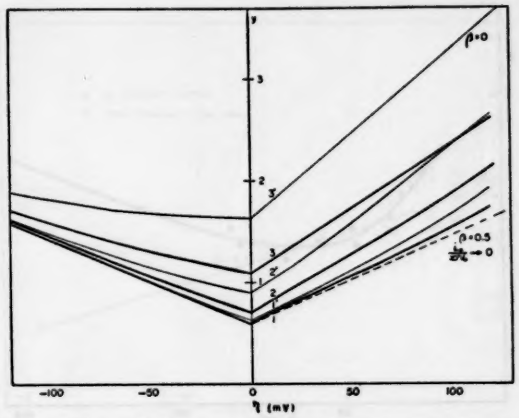

FIG. 9. Theoretical curves of y *vs* η in case of an increasing surface diffusion contribution. ——— Theory derived in this work. ——— Mehl-Bockris approximation. $i_0/FV_0=0.1$ (1 and 1'); 1.0 (2 and 2'); 10 (3 and 3').

The present second approximation for the theory of surface diffusion has still been derived under the assumption that the metal surface does not change with passage of current and therefore that v_0 and i_0 remain constant. However, the experimental η_a-t relations indicate that v_0 is increasing with each pair of high current density pulses applied. In fact, v_0 is roughly linear with i, and as a result of this, in Fig. 6, the slopes of the relation p [Eq. (6)] as a function of t are changing with current density, whilst the intercept remains approximately constant.

These discrepancies result from the approximate assumptions noted above. That the theory of slow surface diffusion provides an interpretation of the essentials of the low-current density behavior during deposition and dissolution at electrodes prepared by quenching is evidenced by (i) The satisfactory representation of the η_a-t relation at each current density given by Eq. (6); (ii) The fair constancy of the $c_{ad}{}^0$ value obtained for different current densities with the same conditions of electrode preparation; (iii) The agreement obtained between the i_0 value calculated utilizing the equations of the surface diffusion theory[29] with the values of this quantity obtained independently by means of extrapolation of the $\eta_a-\log i$ relation. The fact that the change of v_0 with i is irreversible is evidence for the hypothesis that this is due to a change brought about in the surface by polarization at the previous current densities in making a series of sweeps. It would not be consistent with an explanation of the anomalous change of v_0 with i dependent upon an effect *during* the early transient, which the theory aims to interpret. (The change of surface during a given sweep may be supposed to arise in the steady-state section.)

If the change in v_0 as obtained from experimental η_a-t relations (Table III) is taken into account in evaluating y from (20) it is seen in Fig. 10—that the corrected $y-\eta_a$ relation, thus calculated, reasonably

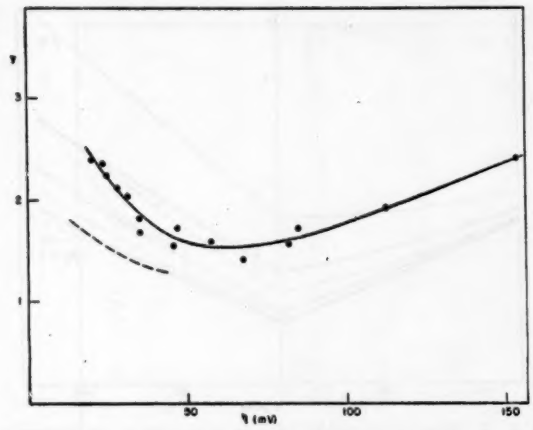

FIG. 10. Typical $y-\eta_a$ curve in the presence of surface diffusion effects.

follows the experimental curve. The remaining difference may be ascribed to an increasing i_0 with the activation due to successive pulses. This concept is consistent with the i_0 values reported in this work for "activated" electrodes, which are greater than those of Mehl and Bockris, who worked with less disturbed Ag surfaces.

(*ii*) *Dependence of surface diffusion polarization upon character of the electrode surface.*—From the results of Fig. 10 it is clear that the surface diffusion contribution to the overpotential in systems of high purity has significance only at low overpotentials (<50 mv). These effects became increasingly significant and long lasting as the purity of the solution is decreased and are therefore likely to play a predominant role in the rate control of the over-all process in systems in which inhibiting impurities are present.

3. Transfer Phenomena

(*a*) *Transfer Overpotential-Time Relation*

In the absence of surface diffusion effects, i is given by

$$i=c_{DL}(d\eta_a/dt)+i_0\{\exp[-(\beta zF/RT)\eta_{a,t}] -\exp[[1-\beta)zF/RT]\eta_{a,t}]\}. \quad (22)$$

Solving (22), (cf. Roiter, Juza, and Polujan[6]) and rearranging

$$q=\log\frac{[\exp(-\eta_{a,\infty}/b')+\exp(\eta_{a,t}/b')][\exp(\eta_{a,\infty}/b')-1]}{[\exp(\eta_{a,\infty}/b')+\exp(\eta_{a,t}/b')][\exp(-\eta_{a,\infty}/b')+1]} =t/2.3\tau_{DL} \quad (23)$$

where $b'=RT/\beta F$ and

$$\tau_{DL}=\{b'/[\exp(-\eta_{a,\infty}/b')+\exp(\eta_{a,\infty}/b')]\}(C_{DL}/i_0). \quad (24)$$

The value of β used in each case was that determined from the steady-state η_a-i relation of the corresponding experiment (cf. the following). A plot of q against t is shown in Fig. 11. It is linear, thus confirming, for the first time, the applicability of (23).

Mean C_{DL}/i_0 values as well as

$$4\tau_{DL}^0=4(RT/F)(C_{DL}/i_0)$$

representing the approximate§ rise time of the potential are given in Table II. From C_{DL}/i_0 and the C_{DL} values obtained from (11) at $t\to 0$, i_0 values were evaluated and are presented in Table II (Column 8, 1).

(*b*) *Steady-State $i-\eta_a$ Relation*

Rearranging (22) at $t>4\tau_{DL}$ [i.e., $C_{DL}(d\eta_a/dt)\to 0$] gives (for the anodic process)

$$y=\log[\{\exp[(zF/RT)\eta_a]-1\}/i] =(\beta zF/2.3RT)\eta_a-\log i_0. \quad (25)$$

The $y-\eta_a$ relation should be linear over the whole η_a region (contrast the Tafel plot) provided that the process is transfer controlled and that β is constant with change of potential. A plot of y against η_a allows a direct evaluation of i_0 and β.

Typical $y-\eta_a$ relations in the presence and absence of surface diffusion effects are shown in Figs. 10 and 12, respectively. When surface diffusion is negligible, (25) is seen to be applicable to about 50 mv. Values of i_0 and β are shown in Table II (Column 8, 2, and 9).

At the lowest concentration (0.001N $AgClO_4$), i_0 and β were obtained from the anodic polarization data at $t>\tau_c$, Eq. (25) being modified to

$$y'=\log[\{\exp[(F/RT)\eta]-[(\tau_c^{\frac{1}{2}}+t^{\frac{1}{2}})/\tau_c^{\frac{1}{2}}]\}/i] =(\beta F/2.3RT)\eta-\log i_0. \quad (26)$$

For each i value, τ_c was evaluated from $\tau_c^{\frac{1}{2}}i=$const, obtained from a cathodic $\eta-t$ relation.

At higher overpotentials (Fig. 12), the $y-\eta_a$ relation deviates towards a second linear relation with slope

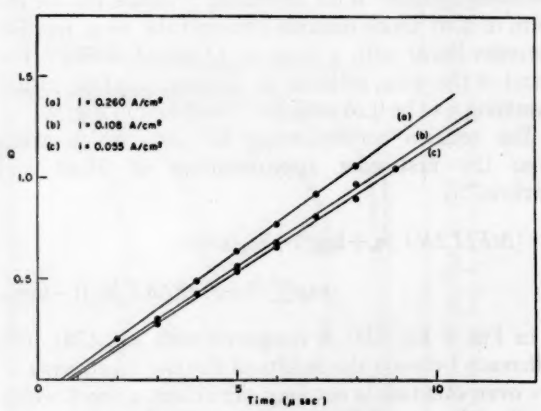

FIG. 11. Charging curves in the course of the transfer controlled anodic polarization. Ag in 0.364N $AgClO_4$+1N $HClO_4$ solution.

§ $\tau_{DL}^0\simeq\tau_{DL}'$ at $\eta_{a,\infty}\to 0$ (<5mv) and as such is defined elsewhere

$F/2.303RT$. *Cathodic and anodic relations coincided.* (See the following.)

The $\log i_0 - \log c_{Ag+}$ relation is shown in Fig. 13. The slope of about 0.5 agrees with the β values of the individual experiments (Table II).

(c) *Current Density-Potential Relation at High Current Densities*

The plot of the steady-state η_a against $\log i$ does not have an appreciable linear section. (Cf. the corresponding plots on the systems Cu—$CuSO_4$, which do give a clear linear relation.[16]) Figure 4 shows that the $i-\eta_a$ relation is characterized by (i) The close identity of cathodic and anodic lines; (ii) The deviations of these lines from the usual exponential relation—in the overpotential range above 50 mv, and the tendency toward an apparent limiting current density (for both anodic and cathodic lines) at the highest overpotential region.

The following mechanisms are not consistent with these results:

(a) Concentration overpotential in the solution because the times at which the measurements were taken were much shorter than the observed transition times.

(b) Surface diffusion polarization, since the experimental cathodic and anodic relations are identical in the high regions in contrast to the indications of Eq. (19) and Fig. 8.

(c) Ohmic control through a surface film, as this would give unusual capacitances; and because the Wachstumwiderstands polarization[4] (resistance polarization at the point of growth) may no longer be considered feasible.[8]

These facts suggest that the transfer process is rate-controlling, in these high i and η_a regions, even though the $\eta_a - i$ relation is not logarithmic. It therefore becomes necessary to determine under what conditions this type of rate control can give $i-\eta_a$ relations of the type of Fig. 4.

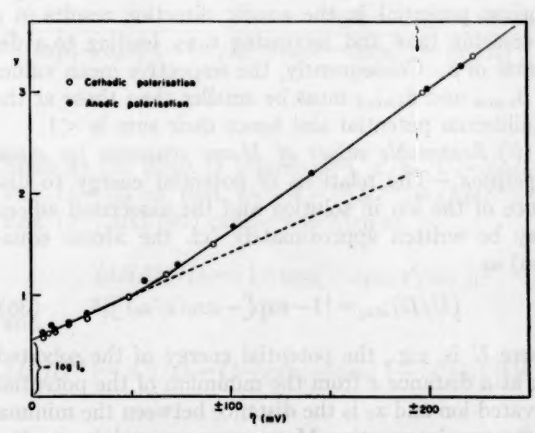

FIG. 12. Typical $y-\eta_a$ relation in the absence of surface diffusion effects. - - - - trend of the relation in case of a constant $\beta=0.5$.

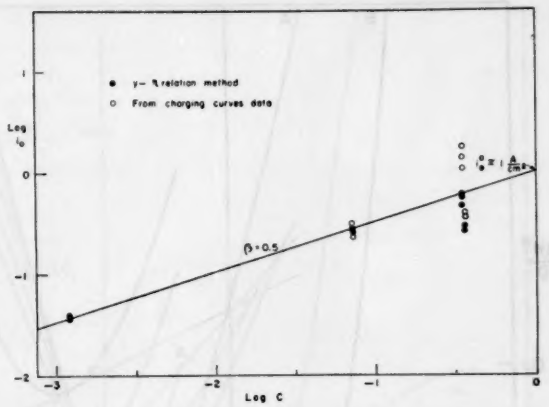

FIG. 13. The concentration dependence of the exchange current density.

(i) *Consideration of the symmetry factor.*—The two definitions of β available in the literature have not previously been shown to be equivalent.

Thus, according to the *potential energy curve view* (Fig. 14)

$$\beta_c = \tan\gamma/(\tan\gamma+\tan\theta);$$

$$\beta_a = \tan\theta/(\tan\gamma+\tan\theta). \qquad (27)$$

Here, β_c and β_a are differential quantities.

According to the *symmetry* view (Fig. 14)

$$\beta_c = x'/x_0. \qquad (28)$$

From Eq. (27) and Fig. 14

$$\beta_c \doteq \frac{\langle \Delta H_1^{0*} \rangle/(x_0-x')}{(\langle \Delta H_1^{0*} \rangle/x') + [\langle \Delta H_1^{0*} \rangle/(x_0-x')]} = x'/x_0. \qquad (29)$$

As a first approximation the two definitions are therefore equivalent provided that the potential energy curves do not have large radii of curvature at their minima.

From the above definitions it is clear that a Tafel relation is only to be expected if, over the range of the potential measurement, $\tan\gamma$ and $\tan\theta$ are constant. Qualitatively, this will be more likely to occur when the heat of activation is high compared with the potential change involved. When this is not the case, the differential β_c and β_a obviously change with potential (Fig. 14).

Consider the effect of potential upon current for such a system. Let $A-A$ (Fig. 14) be the potential energy-distance curve for the initial state of the transfer reaction which corresponds to an equilibrium galvani p.d. between the electrode and solution. The partial current density for, e.g., the transfer reaction *to* the electrode is of the form

$$i = KC_{Ag+} \exp(-\langle \Delta H_2^{0*} \rangle/RT). \qquad (30)$$

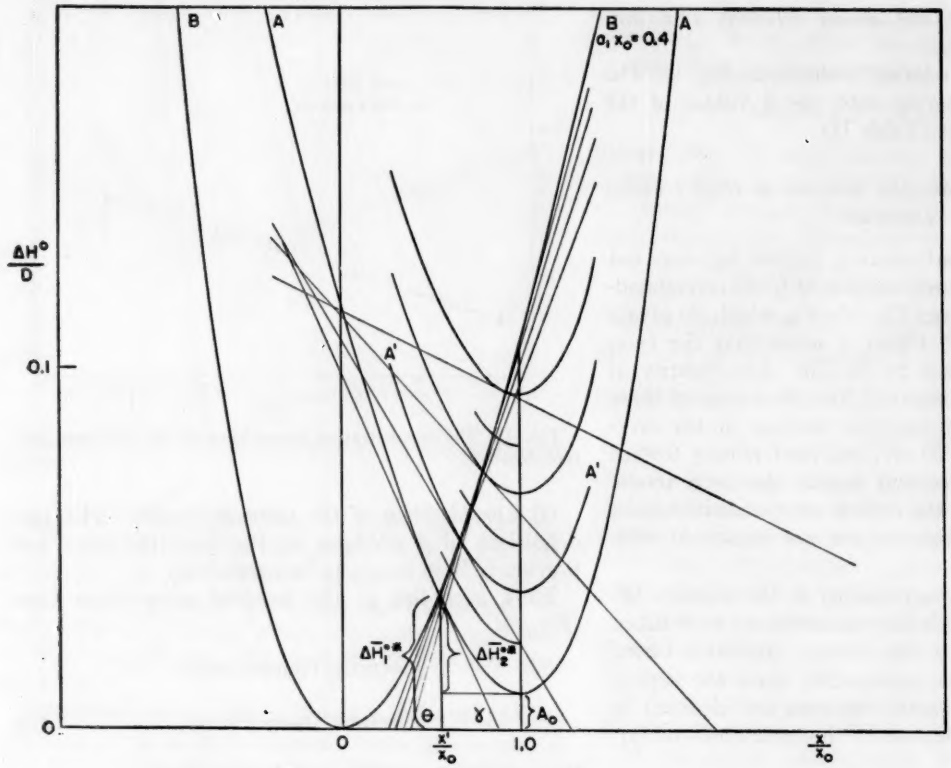

FIG. 14. The potential energy-distance relations (Morse functions with $ax_0=0.4$).

Let the potential be made $d\eta$ more negative. $A-A$ becomes $A-A'$. Thus,

$$i+di=KC_{As+}\exp\{[-\langle\Delta H_2^{0*}\rangle+\beta_{c,\eta}d\eta F]/RT\} \quad (31)$$

and

$$1+(di/i)=1-(\beta_{c,\eta}F/RT)d\eta. \quad (32)$$

Integrating (32) between i_0 and i and between 0 and η

$$\ln(i/i_0)=-(F/RT)\int_0^{\eta}\beta_{c,\eta}d\eta. \quad (33)$$

However, from the usual formulation of the Butler-Volmer equation,

$$\ln(i/i_0)=-(F/RT)\beta\eta. \quad (34)$$

From (33) and (34)

$$\beta=(1/\eta)\int_0^{\eta}\beta_{c,\eta}d\eta. \quad (35)$$

Consequently, the symmetry factor β, as normally used in the Butler-Volmer equation, is the mean value of the $\beta_{c,\eta}$ over the potential range $0-\eta$.||

Since by Eq. (27), $\beta_c+\beta_a=1$, then the sum of all the corresponding mean values of Eq. (35) at any given potential must also be unity, i.e., $\beta_{c,\text{anod}}+\beta_{a,\text{anod}}=1$ and $\beta_{c,\text{cath}}+\beta_{a,\text{cath}}=1$. However, a different conclusion is reached if the symmetry factors considered do not refer to a given current density in the *same* direction but (as usually the case in an experimental determination), those referring respectively to cathodic and anodic currents, at the same *numerical* values of η's with different signs. Thus, from Fig. 14 an increase of i in the cathodic direction tends to cause a decrease of β_c because [cf. Eq. (27)] of increasing $\tan\theta$ and decreasing $\tan\gamma$. Conversely, departure from the equilibrium potential in the anodic direction results in a decreasing $\tan\theta$ and increasing $\tan\gamma$ leading to a decrease of β_a. Consequently, the respective mean values of $\beta_{c,\text{cath}}$ and $\beta_{a,\text{anod}}$ must be smaller than those at the equilibrium potential and hence their sum is <1.

(*ii*) *Reasonable values of Morse constants for metal deposition.*—The relations of potential energy to distance of the ion in solution and the associated adions may be written approximately (cf. the Morse equation) as

$$(U/D)_{x/x_0}=\{1-\exp[-ax_0(x/x_0)]\}^2 \quad (36)$$

where U is, e.g., the potential energy of the solvated ion at a distance x from the minimum of the potential solvated ion and x_0 is the distance between the minima of the two intersecting Morse curves pertaining to the ion and its corresponding adion. Let x' represent the distance between the minimum of the curve BB (in

|| Thus, β, as defined by (35) is analogous to a mean "efficiency factor."

Fig. 14) and the intersection point of curves BB and AA. Then,

$$(U/D)_{x'/x_0}=(\langle\Delta H_1^{0*}\rangle/D_1). \quad (37)$$

Also, from (36) and (37)

$$ax_0=-\frac{2.3}{x'/x_0}\log[1-(\langle\Delta H_1^{0*}\rangle/D_1)^{\frac{1}{2}}]. \quad (38)$$

Let it be assumed that $(x'/x_0)=0.5$. (Little change in ax_0 occurs with x'/x_0 from 0.3 to 0.7.)

$\langle\Delta H^{0x}\rangle$ is known to vary from about 3–20 kcal mole^{-1} and D has the order of magnitude of about 100 kcal mole^{-1}. Thus, the order of magnitude of ax_0 would be, from (38), between

$$(ax_0)_{(\langle\Delta H_1^{0*}\rangle/D_1)=0.03}=0.36$$

and

$$(ax_0)_{(\langle\Delta H_1^{0*}\rangle/D_1)=0.02}=1.2.$$

Hence, evaluation in the following discussion, will be made for this range of the numerical values with special emphasis on the lower value because this would be the one most relevant to high i_0 values.

(iii) Evaluation of the dependence of β on overpotential. —Consider Fig. 14. The two curves AA and BB pertaining to solvated ions and the adions, respectively, can be approximately represented by the equations:

$$U_1=D_1\{1-\exp[-a_1x_0(x/x_0)]\}^2$$

$$U_2=D_2(1-\exp\{-a_2x_0[1-(x/x_0)]\})^2+A. \quad (39)$$

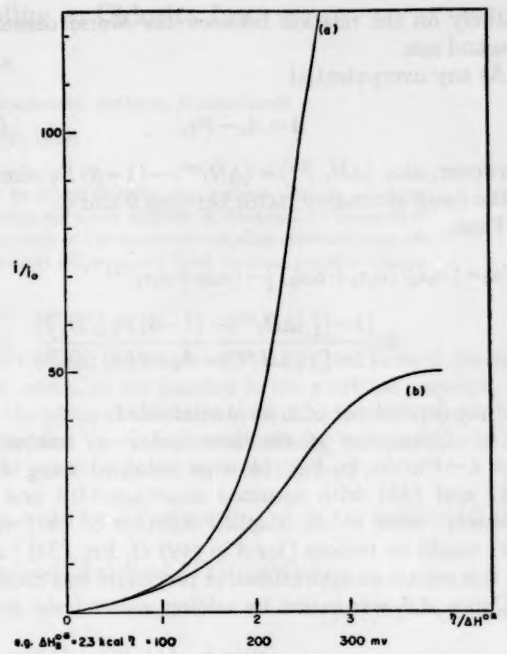

FIG. 15. η_a-i relation as predicted by the Butler-Volmer equation with constant β (a) and with β varying with η (b).

Then,

$$\tan\theta=(dU_1/dx)_{x'}=2D_1a_1\{\exp[-a_1x_0(x'/x_0)]-\exp[-2a_1x_0(x'/x_0)]\} \quad (41)$$

and

$$\tan\gamma=(dU_2/dx)_{x'}=-2D_2a_2(\exp\{-a_2x_0[1-(x'/x_0)]\}-\exp\{-2a_2x_0[1-(x'/x_0)]\}). \quad (42)$$

From (41) and (42)

$$\beta_c=\frac{(-\tan\gamma)}{(-\tan\gamma+\tan\theta)}=\frac{\exp\{-a_2x_0[1-(x'/x_0)]\}-\exp\{-2a_2x_0[1-(x'/x_0)]\}}{(\exp\{-a_2x_0[1-(x'/x_0)]\}\exp\{-2a_1x_0[1-(x'/x_0)]\}+[(D_1a_1)/(D_2a_2)]\{\exp[-a_1x_0(x'/x_0)]-\exp[-2a_1x_0(x'/x_0)]\}} \quad (43)$$

Since at the point of intersection, x'/x_0, $U_1=\langle\Delta H_1^{0*}\rangle$ and $U_1=U_2$ so that $U_2-A=\langle\Delta H_2^{0*}\rangle=\langle\Delta H_1^{0*}\rangle-A$, Eqs. (39) and (40) can be rewritten as

$$\langle\Delta H_1^{0*}\rangle/D_1=\{1-\exp[-a_1x_0(x'/x_0)]\}^2 \quad (44)$$

and

$$(\langle\Delta H_1^{0*}\rangle-A')/D_2=(1-\exp\{-a_2x_0[1-(x'/x_0)]\})^2. \quad (45)$$

Solving (44) and (45) for $a_1x_0(x'/x_0)$ and $a_2x_0[1-(x'/x_0)]$ respectively, subtracting the resulting equations, and rearranging one obtains

$$x'/x_0=[a_2x_0/(a_1x_0+a_2x_0)]-(a_1x_0+a_2x_0)^{-1}\cdot\ln\frac{[1-(\langle\Delta H_1^{0*}\rangle/D_1)^{\frac{1}{2}}]}{\{1-[(\langle\Delta H_1^{0*}\rangle-A)/D_2]^{\frac{1}{2}}\}}. \quad (46)$$

x'/x_0 evaluated from (46) can be inserted into (43) and β_c value obtained.

At equilibrium the constant A is

$$A_0=F_{\text{ion}}^0-F_{\text{ad}}^0 \quad (47)$$

and unless A_0 is very significant compared to $\langle\Delta H_1^{0*}\rangle$ and $D_1\neq D_2$, x'/x_0 and hence $\beta_{c,\text{rev}}$ are seen to depend

entirely on the relation between the Morse constants a_1x_0 and a_2x_0.

At any overpotential

$$A = A_0 - F\eta. \tag{48}$$

However, also $\langle \Delta H_{1,\eta}{}^{0*} \rangle = \langle \Delta H_1{}^{0*} \rangle - (1-\beta) F\eta$ where β is the mean symmetry factor between 0 and η.

Thus,

$$x'/x_0 = [a_2x_0/(a_1x_0+a_2x_0)] - (a_1x_0+a_2x_0)^{-1} \cdot \ln \frac{\{1-[[\langle \Delta H_1{}^{0*} \rangle - (1-\beta) F\eta]/D_1]^{\frac{1}{2}}\}}{\{1-[(\langle \Delta H_1{}^{0*} \rangle - A_0 + \beta F\eta)/D_2]^{\frac{1}{2}}\}} \tag{49}$$

and the dependence of β_e on is established.

(*iv*) *Calculation of the theoretical $i-\eta_a$ relation at high i.*—Curves in Fig. 14 were obtained using Eqs. (44) and (45) with assumed $a_1x_0 = a_2x_0 = 0.4$ and an arbitrary value of A_0. Explicit solution of (43) with (49) would be tedious [for β in (49) cf. Eq. (35)] and for this reason an approximative procedure was used.

Curve AA was raised by adding successively small equal values of $\eta F/D$. In each case x'/x_0 was calculated from (49) taking as β the mean value of β_e from 0 to η previously calculated (or $\beta_{e,rev}$ for the first $\eta F/D$ added). The calculated x'/x_0 value was then introduced into (43) and the β_e value obtained. The mean β' value between 0 and η was then evaluated to be both used for the calculation of x'/x_0 at the next $\eta F/D$, and employed in equation (22) at $(d\eta/dt) \to 0$. This gave rise to the calculated $i-\eta_a$ relation shown in Fig. 15. The shape of the theoretical relation (b) in Fig. 15 is seen to reproduce the tendency towards a transfer controlled limiting current established experimentally (cf. Fig. 4).

ACKNOWLEDGMENTS

The authors wish to signify their gratitude to the International Nickel Company for financial support during the work; and to the University of Belgrade for agreeing to a leave of absence for one of them (A.R.D.). They also wish to thank Dr. E. Blomgren for substantial aid during the development of the instrumentation used in this work.

THE JOURNAL OF CHEMICAL PHYSICS VOLUME 32, NUMBER 2 FEBRUARY, 1960

Nuclear Quadrupole Coupling in Chlorite Ion

J. L. RAGLE

Department of Chemistry, University of Massachusetts, Amherst, Massachusetts

(Received August 26, 1959)

Chlorine pure quadrupole spectra have been observed in silver chlorite and sodium chlorite at room temperature. The observed coupling constant of 108.16 mcps for silver chlorite is discussed in terms of a simple model of the electronic structure, in which the magnitude of the apparent coupling constant may be understood as resulting from a highly asymmetric field gradient ellipsoid and from residual positive charge on the chlorine atom.

THE purpose of this note is to report preliminary results on nuclear quadrupole coupling in two chlorite ion salts. The Cl^{35} and Cl^{37} pure quadrupole spectra have been observed in solid sodium chlorite and silver chlorite at room temperature. Frequencies of these resonances, together with some previously unreported low temperature data of Dodgen and Ragle, are given in Table I. The high values of the apparent quadrupole coupling constant, near that of one unpaired p electron, are to be partly attributed to residual positive charge on the chlorine atom. Depending on the details of the electronic charge distribution, the asymmetry of the field gradient may also contribute a sizable amount to the apparent value of the coupling constant.

One may carry out a naive analysis of the electronic structure in a straightforward way. Note (Figure 1) that in crystalline $AgClO_2$, the metal ion is close to the chlorine atom and is coplanar with the chlorite ion, and that the observed oxygen-chlorine-oxygen bond angle is $116°\pm5°$.[1,2] These observations suggest the use of hybrid orbitals which partake of no out-of-plane character. Since the components of the field gradient tensor are most sensitive to the details of the wave function near the nucleus, it may not be too unreasonable to use the prepared chlorine atomic orbitals to obtain a crude value of the coupling constant and asymmetry parameter. Assuming no d character, the angular forms of these wave functions are

$$t_0 = \cot\theta\{\psi_{3s} - [(1-\cot^2\theta)^{\frac{1}{2}}/\cot\theta]\psi_{3p_x}\}$$

$$t_\pm = 2^{-\frac{1}{2}}(1-\cot^2\theta)^{\frac{1}{2}}\{\psi_{3s} + [\cot\theta/(1-\cot^2\theta)^{\frac{1}{2}}]\psi_{3p_x} \pm [1/(1-\cot^2\theta)^{\frac{1}{2}}]\psi_{3p_z}\}$$

where the orbital t_0 is directed toward the nearest neighbor silver ion, and the orbitals $t_\pm$ are directed toward the oxygen atoms. (See Figure 1.) The angle θ which occurs in these expressions is one-half the O—Cl—O bond angle.

Assigning A as the number of electrons in the orbitals directed toward the oxygen atoms, B as the number of electrons in the single orbital directed toward the silver ion, and C as the number in the p orbital perpendicular to the plane of the ion, one obtains the following expressions for the three nonvanishing components of the field gradient at the chlorine nucleus[3]:

$$\phi_{zz} = \phi_0(1+\epsilon)^\rho[A(\cot^2\theta - \tfrac{1}{2}) + B(1-\cot^2\theta) - (C/2)]$$

$$\phi_{yy} = \phi_0(1+\epsilon)^\rho[-(A/2)(\cot^2\theta+1) - (B/2)(1-\cot^2\theta) + C]$$

$$\phi_{xx} = \phi_0(1+\epsilon)^\rho[A(1-\tfrac{1}{2}\cot^2\theta) - (B/2)(1-\cot^2\theta) - (C/2)].$$

In these expressions, ϕ_0 is the field gradient expected from one unpaired p electron, and the factor $(1+\epsilon)^\rho$ accounts for changes in ϕ_0 from the value characteristic of the free atom as a result of residual positive charge on the chlorine.[4] Assuming that both lone pair orbitals are filled, i.e., that no double bond character exists in the chlorine-oxygen linkages, and that no covalent bonding occurs with the silver ion, one obtains a residual charge of $\rho \leqq +1$ on the chlorine atom from the data of Table I. Under the above assumptions, one also obtains an asymmetry parameter of $\eta \leqq 0.73$, independent of the value of A, which will cause an upward shift of approximately 8% in the apparent coupling constant. It is interesting to note that the asymmetry parameter depends very strongly on the value taken for the O—Cl—O angle. Figure 2 shows the dependence of the field gradient components and the asymmetry parameter on this angle, assuming $A=1$ and B, $C=2$. Although the asymmetry parameter for spin $\frac{3}{2}$ nuclei may be determined by studies of the Zeeman effect of the pure quadrupole spectrum of single crystals, and although this datum is of particular interest here, some difficulty will probably be experienced in carrying out such measurements (*vide infra*).

If we relax our restriction on C by allowing double bond character,[5] charge will be withdrawn from the

[1] Curti, Riganti, and Locchi, Acta Cryst. **10**, 687 (1957).

[2] The crystal structure of the sodium salt does not appear to be known in detail. Mathieu [J. P. Mathieu, Compt. rend. **234**, 2272 (1952)] has given the value of 110° for the O—Cl—O bond angle for $NaClO_3 \cdot 3H_2O$ from spectroscopic data.

[3] T. P. Das and E. L. Hahn, *Nuclear Quadrupole Resonance Spectroscopy* (Academic Press, Inc., New York, 1958), p. 119 ff.

[4] C. H. Townes and A. L. Schawlow, *Microwave Spectroscopy* (McGraw-Hill Book Co., Inc., New York, 1955), p. 239.

[5] L. Pauling, *Nature of the Chemical Bond* (Cornell University Press, Ithaca, New York, 1948), p. 246.

TABLE I. Cl^{35} pure quadrupole frequencies in $AgClO_2$ and $NaClO_2$

Temperature	$AgClO_2$	$NaClO_2 \cdot XH_2O$[a]
77°K	...	53.33±0.08 Mcps
197°K	...	52.60±0.08 Mcps
297°K	54.08±0.07 Mcps	51.82±0.06 Mcps

[a] The sample of $NaClO_2$ was obtained from the Matheson Company, and was used without further purification. The extent of hydration is unknown.

p_π atomic orbital on the chlorine. The effect of this change is to decrease the magnitudes of both the asymmetry parameter and the components of the field gradient tensor, as shown in Fig. 3. This will in turn necessitate choice of a smaller value of A (increase in residual positive charge on the chlorine) to fit the pure quadrupole data. However, both bond energies[6] and the observed chlorine-oxygen bond lengths[1] imply that little double bond character exists. Covalent bonding between the silver and chlorine will likewise lead to a decrease in the magnitudes of the field gradient components, but will lead to an upward shift in the asymmetry parameter which will more than compensate for the first effect. This will require choice of a larger value for A. Such covalent bonding is suggested by the small silver-chlorine distance, as well as by the intense color of the solid material. However, in view of the crude nature of the model employed here, it does not appear desirable to attempt further refinement of the electronic structure calculation. The results cited above ($\rho \leqq +1$, $\eta \leqq 0.73$) are of course not unique, because of the multiplicity of parameters which enter into the theoretical description of the model employed here.

Determination of the asymmetry parameter from single crystal work on the silver salt will be difficult, if not experimentally impossible, since this material crystallizes from solution in small, extremely thin platelets. Its explosive nature in the dry state also makes it awkward to work with. One of two samples prepared by the author exploded due to carelessness in handling. The sodium salt may be obtained commercially in impure form, while the silver salt is easily prepared by precipitation from aqueous solutions of the sodium salt with silver nitrate. Purification may be effected by recrystallization from water. A sample of lead chlorite has been prepared in a similar fashion, but no

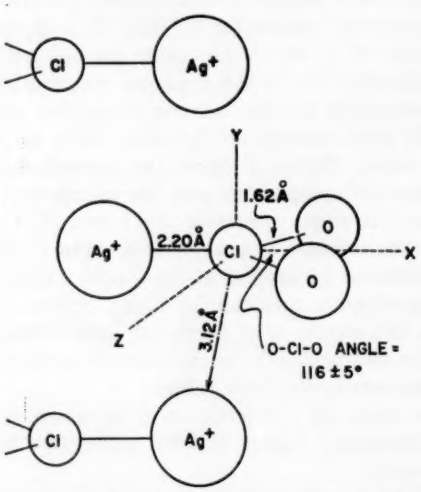

FIG. 1. A portion of the crystal structure of $AgClO_2$, showing distances and relative positions. Two additional silver ions are situated just off the z axis, one at a distance of +3.1 A from the chlorine and the other at −3.1 A.

[6] J. Duchesne and L. Burnelle, J. Chem. Phys. **21**, 2005 (1953).

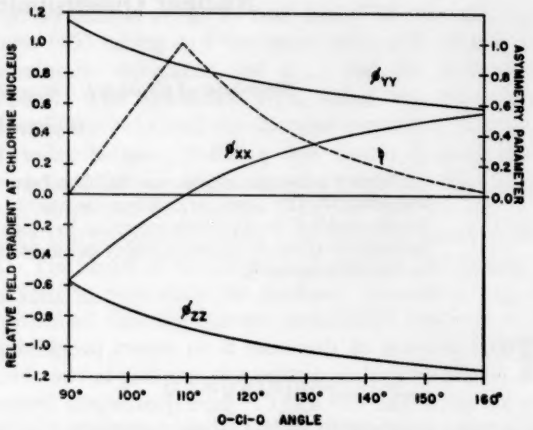

FIG. 2. Asymmetry parameter and principa components of field gradient tensor as a function of the O—Cl—O angle. Field gradients are in units of the chlorine atomic field gradient ϕ_0.

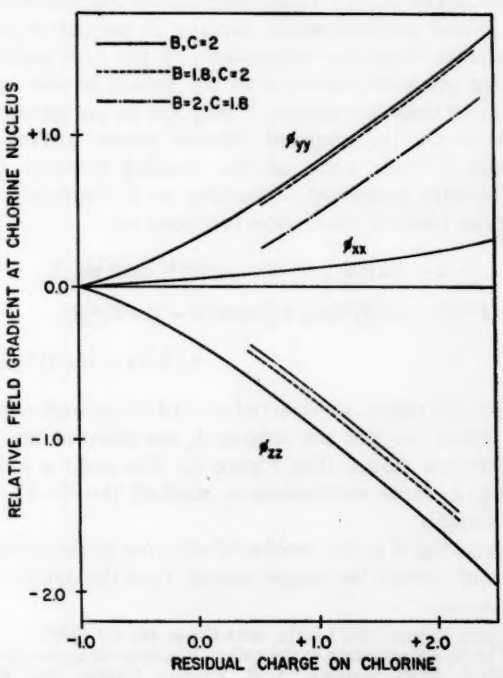

FIG. 3. Principal components of field gradient tensor as a function of the residual charge on the chlorine atom.

pure quadrupole resonance has been found at the time of writing. Further work on this and other salts of chlorite ion is in progress.

The pure quadrupole spectra were observed with a conventional superregenerative spectrometer, and frequencies were measured with a surplus BC-221 heterodyne beat frequency meter. Estimated errors in the frequency measurements represent uncertainty in distinguishing side frequencies from the principal spectrometer response.

THE JOURNAL OF CHEMICAL PHYSICS VOLUME 32, NUMBER 2 FEBRUARY, 1960

Empirical Intermolecular Potential for Inert Gas Atoms

HAROLD W. WOOLLEY

National Bureau of Standards, Washington, D. C.

(Received September 16, 1959)

Transport and thermodynamic calculations for gases at high temperature call for reliable interaction potentials at close approach. Potentials for the noble gases can be extrapolated approximately, yet with some reliability, from the empirical fit of properties in the ordinary range, using a screened Coulomb repulsion and a dispersion attraction reduced by a suitable factor at close approach. Parameters for this potential can be obtained approximately from the known parameters for the exp-six potential. The resulting empirical coefficient for the Coulomb term is found to be of the general order of magnitude given by the product of the nuclear charges. If the theoretical Coulomb repulsion is used, the screening exponent may alternatively be chosen on the basis of other empirical parameters.

I. INTRODUCTION

MOLECULAR interactions are so dependent on details concerning interacting molecules that no uniquely best general empirical potential for the correlation of all gas properties for simple gases is to be expected. Lennard-Jones 6–12 and 6–9 potentials are often used but theory and experimental results on some substances indicate that the repulsion energy can be represented better if an exponential function is used. With the dispersion energy represented somewhat satisfactorily with the inverse sixth power term, Mason[1] and Rice and Hirschfelder[2] have used a conveniently expressed potential function

$$\phi(r)=[\epsilon/(1-6/\alpha)]\{(6/\alpha)\exp[\alpha(1-r/r_m)]-(r_m/r)^6\} \quad (1)$$

which can be regarded as a simplification of a potential used by Buckingham and Corner.[3] Mason and Rice[4,5] have determined values of α, r_m, and ϵ/k for a number of gases, based on second virial, transport, and crystal data. Although the properties fitted are represented satisfactorily in the regions of observation, the extrapolation of predicted values to very high temperature encounters a logical difficulty due to the spurious maximum in the exp-six potential at small distances of separation. While the use of an infinite potential for all smaller radii has permitted satisfactory virial calculations for ordinary temperature ranges, a still more realistic potential is needed if it is desired to extend calculations indefinitely upward to higher temperature.

In the ordinary extreme of close internuclear approach between noble gas atoms, the repulsion energy varies as the inverse first power of the separation distance. At greater separation, this repulsion is reduced, largely because of screening effects of the electrons. While the use of a repulsion energy of such proper limiting form seems appropriate, the usual inverse sixth power attraction term would still overpower it at close approach and give an improper behavior. The Buckingham-Corner adjustment of a factor $\exp[-4(r_m/r-1)^3]$, included in the attractive term for $r<r_m$ and omitted for $r>r_m$, removes this difficulty but has the inconvenience of using different analytical forms in different regions.

II. SELECTION OF A POTENTIAL FUNCTION

A function of considerable adaptability in introducing the analytic adjustments can be arranged in the form

$$U/\epsilon=[(1+\sum_n\gamma_n)/(1+\sum_n\gamma_n-\nu+\mu)]\{[(\nu-\mu)/(1+\sum_n\gamma_n](r_m/r)[\prod_n F_n(r)/\prod_n F_n(r_m)]-(r_m/r)^\nu[f(r)/f(r_m)]\} \quad (2)$$

where γ_n is the value of $-r_m F_n'(r_m)/F_n(r_m)$ and μ is $r_m f'(r_m/)f(r_m)$. The unspecified factors $F_n(r)$ are considered to represent effects due to screening of the nuclear charge by the electrons and in a simplest form

[1] E. A. Mason, J. Chem. Phys. **22**, 169 (1954).
[2] W. E. Rice and J. O. Hirschfelder, J. Chem. Phys. **22**, 187 (1954).
[3] R. A. Buckingham and J. Corner, Proc. Roy. Soc. (London) **A189**, 118 (1947).
[4] E. A. Mason and W. E. Rice, J. Chem. Phys. **22**, 843 (1954).
[5] E. A. Mason and W. E. Rice, J. Chem. Phys. **22**, 522 (1954).

using only one such factor $F_n(r)/F_n(r_m)$ is taken as $\exp[\gamma(1-r/r_m)]$. The factor $f(r)$ is a function to be suitably chosen so as to remain near its value at equilibrium separation for all greater distances while going to zero suitably rapidly as the internuclear separation goes to zero. The resulting potential with $\nu=6$ and with the single $F_n(r)$ mentioned becomes

$$U/\epsilon=[(1+\gamma)/(\gamma-5+\mu)]\{[(6-\mu)/(1+\gamma)]+(r_m/r)\exp[\gamma(1-r/r_m)]-(r_m/r)^6(f/f_m)\}. \quad (3)$$

Frost and Woodson[6] have suggested that the $1/r^\nu$ catastrophe be avoided by subtraction of

$$a^\nu A_{\nu-1}(ar)/(\nu-1)!$$

from the $1/r^\nu$, in case the repulsion potential is of the form $[(c/r)+b]e^{-ar}$, with the function

$$A_{\nu-1}(\alpha)=\int_1^\infty e^{-\alpha x}x^{\nu-1}dx=[(\nu-1)!/\alpha^\nu]e^{-\gamma}\sum_{k=0}^{\nu-1}\alpha^k/k!.$$

In the present application, this is equivalent to using

$$f=1-[1/(\nu-1)!](\gamma r/r_m)^\nu A_{\nu-1}(\gamma r/r_m)$$
$$=1-\exp(-\gamma r/r_m)\sum_{k=0}^{\nu-1}(\gamma r/r_m)^k/k! \quad (4)$$

which leads to $\mu=\mu_\nu$ where

$$\mu_\nu=\gamma^\nu e^{-\gamma}/(\nu-1)![1-\gamma^\nu A_{\nu-1}(\gamma)/(\nu-1)!]$$
$$=\gamma^\nu e^{-\gamma}/(\nu-1)![1-e^{-\gamma}\sum_{k=0}^{\nu-1}\gamma^k/k!]. \quad (5)$$

Before their proposal was published, a somewhat similar correction factor was examined, suggested by physical considerations. It was desired to take the attractive term to be proportional to the product of polarizabilities of the interacting molecules, with the estimates of polarizability based on the squares of mean square radii evaluated only within nonintersecting spheres centered on the nuclei. Thus, it was supposed that each estimated polarizability α could be adjusted in the ratio*

$$\alpha/\alpha_\infty=[1-e^{-\beta r}\sum_{k=0}^{2n+2}(\beta r)^k/k!]^2/[1-e^{-\beta r}\sum_{k=0}^{2n}(\beta r)^k/k!]^2 \quad (6)$$

based on Slater-type functions $\psi=r^{n-1}e^{-\beta r}$. With like atoms with $n=1$, this suggests

$$f=[1-e^{-\beta r}\sum_{k=0}^{4}(\beta r)^k/k!]^4/[1-e^{-\beta r}\sum_{k=0}^{2}(\beta r)^k/k!]^4 \quad (7)$$

or

$$f=\left[1-\frac{1}{4!}(\gamma r/r_m)^5A_4(\gamma r/r_m)\right]^4\Big/\left[1-\frac{1}{2!}(\gamma r/r_m)^3A_2(\gamma r/r_m)\right]^4$$
$$=[1-\exp(-\gamma r/r_m)\sum_{k=0}^{4}(\gamma r/r_m)^k/k!]^4/[1-\exp(-\gamma r/r_m)\sum_{k=0}^{2}(\gamma r/r_m)^k/k!]^4 \quad (8)$$

leading to $\mu=4\mu_5-4\mu_3$ where μ_5 and μ_3 are again given by Eq. (5).

Objection could be made that this must give an exaggerated estimate for the reduction in polarizability, since the electron cloud may more nearly be but slightly displaced initially rather than being effectively limited to so greatly diminished a region of space. Indeed, the net charge displacement is expected to be of a second-order nature, on the basis that the closed shells contain like numbers of electrons of opposite spins so that first-order effects cancel. We have also ignored the effect on the London forces due to change of ionization energy with distance.

A function appearing easier to calculate but having similar behavior was suggested by the net eighth power of the radius at close approach given by Eq. (7). Taking

$$f=[1-\exp(-\gamma r/r_m)]^8 \quad (9)$$

one has $\mu=8\gamma(e^\gamma-1)^{-1}$, so that the potential then takes the form

$$U/\epsilon=\frac{1+\gamma}{\gamma-5+8\gamma(e^\gamma-1)^{-1}}\left[\frac{6-8\gamma(e^\gamma-1)^{-1}}{1+\gamma}(r_m/r)\right.$$
$$\left.\cdot\exp[\gamma(1-r/r_m)]-(r_m/r)^6\left(\frac{1-\exp(-\gamma r/r_m)}{1-e^{-\gamma}}\right)^8\right]. \quad (10)$$

III. COMPARISON AMONG FUNCTIONS AND DATA

A graphical comparison of the different f's suggested is provided in Fig. 1, where the function proposed by Frost and Woodson is seen to be closer than the present eighth power function to the one based directly on the quasi-physical estimate for the polarizability effect. The use of $\gamma/2$ rather than γ in the present eight power f would give a function

$$f=[1-\exp(-\gamma r/2r_m)]^8 \quad (11)$$

more closely agreeing numerically with the estimate of Eqs. (6) to (8), but it would sacrifice an advantage,

[6] A. A. Frost and J. H. Woodson, J. Am. Chem. Soc. **80**, 2615 (1958).

* Elsewhere throughout this paper, α is the usual parameter in the exp-six potential.

now to be discussed, of ease of convertibility of known parameters obtained for the exp-six potential.

For a thorough study of the potential, one wants tables of virial coefficients and of functions for transport property estimation. A simpler preliminary step may be taken, however, involving a comparison between this potential and the exp-six potential in the general region of the equilibrium separation, r_m. For this purpose, values of γ have been determined such that derivatives of the simpler potential obtained by omitting the f factors are identical with those for the exp-six function for various values of α. Similarly, values of γ have been obtained for which the close approach distance σ for the same energy as at infinite separation is identically the same as for various integer values of α. These corresponding values of α and γ have been assembled in Table I with values of γ given by

$$\gamma=\alpha-0.935-3.3/\alpha \qquad (12)$$

also, which is found to be a convenient formula for estimation purposes. The approximate agreement between the three γ's based on different details of the potential, supported by further agreement at slightly smaller separations, suggests that, in the absence of appreciable effects from the functions f, usable estimates for parameters can be obtained from those for the exp-six function by retaining r_m and ϵ unchanged, and using Eq. (12) for the value of γ. Slightly more complicated formulas for γ in case there is appreciable contribution by the functions f could also be obtained.

The potential function is shown in a compact way in the potential energy valley and up to very high energies in Fig. 2. The ordinate plotted linearly is $\log_{10}(U/\epsilon+2)$, whose unit steps are decades for $U/\epsilon+2$, and the abscissa is r/r_m. In addition to the function given by Eq. (10) for integer values of γ, shown by solid curves

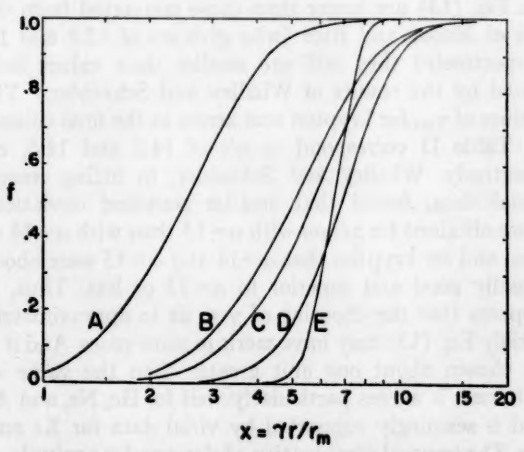

FIG. 1. Factors f to improve the attractive potential at close approach. *A*, Eq. (9); *B*, Eq. (11); *C*, Eq. (4), the factor of Frost and Woodson; *D*, Eq. (8); *E*, the Buckingham-Corner factor shown for $\gamma=10$.

TABLE I. Corresponding values of α and γ.

α	γ (a)	(b)	(c)	(d)
11	9.85	9.79	9.763	9.765
12	10.86	10.81	10.790	10.790
13	11.88	11.82	11.812	11.811
14	12.89	12.83	12.830	12.829
15	13.90	13.85	13.845	13.845

[a] To fit U_m''.
[b] To fit U_m'''.
[c] To fit σ/r_m.
[d] By Eq. (12).

from $\gamma=10$ to $\gamma=15$, Lennard-Jones 6–12 and 6–9 potentials are shown by dashed curves. For comparison, the scattering data results of Amdur and others[7–12] and of Berry[13,14] are also shown, reduced to suitable units for the graph using principally values of ϵ and r_m of Mason and Rice[4] and, in the case of helium, of Kilpatrick, Keller, and Hammel.[15]

For helium, the value of γ converted from the α of Kilpatrick, Keller, and Hammel is 11.2 as listed in the second column of Table II. This is seen to agree fairly well with the lower energy data of Amdur[7] for helium in Fig. 2.

In the case of neon, it may be noted that there is approximate numerical agreement between the converted value for γ, namely 13.3, and the value from this graph of Amdur's neon potential[9] just under the $\gamma=13$ curve and the upper energy value of Berry's neon potential function at close approach.[13]

For argon, the numerical agreement is not as close. Here the converted value of γ from Mason and Rice's α is 12.8, while the data of Amdur[10] for argon indicate a little less than 11. The data of Berry[14] are very near to the $\gamma=12$ curve, intermediate between the other two values.

In the cases of krypton and xenon, the curves for Amdur's scattering data[11,12] differ more drastically from local parallelism with the family of curves given here, although in the single case of krypton the high energy end does just reach the $\gamma=11$ curve and so might be considered almost in agreement here with the 11.1 based on the α of Mason and Rice.

It might seem that there should be fairly close agreement between the empirical function obtained by fitting experimental data and the limiting Coulomb repulsion at very close approach. On the other hand, it might be considered satisfactory if the energy would

[7] I. Amdur and A. L. Harkness, J. Chem. Phys. **22**, 664 (1954).
[8] I. Amdur, J. Chem. Phys. **17**, 844 (1949).
[9] I. Amdur and E. A. Mason, J. Chem. Phys. **23**, 415 (1955).
[10] I. Amdur and E. A. Mason, J. Chem. Phys. **22**, 670 (1954).
[11] I. Amdur and E. A. Mason, J. Chem. Phys. **23**, 2268 (1955).
[12] I. Amdur and E. A. Mason, J. Chem. Phys. **25**, 624 (1956).
[13] H. W. Berry, Phys. Rev. **99**, 553 (1955).
[14] H. W. Berry, Phys. Rev. **75**, 913 (1949).
[15] Kilpatrick, Keller, and Hammel, Phys. Rev. **97**, 9 (1955).

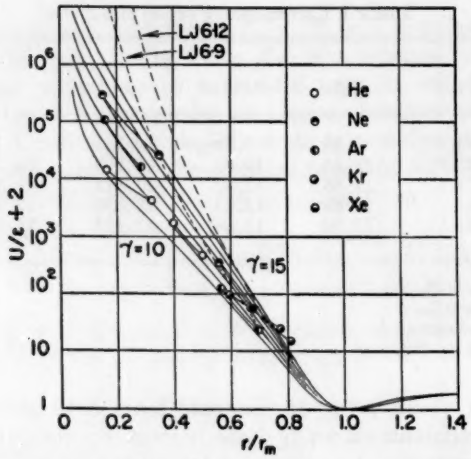

FIG. 2. The potential function given by Eq. (10) with integer γ from 10 to 15. Lennard-Jones 6–12 and 6–9 potentials and inert gas scattering data are also shown.

show qualitative agreement here in approaching infinity as $1/r$, even with a nonphysical proportionality factor. Nevertheless, it is of some interest to note whether this factor as obtained empirically is of the same order of magnitude as the theoretical value. Identification of the limiting $1/r$ form with the internuclear repulsion at close approach gives the estimated product of atomic numbers as

$$(Z_1Z_2)_{calc}=[(6-\mu)e^{\gamma}/2(\gamma-5+\mu)] \cdot (1/R_\infty)(k/hc)(\epsilon/k)(r_m/a_0) \quad (13)$$

where R_∞ is the Rydberg constant; 109 737 cm^{-1} and a^0 is the radius of the first Bohr orbit for hydrogen, 0.5292 A, while hc/k is 1.4388 cm deg. Values of these Z_1Z_2 products calculated from Eq. (13) are compared with the actual Z_1Z_2 products for colliding pairs in the fifth and sixth columns of Table II. For small atoms the values of $(Z_1Z_2)_{calc}$ thus obtained are larger than the actual Z_1Z_2 products; for large atoms the relative sizes are reversed. For argon, the scattering data and the thermal and transport data together appeared to favor a γ near to 12 rather than the 12.8 listed in Table II on the basis of the Mason and Rice correlation alone. If this value $\gamma=12$ be used, the $(Z_1Z_2)_{calc}$ obtained is near 400 corresponding to about 20 for the Z's, thus agreeing fairly well with the actual $Z=18$ for this case. The appreciable shift in $(Z_1Z_2)_{calc}$ as a result of this change in γ shows the great sensitivity to γ in affecting this adjustment. Accordingly, it appears appropriate to examine a reversed procedure of fitting. The last column of Table II shows approximate values for γ obtained by such a reversed calculation procedure, based on the Z_1Z_2 actually occurring and using the other empirical parameters previously known. These values of γ_{est} were obtained by interpolating in Table III, which gives corresponding values of γ and of

$$\log_{10}\frac{Z_1Z_2(hc/k)R_\infty}{(\epsilon/k)(r_m/a_0)},$$

taken as equal to

$$\log_{10}\frac{[6-8\gamma(e^{\gamma}-1)^{-1}]e^{\gamma}}{2[\gamma-5+8\gamma(e^{\gamma}-1)^{-1}]}$$

in accord with Eq. (13).

TABLE II. Constants for the intermolecular potentials for various pairs of molecules.

	γ[a]	ϵ/k (°K or C)	r_m (A)	$(Z_1Z_2)_{calc}$	Z_1Z_2	γ_{est}
He—He	11.2	7.563	3.189	10.2	4	10.1
Ne—Ne	13.3	38.0	3.147	310	100	12.1
Ar—Ar	12.8	123.2	3.866	797	324	11.8
Kr—Kr	11.1	158.3	4.056	250	1296	13.0
Xe—Xe	11.8	231.2	4.450	728	2916	13.4

[a] Converted from empirical values of α, the exp-six parameter.

TABLE III. Correspondence between γ and the Coulomb repulsion.

γ	$\log_{10}\frac{Z_1Z_2(hc/k)R_\infty}{(\epsilon/k)(r_m/a_0)}$
9	3.782
10	4.121
11	4.476
12	4.844
13	5.220
14	5.603
15	5.991
16	6.384

The values of γ_{est} for the first three colliding pairs in Table II are lower than the corresponding values in column 2 based on the findings of Mason and Rice. While the values of γ_{est} for krypton and xenon based on Eq. (13) are larger than those converted from the α's of Mason and Rice (who give α's of 12.3 and 13, respectively) they still are smaller than values indicated by the results of Whalley and Schneider.[16] The values of γ_{est} for krypton and xenon in the final column of Table II correspond to α's of 14.2 and 14.6, respectively. Whalley and Schneider, in fitting second virial data, found that smaller standard deviations were obtained for xenon with $\alpha=15$ than with $\alpha=14$ or less, and for krypton that $\alpha=14$ and $\alpha=15$ were about equally good and superior to $\alpha=13$ or less. Thus, it appears that the choosing of γ so as to approximately satisfy Eq. (13) may have merit in some cases. And if it be chosen about one unit greater than the value so obtained, it agrees particularly well for He, Ne, and Ar and is seemingly supported by virial data for Kr and Xe. The unusual combination of slope and magnitude of

[16] E. Whalley and W. G. Schneider, J. Chem. Phys. **23**, 1644 (1955).

the experimental scattering results shown in Fig. 2 for these last two interactions might perhaps be considered as suggesting the need for higher values for γ for separations near r_m. A need for narrowing the potential well in the case of xenon has been mentioned by Amdur and Schatzki.[17] Indeed one would suppose that the form of a truly valid potential function would show a dependence on the principal quantum numbers for the electrons playing the major role in its origin.

It is appropriate to point out that the good quality of potential function representation shown in Fig. 2 is not sufficient to imply that Eq. (10) is a unique form which must be adopted. Consideration of the relative positions of curves A to D in Fig. 1 suggests that a useful modification of the f taken from Frost and Woodson might in some cases be to use 2γ in place of γ in Eq. (4), giving

$$f=1-\exp(-2\gamma r/r_m)\sum_{k=0}^{r-1}(2\gamma r/r_m)^k/k!, \qquad (14)$$

with μ obtainable from Eq. (5) by replacing γ by 2γ. The position of the corresponding curve in Fig. 1 would be to the right of curve A by exactly the amount that curve C is to the right of curve B, since the abscissas are logarithmic. With this proximity to curve A, the value of f near $r=r_m$ would be so near unity, with any typical γ, that parameter values could be taken essentially the same as for Eq. (10) on the basis of known parameters for the exp-six potential. The resulting potential would be only moderately changed from the graph in Fig. 2. Accordingly, we propose that Eq. (3) might be used with the f given by Eq. (14) in case available calculation procedures would favor its use.

One of the desirable uses for a potential function such as Eq. (10) is to predict reasonably reliable empirical potential interaction energies based on virial and transport data for use in calculations for much higher temperatures. It is naturally to be recognized that the extrapolation to regions of close approach cannot be expected to give highly accurate potentials but still should be useful for rough estimates. This is perhaps well illustrated by the He-He interaction for which various theoretical calculations have been reported. If the empirical parameters used in showing the scattering data in Fig. 2 are retained, it is possible to regard various numerical estimates for the interactions as indicating approximate values of γ. Thus, the calculations of Huzinaga[18] in the region of r/r_m near 0.2 and 0.3 indicate a γ only slightly above the 11.2 empirically obtained from the virial and transport data. The subsequent calculations of Hashino and Huzinaga[19] raise this slightly but not quite so much as to coincide with those of Griffing and Wehner[20] or Sakamoto and Ishiguro[21] whose values are slightly below Slater's[22] in this same separation region and like his would indicate a γ slightly under 12. The results of Rosen[23] for this region plot much closer to the experimental data (8). The numerical results of Lynn,[24] and the semi-empirical function of Buckingham[25] to which Lynn's calculations were adjusted, similarly suggest a change to lower values of γ at close approach. It is probably significant that for r/r_m as small as 0.1, the numerical magnitude of Buckingham's function suggests a γ only slightly more than 10, which agrees well with γ_{est} in Table II, since both results involve estimates depending in some way on the magnitude of the internuclear repulsion at close approach.

[17] I. Amdur and T. F. Schatzki, J. Chem. Phys. **27**, 1049 (1957).

[18] S. Huzinaga, Progr. Theoret. Phys. **18**, 139 (1957).
[19] T. Hashino and S. Huzinaga, Progr. Theoret. Phys. **20**, 631 (1958).
[20] V. Griffing and J. F. Wehner, J. Chem. Phys. **23**, 1024 (1955).
[21] M. Sakamoto and E. Ishiguro, Progr. Theoret. Phys. **15**, 37 (1956).
[22] J. C. Slater, Phys. Rev. **32**, 349 (1928).
[23] P. Rosen, J. Chem. Phys. **18**, 1182 (1950).
[24] N. Lynn, Proc. Phys. Soc. (London) **72**, 201 (1958).
[25] R. A. Buckingham, Trans. Faraday Soc. **54**, 453 (1958).

Electron Spin Resonance Studies of the Potassium Salt of *m*-Dinitrobenzene Negative Ion*

RAYMOND L. WARD

Lawrence Radiation Laboratory, University of California, Livermore, California

(Received September 28, 1959)

A detailed analysis of the electron spin resonance spectrum for the potassium salt of *m*-dinitrobenzene negative ion in DME is presented. Isotopic substitution has been performed in various positions in the molecule. *m*-Dinitrobenzene negative ion exhibits only *one* nitrogen hyperfine interaction of 9.0 gauss, and possesses proton hyperfine interactions of 4.6 gauss for the number 2, 4, and 6 protons and 1.2 gauss for the number 5 proton. The hyperfine spectrum is different for each of the alkali metals, Li, Na, K, Rb, and Cs, but still retains only *one* nitrogen hyperfine interaction. An enriched Li^6 metal salt of *m*-dinitrobenzene indicates no alkali metal hyperfine interaction.

I. INTRODUCTION

POLYATOMIC free radicals, which contain nitrogen atoms, have been found in many cases to possess a dominant nitrogen hyperfine interaction.[1–6] This nitrogen hyperfine splitting, ~9–17 gauss, is usually two to three times larger than any proton hyperfine splitting observed in the same molecule. It is well known that the widths of absorption peaks of proton hyperfine interactions in polyatomic free radicals in dilute solution are quite narrow. Nitrogen-containing polyatomic free radicals, however, possess absorption peaks that are at least an order of magnitude broader than proton peaks. A comparison of the nitrogen absorption peaks in N^{14}-and N^{15}-substituted compounds indicates that this breadth is not due to an electric quadrupole relaxation mechanism.

It is now generally accepted that the isotropic hyperfine interaction, which occurs between the unpaired electron and the protons that lie in the plane of the ring of an aromatic free radical, is due to a $\sigma-\pi$ configuration interaction.[7–10] To describe this isotropic hyperfine interaction it is necessary that the total wave function contains an admixture of an excited-state configuration which will yield an unpaired electron density at the proton in question. This admixture must possess the same symmetry as the ground state of the molecule, and the total wave function must remain an eigenfunction of S^2 and S_z. As pointed out by Weissman,[7] the matrix elements that describe this isotropic hyperfine interaction are linearly dependent upon the mixing parameter and therefore only small admixtures of excited-state configurations are required to account for the proton hyperfine splittings. McConnell and Chestnut[11] have recently presented an elegant treatment of isotropic hyperfine interactions.

In the case of polyatomic free radicals containing nitrogen atoms, such as nitrobenzene negative ion,[5,6] it is not necessary to invoke configuration interaction to produce odd electron density at the nitrogen nucleus. The spatial overlap of the P_z functions of the carbon and nitrogen atoms is sufficient to produce appreciable odd electron density on the nitrogen. The isotropic hyperfine interaction, which is observed in dilute solutions, is thus a measure of the "*S*" character of the total wave function at the nitrogen nucleus.

The earlier survey work on aromatic negative ions containing nitrogen atoms indicated that it would be necessary to invoke both nitrogen and proton hyperfine splittings to interpret the observed spectra.[3,4] The first interpretation, by means of isotropic substitution, was reported a few years ago.[12] Weissman made a partial interpretation of Wuster's salts by means of deuterium, substitution, and recently Tuttle has reported the complete interpretation of Wuster's Blue Ion.[13] Tuttle's analysis indicates that there is appreciable odd electron density in the ring and in the methyl groups attached to the nitrogens, but there is no odd electron density on the nitrogens. An analysis of the hyperfine spectrum of nitrobenzene negative ion indicates both nitrogen and proton hyperfine interactions.[5,6]

An analysis of the complex hyperfine structure of the potassium salt of *m*-dinitrobenzene in 1,2-dimethoxyethane (DME) is presented in this paper. This analysis has brought to light many new and unsuspected interactions both in the magnetic properties of the negative ion and in the chemistry of its preparation.

* This work was performed under the auspices of the U. S. Atomic Energy Commission.

[1] Hutchison, Pastor, and Kowalsky, J. Chem. Phys. **20**, 534 (1952).
[2] Pake, Townsend, and Weissman, Phys. Rev. **85**, 682 (1952).
[3] Chu, Pake, Paul, Townsend, and Weissman, J. Phys. Chem. **57**, 504 (1953).
[4] Pake, Weissman, and Townsend, Discussions Faraday Soc. **19**, 147 (1955).
[5] R. L. Ward and M. P. Klein, J. Chem. Phys. **28**, 518 (1958).
[6] R. L. Ward, J. Chem. Phys. **30**, 852 (1959).
[7] S. I. Weissman, J. Chem. Phys. **25**, 890 (1956).
[8] H. M. McConnell, J. Chem. Phys. **24**, 764 (1956).
[9] H. S. Jarrett, J. Chem. Phys. **25**, 1289 (1956).
[10] R. Bersohn, J. Chem. Phys. **24**, 1066 (1956).
[11] H. M. McConnell and D. B. Chestnut, J. Chem. Phys. **28**, 107 (1958).
[12] S. I. Weissman, J. Chem. Phys. **22**, 1135, (1954).
[13] T. R. Tuttle, Jr., J. Chem. Phys. **30**, 331 (1959).

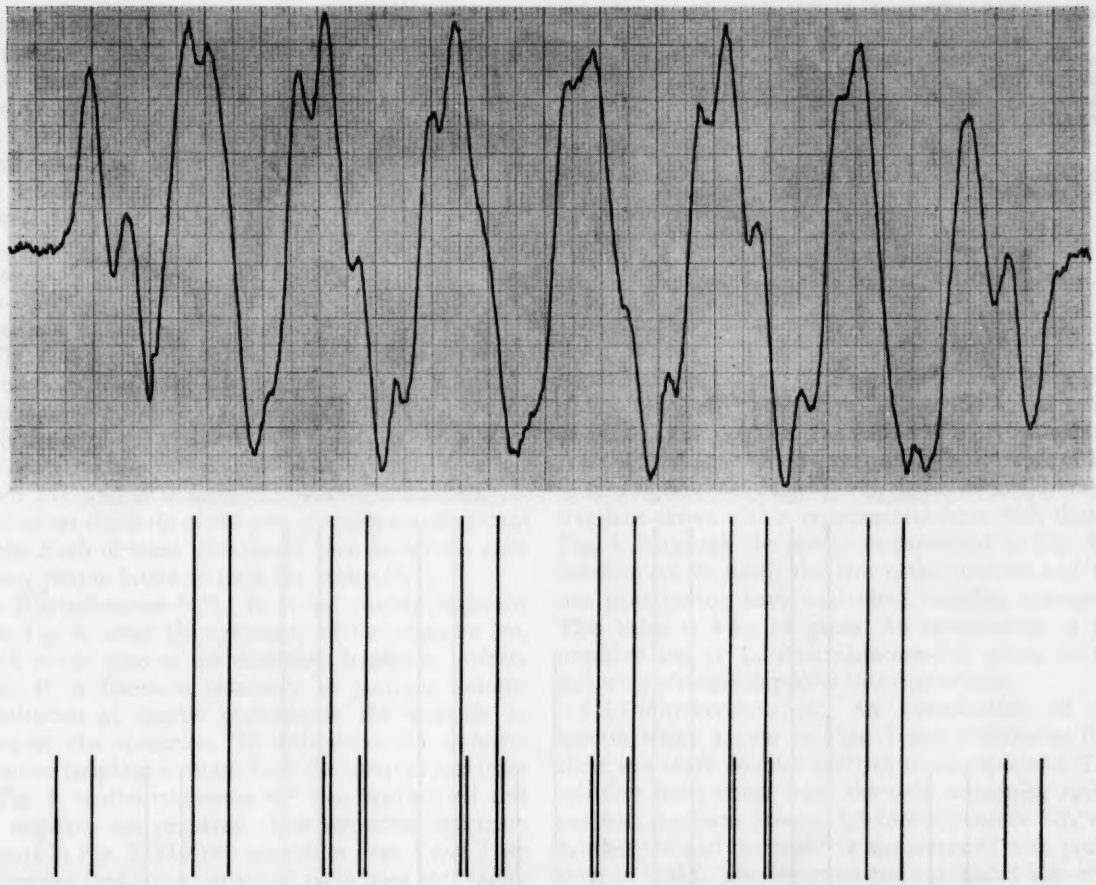

FIG. 1. Observed spectrum of K-m-dinitrobenzene negative ion in DME (above) and calculated spectrum (below).

II. EXPERIMENTAL METHODS AND PREPARATIONS

The following compounds were used in the study of m-dinitrobenzene negative ion in DME:

m-Dinitrobenzene. Reagent grade obtained Eastman Kodak Company.

m-Dinitrobenzene-N_2^{15}. Baker and Adamson's reagent grade benzene was nitrated with a mixture of 95+% N^{15} potassium nitrate, obtained from Bio-Rad Laboratories, and sulfuric acid.

m-Dinitrobenzene-d_4. Benzene-d_6, 99% deuterium obtained from Merck and Company, Limited, was nitrated with a mixture of sulfuric acid and potassium nitrate.

m-Dinitrobenzene-d_4-N_2^{15}. Benzene-d_6, 99% deuterium obtained from Merck and Company, Limited, was nitrated with a mixture of 95+% N^{15} potassium nitrate, obtained from Bio-Rad Laboratories, and sulfuric acid.

1,3-Dinitrobenzene-4-d_1. Paranitrobenzene-d_1 was prepared by the method of Alexander and Burge[14,15] and nitrated with a mixture of sulfuric acid and potassium nitrate.

1,3-Dinitrobenzene-5-d_1. 3,5-Dinitroaniline was prepared from 3,5-dinitrobenzoic acid, obtained from Eastman Kodak Company, by using the Schmidt reaction.[16] The 3,5-dinitroaniline was then reduced by the method described by Kornblum.[17]

1,3-Dinitrobenzene-2-d_1 and 1,3-dinitrobenzene-4-d_1 mixture. Orthonitrobenzene-d_1 was prepared by the method of Alexander and Burge[14,15] and nitrated with a mixture of sulfuric acid and potassium nitrate.

In the synthesis, which consisted of a diazotization reaction of an aniline compound followed by a reduction with hypophosphorous acid, all labile protons in the reaction mixture were replaced by deuterium atoms. This allows a maximum amount of deuterium to be substituted for the corresponding proton. A mixture of 1,3-dinitrobenzene-2-d_1 and 1,3-dinitrobenzene-4-d_1 was prepared instead of pure 1,3-dinitrobenzene-2-d_1, because of the inability to isolate the desired product.

[14] E. R. Alexander and R. E. Burge, Jr., J. Am. Chem. Soc. 72, 3100 (1950).

[15] See also Dauben, Pimental, and Vaughan, J. Am. Chem. Soc. 77, 2886 (1955).

[16] H. Wolff, *Organic Reactions*, Roger Adams, editor (John Wiley & Sons, Inc., New York 1946), Vol. III, p. 307.

[17] N. Kornblum, *Organic Reactions*, Roger Adams, editor, (John Wiley & Sons, Inc., New York, 1944), Vol. II, p. 296.

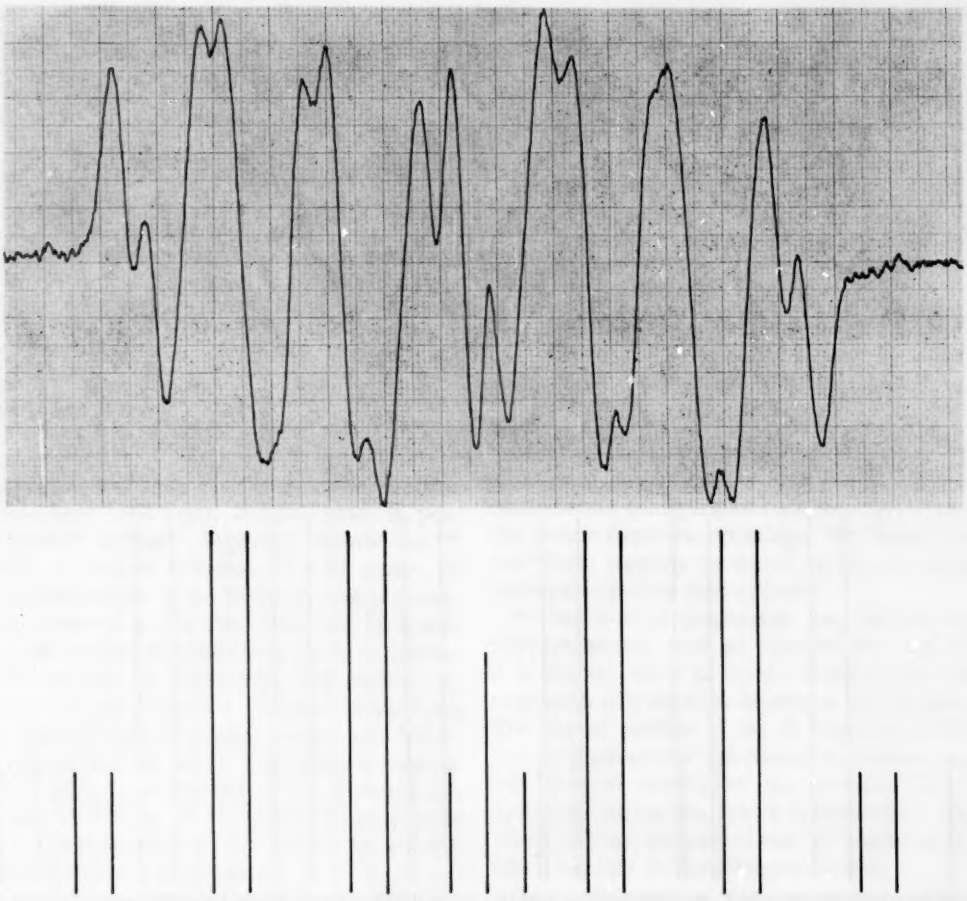

FIG. 2. Observed spectrum of K-*m*-dinitrobenzene-N_2^{15} negative ion in DME (above) and calculated spectrum (below).

All samples used in the preparation of the negative ions were recrystallized and dried by pumping. The preparation of the negative ion has already been described elsewhere.[18]

The electron spin resonance measurements were performed in a conventional spectrometer operating at 9300 Mc/sec with a low frequency of field modulation and a synchronous detector.

All spectra presented were recorded as the derivative of the absorption as a function of the magnetic field. Each spectrum was calibrated with an auxiliary proton resonance probe as the spectrum was being recorded. The proton coupling constants were roughly determined from the corresponding isotopic negative ion, and then were refined by comparison with the spectra in Figs. 1 and 2. The splittings observed were obtained by measuring distances between the maximum of different peaks. The over-all length of the hyperfine pattern was difficult to measure due to difficulty in distinguishing the tails of the absorption curves from the base line, and in the case of the deuterated species there was a small amount, ~10 to 15%, of the undeuterated material present, and in all cases its hyperfine pattern extended slightly beyond that of the deuterated negative ion. The lengths of the *m*-dinitrobenzene and *m*-dinitrobenzene-N_2^{15} negative ion hyperfine spectrum, measured from the first inflexion to the last inflexion, are listed in Table I.

[18] Paul, Lipkin, and Weissman, J. Am. Chem. Soc. **78**, 116 (1956).

III. EXPERIMENTAL RESULTS ON THE POTASSIUM SALT OF *m*-DINITROBENZENE DISSOLVED IN DME

The reaction between an alkali metal and an aromatic hydrocarbon containing a nitro group dissolved in 1,2-dimethoxyethane at room temperature produces a colored solution which in the concentration range 10^{-3} to 10^{-4} *M* usually yields a very complex hyperfine spectrum. However, a few of the nitro compounds already studied, among them *p*-dinitrobenzene, yield a colored solution which shows no electron spin resonance.

The hyperfine structure of nitrobenzene negative ion prepared with potassium in DME has been interpreted as mentioned in the foregoing.[5,6] The nitrogen coupling constant is 11.1 gauss, and the coupling constant for the equivalent two ortho and one para pro-

tons is 3.7 gauss. A value of ≤ 0.65 gauss was estimated for the meta protons by line-width considerations. A simple-minded valence-bond picture of nitrobenzene negative ion agrees with the equivalence of the two ortho and the para protons, and allows an appreciable density on the nitrogen atom. This picture also predicts zero density for the two meta protons. It would be of interest to determine how far this simplified valence-bond picture extends in the nitrobenzene negative ion series.

m-Dinitrobenzene. The hyperfine spectrum for the potassium salt of *m*-dinitrobenzene in DME appears in Fig. 1. If the assumption that the nitrogen hyperfine interactions dominate the spectrum, as they do for nitrobenzene negative ion, one would expect either an equivalence of the two nitrogens and therefore a basic five-line structure of 1:2:3:2:1 intensity ratios, or between five and nine lines of different intensities depending on the ratio of the two nitrogen coupling constants. Each of these lines would then be further split by any proton interactions in the molecule.

m-Dinitrobenzene-N_2^{15}. It is not readily apparent from Fig. 1, using the symmetry of the negative ion, which nuclei possess the dominant hyperfine interactions. It is therefore necessary to perform isotopic substitution at specific positions in the molecule to interpret the spectrum. To determine the nitrogen hyperfine coupling constant from the complex spectrum of Fig. 1, *m*-dinitrobenzene-N_2^{15} was synthesized and the negative ion prepared. This hyperfine spectrum appears in Fig. 2. The two spectra in Figs. 1 and 2 are so complex that a comparison of them does not readily yield a choice for the two nitrogen coupling constants.

m-Dinitrobenzene-d_4 and *m*-Dinitrobenzene-d_4-N_2^{15}. It would be exceedingly helpful to be able to observe the nitrogen hyperfine interactions without the additional splittings due to the protons. As noted in the report on nitrobenzene negative ion,[6] deuterium substitution in the molecule simplified the spectrum whenever no deterium splitting was observed. Following this line of reasoning, *m*-dinitrobenzene-d_4 and *m*-dinitrobenzene-d_4-N_2^{15} were synthesized and the corresponding negative ions prepared. The hyperfine spectra of these negative ions appear in Fig. 3. These spectra give the very interesting and somewhat unexpected results that only one nitrogen atom possesses any odd electron density. The ratio of the splittings for the N^{15} and N^{14} isotopes is $9.0/12.5=0.72$. This agrees quite well with the ratio of the nuclear gyromagnetic ratios for these two isotopes.

The absence of two nitrogen hyperfine interactions in the *m*-dinitrobenzene negative ion initiated a more thorough study of the potassium salt's hyperfine pattern. Various deuterated species were synthesized as noted in Sec. II.

1,3-Dinitrobenzene-4-d_1. The negative ion of 1,3-dinitrobenzene-4-d_1 was prepared and its hyperfine spectrum appears in Fig. 4. The calculated spectrum appears in the bottom part of Fig. 4. It has been possible under better resolution, but poorer signal noise, to resolve the doublets that appear in the calculated spectrum. The hyperfine spectrum of the mixture of 1,3-dinitrobenzene-2-d_1 and 1,3-dinitrobenzene-4-d_1 negative ions agrees within experimental error with that of Fig. 4. Although the spectrum presented in Fig. 4 is inconclusive in itself, the two ortho protons and the one para proton have equivalent coupling constants. This value is 4.6 ± 0.1 gauss. An examination of the negative ion of 1,3-dinitrobenzene-5-d_1 given in the following strongly supports this equivalence.

TABLE I. Coupling constants and lengths of hyperfine patterns for the K salt of *m*-dinitrobenzene in DME.

	Coupling constants[a]	Length of hyperfine pattern[a]
m-dinitrobenzene	$A_N14=9.0\pm0.1$	31.1 ± 0.4
m-dinitrobenzene-N_2^{15}	$A_N15=12.5\pm0.1$	26.0 ± 0.4
1,3-dinitrobenzene-5-d_1	A_{p-5}[b]$=1.2\pm0.1$	
1,3-dinitrobenzene-4-d_1	$A_{p-2}=4.6\pm0.1$	
	$A_{p-4}=A_{p-6}=4.6\pm0.1$	

[a] Measured in gauss.
[b] A_{p-5} is the coupling constant for proton No. 5, etc.

1,3-Dinitrobenzene-5-d_1. An examination of the spectra which appear in Figs. 1 and 2 indicates that there is a small doublet splitting to be explained. This splitting must come from the only remaining spin-$\frac{1}{2}$ particle, the meta proton. 1,3-Dinitrobenzene-5-d_1 was synthesized and the negative ion prepared with potassium in DME. The observed and calculated hyperfine spectrum appears in Fig. 5. This spectrum establishes that the doublet splitting is due to the meta proton, and this spectrum also demonstrates quite nicely the equivalence of the two ortho and the para protons. The coupling constant for the meta hydrogen is 1.2 ± 0.1 gauss.

IV. DISCUSSION OF THE K SALT OF *m*-DINITROBENZENE IN DME

It is now possible to construct the hyperfine spectrum for the potassium salt of *m*-dinitrobenzene and *m*-dinotrobenzene-N_2^{15} in DME with the coupling constants derived from the isotopic substitution. These spectra appear in the bottom parts of Figs. 1 and 2. Even though an intensity comparison is somewhat difficult owing to the observation of the derivative of the absorption spectrum, it can be seen that the theoretical spectrum agrees quite well with the observed spectrum.

The coupling constants, listed in Table I, give an odd electron density map at the positions of the magnetic nuclei in the molecule. Unfortunately, it is not possible to predict how much of the odd electron density resides on the oxygens of the nitro group, and therefore a correlation between the total unpaired density on the molecule and the total observed splitting is not possible at this time.

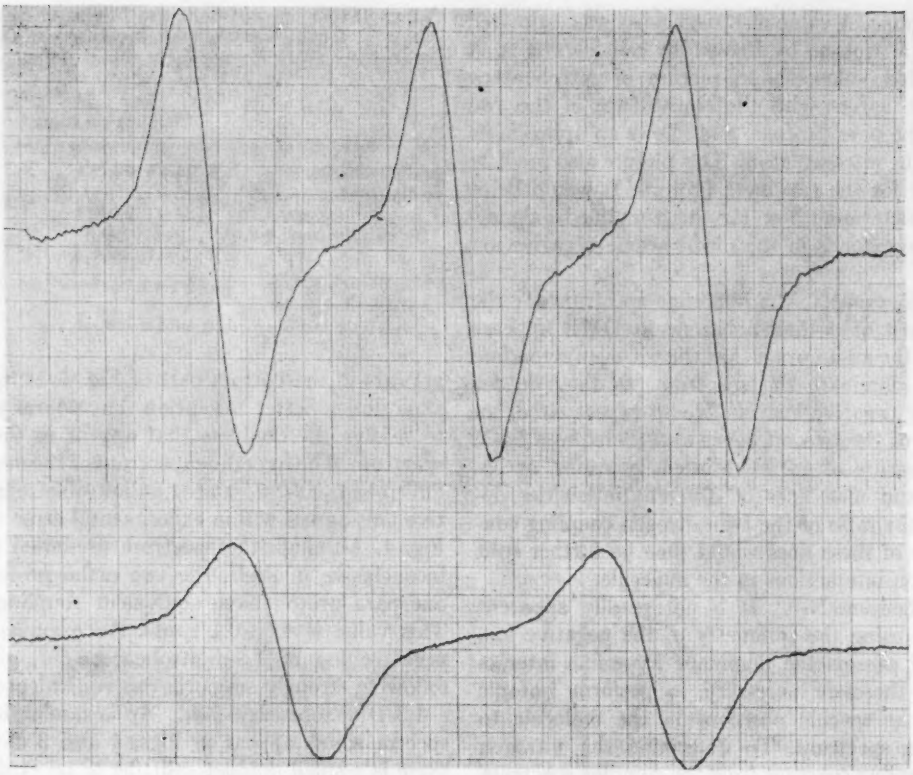

FIG. 3. Observed spectrum of K-*m*-dinitrobenzene-d_4 negative ion in DME (above) and observed spectrum of K-*m*-dinitrobenzene-d_4-N_2^{15} in DME (below).

As mentioned in the foregoing, a study of *m*-dinitrobenzene negative ion with respect to a simplified valence-bond picture is of interest. In this case the valence-bond picture predicts, for a planar negative ion, two separate sets of resonance structures. If the exchange between these two sets is slow, compared to the reciprocal of the nitrogen hyperfine splitting (expressed as a frequency), there would be only one nitrogen hyperfine interaction observed. This theory would also predict equal density on the two ortho protons and the one para proton and zero density on the meta proton. Experimentally it is observed that there is odd electron density on the meta proton. This fact therefore tends to throw doubt on this interpretation.

The interesting observation that only one nitrogen atom in *m*-dinitrobenzene negative ion has appreciable odd electron density raises the question: Is this a peculiarity of the *m*-dinitrobenzene negative ion or do other similar compounds behave in the same manner? It has been observed in this laboratory that many polynitro aromatic free radicals exhibit this single nitrogen hyperfine interaction.[19] A notable example is the series of nitromesitylene negative ions. Nitromesitylene, dinitromesitylene, and the trinitromesitylene negative ions each contain one dominant nitrogen hyperfine interaction of 16.5, 14.6, and 12.6 gauss, respectively. Each negative-ion hyperfine spectrum also contains appreciable proton splitting. The very well-resolved trinitromesitylene negative-ion spectrum contains a basic triplet with each of the triplet peaks split into ten lines of intensities approaching the binomial coefficients.

[19] R. L. Ward (unpublished observations).

V. POSITIVE ION EFFECT

The negative ions reported in this paper were prepared with potassium metal because of the ease in handling the metal and also because previous experience indicated that its perturbation on the negative ion was small. It has been reported that the hyperfine pattern of sodium preparations of naphthalene negative ion in tetrahydrofuran differ from the spectra of salts of the other alkali metals.[20] A resolvable sodium hyperfine interaction has also been observed in the sodium salt of benzophenone in DME,[21] and a possible sodium hyperfine interaction has been observed in the sodium salt of nitrobenzene in DME.[5]

To determine the possibility of a positive ion effect, the entire series of alkali metals, Li, Na, K, Rb, and Cs, were used to prepare the negative ion of *m*-dinitrobenzene in DME. The colors of the solutions vary from

[20] R. L. Ward and S. I. Weissman, J. Am. Chem. Soc. **79**, 2086 (1957).

[21] F. C. Adam and S. I. Weissman, J. Am. Chem. Soc. **80**, 1518 (1958).

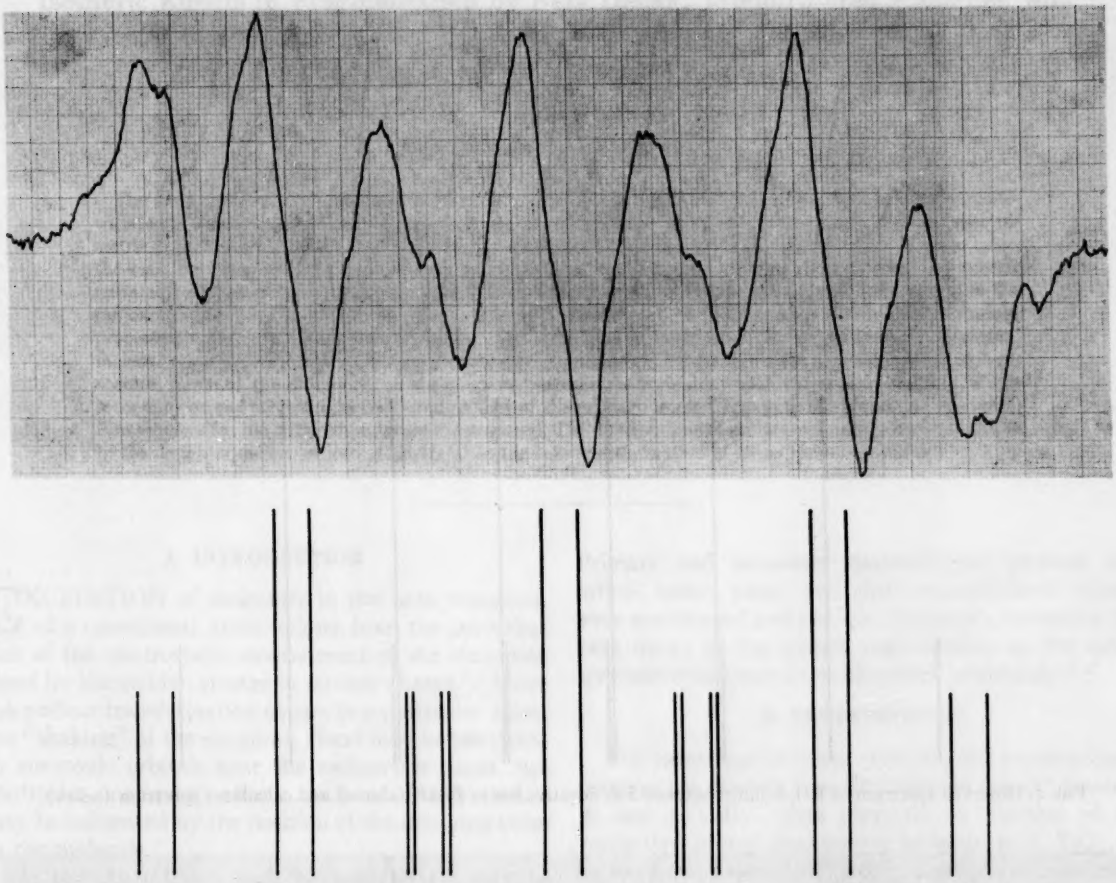

FIG. 4. Observed spectrum of K-1,3-dinitrobenzene-4-d_1 negative ion in DME (above) and calculated spectrum (below).

a light yellow for the Li salt to a dark orange for the Cs salt. The hyperfine spectra, observed in dilute solution, are different for each alkali metal salt. As an example, the hyperfine spectrum of the Li salt of m-dinitrobenzene in DME given in Fig. 6 should be compared with that of the K salt in Fig. 1. The differences in the spectra may be due to a variation in the nitrogen or proton coupling constants for each metal, or to an alkali metal hyperfine interaction. It should be possible to distinguish between these various effects by again restorting to isotopic substitution.

An investigation of the d_4 compound will yield information about the nitrogen hyperfine interaction. The negative ion of m-dinitrobenzene-d_4 was prepared in DME with each of the alkali metals, and in each case a basic triplet was observed with the splitting varying between 9 and 10 gauss for the entire series of metals. In each case, therefore, there is appreciable odd electron density on only one nitrogen and its coupling constant varies only slightly with each metal.

Although the nitrogen coupling constants vary only slightly with alkali metal, it is possible that a proportional change in the smaller proton coupling constant would produce a very different looking hyperfine spectrum. Because of the smallness of the change of the nitrogen coupling constant for each alkali metal, no accurate value for this change has been determined at this time, and no work has been performed on the deuterated species *vs* alkali metal to see if the proton coupling constants remain in the same ratio. Further work will be performed on this alkali metal effect at a later date.

The availability of a sample of Li metal enriched in Li^6 enabled us to prepare the negative ion of m-dinitrobenzene with this enriched metal. The result was that the hyperfine pattern was not distinguishable from that of the negative ion prepared with Li metal of normal isotopic composition. This eliminates, for the case of Li, the existence of an alkali metal hyperfine interaction and therefore implies no odd electron density on the Li.

VI. EXCHANGE REACTIONS

Previously it was reported that an electron transfer reaction between naphthalene negative ion and unreduced napthahalene produced a loss of resolution in the hyperfine pattern.[20] A similar effect occurs in the m-dinitrobenzene negative ion case where the presence of unreduced m-dinitrobenzene removes the smallest

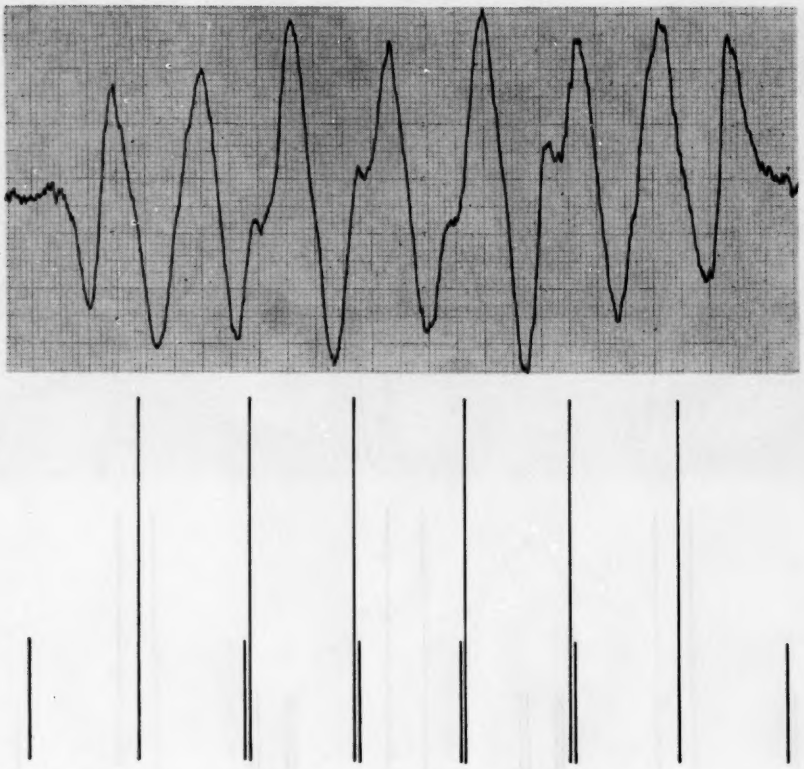

FIG. 5. Observed spectrum of K-1,3-dinitrobenzene-5-d_1 negative ion in DME (above) and calculated spectrum (below).

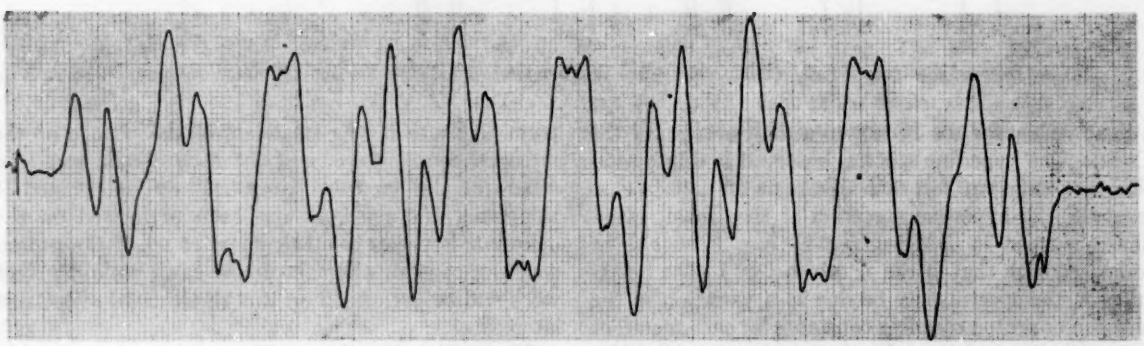

FIG. 6. Observed spectrum of Li-*m*-dinitrobenzene negative ion in DME.

resolvable structure in the spectrum leaving a basic eight-line spectrum. Assuming a second-order rate law, the rate constant is estimated to be of the order of 10^8 to 10^9 liters/mole-sec.

ACKNOWLEDGMENTS

I wish to thank M. P. Klein and B. E. Holder for many helpful discussions and C. J. Dooley for help in the synthesis of the deuterated compounds.

THE JOURNAL OF CHEMICAL PHYSICS VOLUME 32, NUMBER 2 FEBRUARY, 1960

Isomeric Effects in Fragmentation by Beta Decay: Monotritiated Propanes and Toluenes*

S. WEXLER, G. R. ANDERSON,† AND L. A. SINGER‡

Physics Division, Argonne National Laboratory, Lemont, Illinois

(Received June 9, 1959)

The spectra of positively charged fragments from beta decay of tritium in primary and secondary monotritiated propane and in *o*-, *m*-, *p*-, and α-monotritiated toluene have been determined by mass spectrometric techniques. Although the number of products from decomposition of each molecule is quite large, the mass patterns from the two propanes are fairly similar while the four mass spectra from the isomeric tritiated toluenes are very nearly the same. These results suggest that the influence of the location of the radioactive atom in the molecule on the fragmentation following beta decay is often obscured by secondary processes, such as radiationless transitions, H-atom migration, and other rearrangements of the excited molecular ion before breakup. However, there are significant differences within the two groups of mass spectra. Some of the differences in the propane patterns are consistent with the greater stability of the secondary propyl structure as compared to that of the primary isomer. Energetically plausible decomposition schemes for the tritiated propanes are proposed. The distributions of excitation energies made available to the daughter molecular ions $(C_3H_7He^3)^+$ in the beta transformation of H^3 to He^3 are estimated.

A. INTRODUCTION

EXCITATION of molecules in the beta transition of a constituent atom follows from the perturbation of the electrostatic environment of the electronic cloud by the sudden change in nuclear charge.[1–3] Since the nuclear transformation occurs in a particular atom, the "shaking" of the electronic cloud may be restricted to electronic orbitals near the radioactive atom. Accordingly, molecular effects such as fragmentation may be influenced by the position of the decaying atom in the molecule.

On the other hand, such isomeric effects may be obscured by radiationless transitions, H-atom migration or other rearrangements[4–6] in the excited molecular ion prior to breakup. Rapid randomization of excitation energy is postulated in the quasi-equilibrium theory of unimolecular dissociation.[7–10]

To study the way in which the location of the radioactive atom in the molecule influences the fragmentation following beta decay, we have tagged with tritium the simplest alkane and aromatic species in which the positions on the carbon skeleton can be distinguished. Primary and secondary monotritiated propane and ortho-, meta-, para-, and alpha-monotritiated toluene were synthesized and the ionic fragments formed by the beta decay of the tritium were studied by the mass-spectrometric procedures described previously.[11,12]

B. EXPERIMENTAL

The mass spectrometer with special constructional features has already been described in detail.[11] Gaseous *p*- and *s*- C_3H_7T were prepared by reaction of the respective propyl magnesium bromide with T_2O; the *o*-, *m*-, *p*-, and α-monotritiated toluenes were also made by reaction between T_2O and the respective Grignard reagent. The syntheses were performed in a vacuum line to ensure samples of high specific activity. It is estimated that more than 80% of the molecules were tagged with tritium. The tritiated propanes were separated from the ethyl ether solvent by passing the vapors through successive traps at −125°C and −195°C. Purification of the active toluene from the ethyl ether solvent and from possible products from self-ionization during the preparation (e.g., propane, ethane and butane) was accomplished by repeated fractional distillations from a cold trap at −55°C to one at −195°C. The manufacturer (Eastman Kodak Co.) of the bromotoluenes used in preparing the Grignard reagents asserts that each of the bromo isomers contains less than 0.5% of any of the other three. Reaction of the respective Grignard reagents with water results in no rearrangement; the MgBr group is merely replaced by H.[13–15]

* Work performed under the auspices of the U. S. Atomic Energy Commission.

† Resident Student Associate (summer). Present address, University of Iowa, Iowa City, Iowa.

‡ Resident Student Associate (summer). Present address, University of California at Los Angeles.

[1] M. Wolfsberg, J. Chem. Phys. **24**, 24 (1956).
[2] M. Cantwell, Phys. Rev. **101**, 1747 (1956).
[3] H. M. Schwartz, J. Chem. Phys. **23**, 400 (1955).
[4] A. Langer and P. Johnson, *Symposium on Use of Isolopes in Petroleum Chemistry* (American Chemical Society, 1950), p. 23.
[5] D. P. Stevenson and C. D. Wagner, J. Chem. Phys. **19**, 11 (1951).
[6] J. Collin and F. P. Lossing, J. Am. Chem. Soc. **80**, 1568 (1958).
[7] Rosenstock, Wallenstein, Wahrhaftig, and Eyring, Proc. Natl. Acad. Sci. U. S. **38**, 667 (1952).
[8] Friedman, Long, and Wolfsberg, J. Chem. Phys. **27**, 613 (1957).
[9] A. Bruce King and F. A. Long, J. Chem. Phys. **29**, 374 (1958).
[10] W. A. Chupka, J. Chem. Phys. **30**, 191 (1959).
[11] S. Wexler and D. C. Hess, J. Phys. Chem. **62**, 1382 (1958).
[12] S. Wexler, J. Inorg. Nuclear Chem. **10**, 8 (1959).
[13] L. Friedman and J. Turkevich, J. Chem. Phys. **17**, 1012 (1949).
[14] McMurry, Thornton, and Condon, J. Chem. Phys. **17**, 918 (1949).
[15] C. D. Wagner and D. P. Stevenson, J. Am. Chem. Soc. **72**, 5785 (1950).

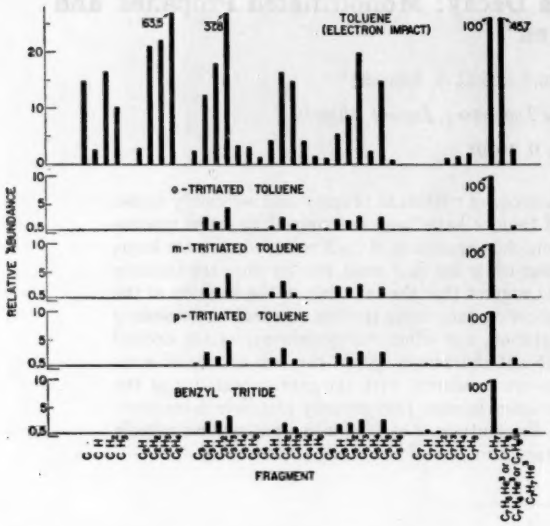

FIG. 1. Comparison of fragment ion yields from beta decay of monotritiated toluenes and from electron impact on untagged toluene.

For several of the isomers, two and three independent samples were prepared. The mass spectra observed were invariant with the sample as well as with the time of standing (sometimes several weeks) of the active sample. Thus, self-radiation appeared not to distort the spectra, at least during the time of the complete experiment. In general, the analyses were performed in haphazard order to avoid any influence of systematic instrumental variations on the patterns observed.

Several experiments were conducted to assess the effects of secondary reactions in the source volume, such as self-ionization and ion-molecule reactions, on the fragmentation patterns. In the studies of s-C_3H_7T, fragments with masses greater than 46 were searched for in order to discover the results of ion-molecule reactions in the source during the experiment and of self-radiation while the active samples were being prepared and retained. No evidence was found for ions containing C_4, C_5 or C_6.

The mass patterns of the two propanes appeared to be insensitive to the source pressure in the range of 5×10^{-6} to 3×10^{-5} mm (as measured with an ionization gauge); for the toluene experiments, the indicated pressure was varied between 8×10^{-6} and 4×10^{-5} mm without noticeable effect on the relative abundances of any of the ions observed except those of masses 94 and 93. The very low relative abundances of the latter two doubled or tripled with increasing pressure in this range. Noting the very high intensity of the equivalent ions on electron bombardment of toluene (Fig. 1), we have concluded that the enhancement is the result of beta ionization of the bulk gas in the source volume. To further assess the distortion of the fragmentation pattern of the tritiated toluene by secondary reactions, dilution experiments with inactive gases were performed. In an experiment in which the partial pressure of the active toluene in the source was 6×10^{-6} and that of oxygen was 2×10^{-5} mm, the O_2^+ peak was only 1% of the $C_7H_7^+$ intensity. In a second such test, part of the fragmentation pattern was measured with the monotritiated toluene at a partial pressure of 1×10^{-6} to 7×10^{-6} mm. Then, the active gas was mixed with inactive toluene and the mixture introduced into the source so that, though the partial pressure of the active gas was unchanged, the total pressure of toluene was now 1.5×10^{-5} mm to 3×10^{-5} mm. The intensities of the fragments, and consequently their relative abundances, were unaltered by the dilution.

In all the studies the source and detector slits of the spectrometer were adjusted to permit resolution of fragments differing by one mass unit.

C. RESULTS

The relative abundances of the positively charged fragments arising from β^- decay of tritium in the two isomeric propanes are given in Table I. For better visual comparison of the data, they are shown in bar form in Fig. 2. The errors listed are standard deviations from the mean value, and reflect the reproducibility of the analyses and estimated errors in the corrections for the varying sensitivity of the detector for ions of different chemical composition. The mass spectrum obtained by impact of 150-v electrons on inactive propane is in-

TABLE I. Fragmentation spectra of p-C_3H_7T and s-C_3H_7T by β^- decay.

m/e	Fragment	Ion yield (%)[a] p-C_3H_7T	s-C_3H_7T
46	$(C_3H_7He^3)^+ + C_3H_7T$	<0.2	<0.2
43	$C_3H_7^+$	41±0.8	56±1.1
42	$C_3H_6^+$	2.2±0.3	3.4±0.4
41	$C_3H_5^+$	29±1.4	7.0±0.7
40	$C_3H_4^+$	1.2±0.1	0.6±0.1
39	$C_3H_3^+$	4.0±0.3	5.3±0.6
38	$C_3H_2^+$	3.7±0.3	3.4±0.4
37	C_3H^+	3.5±0.3	3.8±0.4
36	C_3^+	1.1±0.1	1.1±0.2
29	$C_2H_5^+$	0.6±0.1	2.9±0.5
28	$C_2H_4^+$	0.5±0.1	0.7±0.1
27	$C_2H_3^+$	6.0±0.9	4.3±0.6
26	$C_2H_2^+$	3.2±0.3	3.6±0.4
25	C_2H^+	1.1±0.2	1.7±0.2
24	C_2^+	0.4±0.1	0.9±0.2
15	CH_3^+	1.2±0.2	1.7±0.3
14	CH_2^+	0.8±0.1	0.8±0.1
13	CH^+	0.5±0.05	0.6±0.1
12	C^+	0.4±0.05	0.6±0.1
3	$(He^3)^+$	<0.1	<0.1
3	H_2^+	<0.1	<0.1
1	H^+	0.2±0.05	1.5±0.2
20.5	$C_3H_5^{++}$		0.3±0.1
20	$C_3H_4^{++}$	0.4±0.1	0.4±0.1
19.5	$C_3H_3^{++}$		0.4±0.1
19	$C_3H_2^{++}$	0.7±0.2	0.9±0.2

[a] The yield of each fragment has been corrected for naturally occurring C^{13}.

cluded in the figure. Several characteristics of these data may be pointed out:

(a) Except for a very few of the more than 25 ionic fragments found, notably $C_3H_7^+$ ($m/e=43$), $C_3H_5^+$ ($m/e=41$), $C_2H_5^+$ ($m/e=29$) and H^+, the ionic mass patterns from beta decay in the two propane isomers are quite similar to each other but differ markedly from that obtained by electron impact on C_3H_8.

(b) The low yield of the daughter ions formed as a direct result of the beta transformation, i.e., $(C_3H_7He^3)^+$ and the prominence of the propyl ion is reminiscent of the behavior of CH_3T[16] and C_2H_5T.[11] Apparently, the daughter molecular ion invariably dissociates to give neutral helium.

(c) The intensity of the $C_3H_7^+$ relative to the other fragments is much lower than the yields of the corresponding ions from CH_3T and C_2H_5T. (The ion yields are 41% for p-$C_3H_7^+$, 56% for s-$C_3H_7^+$, 83% for CH_3^+, and 80% for $C_2H_5^+$.)

(d) Rupture of C—C bonds appears to be much more frequent in dissociation of propane by electron impact than in dissociation through β^- decay. Note the enhanced yields of the ions containing two and one carbon atoms in the case of electron bombardment.

(e) The very low abundances of $(He^3)^+$, H^+, and H_2^+ imply that de-excitation of the products of nuclear decay may be by loss of neutral helium and atomic and molecular hydrogen. The mechanism of fragmentation appears to be the same as that in electron impact.

Data on the four monotritiated toluenes are presented in Table II and Fig. 1. The results of electron bombardment studies on untagged toluene are shown in the figure. Although measurements were not made on several ions of very low intensity in the C_7 group from the meta compound, their relative intensities as obtained by magnetic scanning were roughly the same as they were from the other toluenes. We note a striking similarity among the four mass patterns; apparently the position of the tritium in the toluene structure is of minor importance in determining the modes of fragmentation. Again, the principal fragment is the ion from the dissociation of the immediate daughter of the nuclear transformation; the He comes off neutral, as was found previously in the tritiated alkanes. Furthermore, the ion yields of $C_7H_7^+$ (including ions containing C^{13}) are 78, 79, 76, and 79% from o-, m-, p-, and α-monotritiated toluene, respectively, in good agreement with the yields of the corresponding fragments from CH_3T,[16] C_2H_5T,[11] and C_6H_5T.[17] As in the alkanes, the dissociation of the ring structure proceeds through C—C bond ruptures and H or H_2 abstraction. Comparison with the pattern from electron impact on inactive toluene reveals that the aromatic structure is considerably more resistant to decomposition by beta decay of tritium than by electron impact. However, the types of ionic fragments deriving from the two different methods of exciting the toluene molecule are the same.

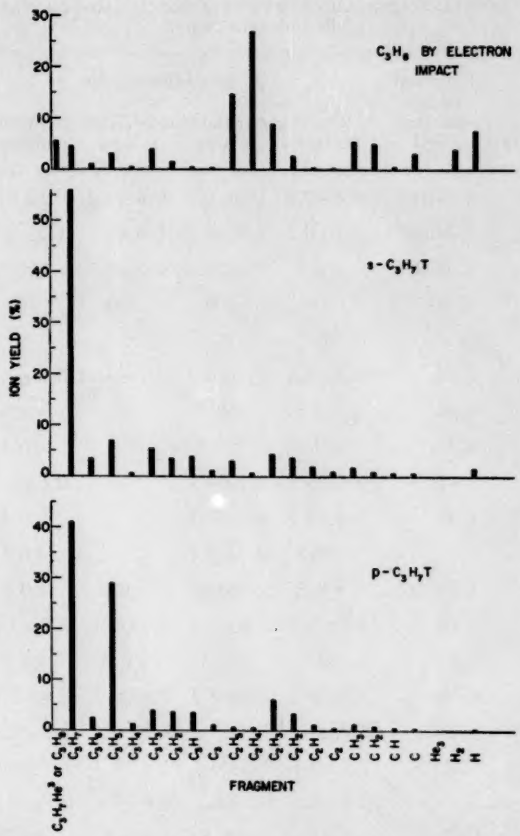

FIG. 2. Comparison of fragment ion yields from beta decay of monotritiated propanes and from electron impact on untagged propane.

In neither the propane nor the toluene studies were doubly ionized fragments observed in more than very minor amounts. Ionization by the "shaking" process in β^- decay in monitritiated compounds may be a negligible effect. But doubly charged ions may have dissociated by Coulombic repulsion in the source, and thus may have escaped detection.

D. DISCUSSION

In a β^- transition the nuclear charge increases by one unit, and in the absence of further ionization the transformed daughter atom will bear a single positive charge. If the decaying atom is a constituent of an isolated molecule, a molecular ion with an electronic charge of +1 will be the immediate product. By virtue of the nonadiabatic nature of the beta decay process,[18] however, the daughter ion may be left in a state of electronic excitation. Because the β^- particle leaves the isolated molecule in a time very short relative to the

[16] A. H. Snell and Frances Pleasonton, J. Phys. Chem. **62**, 1377 (1958).

[17] Carlson, Pleasonton, and Snell, Boston Meeting, Am. Chem. Soc. 1959; T. H. Carlson, J. Chem. Phys. (to be published).

[18] R. Serber and H. S. Snyder, Phys. Rev. **87**, 152 (1952).

TABLE II. Fragmentation patterns of monotritiated toluenes following beta decay.

m/e	Fragment (singly charged ions)	Relative abundance[a] Benzyl tritide	p-tritiated toluene	m-tritiated toluene	o-tritiated toluene
94	$C_7H_7He^3$	0.4±0.2	0.6±0.2	0.6±0.2	0.5±0.2
93	$C_7H_6He^3$	1.2±0.3	1.9±0.2	1.0±0.2	1.2±0.1
92	$C_7H_5He^3$	<0.5	0.8±0.4	0.5±0.7	<0.5
91	C_7H_7	100	100	100	100
90	b	b	b	b	b
89	C_7H_5	0.5±0.1	0.9±0.1	0.7±0.1	0.6±0.1
88	C_7H_4	<0.5	<0.5		<0.5
87	C_7H_3	<0.5	<0.5		<0.5
86	C_7H_2	0.7±0.1	0.7±0.1		0.6±0.1
85	C_7H	0.9±0.1	0.8±0.1		<0.5
84	C_7	<0.5	0.6±0.1		<0.5
78–72	C_6H_6 to C_6	<0.5	<0.5	<0.5	<0.5
65	C_5H_5	2.9±0.1	2.8±0.3	2.3±0.1	2.7±0.2
64	C_5H_4	<0.5	<0.5	<0.5	<0.5
63	C_5H_3	2.9±0.2	2.9±0.2	2.8±0.1	2.9±0.1
62	C_5H_2	2.3±0.1	1.9±0.2	2.2±0.1	2.1±0.2
61	C_5H	2.0±0.1	2.5±0.1	2.5±0.3	2.3±0.1
60	C_5	0.5±0.1	0.6±0.1	0.6±0.1	0.7±0.1
52	C_4H_4	<0.5	<0.5	<0.5	<0.5
51	C_4H_3	1.4±0.1	1.5±0.1	1.3±0.1	1.4±0.1
50	C_4H_2	2.2±0.2	3.4±0.3	3.3±0.1	2.6±0.1
49	C_4H	0.9±0.1	1.7±0.2	1.3±0.1	1.0±0.1
48	C_4	<0.5	<0.5	<0.5	<0.5
39	C_3H_3	3.6±0.2	4.7±0.5	4.7±0.2	4.4±0.2
38	C_3H_2	2.7±0.2	1.9±0.1	2.2±0.1	1.9±0.1
37	C_3H	2.6±0.2	2.7±0.2	2.2±0.1	2.6±0.1
36	C_3	0.5±0.1	0.7±0.1	0.5±0.1	<0.5
28–24	C_2H_4 to C_2	<0.5	<0.5	<0.5	<0.5
15–12	CH_3 to C	<0.5	<0.5	<0.5	<0.5
3	He^3	<0.5	<0.5	<0.5	<0.5
2	H_2	<0.5	<0.5	<0.5	<0.5
1	H	<0.5	<0.5	<0.5	<0.5

[a] The abundance of each ion has been corrected for naturally occurring C^{13}.
[b] A diffuse peak was observed in the mass region between 90 and 91. Accurate intensity measurements could not be made because of interference from the tail of the peak at $m/e=91$.

periods of electronic motion, the sudden change in nuclear charge causes a perturbation in the electrostatic environment of the electronic cloud.[1–3, 19,20] Usually, the cloud will contract adiabatically to accommodate itself to the increased charge, but sometimes excited electronic states result, the energy for the excitation being taken from the energy of the departing nuclear particle.[18] Calculations on the distribution of this excitation energy have been made only for two atomic cases: the $T\rightarrow(He^3)^+$ and $He^6\rightarrow(Li^6)^+$ transformations.[19,21] The distribution computed from Migdal's relations[19] and that found by Winther[21] show a rapid decrease as the energy of excitation increases, with 67 to 70% of the daughter ions being formed in the ground state. But 25% of the $(He^3)^+$ are calculated to have 20.5 ev of excitation relative to the ground state, while 17% of the Li^+ possess about 60 ev. If the radioactive atom is bound in a molecule, a fair fraction of the daughter molecular ions should undoubtedly be formed in excited states and as in electron bombardment of molecules, the energy may be dissipated in the fragmentation of the molecule.

Since the nuclear transformation occurs in a particular atom of the molecule, the "shaking" of the electronic cloud may possibly be restricted to orbitals near the decaying atom. The theoretical treatments[19,22] have shown that orbital ionization initiated by the beta emission in nuclides with high Z is predominantly from the outermost electron shell. It is therefore likely that excitation involves mainly the bonding and other valence electrons of the transformed atom. Such localized excitation may conceivably be detected by comparison of the fragmentation patterns resulting from beta decay of the atom attached at different places in the molecule. The possibility of observing localized effects is enhanced by the unique course of the fragmentation in beta decay. The data on all tagged polyatomic molecules studied thus far (Tables I and II, references 11, 16, and 17) show that the immediate daughter molecule-ions from the beta transition are essentially absent, while the yields of the ions formed by loss of neutral He^3 are high and correspond roughly to the values expected for the fractions of beta transitions to states with little or no excitation.[11,17] Accordingly, the latter are probably the initial fragment ions from breakup of the respective daughter molecule-ions, and are consequently the precursors or "parents" of the other fragments observed. But the initial fragment ions may differ in structure and stability if they are the result of the decay of atoms attached at different places in the molecule. In the studies reported here, the initial fragment ions are p-$C_3H_7^+$ and s-$C_3H_7^+$ from the two monotritiated propanes, and one benzyl ion and three different tolyl ions from the four monotritiated toluenes. These groups of ions differ both in structure and stability.[23,24] Therefore, the fragmentation patterns may

[19] A. Migdal, J. Phys. (U.S.S.R.) **4**, 449 (1941).
[20] E. L. Feinberg, J. Phys. (U.S.S.R.) **4**, 423 (1941).
[21] A. Winther, Kgl. Danske Videnskab. Selskab. Mat.-fys. Medd. **27** (2) (1958).
[22] J. S. Levinger, Phys. Rev. **90**, 11 (1953).
[23] J. L. Franklin and F. H. Field, *Electron Impact Phenomena and The Properties of Gaseous Ions* (Academic Press, New York, 1957), p. 226.
[24] F. H. Field and J. L. Franklin, J. Chem. Phys. **22**, 1895 (1954).

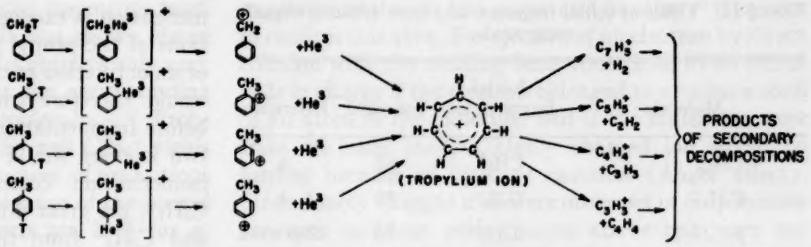

FIG. 3. Proposed partial decomposition schemes for isomeric tritiated toluenes following β^- decay.

very well be different. Such specificity of excitation may have been the cause of the different fragmentation patterns observed in electron-impact studies on isomeric alcohols[8] and halides[25] in which the carbon skeleton is unaltered. As expected, there are wide variations in the fragmentation patterns of isomers with differing carbon skeletons.[25]

However, two processes which may take place between the excitation of the molecule and its fragmentation may obscure the effects of localized excitation. Radiationless transitions occur in times much shorter than periods of vibrational motion. Such transitions have been postulated in the quasi-equilibrium theory of unimolecular dissociation[7] as the vehicle by which excitation energy is rapidly and randomly distributed throughout the molecule. Secondly, migration of hydrogen atoms over the carbon skeleton, or other rearrangements,[26,27] will vitiate structural differences of the initial fragment ion. Consequently, the experiments reported here may act as a test of the quasi-equilibrium model, for similarity of the fragmentation patterns may indicate that there is indeed a time interval between the excitation process and the dissociation process, and that the energy is randomly distributed in the molecule during this delay time. The over-all similarity of the fragmentation patterns from beta decay of tritium in the two isomeric propanes (Fig. 2) and expecially in the four monotritiated toluenes (Fig. 1) suggest that localized excitations are often obscured by random distribution of the excitation energy and by rearrangements prior to decomposition. More than 25 different ionic fragments were detected from each of the two propanes. The yields of some of the ions containing three carbon atoms (particularly $C_3H_7^+$ and $C_3H_5^+$), of $C_2H_5^+$, and of H^+ may be considered to be significantly different, but in general there are no great differences between abundances of the corresponding ions. The mass spectra from the four toluenes, in which more than 35 different species were found, are also very similar despite the difference in structures of the initial fragment ions (*o*-, *m*-, and *p*-tolyl and benzyl). The abundances of the $C_4H_2^+$, $C_3H_3^+$, and $C_3H_2^+$ fragments from benzyl tritide may be significantly different from those of the corresponding ions from the ring substituted toluenes. But there are no profound differences in the four mass spectra.

A strikingly similar observation has been made in studies on electron impact of monodeuterated toluenes. Evidence has been presented to support the view that prior to fragmentation the tolyl and benzyl structures expand to a seven-membered ring, the tropylium ion, in which the hydrogens and carbons, respectively, are indistinguishable.[27–29] The like mass patterns observed in the experiments reported here make it quite possible that the beta decay of tritium in toluene may also lead predominantly to this structure as shown in the plausible scheme of decomposition proposed in Fig. 3: excited tolyl or benzyl ions, formed by immediate loss of neutral He^3 from the daughter molecule-ions, may also rearrange to the tropylium structure which in turn is the common precursor of all the other fragments. However, the few dissimilarities (particularly in the benzyl tritide pattern) suggest that there may be other mechanisms of fragmentation besides the one with tropylium ion as intermediate. The similarity of the behavior of toluene under electron impact and beta decay makes it appear that the same excited states are formed by the two entirely different methods of exciting the molecule.

The absence of large effects attributable to the location of the tritium atom in the fragmentation of the toluene molecule by beta transformation should be noted. Apparently, such aromatic characteristics as hyperconjugation[30] and the variation of charge from carbon to carbon atom in the ring[31] are without great influence on the modes of disruption of the excited molecule-ion. In addition, the structure of the initial fragment ion is of minor importance in determining the modes of fragmentation, for the mass patterns are quite similar despite the difference between the benzyl and tolyl ions. Thus, the behavior of isolated aromatic organic ions seems to have only a limited correlation with their reactions (such as substitution and solvoly-

[25] American Petroleum Institute Research Project 44, *Catalogue of Mass Spectral Data* (Carnegie Institute of Technology (1953)).
[26] D. P. Stevenson, J. Chem. Phys. **19**, 17 (1951); Trans. Faraday Soc. **10**, 35 (1953).
[27] Rylander, Meyerson, and Grubb, J. Am. Chem. Soc. **79**, 842 (1957).
[28] P. N. Rylander and S. Meyerson, J. Chem. Phys. **27**, 1116 (1957).
[29] S. Meyerson and P. N. Rylander, J. Chem. Phys. **27**, 901 (1957).
[30] V. J. Shiner, Jr., and E. Campaigne, *Conference on Hyperconjugation* (Pergamon Press, New York, 1959).
[31] G. W. Wheland, J. Am. Chem. Soc. **64**, 900 (1942).

TABLE III. Yields of initial fragment ions from tritiated organic compounds.

Molecule	Initial fragment ion	Ion yield	Reference
CH_3T	CH_3^+	83	a
C_2H_5T	$C_2H_5^+$	80	b
p-C_3H_7T	$C_3H_7^+$	56	This work
s-C_3H_7T	$C_3H_7^+$	41	This work
C_6H_5T	$C_6H_5^+$	72	c
o-$C_6H_4TCH_3$	$C_7H_7^+$	78	This work
m-$C_6H_4TCH_3$	$C_7H_7^+$	79	This work
p-$C_6H_4TCH_3$	$C_7H_7^+$	76	This work
$C_6H_5CH_2T$	$C_7H_7^+$	79	This work

[a] A. H. Snell and Frances Pleasonton, J. Phys. Chem. **62**, 1377 (1958).
[b] Sol Wexler and D. C. Hess, J. Phys. Chem. **62**, 1382 (1958).
[c] Carlson, Pleasonton, and Snell, Boston Meeting, Am. Chem. Soc. (1959); T. H. Carlson, J. Chem. Phys. (to be published).

sis) in solution, a finding first commented upon by Franklin and Field[24] in their studies on electron impact of several aromatic hydrocarbons.

Though the over-all mass spectra arising from beta decay in the two isomeric propanes are similar, the yields of the $C_3H_7^+$ and $C_3H_5^+$ ions (Table I) are significantly different. Such a large variation may be understood in terms of the relative stabilities of the two propyl ion structures and the energies required for their decomposition into $C_3H_5^+$. The heat of formation of s-$C_3H_7^+$ is measured as 190 kcal/mole while that of p-$C_3H_7^+$ is calculated by the group-orbital method to be 216 kcal/mole.[23] The value of ΔH_f for $C_3H_5^+$ is about 220 or 230 kcal/mole.[22] Thus, the endothermicity of the decomposition of p-$C_3H_7^+$ to $C_3H_5^+$ is only 4 to 14 kcal/mole while the energy necessary to abstract H_2 from the secondary structure is 30 to 40 kcal/mole. If we assume that the distribution of excitation energies is the same in the two isomeric propyl ions, it is clear that more of the primary than secondary propyl ions will have the required energy to decompose into allyl ions. In the light of the preponderance of beta transitions to states of low excitation energy[11] (see below), it may not be surprising that a small difference of endothermicities will cause a marked difference in the fractions of the propyl ions which decompose.

On the assumption that the distribution of excitation energies made available to the daughter molecular ion by the beta emission is the same for both propyl isomers, the differences in ion yields of $C_3H_7^+$ and $C_3H_5^+$ set a lower limit on the activation energy for the isomerization from p-$C_3H_7^+$ to s-$C_3H_7^+$. Since the secondary propyl structure possesses less internal energy than its primary isomer, the p-$C_3H_7^+ \rightarrow s$-$C_3H_7^+$ isomerization is exoergic; but all the decomposition reactions of the propyl ions are endoergic. In the absence of an activation energy, almost all the p-$C_3H_7^+$ formed would therefore convert to the secondary structure before fragmentation. Then, the mass spectra from the two isomers would be expected to be similar. Since isomerization competes with decomposition of p-$C_3H_7^+$, the great differences in ion yields of the $C_3H_7^+$ and $C_3H_5^+$ from the two isomers coupled with the endothermicity calculated above for the p-$C_3H_7^+ \rightarrow C_3H_5^+ + H_2$ reaction (which requires much less energy than do other decompositions) requires that the activation energy for the isomerization from the primary propyl ion to the secondary propyl ion be not much less (and possibly greater) than the energy necessary for abstraction of H_2, about 0.4 ev or 9 kcal/mole. By comparison, Collin and Lossing[6] estimate that the activation energy for H-atom rearrangement in the propyne ion is appreciably less than 9 kcal/mole. But activation energies for H-atom migration would be expected to vary widely among molecular ions. Note, for example, the much larger energy required for the s-$C_3H_7^+ \rightarrow p$-$C_3H_7^+$ isomerization.

Further evidence than an energy of activation may be involved in hydrogen atom migrations may possibly be found in the differences in yields of the $C_2H_5^+$ and $C_2H_3^+$ ions from the two isomeric propanes, although the sums of these two ion yields are approximately equal. The formation of $C_2H_5^+$ from s-$C_3H_7^+$ by simple C—C bond rupture requires an H-atom rearrangement, while its formation from the normal propyl ion does not. Again, if the distributions of excitation energies are in the appropriate region and are the same in the two isomers, more of the $C_2H_5^+$ from the normal propyl ion than of the ethyl ion formed from s-$C_3H_7^+$ will have the energy necessary for conversion to $C_2H_3^+$, if an energy of activation is required for the hydrogen migration in the formation from s-$C_3H_7^+$, as the data (Table I) indicate.

In Table III are listed the yields of the fragment ions produced by loss of neutral He[3] from the daughter molecule-ions in the beta decay of all the monotritiated organic molecules which have been studied to date. In view of the observation that the direct daughter ions from the beta transitions are in very low abundances while the yields of the initial fragment ions are very high and of the order of that expected theoretically for beta transitions in atoms to ground states of daughters,[11,19,21] the intensities of the initial fragment ions may be regarded as representing molecular transitions to low-lying energy states. The fair constancy of this fraction for most of the tritiated organic molecules studied would support the contention that the probability of beta transition to electronic levels of the daughter molecules near the ground state is relatively insensitive to molecular wave functions; and accordingly in 70–80% of the decays of tritium in any molecule, the daughter is formed with little or no excitation. If this

[22] Reference 23, p. 258.

be so, the low ion yields of the propyl fragments must be due to partial decomposition. It was shown above that the abstraction of H_2 from $C_3H_7^+$ requires only very low energies, much lower than for the corresponding fragmentation reaction in other molecules.[11,17] Probably, therefore, the sum of the $C_3H_7^+$ and $C_3H_5^+$ yields is a truer representation of the fraction of transitions to low-lying states than is the abundance of the propyl ion alone. From Table I these sums are 70% for *n*-C_3H_7T and 63% for *s*-C_3H_7T, numbers which are somewhat more in agreement with the yields measured for other tritiated compounds.

Because the evidence presented above points to the initial fragments in the beta decay studies as the precursors of the other ions in the observed mass spectra, comparison with the behaviors of the free radicals CH_3, C_2H_5, C_3H_7 and C_7H_7 under electron impact would be more appropriate than comparisons with the untagged molecule (Figs. 1 and 2). Unfortunately, present techniques for observing free radicals[33,34] have been inadequate for study of their fragmentation by electron bombardment.

Since virtually nothing is known about the energy of the C—He bond, one can only speculate about the reasons for the essentially complete breakup of this linkage in the beta decay process. Arguments were presented[11] earlier to support the view that in beta decay in C_2H_5T the $(C_2H_5He^3)^+$ ion was formed in nonbonding regions of the bound potential energy hypersurfaces of the ion. An alternative explanation may be that, although the parent molecule and daughter ion are isoelectronic, the energy of the C—He bond is very nearly zero in the ground and excited electronic states of all molecular ions containing helium. For the recoil from the beta emission may be responsible for rupture of the carbon—helium bond. But, because of the spread of beta energies from tritium, some 8% of the recoil energies are less than 0.18 ev. Consequently, the strength of the C—He^3 bond must be very low to account for breakup of this linkage in virtually every beta transition. The weakness of the C—He^3 bond would be in sharp contrast to the generally bound character of the $(H{:}He)^+$ ion formed in beta decay.[12,35] It is of interest to note that the observation of the charge remaining with the organic fragment is in accord with the difference of ionization potentials of helium and organic fragment, that of He being much higher.

Migdal[19] and Feinberg[20] have given theoretical arguments to show that ionization by direct collision of the beta with orbital electrons (as the nuclear particle passes through the electronic cloud of the emitting atom) is negligible compared to the probability of ionization by the shaking process. The experimental results presented in this paper and in others[11,17] appear to confirm this view. For ejection of an electron by direct collision with the exciting beta would lead to an ion of $+2e$ in charge if the electron belonged to a valence shell of an atom in the molecule. But if the ionization were from an inner shell, a highly charged ion would be formed because of vacancy cascades (Auger effect). Since doubly charged ions were observed in only minute amounts and ions with charges above two were not found, it appears that ionization by direct collision is a relatively minor effect in beta decay. In addition, it will be recalled that the yields of the initial fragment ions formed in the beta decay of monotritiated organic compounds are in fairly good agreement with the probability predicted for transitions to electronic states of little or no excitation in atoms. The theoretical values[19,21] were derived on the basis that the sudden change in nuclear charge caused the excitation. Since there is such experimental and theoretical agreement that a high fraction of the beta transitions lead to species of low excitation energy, these and other results may be considered as evidence for the "shaking" model. This characteristic is not peculiar to tritium decay, for beta emission by $C^{14}O_2$ and 1,2-$C_2H_4BrBr^{82}$ also give rise mainly to daughters of low excitation energy.[11,16]

E. ESTIMATION OF THE DISTRIBUTION OF EXCITATION ENERGIES IN THE BETA DECAY OF MONOTRITIATED PROPANES

In brief résumé of previous discussions of excitation and ionization by beta decay,[1–3,11,18–22] the rapid ejection of the beta particle from the radioactive atom produces a sudden change in nuclear charge. This sudden change perturbs the electrostatic environment of the electrons of the molecule and may lead to excited electronic states of the daughter molecule-ion. The excitation energy may be dissipated in fragmentation. For simplicity, it is assumed[11] that the "shaking" of the electronic cloud in beta emission in monotritiated compounds is confined to the pair of electrons bonding the tritium to the carbon atom and that these "belong" to the tritium. In this "loose-coupling" or atomic model, accordingly, a T^- ion is assumed to transform to the ground state or one of the several excited electronic states of neutral He^3, and any excitation is transferred to the organic fragment before rupture of the C—He^3 bond. The excitation energy is then dissipated in various decomposition modes of the initial fragment ion. The transformation $T^- \rightarrow He + \beta^- + \nu$ is similar to $He^6 \rightarrow (Li^6)^+ + \beta^- + \nu$, for which Winther[21] has calculated the probabilities of atomic transitions to various electronic states of $(Li^6)^+$. By analogy with Winther's results we would predict that 67% of the helium atoms will be formed in their ground states, 17% with energies 20.5 ev above the ground level, and a rapidly decreasing percentage of He^3 with higher excitation energy up to and exceeding the ionization potential of helium (24.6

[33] Lossing, Marsden, and Farmer, Can. J. Chem. **34**, 701 (1956).
[34] G. C. Eltenton, J. Phys. & Colloid Chem. **52**, 463 (1948), and earlier papers.
[35] Snell, Pleasonton, and Leming, J. Inorg. & Nuclear Chem. **5**, 112 (1957).

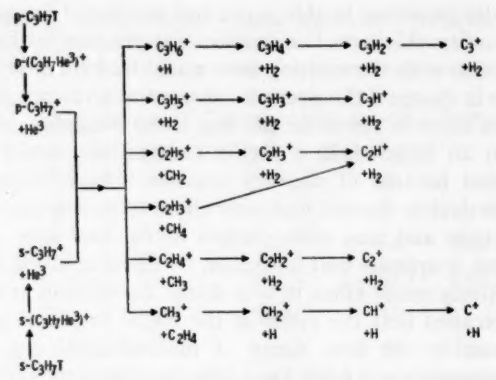

FIG. 4. Proposed breakdown schemes for isomeric tritiated propanes.

ev). The atomic model described here would therefore lead us to expect 65–70% of the daughter ions from beta decay of monoitritiated compounds to have no excitation energy, 15–20% to acquire 20.5 ev, and a smaller percentage to receive a larger energy. But, if there is only partial transfer of energy from the helium to the organic fragment prior to dissolution of the C—He^3 bond, a spread of excitation energies extending from 0 to beyond 20.5 ev would be expected in the initial fragment ion. From Winther's calculations and Migdal's equation[19] for atomic tritium, one may expect the distribution of excitation energies to drop off in exponential fashion as the energy increases.

An alternative method of estimating the distribution of excitation energies produced in the daughter molecular ion by the beta emission will now be described. A comparison of this distribution with the foregoing may indicate the degree to which the "loose coupling" model describes the mechanism of molecular changes accompanying beta decay in a constituent tritium atom. The method will be applied to the two isomeric monotritiated propanes and to monotritiated ethane, for which a fragmentation pattern resulting from β^- decay has already been published.[11] Unfortunately, the thermal and electron-impact data necessary for these estimates are not available for the monotritiated toluenes.

As the first step in the estimation of the distribution of excitation energies from β^- decay in C_3H_7T, an energetically plausible mechanism for the decomposition of the daughter ion is necessary. The one proposed is shown in Fig. 4. The choice of mechanism is made according to some of the percepts of the quasi-equilibrium theory of unimolecular dissociation,[7,36,37] which among other things proposes that an excited molecular ion dissociates by successive, competing, unimolecular reactions. Energetic considerations (namely, that the energy of activation as given by appearance potentials in electron impact studies must equal or exceed the heat of each particular unimolecular decomposition) were the principal bases for the selection of the proposed decomposition sequence, but the presence of metastable ions in mass spectra produced by electron impact also aided in the choice. It is seen that the competitive modes of decomposition are the same as proposed[7,36,37] for $C_3H_8^+$ in electron impact studies except that the "parent" in beta decay is the initial fragment ion, $C_3H_7^+$. The reasons for selection of $C_3H_7^+$ rather than the daughter ion, $(C_3H_7He^3)^+$, as the parent ion of the fragments have been given above. Subsequent secondary reactions other than H_2 elimination (except for dissociation of the C_1 group of ions) have been ignored. Recent experimental results of Kaminsky and Chupka[38] show that H_2 elimination is the dominant mode of fragmentation of the secondary ions. Further, their data indicate that the scheme of breakup of propane by electron bombardment is for the most part exactly as given by the theoretical considerations of Rosenstock *et al.*[7] However, it must be recognized that the acceptance of H_2 elimination as the only type of secondary reaction is a crude approximation, since the secondary ions undoubtedly also dissociate by several competing decomposition reactions.

Accepting the decomposition scheme in Fig. 4, we now assume that every ion of a given type decomposes into the next ion in the sequence of successive decompositions when it has an excitation energy equal to or greater than the minimum energy required for its breakup into the next ion. A histogram of the experimental ion yields (Table I) may then be made on an energy scale which represents excitation energy of the molecular ion $(C_3H_7He^3)^+$ formed in the beta transformation, for a particular fragment ion will appear in the histogram when sufficient energy resided in the immediate daughter ion to equal or exceed the energies of activation of all the successive decompositions leading to the formation of the fragment. The area under the rectangle for each fragment is made proportional to the experimental ion yield. The energy limits of each rectangle are determined by electron impact data on appearance potentials:[39] the lower energy limit of the block is determined by the appearance potential of the particular fragment minus the appearance potential of the propyl ion, while the upper limit is set by the appearance potential of the decomposition daughter less that of the propyl ion. The activation energy for rupture of the C—He^3 bond is taken to be zero in view of arguments presented earlier in this paper. In using appearance potential data (from electron impact on C_3H_8)[39] to evaluate activation energies for the various unimolecular decompositions, we are assuming that they repre-

[36] H. M. Rosenstock, thesis, University of Utah (1952), (unpublished).
[37] A. Kropf, thesis, University of Utah (1954), (unpublished).
[38] W. A. Chupka and M. Kaminsky, Bull. Am. Phys. Soc., Ser. II, **4**, 235 (1959).
[39] J. L. Franklin and F. H. Field, *Electron Impact Phenomena and the Properties of Gaseous Ions* (Academic Press, New York, 1957), pp. 247–260.

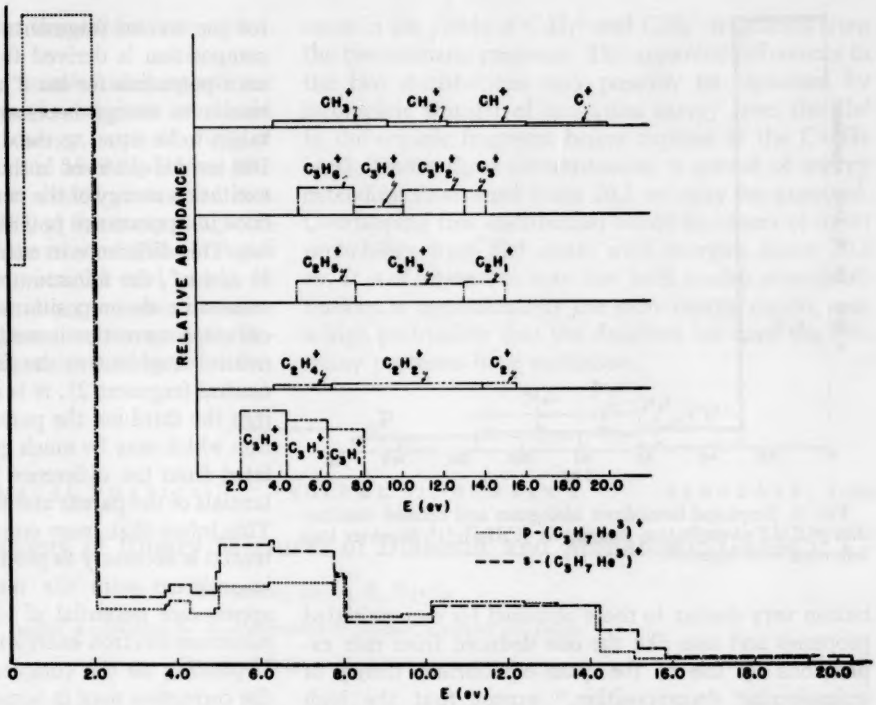

FIG. 5. Empirical breakdown histogram for $(s-C_3H_7He^3)^+$ and derived distributions $p(E)dE$ of excitation energies in primary and secondary $(C_3H_7He^3)^+$ daughter ions following beta transformation. For convenience $C_3H_7^+$ has been omitted from the histogram.

sent accurate thermochemical data. As Friedman *et al.*[40] have pointed out, dissociation energies in agreement with those obtained from thermochemical data are generally derived from appearance potentials. In order to use the yields of the end ions of the decomposition sequencies (e.g., C_3^+ and C_3H^+ in Fig. 4) in the plots, we have taken their blocks to be not much different in height from their respective immediate precursors. This device is based on the reasonable assumption that the high end of the energy distribution does not vary greatly. Summing the areas under the different blocks gives an integral curve which represents the distribution of excitation energies of the $(C_3H_7He^3)^+$ daughter. This follows from the acceptance of the idea that the daughter ion from the beta transition will decompose stepwise to a given fragment ion in a sequence when the excitation energy originally in the daughter is sufficient to provide the activation energies required for all the reactions leading to the particular ion. Since there are six competing breakup processes into which excitation energy in $C_3H_7^+$, and therefore in $(C_3H_7He^3)^+$, may be funneled, the ion yield blocks for all six sequences must be added to arrive at an over-all excitation curve. The use of a histogram implies the assumption that if the energy is insufficient for the decay chain to continue, the energies of the ions at the end of the chain are distributed uniformly between zero and the minimum energy for the next step in the sequence of decompositions.

[40] Friedman, Long, and Wolfsberg, J. Chem. Phys. **26**, 714 (1957).

Figure 5 shows the results of this procedure for the beta transition in s-C_3H_7T. It is seen that the evaluated distribution $p(E)\,dE$ is highly weighted toward low excitation, with 56% of the $(C_3H_7He^3)^+$ being formed with less than 2.1 ev. The distribution beyond 2 ev is fairly flat, extending up to about 18 ev before tailing off to zero. The structure found in the excitation curve is probably without significance because of the crudeness in the use of histograms, and the neglect of decomposition modes other than H_2 elimination for the secondary fragments. A similar excitation curve, evaluated for p-C_3H_7T, appears in the same figure. An added uncertainty arose here in that isomerization of p-$C_3H_7^+$ to s-$C_3H_7^+$ and H_2 abstraction from p-$C_3H_7^+$ both require very little energy (see preceding discussion). For the purposes of this calculation it was assumed that when the excitation energy of the p-$C_3H_7^+$ exceeded about 0.4 ev (the endothermicity of the p-$C_3H_7 \rightarrow C_3H_5^+ + H_2$ reaction), part of the primary propyl ions isomerize and the others decompose into allyl ions. The division was based on the assumption that the primary processes requiring higher energies involved only the secondary propyl structure. On this basis, 78% of the normal ions were taken to have isomerized. We again find an excitation curve with high probability for low energies and a rather flat distribution extending up to ~15 ev before decreasing slowly to zero.

In Fig. 6 are the histograms and the integral excitation curve derived from the previously reported data[11] on monotritiated ethane. Here we find an energy distri-

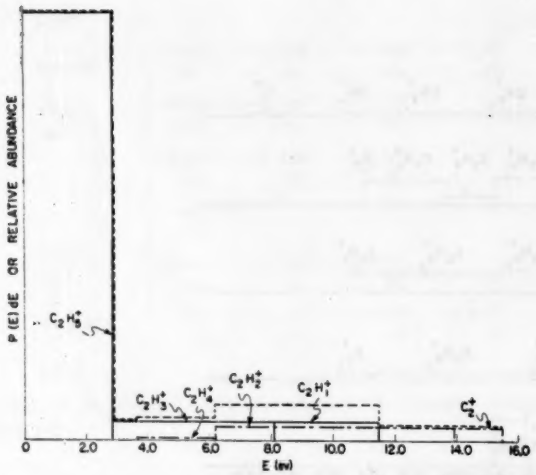

FIG. 6. Empirical breakdown histogram and derived distribution $p(E)dE$ of excitation energies in $(C_2H_6He^3)^+$ daughter ions following beta emission.

bution very similar to those obtained for monotritiated propanes and also like the one deduced from rate expressions by use of the quasi-equilibrium theory of unimolecular decomposition,[11] except that the high energy end of the distribution now is much lower, being about 16 ev rather than the approximately 39 ev estimated previously. This discrepancy may be accounted for by an apparent inconsistency which occurs in the usual application of the statistical theory.

Previous uses of the theory[7–9,11] have generally been based on the assumption that of the excess energy (the energy above the minimum necessary for decomposition) distributed at random throughout an ion, the fraction which will be found in the product ion on dissociation is the ratio of the number of vibrational modes in the daughter ion to that in the parent ion. The remaining fraction of the excess excitation energy was assumed to go with the neutral fragment formed in the decomposition process. In the estimation of an excitation energy distribution for the parent ion, it was customary to compensate for energies lost to the various neutral fragments formed in the successive unimolecular decompositions. However, the minimum energies required for the successive decompositions are usually obtained from experimental appearance potentials. These values must therefore reflect energies taken by the neutral products. For example, in the successive decompositions,

parent ion$\rightarrow$ion 2 + neutral fragment 2

$\downarrow$

ion 3+neutral fragment 3,

ion 3 will be formed when the excitation energy of the parent ion exceeds the minimum energy e_0' of the first breakup and the energy then left in ion 2 exceeds e_0'' for the second fragmentation. The e_0' for the first decomposition is derived from the difference in appearance potentials for ion 2 and the parent ion, while the minimum energy necessary for the second reaction is taken to be equal to the difference for ion 3 and ion 2. But ion 3 is observed in the mass spectrometer when the excitation energy of the parent ion just equals the difference in appearance potentials of ion 3 and the parent ion. This difference in energy is readily seen to be equal to $e_0'+e_0''$, the minimum energies required for the two successive decompositions. If, as was the usual procedure, a correction is made for the energy taken by the neutral fragment in the first of the two breakups (by neutral fragment 2), it is clear that to decay stepwise into the third ion the parent ion will require an excitation which may be much greater than the energy calculated from the difference between the appearance potentials of the parent and the third ions in the sequence. This infers that more energy than the appearance potential is necessary to produce ion 3, which is obviously inconsistent with the meaning of the experimental appearance potential of ion 3, namely that it is the minimum electron energy necessary to produce the ion. Depending on the complexity of neutral fragment 2, the correction may in some cases double the excitation energy required of the parent. Clearly, continued increasing of the energy in the parent ion to "correct" for those amounts carried away by neutral fragments formed farther along in the sequence will make the discrepancy with observation greatest for the ion formed at the end of the successive series of decompositions. Because of the usual number of decays in a sequence for monotritiated propane (Fig. 4) and ethane,[11] and the types of neutral fragments, the parent ion will usually require by this procedure an excitation energy about twice that given by appearance potentials to give rise to the end ions of the sequences. Since the empirical approach outlined above uses the experimental appearance potentials directly in preparing the breakdown curves, the excitation energy of the parent ion is not increased to compensate for energies taken by the neutral fragments. It was recognized implicitly that the magnitudes of the appearance potentials already reflected energies lost to the neutral fragments. Thus, we see why the energy scale for the distribution of excitation energy of the $(C_2H_6He^3)^+$ ions estimated in this paper is contracted in comparison with that estimated[11] by following the procedure outlined by Rosenstock *et al.*[7] The arguments presented here make it appear that the distribution of excitation energies ending at 14–20 ev is the more nearly correct one. The foregoing discussion may also serve to explain the finding of Kaminsky and Chupka[38] that the observed range of excitation energies of the parent ions produced by electron impact in propane is about half that estimated by Rosenstock. Note that the weakness in the application of the theory pointed out here is independent of Chupka's[10] finding that the ions decompose more

rapidly than indicated by the theoretical rate expressions.

It will be recalled that the "atomic" model predicted that the energy distribution in the daughter ion should decrease exponentially with energy, with 65–70% of the ions having no excitation and 15–20% having 20.5 ev. The empirical method just described resulted in a distribution in which about 60% of the decay daughters possessed less than 2.1 ev and the remaining had energies distributed fairly evenly between 2.1 and about 18 ev. However, as brought out in a previous discussion (see Sec. D), below 2.1 ev there may be a rapidly decreasing probability function as evidenced by the differences in ion yields of $C_3H_7^+$ and $C_3H_5^+$ fragments from the two isomeric propanes. The apparent differences in the two distributions may possibly be explained by incomplete transfer of excitation energy from the He^3 to the organic fragment before rupture of the C—He bond. Under these circumstances, a spread of energy extending downward from 20.5 ev may be expected. Overlapping this distribution would be others of lower probability from He^3 states with energies above 20.5 ev. It is of interest to note that both models give distributions in approximately the same energy region, with a high probability that the daughter ion from the beta decay possesses little excitation.

THE JOURNAL OF CHEMICAL PHYSICS VOLUME 32, NUMBER 2 FEBRUARY, 1960

Thermal Conductivity of Binary Mixtures of Diatomic and Monatomic Gases

B. N. Srivastava and A. K. Barua

Indian Association for the Cultivation of Science, Calcutta 32, India

(Received August 21, 1959)

Thermal conductivity of the binary mixtures of O_2—He, O_2—Ne, O_2—Kr, and O_2—Xe have been measured at 30°C and 45°C for various compositions by using the thick-wire-variant of the hot-wire method. For pure O_2 the experimental value of the thermal conductivity is lower than that given by the recent theory of Hirschfelder based on the assumption of local chemical equilibrium, and consequently the values calculated from Hirschfelder's formula for the mixture conductivities are also expected to be higher than the experimental values which is actually found to be so for the mixtures investigated here. The agreement becomes excellent when the experimental values of the conductivity of pure O_2 are used to calculate the mixture conductivities. The formula for the mixture conductivities has been tested in detail and was found to give satisfactorily the composition dependence. The simpler formula for the thermal conductivity of gas mixtures given by Mason and Saxena has also been tested.

1. INTRODUCTION

THERMAL conductivity of polyatomic gases and gas mixtures is of considerable importance for the theory, as of all the transport properties the thermal conductivity is most suitable for deriving information about the internal degrees of freedom of the molecules. Eucken[1] was the first to explain thermal conductivity of a polyatomic gas from simple intuitive arguments whose inadequacy was later pointed out by several workers.[2,3] Hirschfelder[4] has recently given a formal treatment of the thermal conductivity of a polyatomic gas and has obtained a modified Eucken expression. The theoretical ideas underlying his derivation and the limitations of this treatment have been discussed in some detail by Srivastava and Srivastava.[5]

For polyatomic gas mixtures both like and unlike interactions are to be considered, and consequently the theoretical treatment is more complicated. Hirschfelder,[6] by an extension of the foregoing method, has obtained an expression for the thermal conductivity of polyatomic gas mixtures which has not yet been extensively tested.[4,5,7]

Srivastava and Srivastava[5] reported the thermal conductivity of O_2, N_2, H_2, and of the mixtures O_2-A, N_2–A, H_2-A at 38°C and compared their data with Hirschfelder's theory. It was observed that for a pure polyatomic gas at ordinary temperatures Hirschfelder's theory gives a higher value of the thermal conductivity than that given by experiments. For mixtures, fair agreement was obtained with theory when the experimental values of the thermal conductivity of the pure polyatomic gases were used to calculate the mixture conductivities. Some discrepancy was, however, ob-

[1] A. Eucken, Physik. Z. **14**, 324 (1913).
[2] S. Chapman and T. G. Cowling, *The Mathematical Theory of Non-Uniform Gases* (Cambridge University Press, New York, 1952).
[3] K. Schäfer, Z. physik. Chem. (Leipzig) **B53**, 143 (1943).
[4] J. O. Hirschfelder, J. Chem. Phys. **26**, 274, 282 (1957).
[5] B. N. Srivastava and R. C. Srivastava, J. Chem. Phys. **30**, 1200 (1959).
[6] J. O. Hirschfelder, *Sixth Symposium (International) on Combustion* (Reinhold Publishing Corporation, New York, 1957), p. 351.
[7] E. A. Mason and S. C. Saxena, Phys. Fluids **1**, 301 (1958).

TABLE I: Constants of the conductivity cell.

	30°C	45°C
Length of the cell wire ($2l$)	5.9978 cm	5.9987 cm
Radius of the cell wire (r_1)	0.00500 cm	0.00500 cm
Internal diameter of the tube ($2r_2$)	0.3048 cm	0.3048 cm
External diameter of the tube ($2r_3$)	0.5915 cm	0.5915 cm
Resistance of the cell wire (R_0)	0.83518Ω	0.88012Ω
Temperature coefficient of resistance α of the platinum wire	0.00360°C^{-1}	0.00358°C^{-1}
Thermal conductivity λ of the platinum wire in cal cm^{-1} sec^{-1} °C^{-1}	0.167	0.168
Cell constant $(1-C)$	0.9942	0.9941

served between the experimental value of diffusion coefficient for O_2-A and that obtained from a treatment of the conductivity data. It was therefore felt that more extensive comparison with the theory would be most desirable. With this purpose, measurements of the thermal conductivity of O_2 and of the mixtures O_2-He, O_2-Ne, O_2-Kr, O_2-Xe have been carried out and are reported in this paper. The experiments have been done at two temperatures which serves as a useful check on the accuracy of observations.

2. APPARATUS AND THEORY

The method adopted is the thick-wire variant of the hot-wire method, a theory for which has been fully worked out by Kannuluik and Martin[8] and Kannuluik and Carman.[9] The procedure adopted is similar to that of Srivastava and Saxena[10] and Srivastava and Srivastava.[5] In order to increase the accuracy of the observations, the conductivity cell of stainless steel with Perspex seal was made longer and a thinner platinum wire was used as the cell wire. The bore of the cell was uniform to 1/1000 inch over its whole effective length. The temperature coefficient of resistance α of the platinum wire was determined by measuring the resistance of another piece of the same specimen at 0°C, 30°C, 45°C, and 100°C and these were found to be 1.4561Ω, 1.6234Ω, 1.6938Ω, and 2.0093Ω, respectively. The values of the cell constants at 30°C and 45°C are given in Table I.

As shown by Kannuluik and Martin,[8] the solution of the differential equation for heat flow can be written in the form

$$f(\beta l)=[1/(\beta l)^2][1-(\tanh\beta l/\beta l)]=\frac{2\pi r_1^2\lambda J(R-R_0)}{R_0^2I^2\alpha l}, \tag{1}$$

with

$$\beta^2=(2h/r_1\lambda)-(I^2R_0\alpha/2\pi r_1^2Jl\lambda),$$
$$h=K_u/[r_1\ln(r_2/r_1)], \tag{2}$$

where R is the resistance of the wire when a current of I amp is flowing through it, R_0 is the resistance of the cell wire at bath temperature for $I=0$. λ, K_u are the thermal conductivities of the wire and the gas, respectively.

If the hot-wire cell is highly evacuated, the conduction loss through the gas is replaced by the radiation loss h_r, and will in general be small so that β will also be small. Under such conditions Eq. (1) may be expanded out to yield

$$\lambda=\tfrac{1}{6}\frac{RR_0^2I^2\alpha l}{\pi r_1^2J(R-R_0)}\left(1+\tfrac{1}{30}\frac{RI^2\alpha l}{h_r r_1^2\lambda J}\right)\left(1-\tfrac{4}{5}\frac{h_rl^2}{r_1\lambda}\right). \tag{3}$$

For determining λ another conductivity analyzer was constructed without introducing mercury anywhere and the system evacuated to better than 10^{-4} mm of Hg by an oil-diffusion pump. λ was obtained by solving Eq. (3) by successive approximations, and the observed values were found to agree with the standard values.[11]

3. EXPERIMENTAL RESULTS

Thermal conductivity of mixtures of a diatomic and a monatomic gas have been measured by Weber[12] for N_2-A, by Ibbs and Hirst[13] for H_2-A, and recently by Srivastava and Srivastava[5] for O_2-A, N_2-A, H_2-A. For pure O_2, however, there are a number of accurate measurements.[5,14,15] In the present investigation we

TABLE II. Thermal conductivity K of O_2—He mixture in cal·cm^{-1}·sec^{-1} °C^{-1} at 30°C.

% of monatomic gas	I in ma	$R-R_0$ in mΩ	$K_u\times10^5$	$K_u'\times10^5$	$K'\times10^5$	$K\times10^5$
100	205.94	5.934	36.94	36.82	36.58	36.37
87.62	201.46	7.126	28.96	28.88	28.61	28.40
68.41	210.18	11.44	19.84	19.72	19.54	19.42
56.81	203.99	12.72	16.51	16.42	16.18	16.09
33.81	200.64	17.74	11.49	11.40	11.28	11.21
20.59	196.83	20.26	9.412	9.341	9.231	9.182
13.84	200.54	24.07	8.142	8.041	7.960	7.801
0	205.64	32.05	6.612	6.510	6.461	6.442

[8] W. G. Kannuluik and L. H. Martin, Proc. Roy. Soc. (London) **A141**, 144 (1933); **A144**, 496 (1934).
[9] W. G. Kannuluik and E. H. Carman, Proc. Phys. Soc. (London) **B65**, 701 (1952).
[10] B. N. Srivastava and S. C. Saxena, Proc. Phys. Soc. (London) **B70**, 369 (1957).
[11] *International Critical Tables* (McGraw-Hill Book Company, Inc., New York, 1928).
[12] S. Weber, Ann. Phys. **54**, 325, 437 (1917).
[13] T. L. Ibbs and A. A. Hirst, Proc. Roy. Soc. (London) **A123**, 134 (1929).
[14] H. L. Johnston and E. R. Grilly, J. Chem. Phys. **14**, 223 (1946).
[15] F. G. Keyes, SQUID Tech. Rept. **37**, Massachusetts Institute of Technology (April, 1952).

TABLE III. Thermal conductivity K of O_2—He, O_2—Ne, O_2—Kr, O_2—Xe in cal·cm^{-1}·sec^{-1}·°C^{-1} at 30°C.

Gas pair	O_2—He		O_2—Ne		O_2—Kr		O_2—Xe	
	% of He	$K\times10^5$	% of Ne	$K\times10^5$	% of Kr	$K\times10^5$	% of Xe	$K\times10^5$
	100	36.37	100	11.61	100	2.245	100	1.294
	87.62	28.40	77.49	10.20	74.10	2.928	87.13	1.593
	68.41	19.42	57.64	8.967	62.15	3.255	72.65	2.155
	56.81	16.09	40.96	8.149	49.78	3.921	58.79	2.783
	33.81	11.21	23.66	7.441	36.31	4.396	42.41	3.458
	20.59	9.177	13.98	7.094	26.31	4.852	26.38	4.312
	13.84	7.802	0	6.442	10.21	5.971	13.17	5.270
	0	6.442			0	6.442	0	6.442

TABLE IV. Thermal conductivity K of O_2—He, O_2—Ne, O_2—Kr, O_2—Xe mixtures in cal cm^{-1}·sec^{-1}·°C^{-1} at 45°C.

Gas pair	O_2—He		O_2—Ne		O_2—Kr		O_2—Xe	
	% of He	$K\times10^5$	% of Ne	$K\times10^5$	% of Kr	$K\times10^5$	% of Xe	$K\times10^5$
	100	37.68	100	12.05	100	2.325	100	1.351
	83.64	27.40	84.03	10.78	89.14	2.656	85.43	1.792
	71.21	20.69	74.20	10.06	73.84	3.123	72.38	2.294
	54.63	16.31	65.15	9.305	60.59	3.423	57.72	2.975
	39.84	12.67	48.44	8.442	47.51	3.434	41.38	3.463
	25.84	9.981	29.93	7.764	15.45	5.720	25.64	4.560
	14.61	8.477	11.52	7.378	0	6.688	12.81	5.529
	0	6.688	0	6.688			0	6.688

have measured the thermal conductivity of O_2-He, O_2-Ne, O_2-Kr, and O_2-Xe at 30°C and 45°C. The gases were supplied by British Oxygen Company, England. O_2, He, Ne were quoted to be spectroscopically pure while Kr and Xe contained traces of impurities. The observations were taken at a pressure of 10 cm Hg as convection and the temperature jump effect were found to be negligible in the pressure range of 6 to 20 cm of Hg. A typical set of observations taken for O_2-He mixture at 30°C is shown in Table II. In the Table K_u indicates the apparent conductivity calculated from Eqs. (1) and (2), K_u' the value of conductivity reduced to the bath temperature, and K' is the value obtained after correcting for radial flow, radiation, and wall effect. Any possible asymmetry in the cell was taken into account by the cell constant C given in the relation $K=K'(1-C)$ which was determined by assuming the value of the conductivity of neon as given by Kannuluik and Carman[9] as standard. K in the Table gives the thermal conductivity after all corrections have been applied.

In Tables III and IV are recorded the observed values of the thermal conductivity of gas mixtures at different compositions. The results for 30°C are plotted in Fig. 1. The curves are nearly straight lines with slight concavity upwards except in the case of O_2-He where the concavity is very marked.

4. COMPARISON WITH THEORY

The simple Eucken expression for the thermal conductivity of a polyatomic gas is given by

$$K=(\eta/M)[f_{\text{trans}}C_{v_{\text{trans}}}+f_{\text{int}}C_{v_{\text{int}}}], \qquad (4)$$

where K is the thermal conductivity, η the viscosity, $C_{v_{\text{trans}}}$, $C_{v_{\text{int}}}$ are the molar specific heats at constant volume corresponding to the translational and the internal degrees of freedom, respectively. f_{trans}, f_{int} represent the transfer factors for the translational and the internal energy. According to the Chapman-Enskog theory which has also been verified by experiments $f_{\text{trans}}=2.5$, and for simplicity, Eucken put $f_{\text{int}}=1$, so that Eq. (4) becomes

$$K=K_{\text{mon}}[(4/15)C_v/R+(\tfrac{3}{5})], \qquad (5)$$

where K_{mon} is the thermal conductivity when the gas is considered as monatomic.

Actually, the internal energy is transferred by a diffusion mechanism so that $f_{\text{int}}=1$ should be replaced by $f_{\text{int}}=\rho D/\eta$ (where ρ is density and D is self-diffusion coefficient of the gas) to yield the modified Eucken expression

$$K=(\eta/M)[(\tfrac{5}{2})C_{v_{\text{trans}}}+(\rho D/\eta)C_{v_{\text{int}}}]. \qquad (6)$$

Hirschfelder[4] has recently derived by a formal treatment the expression

$$K=K_{\text{mon}}[1-\delta_f+\delta_f(C_p/C_{pf})], \qquad (7)$$

where $\delta_f=\rho DC_{pf}/K_{\text{mon}}$, $C_{pf}=5R/2$. Though put in different forms, the expressions (6) and (7) are equivalent. The values of δ_f for different molecular models have been tabulated[4] for different temperatures. It is possible to assign to δ_f an average value of $\delta_f=0.885$

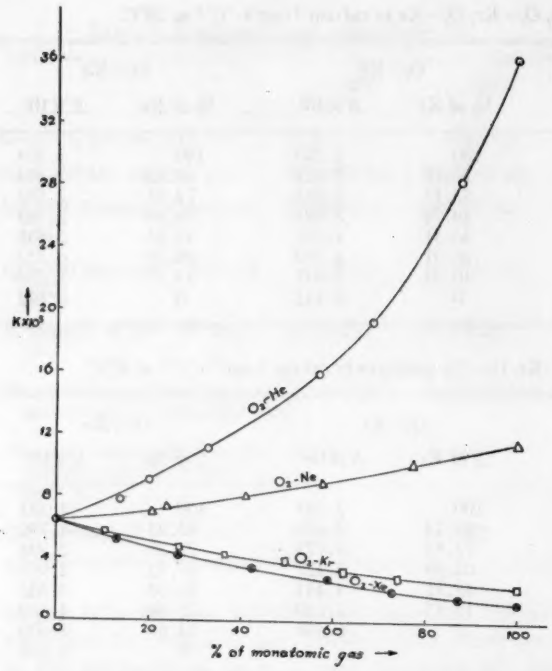

FIG. 1. Thermal conductivity of O_2—He, O_2—Ne, O_2—Kr, and O_2—Xe mixtures at 30°C.

for the Lennard-Jones (12:6) model so that Eq. (7) becomes

$$K/K_{\text{mon}}=0.354C_v/R+0.469. \tag{8}$$

By an extension of the foregoing treatment, Hirschfelder[6] has obtained the following expression for the thermal conductivity of a binary mixture of polyatomic gases:

$$K_{\text{mix}}=K_{\text{mix(mon)}}+[K_1-K_{1\text{ mon}}]\cdot[1+(x_2/x_1)(D_{11}/D_{12})]^{-1}+[K_2-K_{2\text{ mon}}][1+(x_1/x_2)(D_{22}/D_{12})]^{-1}, \tag{9}$$

where K_1, K_2 are the thermal conductivities, D_{11}, D_{22} the coefficients of self-diffusion, and x_1, x_2 the mole fractions of the components 1 and 2 in the mixture. D_{12} is the coefficient of interdiffusion.

If the binary mixture consists of a polyatomic gas denoted by subscript 1 and a monatomic gas denoted by subscript 2, Eq. (9) becomes

$$K_{\text{mix}}=K_{\text{mix(mon)}}+[K_1-K_{1\text{ mon}}][1+(x_2/x_1)(D_{11}/D_{12})]^{-1}. \tag{10}$$

The disadvantages of Hirschfelder's formula [Eq. (9)] are that the calculation is rather laborious and requires the knowledge of the force laws between the molecules. In an attempt to overcome these difficulties, Mason and Saxena[7] have made a number of approximations to arrive at a simpler formula for thermal conductivity of a multicomponent mixture of polyatomic gases and obtained

$$K_{\text{mix}}=\sum_{i=1}^{n}K_i[1+\sum_{j=1,\,i\neq j}^{n}G_{ij}(x_j/x_i)]^{-1} \tag{11}$$

with

$$G_{ij}=(1.065/2\sqrt{2})[1+(M_i/M_j)]^{-\frac{1}{2}}\cdot[1+(K_i^0/K_j^0)^{\frac{1}{2}}(M_i/M_j)^{\frac{1}{4}}]^2, \tag{12}$$

where x_i, x_j represent the mole fractions and M_i, M_j molecular weights of the components i and j, respectively. K_i°, K_j° are the thermal conductivities when the gases are considered to be monatomic. Conductivities K_i°, K_j° are related to the viscosities η_i, η_j by the relation

$$K_i^\circ/K_j^\circ=(\eta_iM_j)/(\eta_jM_i). \tag{13}$$

When η_i and η_j are known experimentally, K_i°/K_j° can be calculated from Eq. (13). In case they are not known, K_i°/K_j° can be calculated from Eq. (8) by using specific heat data. It is also to be noted that we are to use experimental values of K_i and K_j to obtain K_{mix} from Eq. (11).

For comparing our experimental results on O_2, K_{mon} was calculated to the first approximation on the Lennard-Jones (12:6) model (by using the force constants determined from viscosity data) from the relation

$$[K_{\text{mon}}]_1\times10^7=1989.1(T/M)^{\frac{1}{2}}/\sigma^2\Omega^{(2,2)*}(T^*), \tag{14}$$

where T is the temperature in °K, $T^*=kT/\epsilon$, σ and ϵ/k are the potential parameters in A and °K, respectively. The experimental value of the Eucken factor K/K_{mon} can thus be obtained. These are compared with the values of K/K_{mon} calculated theoretically from Eq. (7) by using the value of δ_f given in reference 4 and the values of C_p given in the tables published by the National Bureau of Standards[16] (1955). Again, from a knowledge of the experimental value of K/K_{mon}, $\delta_{f(\text{exp})}$ was calculated from Eq. (7) which gave the value of f_{int} from the relation $f_{\text{int}}=\frac{3}{2}\delta_f$. Similar calculations were made with the data obtained by other workers. The results of these calculations are shown in Table V together with the values of f_{int} calculated on the Lennard-Jones (12:6) model.

For calculating K_{mix} from Eq. (10), $K_{\text{mix(mon)}}$, D_{11}, and D_{12} were calculated on the Chapman-Enskog theory from the expressions given by Hirschfelder, Curtiss, and Bird.[17] The unlike interactions were approximated by applying the usual combination rules. For the monatomic gases the force constants were taken as those determined from viscosity data[17] excepting the case of Kr for which force constants determined by Saxena[18] from thermal conductivity were

[16] Natl. Bur. Standards (U.S.) Circ. No. 564 (1955).
[17] Hirschfelder, Curtiss, and Bird, *Molecular Theory of Gases and Liquid* (John Wiley & Sons, Inc., New York, 1954).
[18] S. C. Saxena, Indian J. Phys. **29**, 587 (1955).

TABLE V. Eucken factor and values of f_{int} for O_2.

T°K	K_{exp} (Authors)	K_{exp}/K_{mon}	Eucken factor K/K_{mon} from Hirschfelder's Eq. (7)	Eucken factor K/K_{mon} from Eucken's Eq. (5)	Value of $f_{int}=3/2\ \delta_f$ From exptl. data	Value of $f_{int}=3/2\ \delta_f$ From Hirschfelder's tables on L-J (12:6) model
303	Present work	1.324	1.363	1.277	1.166	1.313
318	Present work	1.327	1.369	1.279	1.169	1.313
300	Johnston and Grilly[a]	1.318	1.363	1.278	1.152	1.313
320	Johnston and Grilly[a]	1.323	1.370	1.280	1.153	1.314
273	Keyes[b]	1.323	1.357	1.272	1.185	1.312
311	Srivastava and Srivastava[c]	1.303	1.369	1.280	1.135	1.313

[a] See reference 14.
[b] See reference 15.
[c] See reference 5.

TABLE VI. Thermal conductivity and Eucken-type factor for O_2—He mixture at 30°C.

% of He	$K_{exp}\times10^5$	$K_H\times10^5$ from Eq. (10)	$K_{H'}\times10^5$ with exptl. value of δ_f	$K_{MS}\times10^5$ from Eq. (11)	$\frac{K_{exp}}{K_{mix(mon)}}$	$\frac{K_{H'}}{K_{mix(mon)}}$	y	x
100	36.37	36.37	36.37	36.37	1.000	1.000	...	...
85	27.00	27.00	26.90	27.25	1.019	1.015	1.550	5.667
70	20.14	20.64	20.48	21.21	1.031	1.049	1.002	2.333
55	15.64	16.01	15.82	16.53	1.068	1.081	0.825	1.223
40	12.30	12.40	12.18	12.93	1.133	1.123	0.753	0.667
25	9.642	9.838	9.600	10.08	1.194	1.177	0.702	0.111
10	7.621	7.855	7.584	7.759	1.258	1.248	0.652	0.111
0	6.441	6.703	6.441	6.441	1.323	1.323	...	...

TABLE VII. Thermal conductivity and Eucken-type factor for O_2—He mixture at 45°C.

% of He	$K_{exp}\times10^5$	$K_H\times10^5$ from Eq. (10)	$K_{H'}\times10^5$ with exptl. value of δ_f	$K_{MS}\times10^5$ from Eq. (11)	$\frac{K_{exp}}{K_{mix(mon)}}$	$\frac{K_{H'}}{K_{mix(mon)}}$	y	x
100	37.68	37.68	37.68	37.68	1.000	1.000	...	...
85	27.96	28.00	27.92	28.24	1.023	1.024	1.402	5.667
70	20.83	21.34	21.20	22.06	1.040	1.058	0.904	2.333
55	16.20	16.44	16.29	17.25	1.062	1.082	0.750	1.223
40	12.75	12.92	12.75	13.51	1.116	1.124	0.596	0.667
25	10.00	10.11	9.926	10.52	1.188	1.179	0.625	0.333
10	7.892	7.933	7.743	8.075	1.280	1.260	0.600	0.111
0	6.682	6.885	6.682	6.682	1.327	1.327	...	...

TABLE VIII. Thermal conductivity and Eucken-type factor for O_2—Ne mixture at 30°C.

% of Ne	$K_{exp}\times10^5$	$K_H\times10^5$ from Eq. (10)	$K_{H'}\times10^5$ with exptl. value of δ_f	$K_{MS}\times10^5$ from Eq. (11)	$\frac{K_{exp}}{K_{mix(mon)}}$	$\frac{K_{H'}}{K_{mix(mon)}}$	y	x
100	11.61	11.61	11.61	11.61	1.000	1.000	...	...
85	10.54	10.60	10.56	10.34	1.032	1.034	3.030	5.667
70	9.533	9.648	9.565	9.361	1.067	1.071	1.653	2.333
55	8.825	9.082	8.967	8.552	1.092	1.110	1.340	1.222
40	8.056	8.390	8.247	7.849	1.128	1.155	1.093	0.667
25	7.262	7.495	7.327	7.275	1.204	1.215	0.812	0.333
10	6.698	6.937	6.746	6.749	1.268	1.277	0.706	0.111
0	6.442	6.645	6.442	6.442	1.321	1.321	...	...

TABLE IX. Thermal conductivity and Eucken-type factor for O_2—Ne mixture at 45°C.

% of Ne	$K_{exp}\times10^5$	$K_H\times10^5$ from Eq. (10)	$K_{H'}\times10^5$ with exptl. value of δ_f	$K_{MS}\times10^5$ from Eq. (11)	$K_{exp}/K_{mix(mon)}$	$K_{H'}/K_{mix(mon)}$	y	x
100	12.05	12.05	12.05	12.05	1.000	1.000	...	...
85	10.74	10.94	10.90	10.60	1.019	1.034	2.752	5.667
70	9.895	9.978	9.899	9.521	1.066	1.073	1.452	2.333
55	9.010	9.137	9.027	8.853	1.086	1.088	1.076	1.222
40	8.364	8.703	8.565	8.024	1.116	1.157	0.923	0.667
25	7.589	7.666	7.504	7.453	1.220	1.222	0.742	0.333
10	7.033	7.219	7.036	7.001	1.280	1.280	0.651	0.111
0	6.688	6.885	6.688	6.688	1.326	1.326	...	...

TABLE X. Thermal conductivity and Eucken-type factor for O_2—Kr mixture at 30°C.

% of Kr	$K_{exp}\times10^5$	$K_H\times10^5$ from Eq. (10)	$K_{H'}\times10^5$ with exptl. value of δ_f	$K_{MS}\times10^5$ from Eq. (11)	$K_{exp}/K_{mix(mon)}$	$K_{H'}/K_{mix(mon)}$	y	x
100	2.245	2.245	2.245	2.245	1.000	1.000	...	...
85	2.612	2.706	2.683	2.681	1.043	1.071	5.552	5.667
70	3.005	3.198	3.150	3.172	1.082	1.134	2.602	2.333
55	3.554	3.758	3.682	3.705	1.147	1.189	1.656	1.222
40	4.205	4.401	4.295	4.338	1.290	1.235	1.252	0.667
25	4.968	5.112	4.973	5.069	1.274	1.276	0.957	0.333
10	5.819	5.998	5.821	5.892	1.304	1.304	0.738	0.111
0	6.442	6.645	6.442	6.442	1.321	1.321	...	...

TABLE XI. Thermal conductivity and Eucken-type factor for O_2—Kr mixture at 45°C.

% of Kr	$K_{exp}\times10^5$	$K_H\times10^5$ from Eq. (10)	$K_{H'}\times10^5$ with exptl. value of δ_f	$K_{MS}\times10^5$ from Eq. (11)	$K_{exp}/K_{mix(mon)}$	$K_{H'}$ $K_{mix(mon)}$	y	x
100	2.325	2.325	2.325	2.325	1.000	1.000	...	...
85	2.720	2.843	2.818	2.815	1.042	1.073	4.850	5.667
70	3.155	3.335	3.288	3.254	1.092	1.138	2.525	2.333
55	3.695	3.922	3.848	3.850	1.146	1.194	1.425	1.222
40	4.370	4.586	4.489	4.477	1.210	1.241	1.124	0.667
25	5.150	5.335	5.200	5.204	1.268	1.281	0.895	0.333
10	6.029	6.226	6.056	6.154	1.304	1.310	0.851	0.111
0	6.688	6.885	6.688	6.688	1.326	1.326	...	...

TABLE XII. Thermal conductivity and Eucken-type factor for O_2—Xe mixture at 30°C.

% of Xe	$K_{exp}\times10^5$	$K_H\times10^5$ from Eq. (10)	$K_{H'}\times10^5$ with exptl. value of δ_f	$K_{MS}\times10^5$ from Eq. (11)	$K_{exp}/K_{mix(mon)}$	$K_{H'}$ $K_{mix(mon)}$	y	x
100	1.294	1.294	1.294	1.294	1.000	1.000	...	...
85	1.684	1.758	1.738	1.705	1.059	1.093	6.954	5.667
70	2.223	2.268	2.227	2.254	1.164	1.166	3.195	2.333
55	2.804	2.881	2.815	2.875	1.217	1.222	2.000	1.222
40	3.564	3.625	3.529	3.534	1.233	1.234	1.261	0.667
25	4.301	4.307	4.204	4.541	1.255	1.254	1.161	0.333
10	5.500	5.695	5.524	5.641	1.308	1.314	0.772	0.111
0	6.442	6.645	6.442	6.442	1.321	1.321	...	...

used. The results of these calculations are given in Tables VI to XIII. In these tables, K_H in column 3 are the values of K_{mix} with the theoretical value of δ_f, $K_{H'}$ in column 4 are the values of K_{mix} with the experimental value of δ_f. In columns 6 and 7 are recorded the values of the Eucken-type factor for the gas mixtures. The experimental data were smoothed out graphically.

For calculating K_{mix} for O_2–Ne and O_2–He from the formula of Mason and Saxena[7] given in Eq. (11), K_i°/K_j° were obtained from the viscosity data, and for O_2–Kr, O_2–Xe these were obtained from the heat

TABLE XIII. Thermal conductivity and Eucken-type factor for O_2—Xe mixture at 45°C.

% of Xe	$K_{exp}\times10^5$	$K_H\times10^5$ from Eq. (10)	$K_{H'}\times10^5$ with exptl. value of δ_f	$K_{MS}\times10^5$ from Eq. (11)	$K_{exp}/K_{mix(mon)}$	$K_{H'}/K_{mix(mon)}$	y	x
100	1.351	1.351	1.351	1.351	1.000	1.000	...	...
85	1.813	1.835	1.816	1.759	1.092	1.094	6.536	5.667
70	2.317	2.366	2.325	2.351	1.164	1.168	3.067	2.333
55	2.923	3.003	2.939	2.995	1.218	1.225	1.912	1.222
40	3.711	3.766	3.674	3.762	1.281	1.268	1.095	0.667
25	4.577	4.614	4.588	4.691	1.301	1.299	0.940	0.332
10	5.740	5.903	5.735	5.791	1.319	1.318	0.720	0.111
0	6.688	6.885	6.688	6.688	1.326	1.326	...	...

capacity data. The results of these calculations are given in column 5, Tables VI to XIII.

5. DISCUSSION OF RESULTS

A consideration of the values of the thermal conductivity of O_2 (Table V) shows that the experimental values of the Eucken factor are less than those given by Hirschfelder's Eq. (7) derived on the assumption of local chemical equilibrium, and the corresponding values of f_{int} are also less than the limiting values $\sim$1.3. In order to explain this discrepancy between theory and experiment, let us examine, as done by Hirschfelder,[4] the assumptions involved in the derivation of Eq. (7), *viz.*, (1) validity of the condition of local chemical equilibrium which implies that all reactions (including rotational-translational transfer) are fast, (2) all molecular species have the same binary diffusion coefficients even though they are in different states of excitation, (3) thermal diffusion is negligible.

Of the three assumptions the first one seems to be the most important. Ultrasonic and shock-wave measurements show that actually rotational-translational transfer is much slower than the translational-translational transfer. In fact, it has been found that only 1 collision out of 300 in H_2[19] and 1 out of 20 in O_2[20] leads to an energy transfer between the translational and the rotational degrees of freedom, while practically each collision brings about an exchange of translational energy between the two particles. Because of this slow rate of transfer, local chemical equilibrium between the translational and the rotational states may not be established and therefore the contribution, K_r, of the rotational states to the total thermal conductivity, as pointed out by Waelbroeck and Zuckerbrodt,[21] will be less than that given by Eq. (7), and f_{int} will also be lower. This has also been observed by Waelbroeck and Zuckerbrodt in their experiments on the thermal conductivity of O_2 and H_2 down to very low pressures. Hirschfelder[4] has already pointed out that the condition of local chemical equilibrium will not be valid when the excited states are metastable. For electronically excited states which are metastable, he comes to the conclusion that the thermal conductivity is either anomalously large or small. It may be remarked that at the temperatures of our experiment, electronic excitations will be negligible. The present experimental results show that if the local chemical equilibrium condition does not hold due to a comparatively slow rate of rotational-translational transfer, the thermal conductivity is always less. Eucken's derivation is, however, based on the other extreme case where the interchange between the translational and internal energy occurs so rarely that it can be neglected. The actual values of f_{int} are therefore expected to lie between those given by Eucken and by Hirschfelder, i.e., between 1 and 1.3 which is actually found to be the case. In addition to the foregoing considerations, as has been pointed out by Srivastava and Srivastava,[5] f_{int} will also be less than 1.3 if the rate of energy exchange is slow between the different rotational and vibrational states.

Regarding assumptions (2) and (3), it is apparent that if some of the species are in higher quantum states, their collision diameters will be larger so that the corresponding diffusion coefficients will be lower and f_{int} will also be less. This effect will generally be small as the electronic states are not excited at these temperatures and vibrations are only feebly excited. Thermal diffusion adds a small term to heat transfer by conduction but the quantity of heat thus transferred rarely exceeds a few percent of that carried by ordinary conduction and is usually neglected.

It can be seen from Tables VI to XIII that the values of K_{exp} for the gas mixtures, though close to the values of K_H calculated from Eq. (10), are always less than it. One apparent reason for this as we have discussed previously is that the value of δ_f for O_2, as calculated from Eq. (10), is not correct. The agreement between K_{exp} for the mixtures and the calculated values $K_{H'}$ from Eq. (10) is excellent when the experimental values of δ_f are used.

We can also test the algebraic form of Hirschfelder's Eq. (10) and its dependence on the concentration ratio x_2/x_1 in the following way: Equation (10) may be

[19] E. F. Greene and D. F. Hornig, J. Chem. Phys. **21**, 617 (1953); E. S. Steward and J. L. Steward, J. Acoust. Soc. Am. **24**, 194 (1952).
[20] W. G. Thaler, J. Acoust. Soc. Am. **24**, 15 (1952).
[21] F. G. Waelbroeck and P. Zuckerbrodt, J. Chem. Phys. **28**, 524 (1958).

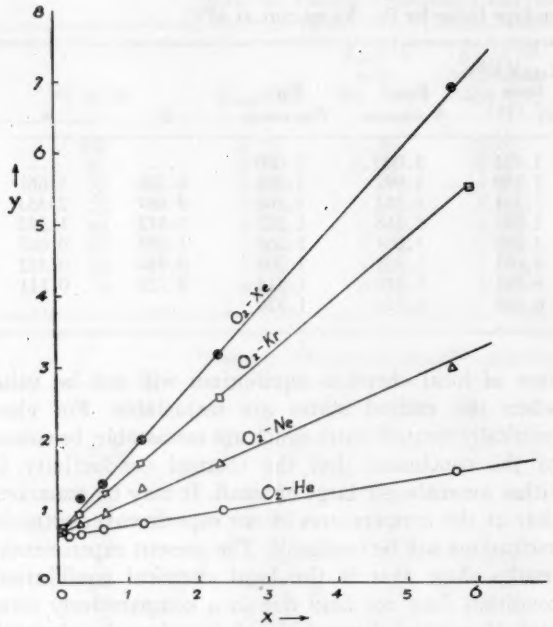

FIG. 2. Graphs showing the relation between y and x at 30°C for O_2—He, O_2—Ne, O_2—Kr, and O_2—Xe mixtures, where $y=1/[K_{mix}-K_{mix(mon)}]$ and $x=x_2/x_1$.

written as

$$K_{mix}-K_{mix(mon)}=\frac{K_1-K_{1\ mon}}{1+(x_2/x_1)(D_{11}/D_{12})} \qquad (15)$$

or $y=mx+c$, where $y=1/[K_{mix}-K_{mix(mon)}]$, $x=x_2/x_1$, $m=(D_{11}/D_{12})/(K_1-K_{1\ mon})$, $c=1/(K_1-K_{1\ mon})$.

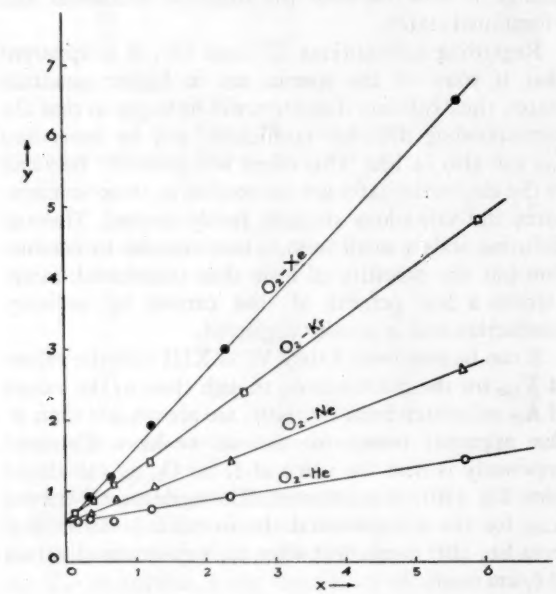

FIG. 3. Graphs showing the relation between y and x at 45°C for O_2—He, O_2—Ne, O_2—Kr, and O_2—Xe mixtures, where $y=1/[K_{mix}-K_{mix(mon)}]$ and $x=x_2/x_1$.

Values of y and x have also been recorded in Tables VI to XIII. When these are plotted (Figs. 2 and 3), the graphs are found to be approximately straight lines as required by the theory. The intercept on the y axis gives the value of K_1 and the slope gives the value of D_{11}/D_{12} from which D_{12} may be obtained. The values of K_1 and D_{12} obtained from Figs. 2 and 3 are recorded in Table XIV. The good agreement obtained between the calculated values of D_{12} and those obtained from the graphs show that the discrepancy observed for O_2-A by Srivastava and Srivastava[5] is not real. We may conclude from the data shown in Tables VI to XIII that Hirschfelder's Eq. (10) can represent correctly the concentration dependence of the thermal conductivity of binary gas mixtures. It is also seen that the agreement obtained with the experimental data by using Mason and Saxena's Eq. (11) is only approximate. The more rigorous formula of Hirschfelder is found to represent the experimental data much better than Eq. (11).

TABLE XIV. Thermal conductivity and interdiffusion coefficients from x y graphs.

T°K	Gas mixt.	$K_1\times10^5$ from graph	$K_{1(exp)}\times10^5$	D_{12} from graph	$D_{12(calc.)}$[a]
303.2	O_2—He	6.381	6.442	0.747	0.762
	O_2—Ne	6.315		0.342	0.340
	O_2—Kr	6.559		0.162	0.154
	O_2—Xe	6.465		0.123	0.125
318.2	O_2—He	6.825	6.688	0.821	0.825
	O_2—Ne	6.628		0.374	0.369
	O_2—Kr	6.707		0.174	0.168
	O_2—Xe	6.825		0.124	0.138

[a] Calculated on the Lennard-Jones (12:6) model.

6. TEMPERATURE COEFFICIENT OF THERMAL CONDUCTIVITY

In Table XV(a) we have recorded the temperature coefficient of thermal conductivity γ of pure gases and gas mixtures calculated from the relation

$$K_2=K_1(1+\gamma t), \qquad (16)$$

where K_2 and K_1 are the thermal conductivities at the higher and the lower temperature, respectively, and t is the temperature interval. As our temperature range is not sufficiently wide, we have also examined closely the accurate thermal conductivity data of Kannuluik and Carman[9] for the monatomic gases extending over a wide range of temperature to find whether γ shows any systematic variation. The γ values calculated from their data are recorded in Table XV(b). It will be seen that γ increases with decreasing temperature. From Table XV and XV it may also be seen that at the same temperature γ increases with the mass of the

TABLE XV. (a) Temperature coefficient of thermal conductivity at 310.5° K.

% of monatomic gas	Gas mixture O_2—He	O_2—Ne	O_2—Kr	O_2—Xe
100	0.0024 (exptl.) 0.0019 (calc)	0.0025 (exptl.) 0.0024 (calc)	0.0025 (exptl.) 0.0031 (calc)	0.0030 (exptl.) 0.0032 (calc)
55	0.0023	0.0023	0.0027	0.0028
0	0.0026	0.0026	0.0026	0.0026

(b) Temperature coefficient of thermal conductivity γ in $°C^{-1}$ from Kannuluik and Carman's[a] data.

$T°K$		He	Ne	A	Kr	Xe
535	Exptl.	0.0012	0.0012	0.0013	0.0016	0.0016
	Calc	0.0012	0.0012	0.0012	0.0016	0.0016
432	Exptl.	0.0016	0.0015	0.0018	0.0021	0.0020
	Calc	0.0016	0.0016	0.0016	0.0019	0.0024
323	Exptl.	0.0020	0.0020	0.0028	0.0030	0.0037
	Calc	0.0019	0.0022	0.0025	0.0030	0.0031
234	Exptl.	0.0030	0.0032	0.0039	0.0044	0.0045
	Calc	0.0028	0.0034	0.0037	0.0038	0.0038
142	Exptl.	0.0042	0.0050	0.0063	...	...
	Calc	0.0047	0.0053	0.0065	...	...

[a] See reference 9.

molecule. These variations of γ may be explained in the following way:

According to the Chapman-Enskog theory, thermal conductivity K is given to the first approximation by

$$[K]_1 = AT^{\frac{1}{2}}/\Omega^{(2,2)*}, \tag{17}$$

where A is a constant, T is the temperature in °K and $\Omega^{(2,2)*}$ is a collision integral dependent on temperature and molecular force laws. The temperature coefficient of thermal conductivity is given by

$$\gamma = (1/K)(dK/dT) = [(1/2T) - (1/\Omega^{(2,2)*})(d\Omega^{(2,2)*}/dT)]. \tag{18}$$

In Eq. (18) the first term on the right-hand side always show an increase with decrease of temperature. For calculating the contribution of the second term, we may assume the molecules to obey Lennard-Jones (12:6) model for which the collision integrals $\Omega^{(2,2)*}$ have been calculated[17] as a function of $T^* = kT/\epsilon$, ϵ being the depth of the potential well. We have

$$(1/\Omega^{(2,2)*})(d\Omega^{(2,2)*}/dT) = (k/\epsilon)(d \ln\Omega^{(2,2)*}/dT^*). \tag{19}$$

A plot of $\ln\Omega^{(2,2)*}$ *vs* T^* shows that $d \ln\Omega^{(2,2)*}/dT^*$ is always negative so that the second term will always add up to the first, and further, its magnitude is larger for lower temperatures. This will thus increase the effect of the first term, and the coefficient γ will thus increase with decreasing temperature. The observed increase of γ from He to Xe at any fixed temperature is due to the variation of the second term in Eq. (18) because of the variation of ϵ for the different gases. In Tables XV we have also recorded the γ values for the monatomic gases calculated from Eq. (18) with ϵ values determined from viscosity. The agreement seems to be quite good except for Kr and Xe at low temperatures. For the gas mixtures, the temperature range is not wide enough to justify such detailed examination of γ.

THE JOURNAL OF CHEMICAL PHYSICS VOLUME 32, NUMBER 2 FEBRUARY, 1960

Molecular Diffusion Studies in Gases at High Temperature. IV. Results and Interpretation of the CO_2—O_2, CH_4—O_2, H_2—O_2, CO—O_2, and H_2O—O_2 Systems*

R. E. WALKER AND A. A. WESTENBERG

Applied Physics Laboratory, The Johns Hopkins University, Silver Spring, Maryland

(Received September 14, 1959)

Experimental measurements of the binary diffusion coefficients for the CO_2—O_2, CH_4—O_2, H_2—O_2, CO—O_2, and H_2O—O_2 systems over the nominal temperature range 300–1000° K are reported. The measurements were made by the point source technique. The data have been analyzed in terms of intermolecular potential energies and the rigorous kinetic theory by using the Lennard-Jones (12–6), modified Buckingham (Exp-6), point center of repulsion (inverse power), and the exponential repulsion potential energy functions. It is shown that all four of these functions are capable of fitting the diffusion data with about the same precision (within experimental error). However, the potential energy values themselves which are calculated from these four different fitted models are shown to be widely at variance; especially in the range of interaction corresponding to the lower temperatures. Thus, these results provide an example of the high degree of ambiguity (previously noted by several others) involved in deducing intermolecular potential energies from transport data. The use of such fitted potentials to extrapolate transport data to higher temperatures, on the other hand, is probably a more reliable procedure, and diffusion coefficients for the above five gas pairs (in their unexcited, undissociated states) have been estimated to 3000° K from the potentials based on the 300–1000° K measurements.

INTRODUCTION

In a recent paper[1] (referred to as I) the authors have presented a new method of measuring molecular diffusion coefficients of gases that is well suited for measurements at high temperatures (300–1200°K). Basically, this technique uses concentration profiles determined downstream of a point source of trace gas in a uniform (heated) laminar jet of carrier gas to evaluate the binary diffusion coefficients. In two subsequent publications[2,3] (referred to as II and III) results of using this technique on the He—N_2, CO_2—N_2, and He—A systems were reported, and the measurements interpreted by means of the kinetic theory of gases to obtain intermolecular forces.

The present paper presents similar measurements and analysis for the gas pairs H_2—O_2, H_2O—O_2, CO—O_2, CO_2—O_2, and CH_4—O_2 over the nominal temperature interval 300–1000°K and at atmospheric pressure. The particular choice of gas pairs was motivated by the need for reliable data on the stable species found in the lean methane-oxygen combustion system presently under analysis at this Laboratory, and should find additional application to other hydrocarbon combustion systems as well as the usual thermophysical applications. As in papers II and III, the data have been analyzed with the rigorous kinetic theory of gases to obtain intermolecular forces between the unlike molecules. Four kinds of intermolecular potentials have been used: the point center of repulsion, the Lennard-Jones (12–6), the modified Buckingham (Exp-6)[4], and the exponential repulsion potential for which the collision integrals have recently been computed by L. Monchick of this Laboratory.[5] The comparison of these different results provides an interesting and instructive example of the perils and possibilities of this kind of use of transport data.

EXPERIMENTAL METHODS AND RESULTS

In general, the experimental methods and equipment used for these measurements were identical to those described in I, so that the details are not repeated here. However, certain modifications required by the peculiarities of some of the gas pairs are discussed below.

In all measurements the trace gas was the light component and the carrier gas the heavy component; this arrangement is particularly suited to this technique† and entirely compatible with the gas pairs being studied. The oxygen (hydrogen free) and carbon dioxide (extra dry) were supplied as compressed gases by the Southern Oxygen Company, while the hydrogen (prepurified), methane (commercial), and carbon monoxide (high purity) were supplied by the Mathieson Company. All gases were used directly from the high-pressure container. In general, small amounts of impurities are unimportant in the measurements; however, the sensitivity of the thermal conductivity gas analysis instrument to light gas impurities required that hydrogen-free gases be used.

* Supported under Contract NOrd 7386 with the Bureau of Ordnance, U. S. Navy.

[1] R. E. Walker and A. A. Westenberg, J. Chem. Phys. **29**, 1139 (1958).

[2] R. E. Walker and A. A. Westenberg, J. Chem. Phys. **29**, 1147 (1958).

[3] R. E. Walker and A. A. Westenberg, J. Chem. Phys. **31**, 519 (1959).

[4] For a discussion of these potentials see Hirschfelder, Curtiss, and Bird, *The Molecular Theory of Gases and Liquids* (John Wiley & Sons, Inc., New York, 1954), Chap. I.

[5] Phys. Fluids (to be published).

† Our experience has been that somewhat better precision is attained when the light gas is used as the tracer. This is probably connected with its lower jet momentum and penetration distance in entering the carrier stream.

Improvements in the thermal conductivity gas analysis instrument used for these measurements have been reported elsewhere.[6]

Carbon Dioxide-Oxygen

Diffusion coefficients for the O_2 (trace)-CO_2 system were obtained in exactly the same way as the N_2 (trace)-CO_2 measurements reported in I and II, so that no further comment on the experimental technique is required. The measurements were obtained over the temperature interval 297–1080°K and are reproduced in Fig. 1.

It is worth noting that both sets of diffusion measurements for $D_{CO_2-N_2}$ and $D_{CO_2-O_2}$ are larger than the D_{CO_2-Air} values given by Klibanov *et al.*[7] and previously compared in I. This is an interesting comparison inasmuch as these are the only other diffusion data covering the same temperature range.

An additional comparison between these measurements and values reported in the literature is given in Table I. No significant concentration effects would be expected for the CO_2-O_2 system since the molecular weights are not widely different. (For a discussion of these concentration effects see papers I and II of this series.)

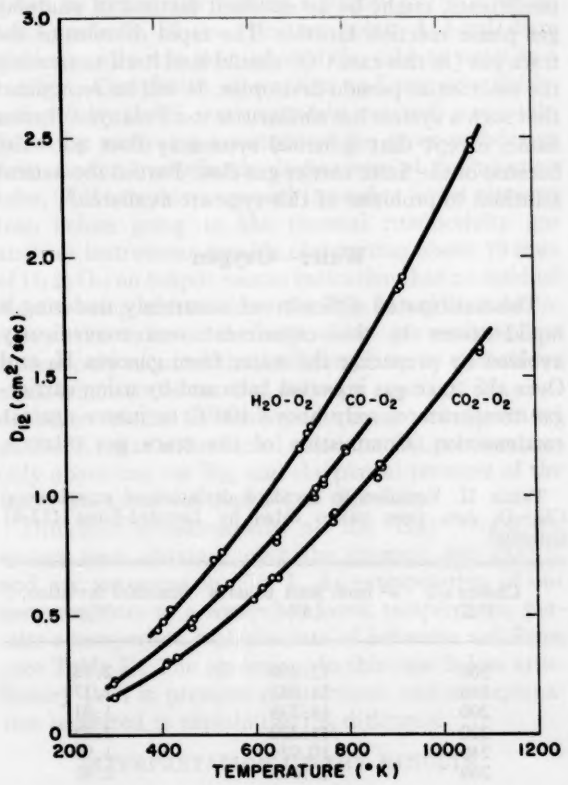

FIG. 1. Diffusion measurements as a function of temperature for the CO_2—O_2, CO—O_2, and H_2O—O_2 systems.

[6] R. E. Walker, Rev. Sci. Instr. **30**, 378 (1959).
[7] Klibanov, Pomerantsev, and Frank-Kamenetsky, J. Tech. Phys. (U.S.S.R.) **12**, 14 (1942).

TABLE I. Comparison of measured diffusion coefficients with previously reported values. $P=1$ atmos.

Gas pair	T (°K)	D_{12} (cm² sec⁻¹) (other work)	D_{12} (cm² sec⁻¹) (this work)	Reference
H_2—O_2	273.2	0.697	0.688[a]	b
H_2O—O_2	308.1	0.282	0.301[a]	c
	329.0	0.318	0.338[a]	c
	352.4	0.352	0.381[a]	c
CO—O_2	273.2	0.185	0.191[a]	b
CO_2—O_2	273.2	0.139	0.137[a]	b
	293.2	0.16	0.153	d

[a] Extrapolated values.
[b] S. Chapman and T. G. Cowling, *Mathematical Theory of Non-Uniform Gases* (The Macmillan Company, New York, 1939).
[c] F. A. Schwertz and J. E. Brow, J. Chem. Phys. **19**, 640 (1951).
[d] L. E. Boardman and N. E. Wild, Proc. Roy. Soc. (London) **A162**, 511 (1937).

Methane—Oxygen

Diffusion measurements for the CH_4 (trace)-O_2 system were made in the usual manner and are presented graphically in Fig. 2. The temperature interval covered was 297–980°K, and no measurements at higher temperatures were possible because spontaneous ignition of the methane in the hot oxygen occurred at about 1020°K. The possibility was raised that prior to ignition there might be some slow reaction occurring in the mixing zone which would render the thermal conductivity gas analysis, and hence the diffusion data, invalid. In order to check this, a Pt—Pt (10% Rh) thermocouple was placed downstream of the injection tube and at various high temperatures the methane flow was alternately turned on and off and the changes in thermocouple reading noted. At no time prior to ignition was a temperature change greater than 2°C observed. From this brief experiment, it was concluded that slow reaction (if any) was of no significance prior to visible ignition.

Since no other diffusion data for CH_4-O_2 have been reported, no comparison is possible.

Hydrogen—Oxygen

Data for the H_2 (trace)-O_2 system are presented in graphical form in Fig. 2. The temperature interval for these measurements was 295–900°K, the upper limit being established (as in the previous case), by the spontaneous ignition of the hydrogen trace in the hot ambient oxygen at about 920°K. The smoothness of the diffusion data approaching this ignition limit tends to indicate that there was no slow reaction in the mixing gas, as did the thermocouple measurements made in the (presumably slower) CH_4-O_2 case discussed previously. No additional proof in the H_2-O_2 case was considered necessary.

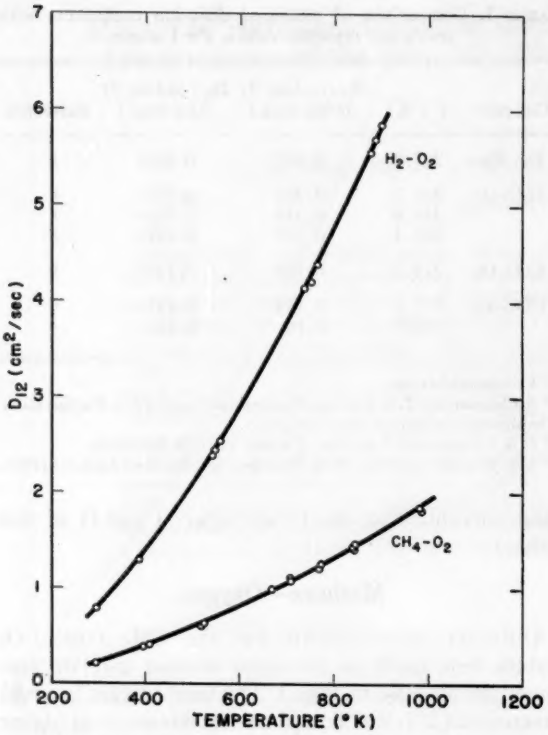

FIG. 2. Diffusion measurements as a function of temperature for the H_2—O_2 and CH_4—O_2 systems.

A comparison between these measurements and a value reported in the literature is made in Table I. The agreement is within the experimental error. No attempt was made to measure the effect of composition on $D_{H_2-O_2}$ by interchanging the trace and carrier gases because of the difficulty in handling large amounts of hydrogen. A theoretical calculation[4] of $D_{H_2(trace)-O_2}/D_{H_2-O_2(trace)}$ yields a value of 1.03 which can be expected to be quite reliable.[2,3]

Carbon Monoxide—Oxygen

Without some chemical change, it is very difficult to analyze quantitatively for the presence of trace amounts of CO in O_2 using thermal conductivity gas analysis. Therefore, in order to get around this difficulty, the sample was first passed over heated platinum gauze to oxidize the CO to CO_2. This combustion furnace was tested at different temperatures‡ while the product composition was monitored with the thermal-conductivity analyzer—in this manner a safe operating temperature was determined at which complete conversion was attained. Because only trace amounts of CO were present, the depletion of the oxygen was negligible and the usual methods of data reduction applied.

Measurements of diffusion coefficients for the CO (trace)-O_2 system were obtained without difficulty up to a temperature of about 800°K. At this point, reproducibility of the measurements became very poor. Detailed sampling and analysis (the usual thermal-conductivity gas analysis with and without conversion of CO to CO_2) revealed that disproportionation of the CO ($2CO \rightarrow CO_2 + C$) in the stainless steel injection tube[8] was occurring in varying amounts at various temperatures above about 700°K. This disproportionation eventually deposited enough carbon to completely plug the injection tube. The measured diffusion coefficients showed that reliable data could be obtained only over the temperature interval 295–800°K, and these are presented in Fig. 1. As before, Table I gives a comparison of our measured values (extrapolated) with values already in the literature.

At temperatures above about 900°K a visible reaction was apparent in the diffusion (mixing) zone, and thermocouple temperature measurements in this region with and without CO trace gas flow showed definitely that a slow gas phase reaction was occurring without a sharp ignition point as in the CH_4-O_2 and H_2-O_2 systems. It seems worth pointing out that detailed measurements of local temperature and composition in a case such as this, along with appropriate diffusion coefficients, might be an excellent method of studying gas phase reaction kinetics. The rapid dilution of the trace gas (in this case CO) should lend itself to treating the reaction as pseudo first order. It will be recognized that such a system has similarities to a Polanyi diffusion flame, except that spherical symmetry does not exist because of the finite carrier gas flow. Partial theoretical solutions to problems of this type are available.[9]

Water—Oxygen

The anticipated difficulty of accurately metering a liquid tracer in this experiment was conveniently avoided by preparing the water from gaseous H_2 and O_2 in the trace gas injection tube and by using carrier-gas temperatures only above 100°C to insure against condensation. Combustion of the trace gas mixture

TABLE II. Variation in standard deviation of experimental CO_2—O_2 data from values fitted by Lennard-Jones (12–6) potential.

Chosen ϵ/k (°K)	σ^2 from least squares (A²)	Standard deviation, S (%)
160	12.259	2.75
180	11.883	2.17
200	11.538	1.81
220	11.220	1.75
240	10.924	1.99
260	10.649	2.41

‡ The temperature of the platinum was not measured directly but rather the voltage to the furnace heating elements.

[8] T. Moeller, *Inorganic Chemistry* (John Wiley & Sons, Inc., New York, 1952), p. 686.

[9] W. Jost, *Diffusion in Solids, Liquids, Gases* (Academic Press, Inc., New York, 1952).

TABLE III. Numerical values of potential parameters for various unlike molecular interactions with associated range of validity and precision of fit to the experimentally measured diffusion data.

	Range of validity		Modified Buckingham (Exp-6)				Lennard-Jones (12-6)			Point center of repulsion			Exponential repulsion		
Gas pair	Min A	Max A	ϵ/k °K	r_m A	α	Std. dev. %	ϵ/k °K	σ A	Std. dev. %	d ergs $\times 10^{10}$A$^\delta$	δ	Std. dev. %	A/k °K $\times 10^{-5}$	ρ A	Std. dev. %
CO_2—O_2	3.09	3.76	165	4.071	12	1.83	213	3.365	1.74	3.75	6.54	2.60	6.5	0.5203	2.94
			202	3.846	14	1.78									
			255	3.616	17	1.74									
H_2—O_2	2.50	2.94	117	3.421	12	0.58	152	2.825	0.63	1.62	7.13	1.01	9.0	0.3948	1.22
			143	3.234	14	0.59									
			183	3.032	17	0.64									
CH_4—O_2	3.08	3.60	145	4.061	12	2.37	182	3.367	2.25	4.56	6.83	3.04	8.0	0.4915	3.30
			170	3.855	14	2.30									
			220	3.612	17	2.25									
CO—O_2	3.01	3.38	40	4.525	12	2.30	91	3.480	1.73	75.6	9.52	1.85	105	0.3392	1.87
			76	4.040	14	1.77									
			110	3.733	17	1.73									
H_2O—O_2	2.78	3.10	55	4.154	12	2.5	80	3.335	1.40	358	11.41	1.46	900	0.2610	1.50
			100	3.567	17	1.4									

containing excess oxygen§ was conveniently accomplished by electrically heating a portion of the injection tube upstream of the injection point. A 5-mil diam platinum wire was inserted into the tube to serve as a catalyst. Completion of reaction and proper stoichiometry (only the H_2 was accurately metered) was established by analyzing a sample of the gases withdrawn from a point immediately downstream of the injection tube. This sample was passed through a liquid nitrogen trap before going to the thermal conductivity gas analysis instrument capable of detecting about 10 ppm of H_2 in O_2; no output was an indication that no residual H_2 was being emitted from the injection tube. Adsorption of the water on the walls of the gas analysis flow system only required that sufficient time be allowed for equilibrium to be reached between readings. No condensation in the thermal conductivity cell (operated at 273°K) was encountered since the cell pressure was only about one cm Hg, and the partial pressure of the water trace was less than 2% of this value.

Diffusion measurements of the H_2O (trace)-O_2 system were obtained over the interval 390–1070°K and are presented in Fig. 1. An extrapolation of our measurements to a somewhat lower temperature, permits a comparison with the data of Schwertz and Brow (see Table I). The agreement in this case is less satisfactory than in previous comparisons, and no explanation is offered to explain the 7% difference.

INTERPRETATION OF THE RESULTS

For gas molecules that have nearly spherically symmetric force fields, the rigorous kinetic theory of gases permits measured transport properties to be related to intermolecular forces.[4] In particular, the measurement of molecular diffusion coefficients as a function of temperature is one of the best known methods of determining intermolecular forces between unlike molecules since, to a very good first approximation, unlike interactions alone determine this transport property. In such an analysis, the procedure is to select a particular analytic function which approximates the actual (unknown) potential energy, and to determine a set of parameters for this function that best reproduces the experimental data. This fitting procedure has already been detailed in II. In the present work, four of the most realistic potential functions have been used to fit the data and then compared with each other. The results afford an interesting example of this type of procedure.

The four potential functions used are the Lennard-Jones (12-6),

$$\phi(r)=4\epsilon[(\sigma/r)^{12}-(\sigma/r)^{6}], \tag{1}$$

the modified Buckingham (Exp-6)

$$\phi(r)=[\epsilon/(1-6/\alpha)][(6/\alpha)\exp\{\alpha(1-r/r_m)\}-(r_m/r)^6], \tag{2}$$

the point center of repulsion,

$$\phi(r)=d/r^{\delta}, \tag{3}$$

and the exponential repulsion,

$$\phi(r)=A\exp(-r/\rho). \tag{4}$$

In these expressions, r is the intermolecular separation distance, and the other quantities (ϵ, σ, α, r_m, d, δ, A, ρ), are constant parameters. For the potential functions given by (1), (2), and (3), the appropriate collision

§ The slight excess of oxygen was unimportant since the carrier gas was also oxygen.

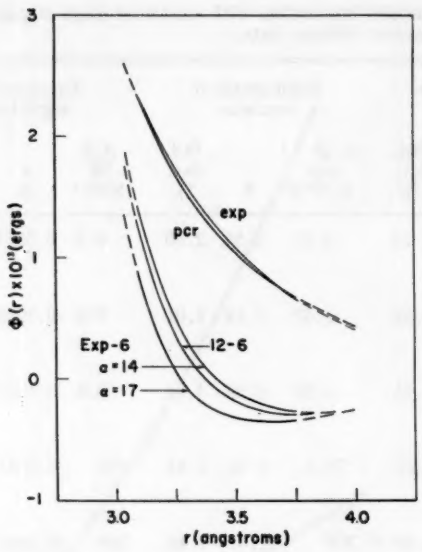

FIG. 3. Potential energy of interaction for CO_2—O_2 using potential parameters listed in Table III.

integrals have already been published.[4,10,11] Collision integrals for the exponential repulsion potential (4), have been recently computed by L. Monchick[5] of this Laboratory and were available to us. Potentials (1) and (2) are realistic functions for low temperature interactions, since they include the London dispersion energy (attractive) term ($\phi \propto r^{-6}$), which has a reasonably firm theoretical basis. Potentials (3) and (4) find particular application to the analysis of high-temperature phenomena where the attractive forces are less important in the molecular collisions. Molecular diffusion coefficients tend to be associated with more penetrating collisions than other transport properties at the same temperature.[12] It should be noted that the above potentials may be used in the case where only one member of the diffusion pair is a polar gas (e.g., H_2O-O_2), since the interaction may still be regarded as effectively spherically symmetric.

The general kinetic theory expressions used in analyzing the diffusion data have been summarized in II. The theory to the second approximation was used in all cases, although this was actually necessary only in the cases where the molecular weights of the two gases in the pair were quite different (H_2-O_2, H_2O-O_2, CH_4-O_2).

To determine the potential parameters that best fitted the experimental measurements, a least squares method was employed. The quantity

$$S=\left(\frac{1}{N}\sum_{n=1}^{N}\left\{\frac{D_{\text{expt}}-[D_{12}]_2}{D_{\text{expt}}}\right\}_n^2\right)^{\frac{1}{2}},$$

was minimized with respect to the parameters involved in the theoretical $[D_{12}]_2$. Because the point center of repulsion potential (3) involves a simple mathematical description of the transport properties, the fitting procedure is straightforward; fitting the other potentials to the data, however, is not so simple. In these cases, the procedure outlined in II was generally followed, i.e., an ϵ, ϵ and α, or A was chosen for the Lennard-Jones, modified Buckingham, or exponential repulsion potentials, respectively, and a value of σ, r_m, or ρ, determined satisfying the least squares requirement. This procedure was repeated for different choices of ϵ, ϵ and α, or A, until a minimum value of S was found. To facilitate this rather tedious operation, the appropriate dimensionless collision integrals were fit to polynominal functions|| in T^* and the entire procedure was programmed on an IBM 650 digital computer. As noted in II, high-temperature transport data are not especially sensitive to the choice of compatible potential parameters, so that the standard deviation S of the measurements varies slowly (generally within experimental error) at its minimum with respect to these parameters (see Table II). For this reason, it was felt that the three parameters for the modified Buckingham (Exp-6) potential could not be unambiguously specified with the available data. Rather, several choices of the parameter α were investigated and are reported below without discrimination. Actually none of the reported potential parameters should be

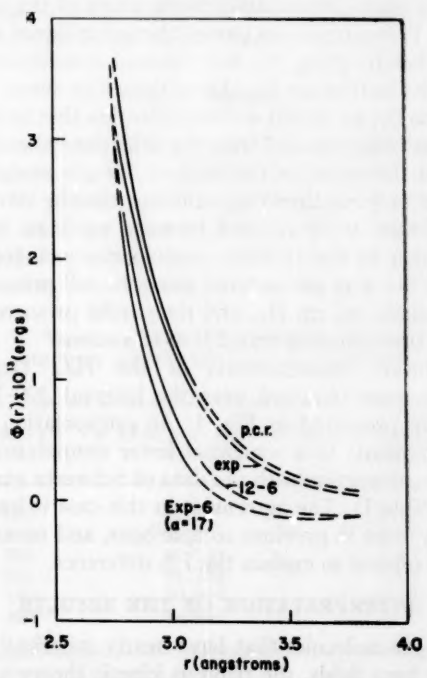

FIG. 4. Potential energy of interaction for H_2O—O_2 using the potential parameters listed in Table III.

[10] E. A. Mason, J. Chem. Phys. **22**, 169 (1954).
[11] E. A. Mason, J. Chem. Phys. **22**, 843 (1954).
[12] J. O. Hirschfelder and M. A. Eliason, Ann. N. Y. Acad. Sci. **67**, 451 (1957).

|| These polynomial expressions are available from the authors.

TABLE IV. Comparison of predicted diffusion coefficients using the various potential functions given in Table III (trace of light gas, $p=1$ atmos).

System	Potential function	Temperature, °K 300	500	1000	1500	2000	2500	3000
CO_2—O_2	12-6	0.161	0.419	1.43	2.84	4.59	6.66	9.01
	Exp-6 ($\alpha=17$)	0.162	0.418	1.42	2.81	4.55	6.58	8.89
	p.c.r.	0.164	0.412	1.44	3.00	5.04	7.54	10.48
	exp	0.164	0.410	1.44	3.04	5.19	7.90	11.15
CH_4—O_2	12-6	0.226	0.581	1.95	3.86	6.23	9.03	12.22
	exp-6 ($\alpha=17$)	0.230	0.593	2.00	3.95	6.38	9.23	12.45
	p.c.r.	0.229	0.574	1.99	4.11	6.88	10.26	14.23
	exp	0.230	0.570	1.99	4.18	7.11	10.77	15.18
H_2—O_2	12-6	0.821	2.09	6.93	13.7	22.2	32.1	43.4
	exp-6 ($\alpha=12$)	0.818	2.07	6.99	14.1	23.1	34.0	46.6
	p.c.r.	0.828	2.06	7.06	14.5	24.3	36.1	50.0
	exp	0.830	2.05	7.10	14.9	25.2	38.1	53.6
CO—O_2	12-6	0.224	0.542	1.73	3.40	5.48	7.93	10.72
	exp-6 ($\alpha=17$)	0.224	0.542	1.74	3.39	5.45	7.88	10.62
	p.c.r.	0.224	0.538	1.76	3.52	5.76	8.44	11.53
	exp	0.225	0.537	1.77	3.57	5.89	8.70	11.99
H_2O—O_2	12-6	0.288	0.692	2.21	4.32	6.96	10.09	13.65
	exp-6 ($\alpha=17$)	0.286	0.691	2.20	4.31	6.93	10.00	13.48
	p.c.r.	0.294	0.691	2.21	4.35	7.05	10.24	13.90
	exp	0.294	0.690	2.21	4.37	7.11	10.38	14.16

considered as being unique in view of the insensitivity of S.

A summary of the potentials fit to the diffusion measurements reported earlier in this paper is given in Table III. Also included is the range of r, over which the determined potential can be expected to be valid (see paper II for a discussion of this rigid sphere range of validity). It will be apparent from a survey of the standard deviations provided in this table, that *all of these intermolecular potentials are about equally successful in fitting the diffusion data within the estimated experimental error*. An equivalent compatibility does not exist, however, between the actual potential energies given by the fitted parameters of Table III. Figures 3 and 4 give examples of typical interactions which illustrate this important fact. Figure 3 is a plot of the CO_2-O_2 potential energy of interaction where the range of validity extends into the "well" created by a combination of attractive and repulsive forces, whereas Fig. 4 is the potential energy of interaction for the H_2O-O_2 system where the range of validity does not extend into the well. It is obvious that, although the repulsive potentials (3) and (4) are quite adaptable to the analysis of high temperature transport data, the corresponding potential energies of interaction so predicted do not include the attractive forces of the interaction, and hence differ significantly from the potential energies predicted by use of the Lennard-Jones (12−6) or modified Buckingham (Exp-6) models. The differences are especially marked when the range of validity is close to the "well." Better agreement between all four potentials exists when the range of validity lies farther up on the (mainly) repulsive part of the curve (note the improved agreement in Fig. 4 as compared to Fig. 3). For more penetrating collisions (i.e., higher temperature) the particular choice of the potential appears to be less critical. It should be emphasized that potentials determined in this way should not be extrapolated much beyond their ranges of validity, especially in the region of the "well." Even within the range of validity, it is impossible to state (without other evidence) which of the potentials is closest to the "true" potential, although it seems likely that potentials such as (1) and (2) which contain an attractive term would be more nearly correct. Conversely, the errors introduced by extrapolation of a transport property to a higher temperature may not be excessive in spite of the disagreement between the various potentials, as is shown in the following section. This point has been made before,[13] but it is well to stress it again.

PREDICTION OF HIGH-TEMPERATURE DIFFUSION COEFFICIENTS

In our previous work[2,3] on the He−N_2 and He−A systems, it was fortunate that detailed information on the intermolecular potential at closer distances of approach (corresponding to higher temperature interactions) had been provided by the molecular beam scattering experiments of Amdur and his co-workers.[14,15] These potentials provided an excellent foundation for predicting high temperature diffusion coefficients ($1000°<T<10\,000°$K) of the unexcited species. The

[13] I. Amdur and J. Ross, Combustion and Flame **2**, 412 (1958).
[14] Amdur, Mason, and Jordan, J. Chem. Phys. **27**, 527 (1957).
[15] Amdur, Mason, and Harkness, J. Chem. Phys. **22**, 1071 (1954).

agreement between our measured values and the scattering predictions in the common temperature interval was quite good.

Unfortunately, no such scattering experiments have been done for the several gas pairs reported here. Table IV gives values to 3000°K for the diffusion coefficients obtained by extrapolation using the rigorous kinetic theory and the various fitted intermolecular potential parameters given in Table III. Although the various intermolecular potentials for a particular interaction are, in general, quite different in themselves, the diffusion coefficients extrapolated from them are not necessarily so, as can be seen by examining Table IV. Which of these extrapolated diffusion coefficients is more nearly correct, is impossible to state.

ACKNOWLEDGMENTS

The detailed analysis of the experimental data was greatly facilitated by the assistance of Mr. S. Favin in performing the various numerical manipulations on the digital computer. His contribution is gratefully acknowleged. The authors are also indebted to Mr. C. Grunfelder for his assistance in the H_2O-O_2 diffusion measurements.

THE JOURNAL OF CHEMICAL PHYSICS VOLUME 32, NUMBER 2 FEBRUARY, 1960

Some Effects of Vapors on Electret Behavior*

J. R. Beeler, Jr.,† J. D. Stranathan, and G. G. Wiseman

Department of Physics, The University of Kansas, Lawrence, Kansas

(Received July 24, 1959)

The effects of various vapors on the growth and decay of electret polarization have been studied. Particular emphasis was given to the effect of water vapor on polyvinyl acetate. The observed effects appear to arise from two causes: (1) a decrease in the relaxation time and an increase in the magnitude of the volume polarization following infusion of vapor into the dielectric; (2) an increase in the transfer of charge by means of interfacial discharge at the dielectric-electrode gap. The infusion of a polar vapor into a nonpolar solid dielectric gave anomalously large values of volume polarization.

The dielectrics studied were polyvinyl acetate, polyethylene, two acrylic resins, and carnauba wax. The vapors used successfully were water and chlorobenzene; unsuccessful attempts were made to use benzene and isopropyl ether.

INTRODUCTION

THE study described here deals with the effects of absorbed and environmental vapor on electret behavior. Previous accounts of these effects[1-3] were incidental to other studies and have either lacked detail or were made at high humidities exclusively. This study was made for relative humidities of 90%, 70%, 50%, 30%, and 0%. Both volume and surface effects were considered, and vapors other than water were used.

EXPERIMENTAL PROCEDURE

The dielectric specimens were tested in dissectible capacitors.[4,5] Unless otherwise stated the specimens were made and tested in pairs, one serving as a control specimen. Matched dissectible capacitors were housed in sealed containers which were immersed in a constant temperature (29.5°C) bath. The test atmospheres containing water vapor were humidified by glycerin-water solutions, and a total pressure of 760 mm Hg was established by admitting dry nitrogen. Charges were measured with a Dershem electrometer and a standard capacitor C in the usual fashion. The measuring circuit, depicted in Fig. 1, permitted charge measurements to be made during both the growth and decay of electret polarization. The stationary (lower) electrode was connected to the positive cable of the high-voltage supply. Hence, according to the customary notation,[2,4] the sign of a heterocharge on the upper dielectric surface is positive and the sign of a homocharge on this surface is negative. The net effective surface charge density σ on the surface, hereinafter called charge density, is taken to be $-Q/A$ where Q is the charge induced on the induction (upper) electrode and A is the area of this electrode. The upper electrode was guarded and both the electrode and the specimens were machined flat in a lathe to increase the accuracy of the charge measurements.

EFFECTS OF WATER VAPOR

The effects of water vapor on electret decay were

* Reported originally, in part, in the doctoral thesis of J. R. Beeler, Jr., March, 1955.

† Now with General Electric Company (ANPD), Cincinnati, Ohio.

[1] A. Gemant, Phil. Mag. **20**, 929 (1935).

[2] F. Gutmann, Revs. Modern Phys. **20**, 457 (1948).

[3] J. W. Wild and J. D. Stranathan, J. Chem. Phys. **27**, 1055 (1957).

[4] M. Eguchi, Phil. Mag. **49**, 178 (1925).

[5] B. Gross, J. Chem. Phys. **17**, 866 (1949).

investigated first. Desiccated disks of Gelva V-7‡ were polarized for from 6 to 10 hr while in a dry nitrogen atmosphere at 760 mm Hg pressure, and allowed to decay (with electrodes short-circuited) for one hour. A glycerin-water solution was then admitted to the test chamber and the decay allowed to continue. Equilibrium moisture in the chamber was attained in about 6 hr. Charge measurements were made at suitable intervals during electret decay. The entire experiment was run for atmospheres of 90%, 70%, and 50% relative humidity. The results of the test at 70% relative humidity are plotted in Fig. 2. Tests at the three values of relative humidity yielded the following results: (1) electret decay is more rapid in a humid than in a dry atmosphere; (2) although not shown by the diagram, specimens which were exposed to water vapor eventually reversed to homocharge polarity in every instance, whereas those maintained dry did not reverse. Both of these effects can be explained by assuming that the potential barrier for the passage of charge across the gap between the electret and the electrode is lowered by the presence of water vapor. During storage of the electret in the short-circuited condition the field within the gap was in such a direction as to deposit negative charge (homocharge) on the upper surface of the dielectric. Also, in this condition, the field in the dielectric itself was opposite to the direction of volume polarization. Thermally and field induced decay of the volume polarization thus leaves the specimen with a net homocharge. Moreover, it will be shown that exposure to moisture increases the volume polarizability of not only Gelva V-7 but also Lucite and Plexiglas.

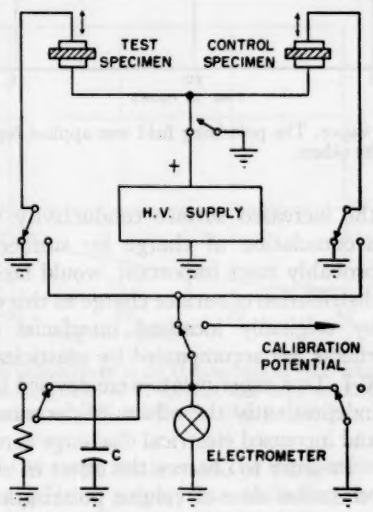

FIG. 1. The power supply was a 30 kv rectified rf supply. The net effective surface charge density σ was measured by lifting the upper electrode (which was grounded except when measurements were being made) from either specimen.

In an attempt to observe the effects of water vapor on the growth as well as the decay of electret polarization, specimens of Gelva V-7 were allowed to acquire their equilibrium moisture in an atmosphere of a particular relative humidity (see Table I). While in this atmosphere they were polarized and short-circuited, after which their surface charges were measured periodically. Fig. 3 shows the results of these measurements. Charge measurements could not be made on the 90% and 100% relative humidity specimens because they became too tacky.

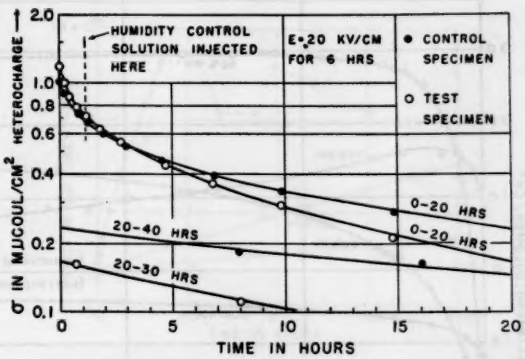

FIG. 2. Decay of σ on Gelva V-7 polarized in a dry atmosphere, in a field of 20 kv/cm applied for 6 hr, and then exposed to water vapor at 70% relative humidity at 29.5° C.

The rapid reversal of electrets which were polarized while containing their equilibrium moisture compared to electrets which were polarized dry, displays the radical change in the volume polarizability of Gelva V-7 caused by water vapor. Evidently the "fast" reversal which has been ascribed to undesiccated Gelva V-7 electrets must be due largely to their water content. The charge behavior of the three test specimens relative to that of the control specimen is consistent with the idea that moisture increases the conduction of charge across the gap and increases the volume polarizability of the material.

What probably happens is the following: (1) the infused moisture renders the volume of the dielectric more polarizable than in the dry state; (2) greater volume polarization for a given applied voltage results in a larger field in the gap; (3) the greater field in the gap (possibly facilitated by moisture in the gap) causes a greater deposition of charge (homocharge) on the dielectric; (4) later, when the capacitor is short-circuited, the volume polarization decays rapidly, leaving the specimen with a large homocharge. The

TABLE I. Measured values of equilibrium moisture with respect to dry weight of Gelva V-7 at 29.5° C.

Relative humidity (%)	Equilibrium moisture (%)	Mers/water molecule
100	3.96	5.28
90	2.94	7.10
70	1.80	11.6
50	1.15	18.1
30	0.70	29.8

‡ A polyvinyl acetate resin manufactured by the Shawinigan Products Corporation, New York.

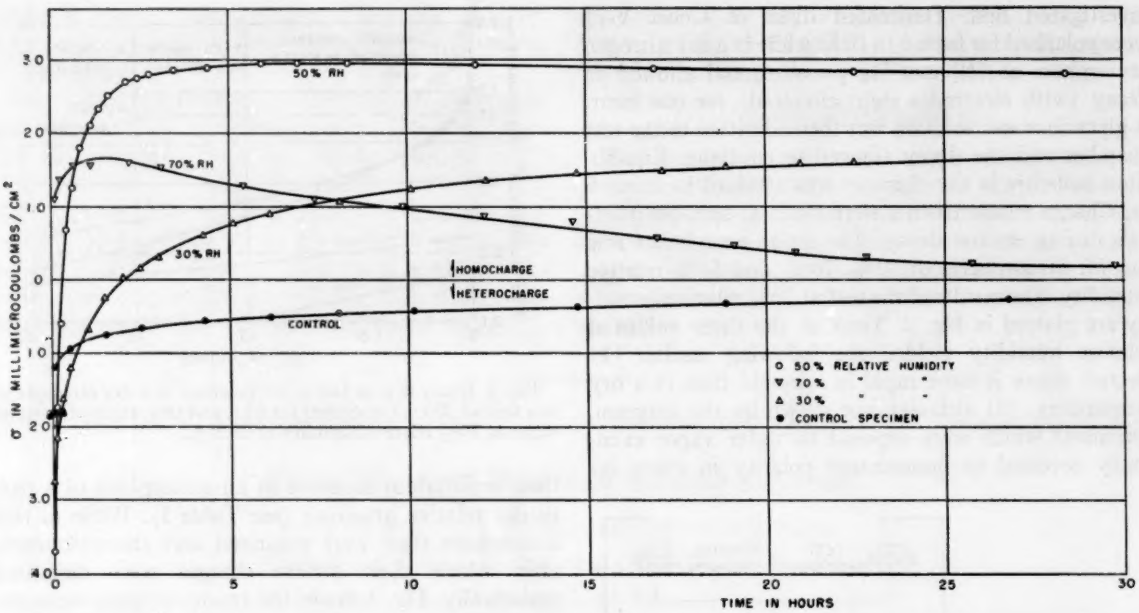

FIG. 3. Variation of σ on Gelva V-7 specimens infused with water vapor. The polarizing field was applied for 6 hours, a field of 20 kv/cm for the 70% relative humidity specimen and 23.5 kv/cm for the others.

eventual decay of net charge (barely observable in Fig. 3 for the 50% relative humidity specimen and quite pronounced for the 70% specimen) arises from the electric field within the specimen and electrical discharge across the gap.

Thus, the changes induced by water vapor on electret behavior arise primarily from two effects: (1) a decrease in the relaxation time of the volume polarization; (2) an increase in electrical discharge across the gap. The mechanism proposed by Gemant,[1] in which the electret is covered by a microscopically thin water layer which acts as a conducting shield, may be important in the latter effect. During both polarization and decay, the increased surface conductivity would allow some accumulation of charge by surface conduction and, probably more important, would facilitate the uniform distribution of surface charge as this charge is deposited by originally localized interfacial discharges. These effects are accompanied by plasticization of the Gelva V-7. Two experiments were devised to test more-or-less independently the effects of decreased relaxation time and increased electrical discharge across the gap.

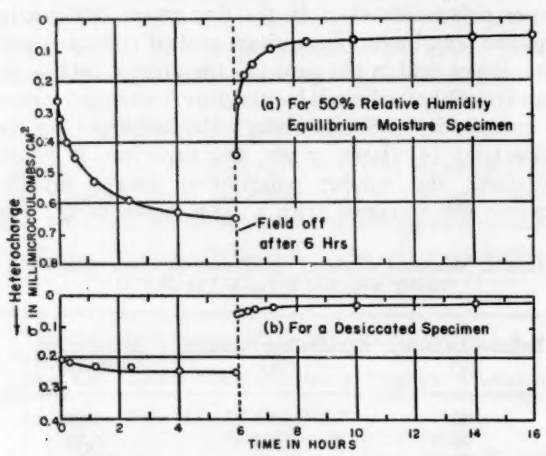
(a) For 50% Relative Humidity Equilibrium Moisture Specimen
Field off after 6 Hrs
(b) For a Desiccated Specimen
Heterocharge
σ IN MILLIMICROCOULOMBS/CM²
TIME IN HOURS

FIG. 4. Variation of σ during polarization and decay for moist and dry Gelva V-7. The polarizing field was 1.1 kv/cm applied for 6 hr.

In order to observe the effect of water vapor on the relaxation time of volume polarization, identical specimens of Gelva V-7 were made. One was allowed to attain equilibrium moisture in a 50% relative humidity atmosphere and the other was desiccated. Both specimens were then subjected to a field of 1100 v/cm for 6 hr, after which they were short-circuited. Polarization under these conditions hopefully restricts discharge across the gap to a negligible amount. The surface charge of each specimen was measured periodically during polarization and depolarization of the dielectric, with the results shown in Fig. 4. The short-time response of the equilibrium-moisture specimen is somewhat greater than that of the dry specimen, a result qualitatively consistent with the results for the 50% relative humidity specimen of Fig. 3.

To observe the effect of water vapor on electrical discharge across the gap, a polystyrene specimen was subjected to a field of 47 kv/cm in a 90% relative humidity atmosphere for 7.3 hr. Since polystyrene is essentially nonabsorptive in the electrical sense, the surface charge measured after removal of the field is essentially all homocharge. After the field was removed

the charge on the specimen was observed in the same atmosphere with the results shown in Fig. 5. The surface charge density on the control specimen of polystyrene was 0.072×10^{-9} coul/cm² throughout the test. Evidently the presence of water vapor enhanced the formation of homocharge. The initial relatively rapid decay of homocharge in the humid atmosphere is the result of electrical discharge across the gap, which ceased after about 40 hr when the surface charge density fell below a threshold value.

Observations of frictionally generated charges on carnauba wax were also made in atmospheres of 90% and 80% relative humidity. These samples maintained their initial (frictional) charge for about 30 min, the time required for the humidity in the chamber to build up to approximately 50%. Except for these initial plateaus, the dissipation of frictional charge from

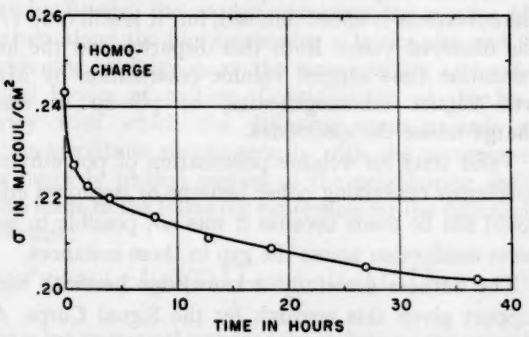

FIG. 5. Decay of σ on polystyrene in an atmosphere of 90% relative humidity. A polarizing field of 47 kv/cm had been applied for 7.3 hr in an atmosphere of 90% relative humidity.

carnauba wax had the same features as the dissipation of field-induced charge from polystyrene, including the flattening at long times. Soak tests of carnauba wax in distilled water revealed only 0.024% water absorption by weight during a 48-hr immersion at 29.5°C. These results suggest that electrical discharge across the gap is the principal mechanism of the decay of an electret's homocharge.

The effects of water vapor on another electret substance, Plexiglas, were also studied. Prior to the studies reported here, considerable variation in the electret-forming properties of different specimens of Plexiglas and Lucite had been observed in these and other§ laboratories.

The polarization response of a sample of Plexiglas was observed immediately after being cut from a sheet that had been stored under normal atmospheric conditions. The sample was then stored in a desiccated oven at 64°C for four months and its polarization response was remeasured. After 9 hr exposure to a polarizing field of 2.14 kv/cm at 64°C, the dried sample attained only about one-third of the surface charge it attained

§ Private communication from H. H. Wieder, National Bureau of Standards, Washington, D. C.

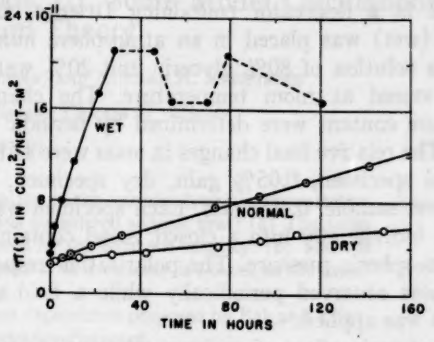

FIG. 6. Effect of moisture on the volume polarization of three Plexiglas samples in a field of 2.03 kv/cm at 35° C.

during an equal period before drying. The dried sample required 20 hr to acquire the same polarization that it attained in one hour before drying.

This same specimen was then stored 14 days in an atmosphere humidified with a solution of 80% glycerin and 20% water at room temperature. During this time it took up 0.273 g of water, about 0.5% of its dried mass. It was then sealed into a chamber containing a dissectible capacitor, and its polarization response measured as before. The moist specimen exhibited a polarization response surprisingly almost precisely the same as it exhibited before desiccation.

The preceding experiment with one Plexiglas sample is necessarily subject to the defect that aging and/or thermal treatment of the sample in the early part of the experiment may affect its subsequent behavior. Accordingly, three specimens were prepared which differed only in their moisture content. Three disks were carefully machined from adjacent regions of a single Plexiglas sheet. One sample (normal) was stored in the normal room atmosphere, the second (dry) was

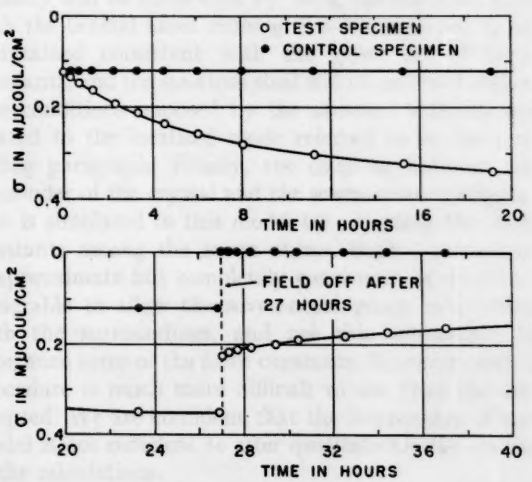

FIG. 7. The rise and decay of heterocharge in a polyethylene specimen containing chlorobenzene vapor (test specimen) and a polyethylene specimen (control specimen). The polarizing field was 1.0 kv/cm applied for 27 hr. The temperature was 29.5° C.

placed in a desiccator containing Drierite, and the third (wet) was placed in an atmosphere humidified with a solution of 80% glycerin and 20% water. All were stored at room temperature. The changes in moisture content were determined by periodic weighings. The relative final changes in mass were as follows: normal specimen, 0.05% gain; dry specimen, 0.25% loss; wet sample, 6.4% gain. Each specimen was then sealed individually into a closed vessel containing air at atmospheric pressure. The polarization response of each was observed periodically while a field of 2.03 kv/cm was applied.

The drastic effect of moisture absorption upon the volume polarization of Plexiglas is evident from the results which are depicted in Fig. 6. (In this figure the function $\pi(t)=P/E+\sigma/E-\epsilon_0$, rather than σ, is plotted. P is the polarization, E the applied electric field, and ϵ_0 the dielectric permitivity of free space.) The effect of moisture in Plexiglas appears to be nonlinear, the response of the wet specimen being disproportionately large. The irregularities in the behavior of the wet specimen beyond 24 hr is due to the typical sporadic discharge across the gap at large values of σ.

EFFECTS OF OTHER VAPORS

A determination of the effects of other vapors, both polar and nonpolar, on Gelva V-7 electrets was attempted, but all of the suitable vapors tried caused the Gelva V-7 to stick to the induction electrode.

As an alternative, attempts were made to study specimens of polyethylene saturated with chlorobenzene, benzene, and isopropyl ether. The use of polyethylene was advantageous because it itself is nonpolar and its conductance and persistent volume polarization are negligible. The polyethylene sample was allowed to attain its equilibrium vapor at an atmosphere 65% saturated with chlorobenzene at 29.5°C. The mass of the absorbed vapor was 7.35% of the mass of the dry polyethylene; this represents 17.5 mers of polyethylene per chlorobenzene molecule. The specimen was polarized at a low voltage to reduce conduction across the gap to a negligible value. The results are shown in Fig. 7.

The kinetic part of the polarization of this sample is seen to be essentially unchanged by infusion with chlorobenzene, but the quasi-static part was greatly increased to a saturation value of about 0.23×10^{-9} coul/cm^2. The Debye expression for the contribution of the chlorobenzene "gas" gives only about 0.01×10^{-9} coul/cm^2 if no internal field correction is made for the surrounding region. If the contribution to the effective field due to full polarization of the surrounding region is allowed for, the computed contribution of the chlorobenzene is about doubled, but it is still only 1/10 the observed value. Both this disparity and the long relaxation time suggest volume polarization by Maxwell-Wagner inhomogeneities, or pile-up of space charge under the electrodes.

Valid tests for volume polarization of polyethylene specimens containing either benzene or isopropyl ether could not be made because it was not possible to suppress conduction across the gap in these instances.

The authors gratefully acknowledge herewith some support given this research by the Signal Corps. Although the problem was undertaken quite independently of a Signal Corps project, early results were sufficiently significant to the project that subsequent aid was judged proper.

THE JOURNAL OF CHEMICAL PHYSICS VOLUME 32, NUMBER 2 FEBRUARY, 1960

On the Dynamical Theory of Diffusion in Crystals. III. Some Model Calculations and Relation to Continuum Theory

A. W. LAWSON, STUART A. RICE,* ROGER D. CORNELIUSSEN, AND NORMAN H. NACHTRIEB

Institute for the Study of Metals, University of Chicago, Chicago 37, Illinois

(Received September 28, 1959)

Some simple models are considered which permit exact evaluation of the various dynamical parameters of the theory of crystal diffusion previously proposed. The models considered suggest that: (a) The jump frequency is insensitive to the normal mode modifications produced by the adjacent vacancy. (b) There is considerable relaxation about a vacancy. (c) The volume of formation of a vacancy is related to the molar volume by $\Delta V^* \approx V/(\gamma_G - \frac{1}{3})$, where γ_G is the Gruneisen constant.

The restrictions of the models are briefly analyzed, and the mass dependence proposed by Bak and Prigogine is compared with the quasi-equilibrium model and the discrepancy discussed.

I. INTRODUCTION

IN two preceding papers,[1,2] we have examined a detailed dynamical model for vacancy diffusion in crystals. Briefly, the model represents the motion of an atom along the line connecting a lattice site and a neighboring vacancy q_1 as the superposition of many normal modes of motion. Consideration of the frequency with which the diffusing atom exceeds a critical amplitude simultaneously with the occurrence of a properly phased motion of the neighboring shell atoms leads to the following expression for the diffusion coefficient:

$$D=\gamma a^2 \nu \phi \exp(-U_0/kT)\prod_j \exp(-U_j/kT)\prod g_{kl}^{(2)}. \quad (1)$$

Here γ is a numerical constant dependent on the crystal structure, a is the lattice constant, and ϕ is the fraction of vacant sites. The frequency ν is related to the contributing normal modes of frequencies $\{\nu_i\}$ by

$$\nu^2=\sum \alpha_{1i}^2 \nu_i^2 / \sum \alpha_{1i}^2, \quad (2)$$

with α_{1i} the contribution of the ith normal mode to a motion along the direction q_1. The energies U_0, U_j are related to the assumed critical amplitudes q_0, q_{j0} which the diffusing atom and the shell atoms must attain to permit passage of the migrating atom by

$$U_0=q_0^2/\sum \alpha_{1i}^2, \qquad U_j=q_{j0}^2/\sum \alpha_{ji}^2. \quad (3)$$

Finally, $g_{kl}^{(2)}$ is the pair-correlation function for atoms k and l, and is expressible in terms of the normal modes of vibration of the crystal. The $g_{kl}^{(2)}$, as in the case of U_0 and U_j, are to be evaluated when the atoms are in the critical positions q_0, q_{j0}.

In the previous papers, attention has been focused on the formal structure of the theory and on methods of deriving *exact relations* between the pressure and temperature dependence[2] of D. In this paper we consider the dynamical theory from the point of view of some simple models. It is our purpose to examine systematically the various terms in Eq. (1) in order to clarify the physical basis of the theory and to develop approximate methods of numerical evaluation.

II. RELATION BETWEEN LATTICE VIBRATIONS AND ν

It is now well established that the vibrational spectrum of a crystal depends on the number and type of imperfections.[3,4] The methods developed by Kirkwood and Stripp and by Montroll and co-workers to study this problem are formally exact, but very complicated. They lead to the important prediction that when a vacancy is created, one localized mode of vibration appears, and all other modes have their vibrational frequencies shifted $0(N^{-1})$. We shall see the localized mode in the simple model considered now, and its role in diffusion will become apparent at this time.

For our purposes, an approximate method of determining the effects of a vacancy on the jump frequency ν will be suitable if it is readily amenable to analysis. Consider then a simple cubic crystal with occasional lattice vacancies. Excise from the crystal some one atom and its six nearest neighbors. This basic group of seven atoms will be our model. The effects of the vacancy will be considered by using the six-atom shell with the central atom missing. All distances are to be maintained consistent with the given set of force constants, and the six-atom shell will be assumed stable. The conditions imposed by the assumed stability are related to the localized mode referred to in the preceding paragraph. Finally, the coupling between the remainder of the crystal and the seven-atom configuration is simulated in this model by adjusting the force constants among the seven atoms. Such a procedure is approximate but completely consistent. It would be preferable to allow the seven-atom group to interact with the surroundings, and use this interaction to determine some of the force constants. However, such a procedure is much more difficult to use than the one adopted. We are confident that the imprecision of our model is not sufficient to alter qualitatively the results of the calculations.

* Alfred P. Sloan Fellow.

[1] S. A. Rice, Phys. Rev. **112**, 804 (1958).

[2] S. A. Rice and N. H. Nachtrieb, J. Chem. Phys. **31**, 139 (1959).

[3] J. G. Kirkwood and K. Stripp, J. Chem. Phys. **22**, 1579 (1954).

[4] E. W. Montroll and R. Potts, Phys. Rev. **100**, 525 (1955).

The seven-atom model system has octahedral symmetry, and its normal modes have been calculated by Liehr and Ballhausen.[5] Let the central atom be labeled by the subscript M and the six peripheral atoms by the subscripts 0, $\cdots$5. Then in terms of the displacements of the atoms along parallel cartesian coordinate systems centered on each atom, the symmetry coordinates are

$$
\begin{aligned}
S_1&=[1/(6)^{\frac{1}{2}}](X_0-X_2+Y_1-Y_3-Z_4+Z_5),\\
S_{2a}&=(1/2\sqrt{3})(X_0-X_2+Y_1-Y_3+2Z_4-2Z_5),\\
S_{2b}&=\tfrac{1}{2}(X_0-X_2-Y_1+Y_3),\\
S_{3a}&=\tfrac{1}{2}(Z_0+Z_1+Z_2+Z_3-4Z_M),\\
S_{3b}&=\tfrac{1}{2}(Y_0+Y_2+Y_4+Y_5-4Y_M),\\
S_{3c}&=\tfrac{1}{2}(X_1+X_3+X_4+X_5-4X_M),\\
S_{4a}&=(1/\sqrt{2})(Z_4+Z_5-2Z_M),\\
S_{4b}&=(1/\sqrt{2})(Y_1+Y_3-2Y_M),\\
S_{4c}&=(1/\sqrt{2})(X_0+X_2-2X_M),\\
S_{5a}&=\tfrac{1}{2}(X_1-X_3+Y_0-Y_2),\\
S_{5b}&=\tfrac{1}{2}(X_5-X_4+Z_0-Z_2),\\
S_{5c}&=\tfrac{1}{2}(X_5-Y_4+Z_1-Z_3)\\
S_{6a}&=\tfrac{1}{2}(Z_0-Z_1+Z_2-Z_3)\\
S_{6b}&=\tfrac{1}{2}(Y_0+Y_2-Y_4-Y_5),\\
S_{6c}&=\tfrac{1}{2}(X_1+X_3-X_4-X_5),\\
R_{1a}&=\tfrac{1}{2}(X_3-X_1+Y_0-Y_2),\\
R_{1b}&=\tfrac{1}{2}(X_4-X_5+Z_0-Z_2),\\
R_{1c}&=\tfrac{1}{2}(Y_4-Y_5+Z_1-Z_3).
\end{aligned}
\tag{4}
$$

The S_{3t} and S_{4t} symmetry coordinates are related to the normal coordinates by

$$S_{3t}=(1/\sqrt{2})(L_{33}Q_{3t}+L_{34}Q_{4t})$$

and

$$S_{4t}=L_{43}Q_{3t}+L_{44}Q_{4t}, \tag{5}$$

where

$$\frac{L_{33}}{L_{43}}=-\frac{4m\lambda_2/M}{[1+(4m/M)]\lambda_6-\lambda_3};$$

$$\frac{L_{44}}{L_{34}}=-\frac{m\lambda_5/M}{[1+(2m/M)]\lambda_2-\lambda_4};$$

$$L_{33}^2+L_{34}^2+(2/m)[1+(4m/M)];$$

$$(1/m)[1+(2m/M)]=\left(\frac{L_{43}}{L_{33}}\right)^2L_{33}^2+\left(\frac{L_{44}}{L_{34}}\right)^2L_{34}^2;$$

$$\lambda_i=4\pi^2\nu_i^2. \tag{6}$$

[5] A. D. Liehr and C. Ballhausen, Ann. Phys. 3, 304 (1958).

The other symmetry coordinates are the same as the normal coordinates. Equations (5) and (6) are valid for the case of a Wilson valence force potential.[5]

In the real crystal, the diffusive path q_1 does not, in general, lie along a normal coordinate. To mimic this behavior in the seven-atom grouping, q_1 is not taken along a bond axis, but rather in the direction of motion of one of the peripheral atoms at an angle of 45° to all bond axes. For, if q_1 were taken along a bond axis, the very high symmetry of the octahedral group would lead to the result that many normal modes would make no contribution to motion along q_1. While the direction chosen is not towards the vacancy, it is preferable in that all modes contribute to the motion. Let K_0 be the force constant for the stretching of the bond between the central atom and a peripheral atom, K_α the force constant for the bending of adjacent bonds, and K_2 the force constant describing the interaction between peripheral atoms on opposite sides of the central atom. From Eqs. (4–6) and the assumption of a Wilson valence potential, it may be shown that[5]

$$
\begin{aligned}
\lambda_1&=(1/m)[K_0+10K_2],\\
\lambda_2&=(1/m)[K_0-2K_2],\\
\lambda_3\lambda_4&=(1/m^2)[(M+6m)/M]2K_\alpha(K_0-2K_2),\\
\lambda_3+\lambda_4&=(1/m)\{[(M+4m)/M]2K_\alpha\\
&\qquad+[(M+2m)/M](K_0-2K_2)\},\\
\lambda_5&=4K_\alpha/m,\\
\lambda_6&=2K_\alpha/m,
\end{aligned}
\tag{7}
$$

for the seven-atom system. As usual, M is the mass of the central atom and m the mass of a peripheral atom. (Here $M=m$ or $M=0$.) When the central atom is absent, three degrees of freedom are lost, and thereby three normal modes vanish. Under these conditions, assuming that the six-atom shell with a central vacancy is stable, we are led to the corresponding frequencies:

$$
\begin{aligned}
\lambda_1&=(K_0'+10K_2)/m,\\
\lambda_2&=(K_0'-2K_2)/m,\\
\lambda_3+\lambda_4&=(1/m)\left(\frac{3K_\alpha(K_0'-2K_2}{2K_\alpha+K_0'-2K_2}\right),\\
\lambda_5&=4K_\alpha/m,\\
\lambda_6&=2K_\alpha/m.
\end{aligned}
\tag{8}
$$

The force constant K_0' is different from K_0. Moreover, the assumption that the six-atom hollow structure is stable implies that K_0' cannot vanish since the hollow shell of atoms would be unstable without an external force such as is provided by the surrounding medium in the crystal. In the model considered, the remainder of the crystal is mimicked by a nonzero value of K_0'. However, then K_0' is not independent of the real force

constants K_α and K_2. In fact,

$$K_0'=2\sqrt{2}K_\alpha+2K_2, \tag{9}$$

when the central atom is missing. Equation (9) gives the minimum value of K_0' for which the six-atom shell is stable. The relationship is obtained by noting which normal modes become degenerate when the central atom is removed, and applying rotational symmetry conditions which make the degenerate modes identical.

For the purposes of computation take $m=100$ amu, with the force constants shown in Table I. These are chosen to give vibrational frequencies of about 10^{12} cps, but are otherwise arbitrary. As can be seen, the chosen force constants vary over a reasonable range. The results of the calculation are shown in Table II. The five cases considered are:

(1) All atoms present, force constants as given in Table I, line 1.

(2) None of the force constants are changed when the central atom is removed, except where required by Eq. (9) to keep the six-atom shell stable.

(3) All force constants are reduced drastically, here by a factor of four. This corresponds to the case when the motions of the atoms surrounding a vacancy become very "soft."

(4), (5) These small changes in force constants attempt to deal with either contraction or dilation of the shell of atoms surrounding the vacancy. In the former case one expects K_2 to decrease, in the latter case to increase. Some change in K_α would be expected also.

Table II indicates that the frequencies of the individual normal modes are rather different in the cases cited. Nevertheless, the frequency ν defined in Eq. (2) is relatively insensitive to the changes in force constants. With one exception, the variation in ν is only 10–20%, whereas the variations in normal mode frequencies are as large as a factor of three. In the model case considered, the vacancy has very little effect on the jump frequency.

If we make the dangerous extrapolation to the real crystal, it would appear that calculations of the frequency ν could be made from the known atomic structure to an accuracy of 10–20% by neglecting the effects of the vacancy. The preceding calculation provides some insight into the moderately successful use of the Debye frequency for ν, since, on *a priori* grounds, the Debye frequency[6] has no direct connection with the motion of an atom along the diffusive trajectory.

Perhaps the quantity of greatest interest is the calculated entropy of vacancy formation. This is given by

$$\Delta S_v=k\sum_i g_i \ln(\nu_i/\nu_i'), \tag{10}$$

TABLE I. Force constants.

Case	Central atom	$K_0'\times10^{-4}$	$K_\alpha\times10^{-4}$	$K_2\times10^{-4}$
1	present	1.00	0.500	0.250
2	absent	1.914	0.500	0.250
3	absent	0.479	0.125	0.0625
4	absent	2.06	0.365	0.500
5	absent	1.81	0.375	0.125

where the sum is over all frequencies of vibration, and g_i is the degeneracy of the ith mode. The calculated values are shown in the last column of Table II. Case 3, corresponding to very soft-shell atom motions, gives much too large an entropy change. By inversion, we conclude that the change in force constants must be less than a factor of four. This then removes the only case for which ν differed by more than 20% due to the presence or absence of a vacancy.

The calculations of ΔS_v presented should be almost independent of material (since only ratios of frequencies are considered), provided that the crystal is simple cubic. Etzel and Maurer[7] found that the entropy of vacancy formation in the simple cubic lattice of NaCl is $3.3k$. This value is rather close to the $3.08k$ computed for the case when there is no change in force constants, except that dictated by stability. The agreement is undoubtedly fortuitous; however, it demonstrates the sensitivity of the entropy of vacancy formation to small changes in vibrational frequencies.

It is pertinent to consider further the agreement between calculation and experiment, and add an amending remark which will serve to connect the model used with our previous general comments. Although the force constants are unmodified for the case in which agreement is obtained, the stability constraint changes most of the frequencies. In particular, ν_1 and ν_2 are increased, in agreement with Rayleigh's theorem,[8] since the removal of the central atom increases the potential energy of the peripheral atoms and thereby changes the ratio of potential to kinetic energy for the vibrating system. The increased frequency ν_1 corresponds to the localized mode of the general theory. As in the one-dimensional lattice, it is a "breathing mode."[4]

The model discussed in this section for the calculation of ν and ΔS_v is approximate in its representation of the coupling to the crystal by suitable atomic force constants. Note, however, that the values given in Table I are much more representative of a crystal than of a molecule. For, in the latter case, it is common for $K_0\approx3-5K_\alpha$, and $K_0\approx10-100K_2$. It should be emphasized that all our numerical deductions must be viewed with reserve because of the simplicity of the model, although the qualitative features are un-

[6] See for example, Nachtrieb, Weil, Catalano, and Lawson, J. Chem. Phys. **20**, 1189 (1952).

[7] H. W. Etzel and R. J. Maurer, J. Chem. Phys. **18**, 1003 (1950).

[8] Lord Rayleigh, *Theory of Sound* (Dover Publications, New York, 1945).

TABLE II.

Case	$\lambda_1\times10^{-26}$	$\lambda_2\times10^{-26}$	$\lambda_3\times10^{-26}$	$\lambda_4\times10^{-26}$	$\lambda_5\times10^{-26}$	$\lambda_6\times10^{-26}$	$2\pi\nu\times10^{-12}$	ΔS_v
1	2.11	0.301	3.20	0.715	1.21	0.603	7.77	...
2	2.66	0.852	0.529	...	1.21	0.603	7.61	3.08k
3	0.665	0.213	0.132	...	0.301	0.151	3.80	19.75k
4	4.25	0.639	0.245	...	0.904	0.452	6.25	7.14k
5	1.84	0.940	0.377	...	0.904	0.452	7.02	6.51k

doubtedly valid. This is the attitude we shall take throughout this paper.

It would be tempting to regard the agreement between calculation and experiment as evidence that the force constants in NaCl are unmodified, and that there is little relaxation about a vacancy. *Such a conclusion would be totally erroneous.* We note that, in a recent paper, Theimer[9] has presented detailed calculations of the entropy of vacancy formation in NaCl. He comes to the conclusion that agreement with experiment can be obtained only if the magnitudes of the shell-atom relaxations are very small, 0.04 to 0.06A. These displacements are of the order of thermal amplitudes, and the resultant volume change is trivially small. Other calculations for the crystalline rare gases[10,11] and for metals[12,13] also show that the relaxation about a vacancy is very small. The weight of evidence from all the detailed calculations would appear to suggest that in fact the relaxation about a vacancy can be neglected to first order.

To what extent are these calculations valid? The work of Theimer[9] and Kanzaki[10] is based on a harmonic model for the crystal, whereas the work of Repani,[11] Girafalco,[12] and Hall[13] is based on computations of static lattice energies. In the static calculations, the force acting on an atom adjacent to a vacancy is, to a large extent, linear in the displacement from the regular lattice position. In this sense, all the cited calculations can give no information about vacancy formation. For, in a completely harmonic crystal, or in one where the restoring force is linear in the displacement as in elastic continuum models, there can be no relaxation. This may be seen either from the elegant arguments of Eshelby,[14] or from direct examination of the lattice dynamics.[2,15] It is the presence of anharmonic forces which is necessary for relaxation to occur.

The necessity for anharmonic forces to effect relaxation may be demonstrated dramatically for the model considered here. The symmetry coordinates given in Eq. (4) are independent of any assumptions made concerning the interatomic potential. It is only in the transition from symmetry coordinates to vibrational frequencies that assumptions are necessary. Consider then that the potential energy of the seven atoms may be expressed as

$$V=(K_0/2)\sum_{i=0}^{5}(\Delta r_i)^2+K_2\sum_{i\neq j,0}^{5}(\Delta r_i)(\Delta r_j)-K_4\sum_{i=0}^{5}(\Delta r_i)^4-K_5\sum_{i\neq j,0}(\Delta r_i)^3(\Delta r_j)-K_6\sum_{i\neq j,0}^{5}(\Delta r_i)^2(\Delta r_j)^2, \quad (11)$$

where the Δr_i are the displacements of the atoms from the equilibrium interatomic spacing. Each of the Δr_i is directed along a bond axis, and therefore

$$\begin{aligned}\Delta r_0&=X_0-X_M,\\ \Delta r_1&=Y_1-Y_M,\\ \Delta r_2&=X_M-X_2,\\ \Delta r_3&=Y_M-Y_3,\\ \Delta r_4&=Z_M-Z_4,\\ \Delta r_5&=Z_S-Z_M.\end{aligned} \quad (12)$$

We now express the cartesian displacements in terms of the symmetry coordinates:

$$\begin{aligned}X_0&=[1/(6)^{\frac{1}{2}}]S_1+[1/2\sqrt{3})\,S_{2a}+\tfrac{1}{2}S_{2b}+(1/\sqrt{2})\,S_{4c},\\ Y_1&=[1/(6)^{\frac{1}{2}}]S_1+(1/2\sqrt{3})\,S_{2a}-\tfrac{1}{2}S_{2b}+(1/\sqrt{2})\,S_{4b},\\ X_2&=-[1/(6)^{\frac{1}{2}}]S_1-(1/2\sqrt{3})\,S_{2a}-\tfrac{1}{2}S_{2b}+(1/\sqrt{2})\,S_{4c},\\ Y_3&=-[1/(6)^{\frac{1}{2}}]S_1-(1/2\sqrt{3})\,S_{2a}+\tfrac{1}{2}S_{2b}+(1/\sqrt{2})\,S_{4b},\\ Z_4&=-[1/(6)^{\frac{1}{2}}]S_1+(1/\sqrt{3})\,S_{2a}+(1/\sqrt{2})\,S_{4a},\\ Z_5&=[1/(6)^{\frac{1}{2}}]S_1-(1/\sqrt{3})\,S_{2a}+(1/\sqrt{2})\,S_{4a}.\end{aligned} \quad (13)$$

To determine the relative magnitudes of the anharmonic and harmonic parts of the potential energy, we require that the relaxation be isotropic and determine the extremum in the potential from

$$\begin{aligned}(\partial V/\partial S_1)_{S_i=0}&=0,\\ S_1&=(6)^{\frac{1}{2}}\langle\Delta r\rangle_{\text{Av}},\end{aligned} \quad (14)$$

[9] O. Theimer, Phys. Rev. **112**, 1857.
[10] H. Kanzaki, Phys. and Chem. Solids **2**, 24 (1957).
[11] G. Nardelli and A. Repanai, Physica **24**, S182 (1958).
[12] L. Girafalco and J. Streetman, Phys. and Chem. Solids **4**, 182 (1958).
[13] G. L. Hall, Phys. and Chem. Solids **3**, 210 (1957).
[14] J. D. Eshelby, in *Solid State Physics*, edited by Turnbull and Seitz (Academic Press, Inc., New York, 1956), Vol. 2.
[15] See for example, F. Seitz, *Modern Theory of Solids* (McGraw-Hill Book Company, New York, 1940).

since only the breathing mode has the proper symmetry to yield an isotropic contraction. The use of Eqs. (11), (12), and (13) and the condition given in Eq. (14) leads to

$$\langle \Delta r \rangle_{Av} = [1/(6)^{\frac{1}{2}}] \left(\frac{K_0 + 10K_2}{\frac{2}{3}K_4 + \frac{10}{3}K_5 + \frac{10}{3}K_6} \right)^{\frac{1}{2}}. \quad (15)$$

The simplest method of estimating anharmonic constants starts from the observation that the extremum in the potential should be near to $a/2$, where a is the lattice spacing. If it is further assumed that $K_4 = K_5 = K_6$, then this condition yields the relationship $K_0 = K_2 = a^2 K_4$. Thus the potential is markedly anharmonic in the vicinity of a vacancy.

We are now in a position to estimate the relaxation about a vacancy. The extent to which an atom adjacent to an empty lattice site moves is determined by the balance between the anharmonic and harmonic forces. It may be imagined that an atom is subjected to the forces of two springs stretched in opposite directions, one of these springs being linear and the other nonlinear. If the displacement of an atom is Δ, then, from Eq. (11) and the condition of isotropy, the balance of forces gives the relation

$$(K_0 + 10K_2)(a + \Delta) = \tfrac{2}{3}(K_4 + 5K_5 + 5K_6)(a - \Delta)^3. \quad (16)$$

When the ratio Δ/a is small, Eq. (16) may be solved readily for Δ/a, with the result

$$\Delta/a = \frac{K_0 + 10K_2 - \frac{2}{3}a^2(K_4 + 5K_5 + 5K_6)}{K_0 + 10K_2 + 2a^2(K_4 + 5K_5 + 5K_6)}. \quad (17)$$

We saw previously that $a^2 K_4 = K_0 = K_2$. The contraction predicted is then $\Delta/a = 11/99$, corresponding to a volume relaxation of 33%. Note that this has been obtained by a condition of consistency with the position of the maximum in the interatomic potential and is not an altogether arbitrary result.

We conclude that there is appreciable relaxation about a vacancy due to the anharmonicity of the potential. This anharmonicity does not affect the jump frequency to first order; the frequency shift $\Delta\nu$ is much less than the frequency itself with $\nu^2 \gg \nu\Delta\nu$.

III. SHELL-ATOM MOTION

The trajectory which a diffusing atom must follow in a face-centered cubic structure requires a phased motion of the near-neighboring atoms to create a hole of sufficient cross-sectional area to permit passage. In this section, we examine some questions dealing with the relationship between the formation of such a hole and the mean thermal amplitudes of the atoms involved.

It is, in principle, easy to calculate the mean-square amplitudes of vibration for a crystal if the vibrational spectrum is known. Moreover, the mean-square amplitude of vibration may be measured by x-ray techniques. For Pb, the results expressed in terms of a Debye temperature, θ_D, and the corresponding amplitude for the crystal with a Debye frequency spectrum,[15]

$$\langle q^2 \rangle = (3h^2/4\pi^2 mk)(T/\theta_D^2) + (h^2/48\pi^2 mk)(1/T), \quad (18)$$

are shown in Table III. It is noteworthy that the root-mean-square amplitude of vibration is quite large in the region where diffusion is measurable (400–600°K). The question of whether or not this amplitude is of a magnitude to permit a hole of sufficient cross section to be opened deserves some examination. For this purpose consider a hard-sphere model of a face-centered cubic crystal. The radius of the hard spheres is chosen to be 1.750 A to correspond to the crystal structure of Pb, the only face-centered cubic structure for which diffusion constants as a function of pressure have been determined.[16] Using the known lattice spacing of 4.950 A, it is easy to compute the required amplitudes of motion of the shell atoms. For example, for a next-nearest neighbor atom to diffuse through the 100 plane requires that the atoms in the 100 plane move about 1.02 A apiece. The much shorter move corresponding to nearest-neighbor diffusion through the 110 plane requires motion of the shell atoms of 0.47 A apiece. The trajectory through the 110 plane clearly requires smaller amplitudes of the shell atoms, but more of them are involved in the total motion than in the case of passage through the 100 plane. It is also clear that the amplitudes required far exceed the root-mean-square amplitude due to thermal motion.

TABLE III. Root-mean-square amplitudes of vibration in Pb.[a]

T(°K)	θ_D(°K)	$\langle q^2 \rangle^{\frac{1}{2}}$ (A)
100	87.2	0.096
200	85.0	0.140
300	81.8	0.178
400	78.0	0.215
500	74.2	0.252
600	70.4	0.292

[a] Private communication from Dr. David Chipman.

It is of interest to convert the description of the shell-atom amplitudes into activation energy language. To do this, note that the probability density for an atom to have a displacement q_j from its lattice site is proportional to $\exp(-q_j^2/kT\sum\alpha_{ij}^2)$. The specific nature of the crystalline structure is contained in the coefficients α_{ij}, and the evaluation of all averages awaits their specification. In Sec. II it was seen that the presence of a vacancy modified but slightly the jump frequency ν, just as if those normal modes which are modified by the presence or absence of an atom add in a random manner to the jump in a specified direction. If this is also correct for the complete crystal, a Debye spectrum will suffice to evaluate $\sum\alpha_{ij}$. By explicit evaluation of the mean-square amplitude using the

[16] Nachtrieb, Resing, and Rice, J. Chem. Phys. 31, 135 (1959).

indicated distribution function, it is found that

$$\langle q^2\rangle = (3kT/4)\sum\alpha_{ij}^2, \tag{19}$$

and by using the equivalent result for the Debye crystal, Eq. (18),

$$\sum\alpha_{ij}^2 = (1/m)\,(h/\pi k\theta_D)^2. \tag{20}$$

Because of the isotropy of the Debye spectrum, this relation is the same for all motions. The latter comment reveals the serious nature of the Debye spectrum approximation in hiding the detailed effects of the lattice. However, it is not unlikely that, although the Debye spectrum is a poor physical approximation to the vibrational spectrum, the average represented in Eq. (20) is little affected. The probability density for a displacement q_j now may be written, using Eq. (19),

$$P^{(1)}(q_j) = (3/4\pi\langle q^2\rangle)^{\frac{1}{2}}\exp[-(3q_j^2/4\langle q^2\rangle)]. \tag{21}$$

With the numerical values of $\langle q^2\rangle$ available from experiment,[15] and those of q^2 from a model, the combination of Eqs. (21) and (1) leads to values of U_0/kT and U_j/kT.

The dynamical model on which Eq. (1) is based assumes a harmonic potential and therefore will overestimate the activation energy seriously. Nevertheless, it is to be hoped that the different diffusive paths discussed are separated widely enough in energy to permit the mechanism to be ascertained. Using the figures in Table III relevant for the temperature 600°K, and using the estimated hard-sphere dilations, the calculated energy of activation for next-nearest neighbor diffusion through the 100 plane is approximately 85 kT_m and that for nearest-neighbor diffusion through the 110 plane approximately 46 kT_m, where T_m is the melting temperature. The calculations mentioned assume a heat of vacancy formation of 6.4 kT_m, the value recently computed for the face-centered cubic crystal of argon,[10] and also a small contribution of order $4kT_m$ due to correlations between atoms. The experimental value of the activation energy for diffusion in Pb is 20.7 kT_m,[16] a factor of two lower than the smaller of the calculated values. The direction and magnitude of the deviation, as expected, are due to the assumption of a harmonic potential for displacements as large as 2.5 A. The real potential always lies below the parabolic potential fit at the minimum. Despite the quantitative disagreement, the qualitative agreement is satisfactory, since the computed energy is in the right range, and the two diffusive paths are sufficiently different energetically to confirm the physical picture which suggests that the nearest-neighbor trajectory through the 110 plane is the one used. It is interesting to note that the energy required to move the diffusing atom will be reduced more drastically from the harmonic value than the corresponding energies for motion of the shell atoms. This is a direct consequence of the differences in the required vibrational amplitudes. If the anharmonic potential defined by Eq. (11) is used with the values of the constants determined by Eq. (15), the computed activation energies are 57 kT_m and 32 kT_m, respectively. In view of the approximate nature of the model, this is very good agreement with experiment. The partition of energy between the various contributions suggested by the model is, approximately, $\Delta H_v \approx 20$–40%, $U_0 \approx 30$–60%, $\sum U_j \approx 15$–25%, $\Delta H_{kl} \approx 5$–10%, in agreement with Koehler's quenching experiments.[17]

Finally, it is pertinent to point out that the change of variables leading to Eq. (21) is related to a description of diffusion in terms of volume fluctuations. Neglecting the differences in units, the role of the free volume is seen to be played by the mean-square thermal amplitude. Both the description in terms of volume fluctuations and the relation of the free volume to thermal amplitudes (or thermal expansion) are in agreement with the simple model used by Turnbull and Cohen[18] to interpret the fluidity of glasses and liquids.

To complete this discussion of shell atom motions, some mention must be made of the computation of the pair correlation functions $g_{kl}^{(2)}$. No calculations have appeared yet in the literature, but related correlation effects have been considered. For example, Barsch[19] has evaluated the deviation of the average of the product of the displacements of two atoms from the product of the root-mean-square average displacements of the same two atoms. The numerical results indicate that in the classical region, $T > \theta_D$, the correlation coefficient,

$$\gamma_{kl} = \langle q_k q_l\rangle / (\langle q_k^2\rangle^{\frac{1}{2}}\langle q_l^2\rangle^{\frac{1}{2}}), \tag{22}$$

is approximately 0.4 at the near-neighbor distance and 0.25 at the next-nearest-neighbor distance. The asymptotic value of γ_{kl} is, of course, zero, as can be ascertained readily from the definition. The relation between $g_{kl}^{(2)}$ and γ_{kl} is not simple since it involves an integration which arises from the statistical definition of the average in the numerator of Eq. (22). Since there will be no occasion to use this relation, it will not be displayed explicitly.

Some physical insight into the nature of the pair-correlation function is provided by the observation that the potential of mean force depends upon the differences in energy required to move an atom with and without normal mode constraints.[1,20] Specifically,

$$g_{12}^{(2)} \propto \exp\left[-(1/kT)\left\{[(\alpha_1^2/\alpha_1'^2)-1]U_1 + [(\alpha_2^2/\alpha_2'^2)-1]U_2 + \frac{2\alpha_1\alpha_2}{\sum\alpha_{1j}\alpha_{2j}}(U_1U_2)^{\frac{1}{2}}\right\}\right], \tag{23}$$

[17] Koehler, Seitz, and Baurle, Phys. Rev. **107**, 1499 (1957).
[18] D. Turnbull and M. H. Cohen (private communication).
[19] G. Barsch, Phys. and Chem. Solids **4**, 27 (1958).
[20] O. P. Manley and S. A. Rice (to be submitted to Phys. Rev.).

where

$$\alpha_j^2=\sum_k \alpha_{jk}^2, \qquad \alpha_j'^2=\sum_k \alpha_{jk}'^2.$$

The coefficient α_{jk} is the weight of the contribution of the kth normal mode to the motion of atom j, while α_{jk}' is the corresponding weight when one atom is not permitted to move. Note that in the limit as the particle separation tends to become indefinitely large, $\alpha_j^2/\alpha_j'^2 \rightarrow 1$, the cross term vanishes, since the coupling between all pairs except close neighbors is zero, and thereby the potential of mean force tends to zero. The normalization constant contains temperature-dependent factors, not indicated in Eq. (23), which make the potential of mean force a free energy. Moreover, since the constraint imposed by fixing the position of one atom is effective only when the pair of atoms is close together, the correlations are seen to depend on the local state of the lattice. To a low order of approximation, the potential of mean force may be thought of as the difference between the local strain energy and the energy required to move each particle independently to its final configuration. Such an interpretation clearly indicates the nature of the cross coupling contained in the pair-correlation function.

IV. CONTINUUM APPROXIMATION

The considerations of Secs. II and III lead to the conclusion that the atomic displacements in the vicinity of a vacancy are considerable. Because of the difficulty of determining the anharmonic part of the pair-interaction potential and the complexity of detailed molecular calculations, we seek to examine a continuum model. By this device, we may hope to supplant the specificities of the dynamical models by the generalities of thermodynamics.

By way of introduction, consider the simple case of the formation of vacancies in a monoatomic homogenous lattice. Let $G(T, P, n_v, N_h)$ be the Gibbs free energy of such a medium containing n_v moles of vacancies and N_h moles of host material in equilibrium at temperature T and pressure p. Then,

$$G=N_h\mu_h+n_v\mu_v, \tag{24}$$

where μ_h and μ_v are, respectively, the chemical potentials of the host material and the vacancies. At equilibrium, $\mu_v=0$, since $\partial G/\partial n_v=0$.

Because the concentration of vacancies is usually less than 1%, a convenient approach is to treat them as perturbations of the unadulterated host. Thus we may write,[21]

$$G=N_h\mu_0+n_vRT\ln(N_v/eN_h)+N_v\psi(p, T), \tag{25}$$

where μ_0 is the chemical potential of the host medium in the absence of vacancies. The function $\psi(p, T)$ contains two contributions, the first of which is $kT\ln N_h$ and arises from the entropy of mixing of holes and atoms. The second contribution is $\alpha(p, T, N_h)$, the change in chemical potential of the host medium due to the addition of one vacancy, but not accounting for the indistinguishability of vacancies. The term α does not contain any contribution from the entropy of mixing.

From Eq. (25), there is obtained by differentiation with respect to N_h,

$$\mu_h=\mu_0-RT(n_v/N_h)=\mu_0-RTx, \tag{26}$$

and, by differentiation with respect to n_v,

$$\mu_v=\psi(p, T)+RT\ln x. \tag{27}$$

Since $\mu_v=0$ at equilibrium, the equilibrium concentration x_e of vacancies is given by

$$x_e=\exp(-\Delta G^*/RT), \tag{28}$$

if the identification $\Delta G^*=\psi(p, T)$ is made. ΔG^* is the isothermal, reversible work required to form a mole of vacancies at constant pressure without allowing the vacancy distribution in the system to relax to its most probable state, i.e., the work required to add additional vacancies at constant mixing entropy.[21] We have made use of the fact that when there are no vacancy-vacancy interactions, α and hence $\psi(p, T)$ are independent of n_v. Note that it has not been necessary to specify the size or shape or any other parameters descriptive of the vacancy. Such a parametric description is necessary only when ΔG^* is to be calculated in terms of the properties of the host medium. To proceed further, and calculate ΔG^*, it will be assumed that elasticity theory is applicable.

Consider now that a process has occurred converting the host substance (without vacancies) into a material with an equilibrium number of vacancies. Of course, the fundamental variables affecting the chemical potential of the medium are the temperature and pressure. The variable n_v is not operationally controllable since it is determined by p and T and the condition $\mu_v=0$. The final state of the system, including vacancies, is one which can in principle be reached (if necessary by extrapolation) by variations of T and p alone. Derivatives with respect to the vacancy concentration, n_v, must be understood to be related fundamentally to derivatives with respect to pressure and/or temperature, although occasionally the variables to be maintained constant during the differentiation do not correspond to ordinary laboratory conditions. From the thermodynamic identities,

$$(\partial\mu_v/\partial p)_{T,n_v,N_h}=(\partial V/\partial n_v)_{T,p,N_h}, \tag{29}$$

and

$$V=N_h(\partial V/\partial N_h)_{p,n_v,T}+n_v(\partial V/\partial n_v)_{p,N_h,T}, \tag{30}$$

it follows that

$$\Delta V^*=(\partial V/\partial n_v)_{p,N_h,T}, \tag{31}$$

[21] See for example, L. Landau and E. Lifschitz, *Statistical Physics* (Oxford University Press, London 1938).

and

$$\bar{V}=\bar{V}_0+x_v\Delta V^*, \tag{32}$$

where $\bar{V}=V/N_h$ is the molar volume. At $T=0°K$, $n_v=0$, and $\mu_h=\mu_0$. Denote by A_0 the value of the Helmholtz free energy in this standard state. If we also take $p=0$ for the standard state, then it can be shown easily[22] that for any other state at pressure p and temperature T,

$$A(p,T)=A_0+\tfrac{1}{2}p^2/B_T+f(T), \tag{33}$$

where B_T is the isothermal bulk modulus. Thus, the increase ΔA^* in the Helmholtz free energy of one mole of host material upon the introduction of one mole of vacancies is

$$\Delta A^*=\tfrac{1}{2}[n_v^2(\partial p/\partial n_v)_{T,N_h,v}^2/B_{T,n_v}]=\tfrac{1}{2}B_{T,n_v}\Delta V^{*2}/\bar{V}, \tag{34}$$

where B_{T,N_v} is the isothermal bulk modulus at constant vacancy concentration. To obtain the free energy ΔG^* from ΔA^*, two other well-known identities may be utilized, namely,

$$\{[\partial/\partial(1/T)](\Delta G^*/T)\}_p=\Delta H^*, \tag{35}$$

and

$$\{[\partial/\partial(1/T)](\Delta A^*/T)\}_v=\Delta U^*. \tag{36}$$

Combining Eqs. (35), (36), and (34) with the identity

$$(\partial n_v/\partial T)_{v,N_h,\mu_v}=(\partial n_v/\partial T)_{p,N_h,\mu_v}+(\partial n_v/\partial p)_{T,N_h,\mu_v}(\partial p/\partial T)_{v,N_h,\mu_v}, \tag{37}$$

it is found that

$$\Delta U^*=\Delta H^*-T(\alpha_p/\beta_T)\Delta V^*, \tag{38}$$

where α_p and β_T are, respectively, the relaxed (equilibrium) values of the isobaric coefficient of volume expansion and the isothermal compressibility.

Now it is convenient to introduce the expression for the difference between the entropy of vacancy formation at constant pressure, ΔS_p^*, and that at constant volume, ΔS_v^*. This is

$$(\partial S_0/\partial n_v)_{p,T,N_h}=\Delta S_p^*=\Delta S_v^*+(\partial S_0/\partial n_v)_{n_v,N_h,T}(\partial v/\partial n_v)_{p,T,N_h}=\Delta S_v^*+(\alpha_{n_v,p}/\beta_{n_v,T})\Delta V^*. \tag{39}$$

Since for small concentrations of imperfections, it is permissible to write $\alpha_p/\beta_T\approx\alpha_{p,n_v}/\beta_{T,n_v}$ from Eqs. (34), (38), and (39),

$$\Delta A^*=\tfrac{1}{2}B_{n_v,T}(\Delta V^{*2}/\bar{V})\approx\Delta G^*. \tag{40}$$

It should be noted that, although Eq. (40) is instantaneously true for all values of T and p, ΔA^* is a rapidly varying function of volume, and the corresponding value of ΔG^* is for a pressure required to maintain a particular volume.

[22] See for example, M. W. Zemansky, *Heat and Thermodynamics* (McGraw-Hill Book Company, New York 1955).

If, in Eq. (39), it is assumed that $\Delta S_v^*\approx 0$, then

$$\Delta S_p^*\approx\alpha_p/\beta_T\Delta V^*. \tag{41}$$

If this approximation is not made,

$$\Delta S_v^*=-(\partial/\partial T)\Delta A^*=[(\partial/\partial v)(\partial p/\partial T)_v]_T(\Delta V^{*2}/2). \tag{42}$$

Using Eq. (42) in conjunction with Gruneisen's relation $\alpha_p/\beta_T=\gamma_G C_v/V$, it is found that

$$\Delta S_v^*=\tfrac{1}{2}(\Delta V^*/\bar{V})[(\alpha_p/\beta_T)\Delta V^*]=\alpha_p\Delta G^*. \tag{43}$$

From Eqs. (43) and (39),

$$\Delta S_p^*=[1+\tfrac{1}{2}(\Delta V^*/\bar{V})](\alpha_p/\beta_T)\Delta V^*, \tag{44}$$

which should yield better agreement with experiment than the approximate relation of Eq. (41), which gives values approximately 25% lower than those obtained from Eq. (44).

Another instructive relation may be derived if it is assumed that ΔV^* scales with the molal volume $\bar{V}$ when the pressure is changed. Consider the equation

$$(1/\Delta G^*)[(\partial/\partial p)(\Delta G^*)]_T=\Delta V^*/\Delta G^*-\left(\frac{\partial \ln B_{n_v,T}}{\partial \ln V}+1\right)(1/B_{n_v,T}). \tag{45}$$

Using Eq. (40) and Gruneisen's theory, it follows from Eq. (45) that

$$\Delta V^*/\bar{V}\approx(\gamma_G-\tfrac{1}{3})^{-1}, \tag{46}$$

or $\Delta V^*/\bar{V}\approx\tfrac{1}{2}$ for a typical metal. Recombining Eqs. (46) and (40) and taking the limit at $T\to 0$ yields

$$\lim_{T\to 0}\Delta G^*=\Delta H^*\approx\frac{B_{n_v,T}{}^0\Delta V^*}{2(\gamma_G-\frac{1}{3})}, \tag{47}$$

where $B_{n_v,T}{}^0$ is the value of the isothermal bulk modulus at the absolute zero of temperature, i.e., in the standard state. Eq. (47) then may be rewritten in the form

$$4\beta\Delta H^*\approx\Delta V^*. \tag{48}$$

To what extent may the above calculations be extended? It is tempting to approximate the volume of activation by including a dilation of the vacancy volume to account for the motional volume.[23] Such a procedure cannot be justified rigorously. While the preceding arguments are rigorous, the calculations of thermodynamic functions for activated states is fraught with uncertainties. Nevertheless, it is interesting to point out that Eqs. (40), (41), and (48), when used as relations between activated quantities, have been shown to be in reasonable agreement with experiment.[23–26] Such agreement suggests that the model of

[23] C. Zener, in *Imperfections in Crystals* (John Wiley & Sons, Inc., New York, 1950).
[24] A. W. Lawson, Phys. and Chem. Solids **3**, 250 (1957).
[25] R. W. Keyes, J. Chem. Phys. **29**, 467 (1958).
[26] A. W. Lawson, J. Chem. Phys. **30**, 1114 (1959).

the activated state as a dilated vacancy is not without physical foundation. However, due to the lack of apparent justification for any extension to the thermodynamics of activated states, we restrict the calculations of this section to the equilibrium properties of vacancies.

Finally, note that the reason we obtain a finite volume of relaxation about a vacancy is that the fundamental formulas in Eqs. (41), (44), and (47), and the Gruneisen relation all contain anharmonic terms in the form of the thermal expansion coefficient or the pressure dependence of the bulk modulus. This is in agreement with the conclusions of Sec. II. Moreover, the estimate of 33% relaxation from the dynamical model is in good agreement with the approximate 50% relaxation predicted by Eq. (46).

V. DISCUSSION

The theory of diffusion can be divided roughly into two overlapping problems. The first of these deals with the mechanism of irreversibility, whereas the second deals with detailed calculations for specific mechanisms. We have avoided the difficulties inherent in the first problem by using an *ansatz*—introducing the irreversibility by fiat. As a typical example of the second grouping, the purpose of this paper has been to implement the dynamical theory presented previously, and to invest the formulas with some physical interpretations borrowed from simple models. In particular, the simple models proposed here suggest that: (a) there is considerable relaxation about a vacancy, (b) the jump frequency is insensitive to the normal mode modifications produced by the adjacent vacancy, (c) the free energy of vacancy formation may be estimated accurately from ordinary elastic constants, (d) the volume change on vacancy formation should be of the order of one-half the molal volume, (e) the correlation energy is a small fraction of the total energy of activation. The considerable concordance between our simple calculations based on several distinct models argues that the deductions (a)–(e) possess a generality not obvious from the models.

The problem of the introduction of irreversibility cannot be dismissed simply by the statement of an *ansatz*. The difficulties inherent in the theory are well known, and here we merely comment that an exact treatment probably will alter the functional dependence but slightly, and affect in a minor way the numerical magnitude of the pre-exponential factor in Eq. (1). From the general theory of Brout and Prigogine,[27] Bak and Prigogine[28] have derived the equations describing diffusion in a one-dimensional system. The mechanical system considered consists of a one-dimensional lattice and a particle which interacts with the lattice. The particle moves in a simple minimum-potential well and is annihilated when it surmounts the barrier. The coupling of the particle to the lattice is of the form $\frac{1}{2}\gamma r^2$, where r is the distance of the particle from its equilibrium position. With a Debye spectrum it is found that

$$D=f(U^\dagger/RT)\,(\kappa\gamma a^2U^\dagger/2\mu C^3m^2RT)\,\exp(-U^\dagger/RT),$$

where κ is a coupling constant, $U^\dagger$ the activation energy, μ is the mass per unit length of lattice, C the velocity of sound, and $f(U^\dagger/RT)$ is bounded between the values 0.82 and unity. Physically, the function $f(U^\dagger/RT)$ is the ratio between the exact value of D and the value for an infinitely high barrier.

The isotope effect predicted by the Bak-Prigogine model is much larger than the predicted by the strong-coupling lattice theories (square root of some reduced mass) or the phenomenological Brownian-motion theories[29] which justify to a certain extent the type of quasi-equilibrium arguments considered in this series of papers. It is clear that the exact mass dependence of D is an intimate function not only of the shape of the barrier but also of the collective motions of the shell atoms which will contribute to make a large reduced mass. The m^2 dependence is therefore likely to be much too large for real crystals. It is also pertinent to point out that the Bak-Prigogine theory validates the quasi-equilibrium approach in the sense that the error in computing the flux when $U^\dagger/RT\geq 15$ is very small. Since for most solids $U^\dagger/RT\geq 20$, the exponential form of solution with $f(U^\dagger/RT)=1$ is very good. Nevertheless, although the exponential term is substantiated, the difference in pre-exponential terms suggests that the detailed nonequilibrium theory differs primarily in questions of the effective coupling between the given particle and the reservoir. This is not unexpected, since it is just such questions which are central to the mechanism of the approach to equilibrium.

ACKNOWLEDGMENT

We are pleased to thank Dr. Howard Reiss of the Bell Telephone Laboratories for several invaluable discussions. We should also like to thank Dr. D. Chipman for permission to use his data on x-ray scattering in Pb prior to publication.

Note added in proof: We are indebted to Dr. R. W. Keyes of Westinghouse Research Laboratories for calling to our attention that Eq. (45) may be integrated directly, yielding

$$\Delta V^*/\bar{V}=[1/(\gamma_G-\tfrac{1}{3})]+C_1(V/\bar{V})^{\gamma_G-\frac{1}{3}}.$$

This equation reduces to our Eq. (45) when the dimensionless constant $C_1=0$. In general ΔV^* is not proportional to $\bar{V}$, but the approximation used by us appears to be good if ΔV^* is pressure independent.

[27] R. Brout and I. Prigogine, Physica, **22**, 621 (1956).
[28] T. Bak and I. Prigogine, J. Chem. Phys. **31**, 1368 (1959).
[29] S. Chandrasekhar, Revs. Modern Phys. **15**, 1 (1943).

Nitrogen Chained Compounds as Intermediates in the Photolysis of Solid HN_3

HAROLD A. PAPAZIAN

Convair Scientific Research Laboratory, San Diego, California

(Received September 23, 1959)

The ultraviolet and visible absorption spectrum of irradiated solid HN_3 has been studied. Gas evolution during warmup of irradiated samples has been analyzed. It is proposed that photolysis in the solid yields NH radicals which react with the matrix to form the nitrogen chained compounds diiminohydrazine (H—N=N—N=N—H), triazene (H_2—N—N=N—H), and the radical H—N=N. The latter is responsible for the blue color and paramagnetism of the solid. Multichained nitrogen compounds are known only as organic derivatives. Here they are formed and stabilized at low temperatures. On warmup of the blue solid, these compounds undergo decomposition yielding the products found from the blue solid.

INTRODUCTION

RICE and Freamo[1,2] found that when gaseous HN_3 was energized, thermally or electrically, and then condensed at liquid nitrogen temperatures, the deposit was colored blue. Later Rice and Grelecki[3] showed that by illuminating solid HN_3 at liquid nitrogen temperature with ultraviolet light, the solid could be colored blue. Recently, it has been shown that solid HN_3 at liquid N_2 temperature also may be colored blue by ion bombardment.[4] The original workers showed that the blue color underwent an irreversible change to white when the temperature of the system was raised, and they reported NH_4N_3 as the only product of the reaction. Rice and his co-workers suggested that the blue color was perhaps due to the NH radical.

Mador and Williams[5] attributed absorption bands at 3500 A and 6500 A to NH and NH_2 radicals, respectively.

Dows, Pimentel, and Whittle[6] studied the infrared spectrum of HN_3 which had passed through a glow discharge before being deposited at −183°C. They found two unidentified intermediates and inferred a third unobserved one which they suggested to be the NH radical.

The present study suggests that the two unidentified intermediates are triazene and diiminohydrazine and that the free radical responsible for the color and paramagnetism of the solid is H–N=N. These conclusions are reached by considering the absorption spectra and the gas evolved from the blue solid. The chemistry which can be attributed to the formation of NH_4N_3 has its analog in the organic chemistry of nitrogen chained compounds.

EXPERIMENTAL

The HN_3 was prepared under vacuum by treating sodium azide with concentrated H_2SO_4. The HN_3 evolved and was passed onto a cold finger, and a purification was carried out by allowing the deposit to warm up, during which time any lower boiling impurities were allowed to come off. When it became obvious that the HN_3 was disappearing, liquid N_2 was reintroduced. A fraction of the remaining HN_3 was then sublimed over to the reaction cold finger.

For the gas evolution studies, both transparent "glassy" and recrystallized "snowy" samples were studied. The recrystallized samples were prepared by allowing the HN_3 to warm up to the point where it began to disappear from the reaction cold finger. During this warmup the sample underwent considerable recrystallization. After irradiation with a G.E. H3FE ultraviolet lamp for the desired length of time, simultaneous measurements of gas evolution, temperature, and pressure (in the apparatus) were recorded. A CEC model 620 mass spectrometer was used to analyze the gases evolved during the warmup. The mass spectrometer leak was tapped into the glass reaction apparatus between the reaction cold finger and the pump used to evacuate the apparatus. This allowed a profile of the evolved gases to be obtained. The outer jacket of the reaction vessel was quartz to allow uv irradiation.

For the absorption spectra a completely transparent "glass" was deposited. A modified universal model Perkin-Elmer 112U spectrophotometer was used to study the spectra between 3300 A and 7600 A. The entire region could not be covered on any one sample because of the necessity of a grating change for the region beyond 6400 A. The cold finger was constructed so that the HN_3 could be deposited on a surface surrounded by liquid N_2. This removed liquid N_2 from the absorption light path. The cold finger had a quartz window to allow uv irradiation. The pressure in the absorption cell was continuously recorded.

RESULTS

Figure 1 shows the evolution of nitrogen during warmup as a function of the time of uv irradiation of recrystallized samples of HN_3. The figure shows four different samples of approximately the same amount of HN_3. The ordinate of the curves are in arbitrary units. Corrections for pressure and pumping speed could not be made on account of the experimental setup.

[1] F. O. Rice and M. Freamo, J. Am. Chem. Soc. **73**, 5529 (1951).
[2] F. O. Rice and M. Freamo, J. Am. Chem. Soc. **75**, 548 (1953).
[3] F. O. Rice and C. Grelecki, J. Am. Chem. Soc. **79**, 1880 (1957).
[4] H. A. Papazian, J. Chem. Phys. **29**, 448 (1958).
[5] J. L. Mador and M. C. Williams, J. Chem. Phys. **22**, 1629 (1954).
[6] Dows, Pimentel, and Whittle, J. Chem. Phys. **23**, 1606 (1955).

The sample irradiated for 2½ minutes showed no apparent color; the 5-minute sample appeared perhaps tinted; the 10-minute sample was blue, and the 20-minute sample was considerably colored. In the warmup of the blue colored samples the color disappeared during the gas evolution step occuring between −160°C and −140°C. The cold finger warmed slowly, and it took on the order of 15 seconds for the color to disappear.

The stepwise reactions occurring during warmup could be stopped by reintroducing liquid N_2 into the cold finger. If the reaction was stopped at the end of any step, then the next step would not appear until the cold finger was warmed to the temperature of that subsequent step.

For longer irradiation times, another step is observed at about −90°C (dashed line, Fig. 1). For the results shown in Fig. 1, this step is observed as a slight change in slope. For irradiation times longer than 2½ minutes the step occurring at −125°C appears as a change in slope, the reaction passing quickly through this region into the reaction occurring at −110°C.

Glassy samples behaved in a very similar manner and in addition showed that the disappearance of the blue color was not accompanied by a recrystallization even though nitrogen gas was evolved. The temperature of recrystallization is very close to −140°C, i.e., the "glass" recrystallized at the beginning of the second step.

The only other gas evolved besides N_2 was H_2. For long irradiations ($\geq$20 min), a trace amount, some 1000 times less than the N_2, was evolved during the color transition step.

We may estimate the relative rates of reaction by the rate of nitrogen evolution as recorded by the mass spectrometer. A rough estimate gives the color transition step to be about an order of magnitude slower than than the subsequent steps at −140°C and −110°C.

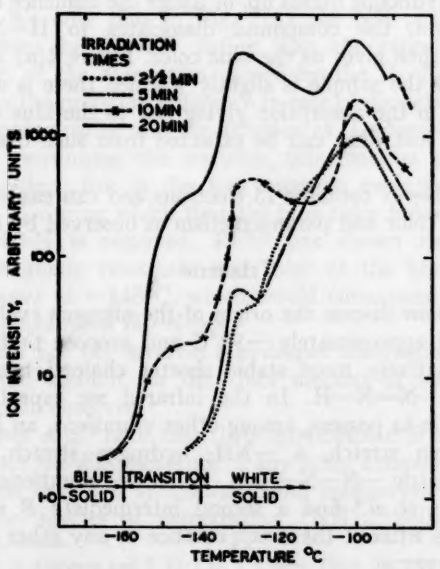

FIG. 1. Nitrogen evolution from irradiated solid HN_3 during warmup.

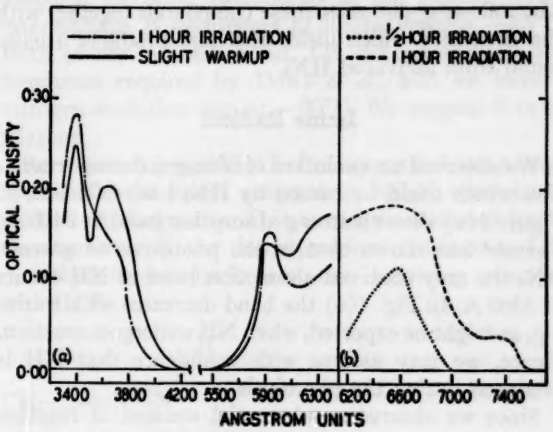

FIG. 2. Absorption spectra of irradiated solid HN_3.

It should be noted here that the reactions yielding the largest part of the gas evolution are present at the shortest irradiation times. The blue color with its gas evolution step appears only after considerable irradiation.

During the irradiation there was a small but steady evolution of nitrogen.

Figure 2 shows the optical absorption spectrum of the blue solid from the range 3300 A to 7600 A. Wavelengths shorter than 3400 A were not measured on this sample but are known from experiments on other samples; the region 6200 A to 7600 A for another sample is shown in Fig. 2(b). From these we can synthesize the entire spectrum. Rice[7] has shown that this is the region of interest, although his spectra did not show detailed bands. The "slight warmup" in Fig. 2(a) was a removal of the liquid N_2 from the absorption cell until gas evolution began, then a quick reintroduction of liquid N_2.

DISCUSSION

The most interesting fact observed in this research is that only nitrogen is given off in any reaction step during the warmup process. The analogous phenomenon is well known in the organic chemistry of nitrogen for chains of three nitrogen atoms or longer.[8] These triazene, tetrazene, tetrazane derivative compounds undergo decompositions with nitrogen evolution. Only the organic derivatives of these compounds are known. We might well expect chains of the parent compounds in the photolysis of HN_3 where it is usually assumed that the first step involves the production of NH. The NH formed can react with the matrix HN_3 yielding such compounds which are stabilized at the low temperatures and decompose during warmup yielding N_2.

[7] F. O. Rice and R. B. Ingall, J. Am. Chem. Soc. **81**, 1856 (1959).

[8] T. W. J. Taylor and W. Baker, *Sidgwick's Organic Chemistry of Nitrogen* (Oxford University Press, London, 1942).

The following discusses these compounds together with the chemistry which yields the final products usually found from activated HN_3.

Imine Radical

We observed an evolution of nitrogen during irradiation which could be caused by $HN_3+h\nu\rightarrow NH+N_2\uparrow$. Figure 2(a) shows a strong absorption band at 3400 A; Thrush[9] has shown that in the photolysis of gaseous HN_3 the only observed absorption band of NH occurs at 3360 A. In Fig. 2(a) the band decreases with warming, as might be expected, when NH undergoes reaction. Hence, we may assume with confidence that NH is produced during the photolysis.

Since we observe a substantial amount of reaction during warmup on samples without any blue color (see Fig. 1), it is unlikely that NH contributes to the color of the solid.

Diiminohydrazine

As an example of the possible type of reaction to a multichained compound which the NH may undergo, we write

$$H-\underset{\cdot\cdot}{\overset{\cdot\cdot}{N}}=N=\overset{\cdot\cdot}{N}: + \underset{\cdot\cdot}{\overset{\cdot\cdot}{N}}-H\rightarrow H-\overset{\cdot\cdot}{N}=\overset{\cdot\cdot}{N}-\overset{\cdot\cdot}{N}=\overset{\cdot\cdot}{N}-H \quad (1)$$

the molecule diiminohydrazine.

In the infrared we expect this molecule to possess, among other vibrations, a hydrogen stretch corresponding to the imino =N—H hydrogen stretching frequency, a hydrogen bending frequency similar to HN_3, and an asymmetric —N=N— stretch.

Imino stretches appear to have a somewhat narrow frequency range,[10] and Colthup[11] gives the range as 3400–3300 cm^{-1}. The hydrogen bending frequency in HN_3 is given[12] as 1150 cm^{-1}. Dows, Pimentel, and Whittle[6] found an unstable intermediate (which they designate *A*) at −183°C to which they attributed two bands, one at 3320 cm^{-1} and another at 1090 cm^{-1}. An examination of their curves shows another small broad band at approximately 1440 cm^{-1}. (This band grows slightly on warming when their second intermediate, designated *B*, appears. This indicates that *B* has a vibration similar to *A*. This is shown below.) From a study of triazenes, LeFevre, O'Dwyer, and Werner[13] indicate that, although generally masked by other vibrations, the —N=N— should absorb around 1406 cm^{-1}. We suggest that the band observed at 1440 cm^{-1} in reference 6 is that vibration, the 3320 cm^{-1} is the imino hydrogen stretch, and the 1090 cm^{-1} is the hydrogen bending frequency in the molecule diiminohydrazine.

The known symmetrical tetrazenes,

$$R_2-N-N=N-N-R_2,$$

form unstable salts with HCl which decompose with the evolution of nitrogen.[8] The azide ion is considered an halogenoid[14] so that we might expect this diiminohydrazine to form a salt with HN_3. Dows *et al.*[6] assign a peak at 2050 cm^{-1} to the asymmetrical N_3 stretch of NH_4N_3. However, other strong bands of NH_4N_3 are not present at −183°C and do not appear until their sample is warmed to −100°C, at which time intermediate *A* disappears. We suggest that the band at 2050 cm^{-1} be assigned to the salt of diiminohydrazine and that intermediate *A* of reference 6 is this compound.

On decomposition of this compound, the 2050 cm^{-1} band is then caused by the product of the decomposition, NH_4N_3. The other strong bands[15] of NH_4N_3 appear at this time (Fig. 2, reference 6). The present work finds considerable N_2 evolution at approximately −110°C which correlates with this decomposition. At this time the small band at 1440 cm^{-1} is replaced by the sharp peak of the N—H bending in NH_4N_3.

H—N=N Radical

The known tetrazanes quite readily undergo equilibrium dissociations.[8] Diiminohydrazine should undergo a tetrazane type dissociation to the free radical H—N=N. This behavior is consistent with the results reported in this paper. For, at short irradiation we get no color and yet get considerable N_2 evolution. On continued irradiation, as the concentration of the diiminohydrazine builds up, or under the influence of the radiation, the compound dissociates to H—N=N which then gives us the blue color. Figure 2(a) shows that as the sample is slightly warmed there is an increase in the absorption giving rise to the blue color; this is just what can be expected from such dissociations.

H—N=N contains 15 electrons and can easily give rise to color and paramagnetism as observed by Rice.[1]

Triazene

We now discuss the origin of the nitrogen evolution step at approximately −90°C and propose that it is the relatively more stable shorter chained triazene, H_2—N—N=N—H. In the infrared we expect this molecule to possess, among other vibrations, an imino hydrogen stretch, a —NH_2 hydrogen stretch, and asymmetric —N—N— and —N=N— vibrations.

Dows *et al.*[6] find a second intermediate *B* which appears without the disappearance of any other com-

[9] B. A. Thrush, Proc. Roy. Soc. (London) **A235**, 143 (1956).
[10] L. J. Belamy, *The Infra-red Spectra of Complex Molecules* (John Wiley & Sons, Inc., New York, 1954).
[11] N. B. Colthup, J. Opt. Soc. Am. **40**, 397 (1950).
[12] D. A. Dows and G. C. Pimentel, J. Chem. Phys. **23**, 1258 (1955).
[13] LeFevre, O'Dwyer, and Werner, Australian J. Chem. **6**, 341 (1953).
[14] T. Moeller, *Inorganic Chemistry* (John Wiley & Sons, Inc., New York, 1952).
[15] Dows, Whittle, and Pimentel, J. Chem. Phys. **23**, 1475 (1955).

pound. To intermediate *B* they assign bands at 3230 cm^{-1} and 860 cm^{-1}. We suggest that the band at 3230 cm^{-1} can be assigned to the hydrogen stretch in $-NH_2$; the vibration at 860 cm^{-1} to the asymmetric —N—N— vibration. In liquid hydrazine the vibration at 873 cm^{-1} has been assigned[16] to the N—N vibration ν_6, and the Raman value is 870 cm^{-1}. As mentioned previously, an examination of their curves shows the small broad band at 1440 cm^{-1} to increase slightly during the appearance of intermediate *B*. As in diiminohydrazine, we assign this to —N=N—. The imino hydrogen stretch occurs with the vibration in the diiminohydrazine.

Further evidence for the existance of triazene is shown from ultraviolet absorption. Klein[17] has shown that several simple organic triazenes have absorptions near 3600 A. We also carried out an experiment which indicated that triazene should absorb at 3600 A. We reduced an aqueous solution of NH_4N_3 successively with Cu, Fe, and Al. Absorption at 3600 A increased successively. Since doing this experiment, we found L. F. Audrieth [J. Chem. Educ. **7**, 2055 (1930)] quoting Dimroth as obtaining triazene by reducing NH_4N_3 in aqueous solution by using a Zn—Cu couple and ammonium chloride. The spectrum in Fig. 2 shows a band at 3600 A which grows during slight warmup. This is the synthesis of triazene caused by the increased mobility of the radicals NH and H—N=N. We can write for the over-all reaction

$$H—N=N+NH+HN_3 \rightarrow H_2—N—N=N—H+\tfrac{3}{2}N_2\uparrow . \qquad (2)$$

During this warmup, a small amount of gas was evolved in the absorption apparatus as required by this equation. We note that in Fig. 2(a) the NH peak does decrease; the increase, rather than, the expected decrease, of the absorption caused by the H—N=N is due to the probable difference in rate of dissociation of diiminohydrazine and the diffusion of H—N=N.

On continuing the warmup, this reaction goes to completion; this is the first nitrogen evolution step (Fig. 1) during which time the blue color fades as the H—N=N is removed. Rice[18] has shown that the paramagnetic resonance and color of the blue solid disappear at −148°C, which would correspond to the disappearance of H—N=N.

Since Eq. (2) involves a hydrogen abstraction step, it could account for the trace amount of hydrogen evolution observed.

Dows *et al.*[6] note that their intermediate *B* appears without the disappearance of any other compound and suggest that *B* is synthesized from unobserved NH or another species of composition $(NH)_x$, both being obscured by other compounds in the deposit. Their intermediate *B* disappears at approximately −83°C. Both of the radicals in Eq. (2) closely resemble the fragments required by Dows *et al.*, and we have a nitrogen evolution step at −90°C. We suggest *B* to be triazene.

An examination of Fig. 2 of reference 6 shows a large increase in the bands assigned to NH_4N_3 when intermediate *B* disappears. This is easily accounted for in the chemistry of the decomposition of triazene. 1,3-dimethyltriazene undergoes the following reaction with HCl[8]:

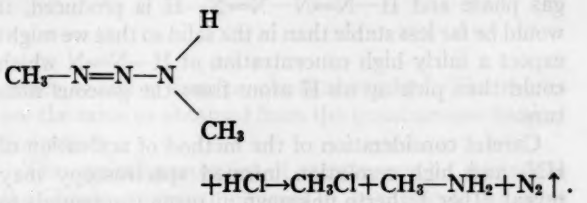

The azide ion being an halogenoid, we may expect triazene to undergo a similar reaction with hydrazoic acid,

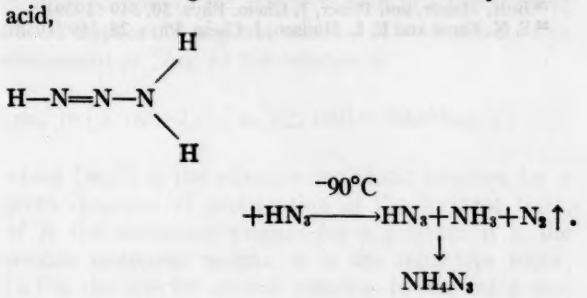

Other Experimental Results

We now discuss the other N_2 evolution steps observed in this research (see Fig. 1). It is not clear to what we may attribute the gas evolution at −140°C and −125°C. It can be seen that, at the shortest irradiation time, the step at −140°C is the least clearly developed step. This may be a compound which is more unstable than diiminohydrazine whose concentration increases with time of irradiation. Such a compound could be the longer chained bisdiazoamine formed by

$$N—H+H—N=N—N=N—H \rightarrow H—N=N—\underset{\displaystyle H}{\underset{|}{N}}—N=N—H. \qquad (3)$$

Figure 1 shows the peak at −140°C to increase with irradiation which is what would be expected from Eq. (3) as NH and H—N=N—N=N—H increase.

The evolution step at −125°C may be the decomposition of diiminohydrazine, its salt decomposing at −110°C.

[16] P. A. Giguere and I. D. Liu, J. Chem. Phys. **20**, 136 (1952).
[17] J. Klein, Compt. rend. **232**, 81 (1951).
[18] F. O. Rice (private communication).

The organic derivatives of the types of compounds discussed herein go through a hydrazine stage in their decomposition.[8] The analogous reactions here can account for the hydrazine azide reported[19] as a product from the blue solid.

In a forthcoming communication it will be shown that the bands at 5900 A and 6200 A are not related to any radicals discussed here, and that they probably arise from the HN_3 matrix. Hence, we may then assign the absorption at 6600 A to H—N=N.

Diimide has been reported[20] as being present in the gaseous discharge of HN_3. If Eq. (1) is operative in the gas phase and H—N=N—N=N—H is produced, it would be far less stable than in the solid so that we might expect a fairly high concentration of H—N=N which could then pick up an H atom from the gaseous mixture.

Careful consideration of the method of activation of HN_3 and high resolution infrared spectroscopy may reveal other hitherto unknown nitrogen compounds to be stabilized at low temperatures.

[19] Bolz, Mauer, and Peiser, J. Chem. Phys. **30**, 349 (1959).
[20] S. N. Foner and R. L. Hudson, J. Chem. Phys. **28**, 719 (1958).

SUMMARY

1. Ultraviolet photolysis of HN_3 at liquid nitrogen temperatures produces NH. Its existance is demonstrated by the absorption band at 3400 A and its behavior with temperature.

2. Reaction between NH and HN_3 at liquid nitrogen temperatures produces diiminohydrazine which partially dissociates to H—N=N. This radical produces the blue color and paramagnetism of the solid.

3. Reaction between H—N=N and NH removes the color from the solid by producing triazene. The largest contribution to the production of NH_4N_3 is the decomposition of triazene.

4. Other longer chained compounds such as bisdiazoamine may also be present.

ACKNOWLEDGMENTS

I am indebted to Dr. A. L. Berlad for his continued encouragement without which this research could not have been completed. It is a pleasure to acknowledge many stimulating discussions with Dr. Thomas Freund throughout the course of the entire problem. Mr. John Pearl rendered outstanding technical assistance.

Optical Rotation of Oriented Helices. II. Calculation of the Rotatory Dispersion of the Alpha Helix*

IGNACIO TINOCO, JR., AND ROBERT W. WOODY†

Chemistry Department, University of California, Berkeley 4, California

(Received October 1, 1959)

The polarizability theory for the average optical rotation of a molecule has been generalized and has been used to calculate the optical rotation along specific directions in the molecule. The optical rotatory dispersion of polyglycine and polyalanine for light incident parallel and perpendicular to the helical axis has been calculated. The predicted dispersion is consistent with most experiments if a left-handed helix is assumed for polybenzyl-L-glutamate and peptides with similar rotatory behavior. The average rotatory dispersion for a helix is not in general qualitatively different from that of a random coil.

INTRODUCTION

ALTHOUGH calculations of the average optical rotation of an α helix have been made,[1–5] estimates of the rotatory dispersion parallel and perpendicular to the helix axis are not available. As these quantities can be measured,[6,7] it is of interest to make the calculation. Furthermore, the previous calculations of the average rotation did not include the effect of side chains. Moffitt[3–5] attempted to calculate the contribution to the rotatory dispersion from the interaction of certain amide transitions. Fitts and Kirkwood made their calculations for an α helix of polyglycine, but they omitted the interactions involving adjacent atoms. We have made calculations for α helices of polyglycine and of polyglycine omitting adjacent atoms; we have also considered the simplest side chain by treating poly-DL-alanine, and right- and left-handed poly-L-alanine. For each of these models we obtained the optical activity along the helical axis $[m_{33}']$; that perpendicular to the helical axis, $[m_{11}']$; and the average, $[m']=([m_{33}']+2[m_{11}'])/3$.

THEORY

We want to extend Kirkwood's[8] polarizability theory for the average optical activity to include the optical activity along specific directions in a molecule. The quantum-mechanical formula for the optical rotation tensor of a molecule, which can be used to derive the desired expression, is available.[9] However, we prefer to use a simpler, classical method. The results are the same as obtained from the quantum-mechanical derivation.

The optical properties of matter can be related to the dipole moment induced in a molecule by unit electric field of the incident light. The optical rotation is proportional to the component of the dipole moment induced parallel to the magnetic field of a plane wave, but 90 degrees out of phase with it.[8] If we designate this component as $(2\pi g/\lambda)$ the rotation is

$$[m_{rr}']=[3/(n^2+2)]\{[\alpha_{rr}]M/100\}=288\pi^2N_0g_r/\lambda^2, \quad (1)$$

where $[m_{rr}']$ is the effective molecular rotation for a given direction of propagation of the incident light; M is the molecular weight—for a polymer it is the residue molecular weight; n is the refractive index; $[\alpha]$ is the specific optical rotation in deg ml/g dm; N_0 is Avogadro's number; λ is the wavelength of light in vacuum; and g_r is the molecular optical rotation parameter. The subscript r refers to a particular direction in the molecule.

The model we choose for a molecule is a collection of point polarizable groups. The dipole induced in group i by the incident light is

$$\mathbf{p}_i=\boldsymbol{\alpha}_i\cdot\mathbf{F}_i+\boldsymbol{\alpha}_i\cdot\sum_k\mathbf{E}_{ik}, \quad (2)$$

where $\boldsymbol{\alpha}_i$ is polarizability of group i; $\mathbf{F}_i$ is the internal electric field of light at group i; and $\mathbf{E}_{ik}$ is the dipole field at point i due to induced dipole at point k.

$$\mathbf{E}_{ik}=\mathbf{T}_{ik}\cdot\mathbf{p}_k=\mathbf{T}_{ik}\cdot\boldsymbol{\alpha}_k\cdot\mathbf{F}_k,$$

$$\mathbf{T}_{ik}=(1/r_{ik}^3)[\mathbf{1}-(3\mathbf{r}_{ik}\mathbf{r}_{ik}/r_{ik}^2)], \quad (3)$$

where $\mathbf{T}_{ik}$ is the dipole interaction tensor; $\mathbf{1}$ is the unit tensor; and $|\mathbf{r}_{ik}|=|\mathbf{r}_k-\mathbf{r}_i|$ equals the distance between group i and k.

The fact that for a given direction of propagation the optical rotation must be independent of the plane of polarization allows us to drop the first term in Eq. (2).

* Supported in part by research grant A-2220 from the National Institute of Arthritis and Metabolic Diseases, Public Health Service.

† National Science Foundation Fellow.

[1] D. D. Fitts and J. G. Kirkwood, Proc. Natl. Acad. Sci. U. S. **42**, 33 (1956).

[2] D. D. Fitts and J. G. Kirkwood, Proc. Natl. Acad. Sci. U. S. **43**, 1046 (1957).

[3] W. Moffitt, J. Chem. Phys. **25**, 467 (1956).

[4] W. Moffitt, Proc. Natl. Acad. Sci. U. S. **42**, 736 (1956).

[5] Moffitt, Fitts, and Kirkwood, Proc. Natl. Acad. Sci. U. S. **43**, 723 (1957).

[6] I. Tinoco, Jr., J. Am. Chem. Soc. **79**, 4248 (1957).

[7] I. Tinoco, Jr., J. Am. Chem. Soc. **81**, 1540 (1959).

[8] J. G. Kirkwood, J. Chem. Phys. **5**, 479 (1937).

[9] I. Tinoco, Jr., and W. G. Hammerle, J. Phys. Chem. **60**, 1619 (1956).

TABLE I. Parameters used in calculating optical rotatory dispersion.

Group	Atom	a(A)	γ(deg)	Z(A)	$\alpha_3-\alpha_1$(A^3)	θ(deg)	ϕ(deg)
amide (NV_1)	N	1.59	27.8	0.89	$1.74\lambda^2/(\lambda^2-\lambda_1^2)$	128	112
amide (NV_2)					$0.98\lambda^2/(\lambda^2-\lambda_2^2)$	38	112
amide					0.375	62	90
amide	C(carbonyl)	1.59	73.8	0.44	0.375	62	90
CH_2	C*	2.29	100.0	1.50	0.603	69	90
CH					0.45	69	90
CH_3	$C_{\beta 1}$	3.34	82.4	2.26	0.75	123	149
CH_3	$C_{\beta 2}$	3.34	117.6	0.74	0.75	57	211

We can also expand the electric field of the incident plane light wave as follows:

$$\mathbf{F}_k=\mathbf{a}_2\mathbf{F}\exp i(\omega t-2\pi\mathbf{a}_1\cdot\mathbf{R}_k/\lambda),$$

$$\mathbf{F}_k=\mathbf{a}_2\mathbf{F}(1-2\pi i\mathbf{a}_1\cdot\mathbf{r}_k/\lambda)\exp i(\omega t-2\pi\mathbf{a}_1\cdot\mathbf{R}_0/\lambda), \quad (4)$$

where $\mathbf{a}_1$, $\mathbf{a}_2$, $\mathbf{a}_3$ is an orthogonal right-handed set of unit vectors in the directions, respectively, of propagation, electric field, and magnetic field; i is $-1^{\frac{1}{2}}$; $\omega=2\pi\nu$ equals circular frequency; $\mathbf{R}_k=\mathbf{R}_0+\mathbf{r}_k$ equals the vector from arbitrary fixed origin to group k; $\mathbf{R}_0$ is the vector from arbitrary fixed origin to convenient point on molecule; and $\mathbf{r}_k$ is the vector from this point to group k.

By substituting Eq. (4) into the second term of Eq. (2) and finding the imaginary component in the direction of the magnetic field we obtain:

$$g_i=-\sum_{k\neq i}(\mathbf{a}_3\cdot\mathbf{a}_i\cdot\mathbf{T}_{ik}\cdot\mathbf{a}_k\cdot\mathbf{a}_2)(\mathbf{a}_1\cdot\mathbf{r}_k)$$

$$g=\sum_{i=1}^{N}g_i \quad (N=\text{number of groups in molecule}). \quad (5)$$

For ease of calculation we assume $\boldsymbol{\alpha}$ is symmetric with symmetry axis along the unit vector $\mathbf{e}$ and principal values α_3 (along $\mathbf{e}$) and α_1. We can write

$$\boldsymbol{\alpha}=(\alpha_3-\alpha_1)\mathbf{ee}+\alpha_1\mathbf{1}. \quad (6)$$

By substituting Eq. (6) into Eq. (5), dropping symmetric terms, and rearranging, we obtain:

$$g_i=(\tfrac{1}{2})(\alpha_3-\alpha_1)_i\sum_{k>i}(\alpha_3-\alpha_1)_kG_{ik}\mathbf{a}_1\cdot(\mathbf{e}_i\times\mathbf{e}_k)(\mathbf{r}_{ik}\cdot\mathbf{a}_1)$$

$$G_{ik}=(1/r_{ik}^3)\{\mathbf{e}_i\cdot\mathbf{e}_k-[3(\mathbf{e}_i\cdot\mathbf{r}_{ik})(\mathbf{e}_k\cdot\mathbf{r}_{ik})/r_{ik}^2]\}. \quad (7)$$

This gives the optical rotation per group i for light incident along $\mathbf{a}_1$. If we divide Eq. (7) by 3, place a dot between the last two parentheses, and delete the $\mathbf{a}_1$'s we have the average optical rotation.[10] This relation was obtained by Kirkwood[8] in 1937. His derivation shows that it is the first term of a more general quantum mechanical expression.

[10] We should point out that in general the relation between the average optical rotation and the optical rotation tensor is not so simple.[9]

CALCULATION

Equation (7) allows us to calculate the optical activity as a function of direction for any molecule for which we know the geometry and for which we are willing to guess the polarizability. For α-helix polypeptides the requirement of known geometry limits us to polyglycine and polyalanine. To consider more complicated side groups we would also have to be willing to guess the configurations of these groups.

We use the geometry of the α helix as given by Pauling and Corey.[11] The position of any atom is specified by the vector:

$$\mathbf{r}=a\cos\gamma\mathbf{i}+a\sin\gamma\mathbf{j}+z\mathbf{k}.$$

The position of the corresponding atom in the next residue of the helix is obtained by adding 100° to γ and 1.5 A to z. The parameters for the α helix[11] are given in Table I. Atom C_{β_1} refers to the right-handed L isomer (or left-handed D) and C_{β_2} refers to the left-handed L isomer (or right-handed D).[12]

The treatment of the polarizability follows Fitts and Kirkwood[2]; the directions and magnitudes of the polarizabilities (Table I) come either from that paper or from Kirkwood.[8] The direction of the symmetry axis $\mathbf{e}$ of the polarizability of a group is related by the angles θ and ϕ to a right-handed rectangular coordinate system fixed to the appropriate atom. This system is specified by three unit vectors.

(axial) $\mathbf{e}_a=\mathbf{k}$

(radial) $\mathbf{e}_r=\cos\gamma\mathbf{i}+\sin\gamma\mathbf{j}$

(tangential) $\mathbf{e}_t=-\sin\gamma\mathbf{i}+\cos\gamma\mathbf{j}$.

The angle θ is the angle between $\mathbf{e}$ and the axial vector

[11] L. Pauling and R. B. Corey, Proc. Natl. Acad. Sci. U. S. **37**, 235 (1952). Other, slightly different, values are also available [Pauling, Corey, Yakel, and Marsh, Acta Cryst. **8**, 853 (1955); L. Brown and I. F. Trotter, Trans. Faraday Soc. **52**, 537 (1956)] but in order to facilitate comparison with previous work[2] we used these.

[12] Bamford, Elliot, and Hanby, *Synthetic Polypeptides* (Academic Press, Inc., New York, 1956), p. 124.

TABLE II. Calculated optical rotatory dispersion for a right-handed α helix. All numbers have been multiplied by 10^9.

	$[m']$			$[m_{33}']$		
Description	a_{11}	a_{12}	a_{22}	a_{11}	a_{12}	a_{22}
All polypeptides	289	−298	178	1419	−930	−268
	a_{10}	a_{20}	a_{00}	a_{10}	a_{20}	a_{00}
Polyglycine (omitting adjacent atoms)	−438	364	130	−289	−1235	−1075
Polyglycine	−825	492	123	−233	−2149	−1445
Poly-DL-alanine	−434	282	90	356	−1488	−810
Poly-L-alanine	−546	245	132	0	−1739	−950
Poly-D-alanine	−323	320	134	711	−1238	−932

and ϕ is the angle between the $\mathbf{e}-\mathbf{e}_a$ plane and the radial vector.

$$\mathbf{e}=\sin\theta\cos\phi\mathbf{e}_r+\sin\theta\sin\phi\mathbf{e}_t+\cos\theta\mathbf{e}_a.$$

The amide polarizability is divided into four terms. The first two terms are centered on the nitrogen; they arise from two transitions[3,4] at $\lambda_1=185$ mμ (NV_1) and $\lambda_2=148$ mμ (NV_2). The magnitude and direction of these transitions were determined by Peterson and Simpson.[13] The last two terms are centered respectively, at the nitrogen and carbonyl carbon; their directions are tangent to the helix at those points. The polarizability of the asymmetric carbon is directed similarly. The polarizability of the β methyl is chosen along the C—C bond. All polarizabilities except the two amide transitions are assumed to be wavelength independent; this should be a good approximation for $\lambda>250$ mμ.

RESULTS

We now have the information needed to use Eq. (7). All that remains is the very tedious summing of all the interactions between all the groups. We included interactions between groups in seventeen residues on either side of the one under consideration.

It is apparent from the wavelength dependence of the polarizabilities that the resulting rotatory dispersion will be of the following form[14]:

$$[m']=\frac{a_{11}\lambda^2}{(\lambda^2-\lambda_1^2)^2}+\frac{a_{12}\lambda^2}{(\lambda^2-\lambda_1^2)(\lambda^2-\lambda_2^2)}+\frac{a_{22}\lambda^2}{(\lambda^2-\lambda_2^2)^2}+\frac{a_{10}}{\lambda^2-\lambda_1^2}+\frac{a_{20}}{\lambda^2-\lambda_2^2}+\frac{a_{00}}{\lambda^2}. \quad (8)$$

The first three terms will be the same for all α-helix polypeptides, while the last three terms will depend on the particular polymer. The results for right-handed helices of five different models are given in Table II. Changing the sign for each term will give the result for the mirror image of the model, e.g., right-handed poly-D-alanine becomes left-handed poly-L-alanine. The numbers in the table have been multiplied by 10^9 and are to be used with λ in cm. It is convenient to present the results in terms of the average rotation $[m']$ and the rotation for light incident parallel to the helical axis $[m_{33}']$. The rotation perpendicular to the helical axis $[m_{11}']$ follows from

$$[m_{11}']=\tfrac{1}{2}\{3[m']-[m_{33}']\}. \quad (9)$$

Each mathematical operation leading to the numbers in Table II was performed at least twice, usually by two different people. We are therefore confident in the accuracy of the numbers.[15] However, these numbers are quite sensitive to the model used. The values of a_{11}, a_{12}, and a_{22} are the most dependable for two reasons. They only involve the interactions of the two known amide transitions, and the induced point-dipole approximation in the polarizability theory is more applicable to the interaction between nonbonded groups.

AVERAGE ROTATORY DISPERSION

The average rotatory dispersion is given as the solid lines in Figs. 1 and 2. Although the absolute magnitude of $[m']$ is not very significant as it is the sum and difference of 6 large numbers, the general wavelength dependence is significant. We notice in Fig. 1 that the dispersion of left-handed poly-L-alanine (curve 5) becomes increasingly negative at low wavelengths while right-handed poly-L-alanine (curve 1) goes through a minimum then turns positive. This behavior is caused by the positive value of a_{11} for a right-handed α helix (therefore negative value for a left-handed α helix) which becomes the dominant contribution to $[m']$ as λ approaches 185 mμ. Similarly, in Fig. 2, right-handed poly-DL-alanine (curve 4) and polyglycine (omitting adjacent atoms) (curve 2) become more positive at low wavelengths while left-handed polyglycine (curve 5) reaches a maximum at $\lambda=250$ mμ and becomes negative at lower wavelengths. Although these calculations show that the most inter-

[13] D. L. Peterson and W. T. Simpson, J. Am. Chem. Soc. **79**, 2375 (1957).

[14] H. Murakami. J. Chem. Phys. **27**, 1231 (1957).

[15] For polyglycine (omitting adjacent atoms) we agree well with Fitts and Kirkwood[2] on a_{11}, a_{12}, a_{22}, and a_{00}. We do not agree on a_{10} and a_{20}, but the resultant values of $[m']$ are not very different from theirs.

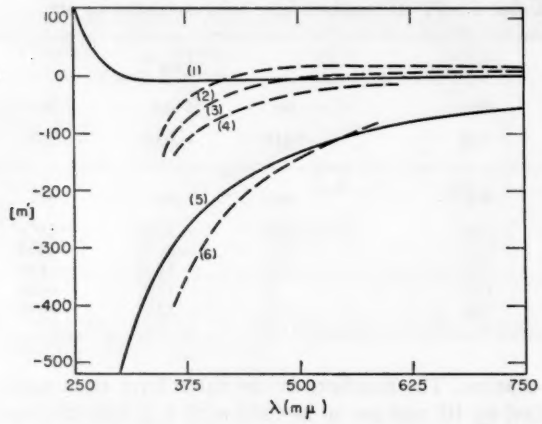

FIG. 1. The average optical rotation *vs* wavelength. The solid curves are calculated: (1) right-handed poly-L-alanine, (5) left-handed poly-L-alanine. The dotted curves are experimental: (2) polybenzyl-L-glutamate in ethylene dichloride,[16] (3) poly-L-glutamic acid in dioxane-water,[16] (4) poly-L-leucine in benzene-*m*-cresol,[19] (6) poly-L-alanine as solid film.[20]

esting wavelength region lies below 350 mμ, the published rotatory dispersion data,[16–20] the dotted lines in Figs. 1 and 2 are for $\lambda > 350$ mμ.

ROTATORY DISPERSION ALONG HELICAL AXIS

The rotatory dispersion for light incident along the helical axis is plotted in Fig. 3. We note that for all 5 models the rotation above $\lambda = 300$ mμ is positive for left-handed helices. We can have some confidence in this result because in contrast to the parameters for the average rotation, the sum of terms in Eq. (8) do not cancel so completely for $[m_{33}']$. All the curves show a sharp change in $[m_{33}']$ for $\lambda \approx 350$ mμ caused by the difference in sign between a_{11} and the other a's. The values of $[m_{33}']$ are about ten times $[m']$; this means that $[m_{11}']$ and $[m_{33}']$ must have opposite signs. These calculated results agree well with the one published experiment[7,21] shown as the dotted line in Fig. 3.

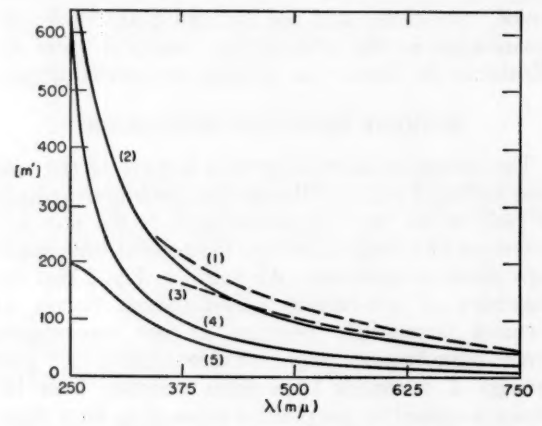

FIG. 2. The average optical rotation *vs* wavelength. The solid curves are calculated: (2) right-handed polyglycine (omitting adjacent atoms), (4) right-handed poly-DL-alanine, (5) left-handed polyglycine. The dotted curves are experimental: (1) polybenzyl-DL-glutamate in dioxane,[18] (3) poly-DL-leucine in benzene-*m*-cresol.[19] These latter curves are for helices with the sense of the poly-L-isomer.

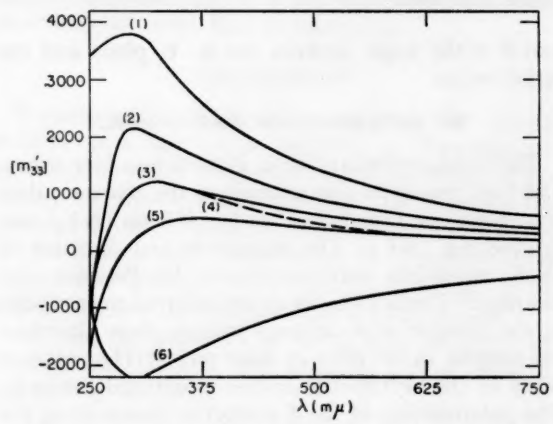

FIG. 3. The optical rotation for light incident along the helical axis *vs* wavelength. The solid curves are calculated: (1) left-handed polyglycine, (2) left-handed polyglycine (omitting adjacent atoms), (3) left-handed poly-DL-alanine, (5) left-handed poly-L-alanine, (6) right-handed poly-L-alanine. The dotted curve is experimental: (4) polybenzyl-L-glutamate in ethylene dichloride.[7]

HELICAL CONTENT AND THE SENSE OF THE HELIX

The aim of many of the optical activity experiments and calculations[1–7,17–20,22–25] in recent years has been to determine both the fraction of residues in a protein or polypeptide present in helices (supposedly α helices) and the sense of these helices. We would like to discuss the previous results in the light of the present paper.

Moffitt and Yang[16,26] derived the following general equation ($MY-9$) for the average rotatory dispersion of a helix.

$$[m'] = \sum_i [a_i \lambda_i^2/(\lambda^2 - \lambda_i^2)] + \sum_i [b_i \lambda_i^4/(\lambda^2 - \lambda_i^2)^2]. \quad (10)$$

[16] W. Moffitt and J. T. Yang, Proc. Natl. Acad. Sci. U. S. **42,** 596 (1956).
[17] J. T. Yang and P. Doty, J. Am. Chem. Soc. **79,** 761 (1957).
[18] P. Doty and R. D. Lundberg, Proc. Natl. Acad. Sci. U. S. **43,** 213 (1957).
[19] Downie, Elliott, Hanby, and Malcolm, Proc. Roy. Soc. (London) **A242,** 325 (1957).
[20] Elliott, Hanby, and Malcolm, Discussions Faraday Soc. **25,** 167 (1958).
[21] Preliminary measurements by K. Yamaoka in this laboratory show that polybenzyl glutamate in dioxane gives similar rotatory behavior.
[22] C. Cohen and A. G. Szent-Gyorgyi, J. Am. Chem. Soc. **79,** 248 (1957).
[23] E. R. Blout and R. H. Karlson, J. Am. Chem. Soc. **80,** 1259 (1958).
[24] M. Idelson and E. R. Blout, J. Am. Chem. Soc. **80,** 4631 (1958).
[25] C. Schellman and J. A. Schellman, Compt. rend. trav. lab. Carlsberg Ser. chim. **30,** 463 (1958).
[26] We shall designate their equations by the notation (MY-).

TABLE III. Parameters for the fit of the calculated and experimental optical rotatory dispersion curves (350 mμ<λ<750 mμ) for [m'] to three empirical equations [Eqs. (11), (12), (13)].

System	a_0	b_0	$k\times10^9$	$k_c\times10^9$	λ_c(mμ)	$k_c\times10^9$	λ_c(mμ)	Ref.
Right-handed poly-L-alanine	...	...	...	...	...	...	...	...
Left-handed poly-L-alanine	−649	56				−294	176	...
Right-handed polyglycine (omitting adjacent atoms)	...	...				231	151	...
Right-handed polyglycine	...	...	250	−283	148	...	...	...
Right-handed poly-DL-alanine	...	...				102	192	...
Polybenzyl-L-glutamate in ethylene dichloride	205	−635	219	−125	280	...	...	(16)
PBLG in chloroform	250	−625	229	−113	275	...	...	(16)
PBLG in dimethyl formamide	200	−660	234	−142	275	...	...	(16)
Poly-L-glutamic acid in dioxane-water	120	−625	248	−188	270	...	...	(16)
Poly-L-leucine in benzene-*m*-cresol	−53	−423	166	−185	250	...	...	(19)
Poly-L-alanine as solid film	−531	−475				−238	275	(20)
Polybenzyl-DL-glutamate in dioxane	680	−500	32	−8.3	300	...	...	(18)
Poly-DL-leucine in benzene-*m*-cresol	592	−513	296	−23	300	...	...	(19)
Polybenzyl-L-aspartate in chloroform	−1533	611	−699	−36	310	...	...	(23)

The second sum contains parameters which primarily depend on the helical skeleton and are independent of side chains. They therefore proposed the equation ($MY-10$)

$$[m']=[a_0\lambda_0^2/(\lambda^2-\lambda_0^2)]+[b_0\lambda_0^4/(\lambda^2-\lambda_0^2)^2] \quad (11)$$

to fit the experimental data. The parameters a_0, b_0, and λ_0 are derivable from the a_i, b_i, and λ_i ($MY-11$), and in certain circumstances b_0 is independent of a_i ($MY-12$). The value of b_0 would then be a measure of the helical content of a polypeptide or protein and its sign would determine the sense of the helix. Experimentally it was found that b_0 was indeed zero for some random coil polypeptides and that it and λ_0 were constant for different helical polypeptides in different solvents. Blout[27] has since found that b_0 is only constant for a certain class of helical polypeptides.

We can apply Moffitt and Yang's equations to our calculated results to see if b_0 is a measure of helical content for these models. Equation (8) can be written in the form of Eq. (10) by the following substitutions:

$$\lambda^2/(\lambda^2-\lambda_i^2)=[1/(\lambda^2-\lambda_i^2)]+[\lambda_i^2/(\lambda^2-\lambda_i^2)] \quad (12)$$

$$\lambda^2/(\lambda^2-\lambda_i^2)(\lambda^2-\lambda_j^2)=[\lambda_i^2/(\lambda_i^2-\lambda_j^2)(\lambda^2-\lambda_i^2)]+[\lambda_j^2/(\lambda_j^2-\lambda_i^2)(\lambda^2-\lambda_j^2)]. \quad (13)$$

If we now calculate b_0 we find that for the parameters given in Table II, b_0 is dependent on side chains. That is, b_0 depends not only on a_{11}, a_{12}, and a_{22}, but it also depends on a_{10}, a_{20}, and a_{00}. Therefore, from these results we do not expect b_0 to be a generally valid measure of either helix content or sense of helix.

We have also attempted to fit the rotatory dispersion curves empirically to Eq. (11) in the wavelength region from 350 to 750 mμ. The value of λ_0 was taken as 212 mμ to agree with previous use of Eq. (11). For the average rotation only the dispersion for left-handed poly-L-alanine could be fitted to this equation and these data could be represented equally well by a one term Drude equation. In fact the data for 3 of the 5 models could be represented by one term Drude equations. The parameters are given in Table III. These results are not consistent with the use of complex *versus* simple dispersion to distinguish helices from random coils.

Fitts and Kirkwood's method,[2] which we have followed, is to compare directly the calculated and observed rotatory dispersion. These authors concluded that poly-γ-benzyl-L-glutamate is a right-handed helix by comparing their calculations for polyglycine (omitting adjacent atoms) with the results of Doty and Lundberg.[18] They essentially compared curves (1) and (2) in Fig. (2), although in their calculations the agreement was even better. The experiment of Doty and Lundberg and other similar experiments[19] (curve 3, Fig. 2) were designed to obtain the rotatory dispersion of a racemic helix having a single screw sense (that corresponding to the L isomer). The implication was that the dispersion obtained would apply to any α helix, that is, be independent of side chains. However, all theories of optical rotation[28] show that the optical rotation of a racemic helix is not the same as that of a helix with no side chains. The racemic helix has contributions to its rotation from the interaction of (a) the D side chains with the backbone of the helix, (b) the L side chains with the backbone and (c) the side chains with each other. Contributions (a) and (b) do not tend to cancel at all, but have the same sign and roughly the same magnitude.

From the discussion above it is clear that we need not expect agreement between Fitts and Kirkwood's calculation and Doty and Lundberg's experiment. Consequently, the conclusion on the sense of the helix is doubtful. Our calculation for a right-handed helix of polyalanine with a random distribution of D

[27] E. R. Blout (personal communication).

[28] W. Kauzmann, Ann. Rev. Phys. Chem. 8, 432 (1957).

TABLE IV. Parameters for the fit of the calculated and experimental optical rotatory dispersion curves (350 mμ<λ<750 mμ) for $[m_{33}']$ to three empirical equations [Eqs. (11), (12), (13)].

System	a_0	b_0	$k\times10^9$	$k_c\times10^9$	λ_c(mμ)	$k_c\times10^9$	λ_c(mμ)	Ref.
Left-handed polyglycine (omitting adjacent atoms)	...	...	2600	−190	250	...	...	...
Left-handed polyglycine	...	...				3650	0	...
Left-handed poly-DL-alanine	3690	−3190	...	...	...	...	...	...
Left-handed poly-L-alanine	2680	−3270	1760	−523	250	...	...	...
Right-handed poly-L-alanine	−5360	3910	−2780	281	212	...	...	...
Polybenzyl-L-glutamate in ethylene dichloride	2470	−737				1120	169	7

and L residues (curve 4, Fig. 2) is again in qualitative agreement with experiment, but the calculated curve for right-handed polyglycine (curve 5, Fig. 2) is not. With only this evidence we would agree with Fitts and Kirkwood, but our other calculations prevent us. We might also point out the possibility that the experiments may have not actually determined the rotation of a racemic α helix. The inclusion of small amounts of D residues in an L helix might cause enough distortion and strain to change the helical optical rotation without changing the sense of the helix.

Looking at Fig. 1 we would decide that benzyl glutamate (curve 2), glutamic acid (curve 3), leucine (curve 4), and alanine (curve 6) formed left-handed helices. The agreement between the calculated curve for left-handed poly-L-alanine (curve 5) and experiment[20] is very suggestive. However, the experiment involves solid films of polyalanine which makes the orientation of the polypeptide uncertain. If the helical axis is primarily perpendicular to the direction of the incident light, the data would still be consistent with left-handed helices as $[m_{11}']$ is negative for them.

Figure 3 also suggests left-handed helices for polybenzyl-L-glutamate. However, data on other polypeptides are needed before a more definite conclusion can be made.

In an attempt to make the comparison between calculation and experiment more quantitative, we have used empirical equations to represent in the wavelength region above 350 mμ all the curves shown in the figures. First a one-term Drude equation was used.

$$[m']=k_c/(\lambda^2-\lambda_c^2). \quad (14)$$

If this equation did not fit the data, the following equation was tried:

$$[m']=[k_c/(\lambda^2-\lambda_c^2)]+(k/\lambda^2). \quad (15)$$

All curves were also represented, if possible, by the Moffitt and Yang equation, Eq. (11) with $\lambda_0=212$ mμ. The parameters, obtained by appropriate graphs of the data, are given in Tables III and IV. No statistical analysis of the parameters was made to determine which equation gave the best representation, and no statistical criteria were established to decide whether the fit of a particular equation were adequate.

All the curves except $[m']$ for right-handed poly-L-alanine could be fit by at least one of the empirical equations and most could be represented by more than one equation. Comparison of the parameters for the experimental and calculated curves however does not seem to provide any new conclusions about the sense of the helix.

Other evidence about the sense of the helix come from x-ray scattering. Arndt and Riley[29] have interpreted their protein x-ray scattering data in terms of left-handed helices. Elliott and Malcolm[30] have recently made some new calculations to compare with x-ray data on poly-L-alanine fibers. Although Brown and Trotter[11] had earlier favored a left-handed helix from these data, Elliott and Malcolm definitely choose a right-handed helix. As the choice also depends on the particular interchain packing assumed, we feel that an independent verification of the helix sense is still required.

DISCUSSION

The form of Eq. (8) applies to any polypeptide (whether helix or random coil) which has no strong chromophore other than the amide. For the helical form of this class of peptides the first three terms will be identical and their calculation will be relatively straightforward. The last three terms depend on the particular polypeptide and are more difficult to calculate. If it were possible to measure the coefficients of the first three terms (a_{11}, a_{12}, a_{22}) for a helical polypeptide we could determine the sense of the helix. Unfortunately, it is not easy to untangle the six coefficients in Eq. (8) from an experimental rotatory dispersion curve.

The problem of a general method of determining helix content is again difficult. We cannot assume that a_{11}, a_{12}, a_{22} are zero for the coil or that they have the same value in the coil form of different polypeptides. Although these terms may be negligible for certain polypeptides in the coil form in certain solvents, proof of this, in general, has not been presented.

If we consider a polypeptide with side chains which

[29] U. V. Arndt and D. P. Riley, Phil. Trans. Roy. Soc. London **A247**, 409 (1955).

[30] A. Elliott and B. R. Malcolm, Proc. Roy. Soc. (London) **A249**, 30 (1959).

exhibit absorption bands whose maxima lie at wavelengths greater than 148 mμ, terms involving these new λ_i must be added to Eq. (8). One new absorption band adds four new terms. The coefficients of these new terms may be negligible if the chromophore on the side chain has enough freedom of rotation; however, in general, they would make a significant contribution to the optical rotatory dispersion. They also make a significant contribution to the difficulty in determining the sense and amount of helix in the polypeptide.

A linear interpolation between points corresponding to 100% and 0% helix has sometimes been used to obtain the helix content of a particular polypeptide. This method is valid only if the regions of helix and the regions of coil in the molecule are large enough so that the fraction of residues in the transition region between helix and coil is small.

Considering $[m_{33}']$ instead of $[m]$, one can become more certain of the helical sense, but the problem of absolute helical content remains intractable.

With these general and rather pessimistic statements as background we can summarize our present results. We have given a simple derivation for a polarizability approximation to the optical activity along specific directions in a molecule. Using this approximation we find good agreement between calculated and observed rotatory dispersion for helical polypeptides. The agreement favors left-handed helices for polybenzyl-L-glutamate (and other peptides with similar rotatory behavior), but it is not conclusive. As most other authors choose right-handed helices (and there has been so much coincidence between experiments and theory in this field in the past), we must point out that our results are based on the use of particular model and a particular theory of optical activity. However, by presenting the results we submit them for further testing. An obvious test is to measure $[m']$ and $[m_{33}']$ for helices of polyalanine in solution from $\lambda = 250$ mμ to 750 mμ.

ACKNOWLEDGMENTS

We wish to thank Professor D. D. Fitts for helpful advice in the early stages of this work. We also appreciate the assistance of Mr. R. Exley, Mr. B. Gong, and Mr. F. Miller in the calculations.

THE JOURNAL OF CHEMICAL PHYSICS VOLUME 32, NUMBER 2 FEBRUARY, 1960

Nature of the Free Electron Model. The Simple Case of the Symmetric Polymethines

H. KUHN, W. HUBER, G. HANDSCHIG, H. MARTIN, F. SCHÄFER, AND F. BÄR

Physikalisch-Chemisches Institut der Universität, Marburg/Lahn, Germany

(Received August 4, 1958)

In the case of the polymethines

$$H_2C{=}CH(CH{=}CH)_{i-1}\overset{\oplus}{C}H_2$$

and

$$H_2C{=}CH(CH{=}CH)_{i-1}\overset{\ominus}{C}H_2$$

the wave functions and energy levels of the π electrons given by the one-dimensional free electron model are compared with those given by more elaborate methods in which the π electrons are treated as electrons in a one- or two-dimensional core potential obtained from nuclear charge and shielding considerations. The results of the three treatments are in good agreement, and thus the reliability of the simple free electron model is justified.

WE can distinguish three stages of refinement in the type of electron gas model used in this laboratory[1]: (a) the one-dimensional free-electron model; (b) the one-dimensional wave shape potential model; (c) the two-dimensional potential trough model. The results of models (a), (b), and (c) shall be compared here in the simple case of the hypothetical ion with resonating structures

$$H_2C{=}CH{-}CH{=}CH{-}CH{=}CH{-}\overset{\ominus}{C}H_2$$

$$\overset{\ominus}{H_2}C{-}CH{=}CH{-}CH{=}CH{-}CH{=}CH_2.$$

[1] See H. Kuhn, Chimia 9, 237 (1955).

In model (a) the π electrons are treated as electrons in the one-dimensional potential well of Fig. 1(a) of length $L = 8l$ where l is the CC $1\frac{1}{2}$—bond distance 1.39 A, and L is the length of the zig-zag line of the CC bonds, including one bond length to either side of each terminal carbon atom. The energy levels $E_n = (h^2n^2)/(8mL^2)$ of the π electron states thus obtained are shown in Fig. 2(a) and the wave functions $\psi_n = (2/L)^{\frac{1}{2}} \sin(ns/L)\pi$ are given in Fig. 3 by dotted lines. Here h = Planck's constant, m = electron mass, n = 1; 2; 3; ···.

In model (b) the π electrons are treated as electrons in a potential $V(s)$ given in Fig. 1(b). Physically, $V(s)$ is the potential of a π electron in the field of the rest of

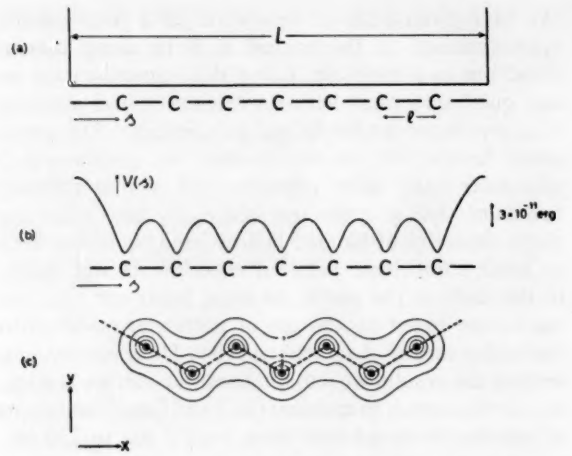

FIG. 1. Potential troughs of models (a), (b), and (c). The levels of the contour lines in the case of model (c) are indicated in units of 10^{-11} erg.

the molecule, averaged over the coordinates orthogonal to the zigzag line connecting the carbon atoms. The potential $V(s)$ is obtained as the sum of contributions of each carbon atom, where the contribution of each carbon atom is found from nuclear charge and shielding considerations,[2] and each CC bond length is assumed to be 1.39 A. With an electric analog computer developed in this laboratory, the wave functions of the stationary states of an electron in this potential can easily be obtained. They are given in Fig. 3 by dashed lines, and the energy levels of these states are shown in Fig. 2(b).

In model (c) the π electrons are treated as electrons in the two dimensional potential $V(x, y)$ of Fig. 1(c). The function $V(x, y)$ represents the potential of a π

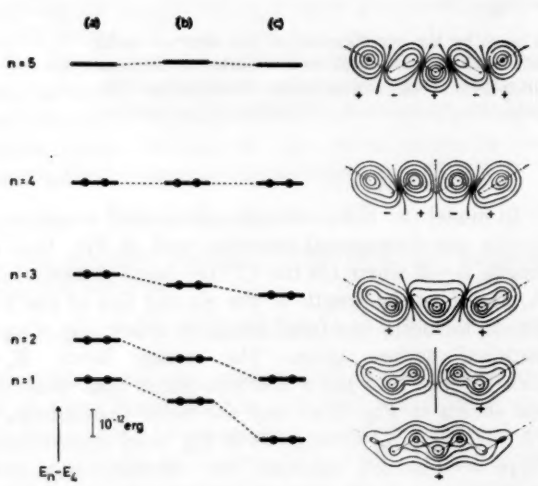

FIG. 2. Energy levels resulting from models (a), (b), and (c) and wave functions from model (c).

[2] Huber, Hornig, and Kuhn, Z. physik. Chem. **9**, 1 (1956); J. Chem. Phys. **25**, 1296 (1956).

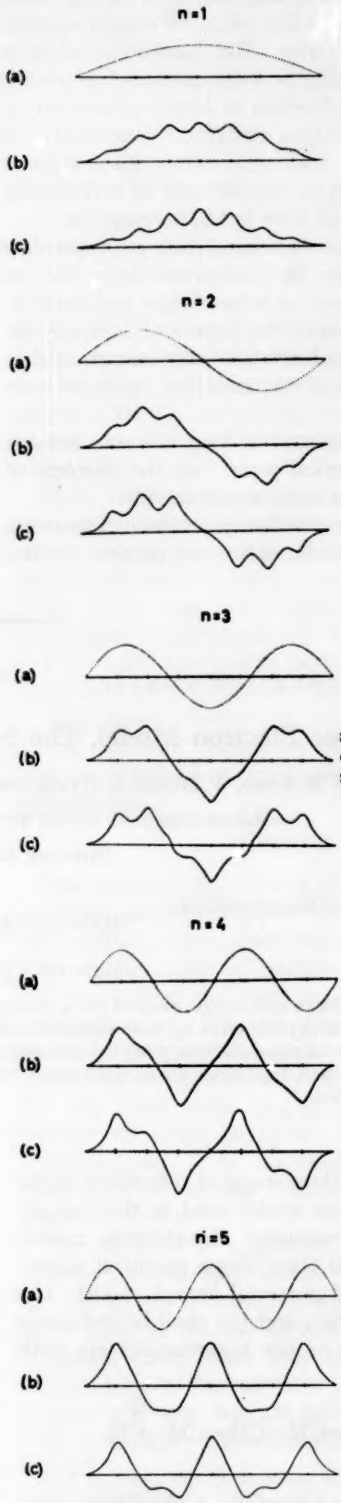

FIG. 3. Wave functions along the zigzag line of the carbon atom skeleton resulting from models (a), (b), and (c).

electron averaged over z, the coordinate perpendicular to the plane of all nuclei of this flat molecule. It is calculated as the sum of contributions of each carbon atom. For finding the contribution of a given atom we made the following assumptions: I. The charge of the atom is completely shielded by other electrons and its contribution is thus neglected if the projection on the xy plane of the position of the electron considered is outside a circle of radius 1.39 A about this atom. II. If this projection is inside that circle, the electron is in the Coulomb field of a charge of 3.25 e_0 (Slater effective charge of carbon) placed in the center of the atom. III. The contribution to be determined is the z average of the potential energy of the electron in this field and this average is found by assuming that the wave function of the electron depends on z as a Slater type p_z atomic orbital. The total potential was obtained by superposing the contributions of each atom, assuming equal CC bond distances of 1.39 A and CCC bond angles of 120°. Again by using an electric analog computer[1] the wave functions and energy levels of an electron in the potential field of Fig. 1(c) can be obtained and they are given in Fig. 2(c). The course of the wave functions along the zig-zag line of the carbon atom skeleton [(dashed line in Fig. 1(c) and Fig. 2)] is shown in Fig. 3 by solid lines. Evidently each one dimensional wave function resulting from models (a) and (b) gives approximately the course of the corresponding two-dimensional wave function along the chain. The positions of corresponding energy levels resulting from the three models (Fig. 2) agree surprisingly well (remember length L in model a) was not adjusted; we simply took $L=8l$ according to the original paper[3]). A similar result was found for other members of the homologous series of polymethines

$$H_2C{=}CH{-}(CH{=}CH)_{j-1}{-}\overset{\ominus}{C}H_2.$$

Table I gives the maximum of the first absorption band of these unknown ions predicted from models (a), (b), and (c), respectively. The table also gives the maximum of the first band of the unknown cations

$$H_2C{=}CH{-}(CH{=}CH)_{j-1}{-}\overset{\oplus}{C}H_2,$$

calculated by assuming the same potential trough as for the corresponding anions. Since each cation has two fewer electrons than the corresponding anion, the first band of the cation results from a transition between the states j and $j+1$, whereas the first anion band results from transition between the states $j+1$ and $j+2$.

TABLE I. Wavelength of the first absorption maximum in millimicrons resulting from models (a), (b), and (c).

	Anion			Cation		
j	(a)	(b)	(c)	(a)	(b)	(c)
1	204	220	275	340	260	230
2	328	330	335	458	390	360
3	453	440	450	581	520	490
4	581	590	550	707	640	620
5	707	690	685	831	810	750

ACKNOWLEDGMENTS

This work has been supported by the Deutsche Forschungsgemeinschaft and by the Deutscher Verband der Chemischen Industrie.

[3] H. Kuhn, Helv. Chim. Acta **31**, 1441 (1948).

Nature of the Free Electron Model. The Case of the Polyenes and Polyacetylenes

F. BÄR, W. HUBER, G. HANDSCHIG, H. MARTIN, AND H. KUHN

Physikalisch-Chemisches Institut der Universität, Marburg/Lahn, Germany

(Received July 7, 1959)

The wave functions and energy levels of the polyenes and polyacetylenes found on the basis of the simple sine curve potential model are compared with those given by more refined methods in which the π electrons are treated as electrons in a one-, two-, or three-dimensional core potential obtained from nuclear charge and shielding considerations. The results of the four treatments are in good agreement, and by considering the electron density distribution along the chain each treatment leads to the same conclusion, that each single bond and each double (or triple) bond in a long-chain polyene (or polyacetylene) must have, respectively, the same length as the single bond and double (or triple) bond in butadiene (or diacetylene). The values of the absorption maxima given by the four models are in good agreement with the experimental values.

IN contrast to the case of the symmetrical polymethines considered before[1] the simplest free electron model does not lead to a suitable description of the polyenes and polyacetylenes, because of the bond alternation found in the latter cases[2]), and the following stages of refinement may be distinguished here: (a) sine curve potential model, (b) one-dimensional wave shape potential model, (c) two-dimensional potential trough model, and in the particular case of the polyacetylenes (d) three-dimensional potential field model.

Let us consider a polyene with j conjugated double bonds. In model (a) the π electrons are treated as electrons in the one-dimensional potential of length $L=(i+\frac{1}{2})(l_1+l_2)$ [Fig. 1(a)] and wave amplitude $V_0=2.4$ ev, where $l_1=1.47$ A (single bond distance) and $l_2=1.35$ A (double bond distance). In models (b) and (c) the π electrons are treated as electrons in the potentials $V(s)$ and $V(x, y)$ given for $j=3$ in Fig. 1(b) and (c), respectively. $V(s)$ and $V(x, y)$ are found in the manner described before[1] by superposing the contributions of each C atom[3]; the foregoing values $l_1=1.47$ A and $l_2=1.35$ A (the values measured in butadiene[4]) have been used for all single and double bond distances and a CCC bond angle of 122° was assumed in the case of model (c).

By using an electrical analog computer[5] the wave functions and energy levels of an electron in these potential fields can be obtained and they are given in Figs. 2 and 3. The course of the two-dimensional wave functions of model (c) along the zig zag line of the carbon skeleton [dashed line in Fig. 2(c)] is shown in Fig. 3(c). The positions of corresponding energy levels (Fig. 2) and the shape of corresponding wave functions (Fig. 3) resulting from the three models agree sur-

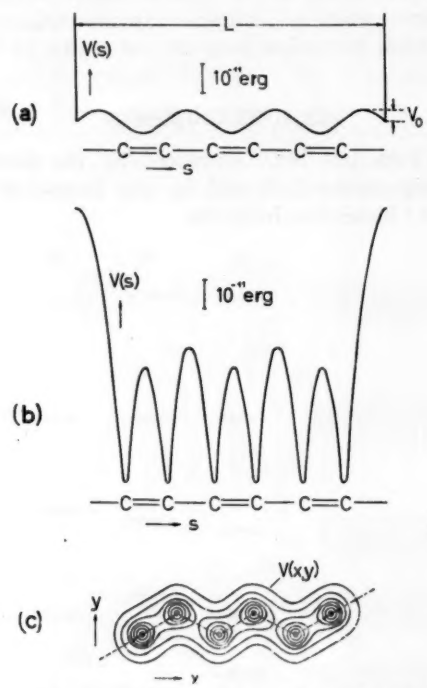

FIG. 1. Polyene with $j=3$. Potential troughs according to models (a), (b), and (c). Contour line spacing in Fig. 1(c): 2.5 10^{-11} erg.

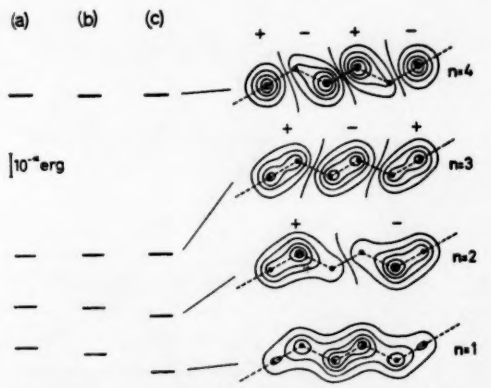

FIG. 2. Polyene with $j=3$. Energy levels resulting from models (a), (b), and (c) and wave functions according to model (c).

[1] Kuhn, Huber, Handschig, Martin, Schäfer, and Bär, J. Chem. Phys. **31**, 467 (1960).
[2] H. Kuhn, J. Chem. Phys. **16**, 840 (1948); **17**, 1198 (1949).
[3] Kuhn, Huber, and Bär, *Calcul des fonctions d'onde moleculaires* (Centre National Recherche Science, Paris, 1958), p. 179.
[4] P. W. Allen and L. E. Sutton, Acta Cryst. **3**, 46 (1950).
[5] Cf. H. Kuhn, Angew Chem. **71**, 93 (1959).

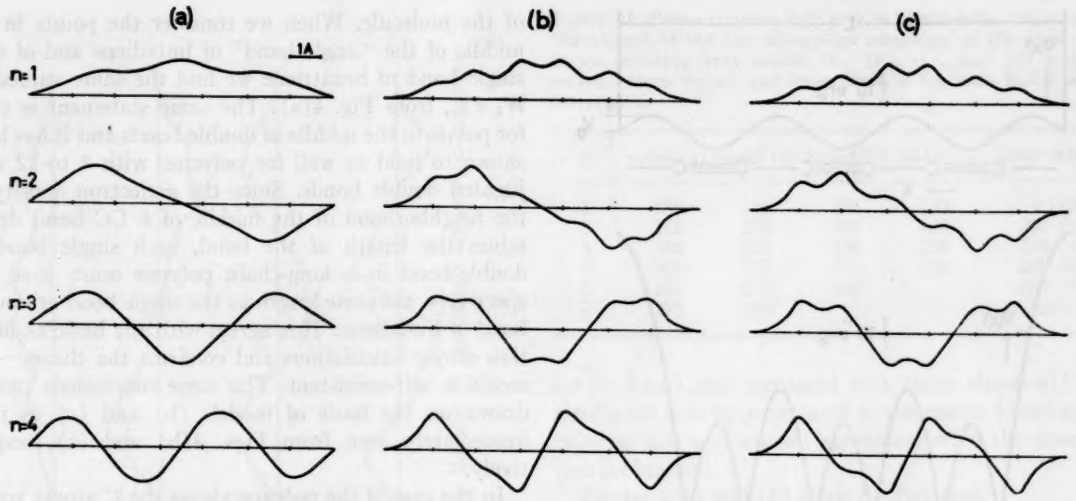

FIG. 3. Polyene with $j=3$. Wave functions according to models (a) and (b). Course of wave functions along the line of the carbon skeleton according to model (c).

prisingly well. A similar result was found for other values of j. For the cases $j=2$ to 12 Table I gives the wavelength λ_{max} of the maximum of the first absorption band resulting from models (a) and (b) as well as the observed data.[6] [In the case of model (c) the λ_{max} values 220 and 290 mμ are found for $j=2$ and 3, respectively.] A good agreement between calculated and observed values is found in each case.

Figures 4(a) and 4(b) show the function,

$$W_1(s)=\sum_{n=1}^{j}2\psi_n^2(s),$$

resulting in the cases $j=2$ and 3 from models (a) and (b). Here $\psi_n(s)$ is the one-dimensional wave function of the nth state normalized such that

$$\int_{-\infty}^{+\infty}\psi_n^2 ds=1.$$

$W_1 ds$ is the probability of finding a π electron (in the ground state of the molecule) in the space between two surfaces (σ_s and σ_{s+ds}) of a certain infinite set of surfaces orthogonal to the carbon atom skeleton; σ_s cuts the zig zag line of the C atoms at point s, σ_{s+ds} at point $s+ds$. Figure 4(c) shows the function

$$W_2(x,y)=\sum_{n=1}^{j}2\psi_n^2(x,y)$$

resulting from model (c), $\psi_n(x,y)$ is the two-dimensional wave function given by model (c) normalized according to

$$\int_{x=-\infty}^{+\infty}\int_{y=-\infty}^{+\infty}\psi_n^2 dxdy=1.$$

$W_2 dxdy$ is the probability of finding a π electron whose projection on the xy plane (plane of the centers of all atoms in the flat molecule) is within the surface element $dxdy$. W_1 and W_2 are measures of the over-all π-electron density distribution along the chain in the ground state

TABLE I. Polyenes with $j=2$ to 12 conjugated double bonds. Wave length of the main maximum of the first absorption band in mμ resulting from models (a) and (b) and observed values (upper and lower limit of the data found in the literature).

j	model (a)	model (b)	observation
2	238	214	217–235
3	286	280	260–282
4	323	333	295–308
5	352	362	326–348
6	377	389	352–371
7	396	417	374–403
8	413	442	396–422
9	428	449	413–447
10	440	465	432–461
11	451	469	449–473
12	460	479	461–482

[6] Cf. reference 3 where the original literature is given.

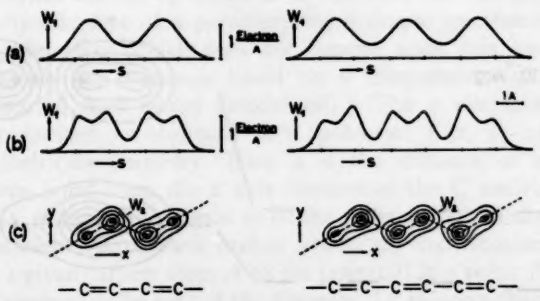

FIG. 4. Polyenes with $j=2$ and 3. Ground state. Charge density distributions of the π electrons according to models (a), (b), and (c). Contour line spacing in Fig. 4(c): 0.35 electrons/A^2. Note the large difference between the density at the single bonds and the double bonds. For $j=3$ one finds the same pronounced difference between alternating short and long bonds (double and single bonds) as in the case of $j=2$.

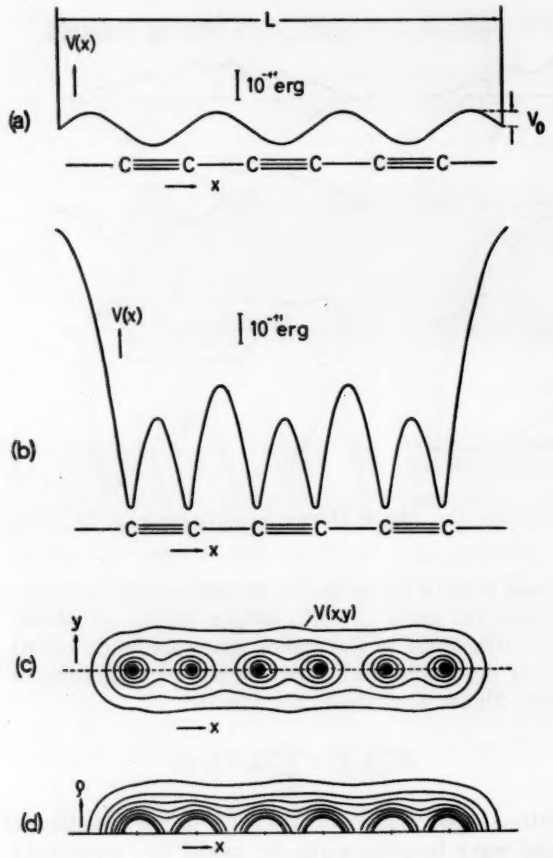

FIG. 5. Polyacetylene with $j=3$. Potential troughs of models (a), (b), (c), and (d). C atoms on x axis; ρ distance of a given point from the x axis. Contour line spacing 2.5×10^{-11} erg in (c) and (d).

of the molecule. When we consider the points in the middle of the "single bond" of butadiene and of each single bond of hexatriene we find the same values for W_1 e.g., from Fig. 4(a). The same statement is valid for points in the middle of double bonds and it has been shown to hold as well for polyenes with 4 to 12 conjugated double bonds. Since the π-electron density in the neighborhood of the middle of a CC bond determines the length of the bond, each single bond or double bond in a long-chain polyene must have, respectively, the same length as the single bond or double bond of butadiene. This agrees with the basic assumption of our calculations and confirms the theory—the model is self-consistent. The same conclusions can be drawn on the basis of models (b) and (c) as it is immediately seen from Figs. 4(b) and (c), respectively.

In the case of the polyacetylenes the C atoms are on a straight line (x axis) and since the correlation of the π_y and π_z electrons is here neglected, the treatment can be restricted to a consideration of the π_z electrons. With models (a), (b), and (c) the potential fields given in Figs. 5(a), (b), and (c) are found in the particular case $j=3$ (j=number of conjugated triple bonds). It is assumed that $V_0=3.4$ ev in the case of Fig. 5(a) and the potentials of Fig. 5(b) and (c) are obtained by using the same contribution for a C atom as in the polyene and polymethine cases. The values $l_1=1.36$ A and $l_3=1.20$ A are used for the length of each single and triple bond, respectively, i.e., the values found in diacetylene.[7] The energy levels and the wave functions thus obtained are given in Figs. 6 and 7. The wavelengths of the absorption maxima obtained by models (a), (b), and (c), respectively, are given in Table II

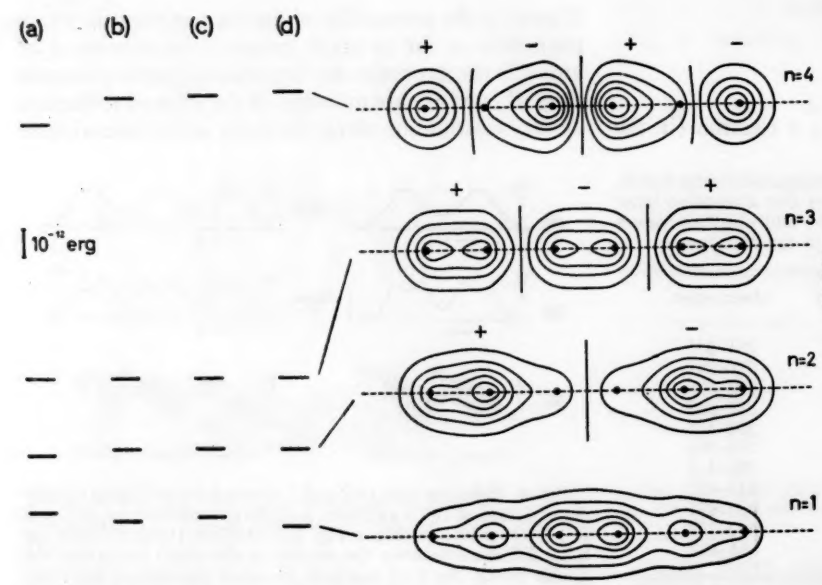

FIG. 6. Polyacetylene with $j=3$. Energy levels resulting from models (a), (b), (c), and (d) and wave functions according to model (c).

[7] Pauling, Springall, and Palmer, J. Am. Chem. Soc. **61**, 927 (1939).

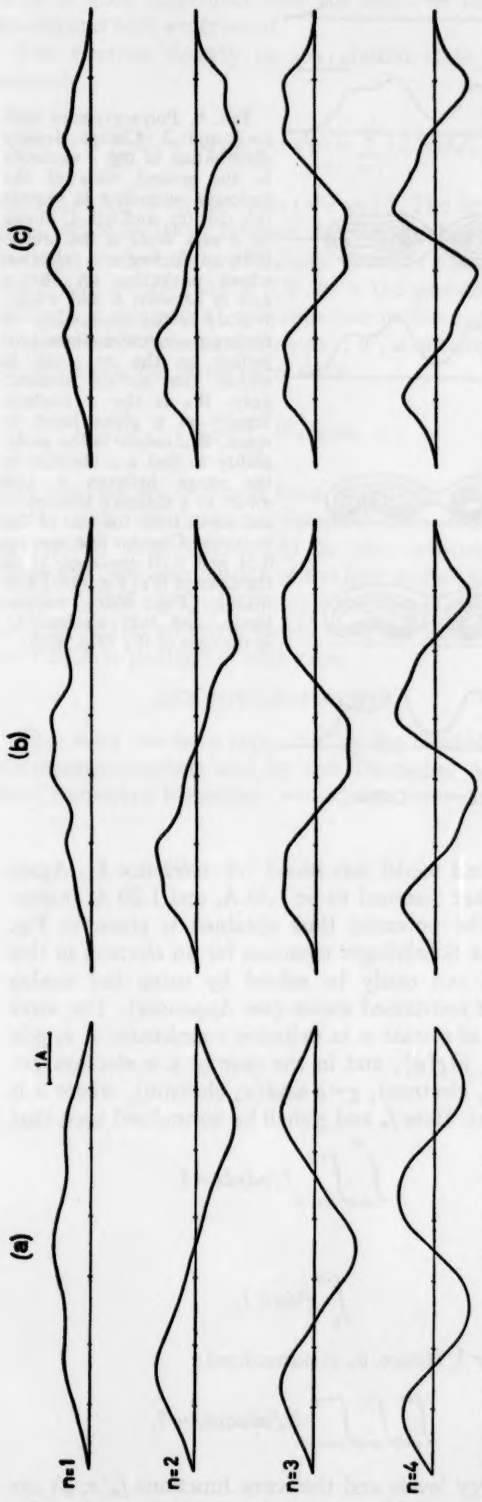

FIG. 7. Polyacetylene with $j=3$. Wave functions according to models (a) and (b). Course of wave functions along the line of the carbon skeleton according to model (c).

TABLE II. Polyacetylenes with $j=2$ to 7 conjugated triple bonds. Wavelength of the first absorption maximum of the main band in $m\mu$ resulting from models (a), (b), (c), and (d) and observed values (upper and lower limit of the data found in the literature).

j	model (a)	model (b)	model (c)	model (d)	observation
2	188	159	155	153	<165
3	222	203	200	199	207–213
4	246	235	234	234	234–240
5	266	257	255	258	260–265
6	282	275	268		284–289
7	295	285			311

for $j=2$ to 7 and compared with those observed.[8] The results are seen to correspond to the results found in the polyene case and a good agreement with the observation is obtained.

Figures 8(a) and (b) show the function,

$$W_1(x)=\sum_{n=1}^{j}4\psi_n^2(x),$$

obtained on the basis of models (a) and (b), respectively. W_1dx is the probability of finding a π electron (in the ground state of the molecule) in the space between two planes perpendicular to the x axis and cutting this axis at points x and $x+dx$, respectively. Figure 8(c) refers to model (c) and shows the functions

$$W_2(x,y)=\sum_{n=1}^{j}2\psi_n^2(x,y) \quad \text{and} \quad W_1(x)=2\int_{-\infty}^{+\infty}W_2dy.$$

W_2dxdy is the probability of finding a π_z electron whose projection on the xy plane is within the surface element $dxdy$. W_1 is easily obtained from W_2 by a numerical integration. The functions W_1 obtained from models (a), (b), and (c) practically agree with each other, and in the manner just indicated the models are found to be self-consistent.

As mentioned before, the two-dimensional potential trough model is based on the assumption that the part of the wave function depending on coordinate z is identical for all π_z electrons in the molecule. In the particular case of a polyacetylene a simple treatment can be given which does not depend upon this hypothesis and which is based on a three-dimensional potential field model [model (d)]. The π electrons are treated as electrons in a potential $V(x,\rho)$ of cylindrical symmetry. Here ρ is the distance of a given point from the x axis connecting the C nuclei. $V(x,\rho)$ is assumed again to be the superposition of the contributions of each carbon atom; the contribution of a given carbon atom A to the potential in a point P is assumed to be zero, if the distance AP is larger than 1.5 A; if the distance AP is smaller than 1.5 A the contribution of atom A to the potential at P is assumed to be identical with the Coulomb potential of a charge

[8] F. Bohlmann, Ber. **86**, 63, 657 (1953); Armitage, Cook, Jones, and Whiting, J. Chem. Soc. **1952**, 2010, 2014, 2883.

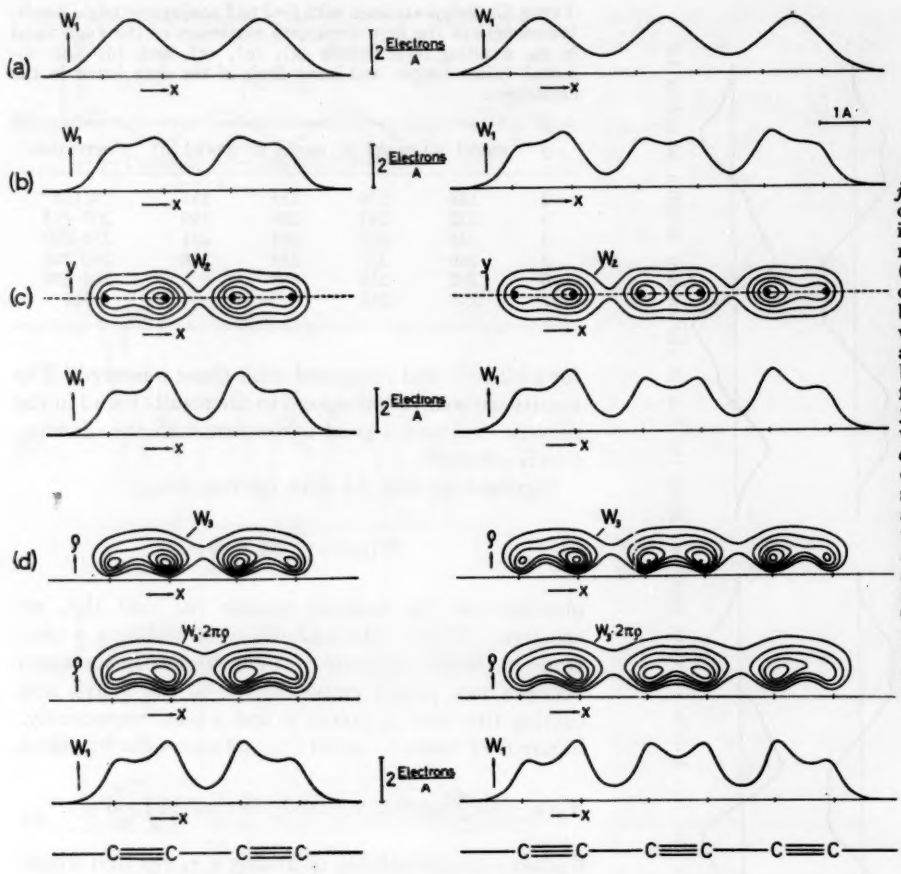

FIG. 8. Polyacetylenes with $j=2$ and 3. Charge density distribution of the π electrons in the ground state of the molecule according to models (a), (b), (c), and (d). C atoms on x axis. W_1dx is the probability of finding a π electron whose projection on the x axis is between x and $x+dx$. W_2dxdy is the probability of finding a π_z electron whose projection on the xy plane is within the surface element $dxdy$. W_3 is the π electron density at a given point in space. $W_3 2\pi\rho d\rho dx$ is the probability to find a π electron in the range between x and $x+dx$ in a distance between ρ and $\rho+d\rho$ from the axis of the molecule. Contour line spacing 0.35 and 0.70 electrons/A^2 in the cases of W_2 [Fig. 8(c)] and $W_3 2\pi\rho$ [Fig. 8(d)], respectively, and 0.26 electron/A^3 in the case of W_3 (Fig. 8(d)).

of 3.25 e_0 located at the center of atom A, the zero of the potential of this charge being fixed to a distance 1.5 A away from the charge. This charge of 3.25 e_0 is the Slater effective charge of carbon, and $-e_0$ is the charge of the electron. These assumptions are closely analogous to the assumptions on which the two-dimensional model was based (cf. reference 1). Again l_1 and l_3 are assumed to be 1.36 A, and 1.20 A, respectively. The potential thus obtained is given in Fig. 5(d). The Schrödinger equation for an electron in this potential can easily be solved by using the analog computer mentioned above (see Appendix). The wave function of a state n in cylindric coordinates x, ρ, ϕ is $\psi_n=f_n(x,\rho)g(\phi)$, and in the case of a π electron $g=a\cos\phi$(π_y electron), $g=a\sin\phi$(π_z electron), where a is a constant. Here f_n and g shall be normalized such that

$$\int_{\rho=0}^{\infty}\int_{x=-\infty}^{+\infty} f_n^2\rho d\rho dx=1$$

and

$$\int_0^{2\pi} g^2 d\phi=1,$$

thus $a=\pi^{-1}$. Hence, ψ_n is normalized:

$$\int_{\phi=0}^{2\pi}\int_{\rho=0}^{\infty}\int_{x=-\infty}^{+\infty}\psi_n^2\rho d\phi d\rho dx=1.$$

The energy levels and the wave functions $f_n(x,\rho)$ are shown in Figs. 6(d) and 9, and in Table II are given the wavelengths of the absorption maxima thus obtained

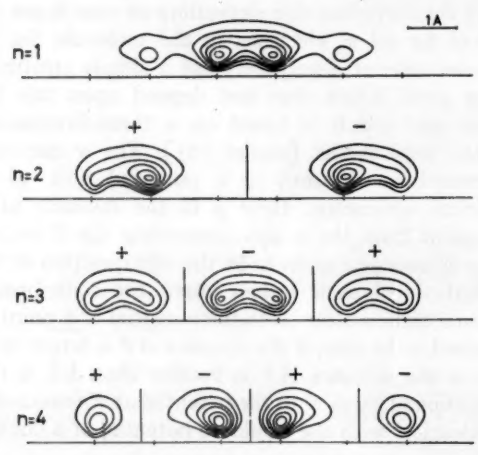

FIG. 9. Polyacetylene with $j=3$. Wave functions $f_n(x,\rho)$ according to model (d).

in the cases $j=2$ to 5. The values calculated are found to be in good agreement with the result of the other models and with experiment.

The electron density in the ground state of the molecule,

$$W_3(x,\rho)=\sum_{n=1}^{j}2f_n^2a^2(\sin^2\phi+\cos^2\phi)=\sum_{n=1}^{j}(2/\pi)f_n^2,$$

is given in Fig. 8 for the cases $j=2$ and 3. The figure also gives $W_3\times 2\pi\rho(W_3\times 2\pi\rho d\rho dx$ is the probability of finding a π electron in the range between ρ and $\rho+d\rho$ and x and $x+dx$) and $W_1(W_1dx$ is the probability of finding a π electron whose projection to the x axis is in the interval between x and $x+dx$); W_1 is obtained from W_3 by numerical integration since

$$W_1=\int_0^\infty W_3 2\pi\rho d\rho.$$

The function W_1 obtained from model (d) practically agrees with the function obtained from model (c) and shows that model (d) is also self-consistent. Thus, the basic assumption of the four models that in a polyacetylene all single bonds have the same lengths $l_1=1.36$ A and all triple bonds have the same lengths $l_3=1.20$ A is justified in each case.

ACKNOWLEDGMENTS

This work has been supported by the Deutsche Forschungsgemeinschaft and by the Deutscher Verband der Chemischen Industrie.

APPENDIX

As shown in the following the problem of solving the Schrödinger equation

$$(1/\rho)(\partial/\partial\rho)[\rho(\partial\psi/\partial\rho)]+(1/\rho^2)(\partial^2\psi/\partial\phi^2)+(\partial^2\psi/\partial x^2)+(8\pi^2\mu/h^2)[E-V(x,\rho)]\psi=0 \quad (1)$$

of an electron (mass μ) in the potential $V(x,\rho)$ of Fig. 5(d) can be reduced to the problem of solving the Schrödinger equation

$$(\partial^2F/\partial x^2)+(\partial^2F/\partial y^2)+(8\pi^2\mu/h^2)[E-V'(x,y)]=0 \quad (2)$$

of an electron in a potential $V'(x,y)$ given in two-dimensional cartesian coordinates. The latter problem can be solved by using the analog computer developed in our laboratory. As is well known, (1) can be separated if we put $\psi=f(x,\rho)g(\phi)$ and the eigenfunctions $g=\text{const}\times\exp(im\phi)$ are found, where $m=0,\ \pm1,\ \pm2,\ \cdots$. For solving the differential equation for the function $f(x,\rho)$ the substitution $f(x,\rho)=F(x,\rho)\times\rho^{-\frac{1}{2}}$ can be introduced and Eq. (2) is then obtained if we set

$$V'=V+(h^2/8\pi^2\mu\rho^2)(m^2-\tfrac{1}{4})$$

and $y=\rho$. In the case of a π electron considered here, $|m|=1$ and thus

$$V'=V+(3h^2/32\pi^2\mu\rho^2).$$

THE JOURNAL OF CHEMICAL PHYSICS VOLUME 32, NUMBER 2 FEBRUARY, 1960

Transmission Measurements with Cold Neutrons in Hydrogenous Liquids*

R. NASUHOGLU† AND G. R. RINGO

Argonne National Laboratory, Lemont, Illinois

(Received September 16, 1959)

Measurements have been made of the transmission cross sections of several series of organic liquids for neutrons in the wavelength region of 5–20 A. These cross sections should show effects from weak bonds, since the scattering cross section of hydrogen is quite sensitive to the binding of hydrogen. Results of the measurements and a description of the helical velocity selector used in making them are given. The results give evidence that the motions of the hydrogens of the methyl group are relatively free in liquids.

I. INTRODUCTION

SINCE Fermi's classic paper[1] on the motion of neutrons in hydrogenous media, it has been realized that the cross section of hydrogen for the scattering of thermal neutrons is quite sensitive to the binding of the hydrogen. For a free (but initially stationary) hydrogen atom, the cross section is about 20 barns; while it is 80 barns for a tightly bound one—i.e., one whose binding energy is greater than the kinetic energy of the incident neutrons. Thus the scattering of cold neutrons which will be of concern here should be affected by possible rotational states that can be excited and to more complicated motions in liquids and solids.

Moreover, another effect makes the hydrogen cross section sensitive to the molecular state of the hydrogen. This arises from the fact that the measured cross section depends on the velocity of the target nuclei. The dependence is easily understood by remembering that the reaction rate is the same in all coordinate systems (in the nonrelativistic approximation). Hence

$$\sigma_{\text{lab}} v_{\text{lab}} = \sigma_0 v_{\text{rel}},$$

where σ_0 is the cross section of a stationary hydrogen atom for a neutron incident on it with velocity v_{rel}. For a gaseous target in which molecular rotation is ignored, this leads by straightforward calculation—including the effects of the center-of-mass motion which are determined by the binding and in this case are simplified by assuming rigid binding—to the result exemplified in Fig. 1 for neutrons of 10 A wavelength or 0.8×10^{-3} ev energy. In other words, in arriving at Fig. 1 we have considered a system having the nuclear properties of the proton and the kinematic properties of a "billiard ball" of the mass of interest. (The curve for a molecule of mass 18 in Fig. 7 shows how the cross section varies as a function of wavelength.) In Fig. 1 increasing mass is roughly equivalent to increasing molecular binding of hydrogen in a more realistic case. Note that the effect of the motion of the target nuclei is somewhat opposite to the effect of the binding and that the highest cross sections are not associated with strong binding (infinite mass) but, when both effects are taken into account, with an intermediate amount even in the simplified calculation of which the results are shown. For the neutrons of long wavelength ($\lambda>10$ A), then, it is roughly true that the greater the binding of the hydrogen the lower the cross section, since the effective mass of the hydrogen turns out to be greater than 3 in essentially every case.

In addition to these two effects a number of other effects, of less importance for hydrogenous materials, influence the cross sections. These include, for example, the coherent scattering, which is sensitive to structural details of the appopriate size. In short, a complete treatment of the scattering of thermal neutrons by any material is a severe test of our understanding of the structure of the material and its dynamic properties. Such treatments are available for the simpler gases.[2] In the case of solids and liquids, however, while the basic neutron interactions all are believed to be well enough known and the general method of handling the problem is probably clear,[3] not enough is known about the properties of the materials involved. In fact, of course, the chief current interest in the scattering of thermal neutrons is to use the scattering as a technique to learn more of the structure and dynamics of solids and liquids. Liquids in particular present an especially difficult problem. While van Hove and Placzek[3] have suggested direct methods for using neutrons to study the average structure of liquids and their vibration spectra, these methods involve the measurement of the spectra of neutrons scattered in particular directions from a sample irradiated by monoenergetic neutrons. This is a comparatively difficult and slow technique.[4] It therefore seemed to be of interest to approach the study empirically and see if any light could be shed by systematic measurements of neutron transmission in liquids. On the ground of their probable sensitivity to details of

* Work performed under the auspices of the U. S. Atomic Energy Commission.

† On leave from the University of Ankara, Ankara, Turkey (now returned).

[1] E. Fermi, Ricerca sci. **7** No. 2,13 (1936). English translation by G. M. Temmer, Document NP-2385, U. S. Atomic Energy Commission TIS Oak Ridge, Tennessee.

[2] R. M. Mazo and A. C. Zemach, Phys. Rev. **109**, 1564 (1958); A. C. Zemach and R. J. Glauber, *ibid.* **101**, 118, 129 (1956).

[3] G. Placzek and L. van Hove, Phys. Rev. **93**, 1207 (1954); L. van Hove, *ibid.* **95**, 249 (1954).

[4] Eisenhauer, Pelah, Hughes, and Palevsky, Phys. Rev. **109**, 1046 (1958); and references therein.

the chemical structure, as discussed above, this study has emphasized long-wavelength neutrons.

II. DESCRIPTION OF VELOCITY SELECTOR

These measurements were made with neutrons monochromatized by a helical velocity selector placed at the Argonne research reactor, CP-5. Since this velocity selector has never been described, a description of it may be of interest.

Basically this neutron velocity selector is the same as the original one, which was constructed by Dunning, Pegram, Fink, Mitchell, and Segrè[5] about 1935. The selector consists of a series of disks with narrow radial slots mounted on a single shaft in such a way that the slots form helical channels running from the first to the last disk, spiraling around the shaft as an axis. If these channels make a complete revolution of the shaft in a distance L, it is obvious that the selector will pass neutrons traveling parallel to the shaft in the right direction and at a velocity given by $v=L\omega/2\pi$, where ω is the rotational velocity of the selector in rad/sec. It is almost as clear that the resolution of such a selector is approximately given by

$$(\Delta v/v)=2\alpha+(a/l)\,(v/R\omega). \qquad (1)$$

where Δv is the full range of velocities passed by the selector; α is the extreme angle that the external collimation permits between any neutron trajectory and the plane passing through the axis of the selector and the center of the collimating system (which is assumed to be symmetrical about such a plane); a is the width of the slots in the selector at the radial distance R from the axis of the selector; and l is the length from entrance to exit disks of the selector. This relation immediately makes it clear why these instruments are most useful with very slow neutrons. Engineering considerations limit the peripheral speed ωR of any rotor to about 200 m/sec (which cannot be exceeded substantially except by elaborate and somewhat risky constructions). Hence, a reasonable value of the velocity resolution when the neutron velocity v is much greater than 200 m/sec can be obtained only at the cost of the loss of intensity attendant on the use of a very narrow angular collimation α.

There are two principal advantages to this variety of velocity selector: (1) it is free from higher or lower order contamination; (2) as compared to the usual time-of-flight instrument, with either a chopper or a pulsed beam, this monochromator delivers neutrons a much greater fraction of the time. This can be very useful when interest is concentrated on a narrow energy range.

Figure 2 shows a cutaway view of the helical velocity selector which was used in this experiment. The rotor of this selector consists of a stack of disks identical to the one partially shown in the figure, mounted with a small key in a helical keyway milled in a shaft of 2-in. diam. The helix of the keyway (which of course determines the pitch of the selector) has a pitch giving it one full turn in 322 in. of shaft. The disks were made by punching sheets of 304 stainless steel about 0.031 in. thick. They were mounted along a total length of 12 in. of shaft. For the first 5 in. at one end, the disks were stacked solidly. For the remaining 7 in. they were cadmium-plated and then mounted in groups of three about 2 in. apart. In order to reduce noise and air resistance each group of slotted disks was put between two blank disks of aluminum. When this rotor was first assembled with the disks held on by large nuts at the two ends of the shaft, it proved impossible to achieve a stable dynamic balance, apparently because of small shifts in the positions of the disks on the shaft. A number of schemes for consolidating the disks and the shaft were tried without success until finally all the disks making up the solid 5 in. section of the rotor were copper-plated then copper-brazed together and to the shaft in a large hydrogen-atmosphere furnace at the General Electric Company in Schenectady, New York.

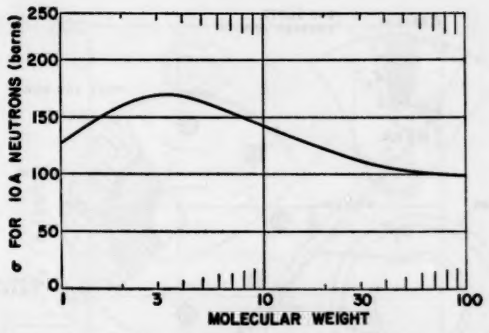

FIG. 1. The scattering cross section in the laboratory frame of reference for 10 A neutrons incident on a hydrogenous gas at 300°K. The hydrogen is assumed to be rigidly bound to a molecule of mass A and the contribution to the cross section is assumed to come entirely from one hydrogen atom per molecule. Rotations are ignored.

Because bearing failure was considered the most risky feature of the operation of the selector, thermistors were placed in the blocks of both rotor bearings to monitor the temperatures. If the temperature rose above about 60°C, the drive was shut off automatically. Prior to this, in a highspeed test of the strength of the disks, the rotor with three disks on it was driven to 12 000 rpm. The disks were not damaged by this but both bearings failed.

The rotor is driven by a 15-hp dc motor through a cogged belt arrangement giving a stepup of 2.568 in rotational speed relative to the motor and a pair of gears giving a further stepup of 2.00. In none of the experiments as yet performed with this selector has the neutron velocity or wavelength been of critical importance. The rotor speed has therefore been measured with a tachometer connected to the driving motor. The

[5] Dunning, Pegram, Fink, Mitchell, and Segrè, Phys. Rev. 48, 704 (1935).

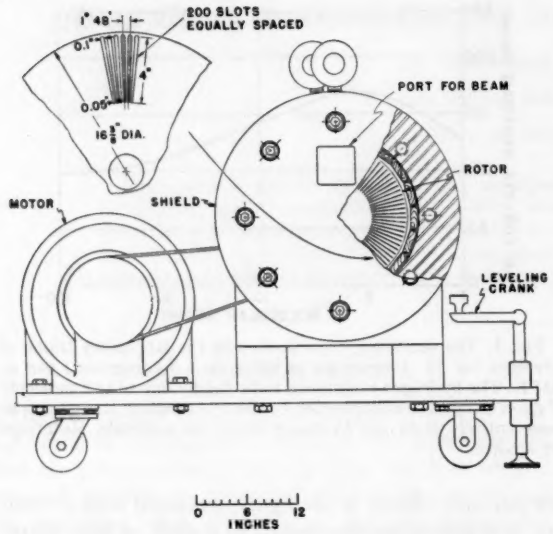

FIG. 2. Sketch of the helical velocity selector as viewed from the neutron source. The neutron beam travels in a direction perpendicular to the plane of the figure.

tachometer was in effect calibrated by measurement of the position of the Bragg cutoff in graphite (6.6 A neutrons)[6] and used to interpolate to other velocities. The driving motor is powered by a motor-generator set. After 10 min or so of operation the speed of the rotor can be held within about 1% with a minimum of attention. There should be no great difficulty in obtaining much closer control if desired.

For shielding against scattered radiation and protection against a rotor failure, the rotor was surrounded by a steel casting about 5 in. thick.

The detector used with this selector was a set of four BF_3 counters, 1 in. in diam and 8 in. long, filled with $B^{10}F_3$ to a pressure of about 25 cm Hg and used with the beam incident on them normal to their length. These detectors, which are quite inefficient for ordinary thermal neutrons, were chosen to discriminate in favor of the very slow neutrons with which this work was concerned. They were used inside a shield consisting of two layers of $\frac{1}{4}$-in. Boral and 8 in. of concrete block. In these circumstances background counting rates were about 200 cpm.

A similar but considerably simpler form of velocity selector has been built by Dash and Sommers.[7] They used a cylindrical rotor with slots milled parallel to its axis, the axis being placed at a small angle ($<10°$) to the direction of a neutron beam. This is a reasonable approximation to a helix and much easier to build. The helical selector can also use this scheme of varying the angle between the neutron beam and the axis of rotation. This might be useful if it were desirable to select neutrons of higher energy than could be passed at the highest usable speed when the beam and axis were parallel. Such a change of course would not circumvent the argument following Eq. (1) so the gain in high-velocity limit would be paid for in resolution.

A helical monochromator which produces pulses of monochromatized neutrons for later use in a time-of-flight apparatus has been built by Jacrot and Gobert[8] and helical monochromators to remove higher order reflections in crystal spectrometers have been built at Columbia University[9] and Saclay.[10] In the last use, of course, it is only necessary that $\Delta v/v<2$.

Some tentative efforts were made to enrich the long-wavelength end of the thermal neutron spectrum available from the thermal column of the Argonne Research Reactor but it was found that no materials placed in the source position inside the thermal column (i.e., at the inner end of a 5-ft hole in the graphite from which the beam was extracted) were better than the graphite itself. Hydrogenous materials in particular were appreciably worse. The idea of cooling the source point,[11] while attractive, was not seriously tried because of the expense. The spectrum of the neutrons coming from the thermal column as it was used is shown in Fig. 3 The temperature of the thermal column was about 50°C in this measurement.

III. MEASUREMENTS

The transmission cross sections of water, a series of alcohols, a series of organic acids, and benzene and cyclohexene were measured in the wavelength range from 5 to 20 A. All the measurements were made at 26° to 28°C in cells with glass windows about 1.5 mm apart. The transparent construction was needed to make sure that the measurements were not falsified by bubbles sticking to the windows.

The results of these measurements are shown in

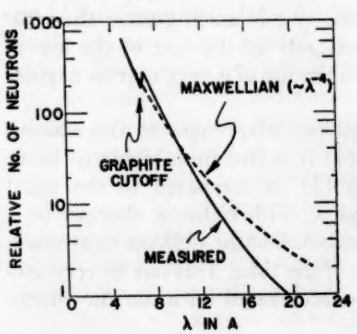

FIG. 3. The long-wavelength portion of the flux spectrum from a thermal column of the Argonne Research Reactor CP-5.

[6] It has been pointed out by F. T. Gould (Rept. CU-179, Columbia University, Department of Physics (October 1, 1958)] that graphite is not an ideal material for this purpose if a high accuracy is desired as its spacing is not extremely constant from one sample to the next [G. E. Bacon, Acta Cryst. **4**, 558 (1951)]. The likely errors in absolute value of wavelength are about ±0.1% which is not of importance for the present work.

[7] J. G. Dash and H. S. Sommers, Rev. Sci. Instr. **24**, 91 (1953).
[8] B. Jacrot and G. Gobert, J. phys. radium **19**, 82 (1958).
[9] F. T. Gould, Columbia University Department of Physics Rept. CU-179 (October 1, 1958).
[10] Hubert, Joly, and Signarbieux, J. phys. radium **19**, 79 (1958).
[11] Butterworth, Egelstaff, London, and Webb, Phil. Mag. **2**, (8) 917 (1957).

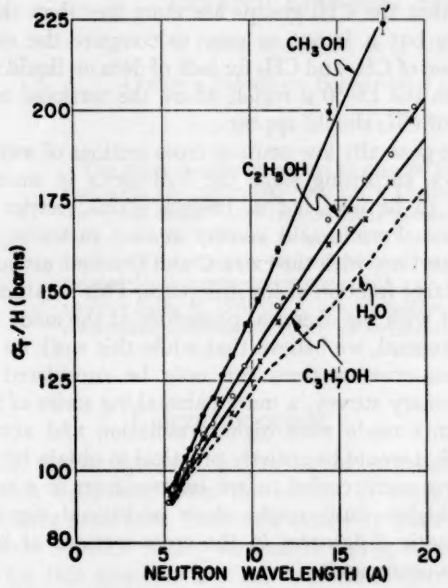

FIG. 4. Transmission cross sections of a series of alcohols. The cross sections shown are the total cross sections divided by the number of hydrogen atoms.

Figs. 4–7 where the transmission cross sections of these organic liquids and water are shown as the total cross section per molecule divided by the number of hydrogen atoms in each molecule. The question of the influence of the carbon and oxygen atoms on these cross sections is of course unsettled, but it seems unlikely that they add more than a few percent[12] and that this small contribution probably does not change much with wavelength (except for the $1/v$ effect). The uncertainties shown are simply the statistical ones. They include no estimate of the systematic uncertainties which arise chiefly, it is believed, from such causes as uncertainty in the thickness of the cell and the wavelength of the neutrons. The relative values of the cross sections should not be appreciably affected by these causes.

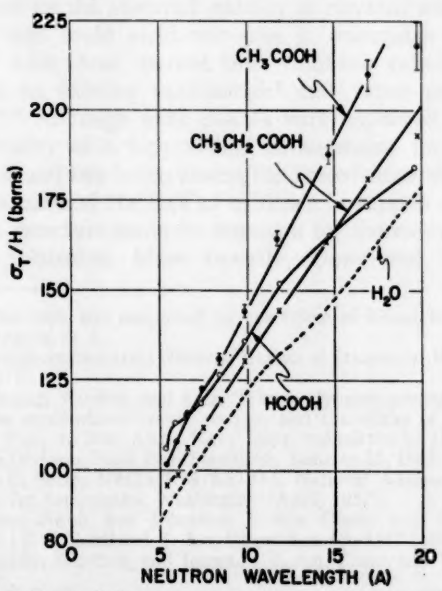

FIG. 5. Transmission cross sections of a series of organic acids, calculated as in Fig. 4.

[12] D. J. Hughes and R. B. Schwartz, "Neutron cross sections," Brookhaven National Laboratory Rept BNL-325 (July 1, 1958, unpublished) second edition.

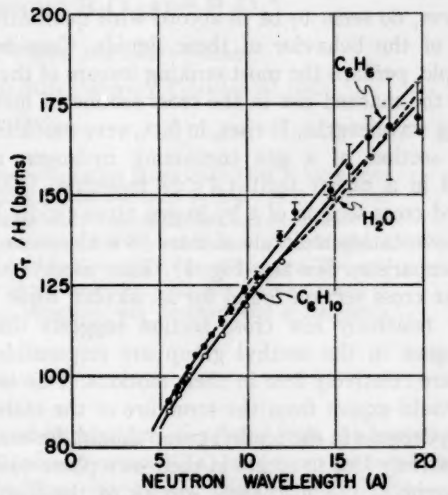

FIG. 6. Transmission cross sections of two cyclic materials calculated as in Fig. 4.

While these results bear out some of the hopes with which this study was started, in that the differences between various materials appear to be quite appreciable, it has not been possible to produce a clear interpretation of all the differences. Some of the major ones,

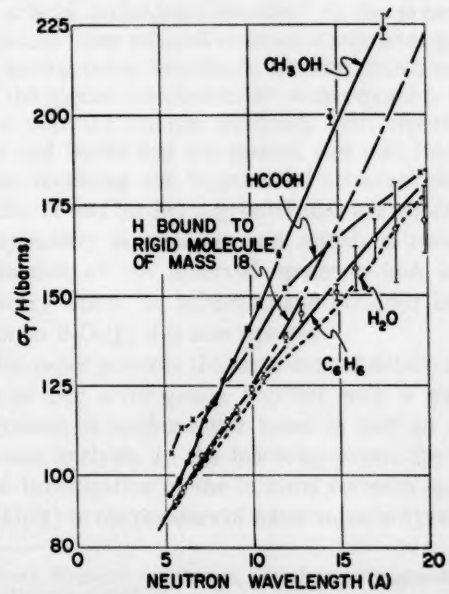

FIG. 7. Comparison of representative curves from previous figures. In the calculated curve for a hydrogen atom bound rigidly to a molecule of mass 18, the conditions are the same as in Fig. 1.

however, do seem to be in accord with qualitative notions of the behavior of these liquids. Consider, for example, perhaps the most striking feature of the set of data: the marked rise in the cross section of methanol at long wavelengths. It rises, in fact, very much like the cross section of a gas containing hydrogen rigidly bound in a rather light ($A<6$) molecule. (The calculated cross section of a hydrogen atom rigidly bound in a nonrotating molecule of mass 18 is shown in Fig. 7 for comparison. See also Fig. 1). That methyl has the highest cross section found for an alcohol while water has a relatively low cross section suggests that the hydrogens in the methyl group are responsible, i.e., they are relatively free in their motions. This is what one would expect from the structure of the molecules. The hydrogens in the methyl group should, for example, be relatively free to rotate in their own plane while the hydrogens of the methylene groups of the higher alcohols cannot rotate without carrying large parts of the molecule with them, a motion which is probably seriously inhibited in liquids. At room temperature, of course, optical vibrations are very little excited.

This notion about the character of the methyl group is supported by the fact that in the region of long neutron wavelengths (where the cross section is most sensitive to the velocity of the hydrogen atoms) the acid with the highest cross section is acetic acid, for which the methyl group is most important. Further evidence is furnished by the infrared spectra of the alcohols.[13] Certainly it is clear from the infrared data that the CH_3 groups are more free than the OH groups but it is not so easy to compare the relative freedom of CH_3 and CH_2 for lack of data on liquid methanol in the 15–50 μ region where the torsional oscillations of CH_3 should appear.

The generally low neutron cross sections of water are not too surprising since the hydrogens in water are likely to be involved in bridges which restrict their motions. Formic acid is very similar to water in its cross section, with the extra C and O atoms accounting for a large fraction of the difference. This is rather consistent with the chemical properties of the acid.

In general, we believe that while this work on slow-neutron cross sections can only be considered as a preliminary survey, a more painstaking series of measurements made with higher resolution and accuracy (which it would be entirely practical to obtain by using a source point cooled to low temperatures in a reactor with higher flux) might show additional significant systematic differences in the cross sections of hydrogenous compounds.

[13] E. K. Plyler, J. Research Natl. Bur. Standards **48**, 281 (1952).

ACKNOWLEDGMENTS

Obviously the design, construction, and placing in operation of the velocity selector involved the help of many people. We are particularly indebted to Mr. N. Hochstetler in the design, to Mr. B. Martinka and Mr. E. Klocek in the construction, and to Dr. V. Culler in placing the device in operation. We are also very much indebted to Dr. S. Wexler for advice on chemical problems.

THE JOURNAL OF CHEMICAL PHYSICS VOLUME 32, NUMBER 2 FEBRUARY, 1960

Infrared Emission Spectra of Gaseous B_2O_3 and B_2O_2*

DAVID WHITE, DAVID E. MANN,† PATRICK N. WALSH, AND ARMIN SOMMER

Cryogenic Laboratory, Department of Chemistry, The Ohio State University, Columbus 10, Ohio

(Received September 18, 1959)

The infrared emission spectra of gaseous B_2O_3 and B_2O_2 in the temperature range 1400–1800°K have been studied in the region 700–4000 cm^{-1}. Distinct bands were found for natural B_2O_3 at 2040, 1302, and 742 cm^{-1}, and the B^{10}—B^{11} isotope shifts measured. From the isotope shift data and other considerations the B_2O_3 molecule has been assigned a V structure having C_{2v} symmetry. A force constant analysis has been made and a frequency assignment is given from which thermal functions have been computed. The calculated force constants are consistent with the high stability of the molecule. Only one emission band of gaseous B_2O_2, at 1890 cm^{-1}, has been observed. A linear $D_{\infty h}$ structure was assumed and a frequency assignment and thermal functions estimated.

I. INTRODUCTION

THE thermodynamic properties of gaseous boric oxide B_2O_3 have been the subject of considerable interest for some time. However, until very recently the complete absence of any structural and spectroscopic data for this molecule has led to various conjectures and speculations regarding its shape and vibrational frequencies. In the early work of Wacker, Woolley, and Fair,[1] several possible structures for B_2O_3 were mentioned but only the D_{3h} bipyramidal configuration was adopted for their computational purposes. Since that time the D_{3h} model has been rather generally accepted and used for further thermodynamic estimates and calculations.[2] The justification for the continued use of this model in thermodynamic work has been supposed to depend chiefly on the observation that only such a compact, highly symmetrical structure could account for the observed stability at elevated temperatures and could yield entropies in reasonable agreement with those derived from third-law calculations based on existing calorimetric[3] and vapor pressure data.[4–7] Although some doubts were expressed as to the reality of a bipyramidal arrangement for three oxygen and two boron atoms, the precedent established by its use and the lack of evidence in support of any given structure made its retention for thermodynamic work plausible. More recently, Dows and Porter[8] observed infrared emission band from the heated vapors of isotopically normal B_2O_3 and from material enriched in B^{10}. They interpreted their results as evidence for the D_{3h} model.

On the other hand, Evans, Wagman, and Prosen[9] have pointed out in a recent review that the heat capacity of liquid B_2O_3 and the heat of fusion are quite uncertain. They show that the existing data could easily lead to an error of a few entropy units if used to compute the entropy of gaseous B_2O_3 at even a moderately elevated temperature, say 1500°K. Clearly, these uncertainties have the effect of vitiating the principal arguments for the bipyramidal model and thereby readmitting for further consideration some of the less symmetrical molecular configurations. Moreover, the conclusions of Dows and Porter and their application of the Teller-Redlich product rule to their data have been questioned on purely theoretical grounds by Taylor.[10]

In a brief preliminary account[11] of the present investigation three infrared emission bands from gaseous B_2O_3 having boron isotopes in natural abundance and from the species enriched in B^{10} were reported. It was shown that the isotopic frequency shift reported by Dows and Porter was not correct, and that their conclusion regarding the bipyramidal structure was not tenable. It was further suggested that a V model with C_{2v} symmetry is plausible and affords a reasonable explanation of the observed spectrum and isotopic frequency shifts. An infrared band obtained in emission from $B_2O_2(g)$ was also reported.

This paper presents the experimental details and results of our investigation together with a complete assignment of fundamentals based in part on a force constant analysis. In the following paper, the results of an investigation of the infrared emission spectrum of $B_2O_3(g)$ in the presence of water vapor are presented.

* This work was supported by the Office of Naval Research, Washington, D. C.

† Permanent address: National Bureau of Standards, Washington, D. C.

[1] Wacker, Woolley, and Fair, "Thermodynamic properties and gaseous equilibria of boron, oxygen, and the oxides of boron," Tech. Rept. to Bur. Aero., Navy Dept., submitted by Heat and Power Division, Natl. Bur. Standards, January 25, 1945.

[2] P. C. Setze, NACA/RM/ES7B14, National Advisory Committee for Aeronautics, Washington (April, 1957).

[3] Kerr, Hersh, and Johnston, J. Am. Chem. Soc. **72**, 4738 (1950); J. C. Southard, J. Am. Chem. Soc. **63**, 3147 (1941).

[4] Speiser, Naiditch, and Johnston, J. Am. Chem. Soc. **72**, 2578 (1950).

[5] Inghram, Porter, and Chupka, J. Chem. Phys. **25**, 498 (1956).

[6] M. O. Scheer, J. Phys. Chem. **61**, 1184 (1957).

[7] A. W. Searcy and C. E. Myers, J. Phys. Chem. **61**, 957 (1957).

[8] D. A. Dows and R. F. Porter, J. Am. Chem. Soc. **78**, 5165 (1956).

[9] Evans, Wagman, and Prosen, Natl. Bur. of Standards Report 6252 (December 1958).

[10] W. J. Taylor, J. Chem. Phys. **28**, 625 (1958).

[11] White, Walsh, and Mann, J. Chem. Phys. **28**, 508 (1958).

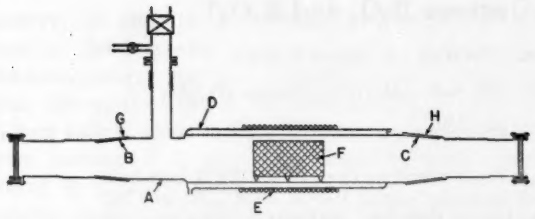

FIG. 1. Furnace for high temperature infrared spectroscopic studies.

II. APPARATUS

The low volatility of both $B_2O_2(g)$ and $B_2O_3(g)$ necessitated the construction of a furnace suitable for the temperature range 1200 to 1800°K. The furnace is designed to operate either *in vacuo* or in an inert atmosphere (argon). A diagram of the furnace is shown in Fig. 1. The main tube A, internal diameter $2\frac{1}{2}$ in. and 12 in. long, the male joints B and C and water jacket D are constructed of Vycor. The induction coil E is powered by a 20-kw oscillator operating in the radio-frequency range and consists of 22 turns of 3/16-in. copper tubing. It is $3\frac{1}{4}$ in. in diameter and $5\frac{3}{4}$ in. long. The molybdenum or platinum tube F, 2 in. in diameter and 4 in. long, in which the hot vapors are produced, is mounted on a molybdenum wire carriage which makes only point contact with the Vycor at several spots. The furnace is sealed at both ends by means of two female T/S Pyrex joints, G and H, to which are connected metal "O" ring flanges, supporting the infrared transmitting windows. To avoid heating as well as coating the windows during operation of the furnace, the T/S joints and window mounts are water-cooled by means of flexible tygon tubing wrapped around these parts. The furnace is evacuated and filled with inert gas through the side arm J. The arrangement of the optical system and accessories is such as to minimize the amount of radiation from the hot refractory tube reaching the spectrometer. The radiation from the hot vapors is focused on the slit of a Model 99 Perkin-Elmer monochromator by means of a plane mirror and a spherical mirror of 9-in. focal length.

III. EXPERIMENTAL

In the previous section it was stated that the refractories in which the hot vapors were generated were either platinum or molybdenum. The platinum tube was used only in investigations below 1475°K because above this temperature it tended to deform rapidly. Above 1475°K, where the majority of the work was carried out, a molybdenum tube was used. The unavailability of molybdenum tubes of large diameter necessitated their fabrication from sheet material. A satisfactory conducting weld was achieved by overlapping the edges of a rolled sheet and melting platinum between them *in vacuo*. To determine if molybdenum is oxidized by $B_2O_3(l)$ at elevated temperatures, the vaporization of $B_2O_3(l)$ from a molybdenum Knudsen cell was investigated by a method similar to that of Speiser, Naiditch, and Johnston.[4] The observed vapor pressures, along with those interpolated from the data of Speiser *et al.* (who used a platinum refractory), are shown in Table I. It is evident from the table that reaction between $B_2O_3(l)$ and molybdenum occurs to a negligible extent.

In testing the furnace it was found that an emission spectrum could not be obtained when the furnace was operated *in vacuo*, presumably because the concentration of hot vapor in the region where the spectrometer was focused was too low. In addition, serious coating of the windows took place. The introduction of argon into the system eliminated these difficulties. However, the intensity of the emission spectrum was found to be strongly dependent on the argon pressure. The variation of intensity of the 2040 cm^{-1} band of $B_2O_3(g)$ as a function of argon pressure, at constant temperature, is shown in Fig. 2. One factor which probably accounts for a large part of the decrease in intensity with increasing pressure is the scattering of the radiation by a fine solid mist which becomes visible at high pressure. This mist is formed by nucleation in the vapor phase, aided by the large convection currents in the system. It interferes with the observation of the spectra, but can be controlled by proper choice of experimental operating conditions, i.e., temperature and inert gas pressure.

To aid in the identification of the emission bands as well as to obtain some thermodynamic information, the intensities of some bands were measured as a function of temperature. It is obvious from the design of the furnace shown in Fig. 1 that temperature can only refer to an average characteristic of the whole tube, owing to the existence of gradients. With proper heating coil design, these gradients can be kept within ± 10 degrees of the average temperature. The temperature of the liquid B_2O_3 was measured at different positions along the length of the tube with a calibrated platinum, platinum-rhodium thermocouple in contact with the liquid. The average reading of the thermocouple was then intercompared with the reading of a Leeds and Northrup optical pyrometer fixed on a certain fiduciary point of the furnace wall, which was then used as a secondary thermometer in most of the experiments. Frequent checks were made to determine if the calibration of the fiduciary point had changed with time. It is

TABLE I. Vapor pressure of $B_2O_3(l)$.

	Pressure (atmos)	
T (°K)	This study	Speiser *et al.*
1409	3.93×10^{-6}	5.06×10^{-6}
1441	5.57×10^{-6}	9.33×10^{-6}
1457	1.63×10^{-5}	1.25×10^{-5}
1492	1.41×10^{-5}	2.37×10^{-5}
1569	6.34×10^{-5}	8.55×10^{-5}
1610	1.05×10^{-4}	1.61×10^{-4}

evident from what has been said in the preceding paragraph that, for the intensity *vs* temperature experiments to have some meaning, the inert gas pressure in the furnace must be held constant.

IV. MATERIALS

The boric oxide containing isotopes in natural abundance was prepared by dehydration of Reagent Grade Matheson, Coleman, and Bell boric acid. The dehydration was carried out in a muffle furnace at 1000°C. The sample was then degassed *in vacuo* in the temperature range 800–1100°C until the water pressure above the sample was less than 1×10^{-4} mm Hg at the highest temperature. The boric oxide enriched in either the B^{10} or B^{11} isotope was prepared in the same way with boric acid samples obtained from the Stable Isotope Division, Oak Ridge National Laboratory.

The $B_2O_2(g)$ was formed in the furnace designed for the spectroscopic work in two ways: by heating a mixture of magnesium oxide and purified boron at approximately 1500°K,[7] and by heating a mixture of B_2O_3 and boron in the same temperature range. The boron was purified by vacuum and sublimation, at 1500°C, of the impurities (chiefly lead, aluminum, and magnesium) in Fisher Scientific Company "purified amorphous boron."[12]

V. EXPERIMENTAL RESULTS

A. B_2O_3

The infrared emission spectra of gaseous natural B_2O_3 and B_2O_3 containing 96%B^{10} in the region 700–4000 cm^{-1} are shown in Fig. 3. Runs were made with samples enriched in B^{11} (98.5%) but the infrared traces are so nearly like those for the natural material that they are not shown. The measured wave numbers are, however, given in Table II along with those for the normal and B^{10} enriched species. Because of the very rapid fall-off in emission intensity with decrease in frequency, the 700-cm^{-1} band required the use of much wider slits (2 mm) and somewhat higher temperatures than were necessary for the detection of the other bands. In view of the low intensity of the 700-cm^{-1} band, it does not seem likely that any bands at still lower frequencies would be detectable in our apparatus. The fact that no emission was detected in the 3000-cm^{-1} region was taken as a clear indication of the absence of water and hydrated species in our sample. Interference from atmospheric absorption in the neighborhood of the 1300-cm^{-1} band was not serious and was taken into account by background correction. The measured wave numbers are values obtained by averaging the results for at least 20–30 runs for each band.

The isotope shift of the highest frequency band is easily reproducible under a large variety of experimental conditions, the uncertainty being no larger than ±3 cm^{-1}. The uncertainties of the isotope shifts

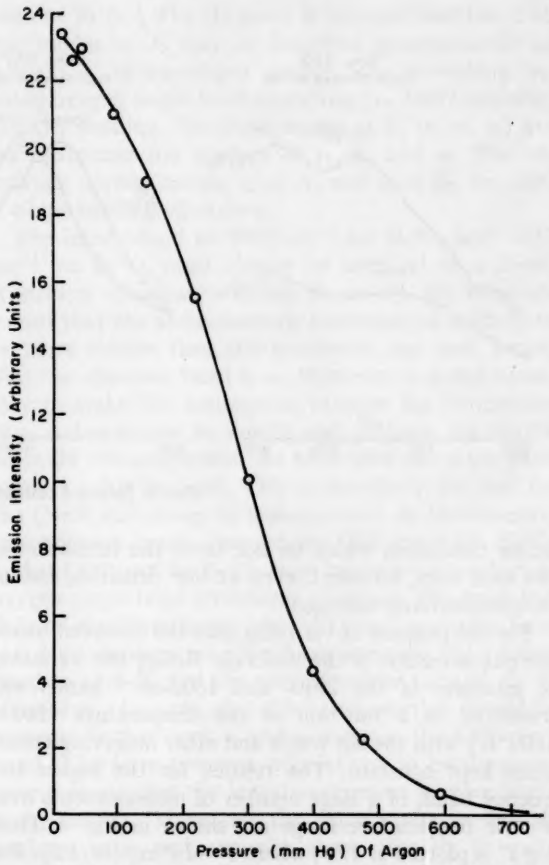

FIG. 2. Variation of intensity of 2040 cm^{-1} band of B_2O_3 with argon pressure at constant temperature.

of the two lower bands are more difficult to estimate, as will be evident from the discussion below. However, they are probably no greater than $\pm20\%$. For the lowest frequency band the uncertainty largely results from the wide slits necessary for its observation. Increasing the temperature failed to increase its intensity appreciably, owing to scattering of the radiation by a solid mist which formed in the hot zone. Lowering of the argon pressure in the furnace did not substantially alter the situation. The presence of the solid suspension also contributed to the uncertainty of the 1300-cm^{-1} band, although in a different way. Here the chief difficulty arose from the strong absorption and emission of the solid at approximately 1280 cm^{-1}. This band, characteristic of the solid, was identified by allowing the windows to become coated and then taking an absorption spectrum of the film. The results are in excellent agreement with those of Sidorov and Sobolev[13] who investigated the infrared absorption spectrum of thin boric oxide films. Although the experimental determination of the isotope shift of the 1300-cm^{-1} band was performed

[12] R. M. Swift and D. White, J. Am. Chem. Soc. **79**, 3641 (1957).

[13] T. A. Sidorov and N. N. Sobolev, Optika i Spectroskiya **3**, 560 (1957).

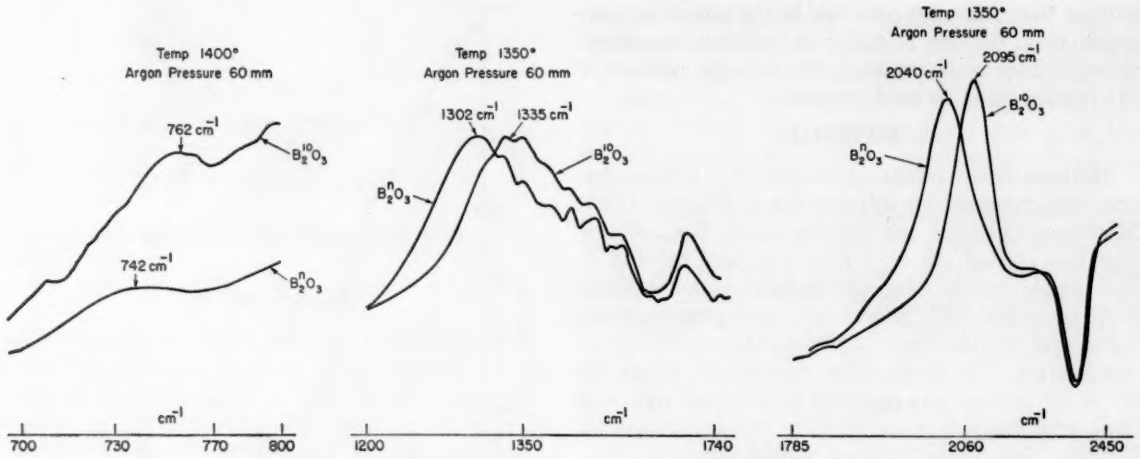

FIG. 3. Infrared emission spectrum of gaseous B_2O_3.

under conditions which do not favor the formation of the solid mist, its effect, even at low densities, cannot be quantitatively assessed.

For the purpose of verifying that the observed bands are characteristic of the molecule B_2O_3,‡ the variation of intensity of the 2040- and 1302-cm^{-1} bands was measured as a function of the temperature (1400–1800°K) with the slit width and other observing conditions kept constant. The results, for the higher frequency band, of a large number of measurements over a wide temperature range are shown in Fig. 4. Here log I' is plotted *vs* $1/T$, where $I'=IT\exp(h\nu/kT)$. I is the observed intensity in arbitrary units, which is proportional to the concentration of excited molecules in the hot zone. The two multiplicative factors T and $I\exp(h\nu/kT)$ relate the observed intensity, in first approximation, to the pressure of the molecule in both ground and excited states. If the band is, indeed, due to gaseous B_2O_3, then from the slope of Fig. 4 one should obtain the heat of vaporization of $B_2O_3(l)$. The value obtained, 76.0±3.5 kcal/mole is in excellent agreement with 77.6±2 kcal/mole derived from precise Knudsen effusion determinations by Speiser *et al.*[4] A similar heat of vaporization, but with larger uncertainty is also obtained from the variation of the intensity of the 1302-cm^{-1} band with temperature.

TABLE II. Observed emission bands for $B_2O_3(g)$.

$B_2^{10}O_3(g)$	$B_2^{11}O_3(g)$ (cm^{-1})	$B_2{}^nO_3(g)$
2095	2035	2040
1335	1300	1302
762	740	742
(~1440)[a]	(~1420)	(~1420)

[a] The frequency given in the brackets is for a shoulder which appears on the 1300 cm^{-1} band (see Fig. 3).

‡ Inghram *et al.*[5] and Scheer[6] have shown that monomeric B_2O_3 is the only gaseous species produced in vaporization of liquid B_2O_3.

B. B_2O_2

Only the emission band, at 1890 cm^{-1}, was observed for $B_2O_2(g)$ in the region 700 to 3000 cm^{-1}. The B_2O_2 was obtained in the furnace either by reaction of boron with magnesium oxide in the temperature range

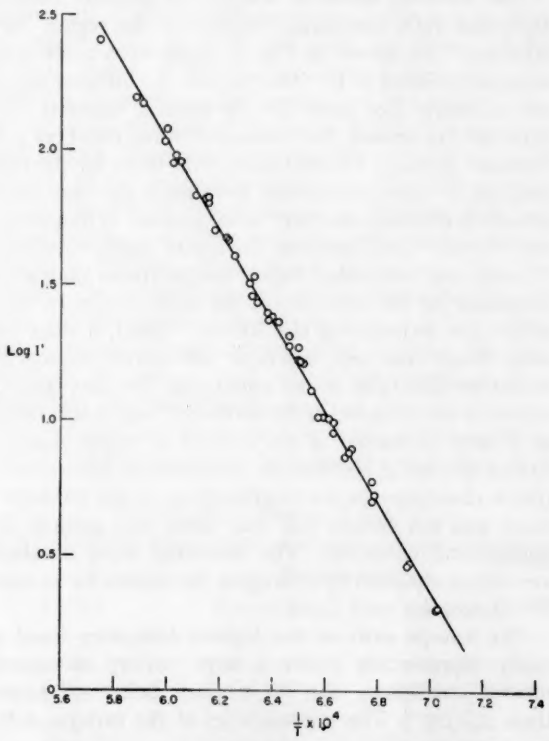

FIG. 4. Variation of intensity of 2049-cm^{-1} band of B_2O_3 with temperature.

1400–1600°K or by reaction of boron with $B_2O_3(l)$ in the same temperature range. The observed intensity of the band under the best conditions was low (approximately 10–15% the high frequency band shown in Fig. 4). Because of this its identification with the molecule B_2O_2 by intensity-temperature measurements could not be made. However, since the same band appears in two *different* reactions which have been shown[5,7] to give rise to the *same* vapor species, there can be little doubt as to its origin.

IV. DISCUSSION

The application of the Teller-Redlich product rule to the isotopic frequency shifts has been given in an earlier publication.[11] It was pointed out there that the observed shifts are such as to require the exclusion of structures with D_{3h} or $D_{\infty h}$ symmetry from further consideration. For D_{3h} symmetry, B_2O_3 would have one infrared active mode in A_2'' and two in E'. For each class the product rule ratio should be 1.0336. The individual observed frequency ratios are $2095/2035=1.0295$, $1335/1300=1.0270$, $762/740=1.0291$. Some pair of the observed frequencies, since they can hardly be other than fundamental modes, must be assigned to species E' of D_{3h}. However, the smallest observed product of the frequency ratios is 1.057. This result is virtually independent of the details of the assignment since any pair of isotopic frequency ratios would give essentially the same result. To get agreement with the theoretical value, the observed ratios would have to be changed by far more than even a very liberal estimate of the uncertainties would allow. Similar arguments lead to the rejection of the $D_{\infty h}$ model. It was also remarked in the earlier report[11] that the presence of a strong emission band in the 2000-cm^{-1} region is a rather clear indication that the molecule contains a boron-oxygen double bond.

This evidence alone would cast doubt on a D_{3h} structure. The spectroscopic results, therefore, strongly favor an extended, bent structure for B_2O_3, though they cannot be used to decide on a particular configuration or symmetry. Almost any molecular geometry with C_{2v}, C_{2h}, or lower symmetry would be acceptable. Other considerations must be used to enable a specific choice to be made. Elementary valency arguments suggest that free B_2O_3 molecules have a V shape with C_{2v} symmetry rather than a W, zigzag, or other extended configuration. It is instructive to note that B_2O_3 is isoelectronic with malononitrile, $H_2C(CN)_2$. The CH_2 group is isoelectronic with oxygen, and the C≡N group with B=O. An approach similar to that used by Walsh[14] for predicting molecular shapes, or even less sophisticated reasoning leads to the same conclusion.

From the assumption of C_{2v} symmetry for B_2O_3 it follows that eight of the nine normal modes of vibration can appear in the infrared: four in A_1, three in B_1, and one in B_2.§ The A_2 mode is infrared inactive. The four modes in A_1 may be described approximately as follows: ν_1, boron-oxygen double bond stretching; ν_2, boron-oxygen single bond stretching; ν_3, OBO bending; ν_4, BOB bending. The three modes in B_1 (ν_5, ν_7, ν_8) are the antisymmetric analogs of ν_1, ν_2, and ν_3. The remaining normal modes, ν_6 of A_2 and ν_9 of B_2, are out-of-plane bending vibrations.

The band found at 2095 cm^{-1} for $B_2{}^{10}O_3$ and 2035 cm^{-1} for $B_2{}^{11}O_3$ must clearly be ascribed to a B=O stretching vibration, whether B_1 or A_1. We have assumed that the antisymmetric fundamental is likely to be more intense than the symmetric one and, hence, that the observed band is ν_6. However, it is not necessary to make this assumption because the frequencies of ν_1 and ν_6 should be similar and, perhaps, nearly the same. In the assignment, we have used the same wave number value for both. This is essentially the case for the C≡N stretchings in malononitrile. In like manner, the emission band observed at 1335 cm^{-1} for $B_2{}^{10}O_3$ and at 1300 cm^{-1} for $B_2{}^{11}O_3$ must be assigned to a boron-oxygen single bond stretching vibration. The weak but definite shoulders found near 1400 cm^{-1} probably have the same explanation. We have assigned the intense band to ν_7 of B_1 and the weak shoulder to ν_2 of A_1. It is possible, of course, that this interpretation should be reversed or that both ν_2 and ν_7 occur in the 1300-cm^{-1} band. The force-constant calculations to be discussed later indicate that the initial assignment is more likely to be correct. Moreover, the calculations as well as analogy with malononitrile show that it is quite improbable that the 762−740-cm^{-1} band arises from a stretching mode.

The XOX symmetric deformation mode in various ethers is usually found near 400 cm^{-1}, and in various related molecules within the limits 300–500 cm^{-1}. In malononitrile the CCC bending is found at a frequency higher than the norm for vibrations of this type.[15] In any case, it may reasonably be expected that the BOB deformation mode of B_2O_3 will occur in this range. The 700 cm^{-1} band would, therefore seem to be much too high to be assigned to ν_4. Moreover, the isotopic frequency shift for ν_4 should be very small. Hence, on this basis alone it is possible to reject the interpretation of the 700-cm^{-1} band as ν_4. It must, therefore, be ascribed to one of the remaining planar bending modes. The magnitude of the observed shift for this band also precludes its assignment to A_2 and probably to B_2 as well. This leaves only ν_3 in A_1 or ν_8 in B_1 as reasonable possibilities. Once again the likelihood that that the antisymmetric fundamental is more intense than the symmetric one suggests the assignment of 762/742 cm^{-1} to ν_8. However, even if this assignment were reversed, neither the force constants nor the other

[14] A. D. Walsh, J. Chem. Soc. **1953**, 2260–2331.

§ The axes have been designated as follows: z is the symmetry axis, and the molecule lies in the xz plane.

[15] F. Halverson and R. J. Francel, J. Chem. Phys. **17**, 694 (1949).

TABLE III. Force constants and fundamental frequencies for $B_2{}^{10}O_3(g)$ and $B_2{}^{11}O_3(g)$.

C_{2v} Species	ν	$B_2{}^{10}O_3$ (ν in cm^{-1})	$B_2{}^{11}O_3$ (ν in cm^{-1})	Force constant[a]
A_1	1	2095[b]	2035[b]	$F_1=15.93$
	2	1447[c] (~1440)	1411[c] (~1420)	$F_2=8.36$[d]
	3	893	873	$F_3=1.33$[d]
	4	311	310	$F_4=4.00$
A_2	5	790	758	$F_5=1.27$[d]
B_1	6	2095[b]	2035[b]	$F_6=15.93$
	7	1335[b]	1300[b]	$F_7=7.60$[d]
	8	762[b]	740[b]	$F_8=1.21$[d]
B_2	9	897	869	$F_9=1.33$[d] $f_{2,4}=1.00$

[a] The force constants are given in units of md/A for the stretching constants, md·A for the bending constants, and in md for the interaction constant.
[b] These are observed values.
[c] These are calculated values. The rather approximate observed values are given in parentheses.
[d] These are based on the averaged values for F_7 and F_8, as discussed in the text.

features of the interpretation would be much affected. The present view has the additional advantage that the assignment of observed fundamentals to B_1 is now complete and can be used to establish a set of force constants from which the A_1 vibrations can be calculated.

Force constants.—The F and G matrices required for the force-constant calculations were constructed by the standard procedures given by Wilson, Decius, and Cross.[16] They agree exactly with those given by Halverson and Francel for malononitrile[15] after allowance is made for the absence of hydrogen atoms and the different identification of the other atoms, and therefore will not be repeated here. In order to simplify the calculations, the boron-oxygen double bond stretching coordinates were factored out of A_1 and B_1 by the usual procedures. The errors introduced by this approximation are small enough to be ignored in the present case. This reduced A_1 to a third-order and B_1 to a second-order problem. The numbering and designation of the principal force constants in each species follows that already given for the fundamentals. Thus, in the A_1 block, F_2, F_3, and F_4, refer to the B—O stretching, OBO bending, and BOB deformation constants, respectively. The observation by Halverson and Francel that a constant is required for the interaction between the B—O stretching and BOB deformation coordinates was noted and the constant $f_{2,4}$ incorporated in the A_1 block. No other interaction constants were used. For the reduction of the G matrices to numerical form, the following molecular constants were assumed for B_2O_3: $r(B{=}O)=1.20$ A, $r(B{-}O)=1.34$ A, $\measuredangle BOB=120°$, and $\measuredangle OBO=180°$.

[16] Wilson, Decius, and Cross, *Molecular Vibrations* (McGraw-Hill Book Company, Inc., New York, 1955).

The force constant obtained from the factored high-frequency element of B_1 and 2095 cm^{-1} fundamental of $B_2{}^{10}O_3$ is 15.93 md/A. A similar result is obtained if the corresponding matrix element and frequency for $B_2{}^{11}O_3$ are used. It may be noted that the B=O stretching force constant is remarkably high, and not far from the common value for the carbon-nitrogen triple bond stretching constant. Since ν_7 and ν_8 have been assigned to B_1, it is possible to solve directly for the force constants F_7 and F_8. Indeed, with the data for both isotopic species at hand, one could solve exactly, not only for F_7 and F_8, but for $f_{7,8}$ as well. However, it was not felt that this would be a useful procedure because the values of all three constants would be quite sensitive to the comparatively large uncertainty in the isotopic separation of the ν_7 and ν_8 bands. Instead, the interaction constant $f_{7,8}$ was fixed at zero and principal constants determined separately from the $B_2{}^{10}O_3$ and $B_2{}^{11}O_3$ data. From the former we found $F_7=7.78$ md/A and $F_8=1.19$ md·A. From the data for the heavier species we obtained $F_7=7.42$ md/A and $F_8=1.23$ md·A. The average values $F_7=7.60$ md/A and $F_8=1.21$ md·A were used for subsequent calculations with the other blocks.

Analogy with the results for malononitrile shows that the symmetrized constants F_2 and F_3 of A_1 are each about 10% larger than the corresponding B_1 constants F_7 and F_8. Hence, for the following calculation on A_1, F_2, and F_3 were given the values 8.36 md/A and 1.33 md·A, respectively. Pilot calculations with these values for F_2 and F_3 and a range of values for F_4 and $f_{2,4}$ showed that the ratio F_4/F_3 could not be far from that found for malononitrile, *viz.*, about 3.5. Moreover, Halverson and Francel[15] found that in their calculation the interaction constant equivalent to $f_{2,4}$ was positive and, if given in units of md, numerically about the same as the symmetrized constant analogous to F_3. Consequently, for the calculations reported here, F_4 and $f_{2,4}$

TABLE IV. Thermal functions of gaseous B_2O_3. (cal deg^{-1} $mole^{-1}$).

T(°K)	$-(F^0-H_0^0/T)$	$H^0-H_0^0/T$	S^0	C_p
50	40.03	7.95	47.98	7.97
100	45.56	8.05	53.61	8.43
200	51.30	8.63	59.92	10.12
273.15	54.08	9.25	63.32	11.81
298.15	54.89	9.49	64.39	12.41
300	54.95	9.51	64.47	12.45
500	60.28	11.55	71.84	16.57
750	65.41	13.83	79.25	19.93
1000	69.66	15.63	85.28	21.91
1250	73.29	17.01	90.30	23.08
1500	76.49	18.09	94.59	23.82
1750	79.34	18.94	98.30	24.31
2000	81.92	19.64	101.56	24.64
2500	86.43	20.68	107.11	25.05
3000	90.27	21.43	111.70	25.29
3500	93.62	21.99	115.61	25.43
4000	96.58	22.43	119.01	25.53
5000	101.65	23.06	124.72	25.63
6000	105.90	23.49	129.39	25.69

were set equal to 4.00 md·A and 1.00 md, respectively. The constants used for A_2 and B_2 were adjusted in a similar manner and set equal to 1.27 md·A and 1.33 md·A, respectively. The results of the complete calculation are given in Table III.

The thermal functions for gaseous B_2O_3 computed from the data in Table III and the molecular constants previously given, are shown in Table IV.

B_2O_2.—Only one band, at 1890 cm^{-1}, was found in the infrared emission spectrum of gaseous B_2O_2. There can hardly be any question that it arises from a B═O stretching mode. It is slightly higher, about 30 cm^{-1}, than the fundamental of the BO molecule in its ground electronic state. Arguments analogous to those used in connection with the structure of B_2O_3 lead to the conclusion that B_2O_2, which is isoelectronic with cyanogen C_2N_2 is linear and has $D_{\infty h}$ symmetry. The B═O force constant is about 13.5 md/A. It is thus quite close to that for BO, which has the value 13.3 md/A; and it is appreciably smaller than the B═O force constant in B_2O_3. Analogy with the C_2N_2 spectrum[17] suggests that the Σ_g^+ B═O stretching mode should have a somewhat higher frequency than the Σ_u^+ mode at 1890 cm^{-1}. We shall assume that it is 2000 cm^{-1}. To estimate the other Σ_g^+ mode a B—B force constant of 4 md/A has been used. This is somewhat greater than the force constant in $B^2(g)$[18] but a larger value is reasonable in view of the value of dissociation energy of B_2O_2 to BO[5,9] This places this Σ_g^+ mode at about 750 cm^{-1}. For any reasonable choice of force constants, it turns out that the frequency of the Π_g mode is about twice that of the Π_u, just as in the case of C_2N_2. A guess which appears reasonable in light of the B_2O_3 calculations is 600 cm^{-1} for Π_g and 300 cm^{-1} for Π_u.

The thermal functions for gaseous B_2O_2 based on the above assignment are given in Table V. The B—B and B═O bond lengths assumed for the calculations are 1.59 and 1.20 A, respectively.

TABLE V. Thermal functions of gaseous B_2O_2 (cal deg^{-1} $mole^{-1}$).

T(°K)	$-(F^0-H_0^0/T)$	$H^0-H_0^0/T$	S^0	C_p
50	33.96	6.96	40.94	7.01
100	38.85	7.19	46.04	8.03
200	44.16	8.37	52.52	10.97
273.15	46.88	9.30	56.20	12.66
298.15	47.73	9.60	57.33	13.14
300	47.79	9.62	57.41	13.16
500	53.20	11.59	64.78	15.64
750	58.22	13.27	71.50	17.45
1000	62.22	14.47	76.69	18.56
1250	65.56	15.36	80.90	19.24
1500	68.42	16.04	84.46	19.67
1750	70.92	16.57	87.52	19.95
2000	73.17	17.01	90.18	20.15
2500	77.04	17.67	94.71	20.39
3000	80.30	18.14	98.44	20.53
3500	83.12	18.48	101.61	20.63
4000	85.61	18.76	104.37	20.67
5000	89.84	19.16	109.00	20.75
6000	93.36	19.41	112.77	20.79

VII. CONCLUSIONS

The high thermal stability of the B_2O_3 molecule has been well known for some time. It may be worthwhile to call attention to the thermodynamic and spectroscopic evidence that bear out this observation. It has already been noted that the force constant for BO in its ground state is about 13.3 md/A and that this is very nearly the value for the B═O stretching constant in B_2O_2. The heats of formation ΔHf_0^0 given by Evans *et al.*[9] for BO(g) and B(g) lead to a bond energy of 187 kcal/mole for the boron-oxygen double bond in BO. The similarity in BO force constants between BO and B_2O_2 suggests that the B═O bond energy is not much different in the two cases. This assumption together with $\Delta Hf_0^0 = -108$ kcal/mole|| for B_2O_2(g) leads to the remarkably high value of 120 kcal/mole for the B—B bond energy in B_2O_2. This is much higher than any of the values suggested by Herzberg[18] or Gaydon[19] for the B—B bond in the B_2 molecule (about 83 kcal/mole). The value obtained from the heats of formation given by Evans *et al.*[9] for B_2(g) and B(g) lead to the even lower value of 65 kcal/mole. Even if allowance is made for the uncertainties in the heats of formation and for the assumption that the B═O bond energy is the same in both BO and B_2O_2, it is clear that the B—B bond in the latter is considerably stronger than in B_2(g). The value of 120 kcal for the B—B bond energy given above is consistent with the lower limit of 100 kcal given by Inghram *et al.*[5] In a similar manner estimates of the bond strengths in B_2O_3 can be made. The heats of formation −207,¶ 134, and 59[20] kcal/mole for B_2O_3(g), B(g), and O(g), respectively, lead to a total heat of atomization of 652 kcal/mole. It will be recalled that the B═O force constant is appreciably larger in B_2O_3 than in either BO or B_2O_2. We may, therefore, take the B═O bond energy in BO, 187 kcal/mole, as a lower limit. This places an upper limit on the B—O bond energy: 139 kcal/mole. It would seem more reasonable to suppose that the B—O bond energy is in the range 120–130 kcal/mole and the B═O bond energy correspondingly higher.

ACKNOWLEDGMENTS

The authors wish to thank Mr. P. Rentzepis for his aid in the preliminary investigations and Dr. Charles W. Beckett for many helpful discussions.

[17] G. Herzberg, *Molecular Spectra and Molecular Structure* II. *Infrared and Raman Spectra of Polyatomic Molecules* (D. Van Nostrand Company, Inc., Princeton, New Jersey, 1945).

[18] G. Herzberg, *Molecular Spectra and Molecular Structure, I. Spectra of Diatomic Molecules* (D. Van Nostrand Company, Inc., Princeton New Jersey, 1950), second edition.

|| The value is 3 kcal higher than the one given by Evans, *et al.*[9] and is based on some later work in this laboratory.

[19] A. G. Gaydon, *Dissociation Energies and Spectra of Diatomic Molecules* (Chapman and Hall, Ltd., London, 1953).

¶ This value is obtained using the data of Reference 4, 6, and 7 and the free energy functions of Table III.

[20] P. Brix and G. Herzberg, Can. J. Phys. **32**, 110 (1954).

Infrared Emission Spectrum of Gaseous HBO_2*

DAVID WHITE, DAVID E. MANN,† PATRICK N. WALSH, AND ARMIN SOMMER

Cryogenic Laboratory, Department of Chemistry, The Ohio State University, Columbus 10, Ohio

(Received September 18, 1959)

The infrared emission spectrum of the vapor phase of the $B_2O_3(l)-H_2O(g)$ system has been studied at elevated temperatures over the region 700–4000 cm^{-1}. Characteristic bands were found near 3680, 2030, and 1420 cm^{-1}, and approximate B^{10}—B^{11} and H—D isotope shifts measured. It is shown that these bands arise from the molecule HBO_2. The intensity of the 2030 cm^{-1} band was studied as a function of both temperature and water pressure. The intensity *vs* temperature measurements lead to a heat of formation, ΔH_0°, of -135.0 ± 3 kcal/mole for $HBO_2(g)$. The spectroscopic data, considered in the light of our analysis of the $B_2O_3(g)$ infrared spectrum, are compatible with the structure

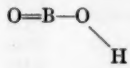

in which the OBO group is linear and the H is off-axis. The force constants are found to resemble those determined for $B_2O_3(g)$. Complete vibrational assignments are given for $HBO_2(g)$ and its trimer $(HBO_2)_3(g)$, a species which has recently been shown to exist in this system. Thermal functions have been computed for both molecules over a wide temperature range.

I. INTRODUCTION

IT has been found that at high temperatures the volatility of liquid B_2O_3 increases markedly in the presence of water vapor, and that the rate of vaporization is strongly dependent on the partial pressure of water.[1,2] This indicates that a reaction takes place and that one or more of the reaction products are stable in the vapor phase. Attempts have been made in this laboratory and elsewhere[2] to identify and estimate the stability of the vapor species by studying the vapor pressure as a function of temperature and partial pressure of water. The system, however, has proved too complex for such measurements to lead to unequivocal conclusions. The composition of the vapor has been found to be strongly dependent on the conditions of the experiment, from which it follows that there must be more than one product species stable in the vapor phase of the B—O—H system at high temperatures. One of these stable species is certainly H_3BO_3, but it can be shown from thermodynamic arguments[3] that it is not important in the reaction at high temperatures and low water pressures. On the other hand, approximate calculations based on average bond energies and related thermodynamic considerations[3] show that under these experimental conditions, a postulated species, HBO_2, could account for the high volatility of B_2O_3 in the presence of water vapor.

In order to elucidate this situation further and determine the structure and stability of the major constituents of the vapor, an investigation of the infrared emission spectrum of the $B_2O_3(l)$—$H_2O(g)$ system was undertaken. The observations and conclusions are reported in detail in this paper. The experimental conditions were such as to favor the formation of HBO_2 (g). The intensities of some of the observed bands were studied as functions of temperature and partial pressure of water, partly with the aim of helping to identify the species present in the vapor. After this investigation was completed, Chupka and Berkowitz,[4,5] using mass spectrometry and somewhat different experimental conditions, demonstrated that the vapor consists almost entirely of $HBO_2(g)$, with a small amount of its trimer, $(HBO_2)_3(g)$, also being found. It will be shown that the observed infrared spectrum is attributable to the monomer, HBO_2, and that the trimer can make only a negligible contribution.

II. EXPERIMENTAL METHODS

The apparatus used in this study was identical with that employed in our investigation of B_2O_3,[6] except for a minor change in the furnace enclosure to permit the introduction of water vapor. A small bulb containing water was attached to one of the end caps by means of a ground joint. The bulb was kept immersed in a bath whose temperature could be controlled so as to maintain constant water pressure in the range 1–20 mm Hg. Pressures were measured with an oil manometer. Rocksalt windows were used at both ends of the furnace enclosure. These gradually deteriorated, but

* This work was supported by the Office of Naval Research, Washington, D. C.

† Permanent address: National Bureau of Standards, Washington 25, D. C.

[1] von Stackelburg, Quantram, and Dressel, Z. Elektrochem. **43**, 14 (1937).

[2] J. L. Margrave, University of Wisconsin (private communication).

[3] Evans, Wagman, and Prosen, Natl. Bur. Standards Rept. No. 6252, December, 1958.

[4] W. A. Chupka and J. Berkowitz, presented at the 135th Meeting of the American Chemical Society, Boston, Massachusetts, April, 1959 (Paper No. 25, Inorganic Division).

[5] W. A. Chupka, Argonne National Laboratory (private communication).

[6] White, Mann, Walsh, and Sommer, J. Chem. Phys. **32**, 481 (1960), preceding article.

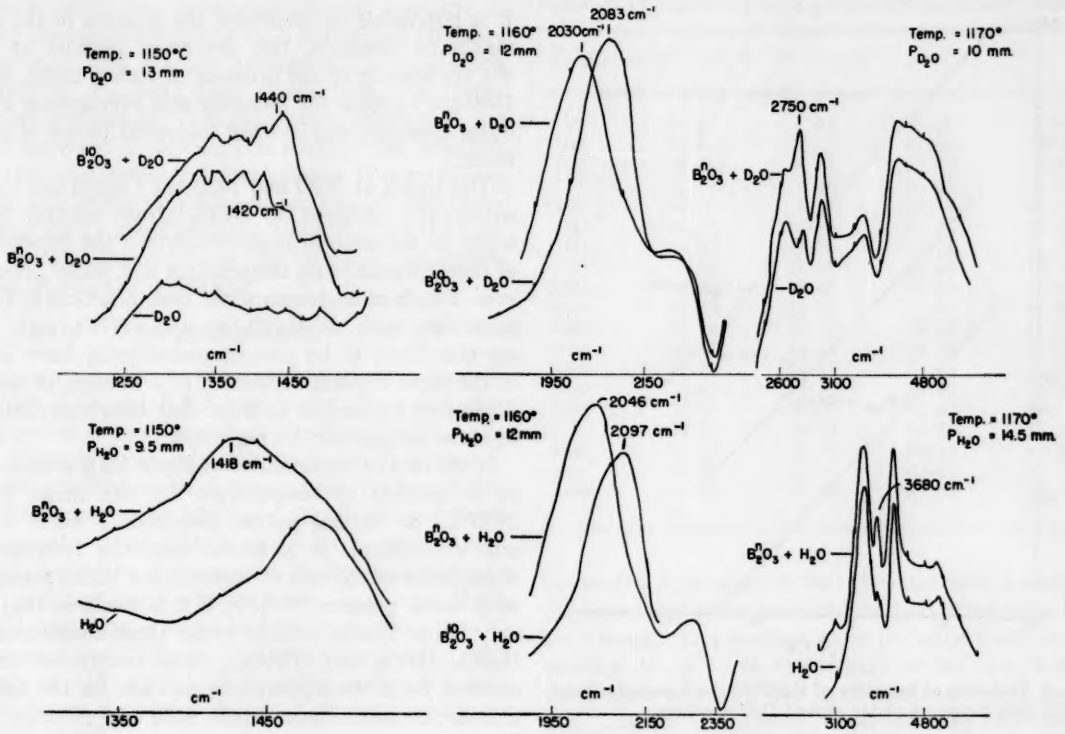

FIG. 1. The emission spectra of the vapor phases of the systems B_2O_3—H_2O and B_2O_3—D_2O at elevated temperatures.

the rate of destruction was remarkably slow even at the highest water pressures.

It was feasible to use a platinum tube to contain the heated liquid B_2O_3 because most of the experiments were carried out at temperatures near 1450°K or less. The B_2O_3 having natural isotopic abundances was prepared by dehydration of reagent Grade Matheson, Coleman, and Bell boric acid by the procedure described in the preceding paper.[6] Samples containing 96% B^{10} were prepared in the same way from isotopically enriched boric acid obtained from the Stable Isotope Division, Oak Ridge National Laboratory.

III. EXPERIMENTAL RESULTS

The infrared emission spectrum of the B_2O_3(l)—H_2O(g) system at temperatures of 1250–1450°K and water pressures of 1–15 mm Hg is shown in Fig. 1. Although the wave number of the strongest band found, that at 2030 cm^{-1}, is very close to that of the most intense B_2O_3(g) band,[6] it can be demonstrated that it must arise from a different vapor species. In the first place, the band is observed with high intensity at temperatures considerably below those necessary to obtain even a very weak B_2O_3(g) emission spectrum. In the second place, its intensity is very strongly dependent on the water pressure, and drops practically to zero when the water vapor is removed from the furnace. Thirdly, the variation of intensity of this band with temperature is considerably different from that observed for B_2O_3(g). The intensity variation with temperature, at several D_2O pressures, is shown in Fig. 2. (D_2O was used instead of H_2O because the emission spectrum of pure H_2O overlaps and distorts the band.) The function $I' = IT \exp h\nu/kT$ is plotted instead of the observed intensity I, to make the ordinate in Fig. 2 proportional to the logarithm of the partial pressure of the emitting vapor species. The data are remarkably consistent and yield a heat of reaction of 39.0±2.5 kcal. This is considerably below the heat of vaporization (78 kcal/mole) of B_2O_3.[7]

To aid in the identification of the major vapor species, an attempt was made to establish the stoichiometry of the reaction by measuring the intensity of the 2030-cm^{-1} band as a function of water pressure. The results of a number of runs are shown in Fig. 3. The slope of the log-log plot should give directly the coefficient of H_2O (g) in the balanced chemical equation in which one mole of vapor species is formed. Although the data are not as precise as might be desired, the average value is clearly between $\frac{1}{2}$ and $\frac{3}{4}$. Boric acid, H_3BO_3, and various larger molecules such as $H_2B_2O_4$ can thus be excluded from further consideration as major vapor species in the hot zone of the furnace, whereas the importance of HBO_2 is strongly indicated. Moreover, some other considerations lend this conclusion additional weight. The magnitude of the frequency suggest that a B=O

[7] Speiser, Naiditch, and Johnston, J. Am. Chem. Soc. **72**, 2578 (1950).

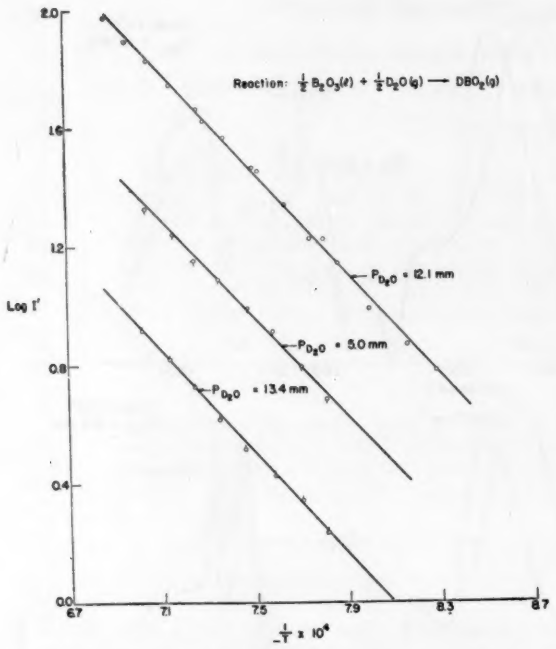

FIG. 2. Variation of intensity of the 2030 cm^{-1} emission band of DBO_2 with temperature for several D_2O pressures.

stretching motion is involved. This too would exclude H_3BO_3, though not necessarily $H_2B_2O_4$. However, the much greater width of this band as compared with that found for the 2040-cm^{-1} band of $B_2O_3(g)$ seems to be an indication that it arises from a relatively small and light molecule.

In a recent mass-spectrometric investigation of the system $B_2O_3(l)$—$H_2O(g)$, Chupka and Berkowitz[4,5] found HBO_2 to be by far the predominant vapor species at H_2O partial pressures up to about 1.5 mm Hg. From the partial pressures of HBO_2 deduced from the observed ion intensities, and the entropies of the molecule derived from this research (v.i.), they obtained 40.0± 2.5 kcal for the heat of the reaction

$$\tfrac{1}{2}B_2O_3(l)+\tfrac{1}{2}H_2O(g)\rightarrow HBO_2(g)$$

in the temperature range 1100–1320°K. This result is in excellent agreement with the value 39.0 kcal found in this investigation and, taken together with the foregoing spectroscopic observations, shows that there can be little doubt that the 2030-cm^{-1} band must be assigned to the molecule HBO_2.

Interpretation of the spectrum in the 3600 cm^{-1} and 1400 cm^{-1} regions is complicated by interference from H_2O emission. This is evident from the traces of the spectrum of pure water vapor at the same temperature and pressure, also shown in Fig. 1. In the 3600 cm^{-1} region (when H_2O was used) a band characteristic of the B_2O_3—H_2O system was identified by comparing a large number of traces at constant H_2O pressure but at different temperatures. Although in this region it is impossible to determine the position of the band maximum precisely, this procedure permits at least the verification of the presence of such a band. In the 1400-cm^{-1} region the blending and overlapping of the water spectrum was lessened somewhat by use of heavy water.

The bands at 3680 and 1420 cm^{-1} could not be unequivocally assigned to HBO_2 (from natural B_2O_3) solely on the basis of measurements of the dependence of their intensities on temperature and water pressure, even if such measurements had been practicable. Other molecules, such as $H_3BO_3(g)$ and $(HBO_2)_3(g)$, that are also likely to be present undoubtedly have bands in the same regions. However, it is possible to use independent arguments to show that their contributions to these spectra can be neglected.

If the rate of vaporization of liquid B_2O_3 is measured as a function of temperature (in the range 1200–1400°K) at various partial pressures of water up to one atmosphere, it is found that the temperature dependence of the rate of vaporization varies markedly with water pressure.[2,8] Now, if it is assumed that the only vapor species present under these conditions are H_3BO_3, HBO_2, and $(HBO_2)_3$, these results can be accounted for if the equilibrium constant for the formation of the latter from liquid B_2O_3 and gaseous H_2O is of the same order of magnitude as that for the reaction†

$$\tfrac{1}{2}B_2O_3(l)+\tfrac{3}{2}H_2O(g)\rightarrow H_3BO_3(g).$$

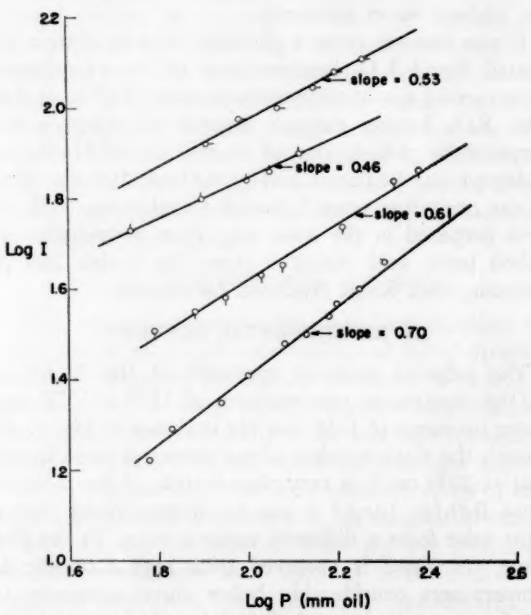

FIG. 3. Variation of intensity of the 2030 cm^{-1} band of DBO_2 with partial pressure of D_2O at constant temperature. (The pressure in mm oil can be converted approximately to mm Hg by division by 14.)

[8] Unpublished observations, this Laboratory.

† This leads to a heat of formation, $\Delta H_0°$, for $(HBO_2)_3$ of −537.0±10 kcal per mole.

Therefore, since the latter equilibrium constant is known,[8] the concentrations of both H_3BO_3 and $(HBO_2)_3$ can be calculated for the average set of conditions ($T=1435°K$, $P_{H_2O}=12$ mm) at which the spectra in Fig. 1 were obtained. This calculation shows that the partial pressure of $HBO_2(g)$ is roughly one hundred times that of either of the other species. It is gratifying to note that recent unpublished preliminary results by Chupka,[5] kindly made available to us, support the foregoing conclusion concerning the ratio of concentrations of H_3BO_3 and $(HBO_2)_3$.

IV. ASSIGNMENT

Arguments similar to those already given in connection with B_2O_3 and B_2O_2[6] lead to the conclusion that HBO_2 probably nas a structure like that of HN_3.[9] The OBO group is supposed linear with the H atom off-axis, and attached to one of the oxygens. We have taken the HOB angle to be 120°, and the B—O and B═O bond lengths to be 1.34 A and 1.20 A, respectively. For C_s symmetry there should be five fundamentals in A' and one perpendicular mode in A''. In HBO_2 the OH stretching is found at 3680 cm^{-1}, while the OD stretch occurs at 2750 cm^{-1} in DBO_2. The B═O stretch appears at 2030 cm^{-1} both in DBO_2 and HBO_2 with normal boron abundance, but at 2083 cm^{-1} in samples enriched in B^{10}.‡

Only one other band was observed, that near 1420 cm^{-1} in the natural species. Within the accuracy of our measurements no change was observed on substitution of D_2O for H_2O. This band, however, appears somewhat shifted when a B^{10}-enriched sample is used. These observations, together with magnitude of the frequency suggest that this band is characteristic of a mode involving a B—O stretch. The measurements are not precise enough for a good estimate of the B^{10}–B^{11} isotope shift to be made, though it appears to be real and appreciable. Actually, one expects two fundamentals in this region. They may be described very crudely as due to the B—O stretching and O—H bending modes. It is possible that they are both present in the broad and weak emission band observed near 1400 cm^{-1} though it is perhaps more probable that the OH bending, likely to be the weaker of the two, falls at lower wave numbers. We have assumed that it occurs near 1250 cm^{-1}. It is found experimentally that there is indeed a band in the vicinity of 1300 cm^{-1} in the HBO_2 (and 1000 cm^{-1} in DBO_2). However, because of its low intensity and its similarity to the pure H_2O (or D_2O) emission in this region, its identification with the molecule HBO_2 (or DBO_2) cannot be made positively. The two remaining fundamentals have been estimated by analogy with HN_3 and from the results obtained for B_2O_3. The parallel mode is placed at 600 cm^{-1}. The frequency assignment for the molecule HBO_2 is summarized in Table I.

TABLE I. Frequency assignment for gaseous HBO_2.

Species	Frequency (cm^{-1})[a]	Approx character of mode
A'	3680	O—H stretch
	2030	B═O stretch
	1420	B—O stretch
	(1250)	O—H bend
	(600)	O—B═O bend
A''	(700)	O—B═O bend

[a] The frequencies given in parentheses have been estimated. The others have been observed in natural $HBO_2(g)$.

TABLE II. Thermal functions of gaseous HBO_2 (cal deg^{-1} $mole^{-1}$).

T(°K)	$-(F°-H_0°/T)$	$H°-H_0°/T$	$S°$	C_p
50	34.35	7.94	42.30	7.94
100	39.86	7.95	47.81	7.98
200	45.41	8.13	53.54	8.82
273.15	47.99	8.44	56.44	9.79
298.15	48.73	8.57	57.31	10.12
300	48.79	8.58	57.37	10.14
500	53.43	9.70	63.14	12.52
750	57.62	11.01	68.63	14.57
1000	60.94	12.08	73.02	15.92
1250	63.73	12.95	76.68	16.85
1500	66.16	13.65	79.82	17.51
1750	68.31	14.24	82.56	17.99
2000	70.25	14.73	84.98	18.35
2500	73.62	15.51	89.14	18.82
3000	76.50	16.09	92.60	19.11
3500	79.02	16.53	95.56	19.30
4000	81.25	16.89	98.14	19.42
5000	85.08	17.41	102.50	19.58
6000	88.29	17.78	106.08	19.66

It did not seem worthwhile, in view of the incompleteness of the data and the low molecular symmetry, to make a detailed force constant analysis. However, some pilot calculations for the A' block, using transferred force constants from the molecule B_2O_3,[6] were made. If the force constant for the B—O—H bonding is chosen to give a frequency for the mode involving the O—H bend in the range 1200–1400 cm^{-1}, it is found that the other calculated frequencies are in fair agreement with the experimental observations.

The thermal functions for the molecule HBO_2 are given in Table II. The calculations were made with the frequency assignment given in Table I and the molecular constants given in the text.

V. DISCUSSION

A. Heat of Formation and Bond Energies of $HBO_2(g)$

From the variation of the intensity of the 2030 cm^{-1} band of HBO_2 with temperature, the heat of the

[8] D. A. Dows and G. C. Pimentel, J. Chem. Phys. **23**, 1258 (1955).

‡ From Fig. 1 it would appear that there is a larger B^{10}—B^{11} isotope shift in this band when D_2O was used in place of H_2O. This, however, is a result of overlapping by the H_2O spectrum.

TABLE III. Estimated frequency assignment for gaseous $(HBO_2)_3$ (C_{3h} symmetry).

Species	Frequency (cm^{-1})
A_1'	550
	1150
	950
	3500
A_2'	1100
	600
	500
A_2''	250
	500
	350
E'	750
	900
	1300
	1000
	600
	450
	3500
E''	350
	200
	1000

TABLE IV. Thermal functions of gaseous $(HBO_2)_3$ (cal deg^{-1} $mole^{-1}$).

T(°K)	$-(F°-H_0°/T)$	$H°-H_0°/T$	$S°$	C_p
50	45.18	8.05	53.24	8.62
100	51.12	9.50	60.62	13.74
200	59.19	14.48	73.67	24.66
273.15	64.24	18.07	82.32	30.97
298.15	65.88	19.24	85.12	32.90
300	66.00	19.32	85.32	33.04
500	77.84	27.34	105.18	44.64
750	90.38	34.55	124.93	52.41
1000	101.05	39.59	140.64	56.69
1250	110.30	43.30	153.61	59.41
1500	118.46	46.15	164.61	61.27
1750	125.75	48.41	174.17	62.59
2000	132.34	50.25	182.59	63.56
2500	143.87	53.05	196.92	64.83
3000	153.73	55.08	208.82	65.59
3500	162.34	56.62	218.97	66.08
4000	169.99	57.82	227.81	66.41
5000	183.09	59.58	242.68	66.81
6000	194.07	60.81	254.88	67.03

reaction

$$\tfrac{1}{2}B_2O_3(l)+\tfrac{1}{2}H_2O(g)\rightarrow HBO_2(g)$$

was found to be 39.0±2.5 kcal/mole at 1350°K or, employing the heat content functions of Table II, $\Delta H_0°=45.5$ kcal/mole. This corresponds to a heat of formation, $\Delta H_0°(f)$, of −135.0±3.0 kcal/mole for $HBO_2(g)$. The B—O and B═O bond energies derived from this result are in close agreement with those deduced for $B_2O_3(g)$. If 130 kcal/mole is assumed for the boron-oxygen single bond energy in $HBO_2(g)$ the boron-oxygen double bond energy has the value 207 kcal/mole.

B. Thermal Functions of the Gaseous Molecule $(HBO_2)_3$

The identification of a trimeric species $(HBO_2)_3$ by Chupka and Berkowitz[4] makes it worthwhile to suggest an assignment and calculate thermodynamic functions for this molecule even if it could have been present only to a very small extent in the $B_2O_3(l)+H_2O(g)$ system under our experimental conditions. The electron diffraction investigation of trimethylboroxole, $(MeBO)_3$, by Bauer and Beach[10] showed that the six-membered OBOBOB ring is planar. More recent work on the Raman spectra of several other boroxoles by Goubeau and Keller,[11] as well as analogy with the spectroscopic results obtained for borazole and its derivatives, provides a convenient basis for guessing a probable vibrational assignment for the trimer. We assume it has C_{3h} symmetry and the following molecular constants: $r(B—O)=1.36$ A, $r(OH)=1.0$ A, $\sphericalangle BOB=120°$; $\sphericalangle BOH=120°$. In this approximation it is assumed that there are no internal rotational degrees of freedom. The estimated frequency assignment for the molecule $(HBO_2)_3$ is shown in Table III.

Thermal functions computed from the frequency assignment in Table III are given in Table IV.

ACKNOWLEDGMENTS

The authors are indebted to Dr. W. A. Chupka for making available to us his preliminary results and to Dr. Charles W. Beckett for many stimulating discussions.

[10] S. H. Bauer and J. Y. Beach, J. Am. Chem. Soc. **63**, 1394 (1941).

[11] J. Goubeau and H. Keller, Z. anorg. u. allgem. Chem. **272**, 303 (1953).

Unimolecular Decomposition of Chemically Activated Ethyl-d_2 Radicals

B. S. RABINOVITCH, D. H. DILLS,* W. H. MCLAIN,† AND J. H. CURRENT†

Department of Chemistry, University of Washington, Seattle 5, Washington

(Received August 24, 1959)

Addition of H atoms to *trans*-ethylene-d_2 produces chemically activated ethyl-d_2 radicals. This choice of the reactant ethylene permits all subsequent secondary processes of the hot ethyl radicals to be counted. The system has been studied between −78° and 160°C, and in most detail at room temperature, as a function of ethylene pressure. Experimental details are similar to those given in previous work on butyl. The relative energy spread of the formed ethyl radicals is here effectively greater than that observed for butyl radical since the thermal spread is not superimposed upon a minimum excess above the critical energy, as was the case for butyl. Nevertheless, relative to high-temperature thermal decompositions, the product ethyl radicals are comparatively monoenergetic, especially at the lowest temperature. The observed rate constant for decomposition k_a was evaluated from the amounts of stabilization *vs* decomposition by C—H rupture. The decomposition rate is compared with theoretical expressions. An isotope effect appears to exist for transfer of H and D in the disproportionation of ethyl-d_2 radicals at 25°.

THE present paper deals with the unimolecular decomposition of energized ethyl-d_2 radicals produced by addition of H atoms to *trans*-ethylene-d_2. The features of this type of experiment, both practical and theoretical, have been pointed out earlier in a study of the decomposition of *sec*-butyl radicals.[1] The chemical activation step, reaction (1), may be followed by both decomposition processes (2) and (3).

$$\mathrm{H}+trans\text{-}\mathrm{C_2H_2D_2}\rightarrow\mathrm{CH_2DC\dot{H}D}^*, \qquad (1)$$

$$\mathrm{CH_2DC\dot{H}D}^* \xrightarrow{k_E} cis\text{-}\mathrm{C_2H_2D_2}\ (trans\text{-}\mathrm{C_2H_2D_2})+\mathrm{H} \qquad (2)$$

$$\xrightarrow{k'_E}\mathrm{C_2H_3D}+\mathrm{D}. \qquad (3)$$

The actual reaction of importance in determining lifetimes for decomposition of the energized ethyl, measured relative to stabilization by (4),

$$\mathrm{CH_2DC\dot{H}D}^*+\mathrm{M}\xrightarrow{\omega}\mathrm{CH_2DC\dot{H}D}+\mathrm{M}, \qquad (4)$$

is reaction (2) the inverse of the formation process; the isotopic labeling of the reactant ethylene permits these events to be counted. The decomposition of ethyl thus differs in an important respect from *sec*-butyl. The latter decomposes by rupture of a C—C bond, and the minimum energy of the energized butyl radicals exceeds the C—C bond dissociation energy by an appreciable amount (~8–10 kcal/mole). The effective energy spread for ethyl radicals should thus be larger than that of butyl formed at the same temperature. If k_a is the observed average rate constant for decomposition at a particular pressure, then $k_a=\omega\cdot D/S$ and $k_{a\infty}/k_{a0}=\langle k_E^2\rangle/\langle k_E\rangle^2=F$ where F, defined by Johnston,[2] gives a measure of the effective energy spread of formed radicals.[1] The dispersion to be anticipated here is thus larger than that found for *sec*-butyl at the same temperature, but still significantly less than that which would arise from a conventional thermal activation process at elevated temperatures.

EXPERIMENTAL

The *trans*-ethylene-d_2 was 99.3% pure, with 0.7% ethylene-d_1 as the impurity. Light ethylene was Phillips research grade and was used without further purification. Tank hydrogen was purified in early work by use of a palladium thimble, and later by passage through silica gel at −195°.

The apparatus and procedure were similar to that described previously,[1] except that the distance from the effusion leak to the hydrogen discharge region was approximately 6 cm. The H atom effusion rate varied around 10^{14}–10^{15} atoms/sec. The percent reaction varied usually from 2–8%. The geometric isomerization of *trans*-ethylene-d_2 was determined by measuring the transmission of the 842-cm^{-1} band of *cis*-ethylene-d_2. Ethylene-d_1 and ethylene-d_3 were determined at 70 v with a Consolidated 21-103 mass spectrometer. The mass 16 peak was examined for evidence of *asym*-ethylene-d_2. Parent peak analyses were also done at low ionizing potential. The isotopic ethane, propane and butane fractions were analyzed at 70 v for some runs. Some check analyses were done on the hydrogen-methane fraction with the mass spectrograph. Other than the composition of the ethylenes, most of the quantitative analyses were made using GLPC.

Solution of the equation of continuity for H atom transport with known values[3] of the rate constant for addition of H to ethylene, shows that atoms were consumed homogeneously at ethylene pressures above 0.1–0.5 mm, depending upon temperature; internal evidence given later indicates that at lower pressures

* Deceased.

† Abstracted in part from thesis to be presented to the Graduate School.

[1] B. S. Rabinovitch and R. W. Diesen, J. Chem. Phys. **30**, 735 (1959); this reference should be consulted for nomenclature, etc.

[2] H. S. Johnston, J. Chem. Phys. **20**, 1103 (1952); H. S. Johnston and J. R. White, *ibid.* **22**, 1969 (1954).

[3] (a) B. deB. Darwent and J. Roberts, Discussions Faraday Soc. **14**, 55 (1953); (b) A. B. Callear and J. C. Robb, Trans. Faraday Soc. **51**, 638 (1955).

TABLE I. Some illustrative product analyses and results.

Temp. °C	−78	−78	−20	−20	25	25	25	25	25
Press. mm	0.40	1.08	0.10	0.26	0.05	0.25	0.25	0.90	1.40
Ethane[a]	1.7	4.1	5.2	3.4	3.4	2.0	2.3	0.69	1.3
Propane	2.5	4.8	9.0	4.7	6.0	2.8	2.8	0.55	0.83
Butane	12	22	21	16	11.5	13.3	17	6.1	8.5
Cis[b]	8.0	4.3	63	38	67	38	48	9.0	5.7
Mono	0.69	...[c]	5.2	2.3	7.3	5.1	3.9	2.2	0.58
Tri	trace	0.00	1.0	1.7	3.5	1.7	1.9	1.0	trace
D/S	0.55	0.15	2.2	1.7	6.0	2.6	2.5	1.3	0.60
h/d	11.8		12.1	16.4	9.2	7.5	12.3	4.1	9.8
$k_a 10^7$ sec^{-1}	0.42[d]	0.30	0.38	0.72	0.46	1.04	0.97	1.85	1.25

[a] All products are in units of 10^{-3} cc of gas at 25° C and have been corrected in the various ways described in the text; the negligible amounts of methane have been omitted.
[b] Also corrected for secondary reaction with H.
[c] Three dots signifies analysis very inaccurate, lost, or not made.
[d] Collision cross sections employed taken from H. W. Melville and J. C. Robb, Proc. Roy. Soc. (London) **A196**, 445 (1949).

reflection of H atoms at the wall occurred to maintain the requirement of homogeneous addition.

Back-effusion corrections are relatively less important in the present system as compared with the butene system, due to the smaller range of product masses here.

RESULTS AND DISCUSSION

Runs were made at −78°, −20°, 25°, and 160° C. Illustrative examples of product composition, etc., and their variation with run conditions are given in Table I. The data are corrected in a manner to be described. All the data are summarized in Fig. I. The results are evidently not characterized by great presion; within their limitations, however, they are consistent. The principal product, other than ethylenes, was butane, with smaller amounts of ethane and propane and traces of methane. Between −78° and 25°, only these were found. Above 25°, some amounts of higher products (C_5 and C_6) also occurred. At very low ethylene pressure or at temperatures below 25°, where the steady state H atom concentration was higher, the amount of propane increased. Ethylene-d_3 was not found at −78° but the amount formed increased at higher temperatures. In a few trial mass spectrographic analyses, HD was not detected in the hydrogen-methane fraction.

Stabilization/Decomposition Ratio

To calculate the amounts of stabilization S and decomposition D of energized ethyl radicals, the reaction mechanism must be formulated.

Primary Process

Reaction (1) is the principal process. The collision efficiency of reaction (1) is[3] $\sim 1.5\times10^{-4}$. That for abstraction by H atoms of H from ethylene or from product butane is much lower,[4] and these processes should not occur; that they do not occur is evidenced by the absence of higher unsaturated products. Another primary process, addition of D atoms arising from reaction (3), is minor and is considered in the following.

Secondary Reactions

The secondary processes which energized ethyl undergoes are reactions (2)–(4). The equilibrium ratio of *cis/trans*-ethylene-d_2 is unity,[5] so it may be assumed that *cis* production is one-half of the total reaction (2). For the simple scheme of reactions (1)–(4), the specific rate ratio for C—H/C—D rupture in $CH_2DÇHD^*$, *h/d*, is given by the ratio of products, *cis/mono*. For several reasons it is necessary to amend this simple ratio and the relative isotopic rates are not accurately known from the present work, nor can the expected dependence of *h/d* on pressure be observed. Nevertheless since reaction (3) is minor, the experimental lifetimes of $CH_2DÇHD^*$ are not significantly affected by the uncertainty attending the isotope effect.

The collision efficiency of reaction (4) is taken as unity for the present. Some aspects of this assumption were discussed previously[1] and are being actively studied in work with butyl. Unlike butyl, ethyl radicals contain no large minimum amount of excess energy above the critical energy required for decomposition and the assumption should be relatively more valid here in view of the low level of the excess thermal energy at the temperatures used.

A possible 1,2 hydrogen rearrangement reaction of $CH_2DÇHD^*$,

$$CH_2DÇHD^* \rightarrow ÇH_2CHD_2^*,$$

[4] A. F. Trotman-Dickenson, *Gas Kinetics* (Academic Press, Inc., New York, 1955), pp. 179, 225.
[5] Douglas, Rabinovitch, and Looney, J. Chem. Phys. **23**, 315 (1955).

which would ultimately give *asym*-ethylene-d_2 on H split-off, does not occur.

Reactions of Stabilized Ethyl Radicals

Experimentally, it is found that the principal reaction of stabilized ethyl is recombination, with concomitant disproportionation:

$$2CH_2DCHD \rightarrow C_4H_6D_4$$

$$\rightarrow cis(trans\text{-})C_2H_2D_2 + C_2H_4D_2 \quad (6a)$$

$$\rightarrow C_2H_3D + C_2H_3D_3. \quad (6b)$$

Assuming that all ethane arises from reactions (6a) and (6b), then the disproportionation/recombination ratio found at pressures above 0.15 mm averages to 0.15 at room temperature, in agreement with results of other workers.[6] The ratio rises to 0.3–0.4 at 0.03–0.05 mm due to the failure of the preceding assumption, as discussed just below. At lower temperature the ratio seems to rise somewhat to ~0.2. Earlier remarks for butyl radicals, regarding thermalization of the hot radicals and possible wall effects, apply here. Production of ethylene-d_1 by reaction (6b) complicates quantitative determination of h/d in energized ethyl-d_2 since the isotope in ethyl disproportionation is not accurately known (Table II). No real difficulty for determination of lifetimes is introduced, however, since reactions (6) may be deduced from (2) and (3) in counting decomposition of ethyl.

Other plausible reactions of ethyl are the following:

$$CH_2DCHD + H \xrightarrow{(a)} C_2H_4D_2^* \xrightarrow{(b)} 2CH_2D, \quad (7)$$

$$\xrightarrow{M} C_2H_4D_2, \quad (8)$$

$$\rightarrow cis\text{-}(trans\text{-})C_2H_2D_2 + H_2, \quad (9a)$$

$$\rightarrow C_2H_3D + HD, \quad (9b)$$

$$CH_2DCHD + CH_2D \rightarrow C_3H_5D_3. \quad (10)$$

Reaction (7) is well known[7] and together with (10) accounts for propane formation. The fact that $C_2H_4D_2^*$ formed by reaction (7a) is ~13 kcal/mole more energetic than the same species produced by inverse (7b), together with the fact that ethane formation from methyl recombination is probably in the fall-off region at these pressures and temperatures,[1,7] suggests that reaction (8) does not compete effectively with (7b). Reaction (10) goes at pressures above 0.1 mm, rather than ethane formation by methyl recombination, because the partial pressure of ethyl, taken as roughly constant throughout the reactor,[1] exceeds that of methyl. For example, at 25° the pressures are roughly 3×10^{-6} and $\sim3\times10^{-7}$ mm, respectively. That the present ethyl radical disproportionation/recombination ratio at room temperature is in the lower range of observed values,[6] at higher reaction pressures, is also *ad hoc* evidence against appreciable amounts of methyl recombination and reaction (8). At lower ethylene pressures, the average H atom concentration in the reactor rises with consequent increase in reaction (7); methyl pressure rises to $\sim10^{-6}$ mm and the apparent ethyl-disproportionation/recombination ratio increases due to methyl recombination. Correction of the total amount of stabilization for this source of ethane is insignificant at higher pressures, and still small (5%) at lower pressures.

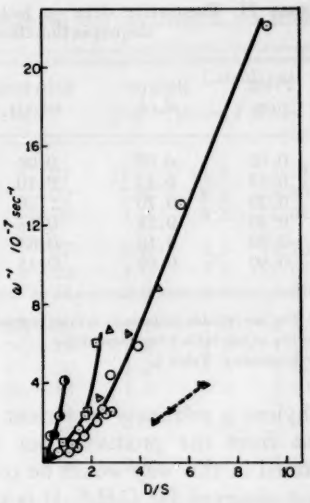

FIG. 1. D/S as a function of ω^{-1}, the average time between collisions. Half-filled circles represent data at −78°C; squares, −20°; circles, 25°; and triangles, early, less reliable data at 25° and 160°, respectively.

It may be noted that, whereas a molecule of butane corresponds to two stabilized radicals, a molecule of propane corresponds to three-halves radicals.

Reactions (9a) and (9b) are energetically plausible and if they occur[8] would further complicate the significance of the ratio *cis/mono*. Toby and Schiff suggest evidence that such reactions are relatively ineffective, while the apparent absence of HD in the products here supports this. A very tentative estimate[8b] for k_9/k_{7a} of ~0.05 further confirms these reactions as negligible for lifetimes.

The occurrence of small amounts (<15–20% butane) of C_5 and C_6 hydrocarbon products at 160° presumably shows an increasing extent of H abstraction reactions (by H atoms rather than by CH_3 or C_2H_5[4]) or of addition of radicals to the double bond. Ethylene isomerization cannot proceed to an appreciable extent by reversible C—C bond formation in any case, since not only is the addition of ethyl to

[6] (a) Smith, Beaty, Pinder, and LeRoy, Can. J. Chem. **33**, 821 (1955); (b) P. J. Boddy and J. C. Robb, Proc. Roy. Soc. (London) **A249**, 518 (1959); Bradley, Melville, and Robb, Proc. Roy. Soc. (London) **A236**, 318 (1956); (c) A. Shepp and K. O. Kutschke, J. Chem. Phys. **26**, 1020 (1957).

[7] E. W. R. Steacie, *Atomic and Free Radical Reactions* (Reinhold Publishing Corporation, New York, 1954).

[8] (a) S. Toby and H. I. Schiff, Can. J. Chem. **34**, 1061 (1956); (b) unpublished results of C. A. Heller and A. S. Gordon. We thank Dr. Heller for permission to quote these.

TABLE II. Illustrative data on isotope effect in ethyl radical disproportionation (25°).

Press mm	Butane[a] d_5/d_4	Ethylene *tri/cis*	Ethane d_3/d_2	X
0.05	0.07	0.06	0.11	0.07
0.15	0.13	0.10	0.25	0.22
0.20	0.10	...[b]	0.16	0.11
0.40	0.14	0.17	0.18	0.09
0.80	0.10	0.03	0.21	0.25
0.90	0.05	0.13	0.18	0.16

[a] The less reliable propane d_4/d_3 ratio is usually between the butane d_5/d_4 ratio and the *tri/cis* ratio when these differ.
[b] Footnote c, Table I.

ethylene a relatively inefficient reaction,[9] as seen here also from the products, but the lifetime of C_4H_9* formed in this way would be considerably longer than that observed for C_2H_5*. It is unnecessary to attempt to assess these side reactions in detail (in their interpretation as stabilization and decomposition products). They count as stabilization products primarily; they are minor in amount and merely make the quantitative aspect of the results a little more approximate at higher temperatures.

Secondary Reaction Due to D Atoms

For the simple scheme of reactions (2) and (4) one has $k_a=\omega\cdot D/S=\omega\cdot\nu$, where ν is the average chain length or number of "offs" of a H atom (providing all H atoms disappear in the gas phase). Because of reaction (3) additional reactions due to D arise:

$$\mathrm{D}+\textit{trans}\text{-}\mathrm{C_2H_2D_2}\rightarrow\mathrm{CHD_2\dot{C}HD}^*,$$

$$\mathrm{CHD_2\dot{C}HD}^*\rightarrow\textit{cis}\text{-}(\textit{trans}\text{-})\,\mathrm{C_2H_2D_2}+\mathrm{D},$$

$$\rightarrow\mathrm{C_2HD_3}+\mathrm{H},$$

$$\mathrm{CHD_2\dot{C}HD}^*+\mathrm{M}\rightarrow\mathrm{CHD_2\dot{C}HD}+\mathrm{M},$$

and to determine the lifetime of dideuteroethyl it is necessary to correct D/S for the amount of *cis* product and of stabilization products which arise from $C_2H_2D_3$*. The stabilization quantity is simply (*mono-tri*), in terms of ethylene reaction products. By use of the approximation[10] $h'/d'=h/d=cis/mono$, where h'/d' is the C—H/C—D specific rupture ratio in ethyl-d_3, the former correction is represented as $(tri\cdot mono/cis)$.

It is fortunate that the various correction factors discussed so far are minor in their effect on the experimental values for lifetimes of ethyl-d_2; because additional corrections enter into some of these factors, and a few new (very minor) corrections appear, due to the disproportionation reaction, ethyl-d_2+ethyl-d_3. These corrections are taken into account in the data of Tables I and II. They further invalidate the quantitative determination of isotope effects for H and D rupture in ethyl decomposition.

From mass-spectrographic analyses of the products an extremely crude and tentative estimate of the hydrogen-deuterium transfer isotope effect in ethyl radical disproportionation (taken as constant for the different radicals) may be obtained, assuming head-to-tail reaction.[11] The steady state concentration ratio of ethyl-d_2 and ethyl-d_3 may be estimated from various product ratios such as 2 butane-d_4/butane-d_5, propane-d_3/propane-d_4 or cis-ethylene-d_2/ethylene-d_3. The ratio per bond of D/H transfer, X, may then be calculated from the observed ratio ethane-d_3/ethane-d_2. Some illustrative data are shown in Table II for 25°. The range of X observed was 0.5–0.07 centered around 0.16. The actual magnitude of X is uncertain, but in any case, is not ~1.4. Similar magnitudes are found from recent data on $H+C_2D_4$.[12]

The expressions for D and S may now be summarized as

$$D=2(\textit{cis-tri}\cdot\textit{mono/cis})+\textit{mono},$$

$$S=2(\text{butane}+\text{ethane})+\tfrac{3}{2}\ \text{propane}+\mathrm{C_5}+\mathrm{C_6}$$
$$+(\textit{tri-mono})+\tfrac{1}{2}\ \text{methane},$$

where the ethylenes which enter in D are net amounts corrected for disproportionation.[13]

The definition of D includes here reaction (3), so k_a is a sum of average rate constants for H and D rupture. At such time as we succeed in making accurate measurements of the relative amounts of reactions (2) and (3), it will be necessary to consider the perturbation

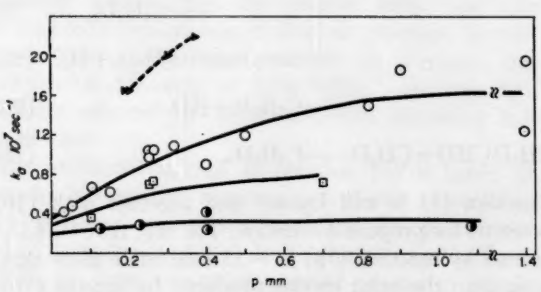

FIG. 2. Plot of k_a *vs* pressure extrapolated to zero pressure.

[9] D. G. L. James and E. W. R. Steacie, Proc. Roy. Soc. (London) **A244**, 289 (1958).
[10] T. B. Flanagan and B. S. Rabinovitch [J. Phys. Chem. **60**, 726 (1956)] find this so for thermally equilibrated species. In the present instance, $C_2H_2D_2$* arises by the process of D addition, not the less energetic H addition as for $C_2H_3D_2$*, and hence h/d is only an upper limit to h'/d'.
[11] M. H. J. Wijnen and E. W. R. Steacie, Can. J. Chem. **29**, 1092 (1951).
[12] A. H. Turner and R. J. Cvetanovic, Can. J. Chem. **37**, 1075 (1959).
[13] In the absence of more nearly complete and accurate analyses, the ratio ethane-d_3/ethane-d_2 was assumed constant at 0.18 for all runs. X was set at an average value 0.17. Then the correction at 25° to *cis* for disproportionation is 0.44 ethane-d_2+0.38 ethane-d_3=0.43 total ethane; the correction to *mono* for disproportionation is 0.27 ethane-d_3=0.04 total ethane; the like correction to *tri* is 0.12 ethane-d_3=0.10 total ethane. At lower temperatures, a *cis* correction=0.5 total ethane is an adequate disporportionation correction.

of the energy distribution function of the formed ethyl-d_2 radicals due to the occurrence of (3), in order to explain the observed isotope effect. Actually, for the present consideration of lifetimes, reaction (3) may be neglected since it constitutes <7–8% of the total decomposition at room temperature and below, and ~12–15% at higher temperatures; the results of this study have quantitative significance only with respect to order of magnitude and not exact magnitude.

Remarks on Shapes of D/S and k_a Plots

Figure 1 summarizes the D/S ratios obtained in all runs. Figures 2 and 3 show the extrapolation of k_a to obtain $k_{a\infty}$ and k_{a0}.

If the mechanism of back reaction was not unimolecular bond scission but involved rather a H transfer reaction of the sort[12]

$$C_2H_3D_2^* + trans\text{-}C_2H_2D_2 \rightarrow cis\text{-}C_2H_2D_2 + C_2H_3D_2$$

the chain length would not be pressure dependent. If some reaction went by this mechanism the plots of Fig. 1 would, for this factor, show an apparent negative intercept with the ordinate. There is no indication of any appreciable effect. For the same reason there is little evidence for a similar bimolecular exchange reaction of deactivated radicals.

The shape of the room temperature plot in Fig. 1 at low pressures is of some importance. The fraction of H atoms that reach the wall at 0.03-mm ethylene begins to approach unity. If H atoms reacted on the wall to produce ethyl then the D/S ratio would tend again to zero at high values of ω^{-1}. Instead the values are normal; thus reflection of H atoms occurs at the wall and the condition of homogeneous reaction in the absence of a heat sink is maintained.

The low pressure shape of the 25° plot also casts light on the practical validity of the assumption of unit collision efficiency for deactivating collisions; where the average energy of the formed radicals is here only several kcal above the critical energy at 25° and correspondingly less at lower temperatures. It is readily apparent, as will be discussed elsewhere, that a collisional energy cascade would give rise to increasingly anomalous (large) values of D/S and k_a at low pressures (Figs. 1 and 3) as the pressure declines. This effect should already be noticeable at $D/S \sim 10$. No significant tendency is observed and instead the data correspond to the naive collisional assumption made; any departure from the assumption appears not to be of practical importance here.

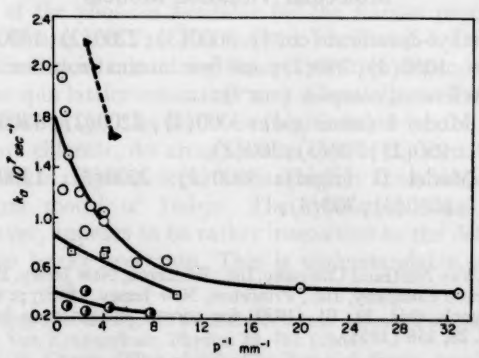

FIG. 3. Plot of k_a *vs* inverse pressure extrapolated to infinite pressure.

TABLE III. Comparison of observed and calculated k_a quantities.

	Temp °C	Obs	Calculated Model I	Calculated Model II
$k_{a\infty}$ 10^6 sec^{-1}	27	18	14.4	3.78
	−20	8.4	8.6	3.00
	−78	4.0	4.8	2.68
k_{a0} 10^6 sec^{-1}	27	3.6	4.8	2.70
	−20	3.0	3.8	2.64
	−78	2.0	3.2	2.56
$k_{a\infty}(T_1)/k_{a\infty}(T_2)$	27/−20	2.1[a]	1.7	1.26
	−20/−78	2.1	1.8	1.12
$k_{a0}(T_1)/k_{a0}(T_2)$	27/−20	1.2[a]	1.3	1.02
	−20/−78	1.5	1.2	1.03
$k_{a\infty}/k_{a0}$	27	5.0	3.0	1.41
	−20	2.8	2.3	1.14
	−78	2.0	1.5	1.05

[a] Calculated assuming no change in collisional stabilization efficiency with temperature.

The increasing curvature of the plots of Figs. 1–3 with rise of temperature is, as it was for *sec*-butyl, a pictorial demonstration of the loosening of quantum restrictions and departure from the relatively monoenergetic distribution of the lowest temperature.

Calculation of k_a

The values of k_a may be calculated as previously,[1] using the treatment of Marcus, once the thermochemistry of the reaction is established and models are chosen to represent the energized molecule and activated complex.

The quantity $\Delta E_0°$, for the reactants $H+C_2H_4$ and product C_2H_5, was calculated as −38 kcal/mole, taking $D_0(C_2H_5—H) = 96$ kcal/mole.[14] The activation energy at 0°K for addition of H to C_2H_4 has been here arbitrarily set at 4 kcal.[3] Hence the critical energy E_0 for decomposition of ethyl, is 42 kcal, and the same value is used for H rupture in dideuteroethyl. Any error in E_0 has small effect on the calculations and does not enter into the more sensitive quantity, E_{min}^+.

Models for the energized molecule and activated complex may be specified. In one version, all vibrations were assumed active. For the complex the (rounded)

[14] *Selected Values of Chemical Thermodynamic Properties*, Natl. Bur. Standards, Circ. 500, 1952; T. L. Cottrell, *The Strengths of Chemical Bonds* (Academic Press, Inc., New York, 1954).

vibration frequencies of ethylene-d_2[15] were used, modified by lowered C=C stretch and torsional frequencies (1300 and 700 cm^{-1}, respectively,) and by the addition of 2 C—H bends at the usual frequencies (rigid model), or reduced frequencies (semirigid model). A simple model of the energized radical is one in which the active internal rotation of a methylene group about the methyl axis is assumed free, which is actually quite plausible since the six minima in the torsional potential function must be very shallow. Recognizing the uncertainty in the numerical results of these experiments, and taking advantage of the tolerance of the rate calculations to approximations in the molecular model, we simplify the calculation by treating as separable the internal rotation and the over-all rotation about the asymmetric top axis,[16] as well as the lesser coupling with the other two rotations. The form of the rate expression of Marcus[17] involving internal rotation then applies, the overall rotations being taken as adiabatic. Any errors in approximations affecting the over-all rotations tend also to cancel for k_a ratios. Vibration frequencies used are given in the Appendix.[18]

The following expressions are obtained for these assumptions:

$$k_E = 2P_1^+ \sum_{E_{v+}=0}^{E^+} P(E_v^+)/hP_1^* N_E^*,$$

$$N_E^* = (8\pi^2 I_r/h^2)^{\frac{1}{2}} \sum_{E_v=0}^{<E} [P(E_v)/(E-E_v)^{\frac{1}{2}}] + (\partial P(E_v)/\partial E_v)_{E_v=E},$$

$$K(E) = N_E^* \exp(-E/RT)dE \Big/ \int_0^\infty N^* \exp(-E/RT)dE,$$

$$k_a = \int_0^\infty \frac{k_E^2 K(E)dE}{k_E+\omega} \Big/ \int_0^\infty \frac{k_E K(E)dE}{k_E+\omega}$$

$$= \int_0^\infty \frac{k_E}{k_E+\omega} \sum_{E_{v+}=0}^{E^+} P(E_v^+) \exp(-E^+/RT)dE^+ \Big/ \int_0^\infty \frac{\sum_{E_{v+}=0}^{E^+} P(E_v^+) \exp(-E^+/RT)dE^+}{k_E+\omega}$$

where P_1^+ is set equal to P_1^*, and I_r is evaluated for a planar radical.

The modified semiclassical integration previously employed[1,17] to evaluate the sums over the vibrational levels is inaccurate and was abandoned in favor of the more accurate direct count.[19] The integrals in k_a were evaluated graphically. The calculated values are compared in Table III with the observed results. Variation of the model has a larger effect on computed k_a ratios than is the case for *sec*-butyl,[1,19] because in the present instance E_{min}^+ has the lower limit zero. Model I gives substantial concordance of the calculated with the observed ratios as well as the absolute rate values. There would be no point in attempting to refine the agreement in view of the experimental uncertainty. It seems that a semi-rigid model describes the activated complex for this reaction and the reverse addition.

The enhanced ratios of $k_{a\infty}/k_{a0}$, relative to those for *sec*-butyl at the same temperatures, shows the anticipated increase in the dispersion of energy of the formed ethyl radicals. However, the absence of any low-lying frequencies in the parent molecule inhibits an even larger effect at these comparatively low temperatures.

It is hoped that more accurate isotopic rate data may be obtained by study of the ethyl-d_3 radical from D+*trans*-$C_2H_2D_2$, and this would provide a further and independent check of the theory and assumed models.

ACKNOWLEDGMENT

We thank the Office of Naval Research for their valuable support.

APPENDIX

Molecular Vibration Models

1. Ethyl-d_2 radical (cm^{-1}). 3000(3); 2200(2); 1300(4); 1050(3); 700(2); one free internal rotation.
2. Activated complex (cm^{-1}):
   Model I (semirigid): 3000(2); 2200(2); 1300(3); 950(2); 700(3); 300(2).
   Model II (rigid): 3000(2); 2200(2); 1300(4); 1050(3); 700(3).

[15] Crawford, Lancaster, and Inskeep, J. Chem. Phys. **21**, 678 (1953).
[16] J. G. Aston, *Physical Chemistry*, H. S. Taylor and S. Glasstone, eds. (D. Van Nostrand Company, Inc., Princeton, New Jersey, 1943), Vol. I, p. 590; G. Herzberg, *Infrared and Raman Spectra* (D. Van Nostrand Company, Inc., Princeton, New Jersey, 1945), p. 491.
[17] R. A. Marcus, J. Chem. Phys. **20**, 359 (1952). See D. R. Herschbach, *ibid.* **31**, 91 (1959) for correct energy levels for internal rotation of two asymmetric parts; also Wilson, Lin, and Lide, *ibid.* **23**, 136 (1955).
[18] I. F. Kovalev, Zhur. Fiz. Khim. **31**, 362 (1957).
[19] Harrington, Rabinovitch, and Diesen, J. Chem. Phys. (to be published).

Chlorine Nuclear Spin-Lattice Relaxation Time in Solid Sodium Chlorate and *p*-Dichloro Benzene*

P. A. BENDER, D. A. JENNINGS, AND W. H. TANTTILA

Physics Department, University of Colorado, Boulder, Colorado

(Received August 3, 1959)

The temperature dependence of the chlorine nuclear spin-lattice relaxation time between the pure quadrupole levels has been measured as a function of temperature in sodium chlorate and paradichlorobenzene. The results are compared with Chang's theory and found to be in good agreement. The Debye temperatures necessary to establish a fit with Chang's theory are 200°K and 90°K for sodium chlorate and paradichlorobenzene, respectively. The measurements were made in the temperature interval 300–10°K.

INTRODUCTION

THE temperature dependence of the spin-lattice relaxation time of nuclei has been treated by Van Kranendonk[1] and by Chang.[2] Van Kranendonk's theory treats the case of nuclei relaxing by means of the interaction of the nuclear quadrupole moment with the time-varying electric field gradients generated by the thermal lattice waves in a crystal. His theory is written for nuclei residing in a crystalline electric field having cubic symmetry. Thus it is directly applicable only to those cases in which the splitting of the spin levels is accomplished by the interaction of the nuclear magnetic moment with a magnetic field. Chang's theory, on the other hand, is somewhat more general and he has adapted it to predicting the temperature dependence of the relaxation time of the chlorine nuclear spin in sodium chlorate. The spin levels of the chlorine nuclei in sodium chlorate are split into two energy levels separated by 30 Mc.

In both Chang's and Van Kranendonk's theory the relaxation process at high temperatures (essentially above 1°K) takes place by the so-called Raman process. A phonon interacts with a nucleus by means of the quadrupole interaction giving off another phonon with the energy of the incident phonon minus the energy change of the nuclear spin. In both theories the temperature dependence of the relaxation time is essentially the same. The temperature dependence of the relaxation time comes principally from the temperature dependence of the phonons available for the Raman process. Both Chang and Van Kranendonk have used a Debye distribution in calculating the temperature dependence of the spin lattice relaxation time. Certainly the Debye distribution for the lattice waves is incorrect for the sodium chlorate. An array such as that of the structure of sodium chlorate departs considerably from the continuum model of Debye. The relaxation time T_1, however, appears to be rather insensitive to the details of the lattice spectrum. This is understandable since the relaxation time T_1 is a function of the integrated effect of all the lattice spectrum. Detailed departures of the lattice spectrum from the Debye spectrum would not bring about a temperature dependence of T_1 sensibly different from that predicted by the Debye spectrum so long as the general features of the Debye spectrum exist in the true lattice spectrum.

The purpose of the investigation of the temperature dependence of T_1 of the chlorine nuclei in sodium chlorate and paradichlorobenzene was to check Chang's theory in the light of the foregoing considerations. The temperature dependence of T_1 for chlorine in paradichlorobenzene was measured so as to exhibit the temperature dependence in a crystal quite different from sodium chlorate. Paradichlorobenzene is a monoclinic molecular crystal with a low melting point (53°C) and the chlorine is bonded to a benzene ring. This low intermolecular bonding energy as well as the difference between the chlorate complex and the paradichlorobenzene molecule would be expected to yield a lattice spectrum whose details would be different from the lattice spectrum for sodium chlorate.

Recently, Briscoe and Squire[3] have measured the relaxation time of iodine nuclei in potassium iodide in the liquid helium region. Their results are consistent with Van Kranendonk's theory. Kraus[4] has measured the temperature dependence of the sodium nuclear relaxation time in sodium chloride. His results are consistent with Van Kranendonk's theory.

Experimental Procedure

The pulsed nuclear induction method was used to measure the relaxation time. This method has been given elsewhere.[5] Our method differed in one important respect. Instead of using a 90° pulse we used a nonsaturating pulse. The method for making T_1 measurements was as follows: The nuclear sample was saturated by repeated pulsing at a fast rate. The pulsing rate was achieved electronically by a fast free-running

* Supported by a grant from the National Science Foundation.

[1] J. Van Kranendonk, Physica **20**, 781 (1954).

[2] C. H. Chang, Office of Scientific Research Repts. (available from Department of Physics, University of Washington, Seattle, Washington).

[3] C. V. Briscoe and C. F. Squire, Phys. Rev. **112**, 1540 (1958).

[4] O. Kraus, Bull. Am. Phys. Soc. Ser. 2, **3**, 166 (1958).

[5] Bloom, Hahn, and Herzog, Phys. Rev. **97**, 1699 (1955). B. Herzog and E. L. Hahn, Phys. Rev. **103**, 148 (1956). M. Bloom, Phys. Rev. **94**, 1396 (1954).

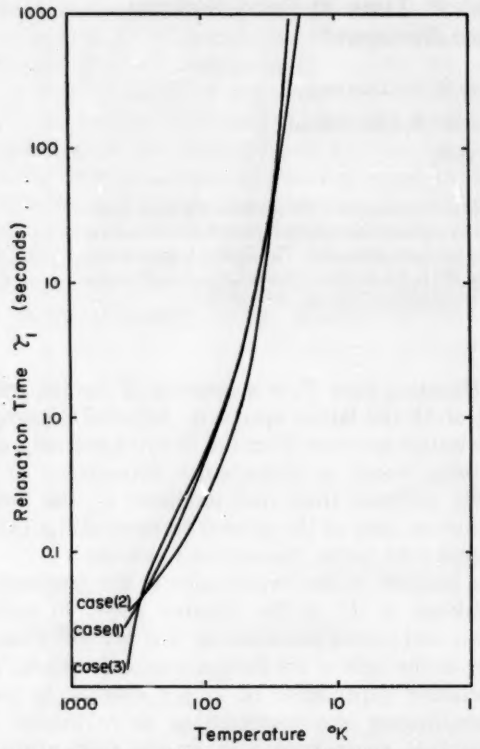

FIG. 1. Comparison of three cases of Chang's theory. Case (1), eqQ, α are assumed temperature independent. Case (2), α is assumed temperature dependent. eqQ depends linearly on T. Case (3), α is assumed temperature dependent. eqQ temperature dependence is assumed to be a parabola.

multivibrator. After the nuclear spins were saturated by the fast pulsing the multivibrator was stopped and a timer started simultaneously. After a period of time a single nonsaturating pulse was initiated by a push-button switch that simultaneously stopped the timer and the free-induction voltage was observed visually on the oscilloscope. This method works well for relaxation times of one second and longer. One need not be concerned about achieving a 90° pulse. The method is expecially suited to making determinations of the relaxation times of nuclear spins between Zeeman levels because the nonsaturating pulse is narrow and has a wide band width. This wide band width alleviates, to some extent, magnetic field drift which occurs during the time between saturation and the subsequent sampling of the spin system by the single pulse.

The temperatures were achieved as follows: The crossed-coil arrangement containing the sample crystal rested above the surface of the helium in the helium double Dewar. Light from a 100-w lamp was permitted to shine on the liquid helium. By varying the voltage on the lamp one could control the amount of helium gas leaving the surface of the liquid helium. To decrease the temperature the light intensity was increased. The temperature measurements were made with a gold-cobalt *versus* copper thermocouple. One junction of the thermocouple was placed in a brass slug that rested in the liquid helium and the other junction was tied to the sample crystal and coated with petrolatum to provide thermal contact between the sample crystal and the function. Several determinations of the relaxation time at one temperature were made. These determinations were made until the relaxation time indicated that essentially all thermal lag in the crystal had disappeared following a change in the temperature.

RESULTS

Chang shows that the main mechanism of quadrupole relaxation of the chlorine nucleus in the sodium chlorate crystal is due to the oxygen atoms. He then shows that the relaxation time T_1 is given by

$$T_1=[\tfrac{3}{2}(cb/MR^2)^2(K/h)^2T^2I_{13}]^{-1}\ \text{sec.}, \qquad (1)$$

where $R=1.46\times10^{-8}$ cm is the distance between the chlorine and the hypothetical nucleus which replaces the oxygen nuclei. The quantity I_{13} is evaluated by numerical integration and is dependent on the Debye temperature. M is the density of the crystal. The quantity cb can be estimated from the thermal expansion of the sodium chlorate crystal and the temperature dependence of eqQ for the chlorine nucleus in the same crystal. The linear thermal expansion coefficient of the

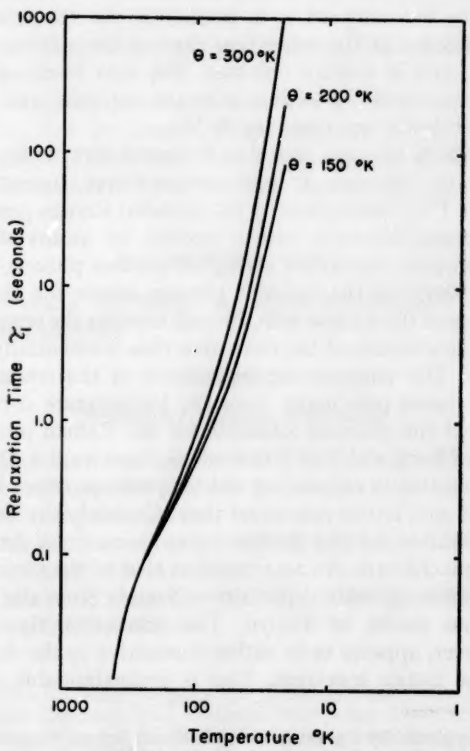

FIG. 2. By using Case (3) of Chang's theory, the effect of choosing different Debye temperatures is shown. All curves were normalized at 297°K to fit the experimental data.

sodium chlorate crystal α is temperature dependent and can be represented by[6]

$$\alpha=\beta_1+2\beta_2(T-298)/°K,$$

where $\beta_1=4.36\times10^{-5}/°K$ and $\beta_2=3.6\times10^{-8}/(°K)^2$. This can be considered as the linear expansion coefficient of the distance between the sodium nucleus and the chlorate group. As the oxygen ions are more tightly bound to the chlorine ion the expansion coefficient of the distance between the chlorine and the oxygen is presumably smaller than that of the crystal as a whole. As there is not enough information to estimate it accurately, Chang writes for the linear expansion coefficient of the chlorate group

$$\alpha^1=f\alpha,$$

where f is a constant smaller than unity.

The values of eqQ of the chlorine nucleus in sodium chlorate have been measured at only three temperatures.[7] Chang fits these three points by a straight line,

$$eqQ=61.78-0.0064T \text{ Mc/sec}, \quad (2)$$

or by a parabola,

$$eqQ=57.72+(15.39-0.03647T)^{\frac{1}{2}} \text{ Mc/sec}. \quad (3)$$

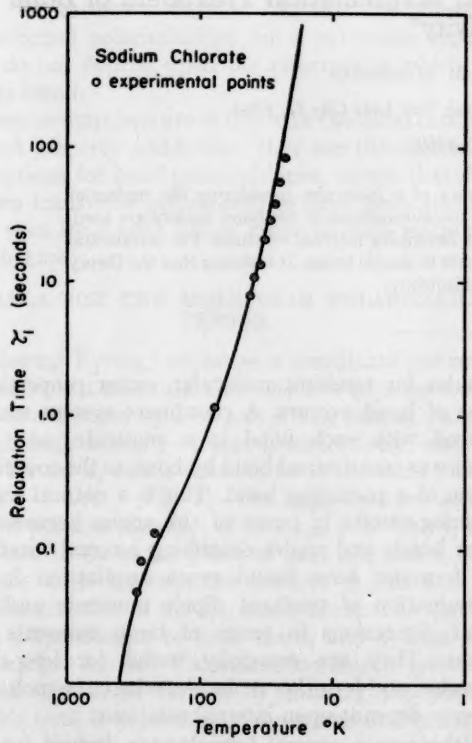

FIG. 3. Comparison of experimental points with Case (3) of Chang's theory, Debye temperature is 200°K.

[6] W. P. Mason, Phys. Rev. **70**, 529 (1946).
[7] Wang, Townes, Schawlow, and Holden, Phys. Rev. **86**, 809 (1952).

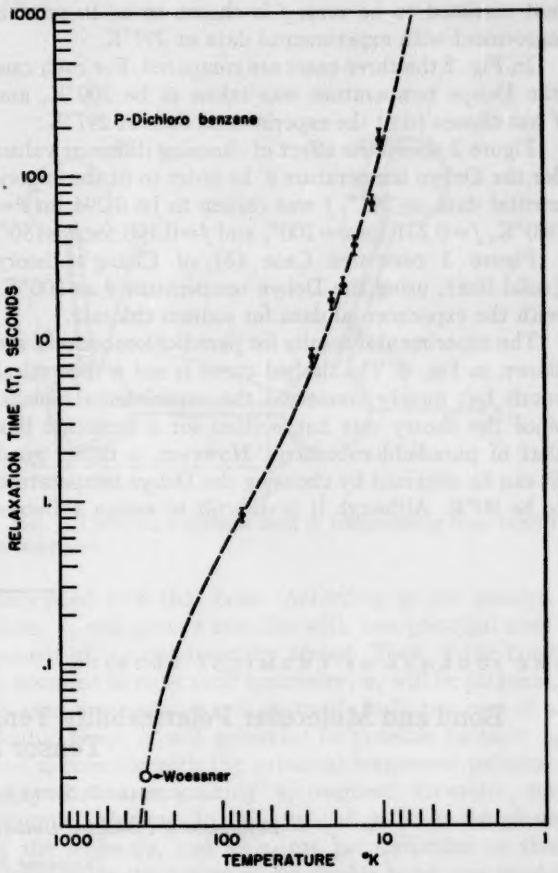

FIG. 4. Temperature dependence of the chlorine nuclear spin-lattice relaxation time in paradichlorobenzene. The dashed line merely connects the experimental points. The relaxation time at 300°K was measured by D. E. Woessner [Ph.D. thesis, University of Illinois (1957)].

In the calculation of the relaxation time due to the sodium Chang found that the computed values were too long for the relaxation mechanism to involve the sodium nuclei. On the other hand, in the calculation of the relaxation time due to the oxygens Chang computed the following three cases.

Case (1).—This is a rough calculation in which

$$f=0.302,\ eqQ=60 \text{ Mc/sec and } \beta_2=0.$$

The temperature dependences of eqQ and α are neglected. In this case we have

$$cb=547 \text{ Mc/sec}=6.05\times10^{-18} \text{ ergs}.$$

Case (2).—The relation between eqQ and T is assumed to be a straight line as given by Eq. 2, but β_2 is not assumed to be zero. The value of f is chosen so that the computed relaxation time at room temperature, 297°K agrees with the experimental value. The appropriate value of f is 0.308.

Case (3).—The relation between eqQ and T is assumed to be a parabola as given by Eq. (3), but β_2 is

not assumed to be zero. f is chosen so as to provide agreement with experimental data at 297°K.

In Fig. 1 the three cases are compared. For each case the Debye temperature was taken to be 200°K, and f was chosen to fit the experimental data at 297°K.

Figure 2 shows the effect of choosing different values for the Debye temperature θ. In order to fit the experimental data at 297°, f was chosen to be 0.294 for $\theta=300$°K, $f=0.231$ for $\theta=200$°, and $f=0.198$ for $\theta=150$°.

Figure 3 compares Case (3) of Chang's theory (solid line), using the Debye temperature θ as 200°K, with the experimental data for sodium chlorate.

The experimental results for paradichlorobenzene are shown in Fig. 4. The dashed curve is not a theoretical result but merely connected the experimental points, since the theory was not written for a structure like that of paradichlorobenzene. However, a rather good fit can be obtained by choosing the Debye temperature to be 90°K. Although it is difficult to assign a Debye temperature to a complex structure such as either sodium chlorate or paradichlorobenzene, the lower melting point and lack of rigidity of the paradichlorobenzene relative to the sodium chlorate does indicate a lower Debye temperature for the paradichlorobenzene.

The theory of Van Kranendonk[1] can be used to fit the experimental points quite well even though the theory was not written for pure quadrupole splitting. There is no question of the essential correctness of either Chang's or Van Kranendonk's theory.

ACKNOWLEDGMENTS

We wish to thank Dr. Richard Kropschot and Mr. Robert Powell of the National Bureau of Standards for assisting us in obtaining calibrated thermocouple leads as well as furnishing us with advice on low temperature measurements. Dr. William Love and Dr. Albert Bartlett loaned us equipment essential to the performance of the experiment.

THE JOURNAL OF CHEMICAL PHYSICS VOLUME 32, NUMBER 2 FEBRUARY, 1960

Bond and Molecular Polarizability Tensors. I. Mathematical Treatment of Bond Tensor Additivity*

RICHARD P. SMITH AND EARL M. MORTENSEN

Department of Chemistry, University of Utah, Salt Lake City 12, Utah

(Received August 10, 1959)

A general equation is obtained for the polarizability tensor of a molecule, considering the molecular tensor to be constructed from bond tensors. Bond-by-bond transformations of the bond tensors are used, so that the general equation involves bond angles and angles describing internal rotations. For tetrahedral hydrocarbons and their derivatives, the general equation reduces to simple forms. It is shown that the theory provides a simple method for the calculation of molecular anisotropy.

INTRODUCTION

EXTENSIVE consideration has been given the problem of the calculation of scalar molecular properties by the simple addition of bond properties. Empirical bond refractions and bond energies, for example, may be added to determine, with a high degree of success, the corresponding molecular properties.

Vector properties also have been considered in terms of bond property additivity. It was suggested by J. J. Thomson[1] that the dipole moment of a molecule be regarded as a vector sum of bond and group moments, and many investigations along these lines subsequently have been made. In 1932 Eyring[2] derived general formulas for resultant molecular vector properties in terms of bond vectors. A coordinate system was associated with each bond in a molecule, and each vector was transformed bond by bond to the coordinate system of a particular bond. This is a natural way of obtaining results in terms of the angles between adjacent bonds and angles describing internal rotations. The formulas have found much application in the determination of resultant dipole moments and molecular dimensions in terms of bond moments and lengths. They are especially useful for long-chain molecules, and for other molecules where the molecular property depends upon internal rotations.

In this paper, general formulas are derived for molecular tensor properties, assuming the molecule to be an assembly of additive bond tensors. Previously, such formulas have been given only for special cases, following the original suggestion by Meyer and Otter-

* Supported in part by the National Science Foundation, and in part by the Standard Oil Company of California through a Predoctoral Research Fellowship held by E. M. M., 1957–1959.

[1] J. J. Thomson, Phil. Mag. **46** [6], 497 (1923).

[2] H. Eyring, Phys. Rev. **38**, 746 (1932).

bein[3] that the polarizability tensor for a molecule might be considered to be a tensor sum of bond and group contributions. We will see that a general consideration of the problem will lead to some useful and interesting results.

In this paper, Eyring's method of assigning a coordinate system to each bond, and of transforming the bond property (in this case a tensor) bond by bond, will be followed. The formulas derived here for the polarizability tensor could also be used for any other molecular property which one wishes to consider in terms of contributions from bond tensors.

ASSUMPTIONS

We assume that each bond in a molecule may be assigned a polarizability tensor with one of the principal axes along the bond axis. The polarizability along this axis is called the longitudinal polarizability, $b^{(1)}$. The other two principal polarizabilities, $b^{(2)}$ and $b^{(3)}$, which are known as the transverse polarizabilities, are perpendicular to the bond direction and to each other. They are assumed to be unequal in general; however, for certain types of bonds, they will ordinarily be taken equal. In the latter case, the bond is said to have axial symmetry, since any axis perpendicular to the bond direction will be a principal axis with the same polarizability. We assume additivity, i.e., that the values of the principal polarizabilities for a particular type of bond do not depend upon the structure in which the bond is found.

These assumptions are in line with the usual concepts of bond property additivity. They are the customary assumptions for bond polarizabilities, except that often the two transverse polarizabilities have been assumed equal even for double bonds, while no such restriction is made here.

FORMULA FOR THE MOLECULAR POLARIZABILITY TENSOR

Following Eyring,[2] we assign a coordinate system to each bond in a molecule. Consider two adjacent bonds which are denoted by $j-1$ and j. The axes x_{j-1} and x_j pass through bonds $j-1$ and j, respectively, and the origin for the x_j axis is taken to be at the atom joining bonds $j-1$ and j (Fig. 1). The angle between axis x_j and the positive direction of axis x_{j-1} is θ_j. The y_j axis is defined to be in the plane of axes x_{j-1} and x_j such that the angle between the positive y_j axis and the negative direction of the x_{j-1} axis is acute. The z_j axis is taken perpendicular to both the x_j and y_j axes such that a right-handed Cartesian coordinate system is formed. The angle formed by rotating the positive z_{j-1} axis until it is parallel to the z_j axis and in such a direction that a right-handed screw progresses along the positive x_{j-1} axis is denoted by ϕ_j.

Consider now the expression for the polarizability tensor α_j of the jth bond in the coordinate system

[3] E. H. L. Meyer and G. Otterbein, Physik Z. 32, 290 (1931).

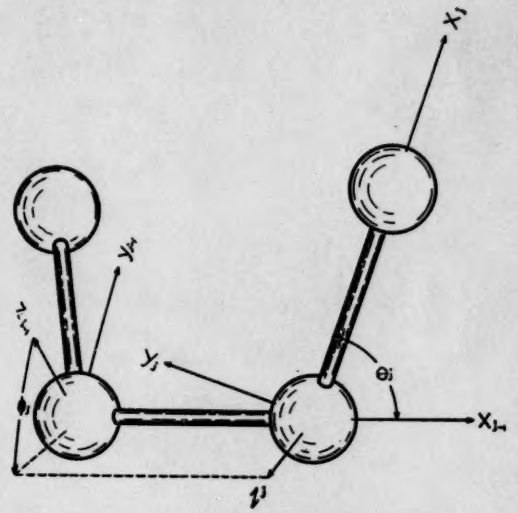

FIG. 1. Coordinate systems used in transforming from bond j to bond $j-1$.

associated with that bond. According to our assumptions, x_j will always coincide with one principal component of the polarizability tensor. Then, if the bond is assumed to have axial symmetry, α_j will be diagonal. If axial symmetry is not assumed, as in the case of a double bond, it will generally be possible to have y_j and z_j coincide with the principal transverse polarizability directions, making α_j diagonal. Consider, for example, ethylene. In this case, all y_j lie in the plane of the molecule, and all z_j are perpendicular to this plane. From the nature of the double bond, one would expect that the principal components of the polarizability tensor perpendicular to the bond direction are parallel to the y_j and z_j axes. Assuming that it is always possible to assign a coordinate system of the type discussed above to each bond such that the coordinate axes for each bond are parallel to the principal axes for that bond, α_j can be represented by the diagonal matrix

$$\alpha_j = \begin{pmatrix} b_j^{(1)} & 0 & 0 \\ 0 & b_j^{(2)} & 0 \\ 0 & 0 & b_j^{(3)} \end{pmatrix} \tag{1}$$

where $b_j^{(2)} = b_j^{(3)}$ for bonds with axial symmetry.

When expressed in the coordinate system of bond $j-1$, the polarizability tensor α_j becomes[4]

$$\mathbf{A}_j \cdot \alpha_j \cdot \mathbf{A}_j^{-1} \tag{2}$$

where $\mathbf{A}_j$ represents the transformation or direction cosine matrix relating the jth coordinate system to the $j-1$st, given by[2]

$$\mathbf{A}_j = \Phi_j \cdot \Theta_j \tag{3}$$

[4] Wilson, Decius, and Cross, *Molecular Vibrations* (McGraw-Hill Book Co., Inc., New York, 1955), p. 359.

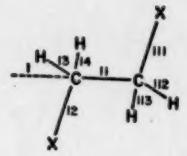

FIG. 2. The use of "bond" *1* in 1,2-dihaloethane.

where

$$\Phi_j=\begin{pmatrix}1 & 0 & 0\\ 0 & \cos\phi_j & -\sin\phi_j\\ 0 & \sin\phi_j & \cos\phi_j\end{pmatrix};$$

$$\Theta_j=\begin{pmatrix}\cos\theta_j & -\sin\theta_j & 0\\ \sin\theta_j & \cos\theta_j & 0\\ 0 & 0 & 1\end{pmatrix}. \tag{4}$$

Likewise, the polarizability α_j transformed to the coordinate system of bond $j-2$ is given by

$$\mathbf{A}_{j-1}\cdot\mathbf{A}_j\cdot\boldsymbol{\alpha}_j\cdot\mathbf{A}_j^{-1}\cdot\mathbf{A}_{j-1}^{-1}. \tag{5}$$

This procedure may be continued so that α_j may be expressed in terms of any coordinate system.

Let us now consider a numbering system for the bonds. A terminal bond may be chosen as a starting point in numbering and may be designated as bond 1. If it is more desirable to choose an internal bond, such as the C—C bond in the case of ethane and its simple derivatives, less difficulty is encountered if one constructs an axis collinear with the axis of the internal bond as in Fig. 2. This axis may then be treated as though it were a terminal bond and may be designated as "bond" *1*. The bonds adjacent to *1* are denoted by *11*, *12*, etc. All bonds adjacent to *12* which have not been previously numered are designated by *121*, *122*, etc. This procedure is continued until all bonds are numbered. Figure 3 shows an example of the numbering in isobutane. For a given molecule, various ways of numbering the bonds in accordance with this system are of course possible. For example, when numbering around rings various possibilities present themselves, and it is not fundamentally important which choice is made.

The general bond will be designated $i_1i_2\cdots i_j$. For bond *112*, $i_1=1$, $i_2=1$, $i_3=i_j=2$. Then the polarizability tensor for the general bond, referred to bond *1*, may be written,

$$\prod_{k=2}^{j}\mathbf{A}_{i_1i_2\cdots i_k}\cdot\boldsymbol{\alpha}_{i_1i_2\cdots i_j}\cdot\prod_{k=j}^{2}\mathbf{A}_{i_1i_2\cdots i_k}^{-1} \tag{6}$$

where $\mathbf{A}_{i_1i_2\cdots i_k}$ is the transformation from the coordinate system of bond $i_1i_2\ldots i_k$ to that of bond $i_1i_2\cdots i_{k-1}$. In certain instances, it may be desirable to transform the polarizability expressed in the coordinate system of bond *1* to some arbitrary set of axes in space (perhaps determined by the symmetry of the molecule). For this purpose, we use a transformation $\mathbf{A}_{i_1}=\mathbf{A}_1$. Introducing this transformation in (6) and summing over all bonds in the molecule, we obtain for the molecular polarizability tensor,

$$\boldsymbol{\alpha}=\sum_{\text{bonds}}\prod_{k=1}^{j}\mathbf{A}_{i_1i_2\cdots i_k}\cdot\boldsymbol{\alpha}_{i_1i_2\cdots i_j}\cdot\prod_{k=j}^{1}\mathbf{A}_{i_1i_2\cdots i_k}^{-1}. \tag{7}$$

Before introducing the explicit form of α_j [Eq. (1)] in Eq. (7), it is convenient to effect the following decomposition of the bond tensor. First, we break up the bond polarizability tensor into the sum of an isotropic tensor and an anisotropic tensor[5]:

$$\boldsymbol{\alpha}_j=\bar{\alpha}_j\mathbf{E}+\begin{pmatrix}\frac{1}{3}(2b_j^{(1)}-b_j^{(2)}-b_j^{(3)}) & 0 & 0\\ 0 & \frac{1}{3}(2b_j^{(2)}-b_j^{(3)}-b_j^{(1)}) & 0\\ 0 & 0 & \frac{1}{3}(2b_j^{(3)}-b_j^{(1)}-b_j^{(2)})\end{pmatrix}. \tag{8}$$

Here $\mathbf{E}$ is the unit tensor, and

$$\bar{\alpha}_j=\tfrac{1}{3}(b_j^{(1)}+b_j^{(2)}+b_j^{(3)}) \tag{9}$$

is the average polarizability of the jth bond. With the further introduction of the quantities

$$\gamma_j=\tfrac{1}{2}(2b_j^{(1)}-b_j^{(2)}-b_j^{(3)}), \tag{10}$$

$$\delta_j=\tfrac{1}{2}(b_j^{(2)}-b_j^{(3)}), \tag{11}$$

Eq. (8) may be reduced to

$$\boldsymbol{\alpha}_j=\bar{\alpha}_j\mathbf{E}+\tfrac{1}{3}\gamma_j\mathbf{F}+\delta_j\mathbf{G} \tag{12}$$

where

$$\mathbf{F}=\begin{pmatrix}2 & 0 & 0\\ 0 & -1 & 0\\ 0 & 0 & -1\end{pmatrix};\qquad \mathbf{G}=\begin{pmatrix}0 & 0 & 0\\ 0 & 1 & 0\\ 0 & 0 & -1\end{pmatrix}. \tag{13}$$

For an axially symmetric bond δ_j vanishes, while γ_j reduces to the bond anisotropy[5] $b_j^{(1)}-b_j^{(2)}$.

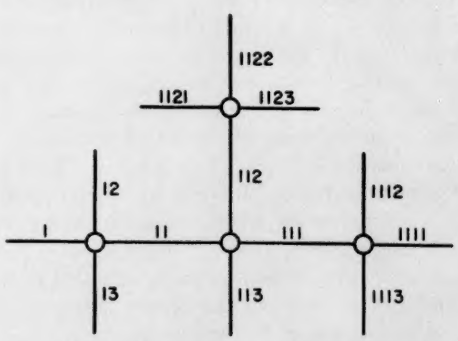

FIG. 3. Bond numbering in isobutane.

[5] E. V. Chalam, Proc. Indian Acad. Sci. **A15**, 190 (1942).

One advantage of the decomposition represented by Eq. (12) is that the bond polarizability tensor components have been factored out of tensors, so that α may be written as a sum of terms in which the bond tensor components appear only in scalar coefficients. For, upon substitution of Eq. (12) into Eq. (7), we obtain

$$\alpha=\mathbf{E}\sum_{\text{bonds}}\bar{\alpha}_{i_1 i_2\cdots i_j}+\tfrac{1}{3}\sum_{\text{bonds}}\gamma_{i_1 i_2\cdots i_j}\mathbf{F}_{i_1 i_2\cdots i_j}+\sum_{\text{bonds}}\delta_{i_1 i_2\cdots i_j}\mathbf{G}_{i_1 i_2\cdots i_j} \quad (14)$$

where

$$\mathbf{F}_{i_1 i_2\cdots i_j}=\prod_{k=1}^{j}\mathbf{A}_{i_1 i_2\cdots i_k}\cdot\mathbf{F}\cdot\prod_{k=j}^{1}\mathbf{A}_{i_1 i_2\cdots i_k}^{-1} \quad (15)$$

$$\mathbf{G}_{i_1 i_2\cdots i_j}=\prod_{k=1}^{j}\mathbf{A}_{i_1 i_2\cdots i_k}\cdot\mathbf{G}\cdot\prod_{k=j}^{1}\mathbf{A}_{i_1 i_2\cdots i_k}^{-1} \quad (16)$$

are tensors involving only the molecular geometry. The first summation in Eq. (14) is simply the mean polarizability of the entire molecule. All terms in the final summation are zero except for contributions made by nonaxially symmetric bonds. If all bonds are isotropic, both the second and third summations will vanish.

Although the bond-by-bond transformations used above may be applied to any molecule and will be very convenient for most complex molecules, certain cases may best be treated by transforming the polarizability tensor for each bond directly to some set of reference axes. If this is done, the decomposition of the polarizability tensor according to Eq. (12) will still be advantageous. Then Eq. (14) will still be valid if we understand $\mathbf{F}_{i_1 i_2\cdots i_j}$ to mean $\mathbf{F}$ transformed directly from the bond coordinate system to the reference system, and similarly for $\mathbf{G}_{i_1 i_2\cdots i_j}$.

TETRAHEDRAL MOLECULES

We now turn our attention to some simplifications in the second summation of Eq. (14) for tetrahedral molecules. It will be shown that the geometry of the tetrahedral arrangement of bonds is such that simple general formulas may be given for such classes of molecules as aliphatic hydrocarbons.

Consider identical axially symmetric bonds *11*, *12*, and *13* which, together with bond *1*, are tetrahedrally arranged about an atom (Fig. 4). The contribution made by the bonds *11*, *12*, and *13* to α is, according to Eq. (14),

$$\mathbf{E}(\bar{\alpha}_{11}+\bar{\alpha}_{12}+\bar{\alpha}_{13})+\tfrac{1}{3}\mathbf{A}_1\cdot(\gamma_{11}\mathbf{A}_{11}\cdot\mathbf{F}\cdot\mathbf{A}_{11}^{-1}+\gamma_{12}\mathbf{A}_{12}\cdot\mathbf{F}\cdot\mathbf{A}_{12}^{-1}+\gamma_{13}\mathbf{A}_{13}\cdot\mathbf{F}\cdot A_{13}^{-1})\cdot\mathbf{A}_1^{-1}.$$

If bonds *11*, *12*, and *13* are of the same type, so that $\gamma_{11}=\gamma_{12}=\gamma_{13}$, we have the combination of terms

$$\mathbf{A}_{11}\cdot\mathbf{F}\cdot\mathbf{A}_{11}^{-1}+\mathbf{A}_{12}\cdot\mathbf{F}\cdot\mathbf{A}_{12}^{-1}+\mathbf{A}_{13}\cdot\mathbf{F}\cdot\mathbf{A}_{13}^{-1}.$$

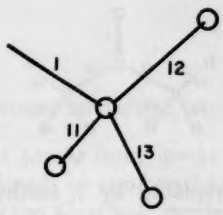

FIG. 4. Tetrahedral arrangement of bonds.

Now for the tetrahedral case $\theta_{11}=\theta_{12}=\theta_{13}=\cos^{-1}(\frac{1}{3})$ and it follows that

$$\mathbf{A}_{11}\cdot\mathbf{F}\cdot\mathbf{A}_{11}^{-1}=\begin{vmatrix} -\frac{2}{3} & (2\sqrt{2}/3)\cos\phi_{11} & (2\sqrt{2}/3)\sin\phi_{11} \\ (2\sqrt{2}/3)\cos\phi_{11} & (\frac{8}{3})\cos^2\phi_{11}-1 & (\frac{8}{3})\cos\phi_{11}\sin\phi_{11} \\ (2\sqrt{2}/3)\sin\phi_{11} & (\frac{8}{3})\cos\phi_{11}\sin\phi_{11} & \frac{5}{3}-(\frac{8}{3})\cos^2\phi_{11} \end{vmatrix}$$

with similar expressions holding for $\mathbf{A}_{12}\cdot\mathbf{F}\cdot\mathbf{A}_{12}^{-1}$ and $\mathbf{A}_{13}\cdot\mathbf{F}\cdot\mathbf{A}_{13}^{-1}$. In view of the relations

$$\phi_{12}=\phi_{11}+120°$$

$$\phi_{13}=\phi_{11}+240°$$

the following identities hold

$$\cos\phi_{11}+\cos\phi_{12}+\cos\phi_{13}=0$$

$$\sin\phi_{11}+\sin\phi_{12}+\sin\phi_{13}=0$$

$$\cos\phi_{11}\sin\phi_{11}+\cos\phi_{12}\sin\phi_{12}+\cos\phi_{13}\sin\phi_{13}=0$$

$$\cos^2\phi_{11}+\cos^2\phi_{12}+\cos^2\phi_{13}=\tfrac{3}{2}$$

and hence,

$$\mathbf{A}_{11}\cdot\mathbf{F}\cdot\mathbf{A}_{11}^{-1}+\mathbf{A}_{12}\cdot\mathbf{F}\cdot\mathbf{A}_{12}^{-1}+\mathbf{A}_{13}\cdot\mathbf{F}\cdot\mathbf{A}_{13}^{-1}=-\mathbf{F}. \quad (17)$$

With the aid of this relationship, considerable simplification of Eq. (14) is easily made for molecules having tetrahedrally arranged bonds.

According to Eq. (14), the polarizability tensor for methane is

$$\alpha=4\bar{\alpha}_{CH}\mathbf{E}+\tfrac{1}{3}\gamma_{CH}[\mathbf{A}_1\cdot\mathbf{F}\cdot\mathbf{A}_1^{-1}+\mathbf{A}_1\cdot(\mathbf{A}_{11}\cdot\mathbf{F}\cdot\mathbf{A}_{11}^{-1}+\mathbf{A}_{12}\cdot\mathbf{F}\cdot\mathbf{A}_{12}^{-1}+\mathbf{A}_{13}\cdot\mathbf{F}\cdot\mathbf{A}_{13}^{-1})\cdot\mathbf{A}_1^{-1}].$$

Here the bonds are assumed axially symmetric, and are numbered as in Fig. 4. With the aid of Eq. (17), this immediately reduces to the familiar result

$$\alpha=4\bar{\alpha}_{CH}\mathbf{E}, \quad (18)$$

i.e., any axis is a principal axis along which the polarizability equals the average polarizability of the molecule.

Let us consider aliphatic hydrocarbon molecules, which are assumed to have all bond angles tetrahedral and all bonds axially symmetric. Any such molecule may be imagined to be constructed by starting with methane and successively replacing particular hydrogen atoms by methyl groups. Suppose the jth bond to be a C—H bond. If the hydrogen atom of this bond is

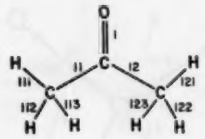

FIG. 5. Bond numbering in acetone.

replaced by a methyl group, the jth bond becomes C—C, and three C—H bonds are added, which may be designated $j1, j2$, and $j3$, respectively. This substitution necessitates the modification of the second summation in Eq. (14) by the addition of

$$-\tfrac{1}{3}\gamma_{CH}\mathbf{F}_j+\tfrac{1}{3}\gamma_{CC}\mathbf{F}_j+\tfrac{1}{3}\gamma_{CH}(\mathbf{F}_{j1}+\mathbf{F}_{j2}+\mathbf{F}_{j3}).$$

Now

$$\mathbf{F}_{j1}+\mathbf{F}_{j2}+\mathbf{F}_{j3}=\mathbf{A}_1\cdots\mathbf{A}_j\cdot(\mathbf{A}_{j1}\cdot\mathbf{F}\cdot A_{j1}^{-1}$$
$$+\mathbf{A}_{j2}\cdot\mathbf{F}\cdot A_{j2}^{-1}+\mathbf{A}_{j3}\cdot\mathbf{F}\cdot\mathbf{A}_{j3}^{-1})\cdot\mathbf{A}_j^{-1}\cdots\mathbf{A}_1^{-1}$$
$$=\mathbf{A}_1\cdots\mathbf{A}_j\cdot(-\mathbf{F})\cdot\mathbf{A}_j^{-1}\cdots\mathbf{A}_1^{-1}=-\mathbf{F}_j$$

by Eq. (17). Thus, conversion of C—H to C—CH_3 makes necessary the addition of

$$(\bar{\alpha}_{CC}+2\bar{\alpha}_{CH})\mathbf{E}+\tfrac{1}{3}(\gamma_{CC}-2\gamma_{CH})\mathbf{F}_j$$

to the polarizability tensor. Considering the result for methane, Eq. (18), in conjunction with this fact, we see that the general expression for the polarizability tensor for any tetrahedral aliphatic hydrocarbon is

$$\boldsymbol{\alpha}=\bar{\alpha}_{\text{molecule}}\mathbf{E}+\tfrac{1}{3}(\gamma_{CC}-2\gamma_{CH})\sum_{CC}\mathbf{F}_j \qquad (19)$$

where $\bar{\alpha}_{\text{molecule}}$ is the sum of the average polarizabilities of all the bonds, and where the sum is taken over C—C bonds only.

Equation (19) holds also if rings are present, provided there is no deviation of bond angles from tetrahedral, e.g., the equation holds for cyclohexane and to a good approximation, for cyclopentane. For a ring may be thought of as being formed by taking an open-chain system, bringing two of the C—H bonds into coincidence, and replacing them by a C—C bond; this modifies the polarizability tensor by adding

$$(\bar{\alpha}_{CC}-2\bar{\alpha}_{CH})\mathbf{E}+\tfrac{1}{3}(\gamma_{CC}-2\gamma_{CH})\mathbf{F}_j$$

where j designates the new C—C bond formed. The terms with CC subscripts are for the new C—C bond, and the terms with CH subscripts are subtracted to allow for the two C—H bonds which are removed.

If a C—H bond is replaced by a C—X bond (X= halogen) then, according to Eq. (14), the polarizability tensor will be modified by the addition of the terms

$$(\bar{\alpha}_{CX}-\bar{\alpha}_{CH})\mathbf{E}+\tfrac{1}{3}(\gamma_{CX}-\gamma_{CH})\mathbf{F}_j$$

where j denotes the bond replaced by a C—X bond. Thus, for halogen-substituted aliphatic hydrocarbons,

$$\boldsymbol{\alpha}=\bar{\alpha}_{\text{molecule}}\mathbf{E}+\tfrac{1}{3}(\gamma_{CC}-2\gamma_{CH})\sum_{CC}\mathbf{F}_j+\tfrac{1}{3}(\gamma_{CX}-\gamma_{CH})\sum_{CX}\mathbf{F}_j \qquad (20)$$

where the summations are over the types of bonds indicated.

TENSOR INVARIANTS

Chalam[5] has considered two invariants related to the polarizability tensor. The first is the spur of the molecular tensor, which he showed to be equal to the sum of the spurs of the bond tensors. This is easily seen to be true in our formalism. Since $\mathbf{F}$ and $\mathbf{G}$ have vanishing spurs, the spurs of these tensors will still vanish after coordinate system transformations. Hence, the theorem readily follows from Eq. (14), where we need consider only the first summation on the right-hand side.

The second invariant considered by Chalam is the quantity,

$$\gamma^2=\tfrac{1}{2}[(A-B)^2+(B-C)^2+(C-A)^2] \qquad (21)$$

where γ^2 is the so-called molecular anisotropy, and A, B, and C are the principal polarizabilities of the molecule. This expression is useful in the theories of light depolarization and the Kerr effect. If the polarizability tensor, in the principal coordinate system, is broken up as an isotropic tensor and an anisotropic tensor as follows,

$$\boldsymbol{\alpha}=\tfrac{1}{3}(A+B+C)\mathbf{E}$$
$$+\begin{vmatrix}\tfrac{1}{3}(2A-B-C) & 0 & 0\\ 0 & \tfrac{1}{3}(2B-C-A) & 0\\ 0 & 0 & \tfrac{1}{3}(2C-A-B)\end{vmatrix},$$

it is readily seen that γ^2 is three-halves the sum of squares of all the terms of the anisotropic tensor. Since the sum of squares of all terms of a symmetric tensor is invariant, γ^2 is invariant. Thus, it is not necessary to know A, B, and C to calculate γ^2. We need only calculate $\boldsymbol{\alpha}$ in any convenient coordinate system by Eq. (14), and then apply the equation

$$\gamma^2=\tfrac{3}{2}\sum_{r,s}\gamma_{rs}^2 \quad (r,s=x,y,z) \qquad (22)$$

where γ_{rs} is the rs component of the anisotropic tensor, the latter being given by the second and third summations in Eq. (14), i.e.,

$$\gamma_{rs}=(\boldsymbol{\alpha}-\bar{\alpha}_{\text{molecule}}\mathbf{E})_{rs}.$$

If every bond is referred directly to the basic coordinate system, a formula given by Chalam is ultimately obtained. For flexible molecules, however, this formula is inconvenient, as it involves the angles between all pairs of bonds in the molecule, rather than

the bond angles and internal rotation angles. Thus, it will often be preferable to use our Eq. (14) in the manner described above for a calculation of the anisotropy.

EXAMPLES

1,2-Dihaloethane, XCH_2CH_2X. For "bond" *1* we take an extension of the C—C bond axis (see Fig. 2). Then, referring all bonds to the coordinate system of "bond" *1*, application of Eq. (20) yields

$$\alpha=\bar{\alpha}_{\text{molecule}}\mathbf{E}+\tfrac{1}{3}X\mathbf{F}+\tfrac{1}{3}Y(\mathbf{F}_{12}+\mathbf{F}_{111})$$

where

$$X=\gamma_{CC}-2\gamma_{CH}$$

$$Y=\gamma_{CX}-\gamma_{CH}$$

provided we take y_1 and z_1 parallel to y_{11} and z_{11}, respectively, so that $\mathbf{A}_{11}=\mathbf{A}_1=\mathbf{E}$. Assuming the molecule to be tetrahedral,

$$\theta_{12}=109°28'$$

$$\theta_{111}=180°-109°28'.$$

Consistent with our other coordinate choices we may choose z_1 parallel to z_{12}. Then,

$$\phi_{12}=0$$

$$\phi_{111}=\phi$$

where ϕ is the angle between the projections of the C—X bonds on the y_1z_1 plane i.e., the plane perpendicular to the C—C bond. Making the above substitutions, we find

$$\mathbf{F}_{12}+\mathbf{F}_{111}=\tfrac{1}{3}\begin{pmatrix}-4 & 2\sqrt{2}(\cos\phi-1) & 2\sqrt{2}\sin\phi\\ 2\sqrt{2}(\cos\phi-1) & 8(\cos^2\phi+1)-6 & 8\sin\phi\cos\phi\\ 2\sqrt{2}\sin\phi & 8\sin\phi\cos\phi & 8\sin^2\phi-6\end{pmatrix}$$

so that the components of the anisotropic tensor are

$$\gamma_{zz}=(\tfrac{2}{3})X-(\tfrac{4}{9})Y$$

$$\gamma_{zy}=\gamma_{yz}=(\tfrac{2}{9})\sqrt{2}(\cos\phi-1)Y$$

etc. Then

$$\gamma^2=\tfrac{3}{2}(\gamma_{zz}^2+\gamma_{zy}^2+\gamma_{yz}^2+\cdots)$$
$$=X^2-(\tfrac{4}{3})XY+(\tfrac{4}{27})(7-4\cos\phi+16\cos^2\phi)Y^2.$$

For the *trans* form, $\phi=\pi$; for the *gauche* form, $\phi=\frac{1}{3}\pi$.

Acetone, CH_3COCH_3. Let the bonds be numbered as shown in Fig. 5, and let ϕ be the C—C—C angle. Let the C=O axis be the x axis in the basic coordinate system to which we ultimately refer all bonds; the y y axis is in the C—C—C plane, and the z axis is perpendicular to this plane. Then, application of Eq. (14) yields

$$\alpha=\bar{\alpha}_{\text{molecule}}\mathbf{E}+\tfrac{1}{3}\gamma_{C=O}\mathbf{F}+\tfrac{1}{3}\gamma_{CC}(\mathbf{F}_{11}+\mathbf{F}_{12})$$
$$+\tfrac{1}{3}\gamma_{CH}(\mathbf{F}_{111}+\mathbf{F}_{112}+\mathbf{F}_{113}+\mathbf{F}_{121}+\mathbf{F}_{122}+\mathbf{F}_{123})+\delta_{C=O}\mathbf{G}.$$

Assuming tetrahedral methyl groups,

$$\mathbf{F}_{111}+\mathbf{F}_{112}+\mathbf{F}_{113}=-\mathbf{F}_{11}$$

$$\mathbf{F}_{121}+\mathbf{F}_{122}+\mathbf{F}_{123}=-\mathbf{F}_{12}$$

[cf. Eq. (17)]. With the use of such relations as

$$\cos\phi_{11}+\cos\phi_{12}=\cos\phi_{11}+\cos(\pi+\phi_{11})=0,$$

we find that $\mathbf{F}_{11}+\mathbf{F}_{12}$ has a simple diagonal form, yielding

$$\alpha=\bar{\alpha}_{\text{molecule}}\mathbf{E}+\tfrac{1}{3}\gamma_{C=O}\begin{pmatrix}2&0&0\\0&-1&0\\0&0&-1\end{pmatrix}$$
$$+\tfrac{1}{3}(\gamma_{CC}-\gamma_{CH})\begin{pmatrix}6\cos^2(\phi/2)-2&0&0\\0&6\sin^2(\phi/2)-2&0\\0&0&-2\end{pmatrix}$$
$$+\delta_{C=O}\begin{pmatrix}0&0&0\\0&1&0\\0&0&-1\end{pmatrix}.$$

It is now trivial to write expressions for the components of α and to calculate derived quantities, such as γ^2.

Bond and Molecular Polarizability Tensors. II. Discussion of Values of Polarizability Parameters for Some Single Bond Involving Carbon*

RICHARD P. SMITH AND EARL M. MORTENSEN

Department of Chemistry, University of Utah, Salt Lake City 12, Utah

(Received August 10, 1959)

It is pointed out that for C—C, C—H, C—O, and C—halogen bonds, the experimental data on molecular polarizability tensors (light depolarization data, Kerr constants, etc.) do not permit evaluation of longitudinal and transverse bond polarizabilities. Only certain linear combinations of these quantities, involving parameters for more than one type of bond, are determinable. The data pertaining to these bonds are discussed in this light. Denbigh's longitudinal and transverse polarizabilities[1] for C—halogen bonds probably are essentially correct, but his C—C and C—H polarizabilities are not meaningful.

INTRODUCTION

IN attempting to simplify the problem of molecular anisotropy, it is natural to begin with the supposition that bonds have characteristic tensor ellipsoids of polarizability, and that the polarizability ellipsoids for molecules may be closely estimated by summing bond ellipsoids. There is no clear evidence for the truth of this provisional assumption. Refraction studies have shown the mean polarizabilities of bonds to be excellent bond constants.[1,2] However, as Bolton[3] has pointed out, it may be that bond polarizability components are not constant, as the ellipsoid representing a bond tensor could appear in different molecules with varying shapes, with the bond still retaining about the same average polarizability.

With this present lack of understanding, it seems best to assume simple tensor additivity of the bond polarizability components, and then to test this assumption by seeing how it works out in practice. In the preceding paper (I),[4] general equations were worked out for the calculation of molecular polarizability components, using the provisional additivity assumption. In this paper, we will see that an examination of these equations readily leads to some interesting conclusions regarding past and future attempts to assign bond ellipsoids from observations on molecular anisotropy.

The bond polarizability ellipsoid idea was first suggested in 1931 by Meyer and Otterbein.[5] Otterbein[6,7] investigated the Kerr constant data for monochlorobenzene and the three dichlorobenzenes. It was found possible to correlate the data for these molecules by assuming characteristic polarizability components for the benzene ring and for the C—Cl bond. Unfortunately, the bond angles for ortho- and metadichlorobenzene were deduced from dipole moment data, assuming strict vector additivity, and hence were incorrect. The Kerr effect measurements were made in solution.

Later, Sachsse[8] made a serious attempt to assign polarizability ellipsoids for C—C, C—H, C—Cl, and C=C bonds, using solution Kerr effect data on simple molecules such as CH_3Cl and CH_2Cl_2. For the molecules studied, he wrote expressions for the molecular anisotropy in terms of the molecular geometry and symbols representing the longitudinal and transverse polarizabilities of the bonds involved. Then the equations were solved simultaneously for the bond polarizability parameters.

In 1939 and 1940, respectively, Wang[9] and Denbigh[1] constructed longer tables of longitudinal and transverse bond polarizabilities, using Sachsse's method of calculation, but with Kerr effect and light depolarization data for gases.

Serious difficulties have presented themselves in these attempts to assign bond polarizabilities. In particular, the C—C bond polarizabilities assigned by Wang and by Denbigh are not reasonable, as Bunn and Daubeny[10] have noted, since the former authors agree in assigning a very large ratio (over 90 in both cases) of longitudinal polarizability to transverse polarizability. This ratio is many times larger than the reasonable ratios (~1 to 3) found for the other bonds for which values were determined. Bunn and Daubeny considered the refractive indices of the hexatriacontane crystal, and found the more realistic ratio 3.67; Bolton,[3] using quantum mechanics, found 1.84.

Wang and Denbigh both determined C—C, C—H, and C=O polarizability components by the method of Sachsse, using simultaneous equations for methane, ethane, and acetone. Thus, by this scheme, the C—C and C—H values are interrelated, and the calculation

* Supported in part by the National Science Foundation, and in part by the Standard Oil Company of California through a Predoctoral Research Fellowship held by E. M. M., 1957–1959.

[1] K. G. Denbigh, Trans. Faraday Soc. **36**, 936 (1940).
[2] B. C. Vickery and K. G. Denbigh, Trans. Faraday Soc. **45**, 61 (1949).
[3] H. C. Bolton, Trans. Faraday Soc. **50**, 1261 (1954).
[4] R. P. Smith and E. M. Mortensen, J. Chem. Phys. **32**, 502 (1960).
[5] E. H. L. Meyer and G. Otterbein, Physik. Z. **32**, 290 (1931).
[6] G. Otterbein, Physik. Z. **34**, 645 (1933).
[7] G. Otterbein, Physik. Z. **35**, 249 (1934).
[8] G. Sachsse, Physik. Z. **36**, 357 (1935).
[9] S.-N. Wang, J. Chem. Phys. **7**, 1012 (1939).
[10] C. W. Bunn and R. de P. Daubeny, Trans. Faraday Soc. **50**, 1173 (1954).

made by Bunn and Daubeny, referred to above, is open to question, since these authors made use of Denbigh's C—H polarizabilities. Of greater importance is a fundamental objection to Wang's and Denbigh's scheme, pointed out by Le Fèvre and Le Fèvre[11]: In order to have enough simultaneous equations, it was necessary to assume axial symmetry for the carbonyl bond. This certainly would not be expected to be a good assumption. In this connection, it should be noted that theoretical calculations made by Bolton[3] indicated different transverse polarizabilities for the C=C bond. We have repeated the Wang and Denbigh calculations for C—H, C—C, and C=O bonds, modified by taking different transverse C=O polarizabilities (with the principal directions assumed to be in the C—C—C plane and out of this plane, respectively), and we have found the results, particularly for the C—C bond, to be quite sensitive to the value assigned for the ratio of the two C=O transverse polarizabilities.

It might be supposed that the C—H bond polarizabilities (together with the C—Cl values) are known from Sachsse's calculations on the methane derivatives or could be determined by bringing these calculations up to date. However, here we encounter a fundamental difficulty. As Le Fèvre and Le Fèvre[11] noted, when we write equations for the molecular polarizability components in terms of bond constants for methane and its chloro derivatives, (assuming these molecules to be tetrahedral), we find that the equations are not soluble, there not being a sufficient number of independent equations. Le Fèvre and Le Fèvre supposed this to be a general problem for tetrahedral halogenated hydrocarbons, although this proposition was not proved. It is proved below to be a general problem, and the formulation given in the preceding paper (I)[4] is shown to be well suited for a clarification.

In view of the impossibility of getting solutions for methane derivatives which are assumed exactly tetrahedral, Sachsse's calculations are invalidated, as the possibility of solving for C—Cl and C—H polarizabilities by this method depends upon the small deviations of the angles from tetrahedral, so that the results obtained are extremely sensitive to the rather uncertain data used. Le Fèvre and Le Fèvre[12] verified this great sensitivity, and we have verified it also.

Recently, Pitzer[13] has discussed the interaction of polarizable units in a molecule, a phenomenon which has largely been ignored. He points out that this phenemonon may account for some of the difficulties which have been encountered in the assignment of bond polarizabilities. We take the viewpoint that the importance of such interactions or of other factors in deviations from additivity cannot be assessed until a scheme assuming strict additivity has been given a fair trial. This will require the analysis of accurate data in terms of "determinable polarizability parameters," as discussed in the following section and illustrated in the remainder of the paper. We do not find the analysis of the experimental data given below to be conclusive, as the uncertainties in the data seem to be too great for any definite conclusions on additivity to be drawn. In the meantime, it must be admitted that deviations from additivity caused by bond interactions may be important, so that simple additivity will prove to be unsatisfactory in many situations. Such has certainly been the case with bond dipole moment vector additivity.

DETERMINABLE POLARIZABILITY PARAMETERS

According to Eq. (19) of I, each component of the polarizability tensor for a tetrahedral hydrocarbon involves the bond polarizability parameters only in the combination

$$\Gamma_{CC} \equiv \gamma_{CC} - 2\gamma_{CH}. \tag{1}$$

Transformation to any coordinate system, including one in which the polarizability tensor is diagonal, will not alter this situation. Now, observable quantities (Kerr constants, light depolarization factors) are expressible in terms of the principal polarizabilities, and therefore in terms of the molecular geometry and Γ_{CC}. It is evident, then, that data for any number of tetrahedral hydrocarbons can only lead to a value of Γ_{CC}. For angles slightly different from tetrahedral, a slightly different linear combination, such as $\gamma_{CC} - 1.9\gamma_{CH}$, would enter the polarizability equations. However, knowledge of this combination and of Γ_{CC} would not permit evaluation of the separate C—C and C—H bond parameters because of great sensitivity of the solution to minor errors in the experimental values of the two slightly different linear combinations. To get a linear combination significantly different from (1), we would have to consider a molecule with angles quite different from tetrahedral, such as cyclobutane. But with the angles somewhat different, it would also be expected that the polarizability components of the bonds would be different.

In a similar way it is easy to see, referring to Eq. (20) of I, that for tetrahedral chlorinated aliphatic hydrocarbons only Γ_{CC} and

$$\Gamma_{CCl} \equiv \gamma_{CCl} - \gamma_{CH} \tag{2}$$

are determinable. Again, deviations of the angles would not be useful, whether small or large.

Since most molecules have approximately tetrahedral and other simple geometrical forms (such as 120° bond angles), we will in a similar way find it to be the general case that it is not possible to assign longitudinal and transverse polarizabilities to bonds in polyatomic molecules, from experimental data on

[11] C. G. Le Fèvre and R. J. W. Le Fèvre, J. Chem. Soc. **1954**, 1577.

[12] C. G. Le Fèvre and R. J. W. Le Fèvre, Chem. & Ind. (London) **1955**, 1121.

[13] K. S. Pitzer, *Advances in Chemical Physics*, edited by I. Prigogine (Interscience Publishers, Inc., New York, 1959), Vol. II, pp. 79–81.

TABLE I. Theoretical expressions for molecular anisotropies.

Molecule[a]	γ^2
C_2H_6	Γ_{CC}^2
C_3H_8	$4/3\Gamma_{CC}^2$
Cyclohexane (chair)	$4\Gamma_{CC}^2$
CH_3X, CHX_3	Γ_{CX}^2
CH_2X_2	$4/3\Gamma_{CX}^2$
C_2H_5	$(\Gamma_{CC}-2\Gamma_{CX})^2$
C_6H_6	γ_b^2
C_6H_5X	$\Gamma_{CX}^2-\Gamma_{CX}\gamma_b+\gamma_b^2$
o-$C_6H_4X_2$, m-$C_6H_4X_2$	$7/4\Gamma_{CX}^2-2\Gamma_{CX}\gamma_b+\gamma_b^2$
p-$C_6H_4X_2$	$4\Gamma_{CX}^2-2\Gamma_{CX}\gamma_b+\gamma_b^2$
CH_3OCH_3	$\Gamma_{CO}^2(1+3\cos^2\phi)$
CH_3OH	$\Gamma_{CO}^2+(3\cos^2\phi-1)\Gamma_{CO}\gamma_{OH}+\gamma_{OH}^2$
H_2O	$\gamma_{OH}^2(1+3\cos^2\phi)$

[a] X=F, Cl, Br, I, CH_3; Γ_{CX} is Γ_{CC} when X=CH_3. All angles are taken to be tetrahedral or 120°, except ϕ, the angle between oxygen bonds.

molecular polarizability components. Only certain linear combinations (*determinable polarizability parameters*) can be assigned. Conversely, the principal molecular polarizabilities are calculable from a suitable set of such linear combinations.

VALUES OF DETERMINABLE POLARIZABILITY PARAMETERS

For the tetrahedral hydrocarbons and chlorinated methanes, the anisotropy γ is proportional to Γ_{CC} and Γ_{CCl}, respectively (Table I), so that these parameters could be estimated by simple averaging of the data. In Table II we have given experimental data for such molecules and also molecules with a few other types of bonds. Cases involving internal rotation, such as *n*-butane and 1,2-dichloroethane, have been omitted in order to avoid the introduction of barrier heights and shapes, which are not known with certainty. It is seen that for aliphatic hydrocarbons the observed quantities vary widely so that simple averaging could not be expected to result in a reliable value of Γ_{CC}. It seemed more appropriate to use the wider range of data embracing C—H, C—C, and C—Cl bonds in a single least-squares treatment, obtaining the best values of Γ_{CC}, Γ_{CCl}, and γ_b, the latter quantity being the benzene anisotropy, taken as the polarizability perpendicular to the ring minus the polarizability in the plane of the ring. The calculations involved the theoretical equations given in Table I, which apply to molecules with C—H, C—C, and C—Cl bonds, and were easily carried out by a successive approximations method conveniently summarized by Wilson.[14] The results for the three parameters, along with some other results discussed below, are given in Table III.

(In Table II, the following definitions apply):

$$\delta^2=2\gamma^2/9\alpha^2$$

$$\rho=6\delta^2/(10+7\delta^2).$$

[14] E. B. Wilson, Jr., *An Introduction to Scientific Research* (McGraw-Hill Book Co., New York, 1952), pp. 220–223.

TABLE II. Experimental molecular anisotropies.

Molecule	α, A^3	$100\,\rho$	$100\,\delta^2$	γ^2, A^6
C_2H_6	4.47[a]	0.50[b]		0.755
		0.80[c]		1.20
			2.3[a]	2.07
		1.6[d]		2.43
C_3H_8	6.29[a]	0.66[b]		1.98
			2.04[a]	3.63
		1.51[e]		4.56
		1.6[d]		4.81
Cyclohexane	10.87[a]			2.02[f]
			0.8[a]	4.25
				5.90[g]
		1.0[d]		9.04
CH_3Cl	4.56[h]	1.54[c]		2.438
CH_2Cl_2	6.48[a,h]	2.43[c]		7.876
$CHCl_3$	8.23[h]	1.28[c]		6.599
C_2Cl_6				9.0[i]
C_6H_6	10.32[j]		7.3[a]	34.99
		4.2[j]		35.28
		6.8[a]		59.00
$C_6H_5CH_3$	12.26[j]	3.9[a]		46.06
			7.9[a]	53.43
		4.6[j]		54.79
o-$C_6H_4(CH_3)_2$	14.1[j]	4.6[j]		72.48
m-$C_6H_4(CH_3)_2$	14.18[j]	4.6[j]		73.30
p-$C_6H_4(CH_3)_2$	14.2[j]		7.7[h]	69.87
				79.62[a,j]
C_6H_5Cl	12.25[j]	4.6[j]		54.70
o-$C_6H_4Cl_2$	14.17[a]	4[a]		63.19
		5[a]		79.96
m-$C_6H_4Cl_2$	14.23[a]	4[a]		63.72
		4.5[a]		72.13
p-$C_6H_4Cl_2$				136.54[a]
CH_3Br	5.55[j]			7.79[i]
$CHBr_3$	11.81[m]	3.1[d]		33.65
C_2H_5Br	7.57[n]	2.3[d]		10.16
C_6H_5Br	13.62[h]	5.3[d]		78.60
		4.83[k]		71.21
1,3,5-$C_6H_3Br_3$				49.98[i]
isoC_3H_7I	11.45[m]	2.3[d]		23.24
CH_3OCH_3[p]	5.16[j]	1.6[j]		3.256
		1.06[c]		2.143
CH_3OH[p]	3.25[k]	1.7[d]		1.374
		1.6[j]		1.292
H_2O[p]	1.454[n]	8.5[o]		1.496

[a] H. A. Stuart and S. v. Schieszl, Ann. Phys. **2** [6], 321 (1948). δ^2 was obtained from Kerr constants measured in the gas phase.

[b] S. Bhagavantam, *Scattering of Light and the Raman Effect* (Chemical Publishing Co., Inc., Brooklyn, 1942), p. 54; Ananthakrishnan's values.

[c] S. Parathasarathy, Indian J. Phys. **25**, 21 (1951). A revision of Parthasarathy's earlier values.

[d] Reference b, pp. 54–55, Cabannes' values.

[e] Reference b, p. 54, Parthasarathy's values.

[f] From polarizability components given by C. G. Le Fèvre and R. J. W. Le Fèvre, J. Chem. Soc. **1956**, 3549.

[g] Reference a, using reported values of polarizability components.

[h] Landolt-Börnstein, Auflage 6, Band I. Teil 3, 1951, p. 509.

[i] From polarizability components given by C. G. Le Fèvre and R. J. W. Le Fèvre, J. Chem. Soc. **1954**, 1577.

[j] H. A. Stuart and H. Volkmann, Ann. Phys. **18** [5], 121 (1933).

[k] Landolt-Börnstein, Auflage 5, Band II, Teil 1, 1931, p. 88.

[l] Ref. j, γ^2 obtained directly from Kerr constant data.

[m] K. G. Denbigh, Trans. Faraday Soc. **36**, 936 (1940). α was obtained by summing the average bond polarizabilities.

[n] A. A. Maryott and F. Buckley, "Table of Dielectric Constants and Electric Dipole Moments of Substances in the Gaseous State" (National Bureau of Standards Circular 537, U. S. Government Printing Office, Washington, 1953).

[o] C. V. Raman and K. S. Krishnan, Phil. Mag. **3** [7], 724 (1927).

[p] C—O—C angle 111°, H—O—C angle 107.3°, H—O—H angle 104.45°, from *Tables of Interatomic Distances and Configuration in Molecules and Ions*, Special Publication No. 11, Chem. Soc. London (1958).

TABLE III. Results of parameter determinations.

Parameter	Value, A^3
Γ_{CC}	1.7[a]
Γ_{CCl}	2.6[a]
γ_{OH}	−6.3[a]
Γ_{CBr}	3.8[b,c]
Γ_{CI}	5.7[c]
Γ_{CO}	1.4[c]
γ_{OH}	1.12[c]

[a] It was not possible to determine whether the signs of these three parameters are correct or should all be simultaneously changed. The selection made seems more reasonable.

[b] 1,3,5-$C_6H_3Br_3$ omitted, as it is inconsistent with the other bromides.

[c] Signs ambiguous, but these choices seem reasonable.

Values of $\Gamma_{CX} \equiv \gamma_{CX} - \gamma_{CH}$ were determined for X = Br, I, and O from the data in Table II for bromides, *iso*-C_3H_7I, and CH_3OCH_3, respectively. A value of γ_{OH}[2] was determined from the H_2O anisotropy. The results (Table III) for the latter two molecules may now be used to check the anisotropy for CH_3OH. The result, $\gamma^2 = 2.04$, is in reasonable agreement with experiment (Table II), considering the wide variation in experimental γ^2 values for other molecules.

VALUES OF BOND LONGITUDINAL AND TRANSVERSE POLARIZABILITIES

This work originally was undertaken with a view to determining whether Denbigh's large longitudinal polarizability and small transverse polarizability for the C—C bond are justified, and if not, to determining better values for these quantities. Longitudinal polarizabilities for bonds are important parameters in a model we have used for calculating charge shifts in molecules due to induction, so that an estimate of the reliability of these parameters seems desirable.[15,16] But we have seen that only Γ_{CC}, not the longitudinal C—C polarizability itself, could be determined from accurate, consistent data, and the present data allow only the roughest estimation of this parameter. Similar statements apply to other bonds, such as C—Cl. It appears that certain longitudinal and transverse bond polarizabilities can only be determined theoretically, as has been attempted in certain cases by Bolton.[3]

[15] Smith, Ree, Magee, and Eyring, J. Am. Chem. Soc. **73**, 2263 (1951).

[16] R. P. Smith and E. M. Mortensen, J. Am. Chem. Soc. **78**, 3932 (1956).

TABLE IV.

C—X	α_{CX}, A^3	$\alpha_{CX}+\frac{2}{3}\Gamma_{CX}$, A^3	b_{CX}^1, A^3
C—Cl	2.59	4.32	3.67
C—Br	3.71	6.24	5.04
C—I	5.77	9.57	8.09[a]
C—O	0.60	1.52	0.84

[a] From reference 15; calculated by assuming the same ratio of transverse to longitudinal polarizability that Denbigh found for several related bonds.

Nevertheless, we may conclude that various of Denbigh's longitudinal and transverse polarizabilities probably are not much in error by the following argument. From the equations

$$\Gamma_{CX} = \gamma_{CX} - \gamma_{CH} \qquad (X = Cl, Br, I, O)$$

$$\gamma_{CX} = b_{CX}^1 - b_{CX}^2 \qquad (X = Cl, Br, I, O, H)$$

$$\alpha_{CX} = \tfrac{1}{3}(b_{CX}^1 + 2b_{CX}^2)$$

we obtain

$$b_{CX}^1 = \alpha_{CX} + \tfrac{2}{3}\Gamma_{CX} + \tfrac{2}{3}\gamma_{CH}. \qquad (3)$$

Here the values of α_{CX}, the average polarizability, are known from bond refraction tables, and estimates of the Γ_{CX} may be obtained from Table III. If the sum of the first two terms is relatively large compared with γ_{CH}, then b_{CX}^1, the longitudinal C—X polarizability, may be determined with fair accuracy. In Table IV we have listed values of α_{CX} and b_{CX}^1 from Denbigh, and also $\alpha_{CX}+\frac{2}{3}\Gamma_{CX}$. We see that Denbigh's b_{CX}^1 values and the $\alpha_{CX}+\frac{2}{3}\Gamma_{CX}$ values will be fairly consistent if $\gamma_{CH} \approx -1$ to $-2A^3$. It appears from Table IV that b_{CX}^1 for the carbon-halogen bonds should be relatively insensitive to γ_{CH}, so that in any case Denbigh's values probably are not much in error.

In order to properly account for the dipole moments of some halogenated aliphatic hydrocarbons, Smith and Mortensen[16] took $b_{CC}^1 = 1.12$ A^3. This is consistent with the Γ_{CC} value in Table III if $\gamma_{CH} = -0.4$ A^3.

From the anisotropy of water we can determine the longitudinal polarizability directly, using the γ_{OH} value in Table III; the result is 1.43 A^3.

Electron Diffraction Study of the Structure of Trimethylphosphine*

L. S. BARTELL, *Department of Chemistry, Iowa State University, Ames, Iowa*

AND

L. O. BROCKWAY, *Department of Chemistry, University of Michigan, Ann Arbor, Michigan*

(Received May 4, 1959)

The structural parameters of gaseous trimethylphosphine, including standard errors, were found to be as follows: center of gravity bond distances were $r_{CP}=1.846_5\pm0.003$ A, and $r_{CH}=1.091\pm0.006$ A; angles were $<$C—P—C$=98.6\pm0.3°$, and $<$P—C—H$=110.7\pm0.5°$; root-mean-square amplitudes of vibration were $l_{CP}=0.054\pm0.003$ A, $l_{CH}=0.073\pm0.006$ A, $l_{P\cdots H}=0.110\pm0.006$ A, and $l_{C\cdots C}=0.084\pm0.005$ A. The methyl groups were observed to be in staggered configurations analogous to those in ethane, with rotational barriers probably 1.5 kcal/mole or higher. A brief structural comparison with halogen derivatives and hydrides is presented.

INTRODUCTION

A SUBJECT of continuing speculation is the structure of trivalent compounds of group V elements. The noteworthy difference in bond angles between hydrides and halides has been discussed in widely different ways.[1] The methyl derivatives, being intermediate between hydrides and halides in several respects, offer useful comparisons. Since the precise structures of these compounds have not been well established, an investigation of some methyl phosphines was undertaken by modern techniques of electron diffraction. Shortly after the analysis of diffraction data for trimethyl phosphine had been carried out, a microwave determination of the structure was reported by Lide and Mann.[2] This offers an excellent opportunity for comparison of the two independent structural methods.

PROCEDURE

A sample of trimethylphosphine was provided by Professor R. W. Parry. Electron diffraction patterns were recorded on Kodak Medium Lantern Slides with an apparatus described earlier,[3] using 40-kv electrons and an r^3 sector. Experimental procedures followed those previously published.[3,4] Indices of resolution of 0.85 and 0.77 were obtained for the 10-cm and 25-cm camera data, respectively. The deviation from unity resulted principally from a uniform delocalization of the specimen throughout the diffraction chamber. Corrections for this effect were taken, conservatively, to be 2/3 of the values calculated with a formula in which the deficiency of the index of resolution was assumed to be due solely to specimen delocalization.[5] Corrections ranged from 0 to 0.002 A.

The data were processed manually by a procedure closely resembling that described previously.[6] The value of b used in the damping function in the radial distribution function was 0.00211. Included in the analysis were corrections for non-nuclear scattering and the failure of the Born approximation. For the latter correction the phase shifts calculated by Ibers and Hoerni[7] were used. Fourier integral termination errors were corrected with the aid of a simple approximation which, to our knowledge, has not been described before. If the Degard damping function $\exp(-bs^2)$ is approximated by the function $C\exp(-cs)$ at the termination of data at s_M and beyond, it is easy to show that the termination ripple, Δf_i, due to peak i, is given approximately by

$$\Delta f_i=\frac{f_i\lambda\{\exp(-\lambda^2 s_M^2/2)\}\{\beta\cos s_M x-x\sin s_M x\}}{(\pi/2)^{\frac{1}{2}}(\beta^2+x^2)}$$

$$=\frac{f_i\lambda\{\exp(-\lambda^2 s_M^2/2)\}\{\sin(s_M x+\theta)\}}{(\pi/2)^{\frac{1}{2}}(\beta^2+x^2)^{\frac{1}{2}}},$$

where f_i is the maximum value of peak i, $\lambda^2=2b+\beta^2$, $x=r-r_i$, $\beta=\lambda^2 s_M$, and $\theta=\arctan(-\beta/x)$. This approximation is adequate for the present purpose as long as $\lambda s_M>\sim 2$, and $|x|<\sim r_i$.

Final parameters were deduced by fitting the experimental radial distribution function with Gaussian peaks, using the method of steepest ascents.[8] Root-mean-square deviations between experimental and calculated curves decreased from about 0.6% to 0.3% of the maximum value of the CP peak over the interval from 1 to 3 A. Internuclear distances are reported in terms of center of gravity parameters, r_g.[9] Standard errors were

* This work was supported in part by the National Science Foundation.

[1] See for example R. S. Mulliken, J. Am. Chem. Soc. **77**, 887 (1955); W. Kolos, J. Chem. Phys. **23**, 1554 (1955); C. E. Mellish and J. W. Linnett, Trans. Faraday Soc. **50**, 657 (1954); and articles to which the above papers refer.

[2] D. R. Lide, Jr., and D. E. Mann, J. Chem. Phys. **29**, 914 (1958).

[3] L. O. Brockway and L. S. Bartell, Rev. Sci. Instr. **25**, 569 (1954).

[4] L. S. Bartell and L. O. Brockway, J. Appl. Phys. **24**, 656 (1953).

[5] L. S. Bartell, J. Appl. Phys. **32**, 252 (1960).

[6] Bartell, Brockway, and Schwendeman, J. Chem. Phys. **23**, 1854 (1955).

[7] J. A. Ibers and J. A. Hoerni, Acta Cryst. **7**, 405 (1954).

[8] R. A. Bonham and L. S. Bartell, J. Chem. Phys. **31**, 702 (1959).

[9] The term r_g corresponds to the $r_g(0)$ of L. S. Bartell, J. Chem. Phys. **23**, 1219 (1955).

calculated as described elsewhere.[8,10] Standard errors quoted for bond angles correspond solely to the uncertainties in the r_g values from which they were calculated and not to possible interpretational uncertainties arising from the operational definition of the angle.

DISCUSSION OF RESULTS

The experimental intensity function is compared in Fig. 1 with the intensity function calculated for a nearly optimum model. The radial distribution curve derived from the experimental intensity function is shown in Fig. 2. If the molecule is assumed to have C_{3v} symmetry, with methyl groups each possessing 3-fold axes approximately coincident with the C—P bonds, the structural parameters can be completely determined from the radial distribution function. The numerical results are listed in Table I.

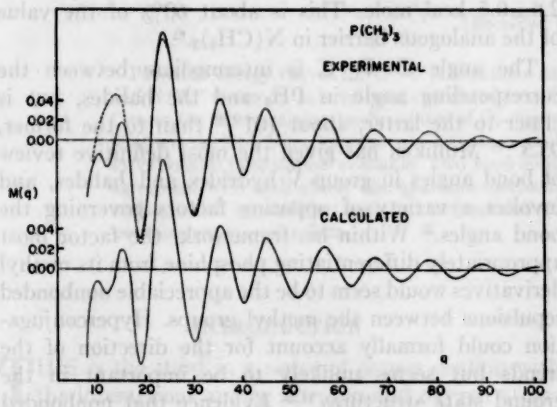

FIG. 1. Reduced intensity curves for trimethylphosphine. The solid lines represent the total scattering function $M(q)$ and the dashed line represents the nuclear scattering function $M_e(q)$. The calculated curve has been multiplied by the experimental index of resolution.

The root-mean-square amplitudes appear to be entirely reasonable in magnitude. The distances and angles agree excellently with the microwave values of Lide and Mann[2] who obtained (assuming $r_{CH}=1.090$ A) $r_{CP}=1.841\pm0.003$ A, $\angle C—P—C=99.1\pm0.2°$, and $\angle P—C—H=111.9\pm1°$.[11] While none of the discrepancies between the microwave and diffraction results are significant according to Cruickshank's criterion,[12] discrepancies of the observed magnitude are likely to arise because of the different operational definitions of lengths and angles involved. For example, if it is

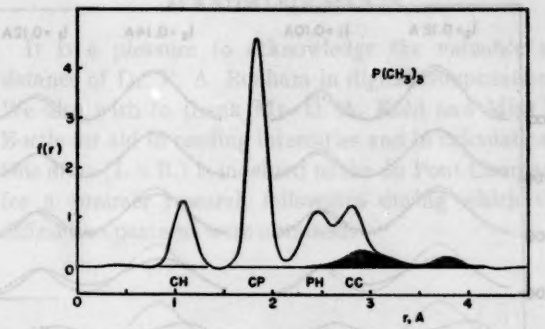

FIG. 2. Experimental radial distribution function for trimethylphosphine. The shaded area indicates the C—H distribution characterizing the restricted rotation of the methyl groups.

considered that the C—P bonds can be described in terms of a Morse potential function with a plausible asymmetry constant a[13] of about 1.8 A^{-1} and $r_g=1.846_5$, the most probable C—P distance r_m is 1.844 A and r_j is 1.839 A (or less if effects of nonbonded repulsions are considered). As a rule spectroscopic r_0 parameters for simple molecules appear to scatter between r_g and r_e, generally falling closer to the latter parameter.

The present structure is also compatible with that deduced in an earlier diffraction study,[14] $r_{CP}=1.87\pm0.02$ A, $\angle CPC=100°\pm4°$, to within the rather large limits of error of the earlier results. The structure of perfluorotrimethylphosphine has been investigated by Bowen,[15] who obtained a C—P bond length of $1.93_7\pm0.017$. This distance, if correct, is remarkably longer than that in $P(CH_3)_3$. An analogous comparison of $N(CH_3)_3$ and $N(CF_3)$ reveals that the C—N distance is shorter by perhaps several hundredths of an angstrom unit in the perfluorinated compound.[16] The C—P bond in $P(CF_3)_3$ merits further attention.

The diffraction C—H distance is 0.025 A shorter

TABLE I. Electron diffraction results for $P(CH_3)_3$

	r_g, A	l, A
C—P	$1.846_3\pm0.003$	0.054 ± 0.003
C—H	1.091 ± 0.006	0.073 ± 0.006
P- -H	2.455 ± 0.006	0.110 ± 0.006
C- -C	2.800 ± 0.005	0.084 ± 0.005

$\angle C—P—C$ $98.6\pm0.3°$ $\angle P—C—H$ $110.7\pm0.5°$

Configuration of methyl groups, staggered.
Barrier to rotation of methyl groups ≥ 1 kcal/mole.

[10] R. A. Bonham and L. S. Bartell, J. Am. Chem. Soc. **81**, 3491 (1959).

[11] Lide reported the angle H—C—H. In the present comparison it seemed preferable to avoid converting the diffraction $\angle P—C—H$ to $\angle H—C—H$, as the operational (r_g) diffraction angles may not transform according to simple geometrical laws. Spectroscopic angles, which are intrinsically no more precisely defined at present, do transform simply (by hypothesis), since the individual angles are not independently defined.

[12] D. W. J. Cruickshank and A. P. Robertson, Acta Cryst. **6**, 698 (1953).

[13] L. S. Bartell, J. Chem. Phys. **23**, 1219 (1955); P. M. Morse, Phys. Rev. **34**, 57 (1929).

[14] H. D. Springall and L. O. Brockway, J. Am. Chem. Soc. **60**, 996 (1938).

[15] H. J. M. Bowen, Trans. Faraday Soc. **50**, 783 (1954).

[16] V. Schomaker quoted by P. W. Allen and L. E. Sutton, Acta Cryst. **3**, 46 (1950); R. L. Livingston and G. Vaughan, J. Am. Chem. Soc. **78**, 4866 (1956).

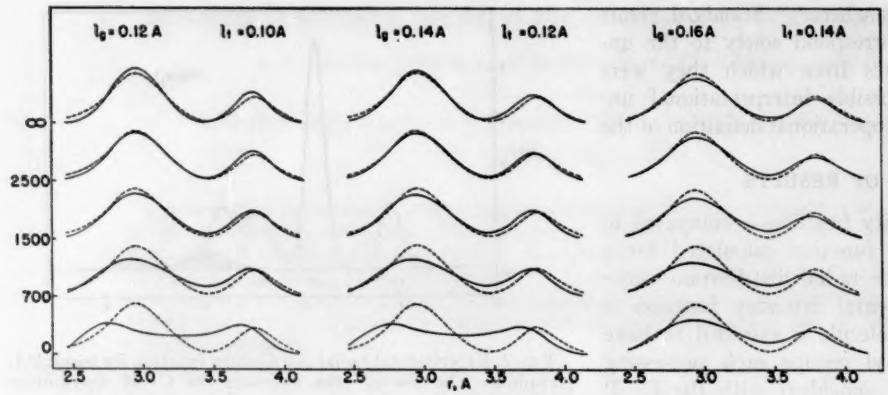

FIG. 3. Radial distribution of C—H distances in trimethylphosphine. The solid lines represent distributions calculated for hindering potentials ranging from free rotation to infinite barriers. V_0 is indicated in cal/mole, and assumed skeletal amplitudes for gauche and trans C—H interactions are shown. The dashed curves correspond to the observed distribution.

than that observed in a recent study[17] of the *n*-hydrocarbons butane through heptane, and approaches in shortness the distance in ethylene.[18] While this difference was also observed in mono- and dimethylphosphine[19] and appears to be significant according to Cruickshank's criterion,[12] there seems to be no obvious reliable explanation. Moreover, the C—H stretching frequencies in $P(CH_3)_3$[20] resemble those of the *n*-hydrocarbons more closely than those of ethylene. Consequently, it is unwise to regard the apparent shortness as established at present.

In addition to providing the main skeletal parameters, the diffraction data clearly indicate the orientation of the methyl groups. The groups are in a staggered configuration entirely analogous to that in ethane or isobutane. It was possible by successive approximations to make the input model in the radial distribution calculation consistent with the output data, including the range from 2.5 to 4.1 A which contains the information on restricted rotation of methyl groups. Plotted in Fig. 3 is this portion of the experimental radial distribution curve from which all contributions except C- -H have been subtracted. By way of comparison, theoretical curves are shown for various skeletal amplitudes of vibration and hindering potentials, assuming the azimuthal probability distribution is proportional to

$$\exp[-V_0\{\cos^2(3\theta/2)\}/RT].$$

Judging from amplitudes observed in other molecules, it is unlikely that the gauche C—H (at $r\sim2.94$ A) skeletal amplitude is less than 0.12 A. It can be seen from Fig. 3 that the gauche amplitude cannot be much greater than 0.14 A. Unfortunately it is not possible to establish the barrier independently of the skeletal amplitude, and there is at present no accurate knowledge of the amplitude. The best fit occurs with a barrier of 2.5 kcal or greater. If the amplitude is as high as 0.14 A the diffraction data do not exclude an infinite barrier. The microwave study[2] confirms the fact that the barrier is substantial, yielding the result 2.6 ± 0.5 kcal/mole. This is about 60% of the value of the analogous barrier in $N(CH_3)_3$.[21]

The angle C—P—C is intermediate between the corresponding angle in PH_3 and the halides, but is closer to the latter, about 101°,[22] than to the former, 93.3°.[22] Mulliken has given the most definitive review of bond angles in group V hydrides and halides, and invokes a variety of opposing factors governing the bond angles.[23] Within his framework, the factor most appropriately differentiating phosphine from its methyl derivatives would seem to be the appreciable nonbonded repulsions between the methyl groups. Hyperconjugation could formally account for the direction of the trends but seems unlikely to be important in the ground state structures.[24,25] Evidence that nonbonded repulsions can indeed account for bond angles and distances in a variety of saturated and unsaturated hydrocarbon derivatives has recently been summarized.[25] It may be noted that the average H—C—H angle in the *n*-hydrocarbons butane through heptane is 7° less than the average C—C—C angle,[26] a difference comparable to that found between the H—P—H and C—P—C angles in the phosphines. A similar but less well documented difference has been found for amines.[22]

The slightly larger angles of the phosphorus halides in comparison with the methyl derivative do not result

[17] Bonham, Bartell, and Kohl, J. Am. Chem. Soc. **81**, 4765 (1959).
[18] L. S. Bartell and R. A. Bonham, J. Chem. Phys. **31**, 400 (1959).
[19] L. S. Bartell, J. Chem. Phys. (to be published).
[20] Rosenbaum, Rubin, and Sandberg, J. Chem. Phys. **8**, 366 (1940).
[21] D. R. Lide, Jr., and D. E. Mann, J. Chem. Phys. **28**, 572 (1958).
[22] L. E. Sutton, *Tables of Interatomic Distances and Configuration in Molecules and Ions* (The Chemical Society, London, 1958).
[23] The empirical generalizations of Mellish and Linnett (reference 1) regarding these compounds fail in the comparison of PF_3 and PH_3, and hence cannot be expected to apply in the case of $P(CH_3)_3$.
[24] M. J. S. Dewar and H. N. Schmeising, Tetrahedron **5**, 166 (1959).
[25] L. S. Bartell, Federov Session on Crystallography, May 26, 1959, Leningrad, U.S.S.R. (to be published).
[26] Reference 17. In the calculation of the angle H—C—H from the angle C—C—H given in the reference, a slight correction has been made for the effect of the large amplitude of vibration of hydrogen atoms.

from larger nonbonded repulsions. In halogen-substituted alkanes and silanes the angle Cl—Y—Cl, as a rule, is slightly smaller, and the angle F—Y—F appreciably smaller than the angle C—Y—C in methyl analogs.[22] In the phosphines the reversal of this order probably results from partial double bonding in the halides and the concomitant tendency (stronger in molecules with only three rather than four bonds) to assume a planar configuration.

ACKNOWLEDGMENTS

It is a pleasure to acknowledge the valuable assistance of Dr. R. A. Bonham in digital computations. We also wish to thank Mr. D. A. Kohl and Miss E. Bortle for aid in reading intensities and in calculations. One of us (L.S.B.) is indebted to the du Pont Company for a summer research fellowship during which the diffraction patterns were obtained.

THE JOURNAL OF CHEMICAL PHYSICS VOLUME 32, NUMBER 2 FEBRUARY, 1960

Interactions between Ground State Oxygen Atoms and Molecules: O—O and O_2—O_2*

JOSEPH T. VANDERSLICE, EDWARD A. MASON, AND WILLIAM G. MAISCH

Institute for Molecular Physics, University of Maryland, College Park, Maryland

(Received June 22, 1959)

Potential energy curves for O—O interactions corresponding to the $X\,^3\Sigma_g^-$, $^1\Delta_g$, $^1\Sigma_g^+$, $^3\Delta_u$, $A\,^3\Sigma_u^+$, $^1\Sigma_u^-$, and $B\,^3\Sigma_u^-$ states of O_2 have been calculated from spectroscopic data by the Rydberg-Klein-Rees method. Curves for the remaining twelve states of O_2 dissociating to ground state atoms have been obtained from relations derived from approximate quantum-mechanical calculations, and checked against the meager experimental information available. Two semi-independent calculations have been made, and are in good agreement with each other. The quantum-mechanical relations also lead to an approximate O_2—O_2 interaction, which is consistent with interactions derived from vibrational relaxation times and from high-temperature gas viscosity data.

INTRODUCTION

THIS is the third in a series of papers dealing with the interactions among nitrogen and oxygen atoms and molecules. Such interactions are not only of importance in the calculation of transport properties of air at high temperatures, but a proper knowledge of them may also lead to a better understanding of the chemistry and physics of the upper atmosphere. Previous papers have dealt with the interactions between nitrogen atoms and molecules[1] and between oxygen and nitrogen.[2] The present paper deals with the calculation of the interaction energies between oxygen atoms and molecules.

The most important interactions for the calculation of transport properties are those between the ground state atoms and molecules. When two ground state oxygen atoms (^3P) collide, they can follow any one of eighteen potential energy curves,[3] corresponding to the spectroscopic states $^1\Sigma_g^+(2)$, $^1\Sigma_u^-$, $^1\Pi_g$, $^1\Pi_u$, $^1\Delta_g$, $^3\Sigma_u^+(2)$, $^3\Sigma_g^-$, $^3\Pi_g$, $^3\Pi_u$, $^3\Delta_u$, $^5\Sigma_g^+(2)$, $^5\Sigma_u^-$, $^5\Pi_g$, $^5\Pi_u$, and $^5\Delta_g$. Spectroscopic data are available on the lowest six bound states, $X^3\Sigma_g^-$, $^1\Delta_g$, $^1\Sigma_g^+$, $^1\Sigma_u^-$, $^3\Delta_u$, and $A^3\Sigma_u^+$, as well as on the bound $B^3\Sigma_u^-$ state, which dissociates into a ground state oxygen atom (^3P) and an excited atom (^1D). Accurate potential energy curves for these states have been calculated by the Rydberg-Klein-Rees (RKR) method.[4] For the other states dissociating to ground state atoms the experimental information is meager. Wilkinson and Mulliken[5] suggest that the $^3\Pi_u$ state predissociates the $B\,^3\Sigma_u^-$ state at $v'=12$ on the left-hand side of the minimum of the $B\,^3\Sigma_u^-$ curve. Here v' is the vibrational quantum number of the $B\,^3\Sigma_u^-$ state. They also mention the possibility of a "forbidden" predissociation of the $B\,^3\Sigma_u^-$ state at $v'=3\frac{1}{2}$ by any of the $^5\Sigma_u^-$, $^1\Pi_u$, or $^5\Pi_u$ states. This "forbidden" predissociation would occur on the right-hand side of the minimum of the $B\,^3\Sigma_u^-$ curve.

Simple quantum-mechanical considerations have been used to determine relations among the eighteen different states of O_2 dissociating to ground state atoms. Once the curves for the six bound states are known, these relations enable the "tails" of the other curves to be determined. The curves so calculated agree with the results of Wilkinson and Mulliken on the predis-

* This research was supported in part by the National Aeronautics and Space Administration.

[1] Vanderslice, Mason, and Lippincott, J. Chem. Phys. **30**, 129 (1959).

[2] Vanderslice, Mason, and Maisch, J. Chem. Phys. **31**, 738 (1959).

[3] G. Herzberg, *Spectra of Diatomic Molecules* (D. Van Nostrand Company, Inc., Princeton, New Jersey, 1950), p. 321.

[4] (a) R. Rydberg, Z. Physik **73**, 376 (1931); (b) O. Klein, Z. Physik **76**, 226 (1932); (c) A. L. G. Rees, Proc. Phys. Soc. (London) **59**, 998 (1947); (d) Vanderslice, Mason, Maisch, and Lippincott, J. Mol. Spectroscopy **3**, 17 (1959).

[5] P. G. Wilkinson and R. S. Mulliken, Astrophys. J. **125**, 594 (1957).

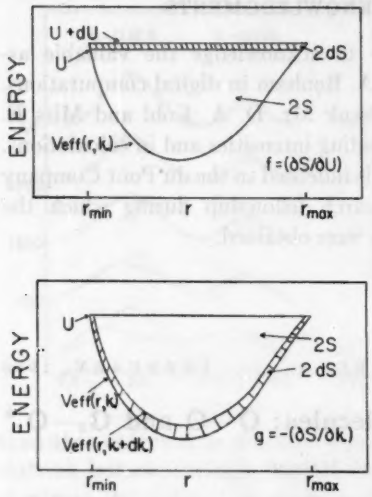

FIG. 1. Graphical interpretation of RKR method.

sociation effects, the only direct experimental checks available. A semi-independent calculation of the "tails," based on the $X^2\Pi$ curve of NO and one O_2 curve, is also in good agreement. These relations have been derived by a modified perfect pairing approximation, previously used[1,2] for N_2 and NO. This modified pairing scheme affords a description in terms of a combination of molecular orbital and valence-bond theory, somewhat along the lines suggested by Linnett.[6] The description further leads to simple relations involving molecules, so that an O_2—O_2 potential can be obtained from results on the O—O interactions. This O_2—O_2 potential is in agreement with other potentials obtained from analysis of high-temperature viscosity data[2] and from analysis of vibrational relaxation time data.[7]

BOUND STATES OF O_2

The potential energy curves for the bound states $X^3\Sigma_g^-$, $^1\Delta_g$, $^1\Sigma_g^+$, $^1\Sigma_u^-$, $^3\Delta_u$, $A\,^3\Sigma_u^+$, and $B\,^3\Sigma_u^-$ were obtained by the RKR method.[4] Although this method has been described in considerable detail in earlier publications,[1,2,4d] it has not been emphasized that the method is quite sensitive to errors in the experimental data in the region near the dissociation limit. To discuss this point, it will suffice here to give a graphical interpretation of the method which follows somewhat along the lines given previously.[4d] The purpose of the method is to obtain values for the classical turning points of the vibrational motion for a given total energy U. The method is formulated in terms of the area $2S$, which is enclosed between the lines of constant energy U and the curve of effective potential energy $V_{eff}(r)$,

$$V_{eff}(r)=V(r)+\kappa/r^2, \qquad (1)$$

where $V(r)$ is the actual potential energy and κ/r^2 is the centrifugal potential term due to rotation (see Fig. 1). The two quantities f and g, defined by

$$f=(\partial S/\partial U)_\kappa \quad \text{and} \quad g=-(\partial S/\partial \kappa)_U, \qquad (2)$$

are then considered. From Fig. 1 it is easy to see that

$$f=\tfrac{1}{2}\int_{r_{min}}^{r_{max}} dr=\tfrac{1}{2}(r_{max}-r_{min}), \qquad (3)$$

$$g=\tfrac{1}{2}\int_{r_{min}}^{r_{max}}(\partial V_{eff}/\partial\kappa)\,dr=\tfrac{1}{2}\int_{r_{min}}^{r_{max}} dr/r^2$$
$$=\tfrac{1}{2}[(1/r_{min})-(1/r_{max})], \qquad (4)$$

where r_{min} and r_{max} are the classical turning points. From these relations it can be seen that a knowledge of $S=S(U,\kappa)$ leads to values of f and g and consequently to values of r_{min} and r_{max}. The RKR method expresses S in terms of the vibrational and rotational constants obtained from analysis of spectroscopic data. Hence once the spectroscopic results are known in a region around U, the function S and consequently r_{min} and r_{max} can be calculated. The method implies that the data are known up to U, since V_{eff} is assumed known up to U in the integration in Eq. (4). This means that the curve has to be built up from the bottom using the spectroscopic data appropriate in each energy region.

It is obvious from the foregoing presentation that f and g are very sensitive to the energy near the dissocia-

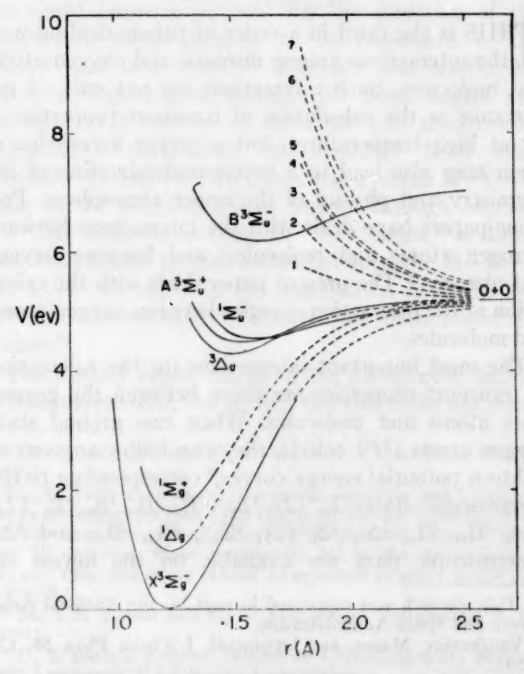

FIG. 2. Summary of O—O interactions. The solid lines have been calculated by the RKR method. The curve numbering is: (1) $^3\Pi_u$ and $^1\Pi_u$; (2) $^5\Pi_g$, $^3\Pi_g$, and $^1\Pi_g$; (3) $^5\Sigma_u^-$ and $^5\Sigma_u^+$; (4) $^1\Sigma_g^+$; (5) $^5\Delta_g$ and $^5\Sigma_g^+$; (6) $^5\Sigma_g^+$; (7) $^5\Pi_u$.

[6] J. W. Linnett, J. Chem. Soc. **1956**, 275.
[7] M. Salkoff and E. Bauer, J. Chem. Phys. **30**, 1614 (1959).

TABLE I. Potential energy of the $X\,^3\Sigma_g^-$ state of O_2.[a]

v	$V(cm^{-1})$	r_{max}(A)	r_{min}(A)	V(ev)
0	787.2	1.262	1.158	0.09761
1	2 344	1.307	1.126	0.2907
2	3 878	1.340	1.106	0.4809
3	5 387	1.370	1.091	0.6680
4	6 873	1.397	1.078	0.8523
5	8 337	1.422	1.067	1.0338
6	9 778	1.445	1.057	1.2125
7	11 196	1.469	1.049	1.3883
8	12 591	1.491	1.041	1.5613
9	13 963	1.513	1.034	1.7314
10	15 313	1.534	1.027	1.8988
11	16 640	1.556	1.022	2.0634
12	17 945	1.577	1.016	2.2252
13	19 227	1.598	1.011	2.3841
14	20 486	1.619	1.006	2.5403
15	21 722	1.641	1.002	2.6935
16	22 934	1.662	0.997	2.8438
17	24 122	1.683	0.993	2.9911
18	25 287	1.704	0.989	3.1356
19	26 429	1.725	0.985	3.2772
20	27 546	1.747	0.982	3.4157
21	28 639	1.768	0.979	3.5512

[a] Experimental data from references 8–12.

tion limit, since small changes in U or κ give large changes in S there. Any errors in the experimental data or inaccuracies in the equations used to fit the data will cause a large error in r. This effect can be seen in the calculated curve for the $B\,^3\Sigma_u^-$ state (see Table VII and Fig. 2), in which the repulsive side of the curve has a positive slope near the dissociation limit. Such a situation does not seem to have occurred before, probably because previous work has not been so close to the dissociation limit.

The results obtained for the bound states by the RKR method are given in Tables I–VII, and the actual curves are shown as the solid lines in Fig. 2. The experimental data were obtained from the following sources: Herzberg,[8a,9] Broida and Gaydon,[8b] Babcock and Herzberg,[10] Lochte-Holtgreven and Dieke,[11] Feast,[12] Herzberg and Herzberg,[13] Hornbeck and Hopfield,[14] Pillow,[15] Brix and Herzberg,[16] Knauss and Ballard,[17] and Herman.[18]

TABLE II. Potential energy of the $^1\Delta_g$ state of O_2.[a,b]

v	$V(cm^{-1})$	r_{max} (A)	r_{min} (A)	V (ev)	T_e+V (ev)
0	751.4	1.272	1.166	0.09318	1.0750
1	2235	1.319	1.134	0.2771	1.2589

[a] Experimental data from reference 13.
[b] T_e is the energy difference between the bottom of the potential curve for the state in question and the bottom of the curve for the $X\,^3\Sigma_g^-$ state.

TABLE III. Potential energy of the $^1\Sigma_g^+$ state of O_2.[a]

v	$V(cm^{-1})$	r_{max} (A)	r_{min} (A)	V (ev)	T_e+V (ev)
0	712.9	1.285	1.176	0.08840	1.7245
1	2118	1.334	1.144	0.2626	1.8987
2	3495	1.371	1.123	0.4333	2.0694
3	4843	1.403	1.107	0.6006	2.2367
4	6164	1.432	1.094	0.7643	2.4004

[a] Experimental data from reference 10.

There is some uncertainty in the numbering of the vibrational levels of the $A\,^3\Sigma_u^+$, $^1\Sigma_u^-$, and $^3\Delta_u$ states. Herzberg[9] has assumed that the first measured band in the $^1\Sigma_u^-\leftarrow{}^3\Sigma_g^-$ system is the 1–0 band and that the first diffuse band observed by Herman[18] at 2913 A is the 0–0 band of the $^3\Delta_u\leftarrow{}^3\Sigma_g^-$ system. Broida and Gaydon,[8b] on the basis of their more recent experimental work on the oxygen afterglow, have concluded that Herzberg's vibrational assignments for the $A^3\Sigma_u^+$ state should be increased by one unit. If Herzberg's numbering is used for these states, the $^3\Delta_u$ curve lies below the $A^3\Sigma_u^+$ curve over the entire region covered in this calculation. The $^1\Sigma_u^-$ curve lies below both at large values of r, but crosses the $^3\Delta_u$ curve at $r=1.718$ A and the $A^3\Sigma_u^+$ curve at $r=1.628$ A. This crossing is in disagreement with the conclusions of Moffitt[19] and of Fumi and Parr,[20] who have calculated that the $^1\Sigma_u^-$ curve lies below the $^3\Delta_u$ curve over the whole region. As pointed out by Herzberg, a shift of two units in the numbering of the $^1\Sigma_u^-$ vibrational bands would lower the $^1\Sigma_u^-$ curve below the other two. On the other hand, the theoretical foundations of the electronic structure calculations are not so well established that the results of Moffitt and of Fumi and Parr can be taken as completely reliable. However, since there appears to be some experimental evidence that Herzberg's vibra-

TABLE IV. Potential energy of the $^3\Delta_u$ state of O_2.[a]

v	$V(cm^{-1})$	r_{max} (A)	r_{min} (A)	V (ev)	T_e+V (ev)
0	454.0	1.557	1.420	0.05630	4.3543
1	1323	1.628	1.385	0.1641	4.4621
2	2141	1.685	1.363	0.2655	4.5635
3	2907	1.739	1.347	0.3605	4.6585
4	3621	1.791	1.334	0.4491	4.7471
5	4284	1.844	1.323	0.5312	4.8292
6	4895	1.898	1.312	0.6070	4.9050

[a] Experimental data from references 9 and 18.

[8] (a) G. Herzberg, Can. J. Phys. **30**, 185 (1952); (b) H. P. Broida and A. G. Gaydon, Proc. Roy. Soc. (London) **A222**, 181 (1954).
[9] G. Herzberg, Can. J. Phys. **31**, 657 (1953).
[10] H. D. Babcock and L. Herzberg, Astrophys. J. **108**, 167 (1948).
[11] W. Lochte-Holtgreven and G. H. Dieke, Ann. Physik **3**, 937 (1929).
[12] M. W. Feast, Proc. Phys. Soc. (London) **A63**, 549 (1950).
[13] L. Herzberg and G. Herzberg, Astrophys. J. **105**, 353 (1947).
[14] G. A. Hornbeck and H. S. Hopfield, J. Chem. Phys. **17**, 982 (1949).
[15] M. E. Pillow, Proc. Phys. Soc. (London) **A67**, 847 (1954).
[16] P. Brix and G. Herzberg, Can. J. Phys. **32**, 110 (1954).
[17] H. P. Knauss and S. S. Ballard, Phys. Rev. **48**, 796 (1935).
[18] L. Herman, Ann. Physik **11**, 548 (1939).
[19] W. Moffitt, Proc. Roy. Soc. (London) **A210**, 224 (1951).
[20] F. G. Fumi and R. G. Parr, J. Chem. Phys. **21**, 1864 (1953).

TABLE V. Potential energy of the $A\,^3\Sigma_u^+$ state of O_2.

v	$V(\text{cm}^{-1})$	r_{max} (A)	r_{min} (A)	V (ev)	T_e+V (ev)
(a) Experimental data and vibrational assignments from reference 8a.					
0	383.1	1.608	1.461	0.04751	4.5343
1	1127	1.683	1.421	0.1397	4.6265
2	1838	1.743	1.397	0.2279	4.7147
3	2513	1.798	1.380	0.3116	4.7984
4	3149	1.853	1.365	0.3905	4.8773
5	3742	1.908	1.351	0.4640	4.9508
6	4284	1.971	1.342	0.5313	5.0181
7	4770	2.043	1.334	0.5915	5.0783
8	5188	2.133	1.327	0.6433	5.1301
9	5524	2.257	1.322	0.6849	5.1717
(b) Experimental data from reference 8a and vibrational assignments from reference 8b.					
0	397[a]	1.600	1.454	0.04923	4.4382
1	1172[a]	1.669	1.412	0.1453	4.5343
2	1916	1.724	1.386	0.2375	4.6265
3	2627	1.775	1.367	0.3257	4.7147
4	3302	1.825	1.351	0.4094	4.7984
5	3938	1.877	1.339	0.4883	4.8773
6	4530	1.931	1.328	0.5618	4.9508
7	5073	1.993	1.319	0.6291	5.0181
8	5559	2.064	1.311	0.6893	5.0783
9	5977	2.154	1.305	0.7411	5.1301
10	6313	2.277	1.300	0.7828	5.1717

[a] These values have been obtained by extrapolation.

tional assignments for the $A^3\Sigma_u^+$ state may be incorrect, we have calculated two potential curves for this state, one using Herzberg's assignments,[8a] and one using the assignments of Broida and Gaydon.[8b] These are given in Tables V(a) and (b). In the subsequent discussion, we have used the curve based on Herzberg's assignments. Our conclusions would be unchanged if the other $A\,^3\Sigma_u^+$ curve were used.

POTENTIAL CURVES AT LARGE DISTANCES FOR BOUND STATES OF O_2

The RKR method gives results only in regions where spectroscopic data are available. It can be seen from Fig. 2 that the solid RKR lines do not extend to large values of r. For many purposes it is necessary to have potential curves at the larger distances.

The $^1\Delta_g$ and $^1\Sigma_g^+$ curves were fitted by Hulburt-Hirschfelder functions[21] at large distances. The Hulburt-Hirschfelder function appears to be about the best empirical potential available, although it does not fit the lowest state ($X\,^3\Sigma_g^-$) very well. These curves for the $^1\Delta_g$ and $^1\Sigma_g^+$ states are shown as dashed lines in Fig. 2. The RKR curves for these states are not known over a large enough range of r to furnish a stringent test of the fit of the empirical potential curves, but an indirect check can be obtained. According to Mulliken[22] (see also Moffitt[19]), the energy splittings between the three lowest states, $X\,^3\Sigma_g^-$, $^1\Delta_g$, and $^1\Sigma_g^+$, should be about equal. Actually, the ratio of the splittings is about 1.48 over the known range. If this ratio is assumed constant for all values of r, then a potential at large r can be calculated for the $X\,^3\Sigma_g^-$ state from the two empirical potential curves for the

TABLE VI. Potential energy of the $^1\Sigma_u^-$ state of O_2.[a]

v	$V(\text{cm}^{-1})$	r_{max} (A)	r_{min} (A)	V (ev)	T_e+V (ev)
0	321.0	1.678	1.517	0.03980	4.5880
1	941.2	1.764	1.476	0.1167	4.6649
2	1522	1.833	1.452	0.1887	4.7369
3	2067	1.899	1.435	0.2563	4.8045
4	2574	1.964	1.421	0.3191	4.8673
5	3042	2.030	1.410	0.3772	4.9254
6	3470	2.098	1.400	0.4303	4.9785

[a] Experimental data from reference 9.

TABLE VII. Potential energy of the $B\,^3\Sigma_u^-$ state of O_2.[a]

v	$V(\text{cm}^{-1})$	r_{max} (A)	r_{min} (A)	V (ev)	T_e+V (ev)
0	348.2	1.683	1.531	0.04318	6.2187
1	1036	1.756	1.486	0.1285	6.3040
2	1701	1.813	1.459	0.2110	6.3865
3	2343	1.865	1.438	0.2905	6.4660
4	2960	1.914	1.420	0.3671	6.5426
5	3553	1.962	1.405	0.4405	6.6160
6	4114	2.009	1.392	0.5101	6.6856
7	4648	2.057	1.380	0.5764	6.7519
8	5149	2.112	1.370	0.6384	6.8139
9	5614	2.172	1.362	0.6961	6.8716
10	6043	2.235	1.353	0.7493	6.9248
11	6431	2.302	1.344	0.7975	6.9730
12	6777	2.386	1.342	0.8403	7.0158
13	7077	2.480	1.338	0.8776	7.0531
14	7332	2.588	1.334	0.9092	7.0847
15	7542	2.721	1.335	0.9352	7.1107
16	7711	2.872	1.340	0.9561	7.1316
17	7844	3.055	1.345	0.9726	7.1481
18	7946	3.270	1.354	0.9853	7.1608
19	8021	3.536	1.364	0.9946	7.1701
20	8074	3.900	1.370	1.0012	7.1767

[a] Experimental data from references 16 and 17.

$^1\Delta_g$ and $^1\Sigma_g^+$ states. This calculated curve, which can be represented by the equation

$$V(r) = -452.4e^{-3.176r} \text{ ev}, \qquad 1.7\text{A} < r < 2.5\text{ A}, \quad (5)$$

is also shown dashed in Fig. 2. This dashed line joins on fairly smoothly to the RKR curve for the ground state, thereby giving an indirect check on the other two curves. The constants for the Hulburt-Hirschfelder curves are given in Table VIII.

The RKR curves for the $^1\Sigma_u^-$, $^3\Delta_u$, and $A^3\Sigma_u^+$ states are known over a large enough range of r to test rigorously any empirical potential function. The $^3\Delta_u$ state was best represented at large distances by a Hulburt-Hirschfelder curve, whereas the $^1\Sigma_u^-$ state was fitted satisfactorily with a Morse curve. The constants

[21] H. M. Hulburt and J. O. Hirschfelder, J. Chem. Phys. **9**, 61 (1941).

[22] R. S. Mulliken, Revs. Modern Phys. **4**, 1 (1932).

for these curves are also given in Table VIII, and the curves themselves are shown dashed in Fig. 2. The $A\,^3\Sigma_u^+$ state (based on Herzberg's assignment) could not be fitted over its whole range by any of the usual empirical functions, but a Morse function could be adjusted to give an excellent fit from 1.74 to 2.26 A, and extrapolation to 2.5 A should be reliable. The equation for this curve is

$$V(r)=0.7267\{\exp[-10.58(r-1.599)]-2\exp[-5.29(r-1.599)]\}\text{ev},\qquad 1.74\text{ A}<r<2.5\text{ A}. \quad (6)$$

RELATIONS AMONG THE STATES OF O_2

A number of approximate but useful relations among the eighteen states of O_2 can be obtained from simple quantum-mechanical considerations. These relations can be used to calculate the long-range "tails" of the curves for the remaining twelve states from the results for the six known bound states discussed in the preceding sections. The results should be fairly reliable since theory is used only to obtain relations among energies and not to calculate directly the energies themselves. Only the p electrons are considered. Similar procedures seemed to work well for N_2[1] and NO,[2] and we might therefore expect it to give good results for O_2 as well.

Since we are interested primarily in the long-range "tails" of the potential energy curves, a correlation among the energies of the various states should presumably be developed by a valence-bond (VB) method, which is generally the best simple method at large internuclear distances,[23] and which gives a description of the molecular states in terms of atomic orbitals (AO's). This involves essentially an electron pairing procedure, which receives its simplest formulation in the perfect pairing approximation,[24]

$$V=\sum_{\substack{\text{orbitals with}\\ \text{paired spins}}}J_{ij}-\tfrac{1}{2}\sum_{\substack{\text{orbitals with}\\ \text{nonpaired spins}}}J_{ij}-\sum_{\substack{\text{orbitals with}\\ \text{parallel spins}}}J_{ij}, \quad (7)$$

where V is the interaction energy and J_{ij} is the exchange integral for two electrons in the atomic orbitals

TABLE VIII. Parameters of empirical functions which give best fit for the bound states of O_2.

$V=D_e[(1-e^{-x})^2+cx^3e^{-2x}(1+bx)-1]$; $x=2\beta(r-r_e)/r_e$

State	D_e(ev)	r_e(A)	2β	c	b
$^1\Delta_g$	4.230	1.2155	3.4203	0.089501	2.6976
$^1\Sigma_g^+$	3.576	1.2268	3.5637	0.098629	2.9187
$^1\Sigma_u^-$	0.6653	1.597	4.8841	0	...
$^3\Delta_u$	0.9154	1.4804	5.4637	0.021247	1.3282

[23] (a) C. A. Coulson, *Valence* (Oxford University Press, New York, 1952), pp. 147–151; (b) Eyring, Walter, and Kimball, *Quantum Chemistry* (John Wiley & Sons, Inc., New York, 1944), pp. 214, 241.

[24] Reference 23a, pp. 166–184.

TABLE IX. Simple MO description of the lower states of N_2 together with their VB energy expressions.

MO's	$X\,^1\Sigma_g^+$	$A\,^3\Sigma_u^+$	$^5\Sigma_g^+$	$^7\Sigma_u^+$
$\sigma_u(2p_{z1}-2p_{z2})$				↑
$\pi_g^-(2p_{x1}-2p_{x2})$		↑	↑	↑
$\pi_g^+(2p_{y1}-2p_{y2})$			↑	↑
$\pi_u^-(2p_{x1}+2p_{x2})$	↑ ↓	↑	↑	↑
$\pi_u^+(2p_{y1}+2p_{y2})$	↑ ↓	↑ ↓	↑	↑
$\sigma_g(2p_{z1}+2p_{z2})$	↑ ↓	↑ ↓	↑ ↓	↑
VB energy expression	$J_{xx}+J_{yy}+J_{zz}$	$J_{xx}+J_{yy}-J_{zz}$	$J_{xx}-J_{yy}-J_{zz}$	$-J_{xx}-J_{yy}-J_{zz}$

i and j. In the foregoing equation terms involving the coulomb integrals have been omitted, since the coulombic interaction between neutral atoms is very small at large internuclear separations. On the other hand, there are many advantages to a molecular orbital (MO) formulation of the problem, since the electronic configurations of molecular states have a very clear and simple description in MO language. This is an important consideration for O_2 with its eighteen states. We therefore try to establish a simple connection between the MO and AO descriptions, such that we can describe the electron configurations in MO language, and from this description write down VB expressions for the interaction energies. Such a connection on a simple level is not trivial, since the MO and the VB or AO descriptions on this level are basically different, inasmuch as the MO description is in terms of *single* electrons and the AO description is in terms of *pairs* of electrons. Of course, in their higher approximations the two descriptions become equivalent,[23] but we are seeking to avoid as much as possible the complications of higher approximations. A further advantage of a simple connection between the MO and the AO descriptions is that it suggests modifications and extensions of the perfect pairing approximation which are necessary for some cases.

Let us first consider a case for which both the VB and the MO descriptions are clear cut, and for which the perfect pairing approximation, Eq. (7), is known to lead to reliable results. The interaction between two ^4S nitrogen atoms, $N(1s)^2(2s)^2(2p_x)(2p_y)(2p_z)$, leads to four possible molecular states, $X\,^1\Sigma_g^+$, $A\,^3\Sigma_u^+$, $^5\Sigma_g^+$, and $^7\Sigma_u^+$. When two N atoms approach each other, the three electrons in the p orbitals of each atom can be paired together in various ways: pairing all three leads to the $X\,^1\Sigma_g^+$ state of N_2; pairing two electrons of one atom with two of the other atom and antipairing the third electrons (spins parallel) leads to the $A^3\Sigma_u^+$ state; and so on until the $^7\Sigma_u^+$ state results from all the p electrons being antipaired. According to Eq. (7) the interaction energies are therefore

$$V(^1\Sigma)=J_{xx}+J_{yy}+J_{zz}=J_{xx}+2J_{yy},$$

$$V(^3\Sigma)=J_{xx}+J_{yy}-J_{zz}=J_{xx},\text{ etc. (see Table IX)}, \quad (8)$$

TABLE X. Simple MO description of the lower states of O_2 together with VB energy expressions.

MO's	$X\,^3\Sigma_g^-$	$^1\Delta_g$	$^1\Sigma_g^+$	$^1\Sigma_u^-$	$^3\Delta_u$	$A\,^3\Sigma_u^+$
$\sigma_u(2p_{x1}-2p_{x2})$						
$\pi_g^-(2p_{x1}-2p_{x2})$	↑		↓	↑ ↓	↑	↑ ↓
$\pi_g^+(2p_{y1}-2p_{y2})$	↑	↑ ↓	↑	↓	↑ ↓	↑
$\pi_u^-(2p_{x1}+2p_{x2})$	↑ ↓	↑ ↓	↑ ↓	↑	↑	↑
$\pi_u^+(2p_{y1}+2p_{y2})$	↑ ↓	↑ ↓	↑ ↓	↑ ↓	↑ ↓	↑ ↓
$\sigma_g(2p_{x1}+2p_{x2})$	↑ ↓	↑ ↓	↑ ↓	↑ ↓	↑ ↓	↑ ↓
VB energy expression	$J_{xx}-J_{yy}$	$J_{xx}-J_{yy}$	$J_{xx}-J_{yy}$	$J_{xx}-3J_{yy}$	$J_{xx}-3J_{yy}$	$J_{xx}-3J_{yy}$

where the x axis lies along the internuclear axis, and by symmetry $J_{xx} \neq J_{yy} = J_{zz}$. In Eq. (8), cross terms such as J_{xy} have been neglected. The reason for doing so is that these terms are smaller than the diagonal terms such as J_{xx}. The exchange term, J, consists of a large number of integrals but, in general, the value of J is roughly proportional to the overlap integral[23b] which by symmetry is zero for the cross terms.

It is clear from Eq. (8) that a knowledge of any two of the states enables one to solve for J_{xx} and J_{yy} and from these the energies of the other two states can be calculated. This has been done for N_2 with excellent results.[1]

It is worth mentioning that a more rigorous scheme would include terms like J_{xy} in Eq. (8). We have not done so since there are not at present sufficient data to evaluate the additional terms which would arise. The inclusion of these additional terms should serve to make the agreement with experiment even better. The results obtained with the present scheme justify this approach—at least until more experimental data become available.

The simple MO description of these four states of N_2 is given in Table IX, together with the VB energy expressions. The MO's, σ_g, π_u^+, π_u^-, π_g^+, π_g^-, and σ_u,† are also shown as approximated by a linear combination of atomic orbitals (LCAO), and it is evident from symmetry that $\pi_u^\pm$ and $\pi_g^\pm$ form two degenerate sets. The relation between the MO and VB descriptions is clear from Table IX: a pair of electrons in a bonding MO leads to a contribution of $+J$ according to the VB perfect pairing approximation, whereas the combination of one electron in a bonding MO plus another electron of the same spin in the corresponding antibonding MO leads to a contribution of $-J$. This latter point has been previously pointed out in some detail by Linnett,[6] who showed that the simple MO wave function for two such electrons, which in Slater determinants is

$$|\,\pi_u^+\alpha \quad \pi_g^+\alpha\,|, \tag{9}$$

is entirely equivalent in the LCAO approximation, except for a normalization factor, to a VB wave function in terms of AO's, which is

$$|\,2p_{y1}\alpha \quad 2p_{y2}\alpha\,|. \tag{10}$$

These simple relations serve as a guide for the more complicated case of O_2. From the MO description of the various molecular states which arise from the interaction of ground state atoms, one should be able to write down the VB expressions for the interaction energies. Since the simple VB description yields results which are in general superior to the simple MO results at large internuclear separations, such a procedure should yield valuable results, as it does for N_2.

The foregoing procedure cannot be applied to O_2 without modification and extension. To illustrate why this is so, we consider the six lowest states of O_2, whose simple MO description is given in Table X. In this simple description there are a number of different electron distributions for the $^1\Delta_g$, $^1\Sigma_g^+$, $^1\Sigma_u^-$, $^3\Delta_u$ and $^3\Sigma_u^+$ states which are degenerate with the ones given in the table. The MO wave functions for these states therefore have to be represented by linear combinations of the wave functions associated with the different electron distributions. Allowance for the use of linear combinations will lead to splitting, causing, for example, the $^1\Sigma_g^+$ state to have a different energy than either the $^1\Delta_g$ or the $^3\Sigma_g^-$ state. This splitting might be looked on as a second-order effect, and it is not included in the present approximation. Such splitting may be fairly large, but we expect that its effects would not be greater in any case than the energy difference between the $^3\Sigma_g^-$ and $^1\Sigma_g^+$ states. Neglecting this effect, then, we see from Table X that there are three electron configurations which did not occur in N_2. These configurations are

$$\begin{array}{lccc} \pi_g^\pm & \uparrow & \uparrow\downarrow & \uparrow\downarrow \\ \pi_u^\pm & \uparrow\downarrow & \uparrow\downarrow & \uparrow \\ & \text{(A)} & \text{(B)} & \text{(C)} \end{array} . \tag{11}$$

The method of treating these electrons from a VB viewpoint is suggested by the work of Linnett.[6] Consider the arrangement (A). As mentioned previously, Linnett has shown that two electrons with α spin, of

† These MO's are also often denoted as $\sigma 2p_x$, $\pi 2p_y$, $\pi 2p_z$, $\pi^* 2p_y$, $\pi^* 2p_z$, and $\sigma^* 2p_x$, respectively.

which one is in a bonding π_u MO and the other is in an antibonding π_g MO, can be considered equivalent to one electron with α spin in each separate AO. If a third electron with β spin is now added to the bonding π_u MO, Linnett has shown that the situation can still be described as the two electrons with α spin occupying AO's and the one electron with β spin occupying the π_u MO. According to Eq. (7) the pair of electrons in the AO's contribute an amount $-J_{vv}$ to the interaction energy. The electron in the bonding π_u MO forms a one-electron bond, and the strength of such a bond is usually about one-half the strength of the corresponding two-electron bond.[23] Thus the total contribution to the interaction energy from the "three-electron bond" of configuration (A) is about $-\frac{1}{2}J_{vv}$.‡ The "three-electron bond" energy has been discussed in the earlier paper[2] on NO, where it was shown that the results obtained on this basis are quite reasonable, and consistent with the meager spectroscopic data and with the large difference in dissociation energy between NO and NO^+.

Consider now the arrangement (B). It is easy to show by the rules of determinants that, within the LCAO approximation, the simple MO wave function

$$|\,\pi_u{}^+\alpha \quad \pi_u{}^+\beta \quad \pi_g{}^+\alpha \quad \pi_g{}^+\beta\,| \qquad (12)$$

is entirely equivalent, except for a normalizing factor, to the simple VB bond wave function

$$|\,2p_{v_1}\alpha \quad 2p_{v_1}\beta \quad 2p_{v_2}\alpha \quad 2p_{v_2}\beta\,|. \qquad (13)$$

According to (13), we can think of the two electrons of α spin on the different atoms contributing an energy of $-J_{vv}$, and similarly for the electrons of β spin, for a total contribution of $-2J_{vv}$. Alternatively, (13) can be interpreted as two electrons on each atom having their spins internally paired, and hence randomly oriented (nonpaired) with respect to the spins of the two electrons on the other atom. According to Eq. (7), this interpretation leads to an energy contribution of $4(-\frac{1}{2}J_{vv}) = -2J_{vv}$, as before.

Finally, the arrangement (C) can also be treated by the Linnett procedure, and is obviously equivalent to one electron with α spin in each AO plus one electron with β spin in the antibonding π_g MO. The two electrons in the AO's contribute $-J_{vv}$ to the energy, but the third electron in the antibonding MO contributes $-\frac{3}{2}J_{vv}$. This has to be so if the configuration

$$\begin{matrix} \pi_g{}^{\pm} & \uparrow \\ \pi_u{}^{\pm} & \uparrow \end{matrix} \qquad (14)$$

is to give a net contribution of $-J_{vv}$ as dictated by the perfect pairing relation. The one electron in the π_u MO has been assumed to contribute $+\frac{1}{2}J_{vv}$, so that the electron in the π_g MO must contribute to $-\frac{3}{2}J_{vv}$ to make the sum be $-J_{vv}$. Thus the total contribution from configuration (C) is $-\frac{5}{2}J_{vv}$. This can also be seen in an even simpler way. Configuration (C) is equivalent to (B) with one electron removed from a bonding MO and hence the energy of (C) is $-2J_{vv} - (+\frac{1}{2}J_{vv}) = -\frac{5}{2}J_{vv}$.

With these rules, then, we can immediately write down the energy expressions for the six lowest states of O_2. These are given in Table X, where we have again set $J_{vv} = J_{zz}$. To the approximation of neglecting splitting, it is seen that the six states break up into two sets of three states each. This is in approximate agreement with experiment, as can be seen in Fig. 2.

The foregoing discussion suggests that the whole method can be formally treated completely on the basis of single electrons, and all reference to electron pairs eliminated. If we assign a contribution to the interaction energy of $+\frac{1}{2}J$ for a single electron in a bonding MO, and $-\frac{3}{2}J$ for a single electron in an antibonding MO, the correct VB energy expression can be obtained simply by adding up the contributions of all the electrons. It seems somewhat paradoxical that an energy expression for electron pairing can be written down in terms of single electron energies, but reference to the preceding discussion and to Tables IX and X shows the validity of the procedure. This result greatly simplifies the problem of writing down energy expressions for large numbers of complicated

‡ Since the arguments used to obtain this value are at best heuristic, the referees have suggested that a more detailed comment should be made. Consider the wave function $|\,a\alpha\, b\alpha\, (a+b)\beta \cdots m\alpha\, n\beta\,|$, where the functions a, b, c, etc., are assumed normalized on the respective atoms. This wave function corresponds to the "three-electron bond" involving the AO's a and b, which are associated with the like atoms A and B. The terms in the interaction energy arising from this three-electron bond are

$$V_3 \approx -(ab\ ab)_H + (ab)_H,$$

where we have as usual neglected the multiple exchange and coulomb integrals, and where

$$(ab\ ab)_H = \int (a_1a_2b_3c_4\cdots)H(b_1a_2a_3c_4\cdots)d\tau,$$

$$(ab)_H = \int (a_1a_2b_3c_4\cdots)H(a_1b_2b_3c_4\cdots)d\tau.$$

We now want to relate this result to the energies of the one-electron bond and of the repulsive two-electron bond with parallel spins. The wave function for the repulsive two-electron bond between a and b is $|\,a\alpha\, b\alpha \cdots n\beta\,|$, and leads to a contribution to the interaction energy of

$$V_2 \approx -(ab\ ab)_H,$$

which we have set equal to $-J_{vv}$. Similarly, the wave function for the one-electron bond between a and b is $|\,(a+b)\alpha \cdots n\beta\,|$, and leads to a contribution to the interaction energy of

$$V_1 \approx (ab)_H,$$

which we have assumed to have half the strength of a normal attractive two-electron bond, or $\frac{1}{2}J_{vv}$. The interaction energy for the three-electron bond is therefore

$$V_3 = V_2 + V_1 = -\tfrac{1}{2}J_{vv}.$$

Thus, the value we have used in this paper is consistent with our assumption regarding the strength of the one-electron bond. In a similar manner it can be shown that the configuration (C) of (11) leads to an interaction energy of $-\frac{3}{2}J_{vv}$.

TABLE XI. Electronic configurations and energy expressions for the upper states of O_2.

State	Electronic configuration (MO)	Energy (VB)	Energy in terms of $^1\Delta_g$ and $^3\Delta_u$
$^3\Pi_u$	$\sigma_g^2(\pi_u^+)^2(\pi_u^-)^2\pi_g^+(\alpha)\sigma_u(\alpha)$	$-\frac{1}{2}(J_{zz}-J_{yy})$	$-\frac{1}{2}V(^1\Delta_g)$
$^1\Pi_u$	$\sigma_g^2(\pi_u^+)^2(\pi_u^-)^2\pi_g^+(\alpha)\sigma_u(\beta)$		
$^5\Pi_g$	$\sigma_g^2(\pi_u^+)^2\pi_u^-(\alpha)\pi_g^+(\alpha)\pi_g^-(\alpha)\sigma_u(\alpha)$	$-\frac{1}{2}(J_{zz}+3J_{yy})$	$-\frac{3}{2}V(^1\Delta_g)+V(^3\Delta_u)$
$^3\Pi_g$	$\sigma_g^2(\pi_u^+)^2\pi_u^-(\alpha)\pi_g^+(\alpha)\pi_g^-(\alpha)\sigma_u(\beta)$		
$^1\Pi_g$	$\sigma_g^2(\pi_u^+)^2\pi_u^-(\alpha)\pi_g^+(\beta)\pi_g^-(\alpha)\sigma_u(\beta)$		
$^5\Sigma_u^-$	$\sigma_g(\alpha)(\pi_u^+)^2(\pi_u^-)^2\pi_g^+(\alpha)\pi_g^-(\alpha)\sigma_u(\alpha)$	$-(J_{zz}+J_{yy})$	$-2V(^1\Delta_g)+V(^3\Delta_u)$
$^3\Sigma_u^+$	$\sigma_u(\alpha)(\pi_u^+)^2(\pi_u^-)^2\pi_g^+(\alpha)\pi_g^-(\beta)\sigma_u(\alpha)$		
$^1\Sigma_g^+$	$\sigma_g^2(\pi_u^+)^2(\pi_u^-)^2\sigma_u^2$	$-2(J_{zz}-J_{yy})$	$-2V(^1\Delta_g)$
$^5\Delta_g$	$\sigma_g(\alpha)(\pi_u^+)^2\pi_u^-(\alpha)(\pi_g^+)^2\pi_g^-(\alpha)\sigma_u(\alpha)$	$-(J_{zz}+3J_{yy})$	$-3V(^1\Delta_g)+2V(^3\Delta_u)$
$^5\Sigma_g^+$	$\sigma_g(\alpha)(\pi_u^+)^2\pi_u^-(\alpha)\pi_g^+(\alpha)(\pi_g^-)^2\sigma_u(\alpha)$		
$^5\Sigma_g^+$	$\sigma_g^2\pi_u^+(\alpha)\pi_u^-(\alpha)\pi_g^+(\alpha)\pi_g^-(\alpha)\sigma_u^2$	$-2(J_{zz}+J_{yy})$	$-4V(^1\Delta_g)+2V(^3\Delta_u)$
$^5\Pi_g$	$\sigma_g(\alpha)(\pi_u^+)^2\pi_u^-(\alpha)\pi_g^+(\alpha)\pi_g^-(\alpha)\sigma_u^2$	$-\frac{1}{2}(5J_{zz}+3J_{yy})$	$-\frac{5}{2}V(^1\Delta_g)+2V(^3\Delta_u)$

molecular electronic states, and we believe it combines the best features of both the MO and VB theories in their simplest forms.

The simple MO description of the other twelve states of O_2 is given in Table XI, together with the energy expressions obtained by the above scheme. As in Table X, we have given only one configuration for each state, although several configurations are possible for many of the states. As mentioned previously, this will lead to splitting so that the states shown as degenerate in Table XI will actually be split, although we do not believe such splitting should be greater than that observed for the three lowest states of O_2.

It is now possible to write expressions for the energies of all the states in Table XI in terms of the energies of any two other states. We choose the $^1\Delta_g$ and $^3\Delta_u$ states since these are the intermediate ones in the two groups of known states. The resulting expressions are given in the final column of Table XI. The energies of these different states in the range from 1.8 to 2.5 A can be represented as follows:

$$^3\Pi_u,\ ^1\Pi_u: V(r)=339\ e^{-3.570r}\ \text{ev}, \quad (15)$$

$$^5\Pi_g,\ ^3\Pi_g,\ ^1\Pi_g: V(r)=717\ e^{-3.565r}\ \text{ev}, \quad (16)$$

$$^5\Sigma_g^+: V(r)=2114\ e^{-3.567r}\ \text{ev}, \quad (17)$$

$$^1\Sigma_g^+: V(r)=1358\ e^{-3.570r}\ \text{ev}, \quad (18)$$

$$^5\Pi_u: V(r)=2455\ e^{-3.567r}\ \text{ev}, \quad (19)$$

$$^5\Sigma_u^-,\ ^3\Sigma_u^+: V(r)=1057\ e^{-3.567r}\ \text{ev}, \quad (20)$$

$$^5\Delta_g,\ ^5\Sigma_g^+: V(r)=1433\ e^{-3.565r}\ \text{ev}. \quad (21)$$

These curves are shown in Fig. 2 as dashed lines. They can, of course, be extrapolated to larger distances than 2.5 A, but at the expense of increased uncertainty in their values.

The only experimental information on any of these curves comes from an analysis of predissociation effects in the $B\ ^3\Sigma_u^-$ curve. Wilkinson and Mulliken[5] find that there is certainly predissociation at the $v'=12$ level of the $B\ ^3\Sigma_u^-$ curve, and it is probable that predissociation takes place in the whole range from $v'=4$ to $v'=12$. According to the correlation rules and the selection rules for predissociation,[25] only the $^3\Pi_u$ state can predissociate the $B\ ^3\Sigma_u^-$ state strongly. Wilkinson and Mulliken suggest that the $^3\Pi_u$ curve predissociates the $B\ ^3\Sigma_u^-$ curve by crossing it to the left of the minimum at $v'=12$. They further suggest that the $^3\Pi_u$ curve comes close to the $B\ ^3\Sigma_u^-$ curve most of the way up the left-hand side of the curve, and that this could explain the probable predissociation in all levels from $v'=4$ to $v'=12$. Our calculated curve for the $^3\Pi_u$ state rises a little too rapidly to pass entirely on the left-hand side of the $B\ ^3\Sigma_u^-$ curve from the minimum to $v'=12$. Extrapolation of our curve inward indicates that it cuts the $B\ ^3\Sigma_u^-$ not only at about $v'=12$, but also right at the minimum. Wilkinson and Mulliken rule out the possibility of a double crossing of the $B\ ^3\Sigma_u^-$ curve by the $^3\Pi_u$ curve, once at the minimum and once at $v'=12$, because of the absence of any observed predissociation effects at the $v'=0$ and $v'=1$ levels. It is therefore probable that our $^3\Pi_u$ curve is slightly too high around the region of the minimum of the $B\ ^3\Sigma_u^-$ curve, but this is easily explained by the approximations we have made.§ Allowance for the effect of splitting would lower our $^3\Pi_u$ curve, and inclusion of the cou-

[25] Reference 3, Chap. VII, Sec. 2.

§ *Note added in proof.*—After this article had been submitted for publication, Dr. Wilkinson called our attention to Dr. P. K. Carroll's work on predissociation in the Schumann-Runge bands [Astrophys. J. **129**, 794 (1959)]. Carroll reports a predissociation at $v'=4$ which apparently is stronger than the predissociation at $v'=12$. He suggests that this may be caused by the $^3\Pi_u$ curve crossing on the right-hand side of the $^3\Sigma_u^-$ curve at $v'=4$. If this is so, then it is difficult to explain the other predissociations ranging from $v'=4$ up to $v'=12$, especially the fact that the probability for predissociation appears to have two maxima, one at $v'=4$ and another at $v'=11$ with a minimum at $v'=9$. Carroll has also found abnormally wide widths for the rotational lines in the 2–0 and 1–0 bands of the Schumann-Runge bands. He feels that this is due to a blending of fine structure components. Our explanation would be that the $^3\Pi_u$ curve crosses at the bottom of the $^3\Sigma_u^-$ curve, as is suggested by our calculations, and then rises along the left-hand branch as Wilkinson and Mulliken suggest.

lombic and overlap integrals dropped from Eq. (7) would cause it to rise fairly sharply at small internuclear separations. If we use the crossing point at $v'=12$ ($V=1.801$ ev, $r=1.342$ A) together with our values for the $^3\Pi_u$ curve at large distances, the equation

$$V(r)=7.61\exp(-0.8224\,r^2)\text{ ev},\qquad 1.34\text{ A}<r<2.5\text{ A}\quad(22)$$

gives an excellent fit. Equation (22) is not entirely correct, however, since it still crosses the $B\,^3\Sigma_u^-$ curve at the minimum, and it is entirely probable that it should pass beneath the minimum. Further evidence for this is the apparent observation by Wilkinson and Mulliken of a weak continuum under the Schumann-Runge bands which may be attributable to the transition $^3\Pi_u\leftarrow{}^3\Sigma_g^-$.

Wilkinson and Mulliken also rule out the crossing of the $B\,^3\Sigma_u^-$ curve by the $^3\Pi_u$ curve at about $v'=3$ on the right-hand side of the minimum, a suggestion made by Flory[26] to explain certain photochemical effects. They suggest that the photochemical results can be explained by a "forbidden" predissociation near $v'=3\frac{1}{2}$ by any of the $^5\Sigma_u^-$, $^1\Pi_u$, or $^5\Pi_u$ curves. Our results indicate that the $^5\Sigma_u^-$ curve crosses the $B^3\Sigma_u^-$ curve right at $v'=3\frac{1}{2}$.

Our results, therefore, are at least not inconsistent with the meager experimental information that is available on the repulsive states which dissociate to ground state atoms. It can further be shown that they are consistent with the previously calculated[2] NO energies, on the assumption that the exchange integrals J are about the same for NO and O_2. Since the energy for the $^2\Pi$ ground state of NO is $V(^2\Pi, \text{NO})=J_{zz}+\frac{1}{2}J_{yy}$, and that for the $^3\Delta_u$ state of O_2 is $V(^3\Delta_u, O_2)=J_{zz}-3J_{yy}$, we can calculate J_{zz} and J_{yy} as a function of distance from the known energies and use the values to calculate the energy of the $^1\Delta_g$ state of O_2. The energies of the $^1\Delta_g$ and $^3\Delta_u$ states in turn determine the energies of all the other O_2 states, as has been shown in Table XI. The $^1\Delta_g$ energies calculated in this way agree with the values of Table VIII quite well. The deviation is 0.010 ev at $r=1.8$ A, rises to 0.041 ev at $r=2.1$ A, and falls to 0.018 ev at $r=2.6$ A. These deviations propagate directly to the other O_2 states as shown by the last column of Table XI. The agreement is certainly within the uncertainty caused by our neglect of splitting.

O_2—O_2 INTERACTIONS

The modified perfect pairing scheme describes interactions between molecules as just the sums of the interactions between the constituent atoms, so that we can calculate approximately the long-range O_2—O_2 interaction from the results of the preceding sections.

[26] P. J. Flory, J. Chem. Phys. 4, 23 (1936).

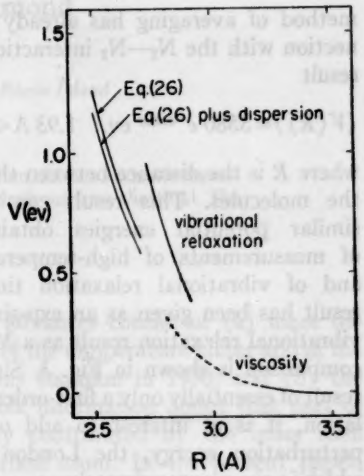

FIG. 3. Average O_2—O_2 interaction as obtained by different methods.

Similar procedures worked well for the N_2—N_2 and N_2—O_2 interactions.[1,2] Consider the interaction of an oxygen atom, $O(2p_x)(2p_y)^2(2p_z)$, with another oxygen atom, $O(2p_x)(2p_y)(2p_z)^2$, each of which is bound to another oxygen to form two oxygen molecules. The interaction of these two configurations will lead to the lowest energy. The electron spins on these two atoms are uncorrelated (nonpaired), and by the perfect pairing relation the net interaction energy between the two atoms is

$$V(\text{O}\cdots\text{O})=-\tfrac{1}{2}J_{xx}-\tfrac{1}{2}(2J_{yy})-\tfrac{1}{2}(2J_{zz})=-\tfrac{1}{2}J_{xx}-2J_{yy},\|\quad(23)$$

or from Table X,

$$V(\text{O}\cdots\text{O})=-\tfrac{1}{4}[7V(^1\Delta_g)-5V(^3\Delta_u)],\quad(24)$$

which can be represented by the expression

$$V(\text{O}\cdots\text{O})=812\,e^{-3.565r}\text{ ev},\quad 1.8\text{ A}<r<2.5\text{ A}.\quad(25)$$

The O_2—O_2 interactions are obtained by adding up all the four pertinent O···O interactions, each of which is given by Eq. (25) with the value of r appropriate for the atom-atom distance. The dependence of the O_2—O_2 interaction on orientation is thus given implicitly by the dependence of the atom-atom distances on the molecular orientations.

In many cases it is useful to have the total O_2—O_2 interaction energy averaged over all orientations. The

|| The referee has pointed out that the interaction energy calculated in this way does not take into account the fact that the values of J_{zz} and J_{yy} depend on the relative orientation of the two O_2 molecules, as well as the fact that at certain orientations the cross terms such as J_{xy} become large. Consideration of extremes of orientations shows that these effects introduce a maximum variation with orientation of about 40% into Eqs. (23)–(25). Neglect of this variation is thus consistent with the other approximations involved, such as neglect of multiple exchange integrals [E. A. Mason and J. O. Hirschfelder, J. Chem. Phys. 26, 756 (1957)], inasmuch as the J's are really treated as disposable parameters to be determined from experiment. Furthermore, the final averaging over all molecular orientations to obtain Eq. (26) also tends to compensate the error.

method of averaging has already been given in connection with the N_2—N_2 interaction,[1] and leads to the result

$$\langle V(R)\rangle = 5580\, e^{-3.355r} \text{ ev}, \quad 1.93\text{ A} < r < 2.70\text{ A}, \qquad (26)$$

where R is the distance between the centers of mass of the molecules. This result can be compared with similar potential energies obtained from analysis of measurements of high-temperature gas viscosity[2] and of vibrational relaxation times.[7] The viscosity result has been given as an exp-six potential, and the vibrational relaxation result as a Morse potential. The comparison is shown in Fig. 3. Since Eq. (26) is the result of essentially only a first-order perturbation calculation, it is of interest to add on the second-order perturbation energy, the London dispersion energy, which is given approximately as

$$\langle V(\text{dis})\rangle = -\tfrac{3}{4}(\bar{\alpha}^2 I/R^6) = -(24.0/R^6) \text{ ev}, \quad R \text{ in A}, \qquad (27)$$

where $\bar{\alpha}$ is the average polarizability of an O_2 molecule and I its ionization potential. The sum of Eqs. (26) and (27) is also shown in Fig. 3. The agreement among the potentials, calculated in three completely independent ways, is excellent. The fact that the potential from vibrational relaxation measurements seems high is to be expected from the approximations made in the theory of vibrational relaxation. This theory is in effect a one-dimensional treatment involving the end-to-end molecular configuration.[27] Since this configuration leads to the largest interaction energy of any configuration, the difference shown in Fig. 3 is not unexpected.

SUMMARY

Potential energy curves for the interactions between two ground state O atoms have been calculated from spectroscopic data and from approximate quantum-mechanical relations. The results obtained from spectroscopic data (RKR method) are given in Tables I–VI for the $X\,^3\Sigma_g^-$, $^1\Delta_g$, $^1\Sigma_g^+$, $^3\Delta_u$, $A\,^3\Sigma_u^+$, and $^1\Sigma_u^-$ states of O_2. The long-range "tails" of the $^1\Delta_g$, $^1\Sigma_g^+$, and $^3\Delta_u$ curves were fitted with Hulburt-Hirschfelder functions, whereas the $^1\Sigma_u^-$ curve was best fitted with a Morse function. The constants for these empirical functions are given in Table VIII. The $A\,^3\Sigma_u^+$ curve was found to be best fitted at large r by Eq. (6), and the $X\,^3\Sigma_g^-$ curve at large r was represented by Eq. (5). Relations among the eighteen states of O_2 dissociating to ground state atoms have been obtained by a modified perfect pairing approximation. This is based on a description of electronic configurations in terms of a combination of AO's and MO's which leads to simple rules for writing down a VB energy expression, given a simple MO description of an electronic state. These relations yield results for the repulsive states of O_2 which have been represented by Eqs. (15) through (21). The repulsive states have been checked against predissociation effects observed in the $B\,^3\Sigma_u^-$ state, and are in agreement with the observations. The curve for the $B\,^3\Sigma_u^-$ state, the upper state of the Schumann-Runge bands, has been calculated by the RKR method with the results shown in Table VII. A partial check has also been made by calculating the O_2 curves in terms of the known curves for the $X\,^2\Pi$ state of NO and the $^3\Delta_u$ state of O_2, with satisfactory agreement.

An O_2—O_2 potential has been generated from the O—O potentials in a manner similar to that used for the N_2—N_2 and N_2—O_2 potentials obtained previously.[1,2] The results are consistent with other potentials obtained from different experimental sources.

It is difficult to assess the absolute accuracy of all the results obtained. However, they are all internally consistent and in agreement with the limited available experimental data.

ACKNOWLEDGMENTS

The authors are extremely grateful to Louis T. Ho, who not only performed a large number of calculations for them, but also checked much of their own work. They are also grateful to Ernest Madsen for checking some of the calculations, and to Dr. Ernest Bauer for communicating the results of his vibrational relaxation calculations before their publication.

[27] (a) E. Bauer, J. Chem. Phys. **23**, 1087 (1955); (b) M. Salkoff and E. Bauer, *ibid.* **29**, 26 (1958).

Density of the Bonding Electrons in Diamond

G. B. CARPENTER

Metcalf Chemical Laboratories, Brown University, Providence 12, Rhode Island

(Received June 26, 1959)

The electron density in diamond, for the bonding electrons only, is derived from old but accurate experimental x-ray diffraction data by subtracting the contribution of the inner shall electrons from the total. The carbon-carbon single bond appears to be very diffuse.

INTRODUCTION

THE possibility of obtaining direct experimental information about the actual shape of a chemical bond has long been an intriguing one, but one which has so far led to only slight results. The reason for this disappointing state of affairs is basically that a chemical bond, when viewed with sufficient perspective, is a relatively minor perturbation of spherical free atoms. This perturbation is near the limit of what can be explored by x-ray diffraction methods.

Diamond offers, however, an unusually favorable situation for direct examination of a bond in this way. First, the carbon atom has low atomic number and large valence, so that the contribution to the diffraction pattern from the inner shell electrons does not so completely overwhelm that from the valence electrons as is usually the case. Second, the thermal motion in diamond is relatively slight and so produces less blurring of the electron density than in any other substance at the same temperature. Third, the highly symmetrical environment of each atom simplifies the problem of separating the effects of thermal motion from those of bonding.

Some of these points were recognized before 1939 by Brill, Grimm, Hermann, and Peters[1] who carried out a series of careful measurements of the intensities of the reflections of x-rays from diamond. From these data, they calculated the electron density in diamond; sharp peaks representing carbon atoms were shown clearly, but the bonds were not every evident.

In 1950, Brill[2] analyzed anew the same data by subtracting from the observed electron density, the density expected for an assembly of spherical carbon atoms. Again only slight indication of the bonds themselves were found; "one-half to three-quarters of an electron has been shifted into each bond," depending on various assumptions about the contributions near the center of an atom in projection.

Recent advances in the interpretation, rather than in experimental methods, have now made it worthwhile to study once more the original data, in order to reveal more clearly what conclusions can be drawn about the electron density within a carbon-carbon single bond. These advances consist of (a) more detailed consideration of the temperature factor and of the scale factor than was common in 1950, and (b) the availability of reliable information about that part of the electron density contributed by the inner shell electrons of the carbon atom. In the present paper, slight adjustments of the original data are made in the light of (a) and the inner shell contribution is removed according to (b). The result is then a map of the density of just the valence electrons in diamond.

CALCULATIONS

Scale and Temperature Factors

The original measurements[1] are divided into three groups made with use of x-rays of three different wavelengths. The group corresponding to the longest wavelength consists of absolute structure factor values, while the other two groups consist of relative values only. Apparently, the second group was placed on the absolute scale by comparison of the values for one reflection common to the first and second group; the third group was similarly related to the first. Preliminary comparison of the resulting structure factors with calculated values suggested that slight inaccuracies remained. Furthermore, the difficulty of making absolute intensity measurements is notoriously great. Consequently, it was decided to introduce a separate scale factor, k_1, k_2, or k_3, for each group of data; the values were adjusted as described in the following.

For the subsequent analysis, it is necessary to know the thermal motion effects with some precision. In view of the high symmetry, and in order to avoid prejudicing the result, a spherically symmetric temperature factor, $\exp[-B(\sin\theta)^2/\lambda^2]$ was assumed.

The four parameters k_1, k_2, k_3, and B were adjusted by a least squares calculation which minimized $\Sigma F_0^2(\ln F_c/F_0)^2$. This quantity is approximately the same as the more obvious $\Sigma(F_0-F_c)^2$, but is more convenient for calculation. Here, the sum is over the 23 measured reflections in the region $(\sin\theta)/\lambda>1$. In this region, the effects of chemical bonds are surely negligible so that the parameters are undistorted by bond effects. Here, $F_0=k_iF_0'$, where F_0' is the value reported originally[1] and $i=1$, 2, or 3 depending on the group to which the reflection belongs; F_0 is then the

[1] Brill, Grimm, Hermann, and Peters, Ann. Physik **34**, 393 (1939).
[2] R. Brill, Acta Cryst. **3**, 333 (1950).

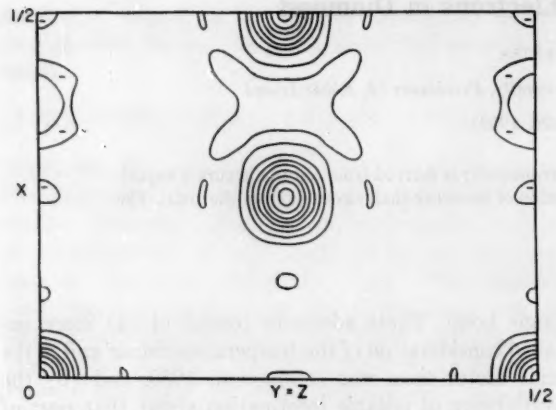

FIG. 1. Total electron density in diamond.

corrected observed structure factor. The quantity $F_c = F_c' \times \exp[-B(\sin\theta)^2/\lambda^2]$, where F_c' is the value calculated for diamond with no thermal motion from the atom form factor for a carbon atom in the valence state.[3]

The results are $k_1 = 1.000$, $k_2 = 0.950$, $k_3 = 1.065$, and $B = 0.1913$ A^2. The fact that the scale factors differ only slightly from unity, although they were determined here by an independent method, is evidence for the accuracy of the original F_0' values.[1] Consequently, the change made here by the use of F_0 is small. This empirical value of B must be compared with a value of 0.15 A^2 given by James[4] on the basis of the Debye temperature for diamond. The slight excess of the empirical value over the theoretical value is attributable to defects both in the theory and in the crystal. The B value corresponds to a rms displacement of a carbon atom of only 0.05 A.

Fourier Syntheses

The data consist of 34 values of $F(hkk)$ out to about 1.65 in $(\sin\theta)/\lambda$, plus the theoretical value of $F(000)$.

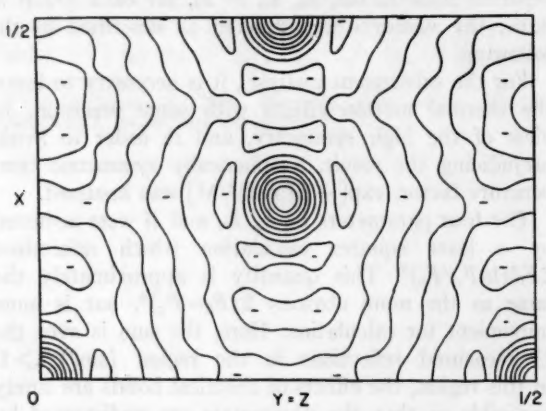

FIG. 2. Inner-shell electron density in diamond.

[3] R. McWeeny, Acta Cryst. 4, 513 (1951).
[4] R. W. James, *The Optical Principles of the Diffraction of X-rays* (G. Bell and Sons, London, England, 1948), p. 225.

Among these is $F(222)$, which would be zero if the carbon atoms were spherically symmetric; the correctness of the value used previously[1,2] and here has been re-confirmed recently.[5] The sign of this reflection was chosen so as to produce a positive contribution in the bonds rather than at atom centers, as seems reasonable; however, the entire effect of $F(222)$ is not great enough to make a significant change in the interpretation of the results.

After this work was completed, a revised value for $F(111)$ appeared[6] which is about 6% lower than the value used here. This produces no important change in the figures; however, the electron density values quoted subsequently are corrected for this small change.

The available data suffice for the calculation of a projection only of the electron density, the projection onto the plane of a and [011]. For convenience in calculation, the crystal was described on tetragonal

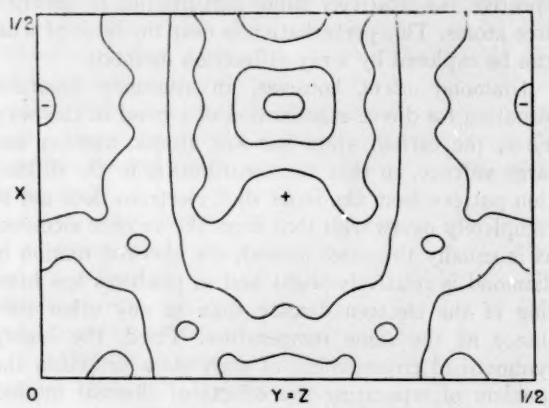

FIG. 3. Bond electron density in diamond.

axes and the projection was along the tetragonal b axis; however, the description of the results is given in terms of the cubic unit cell. The Fourier syntheses were carried out on an IBM 650 computer by means of a program written by the author.

The total projected electron density was calculated from the observed structure factor values modified as described in the preceding section; the result is presented in Fig. 1.

The second projection was computed from the theoretical form factor[7] for the K shell of the carbon atom, modified by the empirical spherical temperature factor; the result is shown in Fig. 2.

The final projection is the difference of the first and second projections, and so represents the projected electron density of the bonding electrons only; the result is shown in Fig. 3. [Actually, this Fourier synthesis was computed separately from $F_0 - F_c$ (K-shell) values, whereas the first was computed as the sum of the second and third.]

[5] M. Renninger, Acta Cryst. **8**, 606 (1955).
[6] R. Brill and H. Zandy, Nature **183**, 1387 (1959).
[7] R. McWeeny, Acta Cryst. **7**, 180 (1954).

RESULTS AND DISCUSSION

The projected electron densities are presented in the form of contour maps in the figures. Each version covers the same region of the crystal; in order to show explicitly the surroundings of one carbon atom, the region shown is four times as large as the asymmetric unit of the projection.

The total electron density is displayed in Fig. 1. The contours are drawn at equal arbitrary intervals of 3.58 electrons/A^2; the negative regions are marked with minuses. This map closely resembles that shown by Brill *et al.*,[1] except that the present version exhibits evidence of diffraction fringes caused by the sharp cutoff of the data at $(\sin\theta)/\lambda=1.65$. These effects were avoided in the earlier work, at the expense of some blurring of the electron density, by introduction of an artificially large temperature factor parameter. Thus, the density at an atom center is here 31.8 electrons/A^2 compared with 18.6 with the artificial temperature effect.[1]

The inner-shell electron density, displayed in Fig. 2, is quite similar to the total density except that the diffraction fringes appear to be more pronounced. The contours are at the same levels as in Fig. 1. In part, the conspicuousness of the fringes is the fortuitous result of small oscillations of the density through zero over large areas of the map; this produces many (zero density) contour lines in these areas where the density is in fact nearly constant. In part, the fringes are really more pronounced because of the sharpness of the core electron clouds. The density at an atom center is 29.4 electrons/A^2.

The bonding electron density is displayed in Fig. 3. Here the contours are spaced only one-fourth as far apart as in Figs. 1 and 2 since the density values are everywhere relatively small. The dominant feature is the general flatness of this map, although it contains twice as many electrons as does Fig. 2. It is necessary to integrate the density over almost the entire area in order to find 4 electrons per atom. There is little evidence for diffraction fringes in this map; these errors were similar in the two previous maps and so almost entirely cancel out in the difference.

Two bonds extend from the central atom (marked by the cross) to the atoms at the bottom corners. These bonds are parallel to the plane of the projection and so are viewed without distortion. Here, in fact, is the best experimentally derived view of a chemical bond yet presented. The bond is remarkably diffuse. The density at an atom center is 2.26 electrons/A^2 while that at the center of the bond is 1.59, and that at a point the same distance from the atom but midway between the two bonds is 0.72 electrons/A^2. Nevertheless, along the perpendicular bisector of a bond, the density rises slowly over a slight maximum at the bond. At the bond center, therefore, the electron density has a saddle point. The projection shows nearly cylindrical symmetry about the bond axis; the deviations are not significantly greater than experimental error, except near the center of an atom where other bonds complicate the picture.

The two other bonds above the central carbon atom make angles of $\pm 54.7°$ with the plane of the projection, so they are seen superimposed and foreshortened. The highest density, 4.84 electrons/A^2, must be halved to allow for the overlapping and multiplied by cos 54.7° to make a rough allowance for the foreshortening; the result, 1.40 electrons/A^2, is close to that at the center of the undistorted individual bonds. Therefore, the peak appearing between the center and the top is not of profound significance. If the density values in this region are simply halved, then they provide a view of a bond which is equivalent by symmetry to a side view of one of the bonds in the lower half of the map.

It is not possible to partition the density near the central atom unambiguously into contributions from the four bonds without the aid of further assumptions.

It is difficult to assess the size of the error to be expected in the result because there is no quantitative discussion of the errors in the original data.[1] If it is assumed, optimistically, that the standard deviation of each structure factor value is about 0.01 electron per one-eighth cell (which is consistent with giving the original values to three decimal places), then the standard deviation in the projected electron density is roughly 0.06 electron/A^2 at general positions, and somewhat more at special positions.[8] To this must be added an unknown error from the theoretical contribution of the inner shell electrons. The total error is then not inconsiderable in Fig. 3 where the interval between contours is only 0.90 electron/A^2. However, it is difficult to think of a more favorable case or a way to make an improvement in the accuracy of measurements. The only obvious improvement would be made by obtaining full three-dimensional data.

ACKNOWLEDGMENT

Financial support for the calculations required in this work was provided by the Office of Naval Research.

[8] D. W. J. Cruickshank and J. S. Rollett, Acta Cryst. **6**, 705 (1953).

THE JOURNAL OF CHEMICAL PHYSICS VOLUME 32, NUMBER 2 FEBRUARY, 1960

Crystal Spectra of Metal Coordination Compounds. I. Tetrahedral Cobalt(II)

J. FERGUSON

Division of Chemical Physics, C.S.I.R.O. Chemical Research Laboratories, Melbourne, Australia

(Received August 7, 1959)

A reflecting microscope has been used to measure the absorption spectra, in polarized light, of a number of cobalt(II) compounds in which the ligands are arranged tetrahedrally. These compounds are Cs_3CoCl_5, cobalt di-*p*-toluidine dichloride, cobalt dipyridine dibromide, and cobalt dipyridine diiodide. The two transitions, $^4A_2 \rightarrow {}^4T_1(F)$ in the near infrared and $^4A_2 \rightarrow {}^4T_1(P)$ in the visible, have been compared in the different compounds and the effect of symmetry discussed. It was also found that the crystal spectra of all but Cs_3CoCl_5 are modified by interaction between the complexes in the crystal so that the energy levels are not accurately described by the field of the ligands only.

INTRODUCTION

CRYSTAL field theory has been successfully used to interpret the absorption spectra of transition metal ions. Most of the experimental work reported so far has been done with solutions and although these give the energy separation between bands they can provide no information about the *polarization* of the electronic transitions. This quantity has significant theoretical interest and provided the mechanism of the transitions is known measurement of crystal spectra in polarized light should simplify the assignments of the bands. For this reason a study of the crystal spectra of metal co-ordination compounds was undertaken and the present paper presents the results obtained with tetrahedral cobalt(II).

The ^4F ground state of Co^{++} is split by a tetrahedral crystal field into three states, $^4A_2(F)$, $^4T_2(F)$, and $^4T_1(F)$. The excited ^4P state is not split by the tetrahedral field and belongs to the representation $^4T_1(P)$. It is usual to put the atomic state from which the level is derived in brackets after the group theory symbol to avoid ambiguity.

In addition to the quartet states there are doublet states in the free ion, the most important of which is the ^2G state which lies close to the ^4P state.

The ground state of Co^{++} in a tetrahedral field is $^4A_2$, followed by $^4T_2$, $^4T_1(F)$, and $^4T_1(P)$. Only the transitions $^4A_2 \rightarrow {}^4T_1(F)$ and $^4A_2 \rightarrow {}^4T_1(P)$ are allowed by the selections rules and these correspond to the bands observed in $CoCl_4^{--}$ at about 5500 and 16 000 cm^{-1}, respectively. It is these bands which are relevant to the present work.

When complexes of the type CoX_2Y_2 are considered, then the near infrared band corresponding to the transition $^4A_2 \rightarrow {}^4T_1(F)$ in CoX_4^{--} should split under the reduced symmetry C_{2v} into three transitions $^4A_2 \rightarrow {}^4A_2$, $^4A_2 \rightarrow {}^4B_1$ and $^4A_2 \rightarrow {}^4B_2$. Each of these is allowed under C_{2v} symmetry and they correspond to polarizations parallel to the z, y, and x molecular axes, respectively. The visible band related to the transition $^4A_2 \rightarrow {}^4T_1(P)$ should also split in the same way.

EXPERIMENTAL

Although the intensities of the transitions are low so that crystal thickness is not necessarily a limiting factor, the crystal size usually makes it impossible to use a macroscopic technique so that it is essential to develop a microspectrophotometric method. A Beck reflecting microscope has been used in the present work, either in conjunction with a Hilger medium quartz spectrograph or a Beckman DK2 spectrophotometer. An enlarged image of the crystal is focussed on the slit of the spectrometer and a piece of polaroid acts as an analyzer. For the near infrared special Polaroid type HR was used. A recorder trace, using the Beckman DK2, is made of the light transmitted through the crystal which is then moved and the trace repeated to get a measure of the light intensity incident on the crystal. The polaroid is most conveniently placed in the sample compartment of the Beckman DK2, or if the spectrum is being photographed, immediately in front of the slit of the spectrograph.

The compounds studied were prepared by methods described in the literature.[1]

CRYSTAL SPECTRUM OF Cs_3CoCl_5

Cs_3CoCl_5 contains the $CoCl_4^{--}$ ion and the crystal structure has been determined.[2] The crystals are deep blue in color because of the strong absorption in the red region. Yamada and Tsuchida[3] have reported its absorption spectrum, also by a microscopic technique, but their measurements were limited to the visible and ultraviolet regions of the spectrum.

The two strongest absorption transitions $^4A_2 \rightarrow {}^4T_1(F)$ and $^4A_2 \rightarrow {}^4T_1(P)$ which occur at about 5500 cm^{-1} and 16 000 cm^{-1}, respectively, are intense and stray light in the microscope optics limits the accurate measurement of peak absorption. The spectra will therefore not be given here. It is important, however, to record the approximate position of the $^4A_2 \rightarrow {}^4T_1(F)$ band in $CoCl_4^{--}$. It lies between 4500 and 7000 cm^{-1}, and there appears to be some evidence from the spectrum to suggest that the band is split into its three

[1] Cobalt di-*p*-toluidine dichloride, reference 5; Cs_3CoCl_5, reference 2; $CoPy_2Br_2$ and $CoPy_2I_2$, A. Hantzsch, Z. Anorg. u. Allgem Chem. **159**, 18 (1927).

[2] H. M. Powell and A. F. Wells, J. Chem. Soc. **1935**, 359.

[3] S. Yamada and R. Tsuchida, Bull. Chem. Soc. Japan **27**, 436 (1954).

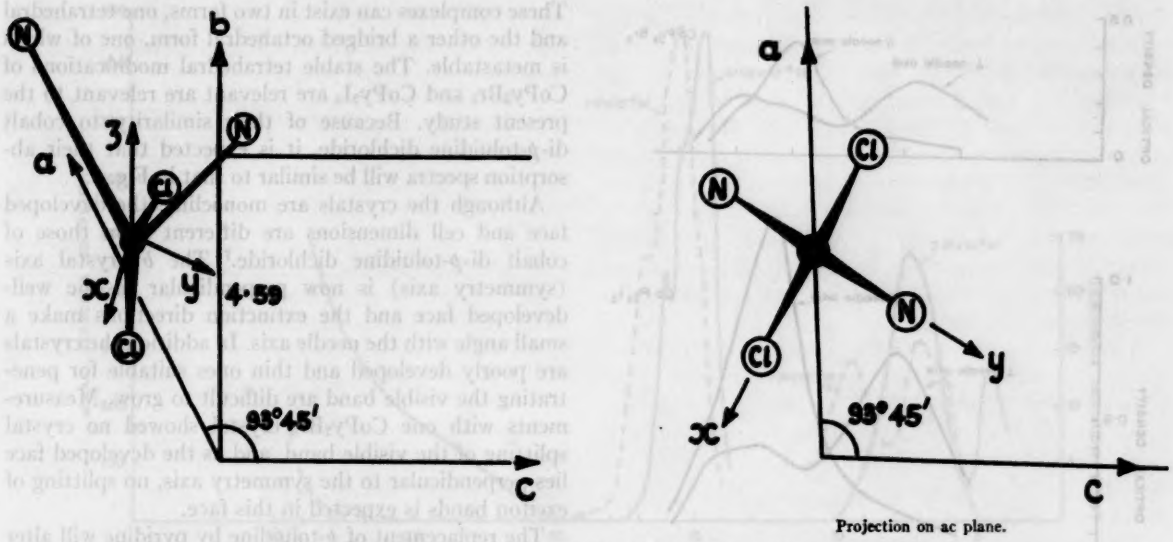

FIG. 1. Crystal structure of cobalt di-*p*-toluidine dichloride and the relation between the crystal and complex axes.

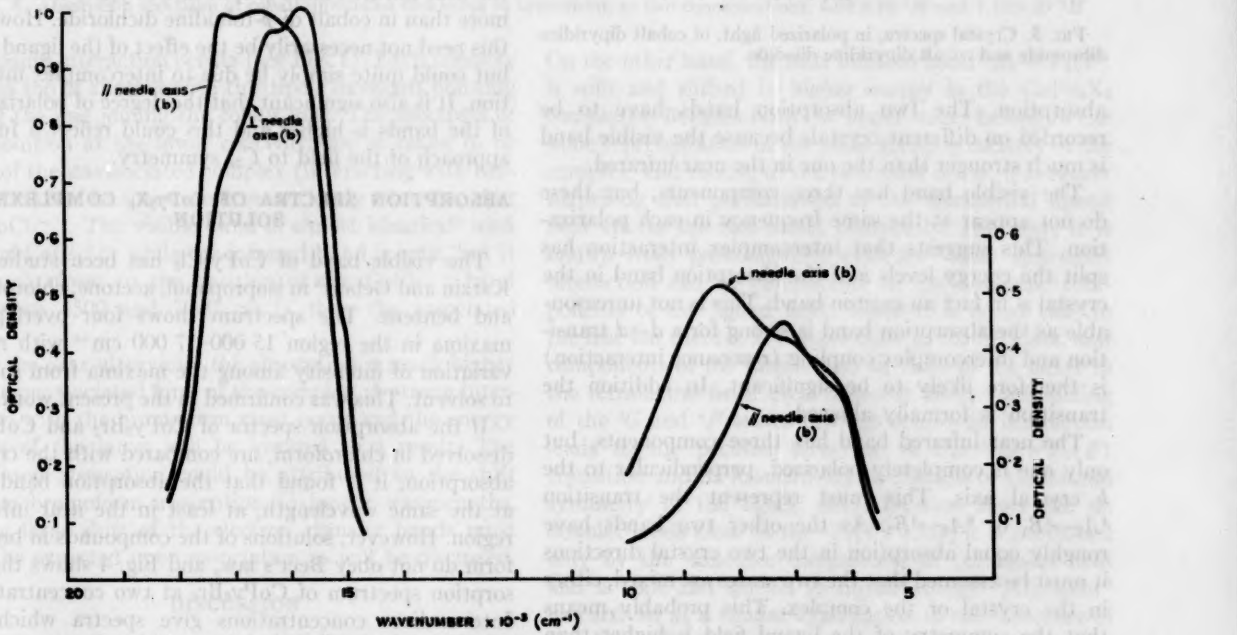

FIG. 2. Crystal spectrum, in polarized light, of cobalt di-*p*-toluidine dichloride.

components. The same band for CoO in ZnO is also split.[4]

The weaker intercombination bands which are easily measured will not be reported here.

CRYSTAL SPECTRUM OF COBALT DI-*p*-TOLUIDINE DICHLORIDE

The crystal structure of cobalt di-*p*-toluidine dichloride has been reported[5] and it is interesting to measure its spectrum in polarized light. If only the nitrogen of the *p*-toluidine is considered then the complex belongs to the point group C_{2v}[6] and the relation between the molecular axes and the crystal axes is shown in Fig. 1. The crystals have the (001) face well developed and the light was incident on this face in the spectral measurements.

Figure 2 shows the crystal spectrum or cobalt di-*p*-toluidine dichloride in the two regions of most intense

[4] D. S. McClure, J. Phys. Chem. Solids 3, 311 (1957).
[5] Bokii, Malinovskii, and Ablov, Kristallografiya 1, 49 (1956).
[6] Eyring, Walter, and Kimball, *Quantum Chemistry* (John Wiley & Sons, Inc., New York, 1944) p. 384.

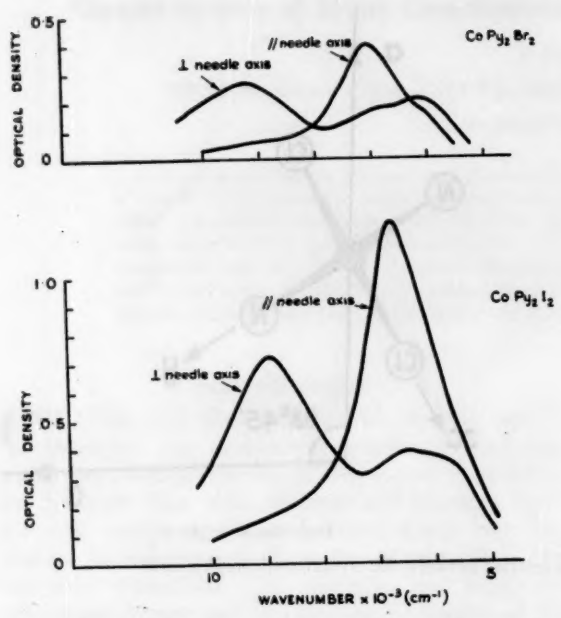

FIG. 3. Crystal spectra, in polarized light, of cobalt dipyridine dibromide and cobalt dipyridine diiodide.

absorption. The two absorption bands have to be recorded on different crystals because the visible band is much stronger than the one in the near infrared.

The visible band has three components, but these do not appear at the same frequency in each polarization. This suggests that intercomplex interaction has split the energy levels and the absorption band in the crystal is in fact an exciton band. This is not unreasonable as the absorption band is strong for a $d-d$ transition and intercomplex coupling (resonance interaction) is therefore likely to be significant. In addition the transition is formally allowed.

The near infrared band has three components, but only one is completely polarized, perpendicular to the b crystal axis. This must represent the transition $^4A_2 \rightarrow {}^4B_1$ or $^4A_2 \rightarrow {}^4B_2$. As the other two bands have roughly equal absorption in the two crystal directions it must be assumed that the two states are mixed, either in the crystal or the complex. This probably means that the symmetry of the ligand field is higher than C_{2v}, but below that of T_d. It should be noted that none of the components of the visible band is completely polarized in the crystal, so that even though the upper state of the visible band belongs to the same representation of the point group as the near infrared band, the effect of the symmetry of the ligand field is different in each case. A possible reason for this will be given in the Discussion.

CRYSTAL SPECTRA OF $CoPy_2X_2$ TYPE TETRAHEDRAL COMPLEXES

Cobalt forms an interesting series of compounds of the type $CoPy_2X_2$, where X = Cl, Br, I, NCS, or NCO. These complexes can exist in two forms, one tetrahedral and the other a bridged octahedral form, one of which is metastable. The stable tetrahedral modifications of $CoPy_2Br_2$ and $CoPy_2I_2$ are relevant are relevant to the present study. Because of their similarity to cobalt di-*p*-toluidine dichloride, it is expected that their absorption spectra will be similar to that in Fig. 2.

Although the crystals are monoclinic the developed face and cell dimensions are different from those of cobalt di-*p*-toluidine dichloride.[7] The b crystal axis (symmetry axis) is now perpendicular to the well-developed face and the extinction directions make a small angle with the needle axis. In addition the crystals are poorly developed and thin ones suitable for penetrating the visible band are difficult to grow. Measurements with one $CoPy_2Br_2$ crystal showed no crystal splitting of the visible band, and as the developed face lies perpendicular to the symmetry axis, no splitting of exciton bands is expected in this face.

The replacement of *p*-toluidine by pyridine will alter the strength of the ligand field and Fig. 3 shows that the near infrared band is split in $CoPy_2Br_2$ and $CoPy_2I_2$ more than in cobalt di-*p*-toluidine dichloride. However, this need not necessarily be the effect of the ligand field, but could quite simply be due to intercomplex interaction. It is also significant that the degree of polarization of the bands is higher and this could reflect a further approach of the field to C_{2v} symmetry.

ABSORPTION SPECTRA OF $CoPy_2X_2$ COMPLEXES IN SOLUTION

The visible band of $CoPy_2Cl_2$ has been studied by Katzin and Gebert[8] in isopropanol, acetone, chloroform, and benzene. The spectrum shows four overlapping maxima in the region 15 000–17 000 cm^{-1} with minor variation of intensity among the maxima from solvent to solvent. This was confirmed in the present work.

If the absorption spectra of $CoPy_2Br_2$ and $CoPy_2I_2$, dissolved in chloroform, are compared with the crystal absorption, it is found that the absorption bands are at the same wavelength, at least in the near infrared region. However, solutions of the compounds in bromoform do not obey Beer's law, and Fig. 4 shows the absorption spectrum of $CoPy_2Br_2$ at two concentrations. Intermediate concentrations give spectra which are intermediate between the two in Fig. 4. Similar behavior is found for $CoPy_2Cl_2$, $CoPy_2I_2$, and $CoPy_2(NCS)_2$. Because the spectrum at the higher concentration is identical (in the near infrared) with that of the crystal, it is assumed to be the spectrum of an associated form.

The complexes are polar and the strong interaction between molecules of the similar complex cobalt di-*p*-toluidine dichloride is shown by its structure, where the short b axis spacing of 4.59A is the direction along which

[7] This information was kindly obtained from an x-ray examination of the crystals by Dr. A. McL. Mathieson.

[8] L. V. Katzin and E. Gebert, J. Am. Chem. Soc. **72**, 5464 (1950).

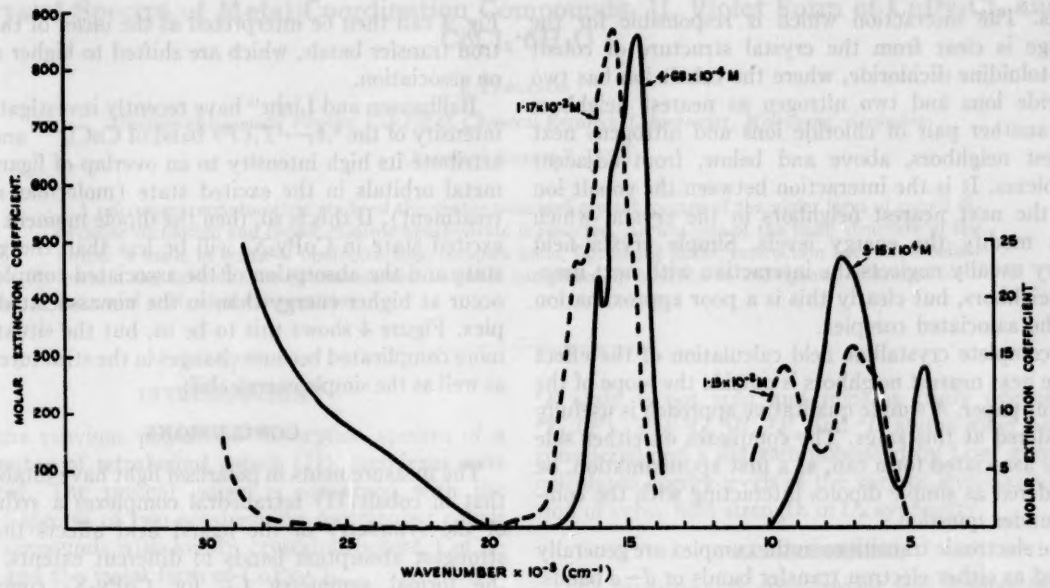

FIG. 4. Absorption spectrum of cobalt dipyridine dichloride in bromoform at two concentrations, $4.68\times10^{-4}M$ and $1.17\times10^{-2}M$.

maximum interaction occurs (see Fig. 1). Each complex sits on top of another with the dipole moments pointing along the line joining the cobalt ions. The spectrum of the solution at the lower concentration is taken to be that of the unassociated complex (interacting with bromoform) and its spectrum is more closely related to that of $CoCl_4^{--}$. The visible band is almost identical[9] with that of $CoCl_4^{--}$, while the infrared band is split, but it is much closer to the position of the $CoCl_4^{--}$ band (between 4500 and 7000 cm^{-1}) than the associated form.

In the near ultraviolet the absorption is much higher in the unassociated form of the complex. A strong interaction with the bromoform must occur and the energy levels of the latter will be lowered as a result. The increased absorption could be attributed to the shift of the bromoform absorption to longer wavelengths, but a large shift of the electron transfer bands must also be expected upon association as will be discussed.

DISCUSSION

Neglecting for the moment the effects of association on the energy levels of the complexes, the spectra show that formal reduction of the symmetry of the ligand field modifies the structure and energy of the transition $^4A_2\rightarrow{}^4T_1(F)$ more than that of $^4A_2\rightarrow{}^4T_1(P)$. Brode[10] has analyzed the visible band corresponding to the transition $^4A_2\rightarrow{}^4T_1(P)$ in $CoCl_4^{--}$ into six overlapping bands and the unassociated forms of $CoPy_2X_2$ show the same type of band structure, and they appear at nearly the same position as in the spectrum of $CoCl_4^{--}$. On the other hand, the near infrared band $^4A_2\rightarrow{}^4T_1(F)$ is split and shifted to higher energy in the $CoPy_2X_2$ complexes. Because both the upper states belong to the same representation of the point group symmetry of the complex, and mixing of the two must occur, it is rather surprising that perturbation of the tetrahedral ligand field affects the two states differently. However, it is known from paramagnetic evidence[11] that spin-orbit interaction can be comparable to the noncubic components of the ligand field. When it is noted that in the free ion there is a ^2G state close to the ^4P state, and components of the former also lie close to the latter in the tetrahedral field, then it seems likely that mixing of the ^2G and ^4P states through spin-orbit interaction leads to the peculiar structure of the $^4A_2\rightarrow{}^4T_1(P)$ transition and its insensitivity to changes of the formal symmetry of the ligand field. Because there are no doublet levels close to the $^4T_1(F)$ state, it is perturbed only by the noncubic components of the ligand field and is split and shifted to higher energy. Jorgensen[12] has arrived at a similar explanation of the structure of the $^4A_2\rightarrow{}^4T_1(P)$ band without considering the near infrared band.

Measurement of the spectra in bromoform solution has strikingly shown how intercomplex interaction modifies the spectra of the compounds of the type $CoPy_2X_2$. The infrared band is still split, but there is a large shift of the components to higher energy (see Fig. 4). This complicates the interpretation of the polarization of the bands in the crystal as it is not clear to what extent the association has modified the energy

[9] C. J. Ballhausen and C. K. Jorgensen, Acta Chem. Scand. **9**, 397 (1955).

[10] W. R. Brode, Proc. Roy. Soc. (London) **A118**, 286 (1928).

[11] S. Koide, Phil. Mag. **4**, 243 (1959); A. Abragam and M. H. L. Pryce, Proc. Roy. Soc. (London) **A206**, 173 (1951); Kambe, Kaide, and Usei, Progr. Theoret. Phys. **7**, 15 (1952).

[12] C. K. Jorgensen, Mol. Phys. **1**, 11 (1958).

levels. The interaction which is responsible for the change is clear from the crystal structure of cobalt di-*p*-toluidine dichloride, where the cobalt ion has two chloride ions and two nitrogen as nearest neighbors and another pair of chloride ions and nitrogens next nearest neighbors, above and below, from adjacent complexes. It is the interaction between the cobalt ion and the next nearest neighbors in the crystal which must modify the energy levels. Simple crystal-field theory usually neglects the interaction with next nearest neighbors, but clearly this is a poor approximation for the associated complex.

A complete crystalline field calculation of the effect of the next nearest neighbors is outside the scope of the present paper. A simple qualitative approach is usefully considered at this stage. The complexes on either side in the associated form can, as a first approximation, be considered as simple dipoles interacting with the complex under question.

The electronic transitions in the complex are generally classed as either electron transfer bands or $d-d$ bands. The dipole moment change between ground and excited state will be large for the first type and zero, or nearly zero, for the second type. Considering the electron transfer bands first, it is easy to see that as the lowest of these will involve excitation of an electron from an orbital, essentially localized on the chloride ion to one mainly $3d$ in character, the dipole moment will be lower in the excited state than the ground state. The interaction energy between the excited state of the complex and the associated complexes will be smaller than for the complex in its ground state, and the absorption transition will appear at a higher energy than in the nonassociated complex. The increased absorption above 20 000 cm^{-1}, of the nonassociated complex in Fig. 4 can then be interpreted as the onset of the electron transfer bands, which are shifted to higher energy on association.

Ballhausen and Liehr[13] have recently investigated the intensity of the $^4A_2 \rightarrow {}^4T_1(P)$ band of $CoCl_4^{--}$ and they attribute its high intensity to an overlap of ligand and metal orbitals in the excited state (molecular orbital treatment). If this is so, then the dipole moment of the excited state in $CoPy_2X_2$ will be less than the ground state and the absorption of the associated complex will occur at higher energy than in the nonassociated complex. Figure 4 shows this to be so, but the situation is more complicated because changes in the structure occur as well as the simple energy shift.

CONCLUSIONS

The measurements in polarized light have established that in cobalt(II) tetrahedral complexes a reduction of the symmetry of the ligand field affects the two strongest absorption bands to different extents. Also, the formal symmetry C_{2v} for $CoPy_2X_2$ complexes results only in a perturbation of the tetrahedral symmetry. More important is the result that association of the complexes modifies the energy levels markedly. The effects of intercomplex interaction are therefore considerable and care must be taken in the analysis of the spectra of other crystalline complexes to ensure that they are not neglected.

ACKNOWLEDGMENT

The author wishes to express his thanks to Dr. A. L. G. Rees and Dr. N. S. Ham for helpful discussions.

[13] C. J. Ballhausen and A. D. Liehr, J. Mol. Spectroscopy **2**, 342 (1958).

THE JOURNAL OF CHEMICAL PHYSICS VOLUME 32, NUMBER 2 FEBRUARY, 1960

Crystal Spectra of Metal Coordination Compounds. II. Violet Form of $CoPy_2Cl_2$ and $CoCl_2 \cdot 6H_2O$

J. FERGUSON

Division of Chemical Physics, C.S.I.R.O. Chemical Research Laboratories, Melbourne, Australia

(Received August 7, 1959)

A microspectrophotometric study of the visible polarized crystal spectra of the violet form of cobalt dipyridine dichloride and cobalt chloride hexahydrate is reported. An analysis of the band structure of the former is made in terms of noninteracting, complex units, but in the latter, interaction between a cobalt ion and the chloride ions on next nearest neighbor complexes, in addition to the ligands, is needed for a successful analysis of the spectrum.

INTRODUCTION

In the previous paper[1] the absorption spectra of a number of tetrahedral cobalt (II) complexes were reported. The present paper is concerned with the crystal spectra of two octahedrally coordinated cobalt (II) compounds with known crystal structure, $CoCl_2 \cdot 6H_2O$ and the violet form of $CoPy_2Cl_2$.

The crystal absorption spectrum of cobalt chloride hexahydrate has previously been reported by Gielessen[2] and Pappalardo.[3] Pappalardo's work was done with unpolarized light and as will be shown the absorption spectrum is so strongly anisotropic that measurements with unpolarized light confuse the analysis of the bands. Gielessen had noted the marked anisotropy of the absorption, but he was not interested in an analysis of the band structure. The present analysis was made possible by the recent crystal structure determination in which it was shown that the basic octahedral unit is $CoCl_2(H_2O)_4$ and not $Co(H_2O)_6^{++}$.[4]

Octahedral Co^{++} complexes are red in color and the spectrum of the ion in water is well known. The spectrum of single crystals of $CoSO_4 \cdot 7H_2O$ has been studied by Holmes and McClure,[5] and it is nearly identical with that of Co^{++} in water. The spectrum of $Co(NO_3)_2 \cdot 7H_2O$ was determined in the present work and it is also the same as Co^{++} in water. The absorption band is broad and asymmetrical, centered at about 500 mμ. It is likely that the asymmetry is linked to a distortion of the water octahedron as a result of the Jahn-Teller effect.[6] This asymmetry is developed to a marked extent in $CoCl_2 \cdot 6H_2O$ and can best be explained by considering the interaction between a Co^{++} ion and the next nearest neighbors as well as the six ligands.

The ground state of the cobalt (II) ion is split under the effect of an octahedral field into three levels, $^4T_{1g}(F)$, $^4T_{2g}(F)$, and $^4A_{2g}(F)$, while the excited ^4P state is not split and remains triply degenerate, $^4T_{1g}(P)$. The ^2G, ^2H, ^2P, and ^2D states must also be considered and a diagram published by Low[7] gives the calculated energy levels of the various levels as a function of cubic field strength in O_h symmetry.

EXPERIMENTAL

The experimental arrangement was similar to that described in I except that a special stage[8] was used to record the spectra at low temperature. The preparation of the cobalt dipyridine dichloride is described in the literature[9] and the cobalt chloride hexahydrate was analytical grade recrystallized from water.

CRYSTAL STRUCTURE OF $CoCl_2 \cdot 6H_2O$

The crystal structure has recently been reported by Mizuno, Ukei, and Sugawara.[4] It is monoclinic with the unit cell dimensions $a=10.34$, $b=7.06$, $c=6.67$ A, and $\beta=122°\ 19'$. Figure 1 shows projections of the $CoCl_2(H_2O)_4$ units (a) on the (010) face and (b) on the (001) face of the crystal. The remaining two molecules of water, which are in the lattice, are not included in the projections. The cleavage plane is parallel to the (001) and this is the well-developed face when the crystals are grown from solution. The projection in Fig. 1(b) is then the relevant one for the spectral measurements as the light was incident on the (001) face. The b crystal axis is parallel to the needle axis and the Co—Cl bonds lie in the ac plane at right angles to the b axis. The crystals are strongly dichroic and appear orange with the electric vector perpendicular to the b axis and mauve with the vector parallel to the b axis. These colors depend, of course, on the crystal thickness. The complex unit belongs[10] to the point group D_{4h} and the arrangement of the four water molecules is square planar.

CRYSTAL STRUCTURE OF $CoPy_2Cl_2$

The structure of the stable violet form of cobalt dipyridine dichloride has been determined by Dunitz.[11]

[1] J. Ferguson, J. Chem. Phys. **32**, 528 (1960); hereafter called I.
[2] J. Gielessen, Ann. Physik **22**, 537 (1935).
[3] R. Pappalardo, Phil. Mag. **4**, 219 (1959).
[4] Mizuno, Ukei, and Sugawara, J. Phys. Soc. Japan **14**, 383 (1959).
[5] O. G. Holmes and D. S. McClure, J. Chem. Phys. **26**, 1686 (1957).
[6] H. A. Jahn and E. Teller, Proc. Roy. Soc. (London) **A161**, 220 (1937); H. A. Jahn, Proc. Roy. Soc. (London) **A164**, 117 (1938).
[7] W. Low, Phys. Rev. **109**, 256 (1958).
[8] Spectrochim. Acta (to be published).
[9] A. Hantzsch, Z. Anorg. u. allgem. Chem. **159**, 18 (1927).
[10] Eyring, Walter, and Kimball, *Quantum Chemistry* (John Wiley & Sons, Inc., New York, 1944), p. 387.
[11] J. D. Dunitz, Acta Cryst. **10**, 307 (1957).

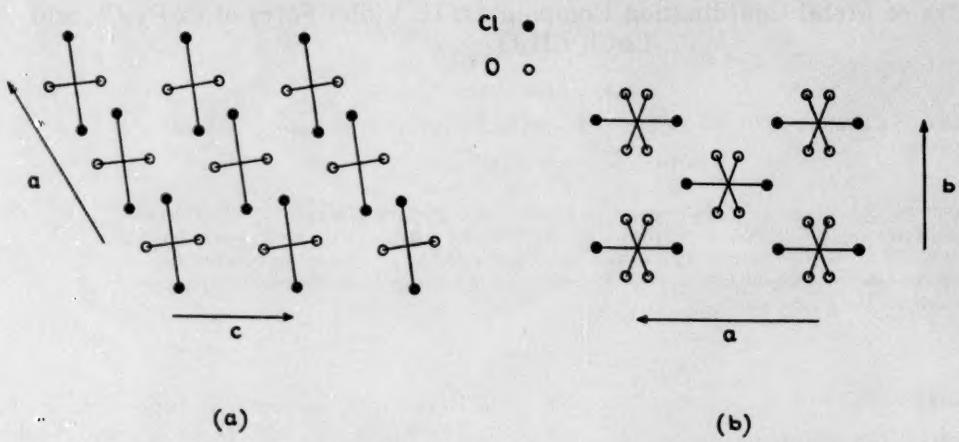

FIG. 1. Crystal structure of cobalt chloride hexahydrate, projections of $CoCl_2(H_2O)_4$ units (a) on the (010) face and (b) on the (001) face.

It is monoclinic with the unit cell dimensions $a=34.42$, $b=17.38$, $c=3.66$ A, and $\gamma=90°$. The structure consists of polymeric chains, running parallel to the c axis (needle axis), each chlorine being shared by two cobalt ions. Figure 2 shows the interatomic distances and angles. The arrangement of the four chloride ions surrounding each cobalt ion is rectangular planar so that the octahedral unit $CoPy_2Cl_4$ has the point symmetry D_{2h}, not D_{4h}. The y complex axis has been taken bisecting the smaller Cl—Co—Cl angle (85.5°) and the z axis coincident with the Co—N direction. The crystals are poorly developed needles showing dichroism.

CRYSTAL SPECTRUM OF $CoPy_2Cl_2$

The absorption spectrum of a single crystal at room temperature is shown in Fig. 3 for light incident on the (100) face. The spectrum appears to be made up of four bands, three of which overlap. Photographs of the spectrum at low temperature, however, show the appearance of a narrow band at about 18 700 cm^{-1}.

CRYSTAL SPECTRUM OF $CoCl_2 \cdot 6H_2O$

The crystal spectrum shows a considerable amount of structure even at room temperature. As well as two broad bands there are other much narrower ones which are further sharpened on cooling the crystal. Figure 4 shows the spectrum at room temperature and low temperature in polarized light. The striking feature about the absorption spectrum is the marked anisotropy of some of the bands, particularly the broad band at about 22 000 cm^{-1}. If the spectrum is taken in unpolarized light it is difficult to observe this band as it has an apparent optical density of about 0.3 (50% transmission) and is broad.

The spectra in Figure 4 were recorded on the Beckman DK2 spectrophotometer and the resolution is not sufficient to resolve the structure of the weak narrow bands. These were obtained from photographs taken with the Hilger medium spectrograph and their positions are given in Table I. They are indicated by arrows in Fig. 4. The positions of these bands agree fairly well with those reported by Gielessen,[2] but include one or two more than those given by Pappalardo.[3]

There is an interesting intensity change and shift of the group of narrow bands on cooling the crystal. Those from 19 800 cm^{-1} to 20 400 cm^{-1} decrease in intensity and the remaining ones increase in intensity. It is likely that the former represent "hot" bands, transitions arising from the vibrationally excited ground state.

DISCUSSION

Band Widths

Both sharp and broad bands often appear in the spectra of transition metal complex ions. The reason for this can easily be seen by considering the dependence of the ground and excited states on the crystal field strength.[12] When the upper state of an electronic transition has the same, or nearly the same, orbital electron configuration as the ground state, then the bands appear sharp.

Pappalardo[3] and Low have calculated the energy levels of both doublet and quartet states of Co^{++} in an octahedral field. These calculations show that three electronic states should be considered for the spectral region covered by the present work. Two of these are quartet states $^4T_{1g}(P)$ and $^4A_{2g}(F)$ and the other is a doublet state $^2T_{1g}(P)$. The appearance of the narrow bands in the spectrum of $CoCl_2 \cdot 6H_2O$ can be linked to the transition from the ground state to the doublet state, because this has essentially the same orbital configuration as the ground state. Spectra of $CoPy_2Cl_2$ at low temperatures show the appearance of a narrow band, but overlap by the more intense broad bands in the same region obscures the detection of others.

Transitions from the ground state to the two quartet states $^4T_{1g}(P)$ and $^4A_{2g}(F)$ should result in broad bands, with the transition to the latter being broader and weaker than the other. In order to identify the bands it is necessary to consider the orientations of the complexes in the crystals.

[12] L. E. Orgel, J. Chem. Phys. **23**, 1824 (1955).

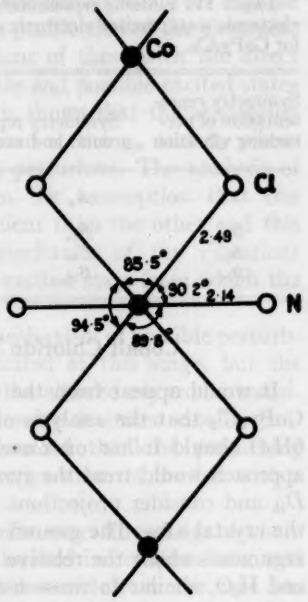

FIG. 2. Crystal structure of cobalt dipyridine dichloride, interatomic distances and angles.

Cobalt Dipyridine Dichloride

$CoPy_2Cl_2$ belongs to the point group D_{2h} because there is a slight rhombic distortion of the tetragonal symmetry. This means that the triple orbital degeneracy of the $^4T_{1g}$ state in octahedral symmetry is removed. The correlations between the irreducible representations of O_h, D_{4h}, D_{2h}, and C_{2h} are given in Table II. It is seen that the components of the ground state are $^4B_{1g}$, $^4B_{2g}$ and $^4B_{3g}$ in D_{2h}. Neglecting the rhombic distortion it is easy to see that from the positions of Cl^- and Py in the spectrochemical series[13] the d_{xz} and d_{yz} orbitals should be less stable than the d_{xy} orbital. This means that the ground state should be doubly degenerate, ^4E_g, with the $^4A_{2g}$ state possibly some few hundred cm^{-1} above it. It seems likely that the rhombic distortion in $CoPy_2Cl_2$ has its origin in the Jahn-Teller effect so that the ^4E_g level is split into $^4B_{2g}$ and $^4B_{3g}$.

A decision must be made as to which band represents the transition to the upper state ^4A_g ($^4A_{2g}$ in O_h). It is assumed that the band at about 16 000 cm^{-1}, polarized perpendicular to the needle axis, represents this transition. This is so because the spectra of $CoPy_4Cl_2$ and $CoPy_4(NCS)_2$[14] show no pronounced splitting of the absorption band, and the components are grouped close together so that a simple tetragonal distortion is unlikely to produce a splitting as large as 3000 cm^{-1} in $CoPy_2Cl_2$. Also, the $^4A_{2g}$ state should lie below the $^4T_{1g}(P)$ state for Dq less than about 1000 cm^{-1} and the ligand field in $CoPy_2Cl_2$ seems certainly less than this; in fact it represents the lowest field of any octahedral complex of cobalt (II) studied in the present work. If we assume, therefore, that the band at 16 200 cm^{-1} is the transition to the upper ^4A_g state, it remains to identify the other bands. For this it is necessary first to consider the projections of the transition moments

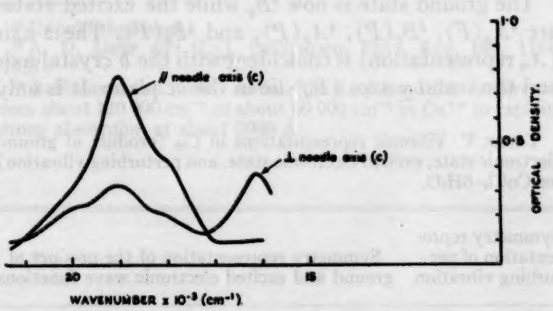

FIG. 3. Crystal spectrum of cobalt dipyridine dichloride in polarized light.

[13] R. Tsuchida, Bull. Chem. Soc. Japan 13, 395 (1938).

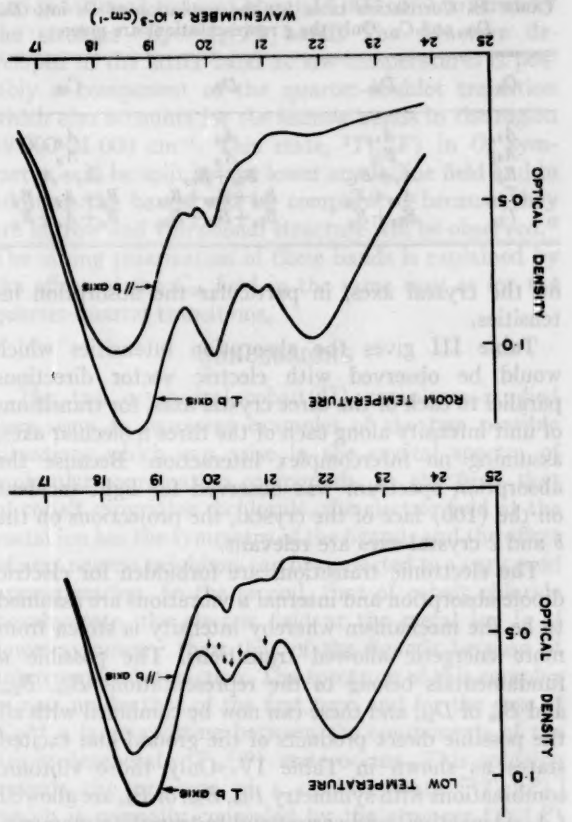

FIG. 4. Crystal spectrum of cobalt chloride hexahydrate at room temperature and low temperature, in polarized light. The arrows show the position of the bands recorded in Table I.

TABLE I. Positions of the narrow bands in the spectrum of $CoCl_2 \cdot 6H_2O$ at low temperature (± 20 cm^{-1}).

19 850 cm^{-1}	20 230 cm^{-1} (*a* pol.)
20 030	20 250 (*b* pol.)
20 120 (*a* pol.)	20 410
20 130 (*b* pol.)	20 580
	20 850

TABLE II. Correlation table for the resolution of O_h into D_{4h}, D_{2h}, and C_{2h}. Only the g representations are given.

O_h	D_{4h}	D_{2h}	C_{2h}
A_{1g}	A_{1g}	A_g	A_g
A_{2g}	B_{1g}	A_g	A_g
E_g	A_g+B_{1g}	$B_{2g}+B_{3g}$	A_g+A_g
T_{1g}	$A_{2g}+E_g$	$B_{1g}+B_{2g}+B_{3g}$	$B_g+A_g+B_g$
T_{2g}	$B_{2g}+E_g$	$B_{1g}+B_{2g}+B_{3g}$	$B_g+A_g+B_g$

on the crystal axes, in particular the absorption intensities.

Table III gives the absorption intensities which would be observed with electric vector directions parallel to each of the three crystal axes, for transitions of unit intensity along each of the three molecular axes, assuming no intercomplex interaction. Because the absorption spectrum was observed for light incident on the (100) face of the crystal, the projections on the b and c crystal axes are relevant.

The electronic transitions are forbidden for electric dipole absorption and internal u vibrations are assumed to be the mechanism whereby intensity is stolen from more energetic allowed transitions. The possible u fundamentals belong to the representations B_{1u}, B_{2u}, and B_{3u} of D_{2h}, and these can now be combined with all the possible direct products of the ground and excited states as shown in Table IV. Only those vibronic combinations with symmetry B_{1u}, B_{2u}, or B_{3u} are allowed (A_{1u} is inactive) and correspond to transition moments along the z, x, and y molecular axes, respectively.

The assignment of the 16 200 cm^{-1} band to an upper ^4A_g state which is polarized perpendicular to the c crystal axis (parallel to b) means that the ground state must be $^4B_{3g}$, since $B_{3g}\times A_g\times(\beta_{1u}, \beta_{2u}, \beta_{3u}) = B_{2u}, B_{1u}, A_u$; zero projection on the c axis, Table III. Either a B_{3g} or B_{2g} ground state is consistent with the interpretation of the rhombic distortion as arising from the Jahn-Teller effect.

The assignment of the other three bands follow from Fig. 3 and Tables III and IV. The highest energy component has nearly equal absorption intensity along the b and c crystal axes and must be assigned to an upper $^4B_{3g}$ state because $B_{3g}\times B_{3g}\equiv A_g$, and from Table I this should result in three active components B_{1u}, B_{2u}, and B_{3u}. The other two bands have the same polarization ratio, roughly 2/1 (c/b) and this is expected for both B_{1g} and B_{2g} upper states.

TABLE III. Squares of the projections (absorption intensities) of unit transitions moments on the crystal axes in $CoPy_2Cl_2$.

Complex axis and representation in D_{2h}		Crystal axis a	b	c
x	(B_{2u})	0.57	0.43	0
y	(B_{3u})	0	0	1
z	(B_{1u})	0.43	0.57	0

TABLE IV. Vibronic representations in D_{2h} (product of ground electronic state, excited electronic state and perturbing vibration) for $CoPy_2Cl_2$.

Symmetry representation of perturbing vibration	Symmetry representation of the product of ground and excited electronic wave functions			
	A_g	B_{1g}	B_{2g}	B_{3g}
β_{1u}	B_{1u}	A_u	B_{3u}	B_{2u}
β_{2u}	B_{2u}	B_{3u}	A_u	B_{1u}
β_{3u}	B_{3u}	B_{2u}	B_{1u}	A_u

Cobalt Chloride Hexahydrate

It would appear from the success of the analysis of $CoPy_2Cl_2$ that the analysis of the spectrum of $CoCl_2\cdot 6H_2O$ should follow on closely similar lines. Such an approach would treat the symmetry of the complex as D_{4h} and consider projections of the molecular axes on the crystal axes. The ground state should be $^4A_{2g}$ from arguments about the relative field strengths of the Cl^- and H_2O, similar to those used for $CoPy_2Cl_2$, and the excited states which fall in the spectral region examined will be $^4A_{2g}(F)$, $^4E_g(P)$ and $^4B_{1g}(P)$. The fundamental vibrations which satisfy the symmetry requirements as perturbers are α_{2u}, β_{2u}, and ϵ_u. However, combinations of these vibrations with the electronic states cannot explain the polarization of the bands in the spectrum. The $\epsilon_u(x, y)$ transition moment projects mainly on the b crystal axis and none of the strong bands is b polarized. In addition the strongly polarized band at 22 000 cm^{-1} is difficult to understand with this scheme. Because of the failure of this model, an attempt was made to include the effect of interactions other than from the six ligands in the octahedron. The next nearest neighbors of the Co^{++} ion are the four Cl^- ions which lie toward the corners of the unit cell, each 4.5A from the Co^{++} ion. When these together with the six ligands are considered, it is easily seen, Fig. 1, that the field around the Co^{++} is C_{2h}. The correlations between D_{4h} and C_{2h} are given in Table I where the twofold axis of C_{2h} is taken to be identical with the twofold axis which bisects the H_2O—Co—H_2O band angle in D_{4h}.

The ground state is now ^4B_g while the excited states are $^4A_g(F)$, $^4B_g(P)$, $^4A_g(P)$, and $^4B_g(P)$. The z axis (A_u representation) is coincident with the b crystal axis and the x and y axes (B_u) lie in the ac plane. It is only

TABLE V. Vibronic representations in C_{2h} (product of ground electronic state, excited electronic state, and perturbing vibration) for $CoCl_2\cdot 6H_2O$.

Symmetry representation of perturbing vibration	Symmetry representation of the product of ground and excited electronic wave functions	
	A_g	B_g
α_u	A_u	B_u
β_u	B_u	A_u

the α_u and β_u vibration fundamentals which are capable of removing the symmetry prohibition of the electronic transition. The combinations of these with the direct products of the ground state and possible excited states are given in Table V. This shows that the absorption bands should be unpolarized if the α_u and β_u vibrations are equally efficient perturbers. The analysis of the spectrum depends on the assumption that one species is much more efficient than the other and this can be related to the mechanics of the vibrations and/or the nature of the excited state from which the intensity is stolen.

Speculation about the mechanism of possible perturbing vibrations is unwarranted at this stage, but the question of the nature of the allowed electronic transitions from which the intensity is stolen can be considered. Usually it is assumed that the perturbing vibration mixes the d^n configuration of the ion with a $d^{n-1}p$ configuration.[15]

There does not appear to be exact knowledge of where the $d-p$ transitions are located in complex ions, and unless they are strongly lowered from the free ion value they must surely lie at too high an energy to be considered for intensity stealing.[16] The possibility then enters that electron transfer states involving essentially ligand to metal transitions are the states from which the intensity for the $d-d$ transitions is stolen. In $CoCl_2(H_2O)_4$ the Co—Cl electron transfer transition should be the most important state from which the intensity is stolen and the spectrum in Fig. 4 can be analyzed on this assumption. The important vibrations will be ones which are essentially Co—Cl stretching modes, α_{2u} in D_{4h} and β_u in C_{2h}. With the β_u vibration as effecting the perturbation then the transitions have the following polarizations: $^4B_g \rightarrow {}^4A_g(F)$, b polarized; $^4B_g \rightarrow {}^4B_g(P)$, a polarized; $^4B_g \rightarrow {}^4A_g(P)$, b polarized; $^4B_g \rightarrow {}^4B_g(P)$, a polarized.

The strongly polarized band at 22 000 cm^{-1} is now interpreted as $^4B_g \rightarrow {}^4B_g(P)$ being a split component of the octahedral band and the one at 18 500 cm^{-1} represents the accidently degenerate pair $^4B_g \rightarrow {}^4A_g(P)$ and $^4B_g \rightarrow {}^4B_g(P)$, the other components of the octahedral $^4T_{1g} \rightarrow {}^4T_{1g}$ transition. The weaker $^4B_g \rightarrow {}^4A_g(F)$ transition is assumed to lie at about 18 000 cm^{-1} covered by the stronger $^4B_g \rightarrow {}^4A_g(P)$ band. The structure developed in the latter band at low temperatures is possibly a component of the quartet-doublet transition which also accounts for the narrow bands in the region 19 000–21 000 cm^{-1}. This state, $^2T_{1g}(P)$ in O_h symmetry, will be split by the lower crystalline field and in addition the bands will be complicated because they are narrow and vibrational structure will be observed.[17] The strong polarization of these bands is explained by the effect of the C_{2h} field in the same way as for the quartet-quartet transitions.

CONCLUSIONS

The two octahedral cobalt(II) complexes studied here seem to represent examples of the two possible situations which can arise in the crystal spectra of molecular coordination compounds. In the first, that of cobalt dipyridine dichloride, the electric field at the metal ion has the symmetry of the ligands and the effect of next nearest neighbors can be neglected to a very good approximation. In the second, that of cobalt chloride hexahydrate, the electric field at the metal ion is of lower symmetry than that of the ligands because of intercomplex interaction. The spectrum of this complex is now unlike that of the first type and for the case of Co^{++} a large splitting between the components of the triply degenerate $^4T_{1g}(P)$ state occurs. This splitting reveals the presence of a doublet state $[^2T_{1g}(P)]$ which is normally concealed by the stronger $^4T_{1g}(P)$ state in the other octahedral complexes.

In I intercomplex interactions were found to modify the absorption spectra of some polar tetrahedral complexes. The crystal spectrum of $CoCl_2 \cdot 6H_2O$ has shown that intercomplex interaction can also be significant in octahedral complexes even though there is a centre of symmetry. This, of course, means that considerable care must be taken in the interpretation of crystal spectra when the crystal structure is not known.

The analysis of the spectrum of cobalt chloride hexahydrate suggests that the mechanism of the $d-d$ transitions in metal complexes can involve electron transfer states as the source of the intensity.

ACKNOWLEDGMENT

The author wishes to thank Dr. A. L. G. Rees and Dr. N. S. Ham for helpful discussions.

[14] Unpublished work.

[15] A. D. Liehr and C. J. Ballhausen, Phys. Rev. **106**, 1161 (1957).

[16] Ballhausen and Liehr[15] assume the $d-p$ transition is lowered from about 120 000 cm^{-1} to about 60 000 cm^{-1} in Cu^{++} to explain strong absorption at about 2000 A.

[17] For example, R. Pappalardo, Phil. Mag. **2**, 1397 (1957).

Kinetic Theory of Moderately Dense Rigid Sphere Fluids. III. The Formulation and Solution of the Transport Equation for Binary Mixtures*

ROBERT A. HARRIS AND STUART A. RICE†

Department of Chemistry and Institute for the Study of Metals, University of Chicago, Chicago 37, Illinois

(Received September 29, 1959)

The theory of the moderately dense rigid sphere fluid is extended to mixtures. The modified Boltzmann equation is derived from the Liouville equation using the technique of time smoothing. The solution of the Boltzmann equation is given in terms of bracket integrals and the entropy production formulated in terms of the perturbation to the distribution function. The bracket integrals are not explicitly evaluated in this paper but a first order result valid for a mixture of spheres of equal diameters gives for the leading term of the diffusion coefficient $D=D^0/g_0^{(2)}(\sigma)$ with D^0 the dilute gas diffusion coefficient, and $g_0^{(2)}(\sigma)$ the pair correlation function evaluated at contact. This leading term is in agreement with the corresponding leading terms for the thermal conductivity and shear viscosity of a one component hard sphere fluid, which also differ from the dilute gas coefficients by the factor $[g_0^{(2)}(\sigma)]^{-1}$. The results quoted in this abstract are the leading terms and do not include all contributions of order v^{-1}.

I. INTRODUCTION

THE kinetic theory of the one component dense rigid sphere fluid was first studied by Enskog.[1] By the use of geometrical arguments and the intuitive notions that there is instantaneous transfer of momentum on collision and that the collision frequency is altered by the shielding of third body molecules, Enskog was able to derive a modified Boltzmann equation for the rate of change of the distribution function in singlet space. It should be emphasized that by the word dense we mean the v^{-1} correction to the dilute gas limit, or the first term in an expansion in terms of the number of molecules in a collision. In the binary collision approximation these two interpretations are interchangeable.

Recently, the theory of the dense rigid sphere fluid has been reanalyzed from several points of view. Collins and Raffel[2] have followed closely the original calculations of Enskog with the modification that the concentration of the centers of the nearest neighbors about a collision sphere is assumed to be given by the reciprocal of the molecular free volume instead of the molecular volume. The free volume, which is calculated from the Eyring-Hirschfelder[3] uniform potential theory of liquids, is an approximate way of handling molecular correlation in dense media. A different investigation by Longuet-Higgins and Pople[4] proceeds by physical arguments from the two assumptions that (a) the spatial pair distribution function depends only on the temperature and density and not on the temperature gradient or rate of strain, and (b) that the velocity distribution function of a single molecule is Maxwellian with a mean equal to the local hydrodynamic velocity and a spread determined by the local temperature. The method used assumes a form for the velocity autocorrelation function and avoids the systematic study of the behavior of the singlet space distribution function. Finally, Rice, Kirkwood, Ross, and Zwanzig[5,6] have established sufficient conditions for the derivation of a modified Boltzmann equation suitable for a dense fluid of rigid spheres. These conditions are found to be (a) that the interval of coarse graining in time (i.e., the basic interval for which the transport equation is valid) be allowed to tend to $+0$, an arbitrarily small but positive quantity, and (b) that the pair correlation function be taken as independent of momentum. The resultant equation differs slightly from that first derived by Enskog: the corresponding shear viscosities are identical but the thermal conductivity calculated by Rice *et al.* differs slightly from that computed by Enskog.[6] Although the differences in transport coefficients are small, the differences in the philosophy of the calculations are considerable.

Aside from the extension of the Longuet-Higgins, Pople treatment by Longuet-Higgins, Pople, and Valleau,[7] little attention has been given to the study of mixtures. Such an investigation is of intrinsically great interest, for the insight it can afford into the molecular nature of the Onsager reciprocal relations.[8] It is the purpose of this and the succeeding papers, to study the properties of the mixed dense rigid sphere fluid with just such an objective in mind.

II. MODIFIED BOLTZMANN EQUATION

The system under consideration, consisting of N_α molecules of species α and N_β molecules of species β,

* The preceding two papers of this series are cited in references 5 and 6.

† Alfred P. Sloan Fellow.

[1] D. Enskog, Kgl. Svenska Vetenskapsakad. Handl. **63**, N4 (1922).

[2] F. C. Collins and H. Raffel, J. Chem. Phys. **22**, 1728 (1954).

[3] Hirschfelder, Curtiss, and Bird, *Molecular Theory of Gases and Liquids* (John Wiley & Sons, Inc., New York, 1954).

[4] H. C. Longuet-Higgins and J. Pople, J. Chem. Phys. **25**, 884 (1956).

[5] Rice, Kirkwood, Ross, and Zwanzig, J. Chem. Phys. **31**, 575 (1959).

[6] S. A. Rice, J. Chem. Phys. **31**, 584 (1959).

[7] Longuet-Higgins, Pople, and Valleau in *Transport Processes in Statistical Mechanics*, edited by I. Prigogine (Interscience Publishers, Inc., New York, 1958), p. 73.

[8] See for example, S. DeGroot, *Thermodynamics of Irreversible Processes* (North Holland, Amsterdam, 1951).

will be described by the normalized specific distribution function $f^{(N)}(\mathbf{R}^{(N)}, \mathbf{p}^{(N)}, t)$ where $\mathbf{R}^{(N)}$ and $\mathbf{p}^{(N)}$ represent the N position and N momentum vectors $\mathbf{R}_{\alpha 1}, \cdots, \mathbf{R}_{\alpha N_\alpha}$, $\mathbf{R}_{\beta 1}, \cdots, \mathbf{R}_{\beta N_\beta}$, $\mathbf{p}_{\alpha 1}, \cdots, \mathbf{p}_{\beta N_\beta}$. The central problem considered in this paper is the determination of the singlet distribution function $f^{(1)}(\mathbf{R}_{\alpha 1}, \mathbf{p}_{\alpha 1}; t)$ where, in general, the n body reduced distribution function is defined by

$$f^{(n)}(\mathbf{R}_\alpha^{(m)}\mathbf{R}_\beta^{(s)}, \mathbf{p}_\alpha^{(m)}\mathbf{p}_\beta^{(s)}; t) = [(N_\alpha - m)!(N_\beta - s)!]^{-1} \int f^{(N)}(\mathbf{R}^{(N)}\mathbf{p}^{(N)}; t) d\mathbf{R}^{(N-n)} d\mathbf{p}^{(N-n)}. \quad (1)$$

The starting point of the calculation is, as usual, the Liouville equation, which has the form

$$(\partial f^{(N)}/\partial t) + \sum_{i=1}^{N} [(\mathbf{p}_k/m_k) \cdot \nabla_{R_k} f^{(N)} + \mathbf{F}_k \cdot \nabla_{p_k} f^{(N)}] = 0, \quad (2)$$

where $\mathbf{F}_k$ is the force acting on molecule k due to all other molecules in the system. The species labeling has been suppressed in Eq. (2) and the sums must be understood to be extended over both species and molecular number.

To obtain the differential equation satisfied by the singlet distribution function of species α, the Liouville equation is reduced by $(N-2)$-fold integration and the use of Green's theorem. If the intermolecular force is pairwise decomposable,

$$\mathbf{F}_k = \sum_{i,j;\alpha,\beta} \mathbf{F}_{ij}^{\alpha\beta}. \quad (3)$$

Then, the result of the reduction is

$$(\partial f^{(1)}/\partial t) + (\mathbf{p}_{\alpha 1}/m_{\alpha 1}) \cdot \nabla_{R\alpha 1} f^{(1)}(\mathbf{R}_{\alpha 1}\mathbf{p}_{\alpha 1}; t) = -(N_\alpha - 1)^{-1} \int \sum_{j,\beta} (N_\beta - \delta_{\alpha\beta}) \mathbf{F}_{1j}^{\alpha\beta} \cdot \nabla_p f^{(2)}(\mathbf{R}_{1\alpha}\mathbf{R}_{2\beta}\mathbf{p}_{1\alpha}\mathbf{p}_{2\beta}; t) d\mathbf{R}_{2\beta} d\mathbf{p}_{2\beta}, \quad (4)$$

where $\delta_{\alpha\beta}$ is the Kronecker delta. Equation (4) contains in a hidden form all the information contained in the Liouville equation and is as difficult to solve. The principal difficulty is, of course, the appearance of $f^{(2)}$ in the integrand of Eq. (4). To obtain $f^{(2)}$ one must know $f^{(3)}$, etc. The basic approximation we shall use to truncate the hierarchy is to limit consideration to binary collisions. The formal mechanism for handling such a procedure is provided by the introduction of time smoothing.[9]

We define a coarse grained distribution function by the relation,

$$\bar{f}^{(N)} = \tau^{-1} \int_0^\tau f^{(N)}(\mathbf{R}^{(N)}\mathbf{p}^{(N)}; t+s) ds, \quad (5)$$

where τ is the interval of coarse graining. It may be readily shown that integration over the time s and integration over the complete phase space $\mathbf{R}^{(N)}$, $\mathbf{p}^{(N)}$, are commutative operations.[9] The integrations over time and reduced phase space, $\mathbf{R}^{(n)}$, $\mathbf{p}^{(n)}$ are not commutative because $f^{(n)}$ satisfies an extended Boltzmann equation rather than a Liouville equation. Explicit coarse graining of Eq. (4) gives

$$\mathfrak{L}\bar{f}^{(1)}(1\alpha) = -[(N_\alpha - 1)\tau^{-1}] \int_0^\tau \int \sum_{j,\beta} (N_\beta - \delta_{\alpha\beta}) \mathbf{F}_{1j}^{\alpha\beta} \cdot \nabla_p f^{(2)}(\mathbf{R}_{1\alpha}\mathbf{R}_{2\beta}\mathbf{p}_{1\alpha}\mathbf{p}_{2\beta}; t+s) d\mathbf{R}_{2\beta} d\mathbf{p}_{2\beta} ds$$

$$\mathfrak{L} = (\partial/\partial t) + (\mathbf{p}_{1\alpha}/m_{1\alpha}) \cdot \nabla_{R_{1\alpha}}, \quad (6)$$

which relates the distribution functions at times t and $t+s$.

As in previous papers,[5,6] it is convenient to introduce a phase space distribution function by the definition

$$f^{(N)}(\mathbf{R}^{(N)}\mathbf{p}^{(N)}; t+s) = \int \cdots \int K^{(N)}(\mathbf{R}^{(N)}\mathbf{p}^{(N)}/\mathbf{R}^{(N)\prime}\mathbf{p}^{(N)\prime}; s) f^{(N)}(\mathbf{R}^{(N)\prime}\mathbf{p}^{(N)\prime}; t) d\mathbf{R}^{(N)\prime} d\mathbf{p}^{(N)\prime}, \quad (7)$$

where $K^{(N)}(s)$ may be shown to satisfy the Liouville equation,

$$(\partial K^{(N)}/\partial s) + \sum_{i=1}^{N} [(\mathbf{p}_k/m_k) \cdot \nabla_{R_k} K^{(N)} + \mathbf{F}_k \cdot \nabla_{p_k} K^{(N)}] = 0, \quad (8)$$

and $K^{(N)}(s)$ is seen to play the role of a transition probability. In addition to the integral relation (1), reduced distribution functions may in general be expressed in terms of the N-body distribution function by

$$f^{(N)}(\mathbf{R}^{(n)}\mathbf{p}^{(n)}, \mathbf{R}^{(N-n)}\mathbf{p}^{(N-n)}; t) = f^{(n)}(\mathbf{R}^{(n)}\mathbf{p}^{(n)}; t) f^{(n/N-n)}(\mathbf{R}^{(N-n)}\mathbf{p}^{(N-n)}; t), \quad (9)$$

[9] J. G. Kirkwood, J. Chem. Phys. 14, 180 (1946).

which defines the relative probability density $f^{(n/N-n)}$. Equation (7) also provides a relationship between distribution functions at the two times t and $t+s$, and may be used to re-express Eq. (6). The use of the definition of $K^{(N)}$ and $f^{(n/N-n)}$ then permits the integrated form of the Liouville equation to be written as

$$\mathfrak{L}\bar{f}^{(1)}(\alpha,1)=-[(N_\alpha-1)\tau]^{-1}\int_0^\tau\int\cdots\int\sum_{j,\beta}(N_\beta-\delta_{\alpha\beta})\,\mathbf{F}_{1j}^{\alpha\beta}\cdot\nabla_{p_\alpha}K^{(2)}(s)f^{(2)}(\mathbf{R}_{1\alpha}'\mathbf{R}_{2\beta}'\mathbf{p}_{1\alpha}'\mathbf{p}_{2\beta}';t)$$
$$\cdot ds d\mathbf{R}_{2\beta}d\mathbf{p}_{2\beta}d\mathbf{R}_{1\alpha}'d\mathbf{R}_{2\beta}'d\mathbf{p}_{1\alpha}'d\mathbf{p}_{2\beta}', \quad (10)$$

and the pair transition probability, $K^{(2)}(s)$, is obtained as a solution of the integrated Liouville equation,

$$\sum_\alpha\left[\frac{\partial K^{(2)}}{\partial s}+\frac{\mathbf{p}_{1\alpha}}{m_{1\alpha}}\cdot\nabla_{R_{1\alpha}}K^{(2)}+\frac{\mathbf{p}_{2\beta}}{m_{2\beta}}\cdot\nabla_{R_{2\beta}}K^{(2)}\right]=-\int\sum_{j,\alpha\beta;\,j\geq 3}[\mathbf{F}_{1j}^{\alpha\beta}\cdot\nabla_{p_{1j}}+\mathbf{F}_{2j}^{\alpha\beta}\cdot\nabla_{p_{2j}}]K^{(2)}(s)d\mathbf{R}^{(N-2)}d\mathbf{p}^{(N-2)}. \quad (11)$$

It is now convenient to introduce the assumption that only binary encounters occur. This is, strictly speaking, rigorously true for rigid sphere fluids with a finite number of particles. However, we wish to also exclude successive correlated binary collisions which will certainly occur if the time interval chosen for coarse graining is sufficiently long. In the limit as $\tau\to+0$ it is plausible that only isolated binary collisions can occur since the number of simultaneous three body collisions must be very small. In the limit $\tau\to+0$ then, the only forces operative are between molecules 1α and 2β. Under these conditions, the right-hand side of Eq. (11) vanishes, and $K^{(2)}(s)$ is the solution of the Liouville equation in pair space. This solution is

$$K^{(2)}(\mathbf{R}_{1\alpha}\mathbf{R}_{2\beta}\mathbf{p}_{1\alpha}\mathbf{p}_{2\beta}/\mathbf{R}_{1\alpha}'\mathbf{R}_{2\beta}'\mathbf{p}_{1\alpha}'\mathbf{p}_{2\beta}';s)$$
$$=\prod_{ik=1\alpha,2\beta}\delta(\mathbf{R}_{ik}-\mathbf{R}_{ik}'-\Delta\mathbf{R}_{ik})\delta(\mathbf{p}_{ik}-\mathbf{p}_{ik}'-\Delta\mathbf{p}_{ik}), \quad (12)$$

where the increments in momenta and positions are to be evaluated from the dynamics of the two body collision. With the aid of an explicit representation of the delta functions, the combination of Eq. (12) with Eq. (10) leads to

$$\mathfrak{L}\bar{f}^{(1)}(\alpha 1)=[(N_\alpha-1)\tau]^{-1}\int_0^\tau\int\sum_\beta(N_\beta-\delta_{\alpha\beta})f^{(2)}(\mathbf{R}_{1\alpha}'\mathbf{R}_{2\beta}'\mathbf{p}_{1\alpha}'\mathbf{p}_{2\beta}';t)$$
$$\prod_{ik=1\alpha,2\beta}\delta(\mathbf{R}_{ik}-\mathbf{R}_{ik}'-\Delta\mathbf{R}_{ik})\frac{\partial}{\partial s}\prod\delta(\mathbf{p}_{ik}-\mathbf{p}_{ik}'-\Delta\mathbf{p}_{ik})ds d\mathbf{R}_{1\alpha}'d\mathbf{R}_{2\beta}'d\mathbf{p}_{1\alpha}'d\mathbf{p}_{2\beta}'d\mathbf{R}_{2\beta}d\mathbf{p}_{2\beta}. \quad (13)$$

Because of the use of (12), Eq. (13) is valid only in the limit $\tau\to+0$. The time interval of duration $+0$ is too short to allow the centers of the mass of the colliding particles to move apart so that we may integrate Eq. (13) to get

$$\mathfrak{L}\bar{f}^{(1)}(\alpha,1)=[(N_\alpha-1)\tau]^{-1}\int\sum_\beta(N_\beta-\delta_{\alpha\beta})[f^{(2)}(\mathbf{R}_{1\alpha},\mathbf{R}_{2\beta},\mathbf{p}_{1\alpha}-\Delta\mathbf{p}_{1\alpha},\mathbf{p}_{2\beta}-\Delta\mathbf{p}_{2\beta};t)-f^{(2)}(\mathbf{R}_{1\alpha}\mathbf{R}_{2\beta}\mathbf{p}_{1\alpha}\mathbf{p}_{2\beta};t)]ds d\mathbf{R}_{2\beta}d\mathbf{p}_{2\beta} \quad (14)$$

with the positions of the colliding molecules the same before and after collision. The integration over volume is now conveniently replaced by an integration over the collision cylinder specified by the impact parameter b, the azimuthal angle ϵ, and the relative velocity $\mathbf{p}_{1\alpha 2\beta}/\mu_{\alpha\beta}$ with $\mu_{\alpha\beta}$ the reduced mass of the colliding pair. If now the pair correlation function defined by

$$f^{(2)}(\mathbf{R}_1\mathbf{R}_2\mathbf{p}_1\mathbf{p}_2;t)=g^{(2)}(\mathbf{R}_1\mathbf{R}_2\mathbf{p}_1\mathbf{p}_2;t)f^{(1)}(\mathbf{R}_1\mathbf{p}_1;t)f^{(1)}(\mathbf{R}_2\mathbf{p}_2;t) \quad (15)$$

is introduced into Eq. (14), the new volume element $dR_{2\beta}=(\mathbf{p}_{1\alpha 2\beta}/\mu_{\alpha\beta})\tau b_{\alpha\beta}db_{\alpha\beta}d\epsilon$ employed, and cognizance taken of the limit $\tau\to+0$, the modified Boltzmann equation becomes after a second time smoothing

$$\mathfrak{L}\bar{f}^{(1)}(\alpha 1)=(N_\alpha-1)^{-1}\int\cdots\int\sum_\beta\frac{p_{1\alpha 2\beta}}{\mu_{\alpha\beta}}(N_\beta-\delta_{\alpha\beta})g_0^{(2)}(\sigma_{\alpha\beta})[\bar{f}^{(1)}(\mathbf{R}_{1\alpha}\mathbf{p}_{1\alpha}-\Delta\mathbf{p}_{1\alpha};t)\,\bar{f}^{(1)}(\mathbf{R}_{2\beta}\mathbf{p}_{2\beta}-\Delta\mathbf{p}_{2\beta};t)$$
$$-\bar{f}^{(1)}(\mathbf{R}_{1\alpha}\mathbf{p}_{1\alpha};t)\,\bar{f}^{(1)}(\mathbf{R}_{2\beta}\mathbf{p}_{2\beta};t)]b_{\alpha\beta}db_{\alpha\beta}d\epsilon d\mathbf{p}_{2\beta}, \quad (16)$$

where we have also used the approximation that the true pair correlation function on contact may be replaced by its local equilibrium value, $g_0^{(2)}(\sigma_{\alpha\beta})$ and $\sigma_{\alpha\beta}$ is the distance apart of the centers of molecules α and β on contact.

III. SOLUTION OF THE MODIFIED BOLTZMANN EQUATION

We now turn to the problem of finding a solution of Eq. (16). As usual, the complexity of the problem demands a perturbation solution. When the gradients of temperature, velocity, and concentration are small, the distribution functions are slowly varying functions of the position coordinates. Under these conditions, the truncated Taylor's series expansion

$$\bar{f}^{(1)}(\mathbf{R}_{2\beta}, \mathbf{p}_{2\beta}; t) = \bar{f}^{(1)}(\mathbf{R}_{1\alpha}\mathbf{p}_{2\beta}; t) + \sigma_{\alpha\beta}\mathbf{k}\cdot\nabla_{R_{1\alpha}}\bar{f}^{(1)}(\mathbf{R}_{1\alpha}\mathbf{p}_{2\beta}; t) \quad (17)$$

may be used to simplify Eq. (16). The vector $\mathbf{k}$ is of unit length and is directed along the line of centers on contact. For the perturbation to the equilibrium distribution function write

$$\bar{f}^{(1)}(\mathbf{R}_{1\alpha}\mathbf{p}_{1\alpha}; t) = \bar{f}_0^{(1)}(1\alpha)[1+\Phi_{1\alpha}]$$

$$\bar{f}^{(1)}(\mathbf{R}_{1\alpha}\mathbf{p}_{1\alpha}-\Delta\mathbf{p}_{1\alpha}; t) = \bar{f}_0^{(1)*}(1\alpha)[1+\Phi_{1\alpha}^*], \quad (18)$$

where the asterisk refers to the function after collision. The unperturbed distribution function $\bar{f}_0^{(1)}$ is conveniently chosen to correspond to local equilibrium in coordinate and momentum space, thereby leading to

$$\bar{f}_0^{(1)}(1\alpha) = [(2\pi m_\alpha kT)^{-3/2}/v_\alpha] \cdot \exp-[\mathbf{p}_{1\alpha}-m_\alpha\mathbf{u}]^2/2m_\alpha kT \quad (19)$$

with $\mathbf{u}$ and v_α^{-1} the local hydrodynamic velocity and local concentration. The use of Eqs. (17), (18), and (19) in Eq. (16) and the neglect of second order terms results in the lengthy equation,

$$\mathfrak{L}\bar{f}^{(1)}(1\alpha) = \sum_\beta[(N_\beta-\delta_{\alpha\beta})/(N_\alpha-1)]g_0^{(2)}(\sigma_{\alpha\beta})\int\cdots\int \bar{f}_0^{(1)}(1\alpha)\,\bar{f}_0^{(1)}(2\beta)\,(p_{1\alpha2\beta}/\mu_{\alpha\beta})\{[\Phi_{1\alpha}^*+\Phi_{2\beta}^*-\Phi_{1\alpha}-\Phi_{2\beta}]$$
$$+\mathbf{k}\sigma_{\alpha\beta}\cdot\{(1/2kT^2)m_\beta[(\mathbf{p}_{1\alpha2\beta}/\mu_{\alpha\beta})\cdot\mathbf{k}]^2-2[(\mathbf{p}_{1\alpha2\beta}/\mu_{\alpha\beta})\cdot\mathbf{k}]\mathbf{k}\cdot[\mathbf{p}_{2\beta}-m_\beta\mathbf{u}]\}\nabla_{R_{1\alpha}}T$$
$$+\mathbf{k}\sigma_{\alpha\beta}\cdot\{-(m_\beta/kT)[(p_{1\alpha2\beta}/\mu_{\alpha\beta})\cdot\mathbf{k}]\mathbf{k}\cdot\nabla_{R_{1\alpha}}\mathbf{u}]\}b_{\alpha\beta}db_{\alpha\beta}d\epsilon d\mathbf{p}_{2\beta} \quad (20)$$

where we have used the following relations:

$$\bar{f}_0^{(1)*}(1\alpha)\,\bar{f}_0^{(1)*}(2\beta) = \bar{f}_0^{(1)}(1\alpha)\,\bar{f}_0^{(1)}(2\beta) \quad (21)$$

$$\nabla_{R_{1\alpha}}\ln[\bar{f}_0^{(1)*}(2\beta)/\bar{f}_0^{(1)}(2\beta)] = (1/2kT^2)\{m_\beta[(\mathbf{p}_{1\alpha2\beta}/\mu_{\alpha\beta})\cdot\mathbf{k}]^2-2(\mathbf{p}_{1\alpha2\beta}/\mu_{\alpha\beta})\cdot\mathbf{kk}\cdot[\mathbf{p}_{2\beta}-m_\beta\mathbf{u}]\}\nabla_{R_{1\alpha}}T$$
$$-(m_\beta/kT)[(p_{1\alpha2\beta}/\mu_{\alpha\beta})\cdot\mathbf{k}]\mathbf{k}\cdot\nabla_{R_{1\alpha}}\mathbf{u}. \quad (22)$$

The left-hand side of Eq. (16) may now be evaluated by substitution of Eqs. (18) and (19), and the subsequent neglect of the terms involving the derivatives of the perturbation function. The use of the equations of change,

$$\partial v_\alpha/\partial t = v_\alpha^2\nabla_{R_{1\alpha}}\cdot(\mathbf{u}/v_\alpha) \quad (23)$$

$$\partial\mathbf{u}/\partial t = -\mathbf{u}\cdot\nabla_{R_{1\alpha}}\mathbf{u}-(1/\rho)\nabla_{R_{1\alpha}}p \quad (24)$$

$$\partial T/\partial t = -\mathbf{u}\cdot\nabla_{R_{1\alpha}}T-(T/2C_v)\sum_\alpha v_\alpha(\partial p/\partial T)\rho\mathbf{1}:\nabla_{R_{1\alpha}}\mathbf{u} \quad (25)$$

leads to the result,

$$\mathfrak{L}\bar{f}_0^{(1)}(1\alpha) = \bar{f}_0^{(1)}(1\alpha)[\{2\mathbf{b}_{1\alpha}+[(v/C_v)(\partial p/\partial T)_\rho-\tfrac{2}{3}](\tfrac{3}{2}-W_{1\alpha}^2)\mathbf{1}\}:\nabla_{R_{1\alpha}}\mathbf{u}+(\tfrac{3}{2}-W_{1\alpha}^2)[(\mathbf{p}_{1\alpha}/m_\alpha)-\mathbf{u}]\cdot\nabla_{R_{1\alpha}}\ln T$$
$$+\{(1/\rho)(2m_\alpha/kT)^{\frac{1}{2}}\nabla_{R1\alpha}p-(2kT/m_\alpha)^{\frac{1}{2}}\nabla_{R1\alpha}\ln v_\alpha\}\cdot\mathbf{W}_{1\alpha}], \quad (26)$$

where ρ is the density, equal to $\sum_\alpha(m_\alpha/v_\alpha)$, v is the mean volume defined as

$$v = \tfrac{1}{2}(v_\alpha+v_\beta), \quad (27)$$

and $\mathbf{W}_{1\alpha}$ is a reduced peculiar velocity given by

$$\mathbf{W}_{1\alpha} = (m_\alpha/2kT)^{\frac{1}{2}}[(\mathbf{p}_{1\alpha}/m_\alpha)-\mathbf{u}] \quad (28)$$

with

$$\mathbf{b}_{1\alpha} = \mathbf{W}_{1\alpha}\mathbf{W}_{1\alpha}-\tfrac{1}{3}W_{1\alpha}^2\mathbf{1}. \quad (29)$$

To complete the formulation of the linearized transport equation the integrals in Eq. (20) must be evaluated. If a polar coordinate system is chosen with $\mathbf{p}_{1\alpha2\beta}/\mu_{\alpha\beta}$ along the polar axis the integrations may be readily carried out.[6] Collecting all terms, the complete line-

arized equation is,

$$\sum_\beta \frac{N_\beta-\delta_{\alpha\beta}}{N_\alpha-1} g_0^{(2)}(\sigma_{\alpha\beta}) \iiint \bar{f}_0^{(1)}(1\alpha)\,\bar{f}_0^{(1)}(2\beta)[\Phi_{1\alpha}{}^*+\Phi_{2\beta}{}^*-\Phi_{1\alpha}-\Phi_{2\beta}]\frac{p_{1\alpha2\beta}}{\mu_{\alpha\beta}} b_{\alpha\beta}db_{\alpha\beta}d\epsilon d\mathbf{p}_{2\beta}$$

$$= \bar{f}_0^{(1)}(1\alpha)\left[\left\{2\mathbf{b}_{1\alpha}+\left(\frac{v}{C_v}\left(\frac{\partial p}{\partial T}\right)_\rho-\tfrac{2}{3}\right)(\tfrac{3}{2}-W_{1\alpha}{}^2)\mathbf{1}\right\}:\nabla_{R_{1\alpha}}\mathbf{u}+(\tfrac{3}{2}-W_{1\alpha}{}^2)\left(\frac{\mathbf{p}_{1\alpha}}{m_\alpha}-\mathbf{u}\right)\cdot\nabla_{R_{1\alpha}}\ln T\right.$$

$$\left.+\left\{(1/\rho)\left(\frac{2m_\alpha}{kT}\right)^{\frac{1}{2}}\nabla_{R_{1\alpha}}p-\left(\frac{2kT}{m_\alpha}\right)^{\frac{1}{2}}\nabla_{R1\alpha}\ln v_\alpha\right\}\cdot\mathbf{W}_{1\alpha}\right]$$

$$+\sum_\beta \frac{N_\beta-\delta_{\alpha\beta}}{N_\alpha-1} g_0^{(2)}(\sigma_{\alpha\beta})\left[\int \frac{m_\alpha}{kT}\bar{f}_0^{(1)}(1\alpha)\,\bar{f}_0^{(1)}(2\beta)\nabla_{R_{1\alpha}}\mathbf{u}:\left(\frac{4\pi\sigma_{\alpha\beta}{}^3}{15}\frac{\mathbf{p}_{1\alpha2\beta}}{\mu_{\alpha\beta}}\frac{\mathbf{p}_{1\alpha2\beta}}{\mu_{\alpha\beta}}+\frac{2\pi\sigma_{\alpha\beta}{}^3}{15}\left(\frac{p_{1\alpha2\beta}}{\mu_{\alpha\beta}}\right)^2\mathbf{1}\right]d\mathbf{p}_{2\beta}$$

$$-\frac{1}{kT^2}\int \bar{f}_0^{(1)}(1\alpha)\,\bar{f}_0^{(1)}(2\beta)\nabla_{R_{1\alpha}}\ln T\cdot\left[m_\alpha\frac{3\pi\sigma_{\alpha\beta}{}^3}{15}\left(\frac{p_{1\alpha2\beta}}{\mu_{\alpha\beta}}\right)^2\frac{\mathbf{p}_{1\alpha2\beta}}{\mu_{\alpha\beta}}-\frac{2\pi\sigma_{\alpha\beta}{}^3}{15}(\mathbf{p}_{2\beta}-m_\beta\mathbf{u})\left(\frac{p_{1\alpha2\beta}}{\mu_{\alpha\beta}}\right)^2\mathbf{1}-\frac{4\pi\sigma_{\alpha\beta}{}^3}{15}(\mathbf{p}_{2\beta}-m_\beta\mathbf{u})\right.$$

$$\left.\cdot\frac{\mathbf{p}_{1\alpha2\beta}}{\mu_{\alpha\beta}}\frac{p_{1\alpha2\beta}}{\mu_{\alpha\beta}}\right]d\mathbf{p}_{2\beta}. \tag{30}$$

From the linear form of Eq. (30), it is clear that the perturbation to the distribution function is

$$\Phi_{1\alpha}=-\mathbf{A}_{1\alpha}\cdot\nabla_{R_{1\alpha}}\ln T-\mathbf{B}_{1\alpha}:\nabla_{R_{1\alpha}}\mathbf{u}+\mathbf{C}_{1\alpha}\cdot\boldsymbol{\gamma}_{1\alpha} \tag{31}$$

where

$$\boldsymbol{\gamma}_{1\alpha}=(1/\rho)(2m_\alpha/kT)^{\frac{1}{2}}\nabla_{R_{1\alpha}}p-(2kT/m_\alpha)^{\frac{1}{2}}\nabla_{R_{1\alpha}}\ln v_\alpha. \tag{32}$$

By substitution of Eq. (31) into Eq. (30) it is found that

$$\sum_\beta \frac{N_\beta-\delta_{\alpha\beta}}{N_\alpha-1} g_0^{(2)}(\sigma_{\alpha\beta})\iiint \frac{p_{1\alpha2\beta}}{\mu_{\alpha\beta}}\bar{f}_0^{(1)}(1\alpha)\,\bar{f}_0^{(1)}(2\beta)[\mathbf{A}_{1\alpha}{}^*+\mathbf{A}_{2\beta}{}^*-\mathbf{A}_{1\alpha}-\mathbf{A}_{2\beta}]b_{\alpha\beta}db_{\alpha\beta}d\epsilon d\mathbf{p}_{2\beta}=\mathbf{K}_\alpha \tag{33}$$

$$\sum_\beta \frac{N_\beta-\delta_{\alpha\beta}}{N_\alpha-1} g_0^{(2)}(\sigma_{\alpha\beta})\iiint \frac{p_{1\alpha2\beta}}{\mu_{\alpha\beta}}\bar{f}_0^{(1)}(1\alpha)\,\bar{f}_0^{(1)}(2\beta)[\mathbf{B}_{1\alpha}{}^*+\mathbf{B}_{2\beta}{}^*-\mathbf{B}_{1\alpha}-\mathbf{B}_{2\beta}]b_{\alpha\beta}db_{\alpha\beta}d\epsilon d\mathbf{p}_{2\beta}=\mathbf{L}_\alpha \tag{34}$$

$$\sum_\beta \frac{N_\beta-\delta_{\alpha\beta}}{N_\alpha-1} g_0^{(2)}(\sigma_{\alpha\beta})\iiint \frac{p_{1\alpha2\beta}}{\mu_{\alpha\beta}}\bar{f}_0^{(1)}(1\alpha)\,\bar{f}_0^{(1)}(2\beta)[\mathbf{C}_{1\alpha}{}^*+\mathbf{C}_{2\beta}{}^*-\mathbf{C}_{1\alpha}-\mathbf{C}_{2\beta}]b_{\alpha\beta}db_{\alpha\beta}d\epsilon d\mathbf{p}_{2\beta}=\mathbf{M}_\alpha \tag{35}$$

where the coefficients $\mathbf{K}_\alpha$, $\mathbf{L}_\alpha$, and $\mathbf{M}_\alpha$ are

$$\mathbf{K}_\alpha=\bar{f}_0^{(1)}(1\alpha)(\tfrac{3}{2}-W_{1\alpha}{}^2)\left(\frac{\mathbf{p}_{1\alpha}}{m_\alpha}-\mathbf{u}\right)+\sum_\beta \frac{N_\beta-\delta_{\alpha\beta}}{N_\alpha-1} g_0^{(2)}(\sigma_{\alpha\beta})\int (1/kT^2)\,\bar{f}_0^{(1)}(1\alpha)\,\bar{f}_0^{(1)}(2\beta)$$

$$\cdot\left[m_\alpha\frac{3\pi\sigma_{\alpha\beta}{}^3}{15}\left(\frac{p_{1\alpha2\beta}}{\mu_{\alpha\beta}}\right)^2\frac{\mathbf{p}_{1\alpha2\beta}}{\mu_{\alpha\beta}}-\frac{2\pi\sigma_{\alpha\beta}{}^3}{15}[\mathbf{p}_{2\beta}-m_\beta\mathbf{u}]\left(\frac{p_{1\alpha2\beta}}{\mu_{\alpha\beta}}\right)^2-\frac{4\pi\sigma_{\alpha\beta}{}^3}{15}[\mathbf{p}_{2\beta}-m_\beta\mathbf{u}]\cdot\frac{\mathbf{p}_{1\alpha2\beta}}{\mu_{\alpha\beta}}\frac{\mathbf{p}_{1\alpha2\beta}}{\mu_{\alpha\beta}}\right]d\mathbf{p}_{2\beta} \tag{36}$$

$$\mathbf{L}_\alpha=-\bar{f}_0^{(1)}(1\alpha)[2\mathbf{b}_{1\alpha}+((v/C_v)(\partial p/\partial T)_\rho-\tfrac{2}{3})(\tfrac{3}{2}-W_{1\alpha}{}^2\mathbf{1})]-\sum_\beta \frac{N_\beta-\delta_{\alpha\beta}}{N_\alpha-1} g_0^{(2)}(\sigma_{\alpha\beta})\int \frac{m_\alpha}{kT}\bar{f}_0^{(1)}(1\alpha)\,\bar{f}_0^{(1)}(2\beta)$$

$$\cdot\left[\frac{4\pi\sigma_{\alpha\beta}{}^3}{15}\frac{\mathbf{p}_{1\alpha2\beta}}{\mu_{\alpha\beta}}\frac{\mathbf{p}_{1\alpha2\beta}}{\mu_{\alpha\beta}}+\frac{2\pi\sigma_{\alpha\beta}{}^3}{15}\left(\frac{p_{1\alpha2\beta}}{\mu_{\alpha\beta}}\right)^2\mathbf{1}\right]d\mathbf{p}_{2\beta} \tag{37}$$

$$\mathbf{M}_\alpha=\bar{f}_0^{(1)}(1\alpha)\mathbf{W}_{1\alpha}. \tag{38}$$

In order to evaluate the coefficients **A**, **B**, **C**, the righthand sides of Eqs. (36) and (37) must be integrated. Let the mole fraction of component α be $x_\alpha = N_\alpha/N$. Then, for $\mathbf{K}_\alpha$ we find

$$K_\alpha = \bar{f}_0^{(1)}(1\alpha)\Big[\Big(\frac{2kT}{m_\alpha}\Big)^{\frac{1}{2}}(\tfrac{3}{2}-W_{1\alpha}^2)\mathbf{W}_{1\alpha}+g_0^{(2)}(\sigma_{\alpha\alpha})\frac{\pi\sigma_{\alpha\alpha}^3}{15v_\alpha}\Big(\frac{2kT}{m_\alpha}\Big)^{\frac{1}{2}}\mathbf{W}_{1\alpha}(5-6W_{1\alpha}^2)$$
$$+\gamma_{\alpha\beta}\frac{1-x_\alpha}{x_\alpha}\frac{\pi\sigma_{\alpha\beta}^3}{15v_\beta}g_0^{(2)}(\sigma_{\alpha\beta})\frac{m_\beta^2}{4\mu_{\alpha\beta}^2}\Big(\frac{2kT}{m_\beta}\Big)^{\frac{1}{2}}Z_{1\alpha}\Big(20-\frac{15m_\beta}{2\mu_{\alpha\beta}}-\frac{6m_\beta}{2\mu_{\alpha\beta}}Z_{1\alpha}^2\Big)\Big],$$

where $\gamma_{\alpha\beta}=1$ when $\alpha\neq\beta$, $\gamma_{\alpha\beta}=0$ when $\alpha=\beta$, and can be written as

$$\gamma_{\alpha\beta}=\log_{10}(10-9\delta_{\alpha\beta}).$$

$\mathbf{Z}_{1\alpha}$ is a new reduced peculiar velocity

$$\mathbf{Z}_{1\alpha}=\sum_\nu (m_\nu/2kT)^{\frac{1}{2}}[(\mathbf{p}_{1\delta}/m_\nu)-\mathbf{u}]\gamma_{\alpha\nu}. \tag{40}$$

By use of the theorem,

$$\int F(|\xi|)\Psi\cdot\xi\xi d^3\xi=(\Psi/3)\int F(|\xi|)\xi^2 d^3\xi, \tag{41}$$

the right-hand side of (37) may be reduced to give for $\mathbf{L}_\alpha$ the relation,

$$\mathbf{L}_\alpha=-\bar{f}_0^{(1)}(1\alpha)\{2\mathbf{b}_{1\alpha}+[(v/C_v)(\partial p/\partial T)_\rho-\tfrac{2}{3}](\tfrac{3}{2}-W_{1\alpha}^2\mathbf{1})-g_0^{(2)}(\sigma_{\alpha\alpha})(2\pi\sigma_{\alpha\alpha}^3/15v_\alpha)[(5+2W_{1\alpha}^2)\mathbf{1}+4\mathbf{W}_{1\alpha}\mathbf{W}_{1\alpha}\}$$
$$-\gamma_{\alpha\beta}[(1-x_\alpha)/x_\alpha]g_0^{(2)}(\sigma_{\alpha\beta})(2\pi\sigma_{\alpha\beta}^3/15v_\beta)(m_\beta^2/4\mu_{\alpha\beta}^2)[(5+2Z_{1\alpha}^2)\mathbf{1}+4\mathbf{Z}_{1\alpha}\mathbf{Z}_{1\alpha}]\}. \tag{42}$$

To determine the functional dependence of $\mathbf{K}_\alpha$, $\mathbf{L}_\alpha$, and $\mathbf{M}_\alpha$ on $\mathbf{W}_{1\alpha}$ and $\mathbf{Z}_{1\alpha}$, we note that a vector or tensor function, $f(\mathbf{x})$ may be written as $f(\mathbf{x})=\mathbf{x}f(|\mathbf{x}|)$. Thus, from Eqs. (33)–(42),

$$\mathbf{C}_{1\alpha}=\mathbf{W}_{1\alpha}C_{1\alpha}(|W_{1\alpha}|), \tag{43}$$

$$\mathbf{A}_{1\alpha}=\mathbf{W}_{1\alpha}A_{1\alpha}^{(1)}(|W_{1\alpha}|)+\mathbf{Z}_{1\alpha}A_{1\alpha}^{(2)}(|Z_{1\alpha}|) \tag{44}$$

$$\mathbf{B}_{1\alpha}=[\mathbf{W}_{1\alpha}\mathbf{W}_{1\alpha}-\tfrac{1}{3}W_{1\alpha}^2\mathbf{1}]B_{1\alpha}^{(1)}(|W_{1\alpha}|)+B_{1\alpha}^{(2)}(|W_{1\alpha}|)\mathbf{1}+[\mathbf{Z}_{1\alpha}\mathbf{Z}_{1\alpha}-\tfrac{1}{3}Z_{1\alpha}^2\mathbf{1}]B_{1\alpha}'^{(1)}(|Z_{1\alpha}|)+B_{1\alpha}'^{(2)}(|Z_{1\alpha}|)\mathbf{1} \tag{45}$$

where Eq. (45) corresponds to the separation of $\mathbf{L}_\alpha$ as follows:

$$\mathbf{L}_\alpha=\mathbf{L}_\alpha^{(1)}+\mathbf{L}_\alpha^{(2)} \tag{46}$$

$$\mathbf{L}_\alpha^{(1)}=-\bar{f}_0^{(1)}(1\alpha)\{2\mathbf{b}_{1\alpha}-g_0^{(2)}(\sigma_{\alpha\alpha})(2\pi\sigma_{\alpha\alpha}^3/15v_\alpha)4[\mathbf{W}_{1\alpha}\mathbf{W}_{1\alpha}-\tfrac{1}{3}W_{1\alpha}^2\mathbf{1}]$$
$$-\gamma_{\alpha\beta}[(1-x_\alpha)/x_\alpha]g_0^{(2)}(\sigma_{\alpha\beta})(2\pi\sigma_{\alpha\beta}^3/15v_\beta)(m_\alpha^2/\mu_{\alpha\beta}^2)4[\mathbf{Z}_{1\alpha}\mathbf{Z}_{1\alpha}-\tfrac{1}{3}Z_{1\alpha}^2\mathbf{1}]\} \tag{47}$$

$$\mathbf{L}_\alpha^{(2)}=-\bar{f}_0^{(1)}(1\alpha)\{[(v/C_v)(\partial p/\partial T)_\rho-\tfrac{2}{3}](\tfrac{3}{2}-W_{1\alpha}^2)-g_0^{(2)}(\sigma_{\alpha\alpha})(2\pi\sigma_{\alpha\alpha}^3/15v_\alpha)[(5+2W_{1\alpha}^2)+\tfrac{4}{3}W_{1\alpha}^2]$$
$$+\gamma_{\alpha\beta}[(1-x_\alpha)/x_\alpha]g_0^{(2)}(\sigma_{\alpha\beta})(2\pi\sigma_{\alpha\beta}^3/15v_\beta)(m_\beta^2/4\mu_{\alpha\beta}^2)[(5+Z_{1\alpha}^2)+\tfrac{4}{3}Z_{1\alpha}^2]\}\mathbf{1}. \tag{48}$$

The standard technique for solving Eqs. (33), (34) and (35) is to expand each scalar function of $|W_{1\alpha}|$ and $|Z_{1\alpha}|$ in a finite series of Sonine polynomials with constant coefficients, with the coefficients regarded as parameters. These coefficients are functions only of the term in the series which they precede. The method is as follows: for each of the A, B, B', and C coefficients there are two equations (one for each species) in a given number of unknown expansion coefficients. Each equation may be multiplied successively by the Sonine polynomial corresponding to one of the expansion coefficients and then integrated over all values of the relevant variables in the allowed domain. The result of this procedure is a set of equations equal in number to the number of unknown expansion coefficients. Any redundancies which arise may be eliminated by the use of the orthogonality relation between any two members of the complete set of Sonine polynomials.

The procedure just sketched was introduced by Hirschfelder and Curtiss[3] and is called a variational method. In fact, it is not necessary to carry out any explicit variations nor to add in conservation conditions as constraints using Lagrange multipliers. These constraints are already implicitly contained in the procedure as outlined.

The Sonine polynomials which will be used are defined by the generating function,

$$S_n^{(m)}(\zeta)=\sum_{j=0}^{m}\frac{(-)^j(m+n)!}{(n+j)!(m-j)!}\zeta^j \tag{49}$$

and are orthogonal with respect to the weighting function $\zeta^n e^{-\zeta}$. The normalization is such that

$$\int_0^\infty \zeta^n e^{-\zeta} S_n^{(m)}(\zeta)\, S_n^{(t)}(\zeta)\, d\zeta=[(m+n)!/m!]\delta_{mt}. \tag{50}$$

Consider first the vector $\mathbf{C}_\alpha$ recalling that $\mathbf{C}_\alpha=\mathbf{W}_{1\alpha}C_\alpha(|\mathbf{W}_{1\alpha}|)$. We expand the scalar function $C_\alpha(|\mathbf{W}_{1\alpha}|)$ as a finite series,

$$C_\alpha(|\mathbf{W}_{1\alpha}|)=\sum_m C_\alpha^{(m)} S_{3/2}^{(m)}(W_{1\alpha}^2) \tag{51}$$

where the expansion coefficients $C_\alpha^{(m)}$ depend only on the index m and the species α. By substitution of Eq. (51) into Eq. (35), it is found that

$$\sum_m\sum_\beta[(N_\beta-\delta_{\alpha\beta}/(N_\alpha-1)]g_0^{(2)}(\sigma_{\alpha\beta})\iiint(p_{1\alpha2\beta}/\mu_{\alpha\beta})\,\bar{f}_0^{(1)}(1\alpha)\,\bar{f}_0^{(1)}(2\beta)\{C_{1\alpha}^{(m)}[S_{3/2}^{(m)}(W_{1\alpha}^{*2})\mathbf{W}_{1\alpha}^{*}-S_{3/2}^{(m)}(W_{1\alpha}^2)\mathbf{W}_{1\alpha}]$$
$$+C_{2\beta}^{(m)}[S_{3/2}^{(m)}(W_{2\beta}^{*2})\mathbf{W}_{2\beta}^{*}-S_{3/2}^{(m)}(W_{2\beta}^2)\mathbf{W}_{2\beta}]\}\,b_{\alpha\beta}db_{\alpha\beta}d\epsilon d\mathbf{p}_{2\beta}=\mathbf{W}_{1\alpha}\bar{f}_0^{(1)}(1\alpha). \tag{52}$$

If the series expansion is truncated after two terms, corresponding to the retention of $C_\alpha^{(0)}$ and $C_\alpha^{(1)}$ only, there are four unknown coefficients. The multiplication of Eq. (52) by $S_{3/2}^{(k)}(W_{1\alpha}^2)\mathbf{W}_{1\alpha}$ and subsequent integration over $d\mathbf{p}_{1\alpha}$ yields

$$\sum_m\sum_\beta[(N_\beta-\delta_{\alpha\beta})/(N_\alpha-1)][g_0^{(2)}(\sigma_{\alpha\beta})/v_\alpha v_\beta][\{S_{3/2}^{(k)}(W_{1\alpha}^2)\mathbf{W}_{1\alpha};\,S_{3/2}^{(m)}(W_{1\alpha}^2)\mathbf{W}_{1\alpha}\}_{1\alpha,2\beta}C_{1\alpha}^{(m)}$$
$$+\{S_{3/2}^{(k)}(W_{1\alpha}^2)\mathbf{W}_{1\alpha};\,S_{3/2}^{(m)}(W_{2\beta}^2)\mathbf{W}_{2\beta}\}_{1\alpha,2\beta}C_{2\beta}^{(m)}=\int W_{1\alpha}^2\bar{f}_0^{(1)}(1\alpha)\,S_{3/2}^{(k)}(W_{1\alpha}^2)\,d\mathbf{p}_{1\alpha} \tag{53}$$

where the bracket notation of Hirschfelder, Curtiss, and Bird[3] has been employed. This is, specifically,

$$\{G;H\}_{1\alpha,2\beta}=-v_\alpha v_\beta\iiint(p_{1\alpha2\beta}/\mu_{\alpha\beta})\,\bar{f}_0^{(1)}(1\alpha)\,\bar{f}_0^{(1)}(2\beta)G(H-H^*)b_{\alpha\beta}db_{\alpha\beta}d\mathbf{p}_{1\alpha}d\mathbf{p}_{2\beta}d\epsilon. \tag{54}$$

Tables of these bracket integrals may be found in the reference cited.

The evaluation of A_α requires a little extra care because of the appearance of two reduced velocities, $\mathbf{W}_{1\alpha}$ and $\mathbf{Z}_{1\alpha}$. Once again, expanding in a finite series of Sonine polynomials,

$$A_\alpha=\sum_m[a_{1\alpha}^{(m)}S_{3/2}^{(m)}(W_{1\alpha}^2)+a_{1\alpha}'^{(m)}S_{3/2}^{(m)}(Z_{1\alpha}^2)]. \tag{55}$$

The substitution of (55) into (33) then gives

$$\sum_m\sum_\beta[(N_\beta-\delta_{\alpha\beta})/(N_\alpha-1)]g_0^{(2)}(\sigma_{\alpha\beta})$$
$$\cdot\Big\{\iiint(p_{1\alpha2\beta}/\mu_{\alpha\beta})\,\bar{f}_0^{(1)}(1\alpha)\,\bar{f}_0^{(1)}(2\beta)[a_{1\alpha}^{(m)}(S_{3/2}^{(m)}(W_{1\alpha}^{*2})\mathbf{W}_{1\alpha}^{*}-S_{3/2}^{(m)}(W_{1\alpha}^2)\mathbf{W}_{1\alpha})$$
$$+a_{2\beta}^{(m)}(S_{3/2}^{(m)}(W_{2\beta}^{*2})\mathbf{W}_{2\beta}^{*}-S_{3/2}^{(m)}(W_{2\beta}^2)\mathbf{W}_{2\beta})]b_{\alpha\beta}db_{\alpha\beta}d\epsilon d\mathbf{p}_{2\beta}$$
$$+\iiint(p_{1\alpha2\beta}/\mu_{\alpha\beta})\,\bar{f}_0^{(1)}(1\alpha)\,\bar{f}_0^{(1)}(2\beta)[a_{1\alpha}'^{(m)}(S_{3/2}^{(m)}(Z_{1\alpha}^{*2})\mathbf{Z}_{1\alpha}-S_{3/2}^{(m)}(Z_{1\alpha}^2)\mathbf{Z}_{1\alpha})$$
$$+a_{2\beta}'^{(m)}(S_{3/2}^{(m)}(Z_{2\beta}^2)\mathbf{Z}_{2\beta}^{*}-S_{3/2}^{(m)}(Z_{2\beta}^2)\mathbf{Z}_{2\beta})]b_{\alpha\beta}db_{\alpha\beta}d\epsilon d\mathbf{p}_{2\beta}\Big\}=\mathbf{K}_\alpha.$$

$$\mathbf{Z}_{2\beta}=\sum_\nu(m_\nu/2kT)^{\frac{1}{2}}[(\mathbf{p}_{2\beta}/m_\nu)-\mathbf{u}]\gamma_{\beta\nu}. \tag{56}$$

The truncation of the expansion in Eq. (55) after the first two terms gives, in this case, eight unknowns. By multiplying each of the equations by $S_{3/2}^{(r)}(W_{1\alpha}^2)\mathbf{W}_{1\alpha}$ and $S_{3/2}^{(r)}(Z_{1\alpha}^2)\mathbf{Z}_{1\alpha}$, a sufficient number of linear equations

is obtained to determine the eight unknown coefficients. The results are

$$\sum_m\sum_\beta[(N_\beta-\delta_{\alpha\beta})/(N_\alpha-1)]g_0^{(2)}(\sigma_{\alpha\beta})(1/v_\alpha v_\beta)[a_{1\alpha}^{(m)}\{S_{3/2}^{(r)}(W_{1\alpha}^2)\mathbf{W}_{1\alpha};\ S_{3/2}^{(m)}(W_{1\alpha}^2)\mathbf{W}_{1\alpha}\}_{1\alpha,2\beta}$$
$$+a_{2\beta}^{(m)}\{S_{3/2}^{(r)}(W_{1\alpha}^2)\mathbf{W}_{1\alpha};\ S_{3/2}^{(m)}(W_{2\beta}^2)\mathbf{W}_{2\beta}\}_{1\alpha2\beta}+a_{1\alpha}{}'^{(m)}\{S_{3/2}^{(r)}(W_{1\alpha}^2)\mathbf{W}_{1\alpha};\ S_{3/2}^{(m)}(Z_{1\alpha}^2)\mathbf{Z}_{1\alpha}\}_{1\alpha2\beta}$$
$$+a_{2\beta}{}'^{(m)}\{S_{3/2}^{(r)}(W_{1\alpha}^2)\mathbf{W}_{1\alpha};\ S_{3/2}^{(m)}(Z_{2\beta}^2)\mathbf{Z}_{2\beta}\}_{1\alpha2\beta}]=\int S_{3/2}^{(r)}(W_{1\alpha}^2)\mathbf{W}_{1\alpha}\cdot\mathbf{K}_\alpha d\mathbf{p}_{1\alpha} \tag{57}$$

$$\sum_m\sum_\beta[(N_\beta-\delta_{\alpha\beta})/(N_\alpha-1)]g_0^{(2)}(\sigma_{\alpha\beta})(1/v_\alpha v_\beta)[a_{1\alpha}^{(m)}\{S_{3/2}^{(r)}(Z_{1\alpha}^2)\mathbf{Z}_{1\alpha};\ S_{3/2}^{(m)}(W_{1\alpha}^2)\mathbf{W}_{1\alpha}\}_{1\alpha2\beta}$$
$$+a_{2\beta}^{(m)}\{S_{3/2}^{(r)}(Z_{1\alpha}^2)\mathbf{Z}_{1\alpha};\ S_{3/2}^{(m)}(W_{2\beta}^2)\mathbf{W}_{2\beta}\}_{1\alpha2\beta}+a_{1\alpha}{}'^{(m)}\{S_{3/2}^{(r)}(Z_{1\alpha}^2)\mathbf{Z}_{1\alpha};\ S_{3/2}^{(m)}(Z_{1\alpha}^2)\mathbf{Z}_{1\alpha}\}_{1\alpha2\beta}$$
$$+a_{2\beta}{}'^{(m)}\{S_{3/2}^{(r)}(Z_{1\alpha}^2)\mathbf{Z}_{1\alpha};\ S_{3/2}^{(m)}(Z_{2\beta}^2)\mathbf{Z}_{2\beta}\}_{1\alpha2\beta}]=\int S_{3/2}^{(r)}(Z_{1\alpha}^2)\mathbf{Z}_{1\alpha}\cdot\mathbf{K}_\alpha d\mathbf{p}_{1\alpha}. \tag{58}$$

The method of evaluation of the B's is identical to the procedure just outlined so we merely quote the results: for $B_{1\alpha}^{(1)}$

$$\sum_m\sum_\beta[(N_\beta-\delta_{\alpha\beta})/(N_\alpha-1)][g_0^{(2)}(\sigma_{\alpha\beta})/v_\alpha v_\beta]$$
$$\times[b_{1\alpha}^{(m)}(1)\{S_{5/2}^{(r)}(W_{1\alpha}^2)(\mathbf{W}_{1\alpha}\mathbf{W}_{1\alpha}-\tfrac{1}{3}W_{1\alpha}^2\mathbf{1});\ S_{5/2}^{(m)}(W_{1\alpha}^2)(\mathbf{W}_{1\alpha}\mathbf{W}_{1\alpha}-\tfrac{1}{3}W_{1\alpha}^2\mathbf{1})\}_{1\alpha2\beta}$$
$$+b_{2\beta}^{(m)(1)}\{S_{5/2}^{(r)}(W_{1\alpha})^2(\mathbf{W}_{1\alpha}\mathbf{W}_{1\alpha}-\tfrac{1}{3}W_{1\alpha}^2\mathbf{1});\ S_{5/2}^{(m)}(W_{2\beta}^2)(\mathbf{W}_{2\beta}\mathbf{W}_{2\beta}-\tfrac{1}{3}W_{2\beta}^2\mathbf{1}\}_{1\alpha2\beta}$$
$$+b_{1\alpha}{}'^{(m)(1)}\{S_{5/2}^{(r)}(W_{1\alpha}^2)(\mathbf{W}_{1\alpha}\mathbf{W}_{1\alpha}-\tfrac{1}{3}W_{1\alpha}^2\mathbf{1});\ S_{5/2}^{(m)}(Z_{1\alpha}^2)(\mathbf{Z}_{1\alpha}\mathbf{Z}_{1\alpha}-\tfrac{1}{3}Z_{1\alpha}^2\mathbf{1}\}_{1\alpha2\beta}$$
$$+b_{2\beta}{}'^{(m)(1)}\{S_{5/2}^{(r)}(W_{1\alpha}^2)(\mathbf{W}_{1\alpha}\mathbf{W}_{1\alpha}-\tfrac{1}{3}W_{1\alpha}^2\mathbf{1});\ S_{5/2}^{(m)}(Z_{2\beta}^2)(\mathbf{Z}_{2\beta}\mathbf{Z}_{2\beta}-\tfrac{1}{3}Z_{2\beta}^2\mathbf{1}\}_{1\alpha2\beta}]$$
$$=\int\mathbf{L}_\alpha^{(1)}:[\mathbf{W}_{1\alpha}\mathbf{W}_{1\alpha}-\tfrac{1}{3}W_{1\alpha}^2\mathbf{1}]S_{5/2}^{(r)}(W_{1\alpha}^2)d\mathbf{p}_{1\alpha} \tag{59}$$

and

$$\sum_m\sum_\beta[(N_\beta-\delta_{\alpha\beta})/(N_\alpha-1)]g_0^{(2)}(\sigma_{\alpha\beta})(1/v_\alpha v_\beta)$$
$$\times[b_{1\alpha}^{(m)(1)}\{S_{5/2}^{(r)}(Z_{1\alpha}^2)(\mathbf{Z}_{1\alpha}\mathbf{Z}_{1\alpha}-\tfrac{1}{3}Z_{1\alpha}^2\mathbf{1});\ S_{5/2}^{(m)}(W_{1\alpha}^2)(\mathbf{W}_{1\alpha}\mathbf{W}_{1\alpha}-\tfrac{1}{3}W_{1\alpha}^2\mathbf{1})\}_{1\alpha2\beta}$$
$$+b_{2\beta}^{(m)(1)}\{S_{5/2}^{(r)}(Z_{1\alpha}^2)(\mathbf{Z}_{1\alpha}\mathbf{Z}_{1\alpha}-\tfrac{1}{3}Z_{1\alpha}^2\mathbf{1});\ S_{5/2}^{(m)}(W_{2\beta}^2)(\mathbf{W}_{2\beta}\mathbf{W}_{2\beta}-\tfrac{1}{3}W_{2\beta}^2\mathbf{1})\}_{1\alpha2\beta}$$
$$+b_{1\alpha}{}'^{(m)(1)}\{S_{5/2}^{(r)}(Z_{1\alpha}^2)(\mathbf{Z}_{1\alpha}\mathbf{Z}_{1\alpha}-\tfrac{1}{3}Z_{1\alpha}^2\mathbf{1});\ S_{5/2}^{(m)}(Z_{1\alpha}^2)(\mathbf{Z}_{1\alpha}\mathbf{Z}_{1\alpha}-\tfrac{1}{3}Z_{1\alpha}^2\mathbf{1})\}_{1\alpha2\beta}$$
$$+b_{2\beta}{}'^{(m)(1)}\{S_{5/2}^{(r)}(Z_{1\alpha}^2)(\mathbf{Z}_{1\alpha}\mathbf{Z}_{1\alpha}-\tfrac{1}{3}Z_{1\alpha}^2\mathbf{1});\ S_{5/2}^{(m)}(Z_{2\beta}^2)(\mathbf{Z}_{2\beta}\mathbf{Z}_{2\beta}-\tfrac{1}{3}Z_{2\beta}^2\mathbf{1})\}_{1\alpha2\beta}]$$
$$=\int\mathbf{L}_\alpha^{(1)}:[\mathbf{Z}_{1\alpha}\mathbf{Z}_{1\alpha}-\tfrac{1}{3}Z_{1\alpha}^2\mathbf{1}]S_{5/2}^{(r)}(Z_{1\alpha}^2)d\mathbf{p}_{1\alpha}. \tag{60}$$

Similarly, the equations for $B_{1\alpha}^{(2)}$ are:

$$\sum_m\sum_\beta[(N_\beta-\delta_{\alpha\beta})/(N_\alpha-1)][g_0^{(2)}(\sigma_{\alpha\beta})/v_\alpha v_\beta][\{S_{1/2}^{(r)}(W_{1\alpha}^2);\ S_{1/2}^{(m)}(W_{1\alpha}^2)\}b_{1\alpha}^{(m)(2)}$$
$$+\{S_{1/2}^{(r)}(W_{1\alpha}^2);\ S_{1/2}^{(m)}(W_{2\beta}^2)\}b_{2\beta}^{(m)(2)}+\{S_{1/2}^{(r)}(W_{1\alpha}^2);\ S_{1/2}^{(m)}(Z_{1\alpha}^2)\}b_{1\alpha}{}'^{(m)(1)}$$
$$+\{S_{1/2}^{(r)}(W_{1\alpha}^2);\ S_{1/2}^{(m)}(Z_{2\beta}^2)\}b_{2\beta}{}'^{(m)(1)}]=\int L_\alpha^{(2)}S_{1/2}^{(r)}(W_{1\alpha}^2)d\mathbf{p}_{1\alpha} \tag{61}$$

and

$$\sum_m\sum_\beta[(N_\beta-\delta_{\alpha\beta})/(N_\alpha-1)][g_0^{(2)}(\sigma_{\alpha\beta})/v_\alpha v_\beta][\{S_{1/2}^{(r)}(Z_{1\alpha}^2);\ S_{1/2}^{(m)}(W_{1\alpha}^2)\}b_{1\alpha}^{(m)(2)}$$
$$+\{S_{1/2}^{(r)}(Z_{1\alpha}^2);\ S_{1/2}^{(m)}(W_{2\beta}^2)\}b_{2\beta}^{(m)(1)}+\{S_{1/2}^{(r)}(Z_{1\alpha}^2);\ S_{1/2}^{(m)}(Z_{1\alpha}^2)\}b_{1\alpha}{}'^{(m)(1)}$$
$$+\{S_{1/2}^{(r)}(Z_{1\alpha}^2);\ S_{1/2}^{(m)}(Z_{2\beta}^2)\}b_{2\beta}{}'^{(m)(1)}]=\int L_\alpha^{(2)}S_{1/2}^{(r)}(Z_{1\alpha}^2)d\mathbf{p}_{1\alpha}. \tag{61}$$

Once the bracket expressions have been evaluated, the perturbation solution of the transport equation is completed. The bracket expressions involving only W's are tabulated in reference 3, but those involving both W and Z must be separately evaluated.[10]

IV. ENTROPY PRODUCTION

We reserve for the following papers the explicit evaluation of the heat flux, stress tensor, and diffusion flux, and focus attention on the microscopic formulation of the entropy flux. To the approximation of considering only binary collisions, the specific entropy may be defined by[3]

$$S=-(k/\rho)\Big[x_\alpha\int \bar{f}^{(1)}(1\alpha)\,\ln \bar{f}^{(1)}(1\alpha)\,d\mathbf{p}_{1\alpha}d\mathbf{R}_{1\alpha} + x_\beta\int \bar{f}^{(1)}(2\beta)\,\ln \bar{f}^{(1)}(2\beta)\,d\mathbf{p}_{2\beta}d\mathbf{R}_{2\beta}\Big]. \quad (62)$$

Cross multiplication by $N_\alpha-1$ and subsequent division by $N=N_\alpha+N_\beta$ serves to bring Eq. (16) into the form,

$$x_\alpha \mathfrak{L}\bar{f}^{(1)}(1\alpha)=x_\alpha J[\bar{f}^{(1)}(1\alpha)\,\bar{f}^{(1)}(2\alpha)] + x_\beta J[\bar{f}^{(1)}(1\alpha)\,\bar{f}^{(1)}(2\beta)] \quad (63)$$

and similarly,

$$x_\beta \mathfrak{L}\bar{f}^{(1)}(2\beta)=x_\alpha J[\bar{f}^{(1)}(2\beta)\,\bar{f}^{(1)}(1\alpha)] + x_\beta J[\bar{f}^{(1)}(2\beta)\,\bar{f}^{(1)}(2\beta)] \quad (64)$$

where the J's are defined as

$$J(\bar{f}^{(1)}(1\alpha)\,\bar{f}^{(1)}(2\beta)) = \iiint (p_{1\alpha 2\beta}/\mu_{\alpha\beta})\,g_0^{(2)}(\sigma_{\alpha\beta})[\bar{f}^{(1)*}(1\alpha)\,\bar{f}^{(1)*}(2\beta) - \bar{f}^{(1)}(1\alpha)\,\bar{f}^{(1)}(2\beta)]\,b_{\alpha\beta}db_{\alpha\beta}d\epsilon d\mathbf{p}_{2\beta} \quad (65)$$

and the positions of molecules 1α and 2β are $\mathbf{R}_{1\alpha}$ and $\mathbf{R}_{2\beta}$ respectively. In contrast to the integral usually defined in dilute gas theory, J involves the molecules at different positions.

If Eqs. (64) and (65) are multiplied by $\ln \bar{f}^{(1)}(1\alpha)$ and $\ln \bar{f}^{(1)}(2\beta)$, respectively, and then integrated over the relevant coordinates, the time rate of change of the entropy becomes

$$\rho\mathfrak{D}_0 S - x_\alpha k[(\mathbf{p}_{1\alpha}/m)-\mathbf{u}]\int \ln \bar{f}^{(1)}(1\alpha)\,\nabla_{R_{1\alpha}}\bar{f}^{(1)}(1\alpha)\,d\mathbf{p}_{1\alpha}d\mathbf{R}_{1\alpha} - x_\beta k[(\mathbf{p}_{2\beta}/m)-\mathbf{u}]\int \ln \bar{f}^{(1)}(2\beta)\,\nabla_{R_{2\beta}}\bar{f}^{(1)}(2\beta)\,d\mathbf{p}_{2\beta}d\mathbf{R}_{2\beta} + k\int \ln \bar{f}^{(1)}(1\alpha)\{x_\alpha J[\bar{f}^{(1)}(1\alpha)\,\bar{f}^{(1)}(2\alpha)]+x_\beta J[\bar{f}^{(1)}(1\alpha)\,\bar{f}^{(1)}(2\beta)]\}d\mathbf{R}_{1\alpha}d\mathbf{p}_{1\alpha} + k\int \ln \bar{f}^{(1)}(2\beta)\{x_\alpha J[\bar{f}^{(1)}(2\beta)\,\bar{f}^{(1)}(1\alpha)]+x_\beta J[\bar{f}^{(1)}(1\beta)\,\bar{f}^{(1)}(2\beta)]\}d\mathbf{R}_{2\beta}d\mathbf{p}_{2\beta}=0 \quad (66)$$

where the operator $\mathfrak{D}_0$ is

$$\mathfrak{D}_0=(\partial/\partial t)+x_\alpha\mathbf{u}\cdot\nabla_{R_{1\alpha}}+x_\beta\mathbf{u}\cdot\nabla_{R_{2\beta}}. \quad (67)$$

Some simple transformations involving integration by parts and use of boundary conditions on $\bar{f}^{(1)}$ permit the separation of the entropy flux from the entropy production. This latter is

$$\eta=-k\Big[\int \ln \bar{f}^{(1)}(1\alpha)\{x_\alpha J[\bar{f}^{(1)}(1\alpha)\,\bar{f}^{(1)}(2\alpha)]+x_\beta J[\bar{f}^{(1)}(1\alpha)\,\bar{f}^{(1)}(2\beta)]\}d\mathbf{R}_{1\alpha}d\mathbf{p}_{1\alpha} + \int \ln \bar{f}^{(1)}(2\beta)\{x_\alpha J[\bar{f}^{(1)}(2\beta)\,\bar{f}^{(1)}(1\alpha)]+x_\alpha J[\bar{f}^{(1)}(2\beta)\,\bar{f}^{(1)}(1\beta)]\}d\mathbf{R}_{2\beta}d\mathbf{p}_{2\beta}\Big]. \quad (68)$$

Equation (68) can be reduced to simpler form when the conditions

$$\int \bar{f}_0^{(1)}(st)\,\Phi_{st}\,d\mathbf{p}_{st}=0$$
$$\int \bar{f}_0^{(1)}(st)\,\Phi_{st}[(\mathbf{p}_{st}/m_t)-\mathbf{u}]d\mathbf{p}_{st}=0$$
$$\int \bar{f}_0^{(1)}(st)\,\Phi_{st}[(\mathbf{p}_{st}/m_t)-\mathbf{u}]^2 d\mathbf{p}_{st}=0 \quad (69)$$

($s=1,2$; $t=\alpha,\beta$)

are used.

It is clear that the derivatives $\mathfrak{L}\bar{f}_0^{(1)}$ vanish when the equilibrium distribution function $\bar{f}_0^{(1)}$ is employed. Therefore,

$$x_\alpha J(\bar{f}_0^{(1)}(1\alpha)\,\bar{f}_0^{(1)}(2\alpha))+x_\beta J(\bar{f}_0^{(1)}(1\alpha)\,\bar{f}_0^{(1)}(2\beta))=0$$
$$x_\alpha J(f_0^{(1)}(2\beta)\,\bar{f}_0^{(1)}(1\alpha))+x_\beta J(\bar{f}_0^{(1)}(1\beta)\,\bar{f}_0^{(1)}(2\beta))=0. \quad (70)$$

The condition expressed in Eq. (70) makes it necessary to carry perturbation terms in the distribution function. Such a procedure must be consistent with the linearize-

[10] R. A. Harris and S. A. Rice (to be published).

tion previously used since if higher order terms are kept in Eq. (20) they would lead to second order contributions to the entropy production. The use of Eq. (18) in Eq. (68) leads to the desired form,

$$\eta=-k\left[\int \ln \bar{f}_0^{(1)}(1\alpha)[x_\alpha J'(1\alpha,2\alpha)+x_\beta J'(1\alpha,2\beta)]d\mathbf{R}_{1\alpha}d\mathbf{p}_{1\alpha}+\int \ln \bar{f}_0^{(1)}(2\beta)[x_\alpha J'(2\beta,1\alpha)+x_\beta J'(2\beta,1\beta)]d\mathbf{R}_{2\beta}d\mathbf{p}_{2\beta}\right], \tag{71}$$

where

$$J'(mn,st)=\iiint (p_{mnst}/\mu_{nt})g_0^{(2)}(\sigma_{nt})\,\bar{f}_0^{(1)}(mn)\,\bar{f}_0^{(1)}(st)[\Phi_{mn}^{*}+\Phi_{st}^{*}-\Phi_{mn}-\Phi_{st}]b_n\,db_n\,d\epsilon d\mathbf{p}_{st} \tag{72}$$

and Eq. (70) has been used to eliminate two terms. Equation (72) is useful only in the gas range since the fundamental definition, Eq. (62), is itself valid only when the deviation of $f^{(2)}$ from an uncorrelated product of the corresponding $f^{(1)}$ is small. Note that the use of Eq. (70) would give $\eta=0$ unless the perturbations to the equilibrium distribution function are retained in the collision integrals. With the perturbation functions known, and $g_0^{(2)}$ expanded as a power series in v^{-1}, Eq. (72) may be used to calculate the entropy production correct to terms of order v^{-1}.

V. DISCUSSION

There is one important case for which we can cut through the formalism of this paper to obtain immediately a first order result. Consider the case of diffusion in a binary hard sphere mixture in which all particles are of equal diameter. Since the equation of state of a hard sphere fluid depends only upon the number density of particles and the diameter of the particles,[8] $g_0^{(2)}(\sigma_{\alpha\beta})=g_0^{(2)}(\sigma_{\alpha\alpha})=g_0^{(2)}(\sigma_{\beta\beta})=g_0^{(2)}(\sigma)$. Except for the terms in the gradient of concentration and pressure, Eqs. (30) then become essentially identical with the one component case for which we previously obtained a solution.[6] From the definition of the matter flux in terms of the distribution function we are led to the leading term $\mathfrak{D}=\mathfrak{D}^0/g_0^{(2)}(\sigma)$ where $\mathfrak{D}^0$ is the dilute gas hard sphere diffusion coefficient. This result is, of course, only the leading term and not complete to order v^{-1}, since terms in the perturbation function also give rise to contributions of order v^{-1}. This result is in agreement with both the thermal conductivity and shear viscosity of a one component hard sphere fluid for which the leading terms are also $[g_0^{(2)}(\sigma)]^{-1}$ multiplied by the corresponding dilute gas coefficient.[6]

We reserve for the following paper the discussion of the entropy production and its relationship to the flux vectors. Here, we merely comment that the detailed hard sphere theory will serve as a useful check of the semiphenomenological approach to the theory of transport in mixtures introduced by Bearman and Kirkwood.[11] In this theory, the detailed calculation of the nonequilibrium distribution function is bypassed by the device of representing the frictional and thermal mean forces in the configuration space of a single molecule as linear functions of the mean velocities and temperature gradients. Bearman, Kirkwood, and Fixman[12] calculated the isothermal heat of transport in terms of equilibrium quantities and self-diffusion coefficients by generalizing the linear relationships to the configuration space of pairs of molecules, and Bearman[13] has used a similar technique to discuss the thermal conductivity of mixtures. It remains to be seen whether the theories developed reproduce properly the v^{-1} dependence for rigid spheres. Such a test may be regarded as indirect evidence for or against the assumed functional dependence of the frictional forces.

[11] R. J. Bearman and J. G. Kirkwood, J. Chem. Phys. **28**, 136 (1958).

[12] Bearman, Kirkwood, and Fixman, Advances in Chem. Phy. **1**, 1 (1959).

[13] R. J. Bearman, J. Chem. Phys. **30**, 835 (1959).

Temperature Dependence of the Chlorine Pure Quadrupole Resonance Frequency in Molecular Crystals*

H. S. GUTOWSKY AND D. W. MCCALL†

Noyes Chemical Laboratory, University of Illinois, Urbana, Illinois

(Received July 13, 1959)

The Cl^{35} pure quadrupole resonance frequency has been observed in polycrystalline CH_2Cl_2, $CHCl_3$,CCl_4, $(CH_3)_3CCl$, and CH_2CCl_2 at temperatures of 77°K and above. In all cases, the resonance frequency decreases at higher temperatures, in qualitative agreement with Bayer's theory for the torsional motions of the molecules. However, a quantitative comparison of the theory with experiment, including Livingston's results at 4 and 20°K, reveals significant discrepancies which are discussed and attributed mainly to the decrease in torsional frequencies at higher temperatures. The resonance was found to "fade out" at temperatures below the transition points in those solids, CCl_4, $(CH_3)_3CCl$, and CH_2CCl_2, where internal or molecular reorientations are known to occur. In the other compounds the resonance was observable up to the melting point. The origin of this phenomenon is discussed briefly.

I. INTRODUCTION

IT is well known[1,2] that the torsional motions of molecules produce significant changes in the nuclear pure quadrupole resonance spectra of solids. Of major concern here is the suggestion[1,3] that torsional oscillations produce the shifts to lower resonance frequencies, observed as the temperature of the sample is increased. According to this model, the shifts result from an averaging, over the molecular motions, of the electric field gradient at the nucleus observed. The amplitudes of the motions and thus the magnitudes of the shifts, with respect to what the resonance frequency would be in a stationary molecule, are greater at higher temperatures.

Most studies of the resonance frequencies have extended over only a limited range of temperatures.[2,4–7] Dean[4,5] has investigated a number of chlorobenzenes, obtaining semiquantitative agreement with the Bayer theory[3]; however, the compounds studied are rather complex and although measurements were made for relatively wide ranges of temperature, liquid nitrogen was the lower limit. Virtually all the other comparisons between theory and experiment have been qualitative in character.[2] For these reasons we undertook a more detailed study of several relatively simple molecules for which Livingston[7] has reported measurements at 4°K and/or 20°K. Thus the data on these compounds now cover their complete solid state temperature range and permit a more extensive check to be made of the Bayer theory.

In addition, two classes of molecular crystal were chosen, those having different solid phases with different dynamic states of the molecules and those having only one solid phase in which molecular motions are restricted to lattice or torsional oscillations. This choice was made with the expectation that motions of large amplitude, such as molecular or CH_3 group reorientations, would produce major effects in addition to the temperature dependent shifts in the resonance frequency predicted by the Bayer theory. This expectation was realized some time ago,[8] when it was found that the chlorine pure quadrupole resonance "faded out" at temperatures far below the melting point in those solids where molecular reorientations are known to occur. However, the resultant hope that the various phenomena might lend themselves to investigating the dynamic structure of solids was not realized until accurate measurements could be made of the pure quadrupole relaxation times. Such measurements have now been accomplished[9] and are to be described in a subsequent paper.[10] Only the initial, qualitative observations of the fade-out are reported here.

II. EXPERIMENTAL DETAILS

The spectrometer used in this work is a frequency modulated (60 cps) superregenerative oscillator of the

* Supported in part by the Office of Naval Research and by a Grant-in-Aid from E. I. du Pont de Nemours and Company.

† National Science Foundation pre-doctoral fellow; now at Bell Telephone Laboratories, Murray Hill, New Jersey.

[1] H. G. Dehmelt and H. Krüger, Z. Physik **129**, 400 (1951).

[2] T. P. Das and E. L. Hahn, *Nuclear Quadrupole Resonance Spectroscopy*, Solid State Physics, Supplement 1 (Academic Press, Inc., New York, 1958). After the completion of our work, Kushida, Benedek, and Bloembergen [Phys. Rev. **104**, (1956)] reported an extensive study of the pressure dependence of the Cu^{63} resonance frequency in Cu_2O and of the Cl^{35} frequency in $KClO_3$ and *p*-dichlorobenzene, each at three different temperatures (−77°C, room temperature, and about 90°C for Cu_2O and $KClO_3$; −77°, 0°, and 25°C for *p*-dichlorobenzene). They found that the temperature dependence includes significant contributions from the volume dependence of the "static" field gradients and vibrational amplitudes. They extended the Bayer theory to include these effects and obtained excellent agreement with their experimental results. Similar studies of the Na^{23} resonance in $NaClO_3$ and $NaBrO_3$ have been reported by H. S. Gutowsky and G. A. Williams, Phys. Rev. **105**, 464 (1957).

[3] H. Bayer, Z. Physik **130**, 227 (1951).

[4] C. Dean and R. V. Pound, J. Chem. Phys. **20**, 195 (1952).

[5] C. Dean (Ph.D. thesis, Harvard University, 1952).

[6] T. C. Wang, Phys. Rev. **99**, 566 (1955).

[7] R. Livingston, J. Chem. Phys. **20**, 1170 (1952); J. Phys. Chem. **57**, 496 (1953).

[8] D. W. McCall (Ph.D. thesis, University of Illinois, 1953), on which this paper is based.

[9] D. E. Woessner (Ph.D. thesis, University of Illinois, 1957).

[10] D. E. Woessner and H. S. Gutowsky (to be submitted to J. Chem. Phys.).

type described by Dean.[5] It was chosen because it gives good signal to noise ratios at the high power levels required by the small gyromagnetic ratios of Cl^{35} and Cl^{37} and favored by their short spin-lattice relaxation times. Circuit diagrams and operating characteristics of the apparatus are given elsewhere.[8]

The cryostat used in the temperature dependence studies consists of a wide-mouthed, 2-liter Dewar flask filled with a bath oil and having an insulating cover of balsa wood. Holes were cut in the latter so that the sample assembly, a centrifugal stirrer, and the coolant could be introduced. The sample assembly is a brass can, containing the sample, with a screw cap having a coax connector on top and the rf coil mounted underneath and immersed in the sample. The temperature measurements were by means of a copper-constantan thermocouple inserted through the top of the can and frozen into the sample.

TABLE I. Temperature dependence of the Cl^{35} pure quadrupole resonance frequency observed in some chloromethanes.[a]

CH_2Cl_2		$CHCl_3$			CCl_4	
T	ν	T	ν_a	ν_b	T	ν
°K	Mc/sec	°K	Mc/sec		°K	Mc/sec
0	36.244	0	38.508	38.508	0	41.170
4	36.243	4	38.506	38.506	20	41.139
20	36.233	20	38.490	38.486	77	40.797
77	35.991	77	38.308	38.254	113	40.554
114	35.691	116	38.128	38.026	126	40.464
121	35.642	125	38.076	37.960	136	40.370
129	35.552	137	38.014	37.880	148	40.278
139	35.419	150	37.942	37.789	152	40.250
153	35.228	165	37.838	37.688		
162	35.086	179	37.758	37.562		
174	34.895	188	37.702	37.482		
		202	37.577	37.346		

[a] The frequencies given for 4° and 20°K are taken from reference 7, and the values for 0°K were obtained by extrapolation.

Medium- and low-boiling petroleum ethers and a mixture called Michie test solvent[11] were used as bath oils. All are flammable liquids at room temperature and have freezing points of about −106, −137, and −160° C, respectively. Liquid nitrogen was used as a coolant; it was merely poured into a small tin can suspended from the Dewar cover and dipping into the bath oil. Thermal equilibrium was established within a few minutes after the coolant had boiled away; thereafter, the temperature increased at a rate convenient for our purpose, and about 6° per hour even at temperatures as low as −160°C. The sample assembly was immersed directly in liquid nitrogen for measurements at that temperature.

The resonance frequencies were measured for the polycrystalline solids with a war surplus BC-221-AN frequency meter, using oscilloscope display. The quench frequency was varied manually in order to distinguish the true resonance from resonances associated with the side band frequencies generated by the quenching circuit. The samples were reagent grade, obtained from commercial sources. The results reported here are for Cl^{35}, because of its greater signal strength; however, the Cl^{37} resonance was observed in some cases, at frequencies in accord with the known magnetogyric ratios.

[11] Available commercially from the Phillips Petroleum Company, Bartlesville, Oklahoma.

TABLE II. Temperature dependence of the Cl^{35} pure quadrupole resonance frequency observed in some methyl chloromethanes.[a]

$(CH_3)_3CCl$		CH_3CCl_3		
T	ν	T	ν_a	ν_b
°K	Mc/sec	°K	Mc/sec	
0	31.207	0	38.275	38.081
20	31.195	20	38.249	38.052
77	31.065	77	38.052	37.829
114	30.932	112	37.856	37.610
124	30.890	121	37.816	37.572
132	30.842	129	37.776	37.504
141	30.802	141	37.712	37.455
149	30.746	148	37.662	
161	30.693	159	37.592	
170	30.628			
178	30.563			

[a] The frequencies given for 20°K are taken from reference 7, and the values for 0°K were obtained by extrapolation.

III. RESULTS AND DISCUSSION

The Cl^{35} resonance frequencies measured for the chloromethanes, CH_2Cl_2, $CHCl_3$, and CCl_4, are given in Table I and those for the methyl chloroethanes, $(CH_3)_3CCl$ and CH_3CCl_3, in Table II. The melting points of the compounds are summarized in Table III along with thermal transition points and the highest temperatures at which the resonance was observed in each solid.

The Fade-Out

In only two cases, CH_2Cl_2 and $CHCl_3$, was the chlorine resonance observable in the solid up to its

TABLE III. Summary of melting points, transition temperatures and fade-out temperatures.

Compound	Melting point, °K	Transition temperature, °K	Fade-out temperature °K
CH_2Cl_2	175	...	(175)
$CHCl_3$ ν_a	210	...	(210)
$CHCl_3$ ν_b	210	...	(210)
CCl_4[a]	250	225	155
$(CH_3)_3CCl$[b]	249	219 183	183
CH_3CCl_3[b] ν_a	240	224 205	160
CH_3CCl_3[b] ν_b	240	224 205	147

[a] Hicks, Hooley, and Stephenson, J. Am. Chem. Soc. 66, 1064 (1944).
[b] Kushner, Crowe, and Smyth, J. Am. Chem. Soc. 72, 1091 (1950).

melting point. Apparently, these solids have no phase transitions; proton magnetic resonance line shape studies[12] indicate that up to their melting points any molecular reorientations in the solids occur at very low frequencies, less than about 10^4 sec^{-1}. On the other hand, the chlorine resonance lines in solid CH_3CCl_3, $(CH_3)_3CCl$, and CCl_4 were observed to fade out at temperatures considerably below their melting points. All three of these compounds have phase transitions which are associated with internal and/or molecular reorientations in the solid. In the case of *t*-butyl chloride $(CH_3)_3CCl$ the fade-out occurs at the lowest of its two known transitions, but in the other compounds, it occurs even lower. Besides the results summarized in Tables I–III, the Cl^{35} resonance of $C_6H_5CCl_3$[13] was found to disappear at 172° K even though it does not melt until 268°K. Dean has mentioned[5] similar behavior for CCl_3CCl_3 but does not comment on the cause. In the last two solids, one would expect either internal or molecular reorientations.[14]

The fade-out is in no way sharp and occurs over a considerable temperature range, about 20°, in all these compounds. Therefore, there is no particular significance to the fact that the ν_b line of CH_3CCl_3 became unobservable at a lower temperature than ν_a, because ν_b is weaker to begin with. The fact that the fade-out apparently occurs only in solids where internal or molecular rotation is either definitely known to occur or is very likely, makes it reasonable that such motions are responsible for the fade-out. The motions could decrease the relaxation times and thereby broaden the resonance beyond detection. The super-regenerative spectrometer used is not well suited for observing line widths; however, the absorption lines did not appear to broaden very much as their intensities decreased. In any event, quantitative measurements of the relaxation times T_1, T_2, and T_2^* are essential for understanding the role of internal and molecular rotation in pure quadrupole resonance. Some such measurements will be discussed in a subsequent publication.[10]

Temperature Dependence of the Resonance Frequency

The effects of torsional oscillations upon the quadrupole resonance frequency have been treated extensively elsewhere[2,3,6,8] and the details will be repeated here only to the degree necessary for our discussion. For simplicity, we assume that the field gradient at the chlorine nucleus has axial symmetry about the C—Cl bond; this is a good approximation.[2] Torsional oscillations of the molecule about an axis (x) perpendicular to the equilibrium position of the C—Cl bond reduces the pure quadrupole resonance frequency to a value ν given by

$$\nu=\nu_Q(1-\tfrac{3}{2}\langle\theta_x^2\rangle), \tag{2}$$

where ν_Q is the resonance frequency for a stationary molecule and $\langle\theta_x^2\rangle$ is the mean square angular displacement of the C—Cl bond from its equilibrium position. $\langle\theta_x^2\rangle$ is given in terms of E_t, the energy of the torsional oscillations, as[15]

$$\langle\theta_x^2\rangle=E_t/4\pi^2I_x\nu_x^2, \tag{3}$$

where ν_x is the torsional frequency and I_x the moment of inertia about the x axis of vibration. For harmonic oscillations E_t is $(v+\frac{1}{2})h\nu_t$. However, the lifetimes of torsional vibrational states are small compared with $1/(\nu_Q-\nu)$ so separate quadrupole resonance lines are not found for the various vibrational states. Instead, θ^2 must be averaged over all the states. This gives

$$\langle\theta_x^2\rangle=(h/4\pi^2I_x\nu_x)\{\tfrac{1}{2}+[\exp(h\nu_x/kT)-1]^{-1}\} \tag{4}$$

and

$$\nu_T=\nu_Q\left\{1-\frac{3h}{8\pi^2I_x\nu_x}\left[\tfrac{1}{2}+\frac{1}{\exp(h\nu_x/kT)-1}\right]\right\}, \tag{5}$$

where ν_T is the resonance frequency at T°K. The term with a coefficient of $\frac{1}{2}$ represents the effects of zero-point vibrations, so that

$$\nu_0=\nu_Q[1-(3h/16\pi^2I_x\nu_x)] \tag{6}$$

and

$$(\nu_T-\nu_0)/\nu_Q=-(3h/8\pi^2I_x\nu_x)[\exp(h\nu_x/kT)-1]^{-1}. \tag{7}$$

Torsional oscillations about a second axis (y) perpendicular to the first and also to the C—Cl bond, contribute a term identical to Eq. (7) but with the appropriate values for I_y and ν_y. If $\nu_x=\nu_y\equiv\nu_t$ and $I_x=I_y\equiv I_t$, the total temperature dependence is given by the following simple equation which includes the effects of both torsional motions

$$(\nu_T-\nu_0)/\nu_Q=-(167.4\times10^{-40})/I_t\nu_t \cdot[\exp(\nu_t/0.686T)-1]^{-1}, \tag{8}$$

where ν_t is in cm^{-1} and I_t in g cm^2.

The percentage change observed in the Cl^{35} resonance of chloroform and methylene chloride is plotted as a function of temperature in Fig. 1, and for *t*-butyl chloride, methyl chloroform and carbon tetrachloride, in Fig. 2. The Bayer theory has been tested by fitting the experimental points with curves calculated by

[12] T. C. Farrar (Ph.D. thesis, University of Illinois, 1959, to be published).

[13] D. W. McCall and H. S. Gutowsky, J. Chem. Phys. **21**, 1300 (1953).

[14] Unpublished NMR studies by C. H. Holm show that the CF_3 groups and also the ring reorient in solid p-$C_6H_4(CF_3)_2$, but at different rates. A comparison of molecular models for this compound and for $C_6H_5CCl_3$ suggests that such motions should also occur in the latter. Internal rotation does not seem likely for CCl_3CCl_3 because of the high barrier [Swick, Karle, and Karle, J. Chem. Phys. **22**, 1242 (1954)], but its molecular symmetry and the mobility of the methyl chloromethanes make it probable that the CCl_3CCl_3 molecule rotates about its C—C axis in the solid.

[15] Eyring, Walter, and Kimball, *Quantum Chemistry* (John Wiley & Sons, Inc., New York, 1949), p. 75.

means of Eq. (8). The adjustable parameters in Eq. (8), I_t and ν_t, were evaluated by using the values for $(\nu_T-\nu_0)$ observed[16] at 77° and 154°K. Upon writing Eq. (8) for these two temperatures and dividing one equation by the other, the ratio R of the frequency changes is found to depend only upon ν_t. A graph of R *vs* ν_t is the simple method used to obtain a value of ν_t from an experimental R. The resulting value for ν_t was then substituted in Eq. (8) along with the value observed for $(\nu_T-\nu_0)/\nu_0$ at 77°K and I_t calculated. Actually, one should use ν_Q in this calculation but the difference is only about 0.1% which is a negligible error in I_t, for our purposes. The values thus obtained for ν_t and I_t were then used in Eq. (8) to calculate the lines drawn in the two figures.

It is seen that the fit of the experimental data by the theoretical curves is semiquantitative at best. In all cases, the frequency decrease observed at 20°K is significantly larger, in absolute value, than that calculated. This is particularly true for $CHCl_3$ and CH_2Cl_2, for which the frequencies observed at 4°K provide a more accurate means of estimating ν_0 than is available for the other compounds. The experimental points between 77° and 154°K generally fall above the theoretical curves and the points at higher temperatures fall below. The high-temperature deviations between theory and experiment are most pronounced for $CHCl_3$ and CH_2Cl_2 for which measurements could be extended to higher temperatures than for the other compounds. In what is apparently the only other case of a molecular crystal for which a quantitative comparison has been attempted[2,5] between the Bayer theory and experiment, similar results were obtained. The experimental slope of the temperature dependence in *p*-dichlorobenzene is smaller than that predicted by the simple theory for lower temperatures (~77°K) and larger at high temperatures (~room temperature).

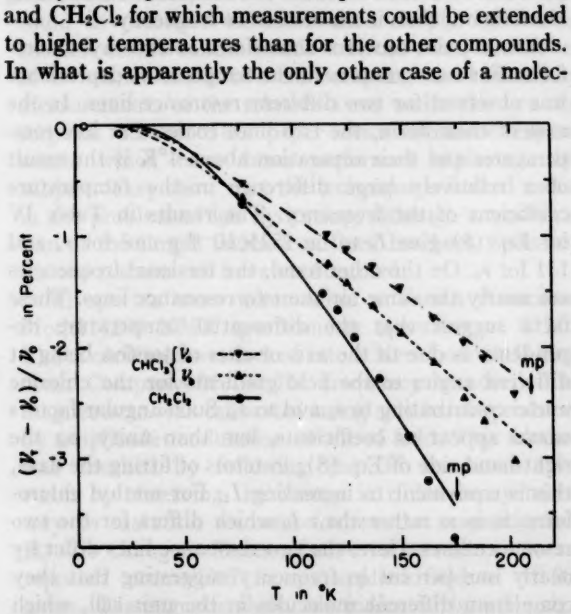

FIG. 1. The percentage change in the Cl^{35} pure quadrupole resonance frequency as a function of temperature in solid chloroform and methylene chloride. The experimental data are represented by the points. The open circles at 4° and 20°K represent the values measured for all three resonances. The curves are those calculated for the simple Bayer theory, by fitting Eq. (8) to the resonance frequencies determined experimentally for 77° and 154°K. The symbol mp indicates the melting points.

[16] The value "observed" at 154°K was taken in most instances from a smooth curve fitted visually to the experimental points obtained at adjacent temperatures.

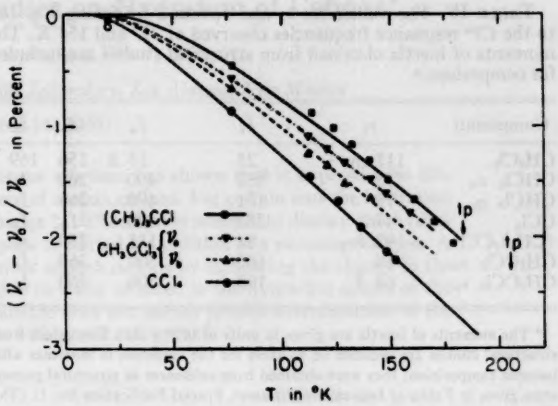

FIG. 2. The percentage change in the Cl^{35} pure quadrupole resonance frequency as a function of temperature in solid *t*-butyl chloride, methyl chloroform and carbon tetrachloride. The experimental data are represented by the points. The open circle at 20°K represents the values measured for carbon tetrachloride and for the two resonance lines of methyl chloroform. The curves are those calculated for the simple Bayer theory, by fitting Eq. (8) to the resonance frequencies determined experimentally for 77° and 154°K. The symbol tp indicates the low temperature transition points in *t*-butyl chloride and methyl chloroform; that of carbon tetrachloride is at 225°K, which is off scale.

Another aspect of the calculations which should be considered is the plausibility of the values obtained for ν_t and I_t. The latter are summarized in Table IV. The torsional frequencies are found to range from 47 to 117 cm^{-1}. This range is reasonable; however, independently obtained values of ν_t do not appear to be available for comparison. On the other hand, the moments of inertia for the free molecules are obtainable from structural studies and are included in Table IV. For each compound except CH_2Cl_2 the three actual moments of inertia are found to be greater than I_t by a factor of at least two. This indicates a serious quantitative discrepancy between experiment and the simple Bayer theory incorporated in Eq. (8). I_t occurs in the denominator of Eq. (8), so the experimental frequency shifts are larger than would be predicted from more reasonable values of I_t, using the same ν_t.

Equation (8) assumes two orthogonal torsional motions, of the same frequency, which produce displacements perpendicular to the C—Cl bond. The actual torsional motions depend upon the crystal structure and molecular symmetry and in most cases these assumptions would not be expected to apply very well. Carbon tetrachloride is simpler than the other compounds in that it is a spherical top and I_t should be independent of the axis about which the

TABLE IV. The values for ν_t and I_t found by fitting Eq. (8) to the Cl^{35} resonance frequencies observed at 77° and 154°K. The moments of inertia obtained from structural studies are included for comparison.[a]

Compound	ν_t	I_t	I_a	I_b	I_c
CH_2Cl_2	117 cm^{-1}	25	15.8	156	169
$CHCl_3$ ν_a	72	152	490	260	I_b
$CHCl_3$ ν_b	70	131	490	260	I_b
CCl_4	47	285	490	I_a	I_a
$(CH_3)_3CCl$	92.5	84	185	250	I_b
CH_3CCl_3 ν_a	68	160	500	360	I_b
CH_3CCl_3 ν_b	64.5	163	500	360	I_b

[a] The moments of inertia are given in units of 10^{-40} g cm^2. The values from structural studies are rounded off to allow for the variation in moments with isotopic composition; they were obtained from references or structural parameters given in *Tables of Interatomic Distances*, Special Publication No. 11 (The Chemical Society, London, 1958).

torsional motions happen to occur. And it is perhaps significant that Eq. (8) fits the experimental data for this compound better than for any of the others. Even so, I_t is found to be 285×10^{-40} g cm^2 which is about half the spectroscopic moment, 490×10^{-40} g cm^2. This aspect of the results makes it impossible to obtain a better fit of the observations by using the spectroscopic moment and two different torsional frequencies rather than the one term form of Eq. (8). Of course, the fit for carbon tetrachloride or any of the other compounds can be improved by using a two-term equation with the I_t's as well as the ν_t's adjustable, but the results would have little or no physical significance without other independent data.

There is another approach to carbon tetrachloride which is more revealing. Because of the molecular symmetry we would expect two identical or near identical torsional frequencies having the same I_t, and the latter should equal the spectroscopic moment. Upon using this assumption to fit Eq. (8) to the frequency shift observed at 77°K, we find a value for ν_t of 38 cm^{-1}. The theoretical curve fits the point at 20°K within experimental error. However, at temperatures above 77°K, the predicted frequency shift is too small. This could occur if ν_t were itself temperature dependent;[17] the point at 154°K would be fitted if ν_t were 36.5 cm^{-1} rather than 38 cm^{-1}. Such a change is reasonable, both in magnitude and in direction. The intermolecular potentials decrease as the crystal expands, and ν_t decreases accordingly. The experimental results for the other compounds can be explained in a similar fashion; however, some of them no doubt have two different torsional frequencies each with its characteristic I_t. In addition, the simple Bayer theory neglects anharmonicities in the potential function which would increase the frequency shifts at the higher temperatures.

It is also possible[2,8] that a continuous distribution of lattice vibrations ν_l contributes to the frequency shifts, especially at low temperatures, as in the Debye treatment of heat capacities. In order to be effective, such motions would need to be "fast enough," i.e., $\nu_l \gg (\nu_Q-\nu)$. Their effects can be calculated by taking the appropriate integral or summation of Eq. (7), as described by Kushida, Benedek, and Bloembergen.[2] We have neglected the effects of the normal, intramolecular vibrations and, as Dean has suggested,[2,5] they would contribute to the frequency change at higher temperatures. A factor probably more important than either of these two is that as much as 5 to 10% of the total field gradient may be of intermolecular origin.[2] This "intermolecular" field gradient depends upon volume, as shown by the results of Kushida *et al.*[2] on *p*-dichlorobenzene, and its contribution to $(\partial \ln\nu/\partial T)_P$ is comparable to that from the temperature dependence of the torsional frequencies. The volume and temperature effects can be separated by careful measurements of the pressure as well as the temperature dependence of the resonance frequencies.[2] Such detailed studies should improve our understanding of intermolecular forces in solids.

The Bayer theory fits the temperature dependence of the frequency observed in those compounds where the fade-out occurs as well as that observed in the other compounds. This implies that the "effective intensity" is more sensitive to the molecular motions causing the fade-out than is the resonance frequency.

A final point concerns chloroform and methyl chloroform. For each compound, the temperature dependence was observed for two different resonance lines. In the case of chloroform, the two lines coalesce at low temperatures and their separation above 4°K is the result of a relatively large difference in the temperature coefficient of the frequency. The results in Table IV for Eq. (8) give I_t to be 152×10^{-40} g cm^2 for ν_a and 131 for ν_b. On the other hand, the torsional frequencies are nearly the same for the two resonance lines. These facts suggest that the differential temperature dependence is due to the axis or axes of torsion being at different angles to the field gradients for the chlorine nuclei contributing to ν_a and to ν_b. Such angular factors would appear as coefficients, less than unity, on the right-hand side of Eq. (8); in terms of fitting the data, this is equivalent to increasing I_t. For methyl chloroform, it is ν_t rather than I_t which differs for the two resonance lines. Here, the two resonance lines differ by nearly one percent in frequency suggesting that they come from different molecules in the unit cell, which could very well have different torsional frequencies.

[17] See H. S. Gutowsky and G. A. Williams, Phys. Rev. **105**, 464 (1957) and references cited therein, particularly that of B. Dreyfus and D. Dautreppe, number 9.

IV. ACKNOWLEDGMENT

We wish to thank Mr. R. E. McClure and Mr. H. D. Hern for their valuable assistance in the development of the instrumentation. The research benefitted from many interesting and profitable exchanges of ideas and information with Dr. J. G. Powles, Dr. L. H. Meyer, and Dr. Myer Bloom.

THE JOURNAL OF CHEMICAL PHYSICS VOLUME 32, NUMBER 2 FEBRUARY, 1960

Nuclear Magnetic Resonance Studies on Hydration of Cations*

JASPER A. JACKSON, JOE F. LEMONS, AND HENRY TAUBE†

University of California, Los Alamos Scientific Laboratory, Los Alamos, New Mexico

(Received October 14, 1959)

A preliminary study of the O^{17} NMR spectra of aqueous solutions has shown that it is possible to distinguish solvent water from water in the hydration sphere of certain cations. For certain ions the hydration water of which is sufficiently nonlabile (lifetime for exchange $>10^{-4}$ sec), it is possible to display the hydration water as a separate NMR peak when the solvent peak is shifted by addition of a paramagnetic ion. A method is suggested for determining the hydration number of such cations by measuring the change in the water available to interact with the paramagnetic ions due to water retained in the hydration sphere of the cations. The enrichment level of the O^{17} at present available does not permit precise determination of the hydration number, but the results are not incompatible with reasonable values.

THE magnitude of the chemical shifts in nuclear magnetic resonance (NMR) spectra which have been reported for oxygen-17[1] led us to hope that the NMR technique would prove useful in establishing the number of water molecules which are directly bound to cations in aqueous solutions. The interaction between an Al^{+++} ion, for example, and the water in the first sphere of coordination is very great, and it seemed reasonable to suppose that this interaction would give rise to a substantial shift in NMR absorption for O^{17} in the bound water as compared to the solvent water. If this shift would occur, the coordination number of the cation could in principle be established simply by taking account of the concentration and the relative number of O^{17} nuclei in the two environments as obtained by measurements of the relative areas under the two absorption curves. This paper describes some experiments which have been performed exploring this subject. They show that the technique is indeed useful in the problem of ion hydration, although a modification of the simple method outlined has been necessary for the systems we have encountered.

All spectra were taken with a Varian Associates Model 4200 NMR spectrometer operating at 6 Mc. The rf oscillator was locked into a New London Instrument Company Model 701 frequency standard. The magnet scan was calibrated using side bands produced by amplitude modulation of the rf field. This method was checked by following the O^{17} resonance from water by observing the change in rf frequency necessary to maintain resonance when the magnetic field H_0 was changed. Shifts relative to solvent water are reported normalized to an applied field of 10 000 gauss. Diamagnetic shifts are indicated by a + sign, paramagnetic shifts by a − sign. Sample temperature was approximately 20°C.

The ion $(NH_3)_5CoOH_2^{+++}$ was chosen for initial study since, for this ion, the question of the number of water molecules directly attached to Co(III) has been settled by the isotope dilution technique,[2] and the exchange of the bound water with solvent water is known[2] to be so slow ($t_{\frac{1}{2}}\sim 28$ hr at 25°C) that there is no danger that the NMR method will be vitiated because of kinetic equivalence of the two kinds of water present. In order to develop a good signal for the bound water, the complex salt was enriched in O^{17}, using as source of this isotope a sample of water containing approximately 1.3% O^{17}.

It was found that a saturated solution of the O^{17}-enriched $(NH_3)_5CoOH_2Cl_3$ shows a well-defined peak at +1.3 gauss. It is interesting to note that this is the first reported observation of a diamagnetic shift for an O^{17} resonance separated from the solvent resonance, although a diamagnetic shift for the solvent peak has been reported by Shulman.[3] The position of absorption by H_2O^{17} in the solvent is not noticeably affected by the complex salt. When F^- rather than Cl^- is the anion, the solubility of the complex cation is much greater. Figure 1 presents the trace[4] obtained with 1.2*M* $(NH_3)_5CoOH_2F_3$ as the solute. The absorption for the bound water in this salt appears at the same position as for the chloride. When enough alkali is added to make the solution basic, a proton is lost from the bound water. The O^{17} in $(NH_3)_5CoOH^{++}$ gives an absorption at +1.6 gauss, the band being somewhat broadened upon the removal of the proton.

An observation which is significant for the experiments to be described later was first made with a solution of $(NH_3)_5CoOH_2Cl_3$. As reported by Shulman,[3,5] paramagnetic ions can bring about substantial changes in the value of the magnetic field strength at which certain other nuclei in solution absorb. The shifts for O^{17} in water brought about by Co^{++} are quite large. Thus when 0.2*M* $Co(ClO_4)_2$ is present in solution, the

* This research was performed at the Los Alamos Scientific Laboratory under the auspices of the U. S. Atomic Energy Commission.

† Permanent address: Department of Chemistry, University of Chicago.

[1] Weaver, Tolbert, and LaForce, J. Chem. Phys. **23**, 1956 (1955).

[2] A. C. Rutenberg and H. Taube, J. Chem. Phys. **20**, 825 (1952).

[3] R. G. Shulman and B. J. Wyluda, J. Chem. Phys. **30**, 335 (1959).

[4] All traces show the derivative of the dispersion curve.

[5] R. G. Shulman, J. Chem. Phys. **29**, 945 (1958).

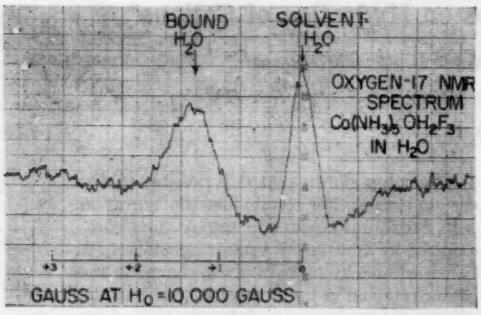

FIG. 1. 1.2*M* $(NH_3)_5CoOH_2F_3$ enriched in O^{17}, dissolved in ordinary water.

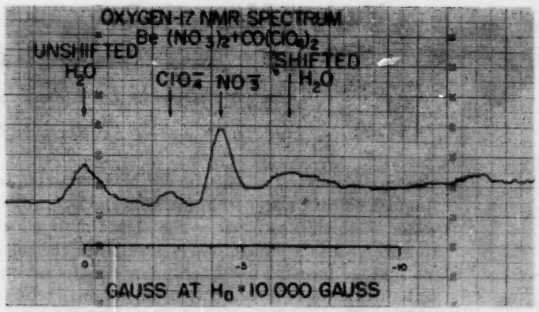

FIG. 3. Composition of solution: 2*M* $Be(NO_3)_2$, 1.4*M* HNO_3, 0.30*M* $Co(ClO_4)_2$.

absorption for O^{17} in solvent water is shifted to -3.3 gauss. However, Co^{++} causes no detectable shift in the peak position for the water bound to Co(III) in the ion $(NH_3)_5CoOH_2^{+++}$, although it does cause a slight broadening of the absorption band. The difference in the response of the two kinds of water to the presence of Co^{++} probably lies in this: the shift in the solvent comes about because of the large number of Co^{++}—OH_2 bonds which are formed (presumably 6 for each Co^{++}) and the rapid exchange between H_2O bonded to Co^{++} and H_2O in the solvent. But it is entirely likely that very few of the H_2O molecules in $(NH_3)_5CoOH_2^{+++}$ are bonded to Co^{++}. That is, species such as

$$\left[(NH_3)_5CoO\overset{H}{\underset{H}{}}Co(H_2O)_n\right]^{6+}$$

are at very low concentration relative to

$$(NH_3)_5CoOH_2^{+++},$$

so that no significant contribution is made by the Co^{++} to the average field which the Co(III)-water experiences. It is, however, interesting that the binuclear species mentioned above can be formed, a conclusion which is indicated[6] by the broadening of the Co(III)-water absorption caused by Co^{++}.

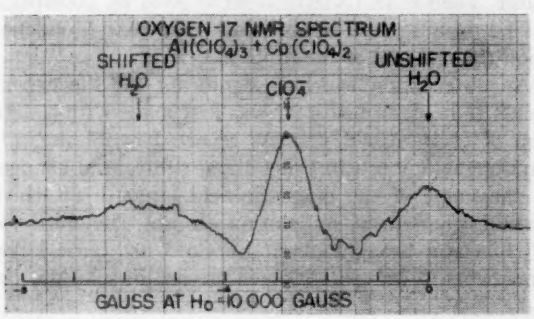

FIG. 2. Composition of solution: 1.6*M* $Al(ClO_4)_3$, 0.5*M* $HClO_4$, 0.24*M* $Co(ClO_4)_2$.

[6] R. E. Connick and R. E. Poulson, J. Chem. Phys. **30**, 759 (1959).

Next, measurements of the NMR absorption of O^{17} were made with aqueous solutions of H^+, Li^+, Be^{++}, Mg^{++}, Ba^{++}, Sn^{++}, Hg^{++}, Ga^{+++}, Bi^{+++}, as perchlorate or nitrate salts. In order to increase the signal-to-noise ratio, the solutions were made up in D_2O which was enriched in O^{17} by a factor of *ca* 2.6 times that of normal water. The cation concentrations were in the range of 2–4*M*. Perchloric or nitric acid was always present in sufficient quantity to suppress the formation of hydrolyzed and condensed species. In each solution, a single absorption band of O^{17} for the solvent and for the oxy-anion are clearly observable. No new peaks are observed, nor is there a detectable change in the position of absorption by O^{17} in solvent water. If a new peak were developed by H_2O bound to Al^{+++}, for example, it should have been clearly observable (thus, upon taking account of the coordination number of Al^{+++}, assumed as 6, and the enrichment level of O^{17} in the bound water, an even stronger signal than for oxygen in the oxy-anion, which is of normal isotopic composition, would have been expected) unless the absorption is masked by that of O^{17} in the solvent, or unless it is so greatly broadened as to escape detection.

By making use of the effects of the kind demonstrated for Co^{++} added to an aqueous solution of $(NH_3)_5CoOH_2^{+++}$, we have been able to distinguish the NMR absorption of O^{17} in hydrate water from that of solvent water at least for certain of the cations referred to in the preceding paragraph. Figure 2 shows a trace which was obtained using a solution containing

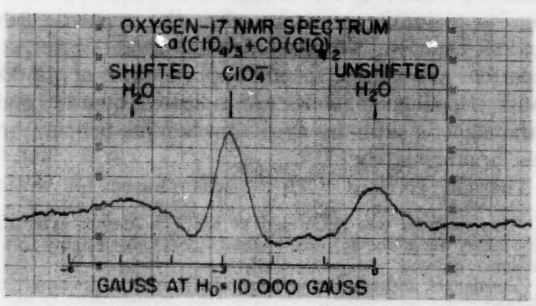

FIG. 4. Composition of solution: 1.8*M* $Ga(ClO_4)_3$, 1*M* $HClO_4$, 0.20*M* $Co(ClO_4)_2$.

Al^{+++}, H^+, and Co^{++}. The absorption by O^{17} in the bulk solvent is shifted -5.7 gauss from the normal position by Co^{++}. Residual absorption at the normal position of H_2O is left, and this we ascribe to the H_2O bound to Al^{+++}. Fe^{++} added to a solution containing Al^{+++} gave essentially the same picture. Traces for solutions containing Be^{++}, H^+, and Co^{++} and containing Ga^{+++}, H^+, and Co^{++} are reproduced in Figs. 3 and 4, respectively. Here also residual absorption at the normal water position as well as shifted solvent water is observed.

Figure 5 shows the trace for a solution containing Mg^{++}, H^+, and Co^{++}. This trace is typical of the remainder of the ions studied. In these cases no residual peak is observed at the unshifted H_2O position.

From the observation that separate hydration peaks are observed for Be^{++}, Al^{+++}, and Ga^{+++}, but not for Mg^{++}, Sn^{++}, Ba^{++}, Hg^{++}, and Bi^{+++}, we conclude from the theory of Gutowsky *et al.*[7] that $t_{\frac{1}{2}}$ for the exchange of water between solvent and hydration shell for Be^{++}, Al^{+++}, and Ga^{+++} exceeds *ca* 10^{-4} sec, and for the others, it is less than *ca* 10^{-4} sec. This measurement for Al^{+++} is compatible with previous independent experiments[8] using the isotopic dilution technique which have shown that $t_{\frac{1}{2}}$ for $Al(H_2O)_6^{+++}$—H_2O exchange in fact exceeds 0.05 sec.

While the traces serve to demonstrate the presence of relatively nonlabile cation-water bonds, the sensitivity of the method at the present level of enrichment of O^{17} is not great enough to decide on the coordination numbers for Be^{++}, Al^{+++}, and Ga^{+++}. The strength of the signals obtained for these ions, on taking account of the line-width, do appear to be compatible with reasonable coordination numbers for these ions (i.e., as 4 for Be^{++} and 6 for Al^{+++} and Ga^{+++}).

It may be possible to determine the amount of water retained by ions with relatively nonlabile hydration water such as Al^{+++} and Be^{++} in another way. Within the accuracy of measurement (3%) the error being due to the broadening of the solvent resonance line by the Co^{++},[6] the shift in the water absorption produced by Co^{++} in a perchlorate solution has been found to be a linear function of the Co^{++} concentration. Thus, if some of the water is held back by a cation such as Al^{+++}, the rest of the water in the solution will come in contact with a Co^{++} more often, thus giving a greater apparent molal shift for the solvent water.

[7] H. S. Gutowsky and C. L. Holm, J. Chem. Phys. **25**, 1228 (1956); H. S. Gutowsky and A. Saika, J. Chem. Phys. **21**, 1588 (1953); Gutowsky, McCall, and Slichter, J. Chem. Phys. **21**, 279 (1953).

[8] H. W. Baldwin and H. Taube (in preparation for publication).

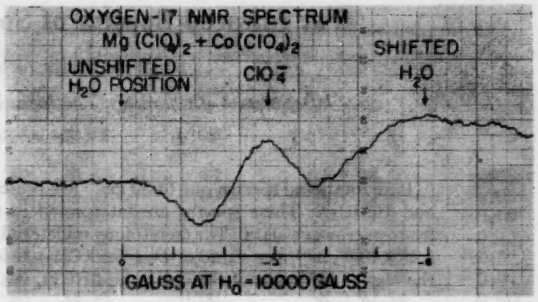

FIG. 5. Composition of solution: 1.8*M* $Mg(ClO_4)_2$, 0.2*M* $HClO_4$, 0.30*M* $Co(ClO_4)_2$.

In order to test this technique, the molal shift for solutions containing only $Co(ClO_4)_2$ was compared with that for solutions containing other cations in addition to the Co^{++} ion. Within the limit mentioned, no change was observed in the molal shift of the solvent water in solutions containing, in addition to Co^{++}, $Ba(ClO_4)_2$ or $Mg(ClO_4)_2$ at the 2 or 3*M* level. This tends to confirm that the exchange of the hydrate water with solvent is so rapid that they are equivalent as far as the present technique is concerned. It also shows that there is no detectable salt effect. For Al^{+++}, Be^{++}, and Ga^{+++} solutions, however, the apparent molal shift for Co^{++} is greater than for Mg^{++} and Ba^{++} and indicates that the former ions do retain water which is not averaged in with the solvent. At the present O^{17} enrichment level the precision of measurements of the shifts is not sufficiently high to use the phenomenon as a means a means of determining the amount of water withheld from the bulk solvent by the Al^{+++} ions, for example, and thus determining the hydration number for these less labile ions. It is obvious that a condition for success of the counting procedure suggested is that the paramagnetic ion retains the same coordination number to water over the whole concentration range.

It is encouraging that the NMR technique has proved useful in distinguishing water of hydration from solvent water. It is hoped that the use of water more highly enriched in O^{17} will make it possible to determine the coordination number for hydrated ions either by the method of relative areas under the absorption curves or by the method of effective molal shift of solvent water.

ACKNOWLEDGMENTS

The authors wish to thank Dr. T. W. Newton for his helpful advice and valuable discussions concerning this work.

Far Infrared Spectra of Some Symmetric Top Molecules*

DEAN W. ROBINSON AND DONALD A. MCQUARRIE

Department of Chemistry, The Johns Hopkins University, Baltimore 18, Maryland

(Received September 21, 1959)

Pure rotational spectra out to 30 cm^{-1} are presented of the gaseous molecules CH_3CN, CH_3CCH, HCF_3, and $(CH_3)_3N$. These spectra are interpreted in view of the rotational constants previously determined from microwave data. The heretofore undetermined value of D_J for CH_3CN has been estimated to be 1.45×10^{-7} cm^{-1}, the value of D_{JK} for $(CH_3)_3N$ is shown to be positive, and the intensity distribution in the high-J subbands of the oblate top, HCF_3, has been estimated to have its center at $K=17$.

INTRODUCTION

OF the long list of gaseous molecules that have been studied by microwave techniques, only a few have rotational constants large enough to yield well-resolved pure rotational spectra by optical methods. Although the transitions between states of high rotational quantum numbers show the largest effects of centrifugal distortion, these transitions in small molecules are for the most part out of the range of microwave spectrometers and so can only be observed using some sort of optical spectroscopy. Unfortunately the wave number resolution attained by optical instruments is at present so far inferior to that easily available to microwave investigators that the latter obtain far better distortion constants from observation of the first few transitions than can be evaluated by optical techniques through observations of transitions between quantum levels in the 50's and 60's.

As for symmetric top molecules, no one has resolved with grating spectrometers any of the subband fine structure arising from centrifugal distortion due to rotation about the figure axis, nor have satellites been resolved unquestionably attributable to molecule in excited vibrational states.* The best that has been done[1] is the fitting of the centers of the subbands to a formula of the linear molecule type,

$$\nu=2BJ'-g(J')^3, \qquad (1)$$

in which B is an apparent rotational constant, g an apparent centrifugal distortion constant, and J' the upper state rotational quantum number. The constancy of B assumes that the center of every subband coincides with the same K in the formula,

$$\nu=2(B_0-D_{JK}K^2)J'-4D_J(J')^3, \qquad (2)$$

so that $B=B_0-D_{JK}K^2$ for all subbands measured. If this were true, then g could be identified with $4D_J$ as has been done previously.[1c,d]

For high J's, over a limited range of J, the fixing of the value of K at the subband centers is probably all right, especially for prolate tops, making determinable both B and D_J.[1c,1d] On the other hand, Palik and Rao were able to fit their excellent methyl halide spectra to within experimental error by a formula, $\nu=2B_0J'-g(J')^3$. Notice that the B_0 here is the microwave B_0 so that their g does not equal $4D_J$, as it could only if the line $K=0$ fell in the middle of every unresolved subband. Actually the apparent center of a subband probably corresponds fairly closely to the maximally populated K level, with some correction for subband asymmetry. This for the methyl halides would seem, from Fig. 2 of reference 1b, to fall between $K=2$ and $K=5$. Palik and Rao state that for $J>20$, the center of gravity lies near $K=6$, 7 or 8, but this estimate was presumably made from measured frequencies rather than from the appearance of their Fig. 2. Although it seems a bit high, the $K=7$ line is, for methyl fluoride, only 0.02 cm^{-1} below the maximally populated $K=3$ due to the crowding of lines at low K's. In the case of an oblate rotor, as is discussed below, where the most highly populated states are those of high K, the choice of the K at the subband centers is more difficult and more critical.

The present paper reports some measurements on four symmetric rotors, two prolate and two oblate, and an interpretation of these in terms of microwave rotational constants. It is clear that such studies cannot compete with microwave spectroscopy for yielding information about these molecules. Nevertheless the spectra are not without interest to spectroscopists as examples of the performance of a new instrument[2] at long wavelengths; and two numerical estimates have been made which must await future verification.

EXPERIMENTAL

Spectra were obtained on an $f/4$, 1 m, vacuum Fastie-Ebert spectrometer[2] of gaseous samples of methyl

* This research was supported by the U. S. Air Force under Contract No. AF 49(638)468, monitored by the Air Force Office of Scientific Research.

† Although Stroup, Oetjen, and Bell (see reference 1d) provisionally assigned lines in the PH_3 spectrum to vibrationally excited molecules, the change in B on vibrational excitation seems extraordinarily large and a Boltzmann factor of about 0.01 for a state at 1000 cm^{-1} seems inconsistent with their exhibited spectrum. G. A. Vanasse and E. V. Loewenstein have interferometrically resolved both "K structure" and lines due to vibrationally excited states in the pure rotation spectrum of NH_3. This was shown at the spring meeting of the Optical Society of America, 1959.

[1] a. N. Wright and H. M. Randall, Phys. Rev. **44**, 391 (1933); b. E. D. Palik and K. N. Rao, J. Chem. Phys. **26**, 1401 (1957); c. R. E. Stroup and R. A. Oetjen, J. Chem. Phys. **21**, 2092 (1953); d. Stroup, Oetjen, and Bell, J. Opt. Soc. Am. **43**, 1096 (1953).

[2] D. W. Robinson, J. Opt. Soc. Am. **49**, 966 (1959).

cyanide, CH_3CN, methylacetylene, CH_3CCH, fluoroform, HCF_3, and trimethylamine, $(CH_3)_3N$. These were observed in the region 30 to 50 cm^{-1} using the first order of a University of Michigan 20° echelette grating with a groove spacing of 27.8 cm^{-1}. The gases were obtained from the Matheson Company and the methyl cyanide from Eastman. All were nominally dried with appropriate agents. The gas cell was 15 cm long with the beam making two passes through; windows were 1/8-in. polyethylene. Filtering of unwanted higher order radiation from the thoria-coated mercury lamp source was accomplished by reflection from a 60° grating ruled with a spacing of about 80 cm^{-1}, one reflection from an aluminum flat ground with 80-mesh emery, passage through one or two thicknesses of black paper taken from a box of Eastman Kodak photographic plates, and the 0.5-mm crystalline quartz detector window. The latter was made 7/32 in. in diameter to accommodate the reduced and transformed image of the slits. These were about 6 mm wide corresponding to spectral slit widths of roughly 0.2 cm^{-1}.

The spectral region involved was calibrated by observation of the spectra of N_2O and CH_3Br, their absorptions having been calculated from microwave data.[3] The known wavelengths were fit by least squares to a linear function of the sin of the measured grating angle. A calibration curve was then constructed from this function. The accuracy of the calibration is believed to be good to 0.02 cm^{-1}; that is, a sharp, easily measured line or subband should have that certainty.

The long wavelength limit of 29.7 cm^{-1} of our spectrometer with the 27.8 cm^{-1} grating permits observation of only the high-J transitions, well above the region of maximum thermal population of J states for the molecules presented.

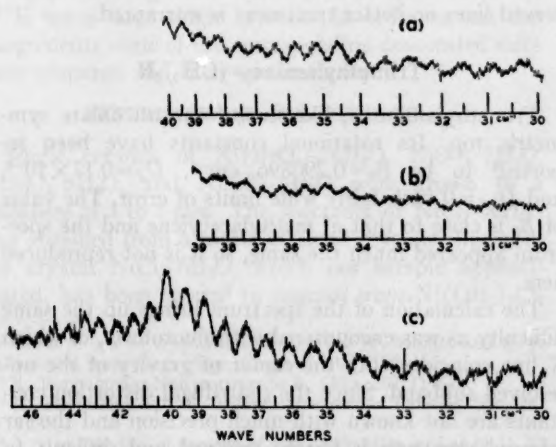

FIG. 1. Far infrared spectra of (a) methyl cyanide, (b) methylacetylene, and (c) fluoroform. Absorption is downward.

[3] Orville-Thomas, Cox, and Gordy, J. Chem. Phys. **22**, 1718 (1954); S. J. Tetenbaum, Phys. Rev. **88**, 772 (1952).

TABLE I. The observed spectrum of methyl cyanide.

J''	ν_{obs}	$(\nu_{calc}-\nu_{obs})$	J''	ν_{obs}	$(\nu_{calc}-\nu_{obs})$
48	29.91 cm^{-1}	0.08 cm^{-1}	61	37.84	0.06
49	30.63	−0.03	62	38.56	−0.05
50	31.21	0.00	63	39.10	0.01
51	31.89	−0.07	64	39.72	0.00
52	32.42	0.01	65	40.45	−0.13
53	33.06	−0.02	66	40.95	−0.02
54	33.67	−0.02	67	41.58	−0.04
55	34.25	0.00	68	42.14	0.00
56	34.88	−0.02	69	42.68	0.06
57	35.48	−0.01	70	43.33	0.02
58	36.09	−0.01	71	43.96	0.00
59	36.62	0.06			
60	37.22	0.07			

DISCUSSION OF SPECTRA

Methyl Cyanide—CH_3CN

The portion of the pure rotation band of methyl cyanide between 29.7 cm^{-1} and 39.2 cm^{-1} is pictured in Fig. 1(a). Methyl cyanide is a prolate top, like the methyl halides, with its larger moment of inertia falling between those of methyl bromide and methyl iodide. It has been studied in the microwave region[4] as have all of its deuterated analogs,[5] nevertheless, to our knowledge the value of D_J has not been reported.

Although the spectra obtained of this molecule are not sharp enough to warrant a definitive calculation of D_J, use of the microwave $D_{JK}=5.94\times10^{-6}$ cm^{-1} and $B_0=0.306839$ cm^{-1} permit[4] D_J to be estimated. As for the choice of K at the subband centers, this is relatively easy. The distribution of molecules in the high-J levels among the various K states for this prolate top is analogous to that for the methyl halides.[1b] Since the most highly populated K states are crowded together at low values of K, it seems certain that the choice of $K=4$ could not introduce an error of more than about 0.1 cm^{-1} if used for the center of gravity of the subbands. These values have been used in Eq. (1) with the result that $D_J=1.45\pm0.3\times10^{-7}$ cm^{-1} best fits the observed data. It is of some support that Kratzer's formula[6] which predicts the D_J's for the methyl halides so well[2a] yields a value of $D_J=1.37\times10^{-7}$ cm^{-1} for methyl cyanide.

The frequencies of the subbands from $J''=48$ to 71 have been calculated from Eq. (2) and the preceding numbers. The observed subbands, averaged from four or five spectra, and the differences from these calculated positions are listed in Table I.

Methylacetylene—CH_3CCH

Methylacetylene is isoelectronic with methyl cyanide but, because of the different disposition of one proton,

[4] Kessler, Ring, Trambarulo, and Gordy, Phys. Rev. **79**, 54 (1950).

[5] Thomas, Sharrard, and Sheridan, Trans. Faraday Soc. **51**, 619 (1955).

[6] A. Kratzer, Z. Physik **3**, 289 (1920).

TABLE II. Observed spectrum of methylacetylene.

J''	ν_{obs}	$(\nu_{calc}-\nu_{obs})$	J''	ν_{obs}	$(\nu_{calc}-\nu_{obs})$
53	30.75	−0.03	59	34.07	0.04
54	31.28	0.00	60	34.67	0.01
55	31.91	−0.06	61	35.26	−0.02
56	32.40	0.01	62	35.87	−0.06
57	33.01	−0.03	63	36.48	−0.11
58	33.54	0.01	64	37.01	−0.07

has a much smaller electric dipole moment as well as a smaller B_0. These effects resulted in a rather poor spectrum as seen in Fig. 1(b). This naturally was difficult to measure.

All of the rotational constants have been reported,[7] namely, $B_0=0.285059$ cm^{-1}, $D_{JK}=5.43\times10^{-6}$ cm^{-1}, and $D_J=0.987\times10^{-7}$ cm^{-1}. These were used as well as $K=4$ to compute the apparent centers of the subbands for $J''=52$ to 64. The best averages of observed absorptions of several spectra are listed in Table II as are the deviations of observed from calculated values. This molecule clearly taxes the ability of the spectrometer to resolve closely spaced lines in this region.

Fluoroform—HCF_3

The spectrum of fluoroform, shown in Fig. 1(c) is the clearest and most easily measured of the four studied. However, its calculation presents a problem not encountered with the prolate tops. All of the rotational constants have been reported,[7] but it is not clear what values of K fall in the centers of gravity of the unresolved subbands. Being an oblate top the term $\exp[-(A-B)K^2/kT]$ in the expression for the thermal population of energy levels increases with increasing K so that the high-K states in a given subband are the most highly populated. Since these are the states that are the most widely spaced by the term $2D_{JK}K^2$ in Eq. (2), the bulk of the intensity of an unresolved subband does not crowd around the origin of the subband. Thus some higher K must replace the $K=4$ used above, and due to the wide spacing of high-K levels, the choice of K is much more critical than was the choice of some K near the subband origin.

TABLE III. Observed spectrum of fluoroform.

J''	ν_{obs}	$(\nu_{calc}-\nu_{obs})$	J''	ν_{obs}	$(\nu_{calc}-\nu_{obs})$
43	30.19	0.08	56	39.08	0.01
44	30.94	0.01	57	39.77	0.00
45	31.61	0.02	58	40.52	−0.08
46	32.26	0.05	59	41.13	−0.01
47	32.99	0.00	60	41.82	−0.03
48	33.67	0.00	61	42.44	0.04
49	34.34	0.01	62	43.11	0.03
50	35.03	0.00	63	43.91	−0.10
51	35.74	−0.03	64	44.57	−0.09
52	36.38	0.01	65	45.26	−0.10
53	37.06	0.00	66	45.86	−0.03
54	37.75	−0.01	67	46.58	−0.08
55	38.41	0.01			

For $J''=55$, a subband near the middle of our observed spectrum, the most intense line would be that for molecules in the state $K=54$ ($K\leq J$ and K's divisible by 3 have a spin statistical weight of twice those not divisible by 3). By the time K fell to 45, the exponential would have dropped to about half this value. On the other hand, at these high K's the spacing of lines going as K^2 would be very large. In order to fit the observed frequencies it was necessary to take the line $K=17$ as the center of gravity of the unresolved subbands. This was determined empirically from the most easily measured subbands and held constant for the calculation of all. With this and the microwave constants[7] $B_0=0.345200$ cm^{-1}, $D_{JK}=-0.602\times10^{-6}$ cm^{-1}, and $D_J=3.77\times10^{-7}$ cm^{-1}, the spectrum was calculated. The observed subband centers and differences from the calculated values are listed in Table III. The negative differences near the end of the table may reflect the error of holding $K=17$, but for these difficultly observed lines no better treatment is warranted.

TABLE IV. Observed spectrum of trimethylamine.

J''	ν_{obs}	$(\nu_{calc}-\nu_{obs})$	J''	ν_{obs}	$(\nu_{calc}-\nu_{obs})$
51	29.96	0.12	60	35.23	0.02
52	30.67	−0.01	61	35.88	0.06
53	31.20	0.03	62	36.51	−0.11
54	31.86	−0.05	63	36.99	−0.03
55	32.34	0.04	64	37.68	−0.15
56	32.94	0.01	65	38.18	−0.07
57	33.50	0.02	66	38.70	−0.02
58	34.06	0.04	67	39.26	−0.01
59	34.69	−0.02	68	39.87	−0.04

Trimethylamine—$(CH_3)_3N$

Trimethylamine is, like fluoroform, an oblate symmetric top. Its rotational constants have been reported[8] to be $B_0=0.290896$ cm^{-1}, $D_J=0.17\times10^{-6}$, and $D_{JK}=0$ with fairly wide limits of error. The value of B_0 is close to that of methylacetylene and the spectrum appeared much the same, so it is not reproduced here.

The calculation of the spectrum brings up the same difficulty as was encountered with fluoroform, of which K line coincides with the center of gravity of the unresolved subband. Since the centrifugal distortion constants are not known with much precision and the far infrared spectrum is barely resolved and difficult to measure, no calculation of this central K can be made. It is clearly seen, however, that unlike fluoroform, trimethylamine has a positive D_{JK}. The quantity $D_{JK}K^2$

[7] C. A. Burrus and W. Gordy, J. Chem. Phys. **26**, 391 (1957).

[8] D. R. Lide and D. E. Mann, J. Chem. Phys. **28**, 572 (1958).

must be taken to be about 1.5×10^{-3} cm^{-1} in order to fit the observed spectrum. This calculation has, of course, used the B_0 and D_J given above and would be very sensitive to variation of D_J out to its limits of error. Nevertheless, B_0 and D_J would both have to be stretched somewhat beyond their limits in order to make D_{JK} negative.

By using the afore-determined $D_{JK}K^2$, the spectrum has been calculated and is compared with that observed in Table IV.

THE JOURNAL OF CHEMICAL PHYSICS VOLUME 32, NUMBER 2 FEBRUARY, 1960

Simultaneous Electronic and Vibrational Transitions in the Spectra of Hydrated Nickel(II) Ion

T. S. Piper and Noretta Koertge

William Albert Noyes Laboratory of Chemistry, University of Illinois, Urbana, Illinois

(Received October 16, 1959)

A series of weak bands at about 19 000 cm^{-1} was found in the visible spectra of the hydrated nickel(II) ion in several crystals. These bands are assigned to simultaneous electronic and vibrational transitions involving the H—O stretching vibration. This assignment was confirmed by observation of an isotopic shift upon deuteration.

THE optical spectra of the ion $Ni(OH_2)_6^{++}$ in crystals and solutions have been investigated repeatedly and interpreted in terms of the crystal field theory.[1–5] The broad bands with $f\sim10^{-4}$ have been assigned to transitions from the ground state $^3A_{2g}(^3F)$ to the excited states $^3T_{2g}(^3F)$, $^3T_{1g}(^3F)$, and $^3T_{1g}(^3P)$ which arise from the configuration $3d^8$ perturbed by an octahedral field. The weak bands or lines have been assigned as transitions to singlet excited states. We report here an investigation of a series of weak bands in the spectra of several hydrated nickel salts; these bands have for the most part escaped detection in previous investigations. The spectra were taken at 77°K using large single crystals. In order to test the assignments some of the corresponding deuterated salts were prepared and their spectra analyzed.

EXPERIMENTAL AND RESULTS

Single crystals of $Ni(BrO_3)_2\cdot6H_2O$, $NiSO_4\cdot7H_2O$, $NiSeO_4\cdot6H_2O$, and $NiSiF_6\cdot6H_2O$ were grown to a thickness of 3 to 5 mm. The spectrum of $NiCl_2\cdot XH_2O$ was obtained from a matte of small crystals. Recently the crystal $NiCl_2\cdot6H_2O$, which our sample approximated, has been shown[6] to contain *trans*-$Ni(OH_2)_4Cl_2$ rather than the hexaquo ion. The deuterated bromate and selenate were prepared by repeated evaporation of the salts with D_2O in vacuum. The isotopic purity of crystals obtained was about 94 atom percent deuterium. Some poor single crystals of the bromate were grown, but a matte of the selenate was used.

The spectra were taken with a Cary double beam recording spectrophotometer. The wave numbers of the bands are accurate to about 10 cm^{-1}. The crystals were mounted in an air-filled cell sealed in a Dewar with optical windows. Cooling of the crystals to 77°K was assured by placing the crystals in contact with a pool of liquid nitrogen.

Figure 1 represents part of the visible spectrum of $Ni(BrO_3)_2\cdot6H_2O$ at 77°K. The band assigned to $^3A_{2g}\rightarrow{}^3T_{1g}$ may be seen to be partially resolved. The wave numbers of the four sharp peaks which occur in pairs are 15 674, 15 813, 16 167, and 16 287 cm^{-1}. These peaks were not significantly shifted upon deuteration. The series of weak bands which appear on the high energy side of this band are depicted in Fig. 2 together with analogous bands of the other crystals. Only the most intense of these bands were observed in the spectra of the deuterated salts because of scattering by the poorly formed crystals.

From the spectra of the salts which gave well formed crystals, the half-widths and extinction coefficients of the most prominent of the weak bands were measured. These data together with the calculated oscillator strengths are collected in Table I. The oscillator strengths of the other members of the series were difficult to obtain since the bands were considerably more diffuse. Their oscillator strengths were estimated at 10^{-8} to 10^{-9}.

[1] For a review of crystal field theory see W. Moffitt and C. J. Ballhausen, Ann. Rev. Phys. Chem. **7**, 107 (1956).
[2] R. Pappalardo, Nuovo cimento **6**, (10), 392 (1957).
[3] H. Hartmann and H. Müller, Discussions Faraday Soc. **26**, 49 (1958).
[4] A recent review of spectra of ions in crystals is that of D. S. McClure, *Solid State Physics* (Academic Press, Inc., New York, 1959), Vol. 9, p. 400.
[5] Calculations of the levels which arise from $3d^8$ in an octahedral field with inclusion of spin-orbit coupling are given by A. D. Liehr and C. J. Ballhausen, Ann. Phys. **6**, 134 (1959).
[6] Mizuno, Ukei, and Sugawara, J. Phys. Soc. Japan **14**, 383 (1959).

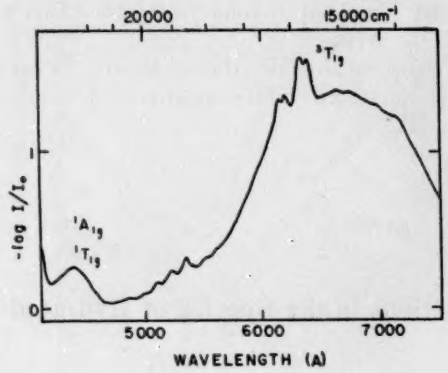

FIG. 1. Visible spectrum of $Ni(BrO_3)_2 \cdot 6H_2O$ at 77°K.

The H—O stretching frequency of $Ni(BrO_3)_2 \cdot 6H_2O$ was observed in the infrared spectrum at 3250 cm^{-1} with a band half-width of 520 cm^{-1}. After deuteration the band was shifted to 2440 cm^{-1}. The analogous band of the selenate was found to consist of two peaks at 3400 and 3240 cm^{-1} with an over-all half-width of 460 cm^{-1}. Deuteration shifted these peaks to 2520 and 2380 cm^{-1}, respectively.

DISCUSSION

Figure 2 indicates that the weak bands in the visible spectra of the hydrated nickel bromate and selenate shift on the average by 790 and 890 cm^{-1}, respectively, to lower wave numbers upon deuteration. These shifts may be compared to those of 810 and 870 cm^{-1}, respectively, observed in the infrared. The isotope effect rules out any assignment of the weak bands as pure electronic transitions to singlet levels.[7] Referring to the spectrum of the bromate it may be seen that the weak bands have an over-all width similar to that of the intense band which occurs some 3000 cm^{-1} lower in energy; furthermore, the spacing of the pair of doublets on the intense band corresponds to that of the weak bands. Therefore, we assign the weak bands to transitions to the electronic level $^3T_{1g}$ with simultaneous excitation of the H—O stretching mode.

The origin of the splittings in the series of weak bands must be sought in the nature of the intense spin-allowed bands. These bands are thought to be envelopes of a series of vibronic transitions. The electronic wave functions of the free ion perturbed by an octahedral field are augmented with odd atomic and molecular orbital functions under the perturbations of asymmetric metal-ligand vibrations, which give rise to nonzero transition probabilities. In confirmation of this, note that the band of $Ni(BrO_3)_2 \cdot 6H_2O$ assigned to $^3A_{2g} \rightarrow {}^3T_{2g}$ is about 2000 cm^{-1} broader than predicted by spin-orbit splitting alone; the four spin-orbit components of $^3T_{2g}$ are calculated[5] to be at 14 027, 14 441, 15 052, and 15 287 cm^{-1} above the ground state. The splittings of the weak bands may then be ascribed to one or more of the following: (1) spin-orbit splitting of the excited electronic state; (2) fields of symmetry lower than cubic which further split the excited electronic state; (3) splittings of the H—O modes and splittings due to hydrogen bonding; (4) lattice vibrations; and (5) metal-oxygen fundamental modes and overtones. The most remarkable aspects of the weak band series which must be accounted for are the relative constancy of the splittings (~480 cm^{-1}) and that in the case of the bromate the series consists of eight bands in a region of 3000 cm^{-1} with a regular variation in intensity.

No single explanation will account for all of the fine structure with the exception of (5). To make this clear we will next examine the other hypotheses. The spin-orbit splittings vary from 200 to 600 cm^{-1} and produce only four components. As to fields of lower symmetry we would expect such fields to show considerable variation from crystal to crystal. In the case of the fluosilicate, the trigonal splittings have been estimated[5] at 50 cm^{-1}. Evidence against moderate or stronger trigonal splittings in this crystal was obtained by examining the spectrum in light polarized parallel and perpendicular to the trigonal axis; no changes in intensity of the weak bands were observed. Finally, considering hydrogen bonding and lattice vibrations, it is again unlikely that these splittings would show much regularity from crystal to crystal. Furthermore, hydrogen bonding broadens the infrared bands by only 500 cm^{-1}.

It is possible that the series of weak bands is a progression of the Ni—O modes in combination with the H—O stretch. The Ni—O modes which are most likely to appear are the asymmetric stretch (T_{1u}) and odd combinations or overtones of the stretches[1,4]; of all the vibrations which can occur in the crystal only the odd stretches produce a large asymmetric field at the nickel ion. The spacings seem reasonable in view of the symmetric stretch (A_{1g}) observed[8] at 394 cm^{-1} in the Raman spectrum of $Zn(OH_2)_6^{++}$.

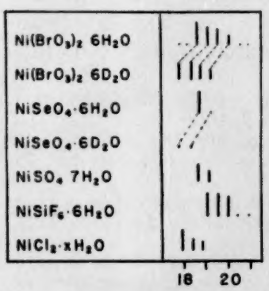

FIG. 2. The wave numbers of the weak bands in thousands of cm^{-1}. The heights of the lines indicate the log of the relative absorbance (log $\log I_0/I$). The spectra were taken at 77°K.

[7] The most prominent of these bands in the spectrum of $NiSiF_6 \cdot 6H_2O$ has been previously observed[2] and has been assigned to $^1T_1$. The spectrum was taken at 4°K and the band was found at 19 350 cm^{-1}. On the other hand the band at 22 770 cm^{-1} shows no isotope effect and is properly assigned[2,4,5] to the levels $^1A_{1g}$ and/or $^1T_{2g}$.

[8] R. Lafont, Compt. rend. **244**, 1481 (1957).

TABLE I. Intensities of the weak bands.

Compound	Crystal system	Wave numbers cm^{-1}	ϵ_{max}[a]	$\Delta\nu_{\frac{1}{2}}$[b] cm^{-1}	Oscillator strength f
$Ni(BrO_3)_2 \cdot 6H_2O$	cubic	18 680	0.06	170	9×10^{-5}
$NiSO_4 \cdot 7H_2O$	orthorhombic	18 690	0.02	240	4×10^{-5}
$NiSeO_4 \cdot 6H_2O$	tetragonal	18 760	0.05	200	9×10^{-5}
$NiSiF_6 \cdot 6H_2O$	trigonal	19 080	0.02	100	2×10^{-5}

[a] The molar extinction coefficient at the band maximum is here defined as $-\log I/I_0$ of a crystal 1 cm thick with a concentration of nickel ions of 1 mole/liter.
[b] The band width at half extinction.

In conclusion, these weak bands in the spectrum of Ni(II) may be assigned to the electronic transition $^3A_{1g} \rightarrow {}^3T_{1g}$ with simultaneous excitation of the H—O stretching frequency. The fine structure is probably due to excitation of Ni—O vibrational modes. Spin-orbit splittings may also contribute to the fine structure.

ACKNOWLEDGMENT

The authors thank the National Science Foundation for a grant in partial support of this research.

THE JOURNAL OF CHEMICAL PHYSICS VOLUME 32, NUMBER 2 FEBRUARY, 1960

Velocity of Compressional Waves in Liquid Hydrogen Fluoride and Some Thermodynamic Properties Derived Therefrom

ROBERT T. LAGEMANN AND C. HARRY KNOWLES*

Department of Physics and Astronomy, Vanderbilt University, Nashville, Tennessee

(Received August 5, 1959)

The velocity of compressional waves (sound waves) has been measured in liquid hydrogen fluoride over the temperature range −15–19°. Using values of density and the specific heat at constant pressure from the literature, values of the following thermodynamic properties have been calculated over the same temperature range: adiabatic compressibility, isothermal compressibility, volume coefficient of expansion, specific heat at constant volume, and the ratio of specific heats.

MEASUREMENTS of certain thermodynamic properties for liquid hydrogen fluoride are nonexistent, probably because of the experimental difficulties inherent in work with that unique and interesting compound. However, many such properties can be calculated if one has available determinations of density, specific heat at constant pressure, and the velocity of compressional waves. It is the purpose of this report to give an account of how the velocity of sound can be measured for the liquid phase and then to present calculated values of some derived thermodynamic properties.

EXPERIMENTAL

Apparatus

The velocity of sound measurements were made by the interferometer method with equipment patterned after that described by McMillan and Lagemann.[1] The chief innovation consisted of a Teflon sylphon[2] inserted as a part of the reflector assembly in such a way that the reflector for the sound waves could be moved about half an inch while at the same time maintaining an almost vacuum-tight system for the hydrogen fluoride under study. As shown in Fig. 1, the sylphon was held in place by two Teflon retaining rings, no gaskets being needed. These rings were tightened into place by means of machine screws made of teflon. Made on a lathe, the screws were useful for about three assemblies of the apparatus before they had to be discarded because of sheared-off threads. All other parts of the interferometer which were in contact with the hydrogen fluoride were of teflon or fluorothene, including the ball and socket joint composing the reflector. The reflector could be set parallel to the bottom of the cup holding the sample simply by pressing it downward against the quartz crystal as measurements were about to begin. Although the system

* Now at Motorola Inc., Phoenix, Arizona.
[1] D. R. McMillan and R. T. Lagemann, J. Acoust. Soc. Am. 19, 956 (1947).
[2] Obtained from the U. S. Gasket Company, Camden, New Jersey, the sylphon measured about two inches both in length and in diameter.

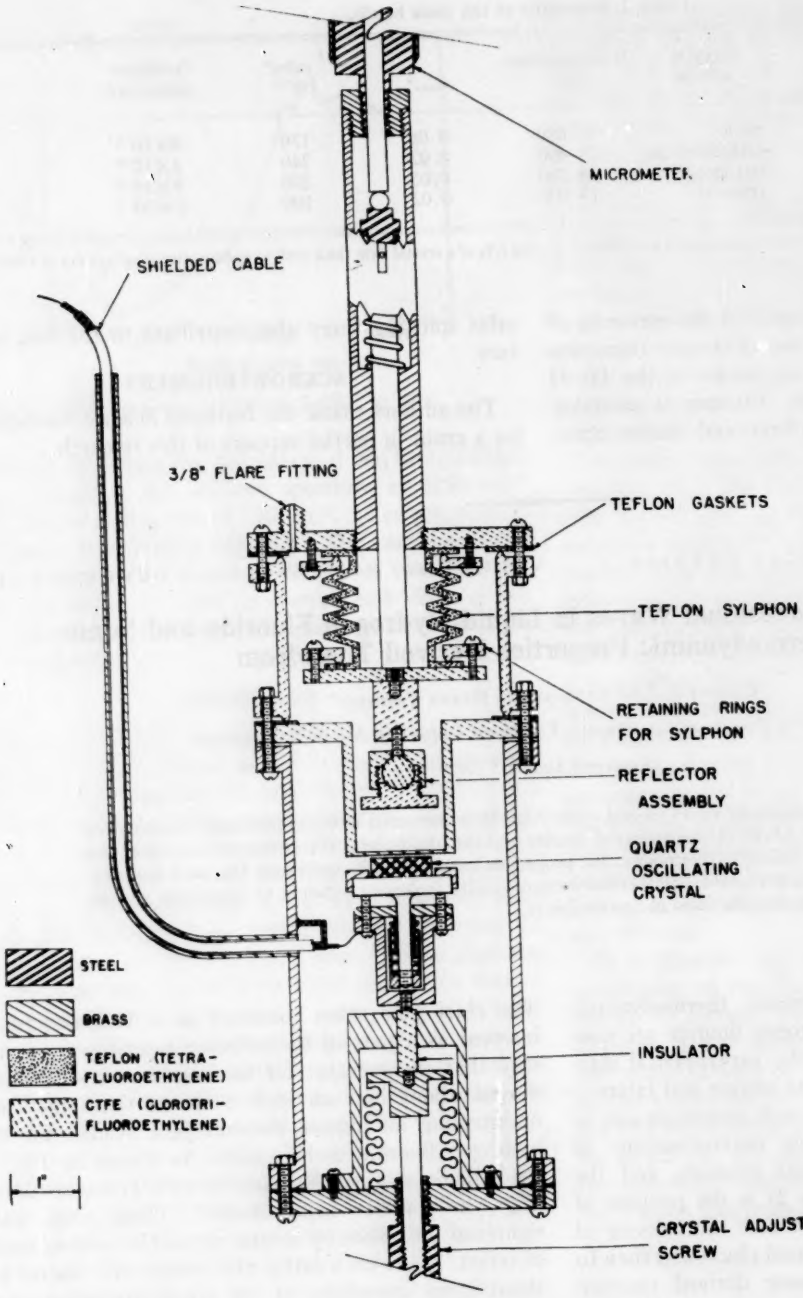

FIG. 1. Cross-section view of the interferometer.

was not fully vacuum-tight, the leak-up rate was only about 1 mm of mercury per hour under a pressure differential of an atmosphere, a rate that decreased as the vapor of the sample became effective when the sample was introduced.

The oscillator-detector circuit was changed somewhat from that used in earlier work[1] and is shown in Fig. 2. The frequency of the oscillator driving the crystal was controlled by the difference frequency between a 4.0-Mc and a 4.5-Mc crystal oscillator circuit. The 500-kc signal, after being tuned by comparison with WWV, varied over a long period of time by only a few cycles per second. Thus the frequency was known to a few parts in 500 000. The positions of the nodal points in the liquid could be repeatedly read to within three parts per 10 000, the least count of the micrometer

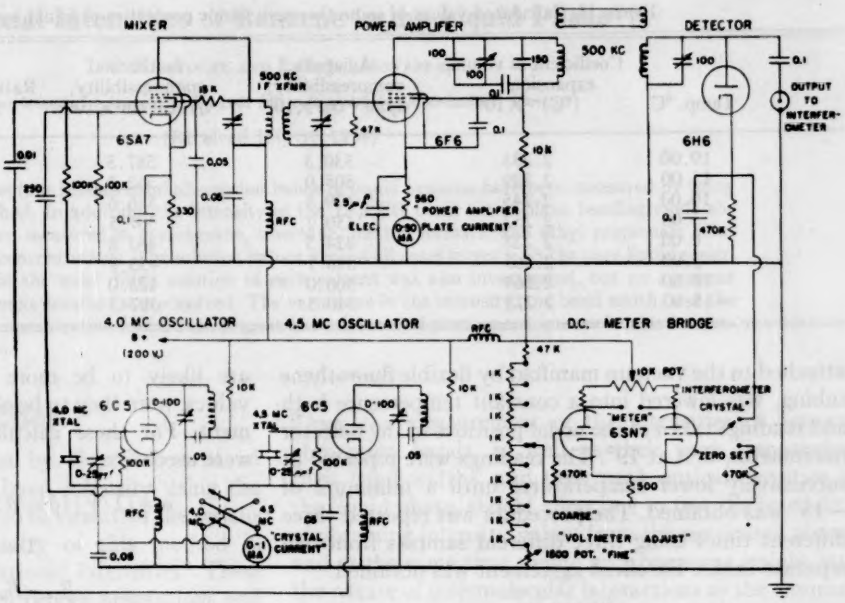

FIG. 2. The oscillator-detector circuit.

being 0.0001 in. The product of the frequency and of the wavelength as determined from micrometer readings gave the velocity of the compressional waves.

Sample

Hydrogen fluoride was obtained from a commercial tank that had been partially emptied. Before a sample was withdrawn, the tank was cooled with a dry ice and dowanol mixture and pumped on. Samples were distilled into a specially constructed fluorothene container attached to a vacuum manifold system which had been constructed of copper and nickel tubing and Hoke monel valves. The line from the tank to this container was of fluorothene, as was the line from the container to the interferometer. A necessary tee-joint was constructed of teflon and, although brass nuts were used to connect the tubing, the liquid hydrogen fluoride did not come into contact with any material except teflon or florothene as it was poured into the interferometer through the flexible tubing. The metal manifold system was fluorinated prior to use, as was the interferometer also. As seen in the fluorothene trap before and after use, the liquid hydrogen fluoride appeared clear and colorless. An infrared spectrum of the vapor give the familiar bands found by Shelton and Nielsen[3] and no others for a cell 10 cm in length filled with gas at atmospheric pressure.

TABLE I. Some physical properties of liquid hydrogen fluoride, experimentally determined.

Temp. °C	Ultrasonic velocity, m/sec	Density[a] g/cc	c_p[b] cal/g °C
19.00	443.2	0.9601	0.6088
15.00	452.1	0.9688	0.6025
10.00	461.5	0.9797	0.5952
5.00	473.5	0.9908	0.5878
0.00	484.9	1.0020	0.5809
−5.00	497.5	1.0134	0.5741
−10.00	516.3	1.0249	0.5675
−15.00	532.3	1.0366	0.5608

[a] J. H. Simons and J. W. Bouknight, J. Am. Chem. Soc. **54**, 129 (1932).

[b] Read from a curve constructed from data given by Hu, White, and Johnston, J. Am. Chem. Soc. **75**, 1232 (1953). All the data except that at 19° are interpolations.

Procedure

The liquid was poured into the interferometer at room temperature, at which point the vapor pressure was about atmospheric. The interferometer, still

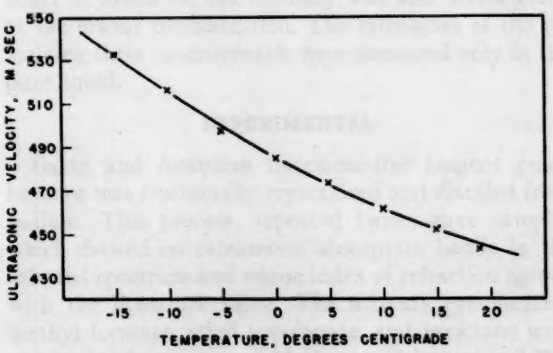

FIG. 3. Ultrasonic velocity as a function of temperature for liquid hydrogen fluoride.

[3] R. D. Shelton and A. H. Nielsen, J. Chem. Phys. **19**, 1312 (1951).

TABLE II. Calculated values of some thermodynamic properties of liquid hydrogen fluoride.

Temp. °C	Coefficient of volume expansion $(°C)^{-1}\times10^3$	Adiabatic compressibility, $dyne^{-1}\ cm^2\times10^{12}$	Isothermal compressibility, $dyne^{-1}\ cm^2\times10^{12}$	Ratio of specific heats, γ	c_v cal/g °C
19.00	2.233	530.3	587.5	1.108	0.5495
15.00	2.239	505.0	562.3	1.113	0.5413
10.00	2.245	479.3	536.6	1.120	0.5314
5.00	2.252	450.2	507.5	1.127	0.5216
0.00	2.258	424.5	481.8	1.135	0.5118
−5.00	2.263	398.7	455.8	1.143	0.5023
−10.00	2.269	366.0	423.0	1.156	0.4909
−15.00	2.273	340.5	397.3	1.167	0.4805

attached to the vacuum manifold by flexible fluorothene tubing, was lowered into a constant temperature bath and readings taken of the nodal positions of the reflector micrometer, first at 19°. The readings were repeated at successively lower temperatures until a minimum of −15° was obtained. The procedure was repeated three different times using three different samples from two separate tanks. Excellent agreement was obtained.

RESULTS

Table I gives the measured values of the ultrasonic velocity of liquid hydrogen fluoride over the temperature range −15–19°. A graphical presentation is shown in Fig. 3. This is the only instance, except for water, in which a nonlinear relation is found between velocity and temperature for a pure compound. It is perhaps worthy of comment to point out that the velocities are among the lowest recorded for any liquid. Table I also gives measurements of the density and specific heat at constant pressure made by other experimenters.

CALCULATIONS

Having measured the velocity of compressional waves and having available determinations of the density and specific heat at constant pressure, it is possible to calculate certain other thermodynamic properties. In fact, it is possible in this way to obtain values which are likely to be more accurate than the measured values, were they to be obtained by conventional equipment. For these calculations the following relations were used:

$$\alpha=(1/V)(\partial V/\partial T)_p=-(1/d)(\partial d/\partial T),$$

$$\mathcal{U}=(dB_{ad})^{-\frac{1}{2}},$$

$$B_{is}-B_{ad}=T\alpha^2/dc_pJ,$$

$$\gamma=B_{is}/B_{ad}=c_p/c_v.$$

In the above, α is the volume coefficient of expansion; $\mathcal{U}$, the ultrasonic velocity; d, the density; B_{ad}, the adiabatic compressibility; B_{is}, the isothermal compressibility; J, the mechanical equivalent of heat, 4.1858 joules per calorie; γ, the ratio of specific heats; c_p, the specific heat at constant pressure; and c_v, the specific heat at constant volume; all measured at the same temperature T. To secure the values of $\partial d/\partial T$ needed to calculate α, it is possible to differentiate the equation given by Simons and Bouknight,[4] which gives density as a function of temperature, with the result that

$$\partial d/\partial T=-0.0022625+2(0.000003125)t.$$

The calculated values of the aforementioned properties are given in Table II.

[4] See reference a in Table I.

Vibrational Intensities of Benzene in the Liquid Phase*†

I. C. HISATSUNE AND E. S. JAYADEVAPPA‡

Department of Chemistry, Kansas State University, Manhattan, Kansas

(Received July 31, 1959)

The intensities of the four fundamental absorption bands in liquid benzene have been measured by using the Wilson-Wells method. In addition, the intensity of the 15-μ CH bond out-of-plane bending mode absorption band has been measured in cyclohexane, isooctane, methyl formate, and ethyl propionate solutions at five different concentrations. The solution values were in all cases larger than the pure liquid result. The effect of iodine in the most dilute solution of each solvent was also investigated, but no apparent difference from the simple solution was observed. The variations in the intensity, the band width, and the peak frequency with concentration found here suggest the existence of pronounced intermolecular interactions in liquid benzene.

INTRODUCTION

THE recent reinvestigation by Overend *et al.* of the 15-μ CO_2 absorption band intensity using the Wilson-Wells method appears to have settled the serious question concerning the validity of this method in obtaining the gas phase vibrational intensities.[1] These investigators showed that with proper precautions and at least for this CO_2 absorption band, the Wilson-Wells method produced an intensity value which was in agreement with those obtained from other methods. However, there still remains an equally serious question as to whether or not such intensity measurements can be carried out in the liquid or solid phases. Moreover, if reproducible intensity values can be obtained in these condensed phases, can such values be correlated sensibly to the vapor phase results? In this paper certain aspects of these problems are discussed.

Absorption intensity measurements in the condensed phases are of particular interest, for they yield not only the usual effective bond moments and their derivatives in dense media, but also information related to intermolecular perturbations.[2] Liquid benzene and its solutions are convenient systems to examine for the latter type of information because intensities of all four fundamental vibrational absorption bands are known in the solid[3] and gas[4,5] phases and because considerable data, both experimental and theoretical, are available for the charge transfer complexes involving benzene.[6] Thus, the measurement of the intensities of benzene absorption bands, as well as their peak frequencies, their band widths, and their peak optical densities in the liquid phase, should allow one to test the feasibility of obtaining intensity values from the condensed phases and at the same time should give one some insight into the nature of intermolecular interactions as the environment of the molecule is changed from the gaseous to a more dense one.

In the experimental results reported here, particular attention was focused on the 15-μ band of benzene which is associated with the CH bond out-of-plane bending normal mode. In this oscillation one expects strong interaction between the CH bonding orbitals and the π-orbitals of the carbon ring,[7] as evidenced by the large difference between the effective CH bond moments calculated from this band intensity and from the other in-plane bending band intensity.[4,5] Thus, if pronounced intermolecular perturbations were present in the condensed phases, then the intensity of this band should very likely be quite different in the gas, liquid, and solid phases, and in solutions of different solvents. We have, therefore, measured the intensity of this band in pure liquid and in solutions of four solvents at five different concentrations. In each of these solvents the effect of iodine on the intensity was also investigated at the lowest concentration. The intensities of the remaining three fundamentals were measured only in the pure liquid.

EXPERIMENTAL

Baker and Adamson thiophene-free reagent grade benzene was fractionally crystallized and distilled from sodium. This process, repeated twice, gave samples which showed no extraneous absorption bands in the infrared spectrum and whose index of refraction agreed with the literature value. The solvents cyclohexane, methyl formate, ethyl propionate, and isooctane were spectro-grade reagents of Matheson, Coleman, and Bell Company. These reagents were used without further purification. The iodine used in this work was a Baker

* Taken in part from a thesis submitted by E. S. J. in partial fulfillment of the requirements for the Ph.D. degree in Chemistry at Kansas State University, 1959.

† Presented at the Symposium on Molecular Structure and Spectroscopy, Ohio State University, Columbus, Ohio, June, 1959.

‡ Present address: Department of Chemistry, Karnatak University, Dharwar, Mysore State, India.

[1] Overend, Youngquist, Curtis, and Crawford, J. Chem. Phys. **30**, 532 (1959).

[2] T. Yoshino, J. Chem. Phys. **24**, 76 (1956).

[3] W. B. Person and C. A. Swenson, Symposium on Molecular Structure and Spectroscopy, Ohio State University, Columbus, Ohio, June, 1959.

[4] J. Overend and B. Crawford, Jr., Symposium on Molecular Structure and Spectroscopy, Ohio State University, Columbus, Ohio, June, 1957.

[5] H. Spedding and D. H. Whiffen, Proc. Roy. Soc. (London) **A238**, 245 (1956).

[6] E. E. Ferguson and F. A. Matsen, J. Chem. Phys. **29**, 105 (1958).

[7] Kross, Fassel, and Margoshes, J. Am. Chem. Soc. **78**, 1332 (1956).

TABLE I. Experimental condition.

Band (cm^{-1})	Prism	Range of effective slit (cm^{-1})	Range of scanning (cm^{-1})
674	KBr	2.9–4.7	600–770
1037	NaCl	2.1–5.1	920–1130
1394, 1485, 1530	NaCl	2.5–9.5	1350–1600
3036, 3072, 3092	LiF	2.1–7.0	2850–3350

and Adamson resublimed reagent grade sample which had been dried in a desiccator over anhydrous phosphorus pentoxide.

Solutions of benzene in various solvents were prepared in calibrated 50-ml volumetric flasks using calibrated pipets. The glass stoppers on these flasks were hand-ground to insure tight fit and thus to prevent evaporation loss of the volatile liquids. None of these solutions was allowed to stand for more than 3 days, and refractive indices were measured periodically to ascertain constancy of the concentrations. In the case of iodine solutions, both benzene and iodine were weighed and then the solvent was added to them.

All spectra were recorded with a Perkin-Elmer Model 12B infrared spectrometer which has been modified for double-pass operation. Pertinent spectral information is listed in Table I. For cell thickness measurements a Perkin-Elmer Model 137 Infracord spectrometer, which we acquired midway in our research schedule, was also used; this instrument was equipped with a NaCl prism. During the recording of the spectrum, the single-beam instrument was flushed continuously with dry air. Absorption by atmospheric water in the 7-μ region was effectively decreased to a constant level by this method. In the measurements of the 15-μ band, the atmospheric CO_2 absorption was made negligible by passing the drying air through Ascarite before it was introduced into the instrument.

The refractive indices of the liquid and solutions were measured with a Bausch and Lomb Abbe-type refractometer which was thermostated at 20°C and equipped with a sodium lamp. Before each measurement, the sample was immersed for a short while in a constant temperature bath kept at 20°C. All measured index values were reproducible to ± 0.0001 unit.

A Perkin-Elmer variable thickness liquid absorption cell with KBr windows was used for all spectral measurements. The cell thicknesses were determined by means of interference patterns[8] obtained on both the single- and double-beam instruments. Before each thickness measurements, the windows on the cell were adjusted for maximum parallelness by observing concentric visible interference fringes at small cell spacings. The estimated uncertainties in these measured cell thicknesses were as follows: ± 0.2 μ for thickness less than 5 μ, ± 0.5 for 5–10 μ, ± 1 for 10–25 μ, and ± 2 for over 25 μ thickness. In several experiments, thicknesses were measured before and after runs, but no significant changes were observed. For cell thicknesses of less than about 6 μ, it often became difficult to identify the interference peaks on the recordings from the single-beam instrument. In such cases, successive measurements were made while the cell was closed; and finally, when the fringes became difficult to identify, the cell was closed by an additional 2 μ on the micrometer scale. The cell thickness was then obtained from a linear thickness *vs* cell micrometer scale plot. These extrapolated values were found to agree within about 0.2 μ with those obtained from the double-beam instrument interference patterns. In two instances, the thickness of the cell was determined from the band area *vs* thickness plot of the 3-μ absorption band. In this case, the cell was filled with benzene, the band area of the 3 μ spectrum measured, and the calculated thickness then used for the measurement of the other absorption bands. In many runs the absorption curves of all four bands were obtained with the same cell setting.

The experimental procedure used in obtaining the spectra was as follows. After the spectrometer had attained equilibrium condition, atmospheric H_2O and CO_2 calibrations were taken. The cell, whose thickness had been determined previously, was filled with the sample and allowed to stand in the radiation beam to attain equilibrium. The zero transmission curve was taken with the beam blocked off. The spectrum of the sample was then recorded twice, one curve superimposed over the other, under conditions of maximum resolution. When the two sets of spectra did not coincide, the run was discarded. During the recording of the spectrum, the cell body temperature was taken with a thermocouple at 5- to 10-min intervals; the temperature was always found to be 25± 2°C. Finally, the background curve was recorded.

The 100% transmission background curve, which can easily be the major source of experimental error, was obtained in the following manner. In liquid benzene runs, all such curves were taken by placing in the infrared beam a KBr window whose transmission was as nearly the same as that of the empty cell. Curves thus obtained were found to coincide or to be parallel with the two wings of the absorption band when the sample thickness was sufficiently small. In instances when weak overlapping bands were present on one of the wings, the remaining clear wing was matched with the background curve. In solution runs on the 15-μ benzene band, this KBr window method gave satisfactory background curves for both isooctane and cyclohexane solvents. However, at larger thicknesses of the cyclohexane solutions, especially when the mole

[8] G. B. B. M. Sutherland and H. A. Willis, Trans. Faraday Soc. 41, 181 (1945).

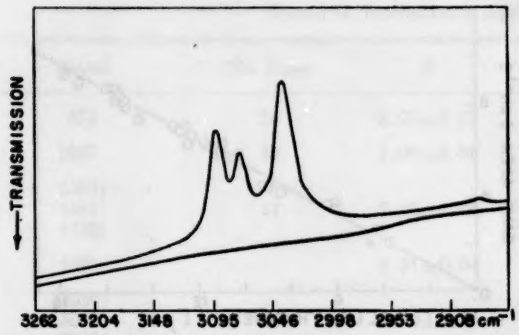

FIG. 1. The spectrum of liquid benzene in the 3-μ region. Background curve obtained with a KBr plate (LiF prism).

fraction of the solvent was large, the background coincided with only the low-frequency wind of the 15-μ band.

There were two solvent bands present at 770 and 640 cm^{-1} in methyl formate solutions. Although these bands did not interfere with the background determination in most cases, in the thick concentrated solvent runs, however, it was necessary to obtain the background curve with the pure solvent in the cell at the same thickness. The second polar solvent, ethyl propionate, gave similar difficulties because of the weak solvent absorption at the same position as the benzene fundamental. In this case two background curves were taken, one with only the solvent at the same thickness and another with the KBr window. The solvent background was then subtracted from the sample curve after the former had been corrected for the proper effective thickness, nl.

RESULTS

A. Liquid Benzene

Typical spectrometer traces of the fundamental absorption bands in liquid benzene are shown in Figs. 1 to 4. From these traces, the apparent percent transmission T_0/T was read off, and logarithms of such values were replotted against frequency in cm^{-1}. The areas beneath these curves were measured with a

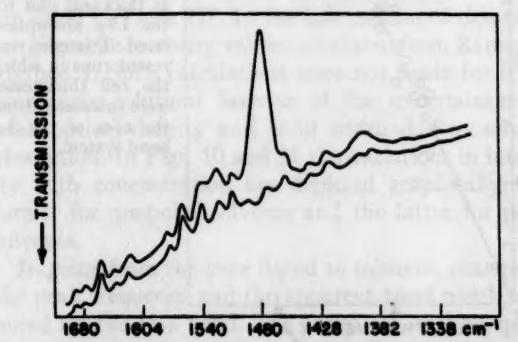

FIG. 2. The spectrum of liquid benzene in the 7-μ region. Background curve obtained with a KBr plate (NaCl prism).

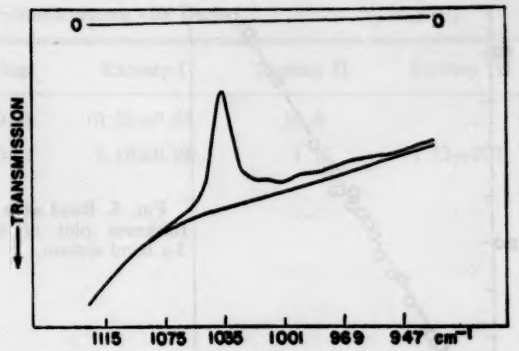

FIG. 3. The spectrum of liquid benzene in the 10-μ region Background curve obtained with a KBr plate (NaCl prism). The zero transmission line (0——0) taken with radiation beam blocked off.

planimeter, and these plotted against thicknesses. Such plots, in which all experimental points fell along straight lines going through the origins, are shown in Figs. 5 to 8. The data for the 3-μ band are for the total area of the three overlapping bands, and those for the 7-μ band contain the weak absorption bands on the wings. In the case of the 10-μ band, the weak absorptions in the low-frequency wing were removed graphically. Since at smaller thicknesses this band was found to be symmetrical with respect to the band center, the overlapping bands were separated by drawing a curve which was symmetric to the high frequency half of the fundamental band. The two points represented by triangles in Figs. 7 and 8 correspond to runs in which the thicknesses were calculated from the area of the 3-μ band.

From the linear area *vs* thickness plots, the apparent intensities of the bands were obtained by taking the slopes of the lines according to

$$B(\text{Darks}) = (2.303/nl)\int \log_{10}(T_0/T)\,d\nu,$$

where B is the apparent intensity, nl the effective path

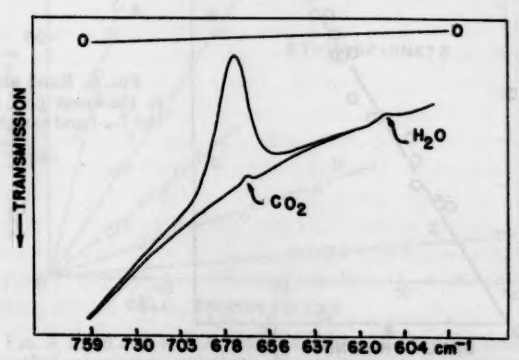

FIG. 4. The spectrum of liquid benzene in the 15-μ region. Background curve obtained with a KBr plate (KBr prism). The zero transmission line (0——0) taken with radiation beam blocked off.

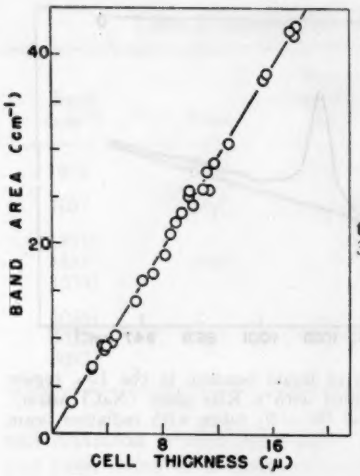

FIG. 5. Band area *vs* thickness plot of the 3-μ band system.

length in terms of concentration in millimoles/cc and thickness in cm. The integration is carried over the entire band. The resulting B values are listed in Table II.

In the case of the 3-μ band, Mair and Hornig[9] have assigned the central peak of the overlapping bands to B_{1u} symmetry, while Brodersen and Langseth[10] have assigned the same band to E_{1u}. The two peaks on the outside have been assigned by both investigating groups to E_{1u} symmetry. Because of this uncertainty in the symmetry of the weak central band, we have made a graphical separation of this peak from the total band area. Again, at smaller thicknesses the two outside peaks were found to be symmetrical about their respective band centers, so that symmetric wings were drawn toward the central band and the area corrected thus. Similarly, for the 7-μ band, the two weak absorption bands on the wings have been assigned by both research groups to E_{1u}, the same as the fundamental, but we have separated these bands in order to facilitate comparison of the intensity to the gas phase result. The apparent intensities of the corrected 3-μ and 7-μ bands are listed in Table II.

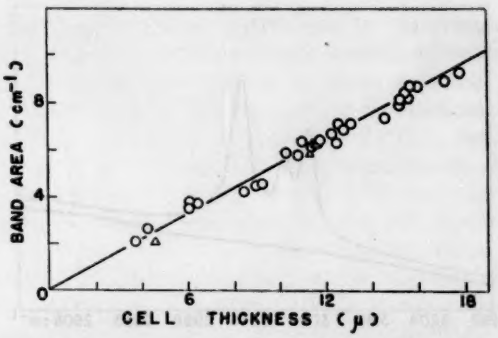

FIG. 7. Band area *vs* thickness plot of the 10-μ absorption band. Triangles represent runs in which the cell thicknesses were calculated from the area of the 3-μ band system.

Both the 10-μ and the 15-μ bands were well isolated from other absorption bands. However, at larger thicknesses the latter band showed asymmetric contour with the high-frequency side having a slightly larger apparent band width. For both of these fundamental bands, wing corrections were made following Ramsay's method.[11] Such corrections were made separately for each half of the 15-μ band because of the asymmetry. We have also calculated the true intensity of these bands according to the three methods given by Ramsay.[11] In this Method I, the intensity is obtained by direct integration of the band, assuming a Lorentz band shape and a triangular slit function. Such integration gives the intensity as a function of the apparent peak optical

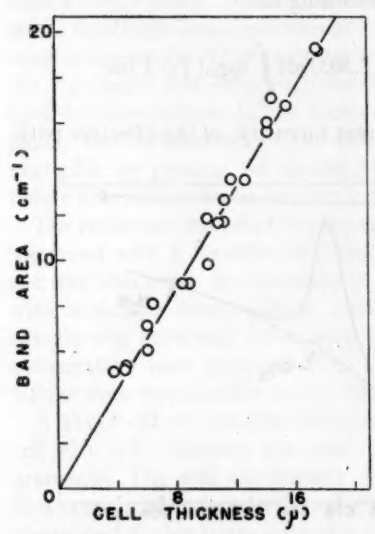

FIG. 6. Band area *vs* thickness plot of the 7-μ band system.

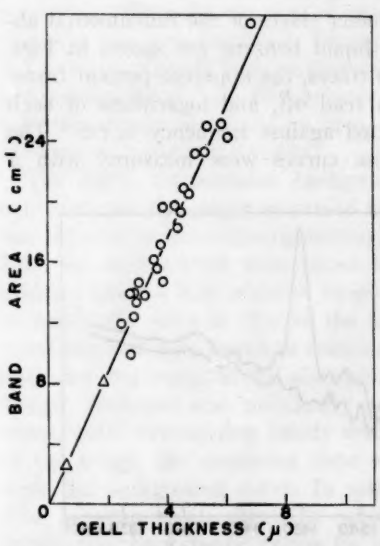

FIG. 8. Band area *vs* thickness plot for the 15-μ absorption band. Triangles represent runs in which the cell thicknesses were calculated from the area of the 3-μ band system.

[9] R. D. Mair and D. F. Hornig, J. Chem. Phys. **17**, 1236 (1949)
[10] S. Brodersen and A. Langseth, Kgl. Danske Videnskab. Selskab. Mat. fys. Skrifter **1**, 1 (1956).
[11] D. A. Ramsey, J. Am. Chem. Soc. **74**, 72 (1952).

TABLE II. Intensities of liquid benzene fundamentals (10^8 Darks).

Band	No. Runs	B	With wings	Ramsay I	Ramsay II	Ramsay III
674	26	8.97±0.13	9.54±0.14	10.58±0.83	10.5	...
1037	30	1.09±0.01	1.15±0.01	1.19±0.08	1.17	1.15±0.01
1394 1481 1530	21	2.24±0.03	...	...	...	...
1481	...	1.91±0.04	...	...	...	...
3036 3072 3092	35	4.99±0.03	...	...	...	...
3036 3092	...	4.44±0.09	...	...	...	...

density, the apparent band width, and the apparent spectral slit. The second method of Ramsay is an extension of the Wilson-Wells method, but one in which the apparent intensity is plotted against apparent peak optical density instead of the effective path length. In this case a linear plot is obtained, and the intercept at peak density of zero gives the true intensity of the band. Ramsay's Method III is based on Bourgin's work in which the area is measured from fractional absorption $1-(T_0/T)$ *vs* frequency plots. This method was applied to only the 10-μ fundamental. The intensity values obtained by these methods were all listed in Table II. It should be noted that values from Ramsay's methods include wing corrections.

The standard errors listed in Table II are based on uncertainties in thickness cited earlier and on estimated errors in optical density measurements. Least square treatment has been applied to all cases except to Ramsay's Method II.

B. 15-μ Band in Solutions

The intensity of the 15-μ band in various solvents at different concentrations was obtained in a manner similar to the pure liquid case. A typical area *vs* thickness plot is shown in Fig. 9. When solvent absorption bands were present, the areas were corrected for them. The resulting intensities which include wing corrections are listed in Table III. In the last column of this table are given the intensity values calculated from Ramsay's Method I. Such calculations were not made for ethyl propionate solutions because of the uncertainties in peak optical density and band width due to solvent absorption. In Figs. 10 and 11 the variations in intensity with concentration are depicted graphically, the former for nonpolar solvents and the latter for polar solvents.

In going from the pure liquid to solution, changes in the peak frequency and the apparent band width were noted for the 15-μ band. The variations of these quantities with concentration are shown in Figs. 12 and 13. In Fig. 12 the ratio of the apparent band width to the apparent peak optical density is plotted against apparent peak optical density. All solution and liquid benzene results, except those points which overlapped completely, are included in this figure. The frequency shifts with respect to the gas phase are shown in Fig. 13. The uncertainties indicated are based on maximum observed deviations form the mean values. We observed only blue shifts in our solution spectra.

The effect of iodine on the 15-μ band of benzene in various solvents was studied for the most dilute solutions only. These results are given in Table IV. The concentrations of iodine used are approximately the maximum amounts which will dissolve in these solutions at 25°C.

DISCUSSION

The agreement we have obtained between the Wilson-Wells method with wing corrections and Ramsay's methods suggests that our experimental values of band area, band width, and peak optical density are consistent. One may now test Debye's equation, given below, which was shown by Polo and Wilson[12] to be applicable

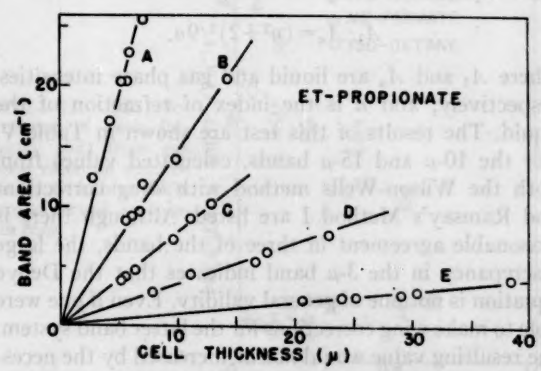

FIG. 9. Band area *vs* thickness plot for the 15-μ band of benzene in ethyl propionate solutions. Concentrations in mmoles/cc: A=5.576, B=2.235, C=1.117, D=0.442, E=0.088.

[12] S. R. Polo and M. K. Wilson, J. Chem. Phys. **23**, 2376 (1955).

TABLE III. Intensity of the 15-μ band in solutions.

Conc. (mmoles/cc)	Mole fraction	n_D^{20}	No. of runs	Intensity (10^3 Darks) with wings	Intensity (10^3 Darks) Ramsay I
		Cyclohexane			
5.582	0.55	1.4602	7	11.08±0.26	12.30±0.83
2.235	0.23	1.4382	5	11.40±0.30	11.60±0.83
1.120	0.12	1.4318	7	13.38±0.46	13.77±1.63
0.444	0.05	1.4285	7	15.39±0.45	15.12±1.38
0.089	0.01	1.4269	7	17.13±0.29	17.08±0.70
		Isooctane			
5.618	0.65	1.4429	6	12.83±0.14	13.49±0.93
2.235	0.32	1.4108	6	15.79±0.25	15.46±1.17
1.122	0.17	1.4002	6	16.56±0.55	17.15±1.91
0.443	0.07	1.3952	5	16.91±0.56	16.10±1.17
0.088	0.01	1.3922	6	17.12±0.27	16.76±0.96
		Methyl formate			
5.589	0.41	1.4239	5	16.08±0.53	17.54±2.31
2.236	0.15	1.3752	7	15.75±0.44	17.24±2.13
1.117	0.07	1.3590	6	16.70±0.44	17.77±1.33
0.443	0.03	1.3504	6	16.23±0.19	17.28±0.72
0.221	0.01	1.3480	6	16.92±0.30	18.30±1.06
		Ethyl propionate			
5.576	0.56	1.4413	6	16.40±0.90	...
2.235	0.24	1.4061	5	15.65±0.88	...
1.117	0.13	1.3954	6	16.47±0.53	...
0.442	0.05	1.3884	5	17.02±1.03	...
0.088	0.01	1.3850	6	16.40±1.29	...

TABLE IV. Intensity of the 15-μ band in iodine-solvent solutions.

Solvent	No. runs	Concentration (mmole/cc) Benzene	Iodine	Intensity (10^3 Darks) With wings	Ramsay I
Cyclohexane	6	0.089	0.016	18.46±0.08	17.29±0.36
Isooctane	6	0.088	0.015	17.87±0.32	16.93±1.90
Methyl formate	5	0.222	0.016	16.60±0.34	18.67±1.12
Ethyl propionate	7	0.888	0.016	16.27±0.92	...

to the comparison of gas phase intensities to those in pure liquids.

$$A_l/A_g=(n^2+2)^2/9n,$$

where A_l and A_g are liquid and gas phase intensities, respectively, and n is the index of refraction of the liquid. The results of this test are shown in Table V. For the 10-μ and 15-μ bands, calculated values from both the Wilson-Wells method with wing corrections and Ramsay's Method I are listed. Although there is reasonable agreement in three of the bands, the large discrepancy in the 3-μ band indicates that the Debye equation is not one of general validity. Even if one were able to make wing corrections for the latter band system, the resulting value would not be increased by the necessary factor of two.

Recently, Schatz[13] calculated the intensity of the 15-μ band in liquid benzene from infrared dispersion measurements to be 14.1×10^3 Darks with an estimated error of about 10%. Although the discrepancy between this value and our Wilson-Wells result is not excessively large in view of the numerous experimental difficulties involved in our method, this difference is probably significant since it is outside the claimed limits of experimental error. That reflection loss of the incident infrared radiation in our work may account for this difference does not appear to be reasonable because of our results in benzene solutions and because such reflections, if significant, would make our value even smaller. At present there are insufficient examples of similar comparisons to decide between these values or to account for this difference.

Our solution work shows that band intensities are indeed dependent on concentrations, but one hardly expected such changes to be as great as the observed factor of two between liquid benzene and very dilute solutions. Furthermore, in all four solutions the intens-

[13] P. N. Schatz, Symposium on Molecular Structure and Spectroscopy, Ohio State University, Columbia, Ohio, June, 1959.

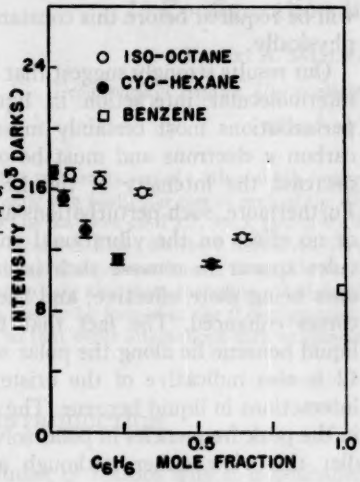

FIG. 10. Intensity *vs* mole fraction plot for 15-μ band in hydrocarbon solvents.

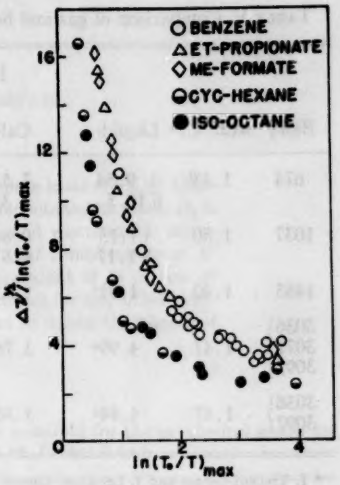

FIG. 12. Band width-peak optical density plot for 15-μ band. This plot includes all experimental points for both liquid benzene and solutions. ($\Delta\nu^{\frac{1}{2}}$ = half-intensity band width).

ity appears to approach a common limit as the mole fraction of benzene becomes zero. This limiting value, which evidently is independent of the nature of the solvent, was found to be 18.4±1.5 (10^3 Darks). One is tempted to call this the "true" band intensity in the liquid phase, but one must still account for the difference between this value and the dispersion result, which is now lower. It may be that the estimated uncertainties quoted by us and by Schatz are conservative, but we prefer to accept these differences as real, although we cannot offer any explanation for these differences without further thorough experimental work on other molecules.

In the nonpolar cyclohexane and in isooctane solutions, one observes a gradual change in band intensity with concentration (Fig. 10). The shift in peak frequency position in these solutions compared to the gas phase value is also apparently not a very sensitive function of concentration (Fig. 13). However, the effect of the polar solvents on both the intensity and peak frequency is quite pronounced as one observes from Figs. 11 and 13. When the benzene mole fraction is about 0.5, the band intensity is already twice as great as that in pure liquid and remains so over a wide range of mole fractions.

The addition of iodine to the most dilute solutions appears to produce no significant effect on the intensity as shown in Table IV. Presumably, the solvent effect outweighed any change in band intensity that the iodine molecule may have caused, and furthermore, the concentration of the benzene-iodine complex was too small. The effect of iodine on the intensity must, therefore, be studied in pure liquid rather than in solutions.

There are three equations which relate solution intensity values to the gas phase result:

Hirota[14]: $$A_s/A_g=[(n_0^2+2)(2\epsilon+1)/3(2\epsilon+n_0^2)]^2,$$

Person[15]: $$A_s/A_g=(1/n_s)[(n_0^2+2)/(n_0^2/n_s^2+2)]^2,$$

Buckingham[16]: $$A_s/A_g=[9n^2/(n^2+2)(2n^2+1)]^2 [1+C_\epsilon(\epsilon-1)/(2\epsilon+1)+C_n(n^2-1)/(2n^2+1)],$$

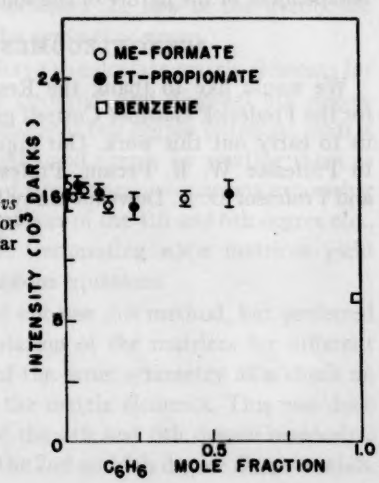

FIG. 11. Intensity *vs* mole fraction plot for 15-μ band in polar solvents.

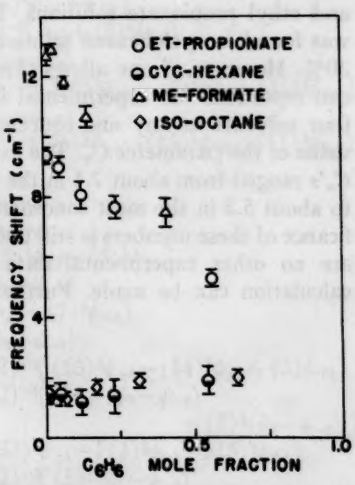

FIG. 13. The dependence of peak frequency shift from gas phase value on concentration. Only blue shifts were observed in solution runs.

[14] E. Hirota, Bull. Chem. Soc. Japan **27**, 295 (1954).
[15] W. P. Person, J. Chem. Phys. **28**, 319 (1958).
[16] A. D. Buckingham, Proc. Roy. Soc. (London) **A248**, 169 (1958).

TABLE V. Comparison of gas and liquid benzene intensities.

Band	n(25°C)[a]	Intensity (10^3 Darks) Liquid	Gas Calc	Gas Exptl. SW[d]	Gas Exptl. OC[e]
674	1.43[b]	i 9.54 ii 10.5	7.5 8.3	8.78	8.5
1037	1.50	i 1.15 ii 1.17	0.86 0.87	0.88	0.85
1485	1.40	1.91[c]	1.53	1.3	1.4
3036 3072 3092	1.47	4.99[c]	3.78	7.56	...
3036 3092	1.47	4.44[c]	3.36	5.98	6.8

[a] J. Vincent-Geisse and J. Lecomte, Compt. rend. **244**, 577 (1957).
[b] Extrapolated from curve in reference a.
[c] No wing corrections included.
[d] Reference 5.
[e] Reference 4.

where n_s, n_0, and n=refractive index of the solution, the solute, and the solvent, respectively; ϵ=dielectric constant of the solvent; C_ϵ and C_n=constants which depend only on the solute; and A_s and A_g=solution and gas phase intensity, respectively. Both Hirota's and Person's equations do not reproduce our experimental data. Although we have used our measured visible refractive indices, the deviations found were great enough to allow us to conclude that these two equations would not give a reasonable fit of our data even if the infrared refractive indices were known. However, Buckingham's equation, in which C_ϵ was taken as zero, did fit our data rather well. Except in the most concentrated solutions, agreement between the calculated and experimental ratios of A_s/A_g was better than about 10% for methyl formate, isooctane, and ethyl propionate solutions. The largest deviation was found in cyclohexane solution where it was about 30%. However, if one allows this deviation, then one can reproduce the experimental intensity ratios in all four solvents at any one concentration with a single value of the parameter C_n. The average values of these C_n's ranged from about 7.4 in the most dilute solutions to about 5.3 in the most concentrated ones. The significance of these numbers is still uncertain, because there are no other experimental data with which similar calculation can be made. Further experimental work will be required before this constant can be interpreted physically.

Our results strongly suggest that there is considerable intermolecular interaction in liquid benzene. These perturbations most certainly must be caused by the carbon π electrons and must be of such nature as to decrease the intensity of the 15-μ absorption band. Furthermore, such perturbations apparently have little or no effect on the vibrational energy. Solvent molecules appear to remove such interactions, with polar ones being more effective; and the band intensity becomes enhanced. The fact that the band widths in liquid benzene lie along the polar solvent curve in Fig. 12 is also indicative of the existence of some strong interactions in liquid benzene. The observed blue shifts in the peak frequencies in polar solvents do not contradict this view either, although a different kind of interaction may be involved here. It will be very interesting to make further studies of these concentration dependences of the CH bond out-of-plane bending mode absorption band intensity in other molecules with π electrons and to ascertain that such dependences are absent or are negligible in absorption bands which are associated with vibrational modes involving no large perturbation of these π electrons.

Although the present work did not settle the question concerning the feasibility of measuring infrared intensities in the liquid phase by using the Wilson-Wells method, it does, nevertheless, indicate some promise that such measurements may be possible in dilute solutions. The marked dependence of intensity on concentration in solutions shows that measurements, in which the cell thickness is kept constant and the concentration alone varied, may not lead to an intensity value which can be interpreted properly. Furthermore, the intensities in pure liquid may differ greatly from solution results, so that one must use such values with considerable caution. One may also conclude from our work that the limiting intensity found here probably is a characteristic property of the absorbing molecule and independent of the nature of the solution.

ACKNOWLEDGMENTS

We would like to thank the Research Corporation for the Frederick Gardner Cottrell grant which enabled us to carry out this work. Our appreciation also goes to Professor W. B. Person, Professor P. N. Schatz, and Professor D. A. Dows for many helpful discussions.

THE JOURNAL OF CHEMICAL PHYSICS VOLUME 32, NUMBER 2 FEBRUARY, 1960

f^2 Configuration in a Crystalline Field

ROBERT A. SATTEN AND JACK S. MARGOLIS

Department of Physics, University of California, Los Angeles 24, California

(Received July 31, 1959)

The matrix representation of a 4th and 6th degree octahedral potential in a complete basis of f^2LSJ functions belonging to a particular row of each of the 5 irreducible representations of the octahedral group O_h is presented. The matrices are 7×7, 3×3, two of 9×9, and 12×12 when spin-orbit and electrostatic interaction are included. Bases for the 5 irreducible representations are presented as linear combinations of M states for integral J values ranging from 0 to 6. Reduced matrix elements (independent of M or row of representation) are also given including a 2nd degree potential as well so that matrices for any other symmetry can readily be formed in the f^2 configuration. Sufficient information is given to define the phases of the states so that other interactions such as spin-orbit can readily be included.

INTRODUCTION

THERE are a number of reasons why it is desirable to have matrix representations of Hamiltonians for f^2 electron systems which include a crystalline field as well as spin-orbit and electrostatic interaction between the two f electrons. To begin with spectra such as of U^{4+} ions have a large crystalline field, probably too large for successful treating of the crystalline Stark splitting by the perturbation of J levels. But even when the field is small as in Pr^{3+} there are a number of good reasons to apply such calculations. Thus in a spectrum in which so many of the levels have been identified it is a good opportunity (a) to test out how good the theory is, (b) to obtain the best parameters, (c) to assess the need for further improvement such an orbit-orbit interaction and configuration interaction. In Tm^{3+} the spectrum is much more uncertain and calculations might play a role in identifying the spectrum. And of course not the least important in setting up such matrices is the fact that machines are available which readily diagonalize fairly large-sized matrices.

The basis of states used for the calculations is $(LSJ\Gamma\rho)$ where ρ indicates the row of the irreducible representation of the symmetry group.

One would only have to calculate matrix elements for say the 4th degree potential and diagonal 6th degree elements. The off-diagonal 6th degree potential matrix elements could be obtained simply by treating them as unknowns in a set of simultaneous equations expressing the fact that the matrices of the 4th and 6th degree etc., potential commute. Commuting $n\times n$ matrices yield $n(n-1)/2$ simultaneous equations.

However, we did not use this method, but preferred to use the commutation of the matrices for different degree potentials of the same symmetry as a check on the correctness of the matrix elements. This was done for the matrices of the 4th and 6th degree octahedral potentials and for the 2nd and 4th degree D_{2h} potentials.

TABLE I. Bases within a J manifold for the octahedral group for values of J from 0 to 6.

	$J=0$	ψ_0
$^1\Gamma_1$	$J=4$	$2(6)^{-\frac{1}{2}}[(14)^{\frac{1}{2}}\psi_0+(5)^{\frac{1}{2}}(\psi_4+\psi_{-4})]$
	$J=6$	$1/4[(2)^{\frac{1}{2}}\psi_0-(7)^{\frac{1}{2}}(\psi_4+\psi_{-4})]$
$^1\Gamma_2$	$J=3$	$(2)^{-\frac{1}{2}}(\psi_2-\psi_{-2})$
	$J=6$	$(1/4)(2)^{-\frac{1}{2}}[(5)^{\frac{1}{2}}(\psi_6+\psi_{-6})-(11)^{\frac{1}{2}}(\psi_2+\psi_{-2})]$
$^2\Gamma_3$	$J=2$	$(2)^{-\frac{1}{2}}(\psi_2+\psi_{-2})$, ψ_0
	$J=4$	$(2)^{-\frac{1}{2}}(\psi_2+\psi_{-2})$
		$(1/2)(6)^{-\frac{1}{2}}[(10)^{\frac{1}{2}}\psi_0-(7)^{\frac{1}{2}}(\psi_4+\psi_{-4})]$
	$J=5$	$(2)^{-\frac{1}{2}}(\psi_2-\psi_{-2})$
		$(2)^{-\frac{1}{2}}(\psi_4-\psi_{-4})$
	$J=6$	$1/8[(22)^{\frac{1}{2}}(\psi_6+\psi_{-6})+(10)^{\frac{1}{2}}(\psi_2+\psi_{-2})]$
		$1/4[(14)^{\frac{1}{2}}\psi_0+(\psi_4+\psi_{-4})]$
$^3\Gamma_4$	$J=1$	ψ_0, ψ_1, ψ_{-1}
	$J=3$	ψ_0, $(8)^{-\frac{1}{2}}[(3)^{\frac{1}{2}}\psi_{\pm1}+(5)^{\frac{1}{2}}\psi_{\mp3}]$
	$J=4$	$(2)^{-\frac{1}{2}}(\psi_4-\psi_{-4})$
		$(8)^{-\frac{1}{2}}[(7)^{\frac{1}{2}}\psi_{\pm1}+\psi_{\mp3}]$
	$J=5a$	ψ_0, $(6)^{-\frac{1}{2}}[\psi_{\pm5}+(5)^{\frac{1}{2}}\psi_{\mp3}]$
	$J=5b$	$(2)^{-\frac{1}{2}}(\psi_4+\psi_{-4})$
		$(1/4)(6)^{-\frac{1}{2}}[3(6)^{\frac{1}{2}}\psi_{\pm1}-(7)^{\frac{1}{2}}\psi_{\mp3}+(35)^{\frac{1}{2}}\psi_{\pm5}]$
	$J=6$	$(2)^{-\frac{1}{2}}(\psi_4-\psi_{-4})$
		$(1/4)(2)^{-\frac{1}{2}}[(6)^{\frac{1}{2}}\psi_{\pm1}-(15)^{\frac{1}{2}}\psi_{\mp3}-(11)^{\frac{1}{2}}\psi_{\pm5}]$
$^3\Gamma_5$	$J=2$	$(2)^{-\frac{1}{2}}(\psi_2-\psi_{-2})$, $\psi_{\pm1}$
	$J=3$	$(2)^{-\frac{1}{2}}(\psi_2+\psi_{-2})$
		$(8)^{-\frac{1}{2}}[(5)^{\frac{1}{2}}\psi_{\pm1}-(3)^{\frac{1}{2}}\psi_{\mp3}]$
	$J=4$	$(2)^{-\frac{1}{2}}(\psi_2-\psi_{-2})$
		$(8)^{-\frac{1}{2}}[\psi_{\pm1}-(7)^{\frac{1}{2}}\psi_{\mp3}]$
	$J=5$	$(2)^{-\frac{1}{2}}(\psi_2+\psi_{-2})$
		$(1/4)(2)^{-\frac{1}{2}}[(15)^{\frac{1}{2}}\psi_{\pm5}-(14)^{\frac{1}{2}}\psi_{\pm1}-(3)\psi_{\mp3}]$
	$J=6a$	$(1/4)(2)^{-\frac{1}{2}}[(11)^{\frac{1}{2}}(\psi_6-\psi_{-6})-(5)^{\frac{1}{2}}(\psi_2-\psi_{-2})]$
		$1/16[(33)^{\frac{1}{2}}\psi_{\pm5}-7(2)^{\frac{1}{2}}\psi_{\pm1}-5(5)^{\frac{1}{2}}\psi_{\mp3}]$
	$J=6b$	$(1/4)(2)^{-\frac{1}{2}}[(5)^{\frac{1}{2}}(\psi_6-\psi_{-6})+(11)^{\frac{1}{2}}(\psi_2-\psi_{-2})]$
		$1/16[3(15)^{\frac{1}{2}}\psi_{\pm5}+(110)^{\frac{1}{2}}\psi_{\pm1}-(11)^{\frac{1}{2}}\psi_{\mp3}]$

TABLE IIA. Reduced matrix elements for second degree potentials $(J \| 3z^2-r^2 \| J')$. In Tables A–F: $(J \| V \| J') = (-1)^{J-J'}.(J' \| V \| J)$.

	$^3P_0$	$^3P_1$	$^3P_2$	$^3F_2$	$^3F_3$	$^3F_4$	$^3H_4$	$^3H_5$	$^3H_6$
$^3P_0$									
$^3P_1$		$-1/5$							
$^3P_2$	$(1/5)(2)^{\frac{1}{2}}$	$(1/10)(3)^{\frac{1}{2}}$	$1/15$						
$^3F_2$		$-2/15$	$(4/315)(3)^{\frac{1}{2}}$	$8/315$					
$^3F_3$		$(8/105)(7)^{\frac{1}{2}}$	$(-1/105)(21)^{\frac{1}{2}}$	$(1/210)(7)^{\frac{1}{2}}$	$1/90$				
$^3F_4$			$4/35$	$(2/945)(3)^{\frac{1}{2}}$	$(1/756)(21)^{\frac{1}{2}}$	$1/126$			
$^3H_4$				$(8/63)(11/30)^{\frac{1}{2}}$	$(-2/45)(11/210)^{\frac{1}{2}}$	$(2/315)(2/55)^{\frac{1}{2}}$	$-52/2475$		
$^3H_5$					$(4/525)(35)^{\frac{1}{2}}$	$(-1/675)(15)^{\frac{1}{2}}$	$(-13/675)(3/22)^{\frac{1}{2}}$	$-1/75$	
$^3H_6$						$(8/1485)(33)^{\frac{1}{2}}$	$(-2/7425)(30)^{\frac{1}{2}}$	$(-1/1650)(55)^{\frac{1}{2}}$	$-1/99$

B. Same as IIA for singlet states.

	$^1S_0$	$^1D_2$	$^1G_4$	$^1I_6$
$^1S_0$				
$^1D_2$	$(-4/15)(3)^{\frac{1}{2}}$	$22/315$		
$^1G_4$		$(-88/6930)(66)^{\frac{1}{2}}$	$-2/385$	
$^1I_6$			$(8/990)(6)^{\frac{1}{2}}$	$-2/99$

C. Reduced matrix elements for fourth degree potentials $(J \| 35z^4-30z^2r^2+3r^4) \| J')$.

	$^3P_0$	$^3P_1$	$^3P_2$	$^3F_2$	$^3F_3$	$^3F_4$	$^3H_4$	$^3H_5$	$^3H_6$
$^3P_0$									
$^3P_1$									
$^3P_2$			$(8/63)(3)^{\frac{1}{2}}$	$-2/567$					
$^3F_2$		$(-2/21)(7)^{\frac{1}{2}}$	$(-1/63)(21)^{\frac{1}{2}}$	$(-2/189)(7)^{\frac{1}{2}}$	$-1/4455$				
$^3F_3$	$(8/9)(2)^{\frac{1}{2}}$	$(1/9)(3)^{\frac{1}{2}}$	$2/63$	$(-4/693)(3)^{\frac{1}{2}}$	$(-1/693)(21)^{\frac{1}{2}}$	$(-1/3465)$			
$^3F_4$	$(16/99)(55)^{\frac{1}{2}}$	$(-8/99)(33/10)^{\frac{1}{2}}$	$(16/99)(110)^{-\frac{1}{2}}$	$(-104/693)(6/55)^{\frac{1}{2}}$	$(13/693)(42/55)^{\frac{1}{2}}$	$(-4/231)(2/55)^{\frac{1}{2}}$	$-4/5445$		
$^3H_4$		$(16/165)(5)^{\frac{1}{2}}$	$(-4/495)(15)^{\frac{1}{2}}$	$(-26/1485)(5)^{\frac{1}{2}}$	$(-2/189)(7/5)^{\frac{1}{2}}$	$(1/693)(15)^{\frac{1}{2}}$	$(-8/231)(66)^{-\frac{1}{2}}$	$-8/31,185$	
$^3H_5$			$(16/99)(3/11)^{\frac{1}{2}}$	$(-16/297)(11)^{-\frac{1}{2}}$	$(-5/297)(7/11)^{\frac{1}{2}}$	$(-10/231)(33)^{-\frac{1}{2}}$	$(-8/38115)(30)^{\frac{1}{2}}$	$(-4/1485)(5/11)^{\frac{1}{2}}$	$-8/49,005$
$^3H_6$									

D. Same as IIC for singlet states.

	$^1S_0$	$^1D_2$	$^1G_4$	$^1I_6$
$^1S_0$				
$^1D_2$		$4/189$		
$^1G_4$	$(16/3)(2/11)^{\frac{1}{2}}$	$(4/231)(6/11)^{\frac{1}{2}}$	$-46/38,115$	
$^1I_6$		$(-16/99)(11)^{-\frac{1}{2}}$	$(-4/847)(6)^{\frac{1}{2}}$	$4/16,335$

E. Reduced matrix elements for sixth degree potentials ($J \| 231z^6 - 315z^4r^2 + 105z^2r^4 - 5r^6 \| J'$).

	$^3P_0$	$^3P_1$	$^3P_2$	$^3F_2$	$^3F_3$	$^3F_4$	$^3H_4$	$^3H_5$	$^3H_6$
$^3P_0$					$-1/3861$				
$^3P_1$					$(10/3861)\,(21)^{\frac{1}{2}}$				
$^3P_2$			$(160/143)\,(110)^{-\frac{1}{2}}$	$(160/3861)\,(3)^{\frac{1}{2}}$	$(200/3861)\,(42/55)^{\frac{1}{2}}$	$1/81081$			
$^3F_2$			$(-4/143)\,(5/3)^{\frac{1}{2}}$	$(-1120/3861)\,(6/55)^{\frac{1}{2}}$		$(-80/1287)\,(2/55)^{\frac{1}{2}}$	$272/4,459,455$		
$^3F_3$			$(40/1287)\,(3/11)^{\frac{1}{2}}$	$(-16/429)\,(5)^{\frac{1}{2}}$	0	$(8/3861)\,(15)^{\frac{1}{2}}$	$(68/1287)\,(66)^{-\frac{1}{2}}$	$1/135,135$	
$^3F_4$		$(-40/429)\,(5)^{\frac{1}{2}}$		$(-160/1287)\,(11)^{-\frac{1}{2}}$	$(-8/429)\,(7/11)^{\frac{1}{2}}$	$(-32/3861)\,(3/11)^{\frac{1}{2}}$	$(16/42,471)\,(30)^{\frac{1}{2}}$	$(10/3861)\,(5/11)^{\frac{1}{2}}$	$5/891,891$
$^3H_4$									
$^3H_5$	$(80/429)\,(66)^{\frac{1}{2}}$	$(20/429)\,(3/11)^{\frac{1}{2}}$							
$^3H_6$									

F. Same as IIE for singlet states.

	$^1S_0$	$^1D_2$	$^1G_4$	$^1I_6$
$^1S_0$				
$^1D_2$			$-4/33,033$	
$^1G_4$	$(320/13)\,(33)^{-\frac{1}{2}}$	$(-160/1287)\,(6/11)^{\frac{1}{2}}$	$(32/14,157)\,(6)^{\frac{1}{2}}$	$-2/891,891$
$^1I_6$		$(400/1287)\,(11)^{-\frac{1}{2}}$		

RESULTS

Table I shows a set of bases for the octahedral group O_h each within a J manifold for values of J ranging from 0 to 6. The results are given as linear combinations of eigenstates of J_z (labeled by M), the z component of angular momentum. These linear combinations were obtained by diagonalizing the 4th degree potential within a J manifold using a JM basis initially. Unless an irreducible representation occurs more than once for a particular J, the eigenvectors within a J manifold of the 4th degree potential are also eigenvectors of the 6th degree potential.

For $J=6$ there are two $^3\Gamma_5$ representations which can be found. The $J=6a$, b sets of bases for $^3\Gamma_5$ are not eigenvectors of the 4th degree potential but only the 6th degree potential. On the other hand for $J=5$ two $^3\Gamma_5$ representations are contained. Two sets of bases for $^3\Gamma_4$ formed from $J=5$ states are readily found by recognizing that any state in the $J=5$ manifold must belong to $^3\Gamma_4$ if it is orthogonal to all the states (already determined) which belong to irreducible representations which are not $^3\Gamma_4$. The two $^3\Gamma_4$ bases are also required to be mutually orthogonal.

Only vectors belonging to one and the same *row* of any particular irreducible representation are used in calculating matrix elements. These are easily picked out by the fact that they are linear combinations of M states which differ by zero or ± 4.

The base vectors in Table I are arranged so that for a given representation the rows correspond, the first row in each case being the one actually used in our calculation of matrix elements.

Table II contains the reduced matrix elements for 2nd, 4th, and 6th degree potentials useful with any symmetry, and Table III presents the matrices of a 4th and 6th degree octahedral potential,

$$V = A\Sigma[(35z^4-30z^2r^2+3r^4)+5(x^4-6x^2y^2+y^4)]$$
$$+B\Sigma[(231z^6-315z^4r^2+105z^2r^4-5r^6)$$
$$-21(x^4-6x^2y^2+y^4)(11z^2-r^2)]$$
$$=(16/3)\pi^{\frac{1}{2}}A\Sigma r^4[Y_{4,0}+(5/14)^{\frac{1}{2}}(Y_{4,4}+Y_{4-4})]$$
$$+32(\pi/13)^{\frac{1}{2}}B\Sigma r^6[Y_{6,0}-(7/2)^{\frac{1}{2}}(Y_{6,4}+Y_{6-4})], \quad (1)$$

where the $Y_{l,m}$ are normalized spherical harmonics and the sum is over the electrons.

To use the nondiagonal reduced matrix elements in Table II it is important to know that they are normalized in such a way that to yield correct matrix elements by the Wigner-Eckart theorem they must be

TABLE III. Matrices of a fourth degree potential V_4 and sixth degree potential V_6 (given by Eq. (1) of octahedral symmetry in a basis of LSJ Γ states belonging to a definite row of Γ. The irreducible representations ${}^1\Gamma_1$, ${}^1\Gamma_2$, ${}^2\Gamma_2$, ${}^3\Gamma_4$, ${}^3\Gamma_5$ are often referred to as A_1, A_2, E, F_1 or t_1, F_2, or t_2, respectively.

${}^1\Gamma_1$, V_4	${}^1G_4$	${}^1I_6$	${}^1S_0$
${}^1G_4$	$\frac{-736}{363}$	$\frac{960}{847}(7)^{\frac{1}{2}}$	$32\left(\frac{2}{231}\right)^{\frac{1}{2}}$
${}^1I_6$		$\frac{-224}{121}$	0
${}^1S_0$			0

${}^1\Gamma_1$, V_4	${}^3H_4$	${}^3F_4$	${}^3H_6$	${}^3P_0$
${}^3H_4$	$\frac{-448}{363}$	$\frac{-80}{33}\left(\frac{2}{55}\right)^{\frac{1}{2}}$	$\frac{640}{2541}\left(\frac{7}{5}\right)^{\frac{1}{2}}$	$\frac{32}{21}\left(\frac{35}{33}\right)^{\frac{1}{2}}$
${}^3F_4$		$\frac{-16}{33}$	$\frac{800}{231}\left(\frac{7}{22}\right)^{\frac{1}{2}}$	$\frac{16}{21}\left(\frac{14}{3}\right)^{\frac{1}{2}}$
${}^3H_6$			$\frac{448}{363}$	0
${}^3P_0$				0

${}^1\Gamma_2$, V_4	${}^3H_6$	${}^1I_6$	${}^3F_2$
${}^3H_6$	$\frac{-64}{99}$	0	$\frac{80}{99}(2)^{\frac{1}{2}}$
${}^1I_6$		$\frac{32}{33}$	0
${}^3F_2$			$\frac{16}{99}$

${}^3\Gamma_3$, V_4	${}^1G_4$	${}^1I_6$	${}^1D_2$
${}^1G_4$	$\frac{-736}{2541}$	$\frac{-192}{847}(35)^{\frac{1}{2}}$	$\frac{32}{77}\left(\frac{10}{11}\right)^{\frac{1}{2}}$
${}^1I_6$		$\frac{608}{363}$	$\frac{-160}{231}\left(\frac{14}{11}\right)^{\frac{1}{2}}$
${}^1D_2$			$\frac{32}{21}$

TABLE III.—*Continued.*

$^2\Gamma_3, V_4$	$^3H_4$	$^3F_4$	$^3H_5$	$^3H_6$	$^3F_2$	$^3P_2$
$^3H_4$	$\frac{-64}{363}$	$\frac{-80}{231}\left(\frac{2}{55}\right)^{\frac{1}{2}}$	$\frac{128}{77}\left(\frac{7}{22}\right)^{\frac{1}{2}}$	$\frac{-128}{2541}(7)^{\frac{1}{2}}$	$\frac{-832}{231}\left(\frac{2}{11}\right)^{\frac{1}{2}}$	$\frac{128}{99}\left(\frac{3}{22}\right)^{\frac{1}{2}}$
$^3F_4$		$\frac{-16}{231}$	$\frac{-16}{77}(35)^{\frac{1}{2}}$	$\frac{-160}{231}\left(\frac{35}{22}\right)^{\frac{1}{2}}$	$\frac{-32}{231}(5)^{\frac{1}{2}}$	$\frac{16}{63}(15)^{\frac{1}{2}}$
$^3H_5$			$\frac{64}{99}$	$\frac{64}{99}\left(\frac{2}{11}\right)^{\frac{1}{2}}$	$\frac{-208}{693}(7)^{\frac{1}{2}}$	$\frac{-32}{77}\left(\frac{7}{3}\right)^{\frac{1}{2}}$
$^3H_6$				$\frac{-1216}{1089}$	$\frac{-160}{693}\left(\frac{14}{11}\right)^{\frac{1}{2}}$	$\frac{160}{231}\left(\frac{42}{11}\right)^{\frac{1}{2}}$
$^3F_2$					$\frac{-16}{63}$	$\frac{16}{21}(3)^{\frac{1}{2}}$
$^3P_2$						0

$^2\Gamma_4, V_4$	$^1I_6$	$^1G_4$
$^1I_6$	$\frac{-512}{363}$	$\frac{-48}{121}(30)^{\frac{1}{2}}$
$^1G_4$		$\frac{-368}{363}$

$^3\Gamma_4, V_4$	$^3P_1$	$^3F_3$	$^3H_4$	$^3F_4$	a^3H_5	b^3H_5	$^3H_6$
$^3P_1$	0	$\frac{8}{21}(7)^{\frac{1}{2}}$	$\frac{64}{99}\left(\frac{33}{14}\right)^{\frac{1}{2}}$	$\frac{-8}{63}(105)^{\frac{1}{2}}$	$\frac{16}{33}(5)^{\frac{1}{2}}$	$\frac{16}{77}(7)^{\frac{1}{2}}$	0
$^3F_3$		$\frac{-8}{99}$	$\frac{-104}{99}\left(\frac{6}{11}\right)^{\frac{1}{2}}$	$\frac{8}{99}(15)^{\frac{1}{2}}$	$\frac{8}{9}\left(\frac{5}{7}\right)^{\frac{1}{2}}$	$\frac{-56}{63}$	$\frac{200}{1089}(11)^{\frac{1}{2}}$
$^3H_4$			$\frac{-224}{363}$	$\frac{-40}{33}\left(\frac{2}{55}\right)^{\frac{1}{2}}$	$\frac{-64}{231}\left(\frac{35}{66}\right)^{\frac{1}{2}}$	$\frac{-224}{231}\left(\frac{6}{11}\right)^{\frac{1}{2}}$	$\frac{-32}{363}(6)^{\frac{1}{2}}$
$^3F_4$				$\frac{-8}{33}$	$\frac{40}{693}(21)^{\frac{1}{2}}$	$\frac{24}{99}(15)^{\frac{1}{2}}$	$\frac{-40}{33}\left(\frac{15}{11}\right)^{\frac{1}{2}}$
a^3H_5					$\frac{-64}{99}$	$\frac{-64}{693}(35)^{\frac{1}{2}}$	$\frac{32}{99}\left(\frac{35}{11}\right)^{\frac{1}{2}}$
b^3H_5						$\frac{64}{99}$	$\frac{-32}{1089}(11)^{\frac{1}{2}}$
$^3H_6$							$\frac{1024}{1089}$

$^3\Gamma_5, V_4$	$^1D_2$	$^1G_4$	$a\,^1I_6$	$b\,^1I_6$
$^1D_2$	$\frac{-64}{63}$	$\frac{16}{77}\left(\frac{10}{11}\right)^{\frac{1}{2}}$	$\frac{-200}{693}\left(\frac{14}{11}\right)^{\frac{1}{2}}$	$\frac{-8}{99}(70)^{\frac{1}{2}}$
$^1G_4$		$\frac{4784}{2541}$	$\frac{-192}{847}(35)^{\frac{1}{2}}$	0
$a\,^1I_6$			$\frac{464}{1089}$	$\frac{16}{99}(55)^{\frac{1}{2}}$
$b\,^1I_6$				$\frac{16}{99}$

TABLE III.—*Continued.*

${}^3\Gamma_5, V_4$	${}^3P_2$	${}^3F_2$	${}^3F_3$	${}^3F_4$	${}^3H_4$	${}^3H_5$	$a\,{}^3H_6$	$b\,{}^3H_6$
${}^3P_2$	0	$\frac{-32}{63}(3)^{\frac{1}{2}}$	$\frac{-8}{3}\left(\frac{5}{21}\right)^{\frac{1}{2}}$	$\frac{8}{63}(15)^{\frac{1}{2}}$	$\frac{64}{99}\left(\frac{3}{22}\right)^{\frac{1}{2}}$	$\frac{-128}{231}\left(\frac{7}{3}\right)^{\frac{1}{2}}$	$\frac{200}{693}\left(\frac{42}{11}\right)^{\frac{1}{2}}$	$\frac{8}{99}(210)^{\frac{1}{2}}$
${}^3F_2$		$\frac{32}{189}$	$\frac{-16}{27}\left(\frac{5}{7}\right)^{\frac{1}{2}}$	$\frac{-16}{231}(5)^{\frac{1}{2}}$	$\frac{-416}{231}\left(\frac{2}{11}\right)^{\frac{1}{2}}$	$\frac{-832}{2079}(7)^{\frac{1}{2}}$	$\frac{-200}{2079}\left(\frac{14}{11}\right)^{\frac{1}{2}}$	$\frac{-8}{297}(70)^{\frac{1}{2}}$
${}^3F_3$			$\frac{8}{297}$	$\frac{40}{231}(7)^{\frac{1}{2}}$	$\frac{-520}{231}\left(\frac{14}{55}\right)^{\frac{1}{2}}$	$\frac{-8}{27}(5)^{\frac{1}{2}}$	$\frac{280}{297}\left(\frac{10}{11}\right)^{\frac{1}{2}}$	$\frac{-40}{297}(2)^{\frac{1}{2}}$
${}^3F_4$				$\frac{104}{231}$	$\frac{520}{231}\left(\frac{2}{55}\right)^{\frac{1}{2}}$	$\frac{-8}{231}(35)^{\frac{1}{2}}$	$\frac{-80}{231}\left(\frac{70}{11}\right)^{\frac{1}{2}}$	0
${}^3H_4$					$\frac{416}{363}$	$\frac{32}{231}\left(\frac{14}{11}\right)^{\frac{1}{2}}$	$\frac{-128}{2541}(7)^{\frac{1}{2}}$	0
${}^3H_5$						$\frac{-128}{297}$	$\frac{-208}{297}\left(\frac{2}{11}\right)^{\frac{1}{2}}$	$\frac{80}{297}(10)^{\frac{1}{2}}$
$a\,{}^3H_6$							$\frac{-928}{3267}$	$\frac{-32}{297}(55)^{\frac{1}{2}}$
$b\,{}^3H_6$								$\frac{-32}{297}$

${}^1\Gamma_1, V_6$	${}^1G_4$	${}^1I_6$	${}^1S_0$
${}^1G_4$	$\frac{19200}{1573}$	$\frac{-4480}{1573}$	0
${}^1I_6$		$\frac{-1280}{4719}$	$\frac{640}{39}\left(\frac{6}{11}\right)^{\frac{1}{2}}$
${}^1S_0$			0

${}^1\Gamma_1, V_6$	${}^3H_4$	${}^3F_4$	${}^3H_6$	${}^3P_0$
${}^3H_4$	$\frac{-87,040}{14,157}$	$\frac{44,800}{1287}\left(\frac{2}{55}\right)^{\frac{1}{2}}$	$\frac{-11,200}{4719}\left(\frac{7}{5}\right)^{\frac{1}{2}}$	0
${}^3F_4$		$\frac{-1600}{1287}$	$\frac{4480}{429}\left(\frac{7}{22}\right)^{\frac{1}{2}}$	0
${}^3H_6$			$\frac{3200}{4719}$	$\frac{320}{429}(33)^{\frac{1}{2}}$
${}^3P_0$				0

${}^1\Gamma_2, V_6$	${}^3H_6$	${}^1I_6$	${}^3F_2$
${}^3H_6$	$\frac{3200}{429}$	0	$\frac{-2240}{429}(2)^{\frac{1}{2}}$
${}^1I_6$		$\frac{-1280}{429}$	0
${}^3F_2$			$\frac{320}{143}$

TABLE III.—*Continued*

	$^3\Gamma_3$, V_6	$^1G_4$	$^1I_6$	$^1D_2$
$^1G_4$		$\frac{-15,360}{1573}$	$\frac{-1920}{1573}(35)^{\frac{1}{2}}$	$\frac{320}{143}\left(\frac{10}{11}\right)^{\frac{1}{2}}$
$^1I_6$			$\frac{1280}{1573}$	$\frac{-1600}{429}\left(\frac{14}{11}\right)^{\frac{1}{2}}$
$^1D_2$				0

	$^3\Gamma_3$, V_6	$^3H_4$	$^3F_4$	$^3H_5$	$^3H_6$	$^3F_2$	$^3P_2$
$^3H_4$		$\frac{69,632}{14,157}$	$\frac{-35,840}{1287}\left(\frac{2}{55}\right)^{\frac{1}{2}}$	$\frac{-1088}{429}\left(\frac{7}{22}\right)^{\frac{1}{2}}$	$\frac{-1600}{1573}(7)^{\frac{1}{2}}$	$\frac{2240}{429}\left(\frac{2}{11}\right)^{\frac{1}{2}}$	$\frac{-960}{143}\left(\frac{3}{22}\right)^{\frac{1}{2}}$
$^3F_4$			$\frac{1280}{1287}$	$\frac{-128}{429}(35)^{\frac{1}{2}}$	$\frac{640}{143}\left(\frac{35}{22}\right)^{\frac{1}{2}}$	$\frac{-320}{429}(5)^{\frac{1}{2}}$	0
$^3H_5$				$\frac{-128}{143}$	$\frac{5600}{429}\left(\frac{2}{11}\right)^{\frac{1}{2}}$	$\frac{-1280}{429}(7)^{\frac{1}{2}}$	$\frac{-320}{143}\left(\frac{7}{3}\right)^{\frac{1}{2}}$
$^3H_6$					$\frac{-3200}{1573}$	$\frac{640}{429}\left(\frac{14}{11}\right)^{\frac{1}{2}}$	$\frac{-160}{429}\left(\frac{42}{11}\right)^{\frac{1}{2}}$
$^3F_2$						0	0
$^3P_2$							0

	$^3\Gamma_4$, V_6	$^1I_6$	$^1G_4$
$^1I_6$		$\frac{-640}{4719}$	$\frac{2240}{4719}(30)^{\frac{1}{2}}$
$^1G_4$			$\frac{-960}{1573}$

	$^3\Gamma_4$, V_6	$^3P_1$	$^3F_2$	$^3H_4$	$^3F_4$	$a\,^3H_5$	$b\,^3H_5$	$^3H_6$
$^3P_1$		0	0	0	0	$\frac{80}{143}(5)^{\frac{1}{2}}$	$\frac{-400}{429}(7)^{\frac{1}{2}}$	$\frac{160}{429}(77)^{\frac{1}{2}}$
$^3F_2$			$\frac{400}{429}$	$\frac{11,200}{1287}\left(\frac{6}{11}\right)^{\frac{1}{2}}$	$\frac{560}{1287}(15)^{\frac{1}{2}}$	0	0	$\frac{2240}{1573}(11)^{\frac{1}{2}}$
$^3H_4$				$\frac{4352}{14,157}$	$\frac{-2240}{1287}\left(\frac{2}{55}\right)^{\frac{1}{2}}$	$\frac{-3808}{429}\left(\frac{35}{66}\right)^{\frac{1}{2}}$	$\frac{1904}{1287}\left(\frac{6}{11}\right)^{\frac{1}{2}}$	$\frac{5600}{14,157}(6)^{\frac{1}{2}}$
$^3F_4$					$\frac{80}{1287}$	$\frac{-2240}{1287}(21)^{\frac{1}{2}}$	$\frac{448}{1287}(15)^{\frac{1}{2}}$	$\frac{-2240}{1287}\left(\frac{15}{11}\right)^{\frac{1}{2}}$
$a\,^3H_5$						$\frac{-320}{429}$	$\frac{-32}{143}(35)^{\frac{1}{2}}$	$\frac{-240}{143}\left(\frac{35}{11}\right)^{\frac{1}{2}}$
$b\,^3H_5$							$\frac{-128}{143}$	$\frac{-2800}{4719}(11)^{\frac{1}{2}}$
$^3H_6$								$\frac{1600}{4719}$

TABLE III.—*Continued*

	$^3\Gamma_5$, V_6	$^1D_2$	$^1G_4$	$a\,^1I_6$	$b\,^1I_6$
$^1D_2$		0	$\frac{-1280}{429}\left(\frac{10}{11}\right)^{\frac{1}{2}}$	$\frac{-1200}{143}\left(\frac{14}{11}\right)^{\frac{1}{2}}$	$\frac{400}{429}(70)^{\frac{1}{2}}$
$^1G_4$			$\frac{4800}{1573}$	$\frac{-12\,000}{14\,157}(35)^{\frac{1}{2}}$	$\frac{-160}{429}(77)^{\frac{1}{2}}$
$a\,^1I_6$				$\frac{-7360}{4719}$	0
$b\,^1I_6$					$\frac{960}{429}$

$^3\Gamma_5$ V_6	$^3P_2$	$^3F_2$	$^3F_3$	$^3F_4$	$^3H_4$	$^3H_5$	$a\,^3H_6$	$b\,^3H_6$
$^3P_2$	0	0	0	0	$\frac{1280}{143}\left(\frac{3}{22}\right)^{\frac{1}{2}}$	$\frac{160}{143}\left(\frac{7}{3}\right)^{\frac{1}{2}}$	$\frac{-120}{143}\left(\frac{42}{11}\right)^{\frac{1}{2}}$	$\frac{40}{429}(210)^{\frac{1}{2}}$
$^3F_2$		0	0	$\frac{1280}{1287}(5)^{\frac{1}{2}}$	$\frac{-8960}{1287}\left(\frac{2}{11}\right)^{\frac{1}{2}}$	$\frac{640}{429}(7)^{\frac{1}{2}}$	$\frac{480}{143}\left(\frac{14}{11}\right)^{\frac{1}{2}}$	$\frac{-160}{429}(70)^{\frac{1}{2}}$
$^3F_3$			$\frac{-240}{143}$	$\frac{-560}{1287}(7)^{\frac{1}{2}}$	$\frac{-11\,200}{1287}\left(\frac{14}{55}\right)^{\frac{1}{2}}$	0	$\frac{-560}{429}\left(\frac{10}{11}\right)^{\frac{1}{2}}$	$\frac{-1680}{429}(2)^{\frac{1}{2}}$
$^3F_4$				$\frac{-400}{1287}$	$\frac{11\,200}{1287}\left(\frac{2}{55}\right)^{\frac{1}{2}}$	$\frac{640}{1287}(35)^{\frac{1}{2}}$	$\frac{2000}{1287}\left(\frac{70}{11}\right)^{\frac{1}{2}}$	$\frac{80}{117}(14)^{\frac{1}{2}}$
$^3H_4$					$\frac{-21\,760}{14\,157}$	$\frac{2720}{1287}\left(\frac{14}{11}\right)^{\frac{1}{2}}$	$\frac{-10\,000}{14\,157}(7)^{\frac{1}{2}}$	$\frac{-80}{1287}(385)^{\frac{1}{2}}$
$^3H_5$						$\frac{320}{143}$	$\frac{1400}{143}\left(\frac{2}{11}\right)^{\frac{1}{2}}$	$\frac{280}{429}(10)^{\frac{1}{2}}$
$a\,^3H_6$							$\frac{18\,400}{4719}$	0
$b\,^3H_6$								$\frac{-2400}{429}$

TABLE IV. Wavefunctions in an $(LSM_L=LM_S=S)$ basis as linear combinations of Slater determinants.

$^3H=(3^+2^+)$
$^3F=1/3[(6)^{\frac{1}{2}}(2^+1^+)-(3)^{\frac{1}{2}}(3^+0^+)]$
$^3P=(1/14)^{\frac{1}{2}}[(3)^{\frac{1}{2}}(3^+-2^+)-(5)^{\frac{1}{2}}(2^+-1^+)+(6)^{\frac{1}{2}}(1^+0^+)]$
$^1I=(3^+3^-)$
$^1G=(1/11)^{\frac{1}{2}}[(5)^{\frac{1}{2}}(2^+2^-)-(3)^{\frac{1}{2}}(3^+1^-)+(3)^{\frac{1}{2}}(3^-1^+)]$
$^1D=(1/21)^{\frac{1}{2}}\{(5)^{\frac{1}{2}}[(2^+0^-)-(2^-0^+)]+(5/2)^{\frac{1}{2}}[(3^--1^+)-(3^+-1^-)]-(6)^{\frac{1}{2}}(1^+1^-)\}$
$^1S=(1/7)^{\frac{1}{2}}[(0^+0^-)-(1^+-1^-)+(1^--1^+)+(2^+-2^-)-(2^--2^+)-(3^+-3^-)+(3^--3^+)]$

multiplied by the following coefficient which we shall designate by the symbol $(j_1j_2m_1m_2;j_1j_2jm)$:

$$(j_1j_2m_1m_2;j_1j_2jm)\equiv(j_1j_2m_1m_2\mid j_1j_2jm)[(j+j_1+j_2+1)!]^{\frac{1}{2}}/[(j_1+j_2-j)!(j+j_1-j_2)!(j+j_2-j_1)!(2j+1)]^{\frac{1}{2}}$$

$$=\sum_k\frac{(-1)^k[(j_1+m_1)!(j_1-m_1)!(j_2+m_2)!(j_2-m_2)!(j+m)!(j-m)!]^{\frac{1}{2}}}{k!(j_1+j_2-j-k)!(j_1-m_1-k)!(j_2+m_2-k)!(j-j_2+m_1+k)!(j-j_1-m_2+k)!}. \quad (2)$$

TABLE V. Matrices of spin-orbit interaction ($\zeta=\frac{1}{2}\zeta_f$) with electrostatic interaction indicated.

$^3P_0$	$^1S_0$	$^3P_1$	$^3F_2$	$^1D_2$	$^3P_2$
$\lvert P-2\zeta$	$4(3)^{\frac{1}{2}}\zeta$	$\lvert P-\zeta$	$F-4\zeta$	$-2(6)^{\frac{1}{2}}\zeta$	0
	S			D	$-3(2)^{\frac{1}{2}}\zeta$
		$^3F_2$			
		$\lvert F-\zeta$			$P+\zeta$

$^3H_4$	$^1G_4$	$^3F_4$	$^3H_5$	$^3H_6$	$^1I_6$
$H-6\zeta$	$2(10/3)^{\frac{1}{2}}\zeta$	0	$\lvert H-\zeta$	$\lvert H+5\zeta$	$(6)^{\frac{1}{2}}\zeta$
	G	$2(11/3)^{\frac{1}{2}}$			I
		$F+3\zeta$			

Note that this coefficient is a normalized Wigner coefficient divided by the strictly M-independent part which is thereby absorbed into the reduced matrix elements. The use of this type of normalization is more convenient than the usual normalization as it saves some calculation time. Also the symmetry properties of the coefficients (2) as well as the reduced matrix elements are simpler. However, normalized Wigner coefficients are always used in transforming from an LSM_LM_S basis to an $LSJM$ basis and these were obtained from Table 2[3] of Condon and Shortley [1]

The *diagonal* reduced matrix elements of Table II have a different normalization (except those of degree 2) than the off-diagonal ones hence they cannot be used with Wigner coefficients in applying the Wigner-Eckart theorem until the proper normalizing factors are provided. Instead the diagonal reduced matrix elements are intended to be used with the Tables of Operator Equivalents given by Stevens.[2] This is to save some computation time.

Another feature of Table II which requires care in using is the fact that it is not entirely symmetric under interchanges of J and J'. Instead the reduced matrix elements satisfy the relation

$$(J \| V \| J') = (-1)^{J-J'}(J' \| V \| J). \qquad (3)$$

Thus Table II is meant to be read with the row label as J and the column label as J'.

[1] E. U. Condon and G. H. Shortley, *The Theory of Atomic Spectra* (Cambridge University Press, New York, 1953), p. 76.

[2] K. W. H. Stevens, Proc. Phys. Soc. (London) **A65**, 213 (1952). Our reduced matrix diagonal elements are what are called α, β, γ by Stevens. See also B. R. Judd, Proc. Roy. Soc. (London) **A227**, 552 (1955) and **241**, 414 (1957), for α, β, γ values for most of the LSJ terms in the f^2 configuration.

In adding the spin-orbit matrices to the crystalline potential one must be careful of phases, i.e., to be sure the spin-orbit matrices were calculated in the same basis of states having the same phases as in the crystalline potential calculation. In order to define the phases, so that our work can be used by others to calculate results for other symmetries or to include other interactions, we present a set of LSM_LM_S wavefunctions for $M_L=L$, $M_S=S$ for the various LS states of the f^2 configuration. These are given as linear combinations of Slater determinants in Table IV. States with other M_L or M_S with the proper phases can be obtained by applying the usual lowering operators.[3] To form $LSJM$ functions with the proper phases as linear combinations of the LSM_LM_S functions one uses Wigner coefficients $(j_1j_2m_1m_2 \mid j_1j_2jm)$ with always $j_1=L, j_2=S$. The spin-orbit matrices in an $LSJM$ basis with our choice of phases are given in Table V; they are the same except for some sign changes as those given by Spedding.[4]

The electrostatic interaction between the two f electrons is diagonal in any basis characterized by L and S and is given in terms of Slater integrals (see reference 1, page 207).

It should be mentioned that G. Goodman[5] has also calculated the matrices of spin-orbit, electrostatic interaction and octahedral ligand field for the f^2 configuration in a basis in which the octahedral potential is diagonal and applied the results to the spectrum of PuF_6. We have compared eigenvalues calculated from our matrices with those of Goodman for the same set of parameters and complete agreement was obtained. However, as a result of making this comparison, we uncovered a numerical error in two of our matrix elements. Thus we are indebted to Goodman for his results which were a help in locating the errors.

ACKNOWLEDGMENT

One of us (RAS) is grateful for the opportunity of spending the summer 1957 in the Chemistry Division at the Argonne National Laboratory, where at the suggestion of Dr. Dieter Gruen this problem was begun and much of the work completed. This work was supported in part by the U.S. Atomic Energy Commission and the U.S. Army Office of Ordnance Research.

[3] Reference 1, p. 48.

[4] F. H. Spedding, Phys. Rev. **58**, 255 (1940).

[5] G. Goodman, Ph.D. dissertation, Harvard (1959).

THE JOURNAL OF CHEMICAL PHYSICS VOLUME 32, NUMBER 2 FEBRUARY, 1960

Dipole Moment Function for HD*

S. M. BLINDER

Applied Physics Laboratory, The Johns Hopkins University, Silver Spring, Maryland

(Received July 27, 1959)

The wave-function method of Trischka and Salwen for computing dipole moment functions is applied to the HD molecule. From data on relative intensities of the weak rotation-vibration transitions, several possible dipole functions are constructed. The one having a maximum coincident with the vibrational potential minimum is believed to be the most reasonable.

TRISCHKA and Salwen[1] have recently given a method for approximating the dipole moment function $M(u)$ of a diatomic molecule in terms of a set of matrix elements R^{00}, R^{01}, $\cdots$, R^{0n}. By their "wave-function method," $M^*(u)$, an approximation to $M(u)$ may be found from

$$M^*(u)=\sum_{n=0}^{N}R^{0n}[\psi_n(u)/\psi_0(u)], \tag{1}$$

where $u=r-r_0$, the displacement from equilibrium nuclear separation. The $\psi_n(u)$ are approximations to the vibrational wave functions. R^{00} is the permanent moment in the vibrational state $v=0$. The other matrix elements R^{0n} are related to observed intensities (integrated over J) of rotation-vibration transitions from the $v=0$ level as follows[2]:

$$I^{0n}/I^{0m}=\nu_{0n}\mid R^{0n}\mid^2/\nu_{0m}\mid R^{0m}\mid^2. \tag{2}$$

If the vibrational levels of the molecule are known, it is possible to determine the relative magnitudes of the R^{0n}. Their signs remain ambiguous. It may be possible, however, to place certain limitations upon the choice of signs from various criteria of physical reasonableness. Presumably, the more terms included in the series (1), the better $M^*(u)$ represents $M(u)$. In addition, a sharp decrease in the magnitudes of successive R^{0n} brings about rapid convergence.

We shall attempt to apply this method to the HD molecule. A dipole moment of order 10^{-3} debye unit arises as a consequence of asymmetric slippage of the electron cloud with nuclear vibration.[3,4] We shall first discuss the validity of representing this effect by a dipole moment function.

$M(u)$ is a function, characteristic of the electronic state of a molecule but independent of the vibrational level, which yields dipole moment matrix elements via integration over vibrational eigenfunctions. For an ordinary heteronuclear diatomic (e.g., HCl) the validity and meaning of such a function are well established. In the case of HD, the moment arises from a vibrational perturbation. It is difficult to demonstrate, by any classical argument, that a vibration-independent dipole function is meaningful, as well, for this molecule. Our quantum mechanical treatment of the problem[5] nevertheless suggests that such a representation is valid for the lower vibrational states of HD. Involved in this conclusion are certain presumptions as to relative magnitude of vibrational and electronic energies. Contingent upon these, a summation procedure reduces dipole moment matrix elements to integrals of a multiplicative operator over vibrational eigenfunctions. This is equivalent to the existence of a dipole function independent of vibrational quantum number. The characteristics dependent on vibrational state are then manifested only in weighted averages over $M(u)$. The foregoing considerations apply only for low vibrational quantum numbers. For highly excited states (when vibrational energy is no longer negligible with respect to electronic energy), our representation of $M(u)$ is no longer adequate.

The experimental data we shall use to construct the dipole function are the intensity measurements on the weak rotation-vibration absorption spectrum of HD.[6] The relative intensities of the transitions 0→1, 0→2, 0→3, 0→4 are roughly indicated by the ratios 1:1.9:0.24:0.08.[7] This is, incidentally, the first known case of intensity reversal for the fundamental and first overtone. The 0→3 and 0→4 intensities are also anomalously large. Generally, the relative intensities of successive overtones fall off sharply (by successive factors approximating 100). This situation was anticipated by Gray and Pritchard[8] for a hypothetical diatomic molecule with dipole function attaining its maximum value near the potential minimum.

The experimental data imply the following rela-

* This work supported by Bureau of Ordnance, Department of the Navy, under NOrd 7386.

[1] J. Trischka and H. Salwen, J. Chem. Phys. **31**, 218, 541 (1959).

[2] See, for example, G. Herzberg, *Spectra of Diatomic Molecules* (D. Van Nostrand Company, Inc., Princeton, New Jersey, 1950), pp. 20–21.

[3] G. C. Wick, Atti accad. naz. Lincei (Ser. 6) **21**, 708 (1935).

[4] S. M. Blinder, J. Chem. Phys. **32**, 105 (1960).

[5] S. M. Blinder, "Dipole Moment of HD, Part II," to be published. This work was reported at the Symposium on Molecular Structure and Spectra, The Ohio State University, June 15–19, 1959.

[6] G. Herzberg, Nature **166**, 563 (1950).

[7] R. A. Durie and G. Herzberg, unpublished work. We are grateful to Dr. Herzberg for permission to use these results.

[8] B. F. Gray and H. O. Pritchard, J. Mol. Spectroscopy **2**, 137 (1958).

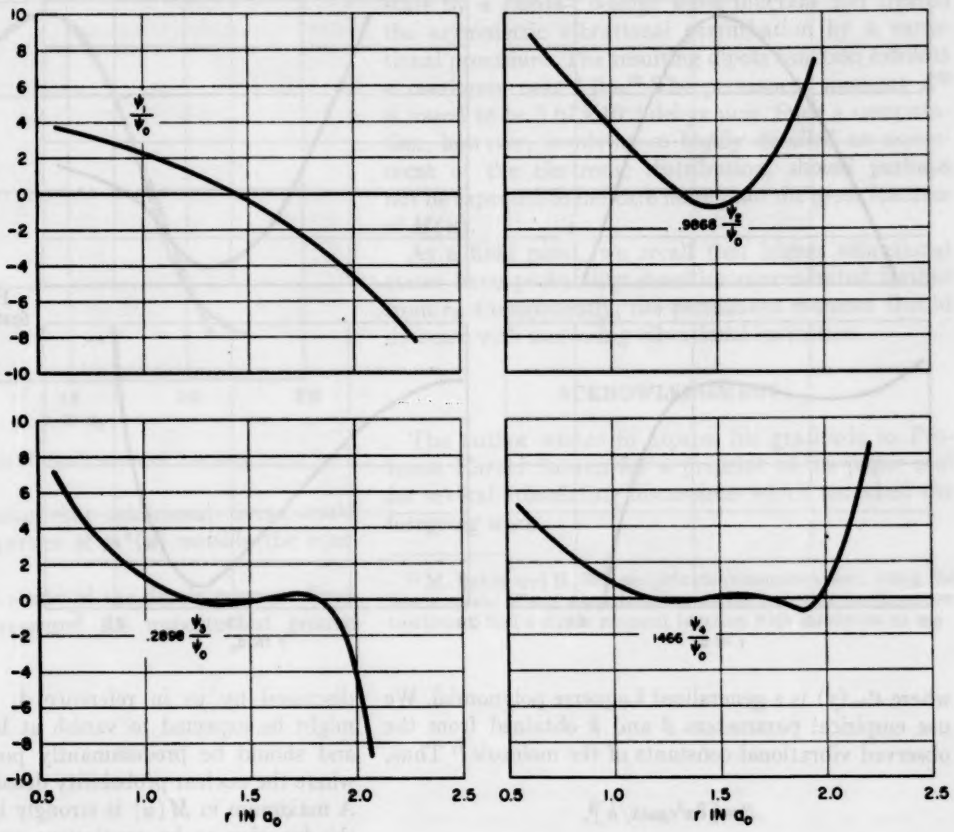

FIG. 1. Wave function ratios.

tionships among the R matrix elements:

$$\nu_{02}\,|\,R^{02}\,|^2/\nu_{01}\,|\,R^{01}\,|^2=1.9,$$
$$\nu_{03}\,|\,R^{03}\,|^2/\nu_{01}\,|\,R^{01}\,|^2=0.24,$$
$$\nu_{04}\,|\,R^{04}\,|^2/\nu_{01}\,|\,R^{01}\,|^2=0.08. \qquad (3)$$

From the vibrational constants for the HD molecule,[9] the frequencies for the hypothetical $J=0$ to $J=0$ transitions are:

$$\nu_{01}=3632\ \text{cm}^{-1},$$
$$\nu_{02}=7087\ \text{cm}^{-1},$$
$$\nu_{03}=10374\ \text{cm}^{-1},$$
$$\nu_{04}=13502\ \text{cm}^{-1}.$$

These yield the relative magnitudes of the R^{0n} with undetermined signs:

$$R^{02}=\pm 0.9868R^{01},$$
$$R^{03}=\pm 0.2898R^{01},$$
$$R^{04}=\pm 0.1466R^{01}.$$

To the approximation that the higher R^{0n} vanish, the dipole function is given by

$$M^*(u)=R^{00}+R^{01}\{[\psi_1(u)/\psi_0(u)]\pm 0.9868[\psi_2(u)/\psi_0(u)]\pm 0.2898[\psi_3(u)/\psi_0(u)]\pm 0.1466[\psi_4(u)/\psi_0(u)]\}. \qquad (4)$$

Regarding the origin and scale of this function as undetermined, the general contour of $M^*(u)$ may still be studied. Accordingly, we define

$$m^*(u)\equiv[M^*(u)-R^{00}]/R^{01}=[\psi_1(u)/\psi_0(u)]\pm 0.9868[\psi_2(u)/\psi_0(u)]\pm 0.2898[\psi_3(u)/\psi_0(u)]\pm 0.1466[\psi_4(u)/\psi_0(u)], \qquad (5)$$

there being an eightfold indeterminacy in the combination of signs. We represent the $\psi_n(u)$ by the Morse eigenfunctions for a nonrotating oscillator[10]:

$$\left.\begin{aligned}\psi_n(u)&=A_n e^{-y/2}y^{(k-2n-1)/2}\mathfrak{L}_{kn}(y)\\ y&=ke^{-\beta u}\\ A_n&=\left[\frac{\beta(k-2n-1)}{n!(k-n-1)!}\right]^{\frac{1}{2}}\end{aligned}\right\} \qquad (6)$$

[9] G. Herzberg, *Spectra of Diatomic Molecules* (D. Van Nostrand Company, Inc., Princeton, New Jersey, 1950), p. 352.

[10] P. M. Morse, Phys. Rev. **34**, 57 (1929); J. L. Dunham, *ibid.* **34**, 438 (1929).

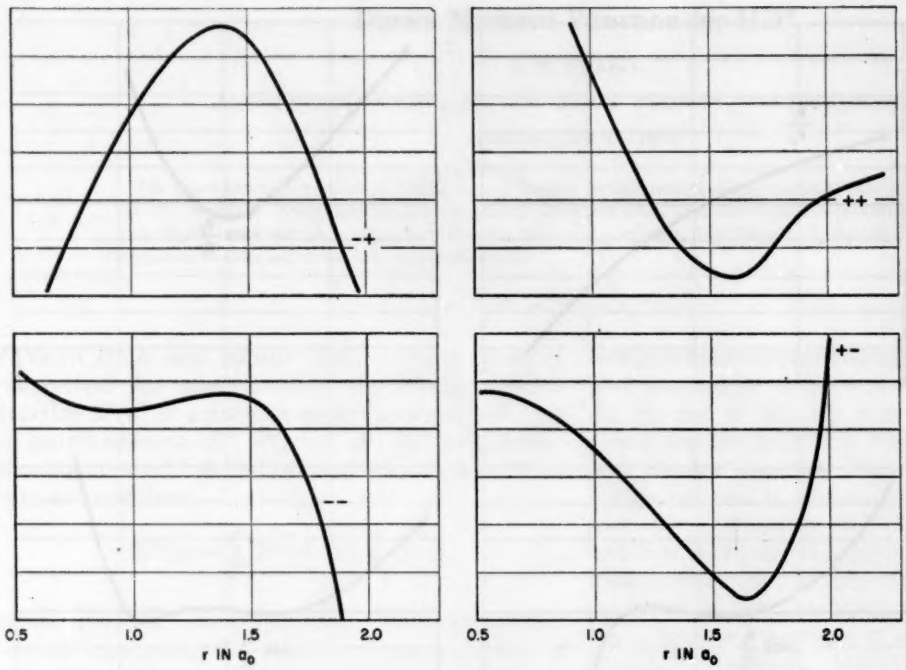

FIG. 2. Combinations of first three functions.

where $\mathfrak{L}_{kn}(y)$ is a generalized Laguerre polynomial. We use empirical parameters β and k obtained from the observed vibrational constants of the molecule.[11] Thus,

$$\beta=[8\pi^2c\mu\omega x/h]^{\frac{1}{2}},$$

$$k=\omega/\omega x, \quad \text{to nearest integer,}$$

where ω is the fundamental vibrational frequency, ωx the anharmonicity, μ the reduced nuclear mass. For the ground state of HD we obtain

$$k=40, \qquad \beta=1.945\times10^8\ \text{cm}^{-1}.$$

The four terms of the function $m^*(u)$ are shown separately in Fig. 1. The four possible combinations of the first three terms are drawn in Fig. 2; these are labeled by the appropriate sign choices. Addition of the fourth term has little effect on the shape of $m^*(u)$ in the equilibrium region $u\approx0(r\approx1.4a_0)$. In particular, the position of the maximum or minimum is not significantly shifted. This term becomes increasingly important, however, for larger values of $|u|$. We may conclude that the expansion (1) converges rapidly in the neighborhood of $u=0$ despite the rather slow decline in the magnitudes of the first few R^{0n}. Outside the equilibrium region, however, more terms would be required to represent the dipole moment function adequately.

We shall next try to decide, on physical grounds, among the alternate representations for $m^*(u)$. As discussed by us in reference 4, the dipole function might be expected to vanish at both $r=0$ and $r=\infty$ and should be predominantly positive in the region where the nuclear probability densities are significant.[12] A maximum in $M(u)$ is strongly indicated, presuming the function to be continuous and smooth. We note that a maximum in $M^*(u)$ may correspond to either a maximum or a minimum in $m^*(u)$ according as R^{01} is positive or negative. The $(-+)$ and $(--)$ representations would then correspond to positive R^{01}, the $(++)$ and $(+-)$, to negative R^{01}. The maximum of the dipole function for these combinations are at $1.40a_0$, $1.38a_0$, $1.60a_0$, and $1.64a_0$, respectively. The $(--)$ representation is unattractive in view of the fact that it does not approach the same limit for $r=0$ and $r=\infty$. Inclusion of more terms might, however, correct the asymptotic behavior. Rigorously then, we cannot make a choice given the available information. As discussed by Trischka and Salwen,[1] knowledge of other matrix elements, for instance the R^{1n}, would be helpful in determining signs. Our guess is that the $(-+)$ representation is the most reasonable. This choice is made appealing by the fact that the dipole maximum occurs at the vibrational potential minimum $(1.40a_0)$ where the nuclear kinetic energy, hence the slippage effect and the contribution to $M(u)$, should be maximized. In addition, inclusion of the fourth term with positive sign (Fig. 3) results in a dipole function which approaches finite limits at both ends. None of the other seven combinations has this property. However, we

[11] Reference 9, p. 101 ff., etc.

[12] In accordance with our convention, a positive dipole function corresponds to the H end of the molecule being positive with respect to the D end.

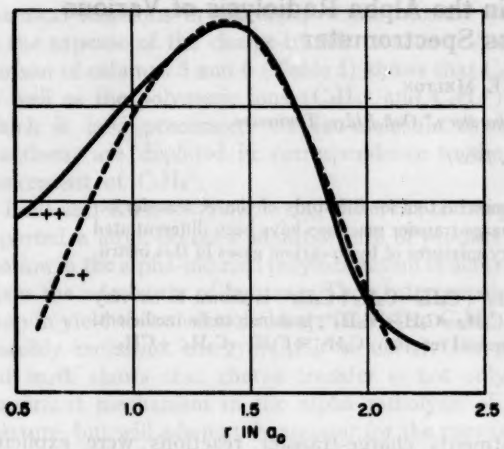

FIG. 3. Shape of dipole moment function.

must again emphasize that additional terms could easily alter the properties of $m^*(u)$ outside the equilibrium region.

In our theoretical study of the dipole moment function,[5] we have represented the unperturbed ground state by a James-Coolidge wave function and treated the asymmetric vibrational perturbation by a variational procedure. The resulting dipole function exhibits a maximum near $1.0a_0$.[13] The permanent moment R^{00} is found to be 5.67×10^{-4} debye unit. Such a computation, however, involving so highly detailed an assessment of the electronic distribution, should perhaps not be expected to indicate more than the gross features of $M(u)$.

As a final point, we recall that higher vibrational states have probability densities concentrated farther from r_0. Consequently, the permanent moment should decrease with increasing vibrational excitation.

ACKNOWLEDGMENT

The author wishes to express his gratitude to Professor Harold Salwen for a preprint of his paper and for several stimulating discussions which launched the foregoing work.

[13] M. Baker and H. Salwen (private communication), using the less accurate Wang wave function and a one-state perturbation treatment, find a dipole moment function with maximum at r_0.

Ion-Molecule Charge Transfer Reactions in the Alpha Radiolysis of Various Hydrocarbons in a Mass Spectrometer

P. S. RUDOLPH AND C. E. MELTON

Chemistry Division, Oak Ridge National Laboratory, Oak Ridge, Tennessee*

(Received July 15, 1959)

The new alpha-particle mass spectrometer proves to be a powerful tool for the study of charge transfer between gaseous ions and molecules. Energetically possible charge-transfer reactions have been differentiated into probable and improbable reactions by employing binary mixtures of hydrocarbon gases in this instrument.

The alpha-particle induced charge-transfer reaction, $C_2H_2^+ + C_6H_6 \rightarrow C_2H_2 + C_6H_6^+$, is shown to be very efficient. In contrast, the charge-transfer reaction, $C_2H_2^+ + C_2H_4 \rightarrow C_2H_2 + C_2H_4^+$, is shown to be inefficient. This inefficiency is discussed in terms of the competing chemical reaction, $C_2H_2^+ + C_2H_4 \rightarrow C_3H_3^+ + CH_3$.

INTRODUCTION

TO establish detailed mechanisms in the radiation chemistry of gaseous mixtures one must consider the possibility of ion-molecule reactions resulting in either chemical change[1] or charge transfer.[2] In a theoretical treatment on mechanisms in the radiation chemistry of gases, Burton and Magee[2] conclude that charge transfer may play a significant role. They further conclude that mere adequacy of energy relationships is not necessarily a sufficient requirement for charge transfer and that a specific mechanism for such a transfer is required.

We have previously described a new alpha-particle mass spectrometer[3] operated at a pressure as high as 0.11 mm in the ionization chamber. This instrument was used to detect and identify ion-molecule reactions resulting in chemical change.[4,5] In the present work, we describe a further application of the same instrument to differentiate ion-molecule reactions into either charge-transfer reactions or chemical reactions. Binary mixtures of acetylene with benzene or ethylene were studied. The acetylene-benzene mixture was selected for initial study since charge transfer had been postulated from chemical evidence to explain the retardation of the alpha-induced polymerization of acetylene by benzene vapor.[6] Hence, a careful investigation of this mixture in the new alpha-particle mass spectrometer was undertaken to test the validity of this postulate.

The importance of ion-molecule charge-transfer reactions in gas phase radiolyses has been the subject of several theoretical discussions.[2,7,8] In view of these treatments charge-transfer reactions were explicitly considered in the previous mass-spectrometric alpha-radiolysis studies of the C_2 hydrocarbons.[4,5] However, data from these studies indicated that charge-transfer reactions played no significant role.

EXPERIMENTAL

Acetylene of 99.99% purity was prepared as previously described.[9] Benzene (Merck, thiophene-free, ACS reagent grade) and ethylene (Phillips Petroleum Company 99.96%) were used without further purification.

The gaseous samples were introduced into the alpha-particle mass spectrometer[3] according to the previously described procedure.[4] Ratios of gaseous mixtures were accurate to within one percent, whereas the absolute pressures given are correct to within about 10 percent. Two pressures in the ionization chamber; 0.01 and 0.1 mm, were employed for the pure gases. For mixtures the total pressure was held at 0.11 mm always maintaining a ratio of 10:1 for the partial pressures of the constituent gases.

RESULTS AND DISCUSSION

When a charge-transfer reaction makes a significant contribution to the absolute intensity of an ion this contribution is readily observed. The data in Table I demonstrate this for the following reaction:

$$C_2H_2^+ + C_6H_6 \rightarrow C_2H_2 + C_6H_6^+. \qquad (1)$$

Consider the absolute intensity for $C_6H_6^+$ in columns 4 and 5. In the mixture (column 5) the intensity of $C_6H_6^+$ is 11-fold that of $C_6H_6^+$ (column 4) at the same partial pressure. This 11-fold increase can only be attributed to the increased concentration of $C_2H_2^+$ which reacts as per reaction (1).

Contrary to the effect observed in the mixture of C_2H_2 and C_2H_4 discussed in the following, competing

* Operated for the U. S. Atomic Energy Commission by the Union Carbide Corporation.

[1] V. L. Tal'rose and A. K. Lyubimova, Doklady Akad. Nauk. S.S.S.R. **86,** 909 (1952).

[2] M. Burton and J. L. Magee, J. Phys. Chem. **56,** 842 (1952).

[3] C. E. Melton and P. S. Rudolph, J. Chem. Phys. **30,** 847 (1959).

[4] P. S. Rudolph and C. E. Melton, J. Phys. Chem. **63,** 916 (1959).

[5] C. E. Melton and P. S. Rudolph, J. Chem. Phys. (submitted for publication).

[6] S. C. Lind and P. S. Rudolph, J. Chem. Phys. **26,** 1768 (1957).

[7] J. L. Magee, J. Phys. Chem. **56,** 555 (1952).

[8] H. S. W. Massey and E. H. S. Burhop, *Electronic and Ionic Impact Phenomena* (Oxford University Press, New York, 1952).

[9] Melton, Bretscher, and Baldock, J. Chem. Phys. **26,** 1302 (1957).

chemical reactions in the $C_2H_2-C_6H_6$ mixture suffer at the expense of the charge-transfer reaction. A comparison of columns 5 and 6 (Table I) shows that $C_2H_2^+$ as well as the polymeric ions ($C_4H_2^+$ and $C_4H_3^+$) for which it is a precursor,[4] via ion-molecule chemical reactions, are depleted in correspondence to the enhancement of $C_6H_6^+$.

Lind and Rudolph,[6] employing different techniques, reported a large decrease in initial rate of product formation in the alpha-induced polymerization of acetylene upon the admixture of benzene. They interpreted this drop in yield to transfer of charge ($C_2H_2^+$ to C_6H_6) and possibly excitation energy ($C_2H_2^*$ to C_6H_6). The present work shows that charge transfer is not only an important mechanism in the alpha radiolysis of this mixture, but will adequately account for the previously observed 32% decrease in initial yield. Thus, our work supports the postulates of Lind and Rudolph.

On the other hand, when charge transfer makes no significant contribution to the absolute intensity of an ion, the data clearly indicates that fact. Consider the energetically possible reaction:

$$C_2H_2^+ + C_2H_4 \rightarrow C_2H_2 + C_2H_4^+ \quad \Delta H = -0.9 \text{ ev.} \quad (2)$$

The $C_2H_4^+$ intensities in both the pure gas and the mixture are equal within experimental error (cf. columns 3 and 4, Table II). This is also true for the intensities of its product ion,[5] $C_3H_5^+$. In these cases the pressure of C_2H_4 is identical. If $C_2H_4^+$ were enhanced by reaction (2), the intensities of $C_2H_4^+$ and $C_3H_5^+$ would necessarily be much higher in the mixture (column 4) because of the 100-fold increase in concentration of $C_2H_2^+$ plus its product ions.[4] Because all product ions in the radiolyses of C_2H_2 come from $C_2H_2^+$ under the present experimental conditions,[4] the increase in intensity of $C_2H_2^+$ was from 32 to 3841 ions/sec. Hence, about 10% of the $C_2H_2^+$ ions are precursors for $C_3H_3^+$ in the mixture. This view is further supported by the values for the total ion intensities in the pure gases and in the mixture. The total ion intensity for the mixture is equal to the summation of the total ion intensities of the pure gases. Thus the intensity of $C_2H_4^+$ is not enhanced by reaction (2).

TABLE I. Experimental results showing charge transfer in the alpha radiolysis of a binary mixture of C_2H_2 and C_6H_6.

			Absolute intensity (ions/sec)		
Mass	Ion	A.P. ev	$1C_6H_6$	$1C_6H_6$ / $10C_2H_2$	$10C_2H_2$
26	$C_2H_2^+$	11.4		305	500
50	$C_4H_2^+$			400	835
51	$C_4H_3^+$			900	1570
78	$C_6H_6^+$	9.2	140	1600	
	Total[a]		140	3906	3841

[a] Total ion intensity of all ions observed, some of which are not shown in this table.

TABLE II. Experimental results pertinent to the possibility of charge transfer in a mixture of acetylene and ethylene.

		Intensity in ions/sec		
(1) Mass	(2) Ion	(3) $1C_2H_4$	(4) $10C_2H_2$ / $1C_2H_4$	(5) $10C_2H_2$
26	$C_2H_2^+$	32	525	500
27	$C_2H_3^+$	70	202	120
28	$C_2H_4^+$	192	166	
39	$C_3H_3^+$		404	
40	$C_3H_4^+$		30	
41	$C_3H_5^+$	30	40	
50	$C_4H_2^+$		575	835
51	$C_4H_3^+$		1250	1570
52	$C_4H_4^+$		170	116
53	$C_4H_5^+$		170	
74	$C_6H_2^+$		40	70
75	$C_6H_3^+$		70	70
76	$C_6H_4^+$		184	290
77	$C_6H_5^+$		180	270
Total		324	4006	3841

The contribution of reaction (2) to the formation of various ions may be obtained from the following relationship:

$$I_t = I_m - I_p, \quad (3)$$

where I_t is the intensity of $C_2H_4^+$ produced by reaction (2); I_m is the sum of the intensity of $C_2H_4^+$ and its product ($C_3H_5^+$) in the mixture; I_p is the sum of the intensities of $C_2H_4^+$ and its product ($C_3H_5^+$) in C_2H_4 alone.

With the values for these quantities in Table II, one obtains:

$$I_m = 166 + 40 = 206,$$

and

$$I_p = 192 + 30 = 222.$$

After substituting these values in Eq. (3), one gets

$$I_t = 206 - 222 = -16.$$

Since this value for I_t is zero within experimental error for these low intensities of ions, it is readily seen that reaction (2) is extremely ineffective and that charge transfer is negligible.

The ion-molecule chemical reaction

$$C_2H_2^+ + C_2H_4 \rightarrow C_3H_3^+ + CH_3 \quad (4)$$

is also energetically possible. In contrast to the charge-transfer reaction (2), the competing chemical reaction (4) is found to be very efficient. Table II shows that $C_3H_3^+$ is found in measurable quantities only in the mixture. Hence, this ion can result only from reaction (4).† We note further that $C_4H_5^+$ for which $C_3H_3^+$ is a precursor[5] also is observed only in the mixture.

† $C_2H_4^+$ is formed by a similar reaction, which does not require separate consideration.

It is obvious from these data that of the two energetically possible reactions (2) and (4), the chemical reaction (4) is vastly more efficient. In fact no evidence was found to substantiate the existence of the charge-transfer reaction (2).

CONCLUSIONS

The study of mixtures at high pressures (up to 0.11 mm) in the new alpha-particle mass spectrometer is particularly elucidating in the explanation of radiolytic reactions. In the present instance, ion-molecule reactions resulting in chemical change are differentiated from those resulting in charge transfer. The probability or improbability of charge-transfer reactions in the alpha radiolysis of binary mixtures of C_2H_2 with C_6H_6 or C_2H_4 has been clearly shown.

We have shown that mere adequacy of energy is an insufficient criterion for postulating ion-molecule charge-transfer reactions and that competing ion-molecule chemical reactions must also be considered when postulating a reaction mechanism.

ACKNOWLEDGMENT

The authors are indebted to Dr. Russell Baldock, Dr. C. J. Hochanadel, and Dr. S. C. Lind of this Laboratory and to Professor M. Burton of Notre Dame University and Professor M. Dole of Northwestern University for constructive criticism and helpful suggestions.

THE JOURNAL OF CHEMICAL PHYSICS VOLUME 32, NUMBER 2 FEBRUARY, 1960

Infrared Spectra of Metal-Chelate Compounds. I. A Normal Coordinate Treatment on Bis-(Acetylacetonato)-Cu(II)*†

KAZUO NAKAMOTO AND ARTHUR E. MARTELL

Department of Chemistry, Clark University, Worcester, Massachusetts

(Received August 14, 1959)

A normal coordinate treatment on the chelate ring of bis-(acetylacetonato)-Cu(II) gives calculated frequencies in good agreement with the observed ones in the 1700 and 350 cm^{-1} range obtained with NaCl, KBr, and CsBr optics. In order to assign the observed bands and to see the coupling between various vibrational modes, the L matrices and the potential energy distribution, $L_{ij}^2F_i$ were calculated for all the in-plane vibrations. The results reveal that (1) the band at 1580 cm^{-1} previously assigned to *asym.* CO stretching is *asym.* CC stretching, (2) the bands at 684 and 654 cm^{-1} formerly suggested to be metal-oxygen stretching modes are metal-oxygen stretching vibrations coupled with ring deformation and CCH_3 bending modes, respectively, and (3) a new band found at 455 cm^{-1} is the *sym.* Cu—O stretching mode. By comparing the force constants of the Cu—O stretching vibration with those of metal-nitrogen and metal-carbon bonds of other compounds, it is suggested that the Cu—O bond in this compound has double bond character.

THE nature of the metal-oxygen bond in the metal chelate compounds of β-diketones has been a subject of considerable interest. Calvin and Wilson[1] originally suggested "benzenoid resonance" which allows partial double bond character for the metal-oxygen bond, although no definite evidence was given from their experimental results. As pointed out by Keller and Parry,[2] however, this structure may not be probable if π-bonding is formed by donation of 3*d*-electrons of the metal to the oxygen, since oxygen has no vacant orbitals. Holm and Cotton[3] recently suggested that π-bonding may be possible if donation of electrons occurs from oxygen to the metal ($0_{p\pi} \rightarrow M_{p\pi,d\pi}$) against the "electrical neutrality principle." Thus, it is highly desirable to obtain experimental data on the bond order of the metal-oxygen bond to see whether π-bonding really exists in these compounds. The stretching force constants of the metal-oxygen bond obtained from the analysis of the vibrational spectra would be useful for this purpose.

On the other hand, studies of the vibrational spectra of the metal-chelates of β-diketones themselves are interesting from the viewpoint of molecular spectroscopy since thus far no normal coordinate treatments have been made on such a chelate ring system, where coupling between various vibrational modes may

* Presented in part before the International Conference on Coordination Chemistry, April 9, 1959 (London).

† This investigation was supported in part by a research grant, H-3246(C1), from the National Heart Institute, Public Health Service.

[1] M. Calvin and K. W. Wilson, J. Am. Chem. Soc. **67**, 2003 (1945).

[2] R. N. Keller and R. W. Parry, *The Chemistry of the Coordination Compounds* (Reinhold Publishing Corporation, New York, 1956), p. 247.

[3] R. H. Holm and F. A. Cotton, J. Am. Chem. Soc. **80**, 5658 (1958).

occur and the concept of "group frequency" may be broken down.

The infrared spectra of the metal-chelate compounds of the β-diketones have been studied extensively by many investigators. For example, Lecomte[4] measured the infrared spectra of a number of metallic acetylacetonates and assigned the bands by assuming the spectra to be derived from the coupled vibrations of two acetone molecules bound together by a chemical linkage. Bellamy and his co-workers[5] attempted to correlate the CO stretching frequencies with the stability of the complex in various β-diketones. Mecke and Funck[6] have made the most complete empirical assignments of the infrared bands of the keto- and enol-forms of acetylacetone and its monovalent metal chelates. Recently more data on the infrared spectra of various β diketones and their metal chelates have been accumulated by other investigators.[7-12]

All these previous measurements, however, have been done only in the NaCl region, and the band assignments have been made only empirically. It is, therefore, desirable to obtain the spectra below 650 cm^{-1} where the metal-oxygen stretching modes may appear. Furthermore, a normal coordinate treatment must be carried out to make theoretical assignments, especially on the metal-oxygen stretching bands as well as to see coupling between various vibrational modes.

In the present paper, the infrared spectrum of bis-(acetylacetonato)-Cu(II) has been obtained in the range between 4000 and 350 cm^{-1}, and a normal coordinate treatment is made for the purpose mentioned above. The effects of changing metals in various β-diketones on the infrared spectra will be discussed in detail in the subsequent paper.

EXPERIMENTAL

Preparation of the Compound

Bis-(acetylacetonato)-Cu(II) was prepared by the reaction between acetylacetone and basic copper acetate. It was first recrystallized from chloroform solution, and was then further purified by sublimation at *ca* 110°C.[8]

Spectral Measurements

A Perkin-Elmer Model 21 infrared spectrophotometer equipped with NaCl or KBr optics was used to obtain the spectra in the range between 4000 and 450 cm^{-1}. The KBr disk method was employed for the preparation of the sample to be measured in this range. For the spectrum between 450 and 350 cm^{-1}, a Perkin-Elmer Model 112 single beam infrared spectrophotometer equipped with CsBr optics was used. In order to avoid water absorption in the air, the whole optical path was flushed by running dry nitrogen. The Nujol mull technique was employed with plates of CsBr. Calibration of the frequency reading was made with polystyrene film (NaCl region), 1,2,4-trichlorobenzene (KBr region), and water vapor for all regions.

TABLE I. Bond distances and angles in metal acetylacetonato complexes.

	$Cu(acac)_2$[a]	$Fe(acac)_3$[b]	Values used in this work
r_1	1.24 and 1.29	1.28	1.28
r_2	1.45 and 1.50	1.39	1.39
r_3	1.50 and 1.55	1.53	1.53
r_4	1.95 and 1.96	1.95	1.95
$\alpha_{12}, \alpha_{12}'$	122° and 134°	119°46′	$\alpha_{12}=\alpha_{12}'=120°$
$\alpha_{23}, \alpha_{23}'$	113° and 118°	...	$\alpha_{23}=\alpha_{23}'=120°$
$\alpha_{31}, \alpha_{31}'$	113° and 130°	...	$\alpha_{31}=\alpha_{31}'=120°$
β	...	132°50′	135°
γ	87°5′	89°50′	90°
δ	119°	132°20′	120°

[a] See reference 14.
[b] See reference 16.
R=1.08 A (taken from ethylene); $\delta=\delta_1=\delta_1'=120°$ was assumed.

METHOD OF CALCULATION

1. Structural Data and Simplified Model

In order to carry out a normal coordinate treatment on such a complicated molecule as the bis-(acetylacetonato)-Cu(II) complex, it is desirable to simplify the system by making reasonable assumptions. Table I compares the bond distances and angles obtained by x-ray analysis on Cu(II)[14,15] and Fe(III) complexes.[16] In the former compound, different bond distances are reported for two C—C and C—O bonds in the same chelate ring. On the other hand, C_{2v} symmetry is reported in the latter. As Holm and Cotton pointed out,[8] the apparent discrepancies of the bond distances found in the former compound might be ascribed to incomplete refinements in the calculations. For this reason, as well as for the purpose of simplifying the calculation, the bond distances and angles were taken from the latter compound.‡

Figure 1 illustrates the molecular model employed in the present calculation.[8] In order to simplify the calculation, a 1:1 complex has been used notwith-

[4] J. Lecomte, Discussions Faraday Soc. **9**, 125 (1950); Duval, Freymann, and Lecomte, Bull. soc. chim. France **19**, 106 (1952).
[5] L. J. Bellamy and R. F. Branch, J. Chem. Soc. **1954**, 4491; L. J. Bellamy, G. S. Spicer, and J. D. H. Strickland, *ibid.* 4653 (1952).
[6] R. Mecke and E. Funck, Z. Elektrochem. **60**, 1124 (1956).
[7] Belford, Martell, and Calvin, J. Inorg. Nuclear Chem. **2**, 11 (1956).
[8] H. F. Holtzclaw, Jr., and J. P. Collman, J. Am. Chem. Soc. **79**, 3318 (1957).
[9] R. West and R. Riley, J. Inorg. Nuclear Chem. **5**, 295 (1958).
[10] R. P. Dryden and A. Winston, J. Phys. Chem. **62**, 635 (1958).
[11] R. West, J. Org. Chem. **23**, 1552 (1958).
[12] Comyns, Gatehouse, and Wait. J. Chem. Soc. **1958**, 4655.
[13] Sacconi, Caroti, and Paoletti, J. Chem. Soc. **1958**, 4257.
[14] Koyama, Saito, and Kuroya, J. Inst. Polytech. Osaka City Univ. **C4**, 43 (1953).
[15] E. A. Shugam, Doklady Akad. Nauk. S.S.S.R. **81**, 853 (1951).
[16] R. B. Roof, Jr., Acta Cryst. **9**, 781 (1956).
‡ Practically, slight differences in bond distances and angles do not cause serious error in the calculations, since the values of the force constants are the main factors in determining the frequencies.

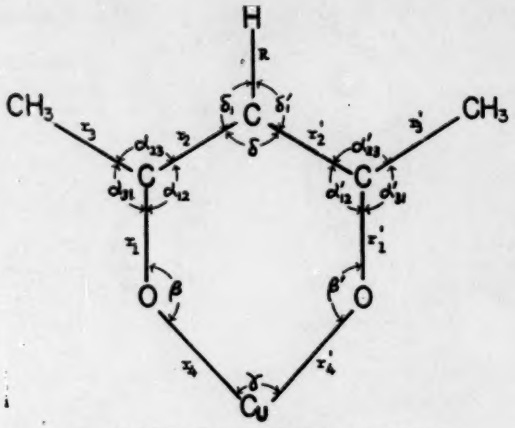

FIG. 1. Molecular model of the 1:1 complex.

standing the fact that the molecule is actually 1:2 complex having a square planar configuration around the central copper atom. This assumption is not serious for most of the vibrational modes except the Cu–O vibration. The methyl group was assumed to be a single atom having the same mass as that of the methyl group.

2. Classification of the Vibrations

This simplified model has twenty-one normal vibrations. Since the symmetry of this model is C_{2v}, the vibrations are grouped into four classes. Furthermore, the in-plane vibrations ($8A_1$ and $7B_2$) are separable from the out-of plane vibrations ($2A_2$ and $4B_1$). In this paper, the fifteen in-plane vibrations are calculated.

The symmetry coordinates are given in Table II and the elements of the **G** and **F** matrices are tabulated in the Appendix. Evidently, both the A_1 and B_2 matrices thus obtained still involve one redundant condition in each species which is a complicated function of the bond distances and angles. It is not necessary, however, to write these two redundant conditions explicitly since they give "zero frequency" in the final calculation. Furthermore, the order of the A_1 matrix was reduced by using a "high-frequency separation" for a C—H stretching mode. Finally, two 8th-order secular equations of the form, $|\mathbf{GF}-\mathbf{E}\lambda|=0$ were solved for each species.

Force Constants

In order to express the potential energy, an Urey-Bradley potential field[17] of the following type was employed:

$$V=\sum_i[K_i'r_{i0}(\Delta r_i)+\tfrac{1}{2}K_i(\Delta r_i)^2]+\sum_i[H_i'r_{ia}^2(\Delta\alpha_i)+\tfrac{1}{2}H_i r_a^2(\Delta\alpha_i)^2]+\sum_i[F_i'q_{i0}(\Delta q_i)+\tfrac{1}{2}F_i(\Delta q_i)^2].$$

Here, Δr_i, $\Delta\alpha_i$, and Δq_i are the changes of the bond length, bond angles, and the distances between nonbonded atoms. The symbols K_i, K_i', H_i, H_i', F_i, and F_i' represent the stretching, bending, and repulsive force constants, respectively. Furthermore, r_{i0}, r_{ia}, and q_{i0} are the values of the distances at the equilibrium positions, and are inserted to make the force constants dimensionally similar. The quantities K_i' and H_i' vanish in the final result, since they can be expressed in terms of F' by the equilibrium condition. F' was taken as $-\frac{1}{10}F$ by assuming that the repulsive energy between the nonbonded atoms is proportional to $1/r^9$. The set of the force constants used in the present calculation is given in Table III. Most of the values were taken from benzene[18] and acetic acid anion,[19] because the results of x-ray analysis indicate that the C—C and C—O bond distances are almost the same as those in benzene and acetic acid anion, respectively. Mecke and Funck[6] also arrived at the same conclusion from a comparison of the stretching frequencies of the C—C and C—O bonds in the enol-form of acetylacetone with those of benzene and acetic acid anion, respectively. The force constants related to the Cu—O

TABLE II. Symmetry coordinates for in-plane vibrations.

Species	Symmetry coordinate	Vibrational mode
A_1	$S_9=\Delta R$	CH str.
	$S_1=(1/\sqrt{2})(\Delta r_1+\Delta r_1')$	CO str.
	$S_3=(1/\sqrt{2})(\Delta r_2+\Delta r_2')$	CC str.
	$S_5=(1/\sqrt{2})(\Delta r_3+\Delta r_3')$	C·CH$_3$ str.
	$S_7=(1/\sqrt{2})(\Delta r_4+\Delta r_4')$	CuO str.
	$S_{11}^a=(1/\sqrt{2})(\Delta\alpha_{23}-\Delta\alpha_{31}+\Delta\alpha_{23}'-\Delta\alpha_{31}')$	C·CH$_3$ bend.
	$S_{13}=(1/2)(\Delta\alpha_{12}+\Delta\alpha_{12}'-\Delta\beta-\Delta\beta')$	ring def.
	$S_{15}=(1/\sqrt{12})(2\Delta\gamma+2\Delta\delta-\Delta\alpha_{12}-\Delta\alpha_{12}'-\Delta\beta-\Delta\beta')$	ring def.
	$S_{17}=(1/\sqrt{2})(\Delta\gamma-\Delta\delta)$	ring def.
	$S_{19}=(\Delta\alpha_{12}+\Delta\alpha_{23}+\Delta\alpha_{31}+\Delta\alpha_{12}'+\Delta\alpha_{23}'+\Delta\alpha_{31}')$	redundant
	$S_{20}=(\Delta\delta+\Delta\delta_1+\Delta\delta_1')$	redundant
	$S_{21}=(\Delta\alpha_{12}+\Delta\alpha_{12}'+\Delta\beta+\Delta\beta'+\Delta\gamma+\Delta\delta)$	redundant
B_2	$S_2=(1/\sqrt{2})(\Delta r_1-\Delta r_1')$	CO str.
	$S_4=(1/\sqrt{2})(\Delta r_2-\Delta r_2')$	CC str.
	$S_6=(1/\sqrt{2})(\Delta r_3-\Delta r_3')$	C·CH$_3$ str.
	$S_8=(1/\sqrt{2})(\Delta r_4-\Delta r_4')$	CuO str.
	$S_{10}^a=(1/\sqrt{2})(\Delta\alpha_{23}-\Delta\alpha_{31}-\Delta\alpha_{23}'+\Delta\alpha_{31}')$	C·CH$_3$ bend.
	$S_{12}^a=(\Delta\delta_1-\Delta\delta_1')$	CH bend.
	$S_{14}=(1/2)(\Delta\alpha_{12}-\Delta\alpha_{12}'+\Delta\beta-\Delta\beta')$	ring def.
	$S_{16}=(1/2)(\Delta\alpha_{12}-\Delta\alpha_{12}'-\Delta\beta+\Delta\beta')$	ring def.
	$S_{18}=(\Delta\alpha_{12}+\Delta\alpha_{23}+\Delta\alpha_{31}-\Delta\alpha_{12}'-\Delta\alpha_{23}'-\Delta\alpha_{31}')$	redundant

[a] These three coordinates are not normalized. This is due to the following reason: When the orders of the original 21st-order matrices were reduced using redundant conditions such as $\Delta\delta+\Delta\delta_1+\Delta\delta_1'\equiv 0$, nonorthogonal matrices such as

$$\mathbf{T}=\begin{pmatrix}+1 & +1 & +1\\ +1 & 0 & 0\\ 0 & +1 & -1\end{pmatrix}$$

were employed. Since **T** is not orthogonal, the **G** and **F** matrices were transformed as follows: $\mathbf{G}^T=\mathbf{TGT}$ and $\mathbf{F}^T=\tilde{\mathbf{T}}^{-1}\mathbf{F}\mathbf{T}^{-1}$.

[17] T. Shimanouchi, J. Chem. Phys. **17**, 245, 734, 848 (1949).

[18] Y. Kakiuchi, Bull. Chem. Soc. Japan **26**, 260 (1953).

[19] K. Nakamura, J. Chem. Soc. Japan **79**, 1411 (1958).

TABLE III. Force constants of bis-(acetylacetonato)-Cu(II) in 10^5 dyne/cm.

Stretching	Bending	Repulsive
$K_1=K(C^{\cdots\cdots}O)=7.20$[a]	$H_1=H(\Delta\alpha_{12})=0.2$[c]	$F_1=F(C\cdots O)=0.50$[a]
$K_2=K(C^{\cdots\cdots}C)=5.46$[b]	$H_2=H(\Delta\alpha_{23})=0.25$[c]	$F_2=F(C\cdots CH_3)=0.40$
$K_3=K(C—CH_3)=3.30$[a]	$H_3=H(\Delta\alpha_{31})=0.31$[a]	$F_3=F(O\cdots CH_3)=0.50$[a]
$K_4=K(Cu—O)=2.25$	$H_\beta=H(\Delta\beta)=0.05$	$F_4=F(C\cdots Cu)=0.05$
	$H_\gamma=H(\Delta\gamma)=0.05$	$F_5=F(O\cdots O)=0.05$
	$H_\delta=H(\Delta\delta)=0.33$[b]	$F_6=F(C\cdots C)=0.37$[b]
	$H_{\delta_1}=H(\Delta\delta_1)=0.20$[b]	$F_7=F(C\cdots H)=0.54$[b]

[a] Acetic acid anion (reference 19).
[b] Benzene (reference 18).
[c] Intermediate values between these two. The value of $K(C—CH_3)$ was increased to take into account the repulsions of the three hydrogens of the methyl group, since in the present calculation, the methyl group was assumed to be a single atom.

bond were determined so as to obtain the best fit between the calculated and observed frequencies.

RESULTS AND DISCUSSION

Frequency

The infrared spectra of bis-(acetylacetonato)-Cu(II) is shown in Fig. 2. The frequencies of the absorption bands in the NaCl region agree in general with those reported by West and Riley.[9] Table IV compares the observed with the calculated frequencies. The agreements are surprisingly good for such a complicated ring system, although the bands corresponding to the calculated frequencies of 373,§ 320, 273, and 197 cm^{-1} could not be observed because these frequencies were outside of our observable region.

As stated above, the coupling between two acetylacetone molecules which exists in actual 1:2 complex was entirely neglected in our calculation. It is obvious, however, that the effect of such coupling is serious only between four Cu—O bonds which form a square planar configuration around the central Cu atom. In order to see the effect of coupling between four Cu—O bonds, two calculations have been made with the same set of the force constants by using a nonlinear triatomic

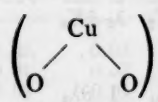

and a square planar (CuO_4) models. A comparison of the Cu—O stretching frequencies obtained by these two calculations indicates that the former model tends to give slightly lower frequencies than the latter. As will be shown later, ν_6 at 455 cm^{-1} (calculated as 457 cm^{-1}) and ν_{14} (calculated as 320 cm^{-1}) are almost pure Cu—O stretching modes of symmetric and antisymmetric types, respectively. Therefore, it is reasonable to assume that both the frequencies may be slightly higher|| if a calculation is made on the actual 1:2 complex.

The bands observed at 1415, 1356, 1020, 781, and 614 cm^{-1} are attributed either to the methyl group or to out-of-plane vibrations which were not treated in the present calculation (see Table IV).

Effect of Coupling

It is anticipated that the usual empirical assignments made by using the concept of "group frequency" may encounter difficulty in a chelate ring system because strong coupling between various vibrational modes may occur. In order to know the nature of the observed bands, it is therefore necessary to determine the mixing ratio of various modes in each band. The **L** matrix defined by the following relation:

$$\mathbf{S}=\mathbf{LQ}, \quad \text{or} \quad \mathbf{Q}=\mathbf{L}^{-1}\mathbf{S}$$

expresses the relative amplitude of each symmetry coordinate in a given normal vibration. (Here, **S** denotes the internal symmetry coordinates, and **Q** represents the normal coordinates.) It should be noted, however, that the dimension of L for the stretching coordinates is different from those for the deformation coordinates. In such a case, it is better to calculate the distribution of potential energy in the internal symmetry coordinates in each normal vibration. The potential energy of the whole molecule for a given normal vibration (Q_λ) is given by

$$V=\tfrac{1}{2}\cdot Q_\lambda^2\sum F_{kl}L_{k\lambda}L_{l\lambda}$$

where $F_{ii}L_{i\lambda}^2$ are the distributions of energies in the coordinate, S_i, in the normal vibration, Q_λ.[20] There-

§ The band at 373 cm^{-1} may be too weak to be observed although it is within our observable region.

|| As a result, slightly smaller Cu—O stretching force constant will be suitable in the 1:2 complex.

[20] Y. Morino and K. Kuchitsu, J. Chem. Phys. **20**, 1809 (1952); Sweeny, Nakagawa, Mizushima, and Quagliano, J. Am. Chem. Soc. **78**, 889 (1956).

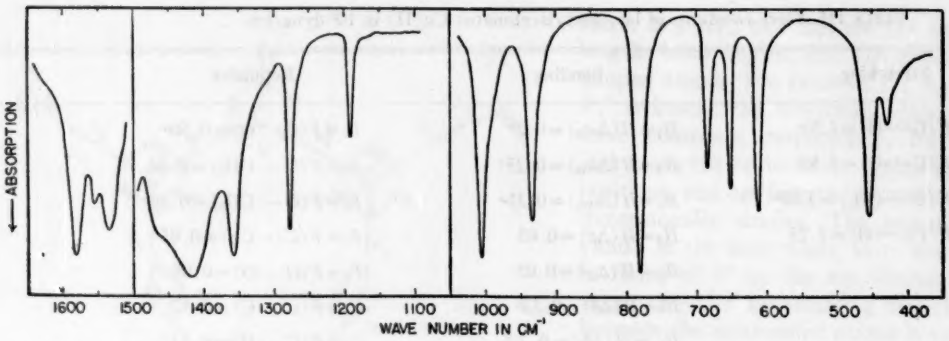

FIG. 2. Infrared spectrum of bis-(acetylacetonato)-Cu(II).

fore, the potential energy distributions, $F_{ii}L_{ai}^2$, have been calculated for all the in-plane vibrations, and the results are shown in Table V, where the number indicates only relative contributions from each symmetry coordinate.

TABLE IV. Comparison of calculated and observed frequencies of bis-(acetylacetonato)-Cu(II) in cm^{-1}.

		Obs.	Calc.	Error (%)
In-plane modes A_1	ν_1	1554	1566	+0.8
	ν_2	1274	1251	−1.8
	ν_3	937	934	−0.3
	ν_4	684	657	−3.9
	ν_5	455	457	+0.4
	ν_6	...	273	
	ν_7	...	197	
B_2	ν_8	1580	1594	+0.9
	ν_9	1534	1500	−2.2
	ν_{10}	1190	1225	+2.9
	ν_{11}	937	881	−6.0
	ν_{12}	654	631	−3.5
	ν_{13}	?	373	
	ν_{14}	...	320	
Out-of-plane-modes[a]		1415		CH_3 deg. def.
		1356		CH_3 sym. def.
		1020		CH_3 rock.
		781		CH out-of-plane bend.
		614		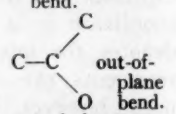 out-of-plane bend.
		427[b]		out-of-plane or ν_{13}

[a] Without calculation, it is almost certain that the three bands at 1415, 1356, and 1020 cm^{-1} bands are due to methyl group [See I. Nakagawa and S. Mizushima, Bull. Chem. Soc. Japan **28**, 589 (1955)]. The band at 781 cm^{-1} shows deuterium shift and was assigned to C—H out-of-plane mode by Mecke and Funck. The band at 614 cm^{-1} is probably due to the

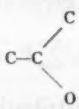

wagging mode, since a similar mode was observed at 616 cm^{-1} for the acetic acid anion [see L. H. Jones and E. McLaren, J. Chem. Phys. **22**, 1796 (1954) or reference 19].

[b] The assignment for this band is ambiguous. It may be one of the out-of-plane ring vibrations or may correspond to the observed band at 373 cm^{-1} (ν_{13}) if it is assumed that the force constants used for ring deformations were too low.

Band Assignments

On the basis of the results shown in Table V, it is now possible to assign the observed bands theoretically. As is seen in Fig. 2, three strong bands appear at 1580, 1554, and 1534 cm^{-1}. The first band at 1580 cm^{-1} (ν_8) is definitely due to asymmetric C—C stretching, and not C—O stretching. This result is particularly interesting since the previous investigators assigned it empirically to the C—O stretching mode. The following bands at 1554 (ν_1), 1534 (ν_9), and 1274 (ν_2) cm^{-1} are *sym.* C—O stretching, *asym.* C—O stretching (coupled with C—H bending), and *sym.* C—C stretching (coupled with C—CH_3 stretching) modes, respectively. The order of the frequencies of these four bands is reasonable since the two C—C stretching frequencies are far apart because two C—C bonds are next to each other and interact strongly, whereas two C—O stretching frequencies are close because two C—O bonds are separated, and interaction between the two stretching coordinates is fairly small.

In order to investigate in detail the reversal of the frequency order of ν_8 and ν_1, we have calculated the Jacobian matrix[21]

$$J_{ah}=\begin{pmatrix} \frac{1}{\lambda_1}\frac{\partial\lambda_1}{\partial K_1} & \frac{1}{\lambda_2}\frac{\partial\lambda_2}{\partial K_1} & \cdots & \frac{1}{\lambda_a}\frac{\partial\lambda_a}{\partial K_1} \\ \frac{1}{\lambda_1}\frac{\partial\lambda_1}{\partial K_2} & \frac{1}{\lambda_2}\frac{\partial\lambda_2}{\partial K_2} & \cdots & \frac{1}{\lambda_a}\frac{\partial\lambda_a}{\partial K_2} \\ \cdots & \cdots & \cdots & \cdots \\ \frac{1}{\lambda_1}\frac{\partial\lambda_1}{\partial K_h} & \frac{1}{\lambda_2}\frac{\partial\lambda_2}{\partial K_h} & \cdots & \frac{1}{\lambda_a}\frac{\partial\lambda_a}{\partial K_h} \end{pmatrix}$$

which expresses the effect of variation of the force constants on the frequencies. As is shown in Table VI, it was found that a fairly large decrease of K(C···C) and increase of K(C···O) are necessary to reverse the order of ν_8 and ν_1. Since the values of K(C···C) and

[21] T. Miyazawa, J. Chem. Soc. Japan **76**, 1132 (1955); I. Nakagawa and T. Shimanouchi, *ibid.* **80**, 128 (1959).

TABLE V. The potential energy distribution $F_{ii}L_{ik}^2$ for each normal mode of vibration.[a]

		Symmetry coordinate								
	Band	S_1	S_3	S_5	S_7	S_{11}	S_{13}	S_{15}	S_{17}	Assignments[b]
A_1 species	ν_1	*1.00*	0.36	0.03	0.02	0.14	0.00	0.07	0.02	CO str.
	ν_2	0.19	*1.00*	*0.85*	0.02	0.08	0.14	0.01	0.00	CC str. + CCH_3 str.
	ν_3	*0.83*	0.37	*1.00*	0.25	0.09	0.40	0.19	0.42	CCH_3 str. + CO str.
	ν_4	0.02	0.00	0.54	*0.97*	0.38	*1.00*	0.04	0.14	ring def. + CuO str.
	ν_5	0.05	0.35	0.52	*1.00*	0.17	0.02	0.17	0.09	CuO str.
	ν_6	0.03	0.07	0.00	0.30	*1.00*	0.02	0.00	0.01	C·CH_3 bend.
	ν_7	0.01	0.00	0.00	0.04	0.01	0.65	*1.00*	0.12	ring def.
		S_2	S_4	S_6	S_{12}	S_8	S_{10}	S_{14}	S_{16}	
B_2 species	ν_8	0.32	*1.00*	0.01	0.09	0.00	0.04	0.00	0.03	CC str.
	ν_9	*1.00*	0.13	0.20	*0.99*	0.03	0.06	0.03	0.04	CO str. + CH bend.
	ν_{10}	0.35	0.20	0.31	*1.00*	0.03	0.00	0.01	0.00	CH bend.
	ν_{11}	0.10	0.10	*1.00*	0.01	0.06	0.02	0.00	0.04	C·CH_3 str.
	ν_{12}	0.01	0.03	0.00	0.01	*0.89*	*1.00*	0.05	0.33	C·CH_3 bend. + CuO str.
	ν_{13}	0.03	0.03	0.03	0.00	0.00	0.27	0.00	*1.00*	ring def.
	ν_{14}	0.08	0.00	0.06	0.00	*1.00*	0.55	0.06	0.04	CuO str.

[a] The values in the table indicate only relative ratios of $F_{ii}L_{ik}^2$ in each band.
[b] A_1 and B_2 species are symmetric and asymmetric types, respectively.

$K(C\cdots O)$ employed in our calculation are based on x-ray data, we conclude that our band assignments are correct in so far as the use of x-ray analysis to estimate force constants is valid.

The band at 1190 cm^{-1} (ν_{10}) is almost the pure C—H in-plane bending mode according to Table V, and furthermore, was shown to be shifted to 875 cm^{-1} by deuteration in monovalent metallic acetylacetonato complexes.[6] Although only one band was observed at 937 cm^{-1} (ν_3, ν_{11}), it may result from overlap of *asym.* and *sym.* C—CH_3 stretching modes which have almost the same frequencies.

The bands at 684 (ν_4) and 654 (ν_{12}) cm^{-1} are of special interest, since Lecomte[4] found that their frequencies are sensitive to a change in the metal ion and suggested that they might be due to the metal-oxygen vibrations. The results of our calculation clearly indi-

TABLE VI. The Jacobian matrices in acetylacetonates.[a]

		K(C—O)	K(C—C)	K(C—CH_3)	K(Cu—O)
A_1	λ_1	*0.08*	0.03	0.00	0.01
	λ_2	0.01	*0.07*	*0.10*	0.00
	λ_3	0.02	0.01	*0.06*	0.03
	λ_4	0.00	0.00	0.04	*0.12*
	λ_5	0.00	0.02	0.05	*0.16*
	λ_6	0.00	0.01	0.00	*0.09*
	λ_7	0.00	0.00	0.00	0.02
B_2	λ_8	0.03	*0.12*	0.00	0.00
	λ_9	*0.06*	0.01	0.02	0.01
	λ_{10}	0.02	0.01	*0.04*	0.01
	λ_{11}	0.01	0.01	*0.18*	0.02
	λ_{12}	0.00	0.00	0.00	*0.18*
	λ_{13}	0.00	0.00	0.01	0.00
	λ_{14}	0.01	0.00	0.01	*0.22*

[a] Only the part of the stretching force constants are shown in the foregoing.

TABLE VII. M—C and M—N stretching frequencies and force constants in various compounds.

Compound	Obs. (cm^{-1})[a]	Calc. force const[b] (10^5 dyne/cm)	Literature
$K_2[Pt(CN)_4]$	505 (IR) 465(R),455(R)	K(Pt—C) = 3.425	c
$K_2[Pt(NO_2)_4]$	450,319,307 (IR) (R) (R)	K(Pt—N) = 3.40	d
$[Pt(NH_3)_4]Cl_2$	538 (R)	K(Pt—N) = 2.804	e
$K_3[Co(CN)_6]$	564,406(R) (IR)	K(Co—C) = 2.33	f
$K_4[Fe(CN)_6]$	585 (IR)	K(Fe—C) = 2.33	f
$Ni(CO)_4$	422,381(R) (IR)	K(Ni—C) = 2.12	g
$Cr(CO)_6$	436,393,373 (IR) (R) (R)	K(Cr—C) = 1.83	h
$Mo(CO)_6$	379,368,334 (R) (IR) (R)	K(Mo—C) = 1.77	h
$[Hg(NH_3)_2]Cl_2$	513(IR)	K(Hg—N) = 1.695	i

[a] IR, infrared; R, Raman.
[b] Only the values obtained by using Urey-Bradley type potential field are listed here.
[c] Sweeny, Nakagawa, Mizushima, and Quagliano, J. Am. Chem. Soc. **78**, 889 (1956).
[d] Nakamoto, Fujita, and Murata, J. Am. Chem. Soc. **80**, 4817 (1958).
[e] Mizushima, Nakagawa, Schmelz, Curran, and Quagliano, Spectrochim. Acta **13**, 31 (1958).
[f] S. Mizushima and I. Nakagawa, Kagaku-no-Ryˆiki **10**, 173 (1956).
[g] H. Murata and K. Kawai, J. Chem. Phys. **26**, 1355 (1957); also, see: L. H. Jones, J. Chem. Phys. **28**, 1215 (1958).
[h] H. Murata and K. Kawai, J. Chem. Phys. **27**, 605 (1957).
[i] Bertin, Nakagawa, Mizushima, Lane, and Quagliano, J. Am. Chem. Soc. **80**, 525 (1958).

TABLE VIII. Force constant, bond distance, and electronegativity.

	Ni—C in $Ni(CO)_4$	Cu—O in $Cu(acac)_2$	Fe—C in $[Fe(CN)_6]^{-4}$
K (10^5 dyne/cm)	2.12	2.25	2.33
r (A)	1.82	1.95	1.89
χ_{metal}	1.6	1.6	1.6
χ_O or χ_C	2.5	3.5	2.5
$[(\chi_M \cdot \chi_{O,C})/r^2]^{3/4}$	1.1	1.3	1.1

cate that the band at 684 cm^{-1} is due to a ring deformation vibration (S_{13}) coupled with Cu—O stretching mode (S_7), whereas the band at 654 cm^{-1} is due to *asym.* C—CH_3 bending (S_{10}) coupled with Cu—O stretching mode (S_8). Thus it is understandable that these two bands are "metal-sensitive." However, they can not be assigned to Cu—O stretching modes.

We have found a new band at 455 cm^{-1} (ν_6) in the bis-(acetylacetonato)-Cu(II) complex. As is seen in Table V, the nature of this band is almost the pure Cu—O stretching mode. Therefore, we assign it to the *sym.* Cu—O stretching mode. This band is "metal-sensitive" and is shifted regularly in the order of stability of the complexes when the metal is changed. The effect of changing the metal on the frequency of this band, and of other bands, will be discussed in a subsequent paper.

According to our calculation, the bands at 373 (ν_{13}) and 197 (ν_7) cm^{-1} are almost pure ring deformation vibrations, although they were not observed in our measurements. The results of the calculation also indicate that there should be two bands at 320 (ν_{14}) and 273 (ν_6) cm^{-1}; the former is the *asym.* Cu—O stretching vibration and the latter is the *sym.* C—CH_3 bending mode.

The Nature of the Copper—Oxygen Bond

Table VII lists the metal-carbon and metal-oxygen stretching frequencies and their force constants, although no metal-oxygen bond has so far been studied. If the Cu—O stretching force constant, 2.25×10^5 dyne/cm used in the present calculation is compared with the values listed in Table VII, it is found that the force constant of the Cu—O bond in bis-(acetylacetonato)-Cu(II) is intermediate between those of the Ni—C bond in $Ni(CO)_4$ and Fe—C bond in the $[Fe(CN)_6]^{4-}$ ion. It is well known that both of the Ni—C and Fe—C bonds in these two compounds have partial double bond character which involve the filled *3d* orbitals of the metals.[22] In bis-(acetylacetonato)-Cu(II), Calvin and Wilson[1] suggested the following "benzenoid resonance":

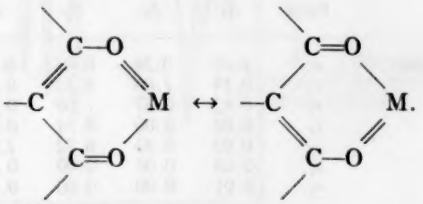

Thus far no theoretical relation between the force constant and the bond energy has been derived even for diatomic molecules.¶ Gordy[23] proposed the following empirical relation:

$$K = aN[(\chi_A \cdot \chi_B)/r^2]^{3/4} + b$$

where χ_A and χ_B are electronegativities of the atoms A and B, respectively; r, bond distance; N, bond order; and a and b, constants. If this relation is applied for the three bonds mentioned above, one finds that the quantity, $(\chi_A\chi_B/r^2)^{3/4}$ has similar values in all of these compounds, as shown in Table VIII. Since the values of the force constants do not differ appreciably, this result seems to suggest that the bond orders of the Ni—C, Cu—O and Fe—C bonds in these three compounds are similar. Friedel *et al.*[24] estimated the bond order of the Ni—C bond as *ca* 1.67. Therefore, it is not unreasonable to suggest from this infrared study that the bond order of the Cu—O bond in bis-(acetylacetonato)-Cu(II) is similar to that of Ni—C bond in nickel carbonyl.

ACKNOWLEDGMENTS

The authors wish to express their sincere thanks to Professor R. C. Lord, Jr., of the Massachusetts Institute of Technology for aid in obtaining the spectra in the CsBr region, and to Dr. I. Nakagawa of Tokyo University for his kind guidance and valuable suggestions throughout our calculations.

---

[22] L. Pauling, *The Nature of the Chemical Bond* (Cornell University Press, Ithaca, New York, 1940).

¶ The force constant, K, is related to the shape of the potentia curve at the bottom, $[K = (d^2V/dr^2)_{r=r_e}]$, whereas the bond energy is measured by the depth of the potential curve. The relation between these two quantities is not simple.

[23] W. Gordy, J. Chem. Phys. **14**, 305 (1946).

[24] Friedel, Wender, Shufler, and Sternberg, J. Am. Chem. Soc. **77**, 3951 (1955).

APPENDIX

G Matrices

A_1

$G_{11}=\mu_c+\mu_0, \quad G_{12}=G_{13}=-(1/2)\mu_c, \quad G_{14}=-(1/\sqrt{2})\mu_0$

$G_{15}=(\sqrt{3}/2)\mu_c(\rho_{r2}+2\rho_{r3}), \quad G_{16}=(1/2\sqrt{2})(\sqrt{2}\mu_0\rho_{r4}-\sqrt{3}\mu_c\rho_{r2})$

$G_{17}=(\sqrt{3}/2)[(\tfrac{3}{2})^{\frac{1}{2}}\mu_c\rho_{r2}+\mu_0\rho_{r4}], \quad G_{18}=(1/\sqrt{2})[\mu_0\rho_{r4}-(\tfrac{3}{2})^{\frac{1}{2}}\mu_c\rho_{r2}]$

$G_{22}=(\tfrac{3}{2})\mu_c, \quad G_{23}=-(\tfrac{1}{2})\mu_c, \quad G_{24}=0,$

$G_{25}=-(\sqrt{3}/2)\mu_c(\rho_{r1}+\rho_{r2}+2\rho_{r3}), \quad G_{26}=(\sqrt{3}/2\sqrt{2})\mu_c(\rho_{r2}-2\rho_{r1})$

$G_{27}=-(3/2\sqrt{2})\mu_c\rho_{r2}, \quad G_{28}=(\sqrt{3}/2)\mu_c\rho_{r2}, \quad G_{33}=\mu_c+\mu_R$

$G_{34}=0, \quad G_{35}=(\sqrt{3}/2)\mu_c(\rho_{r1}-\rho_{r2}), \quad G_{36}=(\sqrt{3}/2\sqrt{2})\mu_c(2\rho_{r1}+\rho_{r2})$

$G_{37}=-(3/2\sqrt{2})\mu_c\rho_{r2}, \quad G_{38}=(\sqrt{3}/2)\mu_c\rho_{r2}, \quad G_{44}=\mu_0+\mu_M$

$G_{45}=(1/\sqrt{2})\mu_0\rho_{r1}, \quad G_{46}=(1/\sqrt{2})(\sqrt{2}\mu_0\rho_{r1}-\mu_M\rho_{r4}), \quad G_4=-[3/(6)^{\frac{1}{2}}]\mu_M\rho_{r4}$

$G_{48}=-\mu_M\rho_{r4}$

$G_{55}=\mu_0\rho_{r1}^2+4\mu_R\rho_{r3}^2+\mu_c(\rho_{r1}^2+\tfrac{5}{2}\rho_{r2}^2+4\rho_{r3}^2-\rho_{r1}\rho_{r2}+2\rho_{r2}\rho_{r3}+2\rho_{r1}\rho_{r3})$

$G_{56}=(1/\sqrt{2})\mu_c(2\rho_{r1}^2-\tfrac{1}{2}\rho_{r1}\rho_{r2}-\rho_{r2}\rho_{r3}+2\rho_{r1}\rho_{r3}-\tfrac{5}{2}\rho_{r2}^2)+(1/\sqrt{2})\mu_0[2\rho_{r1}^2+(1/\sqrt{2})\rho_{r1}\rho_{r4}]$

$G_{57}=[1/(6)^{\frac{1}{2}}]\mu_c(-\tfrac{3}{2}\rho_{r1}\rho_{r2}+3\rho_{r2}\rho_{r3}+\tfrac{15}{2}\rho_{r2}^2)+(\sqrt{3}/2)\mu_0\rho_{r1}\rho_{r4}$

$G_{58}=(1/\sqrt{2})\mu_0\rho_{r1}\rho_{r4}-(1/2)\mu_c\rho_{r2}(5\rho_{r2}+2\rho_{r3}-\rho_{r1})$

$G_{66}=(1/2)\mu_M\rho_{r4}^2+\mu_c(\tfrac{5}{4}\rho_{r2}^2+2\rho_{r1}^2+\rho_{r1}\rho_{r2})+\mu_0(2\rho_{r1}^2+\tfrac{1}{2}\rho_{r4}^2+\sqrt{2}\rho_{r1}\rho_{r4})$

$G_{67}=(1/2\sqrt{3})\{3\mu_M\rho_{r4}^2+\mu_0[3\rho_{r4}^2+(6/\sqrt{2})\rho_{r1}\rho_{r4}]-\mu_c(\tfrac{15}{2}\rho_{r2}^2+3\rho_{r1}\rho_{r2})\}$

$G_{68}=(1/\sqrt{2})\{\mu_c(\tfrac{5}{2}\rho_{r2}^2+\rho_{r1}\rho_{r2})+\mu_0(\rho_{r4}^2+\sqrt{2}\rho_{r1}\rho_{r4})+\mu_M\rho_{r4}^2\}$

$G_{77}=(3/2)\{(\mu_M+\mu_0)\rho_{r4}^2+\tfrac{5}{2}\mu_c\rho_{r2}^2\}$

$G_{78}=(\sqrt{3}/\sqrt{2})\{(\mu_M+\mu_0)\rho_{r4}^2-\tfrac{5}{2}\mu_c\rho_{r2}^2\}$

$G_{88}=(\mu_M+\mu_0)\rho_{r4}^2+\tfrac{5}{2}\mu_c\rho_{r2}^2.$

B_2

$G_{11}=G_{11}^{A1} \quad G_{12}=G_{12}^{A1}, \quad G_{13}=G_{13}^{A1}, \quad G_{14}=-(\sqrt{3}/\sqrt{2})\mu_c\rho_{r2}$

$G_{15}=G_{14}^{A1}, \quad G_{16}=G_{15}^{A1}, \quad G_{17}=-(1/2)\{[(6)^{\frac{1}{2}}/2]\mu_c\rho_{r2}+\mu_0\rho_{r4}\}$

$G_{18}=-(1/2)\{[(6)^{\frac{1}{2}}/2]\mu_c\rho_{r2}-\mu_0\rho_{r4}\}, \quad G_{22}=(5/2)\mu_c, \quad G_{23}=G_{23}^{A1}$

$G_{24}=-(\sqrt{3}/\sqrt{2})\mu_c(2\rho_R+\rho_{r2}), \quad G_{25}=0, \quad G_{26}=-(\sqrt{3}/2)\mu_c(\rho_{r1}-\rho_{r2}+2\rho_{r3})$

$G_{27}=-(\sqrt{3}/2\sqrt{2})\mu_c\rho_{r2}, \quad G_{28}=-(\sqrt{3}/\sqrt{2})\mu_c(\rho_{r1}+\tfrac{1}{2}\rho_{r2}), \quad G_{33}=G_{33}^{A1}$

$G_{34}=(\sqrt{3}/\sqrt{2})\mu_c\rho_{r2}, \quad G_{35}=0, \quad G_{36}=G_{35}^{A1}, \quad G_{37}=(\sqrt{3}/2\sqrt{2})\mu_c\rho_{r2}$

$G_{38}=G_{36}^{A1}, \quad G_{44}=4\mu_H\rho R^2+\mu_c(4\rho_R^2+3\rho_{r2}^2+4\rho_R\rho_{r2}), \quad G_{45}=0$

$G_{46}=(1/\sqrt{2})\mu_c\rho_{r2}(\rho_{r1}-3\rho_{r2}-2\rho_{r3}-2\rho_R), \quad G_{47}=\mu_c\rho_{r2}(\tfrac{3}{2}\rho_{r2}+\rho_R)$

$G_{38}=\mu_c\rho_{r2}(\rho_{r1}+\rho_R+\tfrac{3}{2}\rho_{r2}), \quad G_{55}=G_{44}^{A1}, \quad G_{56}=G_{45}^{A1}$

$G_{57}=-(1/\sqrt{2})\mu_M\rho_{r4}, \quad G_{58}=(1/\sqrt{2})(\mu_M\rho_{r4}+\sqrt{2}\mu_0\rho_{r1})$

$G_{66}=4\mu_R\rho_{r3}^2+\mu_0\rho_{r1}^2+\mu_c(\rho_{r1}^2+\tfrac{3}{2}\rho_{r2}^2+4\rho_{r3}^2-\rho_{r1}\rho_{r2}+2\rho_{r2}\rho_{r3}+2\rho_{r1}\rho_{r3})$

$G_{67}=(1/\sqrt{2})\{\mu_c(\tfrac{1}{2}\rho_{r1}\rho_{r2}-\rho_{r2}\rho_{r3}-\tfrac{3}{2}\rho_{r2}^2)-(1/\sqrt{2})\mu_0\rho_{r1}\rho_{r4}\}$

$G_{68}=(1/\sqrt{2})\{\mu_c(2\rho_{r1}\rho_{r3}-\rho_{r2}\rho_{r3}-\tfrac{1}{2}\rho_{r1}\rho_{r2}+2\rho_{r1}^2-\tfrac{3}{2}\rho_{r2}^2)+\mu_0(2\rho_{r1}^2+(1/\sqrt{2})\rho_{r1}\rho_{r4}]\}$

$G_{77}=(1/2)\{\frac{3}{2}\mu_C\rho_{r_2}^2+(\mu_0+\mu_M)\rho_{r_4}^2\}$

$G_{78}=(1/2)\{\mu_C(\frac{3}{2}\rho_{r_2}^2+\rho_{r_1}\rho_{r_2})-\mu_M\rho_{r_4}^2-\mu_0(\rho_{r_4}^2+\sqrt{2}\rho_{r_1}\rho_{r_4})\}$

$G_{88}=(1/2)\{\mu_C(4\rho_{r_1}^2+2\rho_{r_1}\rho_{r_2}+\frac{3}{2}\rho_{r_2}^2)+\mu_M\rho_{r_4}^2+\mu_0(4\rho_{r_1}^2+2\sqrt{2}\rho_{r_1}\rho_{r_4}+\rho_{r_4}^2)\}$.

μ_C, μ_H, μ_O, μR, and μM are reciprocal masses of C, H, O, R(CH_3), and M(Cu), respectively. ρ_{r_1}, ρ_{r_2}, ρ_{r_3}, ρ_R, and ρ_{r_4} are reciprocals of the bond distances of C$\cdots$O, C$\cdots$C C—R(CH_3), C—H, and M(Cu)—O, respectively.

F Matrices

A_1

$F_{11}=K_1+(t_1^2F_1'+s_1^2F_1)+(t_2^2F_3'+s_2^2F_3)+(t_3^2F_4'+s_3^2F_4)$

$F_{12}=-t_1t_4F_1'+s_1s_4F_1, \qquad F_{13}=-t_2t_8F_3'+s_2s_8F_3$

$F_{14}=-t_3t_{10}F_4'+s_3s_{10}F_4, \qquad F_{15}=-(r_3/2)(t_2s_8F_3'+t_8s_2F_3)$

$F_{16}=(r_2/\sqrt{2})(t_1s_4F_1'+t_4s_1F_1)-(r_3/2\sqrt{2})(t_2s_8F_3'+t_8s_2F_3)-(r_4/\sqrt{2})(t_3s_{10}F_4'+t_{10}s_3F_4)$

$F_{17}=-[r_2/(6)^{\frac{1}{2}}](t_1s_4F_1'+t_4s_1F_1)+[r_3/2(6)^{\frac{1}{2}}](t_2s_8F_3'+t_8s_2F_3)-[r_4/(6)^{\frac{1}{2}}](t_3s_{10}F_4'+t_{10}s_3F_4)$

$F_{18}=0, \qquad F_{22}=K_2+(t_4^2F_1'+s_4^2F_1)+2s_5^2F_6+(t_6^2F_2'+s_6^2F_2)+(t_7^2F_7'+s_7^2F_7)$

$F_{23}=-t_6t_9F_2'+s_6s_9F_2, \qquad F_{24}=0, \qquad F_{25}=(r_3/2)(t_6s_9F_2'+t_9s_6F_2)$

$F_{26}=(r_1/\sqrt{2})(t_4s_1F_1'+t_1s_4F_1)-(r_3/2\sqrt{2})(t_6s_9F_2'+t_9s_6F_2)$

$F_{27}=-[r_1/(6)^{\frac{1}{2}}](t_4s_1F_1'+t_1s_4F_1)+[r_3/2(6)^{\frac{1}{2}}](t_6s_9F_2'+t_9s_6F_2)+[2r_2/(6)^{\frac{1}{2}}](t_6s_5F_6'+t_5s_5F_6)$
$-[R/(6)^{\frac{1}{2}}](t_7s_{12}F_7'+t_{12}s_7F_7)$

$F_{28}=-r_2(t_5s_5F_6'+t_5s_5F_6)+(R/2)(t_7s_{12}F_7'+t_{12}s_7F_7)$

$F_{33}=K_3+(t_8^2F_3'+s_8^2F_3)+(t_9^2F_2'+s_9^2F_2)$

$F_{34}=0, \qquad F_{35}=(r_2/2)(t_9s_6F_2'+t_6s_9F_2)-(r_1/2)(t_8s_2F_3'+t_2s_8F_3)$

$F_{36}=-(r_2/2\sqrt{2})(t_9s_6F_2'+t_6s_9F_2)-(r_1/2\sqrt{2})(t_8s_2F_3'+t_2s_8F_3)$

$F_{37}=(r_2/2(6)^{\frac{1}{2}})(t_9s_6F_2'+t_6s_9F_2)+[r_1/2(6)^{\frac{1}{2}}](t_8s_2F_3'+t_2s_8F_3)$

$F_{38}=0, \qquad F_{44}=K_4+(t_{10}^2F_4'+s_{10}^2F_4)+2s_{11}^2F_5, \qquad F_{45}=0$

$F_{46}=-(r_1/\sqrt{2})(t_{10}s_3F_4'+t_3s_{10}F_4), \qquad F_{47}=[2r_4/(6)^{\frac{1}{2}}](t_{11}s_{11}F_5'+t_{11}s_{11}F_5)-[r_1/(6)^{\frac{1}{2}}](t_{10}s_3F_4'+t_3s_{10}F_4),$

$F_{48}=r_4(t_{11}s_{11}F_5'+t_{11}s_{11}F_5)$

$F_{55}=(r_2r_3/4)(H_2-s_6s_9F_2'+t_6t_9F_2)+(r_1r_3/4)(H_3-s_2s_8F_3'+t_2t_8F_3)$

$F_{56}=(r_1r_3/4\sqrt{2})(H_3-s_2s_8F_3'+t_2t_8F_3)-(r_2r_3/4\sqrt{2})(H_2-s_6s_9F_2'+t_6t_9F_2)$

$F_{57}=[r_2r_3/4(6)^{\frac{1}{2}}](H_2-s_6s_9F_2'+t_6t_9F_2)-[r_1r_3/4(6)^{\frac{1}{2}}](H_3-s_2s_8F_3'+t_2t_8F_3)$

$F_{58}=0, \qquad F_{66}=(r_1r_2/2)(H_1-s_1s_4F_1'+t_1t_4F_1)+(r_2r_3/8)(H_2-s_6s_9F_2'+t_6t_9F_2)+(r_1r_3/8)(H_3-s_2s_8F_3'+t_2t_8F_3)$
$+(r_1r_4/2)(H_\beta-s_3s_{10}F_4'+t_3t_{10}F_4)$

$F_{67}=(r_1r_4/2\sqrt{3})(H_\beta-s_3s_{10}F_4'+t_3t_{10}F_4)-(r_1r_2/2\sqrt{3})(H_1-s_1s_4F_1'+t_1t_4F_1)-(r_2r_3/8\sqrt{3})(H_2-s_6s_9F_2'+t_6t_9F_2)$
$-(r_1r_3/8\sqrt{3})(H_3-s_2s_8F_3'+t_2t_8F_3)$

$F_{68}=0, \qquad F_{77}=(r_1r_2/6)(H_1-s_1s_4F_1'+t_1t_4F_1)+(r_2r_3/24)(H_2-s_6s_9F_2'+t_6t_9F_2)+(r_1r_3/24)(H_3-s_2s_8F_3'+t_2t_8F_3)$
$+(r_1r_4/6)(H_\beta-s_3s_{10}F_4'+t_3t_{10}F_4)+(r_4^2/3)(H_\gamma-s_{11}^2F_5'+t_{11}^2F_5)+(r_2^2/3)(H_5-s_5^2F_6'+t_5^2F_6)$
$-(Rr_2/6)(H_{\delta 1}-s_7s_{12}F_7'+t_7t_{12}F_7)$

$F_{78}=[r_4^2/(6)^{\frac{1}{2}}](H_\gamma-s_{11}^2F_5'+t_{11}^2F_5)-[r_2^2/(6)^{\frac{1}{2}}](H_5-s_5^2F_6'+t_5^2F_6)-(Rr_2/2(6)^{\frac{1}{2}})(H_{\delta 1}-s_7s_{12}F_7'+t_7t_{12}F_7)$

$F_{88}=(r_4^2/2)(H_\gamma-s_{11}^2F_5'+t_{11}^2F_5)+(r_2^2/2)(H_5-s_5^2F_6'+t_5^2F_6)+(Rr_2/4)(H_{\delta 1}-s_7s_{12}F_7'+t_7t_{12}F_7).$

B_2

$F_{11}=F_{11}^{A_1}$, $F_{12}=F_{12}^{A_1}$, $F_{13}=F_{13}^{A_1}$, $F_{14}=0$, $F_{15}=F_{14}^{A_1}$, $F_{16}=F_{15}^{A_1}$

$F_{17}=-\sqrt{3}F_{17}^{A_1}$, $F_{18}=F_{16}^{A_1}$, $F_{22}=K_2+(t_4^2F_1'+s_4^2F_1)+2t_5^2F_6'+(t_6^2F_2'+s_6^2F_2)+(t_7^2F_7'+s_7^2F_7)$,

$F_{23}=F_{23}^{A_1}$

$F_{24}=(R/\sqrt{2})(t_7s_{12}F_7'+t_{12}s_7F_7)$, $F_{25}=0$, $F_{26}=F_{25}^{A_1}$

$F_{27}=F_{28}=F_{26}^{A_1}$, $F_{33}=F_{33}^{A_1}$, $F_{34}=F_{35}=0$, $F_{36}=F_{35}^{A_1}$

$F_{37}=F_{38}=F_{36}^{A_1}$, $F_{44}=(Rr_2/2)(H_{31}-s_7s_{12}F_7'+t_7t_{12}F_7)$

$F_{45}=F_{46}=F_{47}=F_{48}=0$, $F_{55}=K_4+(t_{10}^2F_4'+s_{10}^2F_4)+2t_{11}^2F_5')$

$F_{56}=0$, $F_{57}=-F_{46}^{A_1}$, $F_{58}=F_{46}^{A_1}$, $F_{66}=F_{55}^{A_1}$, $F_{67}=F_{68}=F_{56}^{A_1}$

$F_{77}=F_{88}=F_{66}^{A_1}$, $F_{78}=-\sqrt{3}F_{67}^{A_1}$.

Here

$t_1=(r_2\sin\alpha_{12})/q_{C\cdots O}$ $t_2=(r_3\sin\alpha_{31})/q_{R\cdots O}$ $t_3=(r_4\sin\beta)/q_{C\cdots M}$

$t_4=(r_1\sin\alpha_{12})/q_{C\cdots O}$ $t_5=(r_2\sin\delta)/q_{C\cdots C}$ $t_6=(r_3\sin\alpha_{23})/q_{C\cdots R}$

$t_7=(R\sin\delta_1)/q_{C\cdots H}$ $t_8=(r_1\sin\alpha_{31})/q_{R\cdots O}$ $t_9=(r_2\sin\alpha_{23})/q_{C\cdots R}$

$t_{10}=(r_1\sin\beta)/q_{C\cdots M}$ $t_{11}=(r_4\sin\gamma)/q_{O\cdots O}$ $t_{12}=(r_2\sin\delta_1)/q_{C\cdots H}$

$s_1=(r_1-r_2\cos\alpha_{12})/q_{C\cdots O}$ $s_2=(r_1-r_3\cos\alpha_{31})/q_{R\cdots O}$ $s_3=(r_1-r_4\cos\beta)/q_{C\cdots M}$

$s_4=(r_2-r_1\cos\alpha_{12})/q_{C\cdots O}$ $s_5=\{r_2(1-\cos\delta)\}/q_{C\cdots C}$ $s_6=(r_2-r_3\cos\alpha_{23})/q_{C\cdots R}$

$s_7=(r_2-R\cos\delta_1)/q_{C\cdots H}$ $s_8=(r_3-r_1\cos\alpha_{31})/q_{C\cdots O}$ $s_9=(r_3-r_2\cos\alpha_{23})/q_{C\cdots R}$

$s_{10}=(r_4-r_1\cos\beta)/q_{C\cdots M}$ $s_{11}=\{r_4(1-\cos\gamma)\}/q_{O\cdots O}$ $s_{12}=(R-r_2\cos\delta_1)/q_{C\cdots H}$

$q_{i\cdots j}$ is the distance between nonbonded atoms, i and j.

Paramagnetic Resonance of Ti^{3+}, Cr^{3+}, and Fe^{3+} in $AlCl_3 \cdot 6H_2O$*

EUGENE Y. WONG†

Enrico Fermi Institute for Nuclear Studies, University of Chicago, Chicago, Illinois

Magnetic resonance of single crystals of $TiCl_3 \cdot 6H_2O$, $CrCl_3 \cdot 6H_2O$, and $FeCl_3 \cdot 6H_2O$ diluted with $AlCl_3 \cdot 6H_2O$ was observed. The results in each case were fitted to a spin Hamiltonian.

INTRODUCTION

THE magnetic resonance spectrum of Ti^{3+} in $CsTi(SO_4)_2 \cdot 12H_2O$ was observed by Bijl[1] and discussed by Bleaney and co-workers.[2,3] The Ti^{3+} in this alum has six H_2O molecules arranged as the nearest neighbors at the corners of an octahedron. Most of their discussion concerned the interaction of these nearest neighbors with the central ion. Since in the $AlCl_3 \cdot 6H_2O$ structure the Al^{3+} ion has the same nearest neighbors as the Ti^{3+} in the alum, it appeared that $AlCl_3 \cdot 6H_2O$ would be a good host crystal for a comparative study of the Ti^{3+} ion. The results, which were quite different from those for the alum, fit Bleaney's[2] formula well.

The Cr^{3+} ion has been studied extensively.[4] However no work in $AlCl_3 \cdot 6H_2O$ has been reported. The results reported in this paper are very similar to those which were obtained for all the alums studied except that the width of the lines in the trichloride is considerably reduced, and the 4 hyperfine lines due to the naturally occurring Cr^{53} can be clearly observed.

The magnetic resonance of Fe^{3+} ion in some alums has been studied by Bleaney and Trenam.[5] The results reported here are very similar to one of their results.

The experiments reported here indicate a large axial field for Ti^{3+} and Fe^{3+} but a small axial field for Cr^{3+}. This may be caused by the distortion of the crystal since the ionic radii of Cr^{3+} is closest to Al^{3+} among the 3 ions.[6]

CRYSTAL STRUCTURE AND EXPERIMENTAL DETAIL

The symmetry of the $AlCl_3 \cdot 6H_2O$ crystal has been given by Wyckoff[7,8] as D_{3d}^6. The point symmetry at the Al^{3+} ion sites is C_{3i}. The nearest neighbors of the Al^{3+} ion are six H_2O molecules arranged at the corners of an octahedron. Since the nearest neighbors contribute most of the electrostatic field, the crystal field can be considered as cubic to a first approximation. The rest of the crystal contributes a small superimposed C_{3i} field.

The crystals were grown by evaporating H_2O from solutions of $AlCl_3 \cdot 6H_2O$ and $XCl_3 \cdot 6H_2O$, where X represents Ti, Cr, and Fe. In the case of Ti the crystals were grown in an O_2-free atmosphere. The concentration of the transition ions in the crystals was less than 10^{-4} mole fraction. The c axis of the crystal always lies along the intersection of the two large crystal faces. This assignment of c axis was also confirmed by polarized light.

The experiments were performed at 1.2, 3, and 18 cm. The 1.2- and 3-cm apparatuses were very similar to those reported by Llewellyn.[9] The 18-cm apparatus was used only in the case of the Fe^{3+}. It employed a General Radio type 1218-A UHF oscillator as the microwave source and a partial coaxial cavity as the resonant chamber. The detection system used with the 18-cm apparatus was the same as that used with the 1.2-cm and 3-cm apparatuses. At all wavelengths the magnetic field was measured by simultaneous display of a proton resonance signal and of the electronic resonance signal on a dual-beam oscilloscope.

EXPERIMENTAL RESULTS AND DISCUSSION

Ti^{3+}

No resonance was observed at room temperature. At the boiling points of liquid N_2 and liquid He, a peak about 100 gauss wide was observed. This peak showed no appreciable difference in width at these two temperatures, and did not vary in position for various crystal orientations. The data were described by the spin Hamiltonian $\beta \mathbf{H} \cdot g \cdot \mathbf{S}$, using an isotropic $g = 1.93 \pm 0.002$ for both temperatures.

The cubic field splits the ground term ^2D into an orbital doublet and an orbital singlet. The C_{3i} field plus the spin-orbit interaction splits the orbital triplet further into 3 Kramers doublets. These doublets will be split further by the magnetic field and can be represented by the spin Hamiltonian $\beta \mathbf{H} \cdot g \cdot \mathbf{S}$. For some values of the parameters of the C_{3i} field Bleaney[2] gave the

* This work was supported by the U. S. Atomic Energy Commission.

† Present address: Department of Physics, University of California, Los Angeles 24, California.

[1] D. Bijl, Proc. Phys. Soc. (London) **A63**, 405 (1950).

[2] B. Bleaney, Proc. Phys. Soc. (London) **A63**, 407 (1950).

[3] Bleaney, Bogle, Cooke, Duffus, O'Brien, and Stevens, Proc. Phys. Soc. (London) **A68**, 57 (1955).

[4] K. D. Bowers and J. Owen, Rept. Progr. Phys. **18**, 304 (1955).

[5] B. Bleaney and R. S. Trenam, Proc. Roy. Soc. (London) **A223**, 1 (1954).

[6] R. C. Evans, *An Introduction to Crystal Chemistry* (Cambridge University Press, New York, 1948), p. 171.

[7] Wyckoff, *Crystal Structure* (Interscience Publishers, Inc., New York, 1957), Vol. 2, Chap. X, p. 39.

[8] K. R. Andress and C. Carpenter, Z. Krist. **A87**, 446 (1934).

[9] P. M. Llewellyn, J. Sci. Instr. **34**, 236 (1957).

TABLE I. Experimental results of Cr^{3+} for $AlCl_3 \cdot 6H_2O$ and $AlCl_3 \cdot 6D_2O$.

Temperature	Crystal	g	$\lvert D \rvert/hc$, cm^{-1}	$\lvert A \rvert/hc$, cm^{-1}
room temperature	$AlCl_3 \cdot 6H_2O$	1.977 ± 0.001	0.0327 ± 0.0001	...
	$AlCl_3 \cdot 6D_2O$	1.977 ± 0.001	0.0315 ± 0.0001	...
boiling point of liq N_2	$AlCl_3 \cdot 6H_2O$	1.977 ± 0.001	0.0430 ± 0.0001	$(1.70 \pm 0.01) \cdot 10^{-3}$
	$AlCl_3 \cdot 6D_2O$	1.977 ± 0.001	0.0327 ± 0.0001	$(1.72 \pm 0.01) \cdot 10^{-3}$

following first-order formulas for the g value of the ground doublet:

$$g_{\parallel} = [3(\Delta + \zeta/2)/S] - 1,$$

$$g_{\perp} = [(\Delta - 3\zeta/2)/S] + 1,$$

where Δ = the splitting of the orbital triplet due to the C_{3i} field alone, ζ = the spin-orbit interaction constant, and $S = [(\Delta + \zeta/2)^2 + 2\zeta]^{\frac{1}{2}}$.

The only solution for an isotropic g is $\zeta/\Delta \to 0$ which gives $g = 2$. The experimental result gives an isotropic g within 1%. This indicates that Δ is at least 100 times bigger than ζ, or at least of the order of 10^4 cm^{-1} since ζ equals 153.7 cm^{-1}.[10] If the other Kramers doublets are separated by at least 10^4 cm^{-1} from the ground states, only the ground states can be observed at boiling point temperatures of liquid N_2 and liquid He.

The fact that there was no appreciable change of line width upon cooling from liquid N_2 temperature to liquid He temperature indicates the width is not due to a short relaxation time. The dipole-dipole or exchange broadening cannot give such a width because the paramagnetic ion concentration was too low. The interaction of the $3d^1$ electron with the protons of the H_2O molecules can give a broadening, but if this broadening is 100 gauss the hyperfine structure should be resolved. The most plausible reason for the observed line width is that it may be due to the distortion of the crystal. If this is the case it can also explain the necessity of a rather large Δ to fit Bleaney's formulas. The splitting of the triplet is due not only to the C_{3i} field but also to the distortion field.

Cr^{3+}

The experiment was carried out at 1.2 cm and 3 cm at both room temperature and at the boiling point of liquid N_2. In order to get more conclusive results on the hyperfine structure, $AlCl_3 \cdot 6D_2O$ was also employed as a host crystal. The spectra of these two crystals were very similar except that the $AlCl_3 \cdot 6D_2O$ gave sharper lines as expected. Three main lines accompanied by some weak lines were observed. The origin of some of these weak lines was not identified. Contrary to what Low[11] reported for Cr^{3+} in an MgO crystal, these weak lines did vary in position with various crystal orientations. In the case of $AlCl_3 \cdot 6D_2O$ four of the weak lines were equally spaced and occurred two on each side of the main central line. These weak lines were identified as the hyperfine lines of Cr^{53} since they had the same width as the main central line, and the measured intensity ratio to the main central line was 1 to 40 while the theoretical ratio is 1 to 38 for naturally occurring Cr. In the case of $AlCl_3 \cdot 6H_2O$ the same pattern was observed except that the intensity was too weak to be measured accurately. The results summarized in terms of the spin Hamiltonian

$$\mathcal{H} = \beta g \mathbf{H} \cdot \mathbf{S} + D[S_z^2 - \tfrac{1}{3}S(S+1)] + A\mathbf{I} \cdot \mathbf{S}$$

are listed in Table I.

The crystal field theory of the Cr^{3+} ion has been discussed by various authors[12,13]. In an octahedral field the Russell-Saunders ground term of the Cr^{3+} splits into two orbital triplets and an orbital singlet. The orbital singlet with fourfold spin degeneracy constitutes the ground level. The spin-orbit interaction plus the C_{3i} field splits it further into two Kramers doublets with a small separation. The first term of the Hamiltonian is due to the interaction between the external magnetic field and the $3d^3$ electrons, the second term represents the zero field splitting, and the last term represents the interaction due to the nucleus of the Cr^{53}. Measurements made at intervals of $\pi/20$ from a position with the c axis parallel to $\mathbf{H}$ to a position with the c axis perpendicular to $\mathbf{H}$ fit the spin Hamiltonian to about 1 gauss.

There was no appreciable change of line width upon cooling from room temperature to the boiling point of liquid N_2. In the case of the $AlCl_3 \cdot 6H_2O$ crystals the width of the central peak was about 4 gauss and of the two side peaks was about 16 gauss for a position with the c axis parallel to $\mathbf{H}$. In the case of the $AlCl_3 \cdot 6D_2O$ crystal with central peak was about 2.7 gauss wide, and the two side peaks were about 15 gauss wide, for a position with the c axis parallel to $\mathbf{H}$. Shifting from H_2O to D_2O gave a sharper central peak. This indicated that the width for the central peak may be due to unresolved hyperfine structure caused by the surrounding H_2O or D_2O molecules, However the two side peaks had almost the same width for the H_2O and the D_2O crystals. This means that there must be another cause which gives a width greater than the hyperfine broadening due to the H_2O or the D_2O molecules.

[10] C. E. Moore, *Atomic Energy Levels* (U. S. Government Printing Office, Washington, D. C., 1949), Vol. 1, p. 283.
[11] W. Low, Phys. Rev. **105**, 801 (1957).
[12] R. Finkelstein and J. H. Van Vleck, J. Chem. Phys. **8**, 709 (1940).
[13] R. Schlapp and W. G. Penney, Phys. Rev. **42**, 666 (1932).

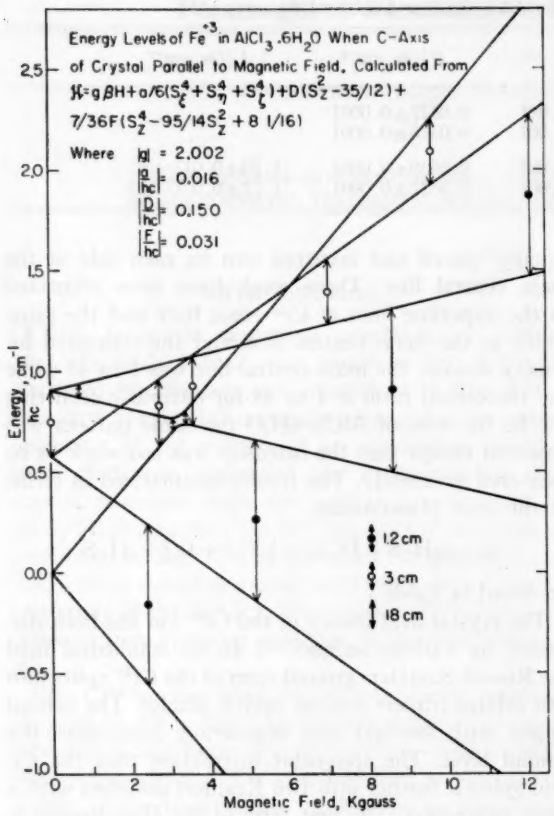

FIG. 1.

A crystal distortion which results in a slight change of D in the spin Hamiltonian can broaden the two side peaks but leave the central peak unaffected. The position of the two side peaks is dependent on D through first-order perturbation, while the position of the central peak has a second-order dependency on D. Since the second-order effect is small the central peak can be considered as unaffected. However this argument is not consistent with all experimental observations. In a position with $\tan\theta=\sqrt{2}$ ($\theta=$ angle between c axis and $\mathbf{H}$) the position of the two side peaks does not have a first order dependence on D, and hence it should be as sharp as the central peak. But the observed width of the two side peaks was about 15 gauss for all crystal orientations. It did not become any sharper at that particular orientation.

Fe^{3+}

No resonance was observed at room temperature, but at the boiling point of liquid N_2 strong resonance was observed. The spectrum obtained at 3 cm and 18 cm was extremely complicated. However, at 1.2 cm the spectrum could be easily identified as a spin equals $\frac{5}{2}$ spectrum with a large zero field splitting. The results summarized in terms of the spin Hamiltonian

$$\mathcal{H}=g\beta H+(a/6)(S_\xi^4+S_\eta^4+S_\zeta^4)+D(S_z^2-35/12)+(7F/36)(S_z^4-\tfrac{95}{14}S_z^2+\tfrac{81}{16})$$

give

$$g=2.002\pm0.002,$$
$$|a|/hc=(1.6\pm0.5)\times10^{-2}\ \text{cm}^{-1},$$
$$|D|/hc=0.150\pm0.002\ \text{cm}^{-1},$$
$$|F|/hc=(3.1\pm0.2)\times10^{-2}\ \text{cm}^{-1}.$$

The other measurements at various crystal orientations were not used because it is difficult to solve the six by six matrix. The energy level diagram calculated from the spin Hamiltonian with the foregoing parameters is shown in Fig. 1. The arrows indicate the observed transitions. The experimental results agree with the spin Hamiltonian to only 5%.

The splitting of the ^6S state has been discussed by various authors.[13–15] However from this experiment no definite conclusion can be drawn about the various mechanisms mentioned by these authors.

The width of the lines varied from 4 to 15 gauss for different transitions. Most of the lines split into two lines of equal intensity when the crystal orientation was varied from the parallel to the perpendicular position. Since there are two Al^{3+} ions in a smallest unit cell, a slight distortion of the two complex ions with respect to each other can account for the splitting. This also means that the width may be due to the crystal distortion.

ACKNOWLEDGMENT

The author wishes to acknowledge the friendly encouragement and helpful discussion of Professor C. A. Hutchison, Jr. The author also thanks Edward Bartal and J. D. S. Danielson for the construction of the instruments used in these experiments.

[14] M. H. L. Pryce, Phys. Rev. **80**, 1106 (1950).
[15] Hutchison, Judd, and Pope, Proc. Phys. Soc. (London) **B70**, 514 (1957).

Hydrogen Formation in the Radiation Chemistry of Water

H. A. MAHLMAN

Oak Ridge National Laboratory, Chemistry Division, Oak Ridge, Tennessee*

(Received September 14, 1959)

The molecular hydrogen yields in concentrated aqueous sodium nitrate solutions by cobalt-60 gamma-ray irradiation have been observed and correlated with the molecular hydrogen yields observed in dilute solutions. The $G(H_2)$ plotted as the cube root of the $NaNO_3$ activity exhibits a sharp break indicative of a change in the mechanism of formation. The predominant process, designated E_1, is readily affected by a scavenging solute. A process of lessor magnitude, designated E_2, is less susceptible to solute scavenging. The sharp break is interpreted as the cessation of the E_1 process. The $G(H_2)$ observed in the $NaNO_3$ solutions at 298° K is correlated with the $G(H_2)$ observed in ice at 77° K. Of paramount importance is the observation that the hydrogen formed by the E_1 process may be eliminated by irradiation of aqueous nitrate solutions at 77° K. The $G(D_2)$ data observed in comparable D_2O—$NaNO_3$ solutions also exhibit the same mechanisms of formation. The isotope effect on the formation of D_2 in D_2O is in qualitative agreement with two initial distributions of the H atoms.

INTRODUCTION

THE interpretations of the radiation chemistry of aqueous solutions have been based upon the premise of solvent decomposition. The assumed initial solvent decomposition products, H atoms and OH radicals, as they diffuse away from their sites of origin, may interact to reform water or the detected molecular products H_2 and H_2O_2.[1] In this paper the dependence of the hydrogen yield upon the concentration of sodium nitrate, an H atom scavenging solute, illustrates the existence of two scavenging efficiencies in deaerated solutions containing potassium bromide which is interpreted as evidence that the hydrogen atoms are formed by two mechanisms. One of these scavenging efficiencies is the same in liquid at 298°K as it is in ice at 77°K.

EXPERIMENTAL

The water used was purified and stored in silica vessels.[2] The chemicals were Baker and Adamson reagent grade and were used without further purification. The concentration of the sodium nitrate solutions studied varied from 6.4×10^{-4} to 9.1 molal and contained 10^{-3} M KBr to protect the molecular hydrogen formed from hydroxyl radical attack.[3] The residual gas volume per sample was reduced to less than 0.001 cc STP by repeated cycles of freezing, evacuating to 10^{-6} mm pressure, and thawing.

All irradiations were made utilizing a cobalt-60 gamma-ray source[4] supplying a dose rate of 6×10^{20} ev, l^{-1}, min^{-1} relative to the ferrous dosimeter value of 15.6 molecules oxidized per 100 ev of absorbed energy.[5] This annularly loaded cylindrical source provided homogeneous irradiations for centrally placed samples. Hydrogen determinations were made by ignition with oxygen on a platinum filament and the hydrogen yield $G(H_2)$, defined as the number of H_2 molecules formed per 100 ev of absorbed energy, was calculated on the basis of total absorbed energy.[6]

RESULTS AND DISCUSSION

Previous studies have indicated that nitrate ions lower the hydrogen yield,[7] and the observed hydrogen yields in aqueous sodium nitrate solutions less than 1.0 molal gave a linear relationship when plotted against the cube root of the $NaNO_3$ thermodynamic activity.[8]

The $G(H_2)$ have now been determined in aqueous $NaNO_3$ solutions from 1.0 molal to 9.1 molal. In Fig. 1 the hydrogen yields are plotted as the cube root of the $NaNO_3$ activity. The activity of the $NaNO_3$ was calculated by using experimentally determined activity coefficients.[9] The cube root plot illustrates the data favorably by allowing an extrapolation to "zero" solute concentration.

From the cube root plot, Fig. 1, it is apparent that the hydrogen yields may be shown as two linear lines with two different slopes. The intersection of these two lines occurs at $(\text{activity})^{\frac{1}{3}}=0.89$ or activity $=0.71$ or 1.30 molal. One process, arbitrarily designated E_1, is readily effected by the $NaNO_3$ scavenger, whereas the second process, designated E_2, is not readily scavenged. The different scavenging efficiencies indicate that the molecular hydrogen is formed by two mechanisms.

The hydrogen yields observed at 298°K in $NaNO_3$ solutions greater than 1.30 molal have particular interest since an extrapolation through these points to

* Operated for the U. S. Atomic Energy Commission by the Union Carbide Corporation.

[1] A. O. Allen, Discussions Faraday Soc. **2**, 79 (1952).

[2] C. J. Hochanadel, J. Phys. Chem. **56**, 587 (1952).

[3] E. R. Johnson and A. O. Allen, J. Am. Chem. Soc. **74**, 4147 (1952).

[4] J. A. Ghormley and C. J. Hochanadel, Rev. Sci. Instr. **22**, 473 (1953).

[5] C. J. Hochanadel and J. A. Ghormley, J. Chem. Phys. **21**, 880 (1953).

[6] H. A. Mahlman and G. K. Schweitzer, J. Inorg. & Nuclear Chem. **5**, 213 (1958).

[7] H. A. Mahlman and J. W. Boyle, J. Chem. Phys. **27**, 1434 (1957).

[8] H. A. Mahlman, J. Chem. Phys. **31**, 993 (1959).

[9] H. S. Harned and B. B. Owen, *The Physical Chemistry of Electrolytic Solutions* (Reinhold Publishing Corporation, New York 1957).

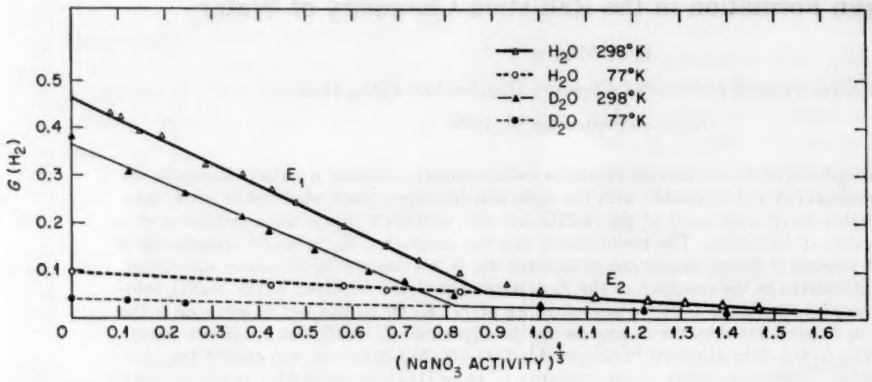

FIG. 1. Hydrogen yields as a function of $NaNO_3$ activity.

"zero" solute concentration has an intercept of $G(H_2) = 0.10$. This intercept is identical with the $G(H_2)$ observed in ice at 77°K. Ghormley and Stewart[10] have also determined that $G(H_2) = 0.10$ in ice irradiated at 77°K. The $G(H_2)$ observed in frozen $NaNO_3$ solutions greater than 1.30 molal at 77°K are the same as the $G(H_2)$ observed when the identical solutions are irradiated at 298°K. Furthermore, the $G(H_2)$ in frozen $NaNO_3$ less than 1.30 molal coincide with the 298°K extrapolation to "zero" solute concentration. This is contrasted to the E_1 portion which is eliminated at 77°K. The hydrogen yields observed in solutions greater than 1.30 molal irradiated at 298°K were also found to be independent of bromide ion concentration as were all solutions irradiated at 77°K regardless of the sodium nitrate concentration.

The $G(D_2)$ observed in comparable $D_2O-NaNO_3$ solutions are also presented in Fig. 1. The activity coefficient for $NaNO_3$ solutions in D_2O was assumed to be the same as in H_2O solutions containing the same mole ratio of solute to solvent. Equal solute molalities in H_2O and D_2O do not contain equal mole ratios of solute to solvent since there is a 10% difference in the densities of H_2O and D_2O. Therefore, the calculation of activity from equal solute molalities and the assumed equal activity coefficients would not be appropriate. The division of the heavy water hydrogen yields into two parts and the observation that a portion of the $G(D_2)$ is readily suppressed by $NaNO_3$ while a lessor amount is quite difficult to scavenge is comparable to the light water data.

At zero solute concentration, the $G(H_2)$ from the E_2 process in H_2O and D_2O is 0.10 and 0.04, respectively. The $G(H_2)$ from the E_1 process is the difference between the total observed $G(H_2)$ and the $G(H_2)$ derived from the E_2 process. These differences are 0.36 and 0.33 for light and heavy water and are not considered to be significantly different from each other.

The molecular hydrogen yield formed by the E_1 process may be a manifestation of the decomposition of excited water molecules into radical pairs H and OH (D and OD) as in the Samuel-Magee theory.[11] The elimination of the molecular hydrogen formed by the E_1 process during irradiation at 77°K suggests an increased back reaction. The radical pairs arising from the decomposition of excited water molecules would be subject to strong caging forces at 77°K. Increased caging would favor a back reaction to form water (ice) and would naturally suppress the observed $G(H_2)$ by the removal of H atoms.

At zero solute concentration, the $G(H_2)$ from the E_1 process in H_2O and D_2O are 0.10 and 0.04 and the difference, 0.06, is considered significant. This difference, 0.06, is qualitatively consistant with the isotope effect proffered by Dainton.[12] He postulated that the initial H atom distribution did not conicide with the OH radical distribution but had an unsymmetrical element, and in D_2O the disparity between the D and OD radical distribution is greater than the corresponding distribution in water. If some of the H atoms arise from the interaction of a water molecule with an electron, then the difference in the rotational relaxation times for H_2O and D_2O enables the electron to diffuse farther away from its site of origin in D_2O. This would result in a broader distribution of D atoms in D_2O than the corresponding H atom distribution in H_2O. Experimental results have verified that $G_{(D)}$ is larger than $G_{(H)}$ and that $G(D_2)$ is less than $G(H)_2$[13] at 298°K. In agreement, the data for the E_2 process show a lower $G(D_2)$ than $G(H_2)$ while the $G(D_2)$ and $G(H_2)$ for the E_1 process are nearly constant.

The insensitivity of the E_2 process to scavengers is an apparent anomaly. However, EPR measurements[14] by Livingston and Weinberger show a specificity of H atom reaction to form H_2 in sulfuric acid solutions irradiated at 77° K and then warmed. The $G_{(H)}$ of

[10] J. A. Ghormley and A. C. Stewart, J. Am. Chem. Soc. **78**, 2934 (1956).

[11] A. H. Samuel and J. L. Magee, J. Chem. Phys. **21**, 1080 (1953).

[12] F. S. Dainton, Radiation Research, Suppl. 1, 1–25 (1959).

[13] H. A. Mahlman and J. W. Boyle, J. Am. Chem. Soc. **80**, 773 (1958); Armstrong, Collinson, and Dainton *et al.*, *Proceedings of the Second International Conference on Peaceful Uses of Atomic Energy*, (United Nations, Geneva, Switzerland, 1958) p. 80; C. N. Trumbore and A. H. W. Aten, Jr., J. Am. Chem. Soc. **78** 4179 (1956); T. J. Hardwick, J. Chem. Phys. **31**, 226 (1959).

[14] R. Livingston (private communication).

stably trapped hydrogen atoms measured at 77° K by EPR is much less than the $G_{(H)}$ calculated from chemical measurements in the identical solutions at 298° K. This discrepancy is indicative of a large back reaction.

This discussion has been based upon the assumption that the initial decomposition of frozen water at 77° K is the same as the initial decomposition of liquid water at 298° K. The major cause of the difference between the effects noted at 77° K and 298° K has been ascribed to the large back reaction occurring at the lower temperature. It is possible, however, that at 77° K fewer radicals have formed and that no extensive back reaction has taken place. Nevertheless, the E_1 process has been eliminated in the frozen system and the E_2 process manifests itself independent of the temperature. Measurements by Piette *et al.*[15] and Ghormley and Stewart[9] indicate that the $G(H_2)$ is constant between 4° K and 173° K.

CONCLUSION

The data indicate that the production of molecular hydrogen during the Co-60 gamma irradiation of aqueous $NaNO_3$ solutions is derived from two mechanisms. The comparable hydrogen yield data for D_2O—$NaNO_3$ solutions also indicates two mechanisms of formation. The major portion (E_1) of the molecular hydrogen yield is readily reduced by the addition of a H atom scavenger, nitrate ion, while the remaining portion (E_2) of the hydrogen yield is less susceptible to the effect of this scavenging solute. The E_1 process may be eliminated by irradiation of aqueous $NaNO_3$ solutions at 77° K or by sodium nitrate concentrations in excess of 1.30 molal. The E_2 process occurs to the same extent in $NaNO_3$ solutions greater than 1.30 molal at 298° K as it does in the identical solutions at 77° K. The molecular hydrogen formed by the E_2 process is independent of the temperature. In sodium nitrate solutions less than 1.30 molal, the molecular hydrogen yield derived from the E_2 process is predicted by an extrapolation of the data observed in sodium nitrate solutions greater than 1.30 molal at 298° K. Additional work is being conducted to elucidate the mechanisms of molecular hydrogen formation for the two processes.

[15] Piette, Rempel, Weaver, and Fournoy, J. Chem. Phys. **30** 1623 (1959).

ACKNOWLEDGMENT

The author wishes to thank C. J. Hochanadel and P. S. Rudolph for their helpful criticism and encouragement in conducting this work. He also wishes to thank J. W. Boyle, M. Burton, and R. Livingston for their comments.

THE JOURNAL OF CHEMICAL PHYSICS VOLUME 32, NUMBER 2 FEBRUARY, 1960

Vibrational Distribution in Late Nitrogen Afterglows

R. A. YOUNG AND K. C. CLARK
Department of Physics, University of Washington, Seattle, Washington
(Received August 31, 1959)

The late portion of long afterglows in nitrogen at a pressure of 1 mm Hg has been investigated spectroscopically, revealing that during 140 sec of decay no change occurs in the characteristic relative vibrational distribution of the N_2 ($B\,^3\Pi \rightarrow A\,^3\Sigma$) 1st positive bands. A common excitation mechanism for all levels is required; it cannot depend upon known metastable particles formed in the initial discharge or generated during the decay.

AFTERGLOWS in active nitrogen consist predominantly of the 1st positive bands of N_2 ($B^3\Pi \rightarrow A\,^3\Sigma$) with particular enhancement of those from vibrational levels near $v'=11$ and 6. In the various theories[1-3] which are proposed to account for the intensity distribution of the characteristic afterglow spectrum, metastable atoms or molecules play a necessary role. The initiating discharge produces several types of such metastable particles, having lifetimes of the order of seconds under usual afterglow conditions.[4] One would expect those details of the spectrum whose excitation utilizes metastable particles to decay with time differently than those features whose excitation does not require metastable particles. It is therefore of interest to look for changes in the afterglow spectrum over times longer than the above lifetimes. Until the present report, none of the many spectrographic investigations has extended to times later than about one second in decay.

EQUIPMENT

The active nitrogen was formed in a static system by a single high-current arc between aluminum electrodes, discharging a capacitance of 36 μf at 4 kv through a triggered Ignitron. Nitrogen made from sodium azide was used at about 1 mm Hg, and the afterglow was observed in a spherical 12-liter bulb whose interior walls were coated with deliquescent phosphorus pentoxide. Efficient transfer of the active nitrogen from the discharge region through a 30-cm connecting tube of 20-mm diameter was effected by the discharge pressure pulse. An external coating of magnesium oxide increased the light collection from the observation bulb by a factor of about 100.

A spectrograph employing a blazed transmission grating of 600 lines/mm and a 25-mm $f/0.95$ objective lens on a Bolex H-16 movie camera was principally used. The entrance slit was 5 cm high, 75 cm from the collimating lens, and sufficiently wide to give 20-A wavelength resolution. Spectrograms of higher resolution at fixed delays were obtained using other instruments, such as the echelle spectrograph discussed in a subsequent paper.[5] The camera arrangement permitted convenient film transport by cable release following multiple exposures on a single frame. Typical spectrograms from several hundred runs are discussed in this paper. Eastman 103a-F and 1-N emulsions were used and were developed in D-19 to a background density of about 0.3. Calibration exposures were placed on each section of film, and used for careful determination of intensities from densitometer records.

Time resolution was provided by a servo-controlled 2.5-mm aperture which moved along the length of the normal spectrographic slit. Its driving system included a photomultiplier, integrator, servo-controlled aperture drive, and position recorder. The aperture briefly remained stationary, then moved at a varying rate which was proportional to the intensity of the 1st positive bands, producing essentially constant photographic density along the slit image as the afterglow decayed. A nonlinear time scale on the photograph necessarily resulted and was determined from continuous chart recordings of the aperture position *versus* time throughout a run of cyclic exposures. In this manner relative variations among the bands are emphasized, while the general decay with time can be obtained from the record of the aperture positions. In cyclic afterglow exposures over hours or days, any malfunction of the servo-aperture control or unwanted deviation of the decay rate is observed on these continuous records, and the run can be discarded. Any departure from uniform exposure along any one line caused by nonuniform illumination or by incomplete aperture sweeps is equally present for all lines and therefore does not affect the ratios of simultaneous intensities.

RESULTS

Figure 1 is a representative time-resolved spectrum of the first positive bands ($B\,^3\Pi \rightarrow A\,^3\Sigma$) excited in the nitrogen afterglow at a pressure of 1 mm Hg and covering the first half-minute of decay. During this interval the afterglow decay changes from the early hyperbolic form characterizing recombination of two active particles to the late exponential decay due to wall losses. Transitions from the various excited vi-

[1] O. Oldenberg, Phys. Rev. **90**, 727 (1953).
[2] Berkowitz, Chupka, and Kistiakowsky, J. Chem. Phys. **25**, 457 (1956).
[3] J. M. Anderson, Proc. Phys. Soc. (London) **A70**, 887 (1957).
[4] J. F. Noxon, "Active Nitrogen at High Pressure" (thesis, Harvard University, 1957).
[5] R. A. Young and K. C. Clark, J. Chem. Phys. **32**, 607 (1960).

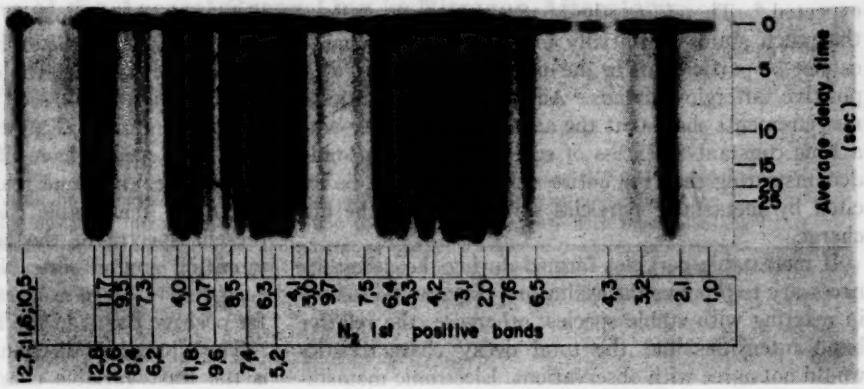

FIG. 1. A time-resolved spectrum of 1st positive bands in N_2 afterglow at 1 mm Hg pressure, resulting from 100 cyclic exposures on 1-N 16-mm film. Band identifications are marked and wavelength increases toward the right. The nonuniform exposure time during decay is indicated by the scale of average time since the discharge and is chosen to give approximately constant density after an initial delay.

brational levels are indicated and show the typical afterglow enhancements near $v'=11$ and 6. While the major bands are detectable in a single decay with 103a-F film, this picture represents the superposition of about 100 decays recorded on 1-N film. It is apparent that the relative intensities maintain a constant ratio. Detailed photometric measurements confirm (within $\pm 10\%$) that no change in the relative distribution of the first positive bands occurs during the 25-sec period. Furthermore, the number of transitions per second from the enhanced $v'=2$ vibrational level of the $B\,^3\Pi$ state is comparable to the number of transitions per second from the $v'=11$, 12 vibrational level.

Figure 2 compares spectrograms of identical afterglows taken on 103a-F film after delays of 2 sec and of 140 sec. The apparent similarity of intensity distributions is striking. Densitometer measurements again show that within $\pm 10\%$ the two spectrograms are identical in relative intensities. Several other spectrograms have been measured with results agreeing with those obtained in Figs. 1 and 2. With longer exposures, several weaker bands become apparent. Most of these can be attributed to the CN molecule (CN violet and red systems) and to NO (the β and γ bands). The oxygen green line (5577A) is a common, though perhaps surprising, occurrence even in the 140-sec-old afterglow. The auroral green line excitation mechanism has been studied and is reported elsewhere.[5]

An unresolved overlap of the CN red system could conceivably distort the measurements of the N_2 1st positive system, although this would seem an unlikely possibility since the spectra are so characteristic of the nitrogen afterglow. However, a clear answer can be given. By using a crossed grating echelle spectrograph with the Bolex camera, one can separate the band heads of these N_2 and CN systems at approximately 1-A resolution with sufficient sensitivity to record the spectrum of afterglow older than 1 min. The spectrum is identical in its general features with those obtained at lower dispersion, and the influence of the CN red system on the measured relative intensities of the N_2 bands is seen not to be appreciable.

DISCUSSION

Theories pertaining to the excitation of the 1st positive bands in active nitrogen employ processes based on the storage of energy by dissociated ground-state atoms and its transfer into the $B\,^3\Pi$ state via 3-body recombination either directly or through the $^5\Sigma$ state.[2] Vibrating ground-state molecules have also been proposed.[3,6] None of these processes has been shown to account for the excitation of low vibrational levels of the $B\,^3\Pi$ at rates comparable with that of the $v'=11$, 12 levels. The local intensity maximum at $v'=6$ has been attributed to reactions involving nitrogen atoms or molecules in metastable electronic states.

The long time over which the same relative intensity distribution has now been observed to persist exceeds the lifetimes of any metastable states which could be

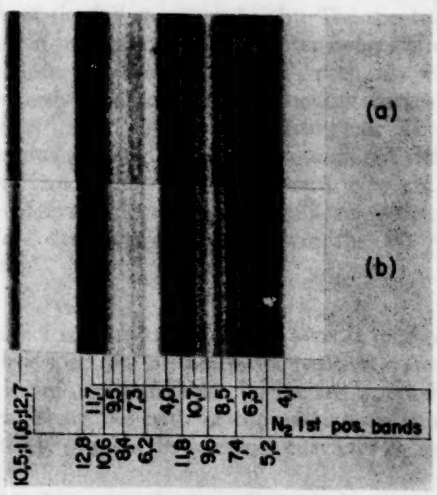

FIG. 2. Comparison of early and late nitrogen spectra at fixed delay times of (a) 2 sec and (b) 140 sec. Spectra represent identical afterglows at 1 mm Hg pressure and are limited to the visible region by the response of the 103a-F 16-mm film used.

[6] S. W. Kash, University of California Institute of Geophysics, Final Report, Contract NGonr-27503, February (1951).

expected.* Therefore, these measurements indicate that such states, if initially formed in the discharge, cannot be participants in the excitation of selective 1st positive afterglow bands. Auxiliary photomultiplier measurements show that the afterglow can decay with a time constant in excess of several hundred seconds, demonstrating that the entire afterglow cannot be excited by metastable particles surviving from the discharge.

If metastable particles formed during the decay are necessary to produce the excitation, they can do so only in reacting with stable species; otherwise, the relative band intensities and the total decay characteristics would not agree with observations. Electronic metastable states can therefore play no part, except as intermediaries, in the production of the 1st positive bands in the afterglow.

Likewise, vibrationally excited ground state N_2 cannot participate in the excitation of the afterglow bands. Although it is conceivable that N_2 may have a vibrational lifetime of 100 sec,[7] this time is improbable in the present conditions; Kaufman and Kelso[8] recently imply that such species have lifetimes of about 0.05 sec. In either case, the same reasoning previously applied to electronic metastable particles, together with the present spectra of the late afterglow, indicates that vibrating ground state N_2 cannot serve either as the energy reservoir or as a reactant in the excitation of the 1st positive bands in the afterglow.

The vibrational distribution of the 1st positive bands is the least variable characteristic of active nitrogen and evidently is determined by the intrinsic nature of the single act of excitation. Theories which utilize more than one excitation mechanism or employ metastable particles, other than as intermediaries, are incorrect in their explanation of the afterglow spectrum.

* Noxon[4] found that about 10^8 to 10^9 collisions with N_2 are required to deactivate metastable electronic states of O, N, N_2, this number corresponding to a mean collisional lifetime of 10–100 sec under the conditions of the present measurements.

[7] S. J. Lukasik and J. E. Young, J. Chem. Phys. **27**, 1149 (1957).
[8] F. Kaufman and J. R. Kelso, J. Chem. Phys. **28**, 510 (1958).

Excitation of the Auroral Green Line in Nitrogen Afterglows

R. A. YOUNG AND K. C. CLARK

Department of Physics, University of Washington, Seattle, Washington

(Received August 31, 1959)

Production of the auroral green line of OI($^1D-^1S$, 5577 A) is observed during long (30-sec) afterglows in a static system containing nitrogen and small amounts of oxygen. Relative to the intensities of the N_2 1st positive bands, the measured intensities of 5577-A and the NOβ bands increase with time. The long period of observation definitely eliminates the initial discharge as a possible source of the metastable oxygen atoms, and their chemical excitation in the afterglow volume is established. A probable process consistent with observations is that involving collision of N atoms with vibrationally excited NO molecules. This mechanism is discussed as a possible source of 5577 A in the airglow.

EXCITATION in the airglow of the auroral green line of atomic oxygen ($^1D-^1S$, 5577 A) is generally regarded as due to luminescent chemical reactions in the atmosphere. Possible excitation reactions have been proposed[1] involving atomospheric constituents known to exist at the observed heights of the airglow. Laboratory chemical excitation of this line has not been clearly distinguished from production in the initial discharge. Intense sources of this line, such as those of McLellan and Shrum[2] and of Noxon[3] undoubtedly rely upon electron collisions to excite the atomic oxygen. The 5577-A line is often observed in active nitrogen generated in a flow system,[4,5] but these observations are limited to such an early portion of the decay that many of the observed ^1S atoms, whose radiative lifetime is about 1 sec,[6] are those formed in the discharge by nonchemical processes.

The present observation of the auroral green line during the later portions of the nitrogen afterglow is the first verifiable instance of its chemical excitation. Production mechanisms applicable to the observations will be discussed.

EXPERIMENT

The experimental equipment is the same as that described in a previous paper[7] dealing with the 1st positive ($B\,^3\Pi \rightarrow A\,^3\Sigma$) bands of the nitrogen afterglow. It employs a very fast spectrograph of low resolution, equipped with a servo-controlled aperture moving along the normal slit. This generates a time-resolved spectrum of uniform density but nonuniform time scale encompassing 30 sec of decay in a static gas system. This aperture arrangement effectively utilizes the afterglow radiation; more importantly, it emphasizes relative changes among the spectral components. Their explicit time dependence can be derived from continuous records of aperture position *vs* time made thoughout the long ($\frac{1}{2}$- to 12-hr) cyclic exposures. Observations were made in a 12-liter bulb coated internally with deliquescent phosphorous pentoxide to reduce surface reactions and externally with magnesium oxide to increase the light collection efficiency.

The 5577-A line was emphasized by leaking oxygen into the nitrogen system, already at about 1 mm Hg, at a rate corresponding to a pressure rise rate of 0.001 mm/hr. A liquid nitrogen trap was necessary to remove nitrogen oxides and other impurities from the gas volume during the long exposures.

Relative measurements of photographic exposure (intensity$\times$time) along a spectral line were made using calibrated densitometer traces. The moving aperture was $\frac{1}{20}$ of the full spectrum height. The spectrum was covered in ten separate densitometer sweeps of equally spaced intervals, from which, on correlation with the continuously recorded aperture motion, curves of exposure *vs* delay time were constructed. The servo system was adjusted to keep the integrated visible 1st positive band of nitrogen at constant exposure. Other bands observed deviating from uniform density were therefore decaying differently than the 1st positive system.

RESULTS

Figure 1 is a reproduction of a typical time-resolved afterglow spectrum of the N_2 1st positive system. The densities of the individual bands are approximately uniform along the path of the moving aperture[7] and collectively provide the reference curve for N_2 shown in Fig. 3.

Figure 2 is a reproduction of a typical spectrum made under the same conditions as before but with about 100 times the exposure in order to show weaker components. These features are the red and violet systems of CN, the β bands of NO, and the auroral green line.

Results of densitometer measurements are displayed in Fig. 3. The photographic exposures are plotted loga-

[1] D. R. Bates, *The Earth as a Planet* (University of Chicago Press, Chicago, Illinois, 1954) edited by G. P. Kuiper, Ch. 12. This volume reviews the observations and theoretical considerations pertinent to the upper atmosphere.

[2] J. C. McLellan and G. M. Shrum, Proc. Roy. Soc. (London) **A114**, 1 (1927).

[3] J. F. Noxon, "Active Nitrogen at High Pressure," (thesis, Harvard University, 1957).

[4] Kurzweg, Bass, and Broida, J. Mol. Spectroscopy **1**, 184 (1957).

[5] M. Brook and J. Kaplan, Phys. Rev. **96**, 1540 (1954).

[6] R. H. Garstang, *The Airglow and the Aurorae* (Pergamon Press, New York, 1955) edited by E. B. Armstrong and A. Dalgarno, p. 324.

[7] R. A. Young and K. C. Clark, J. Chem. Phys. **32**, 604 (1960).

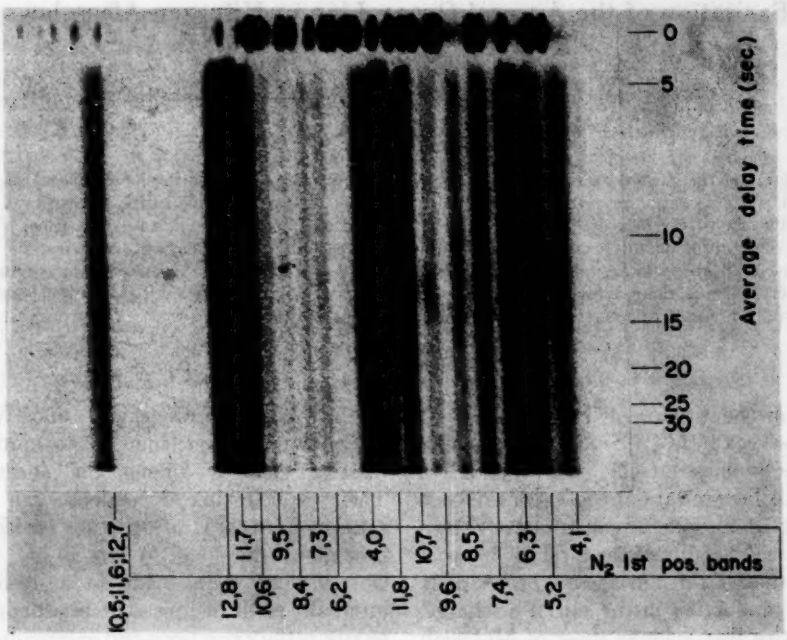

FIG. 1. Time-resolved spectrum of 1st positive bands in N_2 afterglow at 1 mm Hg pressure. Band identifications are marked, and wavelength increases to the right in all spectra. The non-uniform length of exposure is indicated by the scale of average elasped time since the discharge, including an initial delay. This exposure time control produces the approximately constant density shown in Fig. 4.

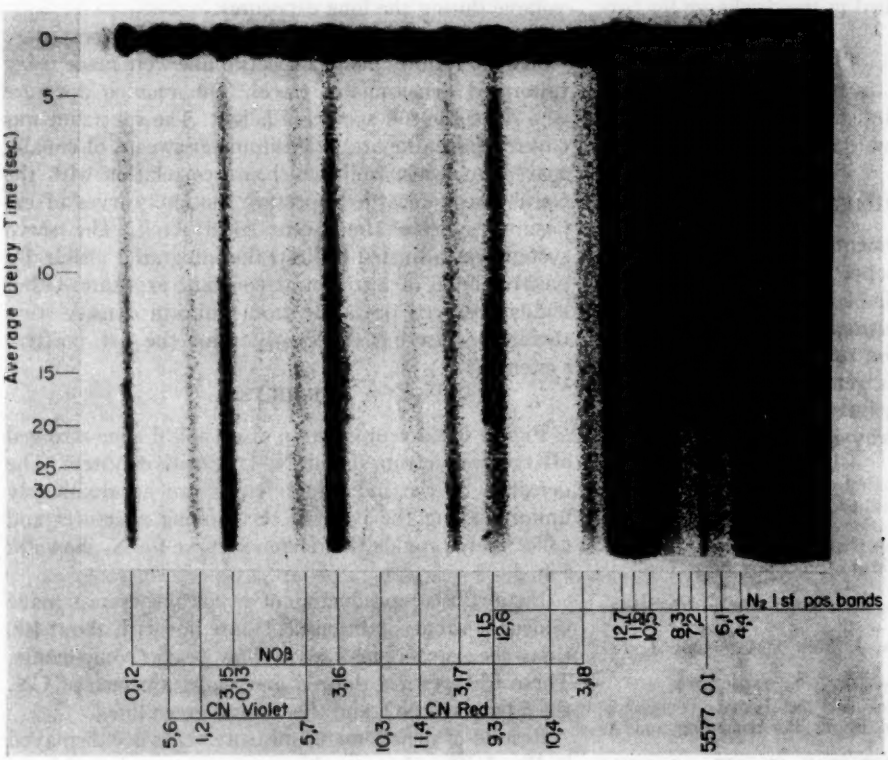

FIG. 2. Strongly exposed time-resolved spectrum showing the progressive increase of OI (5577 Å) and weak NOβ and CN band systems relative to those of N_2. The time scale is identical with that of Fig. 1.

rithmically to permit arbitrary displacement into groups of similar time dependence. The slight variation for the N_2 1st positive bands is attributable to nonuniform illumination and can be taken into account when necessary. The NO bands decay more slowly than the N_2 bands. The 5577-A line decays similarly with the NO bands, showing a definite growth relative to those of N_2. This behavior definitely indicates a chemical excitation not identical with that of the N_2 bands. In this instance the CN bonds also show a similar decay.

The identification of the feature near 5577 A as the auroral green line is based on the following groups of evidence: (1) Its strong occurence coincides critically and reasonably with the addition of suitable traces of oxygen. (2) From calibrations of the low resolution time-resolved spectrograms its wavelength is measured to be 5577 ± 10 A, and its image width is less than that of any other afterglow features and corresponds to that of known line sources. Its position coincides with the green line produced by a Tesla discharge in the observation bulb. (3) From the spectrogram of Fig. 4 the wavelength is found to be 5577.4 ± 0.1 A, in agreement with the known value of 5577.35 A. This corroborative spectrum was taken with crossed echelle and ordinary reflection gratings and a 2-in. $f/1.4$ lens. It represents similar conditions to those of the previous spectrogram but is limited to that portion of the afterglow following the formative discharge by more than 20 sec in order to avoid any possibility of survival of original metastable oxygen atoms.

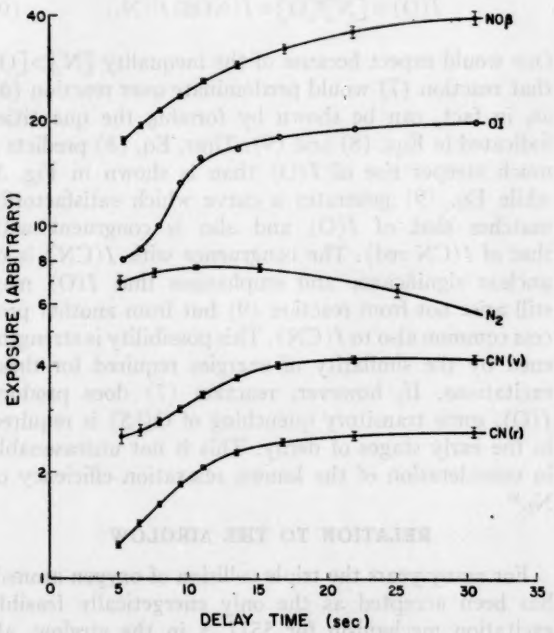

FIG. 3. Comparison of the time dependence of various afterglow emissions shown in Figs. 1 and 2. Curves represent groupings as to source, with the photographic exposures normalized within each group at $t=10$ sec; the separation between groups is arbitrary. This is not a plot of intensity decay because of the common variation in length of exposure, but relative changes between groups are proportional to relative changes of intensity. All features identified in Figs. 1 and 2 except the very weak 1st positives were plotted and used to set the indicated deviations.

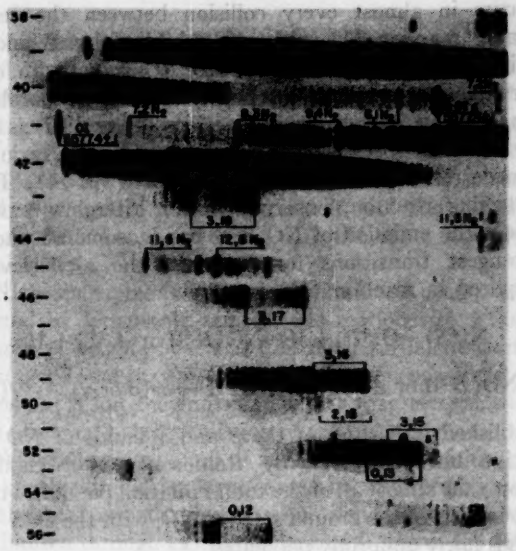

FIG. 4. Echelle spectrogram of nitrogen afterglow after 20-sec of decay, showing strong green line emission. Spectrum orders are numbered at the left margin, and bands of N_2 and NOβ are identified. Only those of N_2 are labeled. The 5577-A line is shown in two orders.

Evidence indicates that the green line is emitted from the volume and not the walls. Intensity measurements of the N_2 bands by suitably collimated photomultipliers show that little, if any, of this associated radiation comes from the wall. If the green line were produced at the wall, it might be highly perturbed, as is the green wall continuum observed by Noxon[3] in systems producing the green line in the volume and as are the shifted emission lines of afterglows condensed on extremely cold surfaces.[8] However, the absence of any observable wavelength shift in Fig. 4 implies a volume emission.

INTERPRETATION

Since the radiative lifetime of the ^1S state of atomic oxygen is approximately 1 sec and Noxon[3] has found that approximately 10^8 collisions are necessary to deactivate this state, the ^1S state then has time to radiate; in any case, observations on the Tesla discharge experimentally establish this fact.

Several processes are conceivable as excitation mechanisms for the oxygen line. One may first consider the spin disallowed reaction

$$NO(^2\Pi, v\geqq 4)+N(^4S)\rightarrow N_2(^1\Sigma)+O(^1S). \quad (1)$$

Since the similar reaction

$$NO(^2\Pi)+N(^4S)\rightarrow N_2(^1\Sigma, v \text{ large})+O(^3P) \quad (2)$$

[8] H. P. Broida and O. S. Lutes, J. Chem. Phys. **24**, 484 (1956).

occurs in almost every collision between the reactants,[9] reaction (1), although inhibited by Wigner's spin conservation rule, still may occur with an observable rate when reactant populations are comparable. The relative importance of reactions (1) and (2) is set by the fixed specific reaction rates and by the ratio of concentrations of NO ($v \geqq 4$) and NO ($v < 4$). The following reaction, observed in the afterglow,[10] produces the emission of NO β, γ bands, some of whose strongest transitions terminate on the $v \geqq 4$ levels required in reaction (1):

$$N(^4S)+O(^3P)+M \rightarrow NO(B\,^2\Pi \text{ or } A\,^2\Sigma)+M$$

$$NO(B\,^2\Pi \text{ or } A\,^2\Sigma) \rightarrow NO(X\,^2\Pi)+h\nu(\beta \text{ or } \gamma). \quad (3)$$

Published intensities of the β and γ bands of NO in active nitrogen given by Robinson and Nicholls[11] show that almost all of the total radiation populates the $v \geqq 4$ levels of the ground state of NO, with the $v = 5-9$ levels fairly uniformly populated.

In the cycle of reaction (3) followed by both (1) and (2), atomic oxygen acts as a catalyst for nitrogen recombination. Atomic nitrogen survives in these experiments only at very small concentrations of atomic oxygen, or, equivalently, of nitrogen oxides.

An alternative source of NO($v=6$) is offered by the reaction,

$$N(^4S)+O_2(^3\Sigma) \rightarrow NO(^2\Pi, v=6)+O(^3P). \quad (4)$$

Although the rate of this two-body reaction is known to be small,[9] it may become important compared to the three-body reaction (3) when sufficient molecular oxygen is present. The cyclic reactions (1), (2), and (3) lead to the following dependence of intensity ratios on concentrations:

$$I(O)/I(N_2) \sim [O]/[N] \sim I(NO\beta)/I(N_2). \quad (5)$$

If [O] is constant, these ratios should increase with time in inverse proportion to [N]. Between times 10 and 30 sec this concentration was measured to decrease by a factor of 4.5, using the square root of the 1st positive intensity recorded by a photomultiplier during the exposure. However, Fig. 3 shows an increase by a factor of only 1.7, indicating that [O] is slowly decreasing at a rate somewhat less than that of [N].

Equation (5) implies that the ratio $I(O)/I(NO\beta)$ remains fixed. However, if NO($v=4$–9) is depopulated by collision or radiation, then this intensity ratio will decrease during the afterglow decay because the relaxation time interval set by reaction (2) increases as [N] decreases. Between the times of 10 and 30 sec shown by Fig. 3, this ratio decreases by 20%, while the interval during which relaxation can occur increases by a factor of 4.5. If one assumes the reasonable values of $[N]=0.001\,[N_2]$ at 10 sec and unity as the probability for reaction (2), the relaxation of NO can conveniently be described as exponential with a decay time of 2.6 msec. The radiative lifetime of NO($v=4$–9) is longer than that of the $v=4$ level, which is 4.1 msec, as estimated from the $\Delta v=1$ absorption bands.[12] Therefore, if the OI (5577 A) line is excited by reactions (1) and (2), these results imply that at least 2×10^4 collisions with N_2 are needed to deactivate NO($v=4$–9).

Another possible excitation mechanism for the green line involves three-body atomic collisions, as suggested by Chapman,[14]

$$O+O+O \rightarrow O_2+O(^1S) \quad (6)$$

$$N+N+O \rightarrow N_2+O(^1S). \quad (7)$$

The curves shown in Fig. 3 offer the possibility of ascertaining the relative importance of these reactions in the afterglow. Reactions (6) and (7),* together with the known excitation mechanisms for the NOβ and N_2 1st positive bands, lead to the following relations respectively,

$$I(O) \propto [O]^3 \propto I^3(NO\beta)\,I^{-\frac{1}{2}}(N_2) \quad (8)$$

$$I(O) \propto [N]^2[O] \propto I(NO\beta)\,I^{\frac{1}{2}}(N_2). \quad (9)$$

One would expect because of the inequality [N]>[O] that reaction (7) would predominate over reaction (6) as, in fact, can be shown by forming the quantities indicated in Eqs. (8) and (9). Thus, Eq. (8) predicts a much steeper rise of $I(O)$ than is shown in Fig. 3, while Eq. (9) generates a curve which satisfactorily matches that of $I(O)$ and also is congruent with that of I(CN red). The congruence with $I(CN)$ is of unclear significance and emphasizes that $I(O)$ may still arise not from reaction (9) but from another process common also to $I(CN)$. This possibility is strengthened by the similarity of energies required for these excitations. If, however, reaction (7) does produce $I(O)$, some transitory quenching of $O(^1S)$ is required in the early stages of decay. This is not unreasonable in consideration of the known relaxation efficiency of N_2.[13]

RELATION TO THE AIRGLOW

For many years the triple collision of oxygen atoms[14] has been accepted as the only energetically feasible excitation mechanism for 5577 A in the airglow, although no corroborative measurements are available.

[9] G. B. Kistiakowsky and G. G. Volpi, J. Chem. Phys. **28**, 665 (1958).
[10] F. Kaufman and J. R. Kelso, J. Chem. Phys. **27**, 1209 (1957).
[11] D. Robinson and R. W. Nicholls, Proc. Phys. Soc. (London) **71**, 957 (1957).
[12] S. S. Penner and D. Weber, J. Chem. Phys. **21**, 649 (1952); and B. L. Crawford, Jr., and H. L. Dinsmore, J. Chem. Phys. **18**, 983 (1950).
* Conversations with W. J. Schade and C. A. Barth concerning the feasibility of reaction (7) are gratefully acknowledged.
[13] Bauer, Kneser, and Sittig, J. Chem. Phys. **30**, 1119 (1959).
[14] S. Chapman, Proc. Roy. Soc. (London) **A132**, 353 (1931).

The reaction sequence (4) followed by (1) may also contribute significantly to the observed green line intensity.

Results from recent rocket and sea level measurements of the green line in the airglow provide the following information: (1) Intensity of the 5577 A radiation is[15] typically $300–600\times10^6$ photons/cm² sec. (2) The radiation occurs in a relatively thin layer[16] between about 95 and 105 km. (3) It has a patchy, inhomogeneous distribution. Recent investigations have also determined the kinetic temperature of 240°K at 100 km and the following concentrations of the reactants: $[N_2]=1.2\times10^{13}$/cm³, $[O_2]=4\times10^{12}$/cm³. Although the ratio $[N]/[N_2]$ is uncertain, a reasonable estimate is 10^{-2}, i.e., $[N]=1.2\times10^{11}$/cm³. With the known rate of reaction (4) and the above values of concentrations, one can compute that NO ($v=6$) is produced at the rate of 3×10^6/cm³ sec. Wigner's spin conservation rule may inhibit reaction (1) relative to (2) by a factor of about 10^{-2}. Reaction (4) followed by reaction (1) would therefore lead to 200 photons/cm³ sec at 5577 A. Uncertainties in [N] and in the effect of Wigner's rule permit flexibility in this estimate by an order of magnitude. If the green line is radiated uniformly from a 10-km layer, this rate produces 200×10^6 photons/cm² sec, in remarkable agreement with the value measured in airglow.

Nitrogen atoms present at 100 km have been transported by large-scale atmospheric motions from their source at heights near 150 km. Such turbulent transport could lead to considerably inhomogeneous distributions of [N] at the emission height, in agreement with the observed patchy emission of the green line.

While the distribution of 5577-A emission within the 10-km thick radiating layer cannot be predicted because of the unknown distribution of N, its upper extent will be limited through (4) by the lack of O_2 above the 100–120 km dissociation region, and its lower boundary will be set through (1) by the diminishing [N].

[15] E. R. Manring and H. B. Pettit, *The Threshold of Space* (Pergamon Press, London, 1957) edited by M. Zelikoff, p. 58.
[16] Koomen, Scolnik, and Tousey, reference 13, p. 217.

Letters to the Editor

THE Letters to the Editor section is subdivided into three parts entitled Communications, Comments and Errata, and Notes. These three sections are all subject to the same limitations on length. The textual material of each Letter is limited to a number of words equal to 950 minus the following: (a) 200 words for each average-sized figure; (b) 50 words for each displayed equation; (c) 7 words for each line of table including headings and horizontal rulings. No proof will be sent to the authors of "Communications" and "Comments and Errata." Proof will be sent to the authors of "Notes." The publication charge for Letters is $30 per page, with a minimum of $30 per Letter. If honored, the Institution will be entitled to 100 reprints without covers. See issues of May–September, 1957, for descriptions of categories.

Communications

Vapor Pressures of the Neon Isotopes*

ETIENNE G. ROTH† AND JACOB BIGELEISEN

Chemistry Department, Brookhaven National Laboratory, Upton, Long Island, New York

(Received December 14, 1959)

IN recent years there has been considerable interest in the measurement of the effect of isotopic substitution on properties associated with the equation of state of condensed phases, e.g., vapor pressure, molal volume, compressibility, etc. Such measurements are of interest *per se* and, in addition, provide a basis for the development of the theory of quantum effects on the equation of state of condensed substances. Studies of the behavior of the neon isotopes have a focal point in this development. There are no complications from statistics, such as in the He^3—He^4 problem. Molecular solids have the complication of coupling between lattice and molecular vibrations as well as translational-rotational coupling.

In their pioneer work, Keesom and Haantjes[1] showed that the quantum effects in solid and liquid neon are sufficiently large to lead to measurable differences in the vapor pressure between Ne^{20} and Ne^{22}. Their results are in definite disagreement with a Debye model for the solid, if one assumes $\theta_D=63°K$ as determined from the heat capacity of the solid.[2] Johns[3] has shown that better agreement with the experimental data is obtained by an anharmonic Einstein lattice, the parameters for which are evaluated by Henkel's method.[4] The parameters used by Johns lead to values for a_0, the lattice constant, ranging between 4.539 and 4.581 A between 0–24°K. This is in definite disagreement with the experimental value of 4.429 A at 4°K.[5] Inasmuch as Johns uses a 14–6 potential, the zero point energy $\frac{3}{2}W$ is a sensitive function of a_0 and increases from 71.7 to 95.4°K as a_0 decreases from 4.564 to 4.429 A. The use of the experimentally determined a_0 in Johns' calculation leads to a difference in vapor pressures of the neon isotopes much greater than that observed by Keesom and Haantjes and suggests a revision in the potential constants of Zucker.[6]

We, therefore, have, undertaken an experimental reinvestigation of the vapor pressures of the neon isotopes over the temperature range 16.4–30.1°K. Measurements were made by differential manometry in a Giauque-Johnston type cryostat modified for temperature stability. The Ne^{20} sample contained 99.9% Ne^{20} and the Ne^{22} sample contained 72.2% Ne^{22}. Extrapolation to pure Ne^{20} and Ne^{22} can be made with sufficient accuracy by the use of Raoult's law. Our results are in substantial agreement with those of Keesom and Haantjes. At 20°K, where the scatter in our data is an order of magnitude smaller than in the data of Keesom and Haantjes, we find $\ln P_{Ne^{20}}/P_{Ne^{22}}$ is 6 % larger than the smoothed line given by them. For solid neon, our data can be represented to a high accuracy by either an Einstein or Debye harmonic lattice with $\theta_D(Ne^{20})=74.6°K$. For the Einstein lattice $\frac{4}{3}\theta_E=75.9°K$. The result may be compared with the value obtained by Henshaw[5] from the Debye-Waller temperature factor, $\theta_D=73°K$, and with the recent calculation of the zero point energy of Ne by Bernardes,[7] from which he obtains $\theta_D=8E_0/9R=73°K$.

A complete description of the experiment and the experimental data will be submitted for publication shortly. We thank Dr. G. R. Grove of the Mound Laboratory of the Monsanto Chemical Company for the enriched neon samples.

* Research carried out under the auspices of the U. S. Atomic Energy Commission.

† Visiting Chemist at Brookhaven National Laboratory 1957–1958. Permanent address: Centre d'Etudes Nucléaires de Saclay, Gif-sur-Yvette, France.

[1] W. H. Keesom and J. Haantjes, Physica **2**, 986 (1935).
[2] K. Clusius, Z. physik. Chem. **B4**, 1 (1929).
[3] T. F. Johns, Phil. Mag. **27**, 229 (1958).
[4] J. H. Henkel, J. Chem. Phys. **23**, 681 (1955).
[5] D. G. Henshaw, Phys. Rev. **111**, 1470 (1958).
[6] I. J. Zucker, J. Chem. Phys. **25**, 915 (1956).
[7] N. Bernardes, Phys. Rev. **112**, 1534 (1958).

Infrared Studies of Dense Forms of Ice

E. R. LIPPINCOTT, *Department of Chemistry, University of Maryland, College Park, Maryland*

AND

C. E. WEIR AND A. VAN VALKENBURG, *National Bureau of Standards, Washington, D. C.*

(Received December 10, 1959)

THE structures of the dense forms of ice have been of considerable interest since the complexity of the system was revealed by Bridgman.[1] McFarlan[2] pro-

duced the various forms under pressure, cooled the system to a temperature sufficiently low that the pressure could be released without reversion to Ice-I, and obtained x-ray patterns in the metastable state at 1 atmos. He found Ice-II and Ice-III to be orthorhombic and to contain distorted oxygen tetrahedra. Data for the higher pressure forms IV, V, and VI were obtained but were not worked out because of their low symmetry.

Recently a high pressure infrared cell using two type-II diamonds in a "squeezer" design has been constructed here.[3] Preliminary infrared patterns differing considerably from that of Ice-I have been obtained and, since these patterns may be of interest, they are reported here. In these studies the specimen was cooled by passing cold nitrogen gas through the supporting steel block, temperatures being measured by a thermocouple placed close to the diamonds. Temperature was controlled by adjusting the flow of gas and in any run varied not more than ± 0.5°C. From observations on cooling near 0°C it was concluded that the temperature of the specimen was not more than 5°C above that registered by the couple.

Spectra obtained are shown in Fig. 1 as recorded successively for liquid water at room temperature and 1 atmos; Ice-I at -7°C and 1 atmos; ice at -26°C and 9000 atmos, obtained by cooling the previous specimen and then compressing; and ice at -27°C and 3000 atmos, obtained by decompressing from 9000 atmos. A pattern of the diamond cell alone is included for comparison. In view of the metastability of the forms of ice reported previously,[1,2] and also observed here, the phases present at the elevated pressures are not certain. The run at 9000 atmos is in the Ice-VI field while the 3000-atmos run is in the Ice-II field but so close to the II–III transition line that the temperature differential between specimen and thermocouple might place the run in the Ice-III field.

In Ice-I the band centered at 3200 cm^{-1} corresponds to the hydrogen bonded O—H stretching mode and the 1630 cm^{-1} band on the shoulder of the diamond band to the H—O—H bending mode. The broad band centered near 850 cm^{-1} corresponds to a libration mode of the molecule. When liquid water is frozen the formation of the strong hydrogen bonds of Ice-I is accompanied by a shift of the stretching band to lower frequencies, a marked apparent decrease in intensity of the bending band and an increase in intensity of the libration band.[4] In the spectrum at 9000 atmos the peak stretching frequency has shifted to 3600 cm^{-1}, the bending band has a greatly increased intensity but has

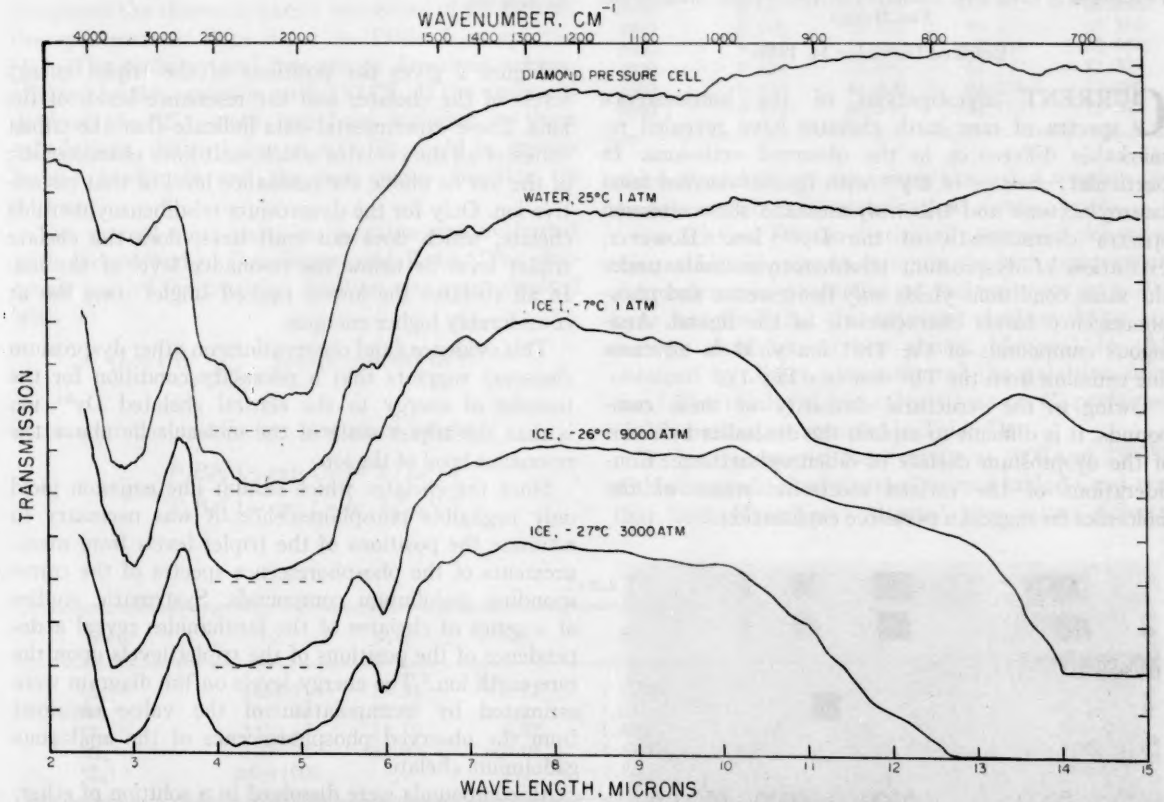

FIG. 1. Infrared patterns for water and ice in the diamond pressure cell. Curves are displaced vertically to avoid overlapping. The zero line for each curve is indicated by the broken line immediately below each curve between 4 and 5 μ. For the bottom curve the abscissa represents the zero line.

not shifted appreciably, and the libration band is either missing or has shifted to lower frequencies. These results are consistent with the interpretation that the hydrogen bonds responsible for the open structure of Ice-I have collapsed and, in the close-packed structure of the dense ice, hydrogen bonding produces a minor effect on the vibration modes. Presumably, weak hydrogen bonds still exist in the dense ice but with the O—H···O angle deviating considerably from 180°.

The spectrum at 3000 atmos is in many respects intermediate between that of Ice-I and that at 9000 atmos. It is not certain that the splitting of the bending band is real because of low intensities associated with frosting of the apparatus in this run.

[1] P. W. Bridgman, *The Physics of High Pressure* (G. Bell and Sons, Ltd., London, 1952), pp. 242, 426.
[2] R. L. McFarlan, J. Chem. Phys. **4**, 60, 253 (1936).
[3] Weir, Lippincott, Van Valkenburg, and Bunting, J. Research Natl. Bur. Standards **63A**, 55 (1959).
[4] P. A. Giguère and K. B. Harvey, Can. J. Chem. **34**, 798 (1956).

Extreme Variations of the Emission Spectra of Dysprosium Chelates

G. A. Crosby and R. E. Whan

Department of Chemistry, University of New Mexico, Albuquerque, New Mexico

(Received December 14, 1959)

Current investigations of the luminescence spectra of rare earth chelates have revealed remarkable differences in the observed emissions. In particular, chelates of Dy^{3+} with ligands derived from benzoylacetone and tribenzoylmethane show emission spectra characteristic of the Dy^{3+} ion.[1] However, excitation of dysprosium tris*di*benzoylmethide under the same conditions yields *only* fluorescence and phosphorescence bands characteristic of the ligand. Analogous compounds of the Tb^{3+} ion yield in all cases line emission from the Tb^{3+} ion (see Fig. 1).

Owing to the structural similarity of these compounds, it is difficult to explain the dissimilar behavior of the dysprosium chelate of dibenzoylmethane. Considerations of the excited electronic states of the molecules do suggest a plausible explanation.

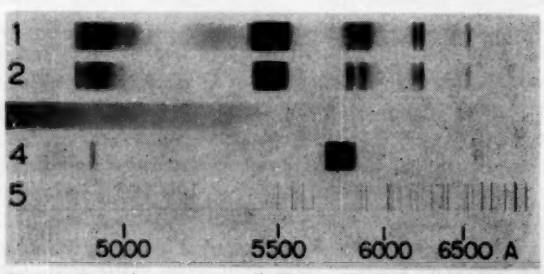

Fig. 1. Emission spectra: (1) TbD_3; (2) TbB_3; (3) DyD_3; (4) DyB_3; and (5) Ne calibration.

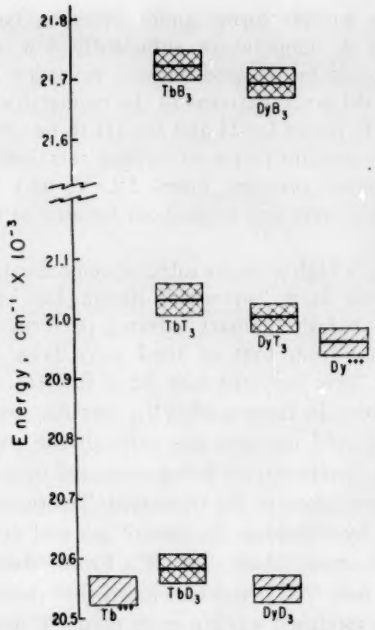

Fig. 2. Energy-level diagram. Tb^{3+} and Dy^{3+} levels are the resonance levels of the ions. All other levels are the triplet state levels for the chelates. Single hatch: measured values; cross hatch: estimated from corresponding Gd chelate (see text). B = benzoylacetonate ion; D = dibenzoylmethide ion; T = tribenzoylmethide ion.

Figure 2 gives the positions of the triplet energy levels of the chelates and the resonance levels of the ions. These experimental data indicate that the triplet states of all the chelates which emit lines characteristic of the ion lie above the resonance level of that respective ion. Only for the dysprosium trisdibenzoylmethide chelate, which does not emit lines, does the chelate triplet level lie below the resonance level of the ion. In all chelates the lowest excited singlet state lies at considerably higher energies.

This evidence (and observations on other dysprosium chelates) suggests that a necessary condition for the transfer of energy to the central chelated Dy^{3+} ion is that the triplet state of the molecule lie above the resonance level of the ion.

Since the chelates which exhibit line emission yield only negligible phosphorescence, it was necessary to estimate the positions of the triplet levels from measurements of the phosphorescence spectra of the corresponding gadolinium compounds. Systematic studies of a series of chelates of the lanthanides reveal a dependence of the positions of the triplet levels upon the rare earth ion.[2] The energy levels on the diagram were estimated by extrapolation of the value obtained from the observed phosphorescence of the analogous gadolinium chelate.

All compounds were dissolved in a solution of ether, 3-methylpentane, and ethanol (5 parts, 5 parts, 2 parts by volume) frozen to 77°K and irradiated with 3650 A

Hg light. Emission spectra were photographed on a Steinheil GH Spectrograph.

Preliminary studies of a variety of chelates of other rare earth ions indicate that this proposed condition for energy transfer may not be applicable to all the other rare earth ions. Further work on this problem is in progress.

[1] G. H. Dieke and Shobha Singh, J. Opt. Soc. Am. **46**, 495 (1956).
[2] R. E. Whan and G. A. Crosby (to be published).

Thermodynamic Properties of C_2*

ROBERT L. ALTMAN

Department of Mineral Technology, University of California, Berkeley, California

(Received December 11, 1959)

RECENT spectroscopic data[1,2] indicate that the $^1\Sigma_g^+$ state of C_2 is about 610 cm^{-1} below the $^3\Pi_u$ state hitherto considered the ground state.[3] Ballik and Ramsay[2] have also provisionally obtained the molecular constants of a new $^3\Sigma^-$ state whose excitation energy is somewhat higher than the $^3\Pi_u$ state. We have recomputed the thermodynamic properties of C_2 with all the spectroscopic data listed in Table I except the $^3\Sigma_u^+$. The enthalpy and free energy functions are unaffected by this omission until 3500°K. If the uncertain data of the $^3\Sigma_u^+$ state had been included in these calculations, the enthalpy at 4000°K would be greater by 0.1 kcal/mole and the free energy function by 0.01 eu.

The ground state partition function was evaluated with the method of Pennington and Kobe.[4] The electronic part of the partition function was approximated with

$$Q_e = 1 + \sum_{i=A,B,\cdots} g_i \exp(-hc/kT\nu_{00}{}^i).$$

Each state has an effective statistical weight

$$g_i = \frac{P_i B_0{}^0[1-\exp(-hc/kT\omega_0{}^0)]}{P_0 B_0{}^i[1-\exp(-hc/kT\omega_0{}^i)]},$$

where P_i and P_0 are the proper statistical weights and the other symbols have their usual significance.[5]

Gurvich and Korobov[6] originally proposed the use of this method in order to compute the high temperature thermodynamic properties of molecular oxygen. We have confirmed that this approach yields enthalpy and entropy data for oxygen almost identical to that obtained by direct summation of the partition function.[7] The results of our calculations on C_2 performed in this manner are reported in Table II.

We have compared these results at 2000 and 2500°K with other published thermodynamic tables[8,9] and note that both Pitzer[8] and Altman[9] give values different

TABLE II. Thermodynamic properties of gaseous C_2.

T deg K	C_p° cal/mole deg K	$H_T^\circ - H_0^\circ$ kcal/mole	$-(F_T^\circ - H_0^\circ)/T$ cal/mole deg K	S_T° cal/mole deg K
100	7.114	0.697	30.945	37.919
200	9.670	1.525	35.923	43.549
298.15	10.311	2.530	39.143	47.628
300	10.300	2.549	39.195	47.692
400	9.472	3.539	41.698	50.545
500	8.868	4.452	43.682	52.587
600	8.593	5.323	45.303	54.175
700	8.501	6.177	46.667	55.492
800	8.496	7.027	47.843	56.626
900	8.530	7.878	48.875	57.628
1000	8.582	8.733	49.796	58.530
1100	8.642	9.594	50.628	59.350
1200	8.706	10.462	51.387	60.105
1300	8.772	11.336	52.085	60.804
1400	8.839	12.216	52.731	61.457
1500	8.907	13.103	53.333	62.069
1600	8.975	13.998	53.898	62.646
1700	9.042	14.898	54.429	63.192
1800	9.108	15.806	54.930	63.711
1900	9.172	16.720	55.405	64.205
2000	9.234	17.640	55.857	64.677
2100	9.293	18.567	56.288	65.129
2200	9.349	19.499	56.700	65.563
2300	9.402	20.436	57.094	65.979
2400	9.451	21.379	57.473	66.381
2500	9.497	22.326	57.837	66.767
2600	9.540	23.278	58.188	67.141
2700	9.579	24.234	58.526	67.501
2800	9.614	25.194	58.853	67.851
2900	9.647	26.157	59.169	68.188
3000	9.676	27.123	59.475	68.516
3500	9.782	31.990	60.876	70.016
4000	9.836	36.897	62.102	71.327
4500	9.855	41.820	63.193	72.486
5000	9.855	46.748	64.175	73.525

TABLE I.

State	ω_e	$\omega_e x_e$	$\omega_e y_e$	B_e	α_e	γ_e	ν_{00}
$^1\Sigma_g^+$ [a]	1854.71	13.34	−0.17	1.81984	0.01765	−0.00023	0[c]
$^3\Pi_u$ [b]	1641.35	11.67	...	1.6326	0.01683	...	610[c]
$^3\Sigma_g^-$ [c]	1470.45	11.19	0.02	1.4985_2	0.01634	...	6243.5
$^1\Pi_u$ [a]	1608.35	12.07_8	−0.01	1.61634	0.0168_6	−0.00005	8268.33
$^3\Sigma_u^+$ [c]	$\Delta G \approx 1900$	...	...	~1.86	...	...	14 300[c]

[a] Reference 3.
[b] J. G. Phillips, Astrophys. J. **108**, 434 (1948).
[c] Reference 2.

TABLE III.

Temp. (°K)	2000	2500
$\Delta(H_T^\circ - H_0^\circ)$ kcal/mole	−1.36[a] −1.53[b]	−1.83[a] −1.78[b]
$\Delta -(F_T^\circ - H_0^\circ)/T$ eu	+0.53[a] +0.47[b]	+0.43[a] +0.31[b]

[a] See reference 8.
[b] See reference 9.

from those of Table II by the amounts shown in Table III. Reference 9 assumed a $^3\Pi_u$ ground state and, therefore, the free energy values would be higher than those of Table II because the $^3\Pi_u \rightarrow {}^3\Sigma_g^-$ transition[1] was not considered.

Drowart *et al.*[10] have reported heats of sublimation for diatomic carbon of 195.8 kcal/mole (2nd law) and 198.0 (3rd law) based upon Pitzer's thermodynamic data. If the data of Table II are used instead, these values are reduced to 194.2 and 196.9, respectively, in excellent agreement with Brewer *et al.*[11]

We are indebted to Professor L. Brewer for making us aware of this problem and for some valuable discussions.

* This work was supported by the Metallurgy and Materials Branch of the U. S. Atomic Energy Commission.

[1] E. A. Ballik and D. A. Ramsay, J. Chem. Phys. **31**, 1128 (1959).
[2] E. A. Ballik and D. A. Ramsay (private communication).
[3] J. G. Phillips, Astrophys. J. **107**, 389 (1948).
[4] R. E. Pennington and K. A. Kobe, J. Chem. Phys. **22**, 1442 (1954).
[5] G. Herzberg, *Spectra of Diatomic Molecules* (D. Van Nostrand Company, Inc., Princeton, New Jersey, 1950).
[6] L. V. Gurvich and V. V. Korobov, Zhur. Fiz. Khim. **30**, 2794 (1956).
[7] H. W. Woolley, J. Research Natl. Bur. Standards **40**, 163 (1948).
[8] K. S. Pitzer and E. Clementi, U. S. Atomic Energy Commission Report UCRL-6875.
[9] R. L. Altman, *Thermodynamic Properties of Propellant Combustion Products* (Rocketdyne Report 669).
[10] Drowart, Burns, DeMaria, and Inghram, J. Chem. Phys. **31**, 1131 (1959).
[11] Brewer, Hicks, and Krikorian (in preparation).

Comments and Errata

Electron Scattering from Iodine Vapor

A. ALMENNINGEN, O. BASTIANSEN, L. FERNHOLT, AND M. TRAETTEBERG

Department of Chemistry, University of Oslo, Oslo, Norway, and The Technical University of Norway, Trondheim, Norway

(Received November 19, 1959)

AN anomalous effect has been reported by I. L. Karle when 40-kv electrons are scattered from iodine vapor.[1] She found that the intensity curve was nearly uniformly shifted towards larger s values, leading to the form $\exp(-ks^2)\ \sin(rs-\phi)/(rs-\phi)$ for the molecular intensity curve. The measured phase ϕ was found to be of the order 0.3, i.e., approximately 17°.

As this effect is of considerable theoretical and practical interest for electron diffraction investigations, we found it worth while to repeat the experiment. Two sets of electron diffraction sector diagrams were taken, using the two accelerating potentials 38.70 kv and 40.884 kv. As we were primarily looking for the phase shift effect only long distance diagrams were taken. The distance between diffraction point and photographic plate was approximately 49 cm. These plates give intensity data from $s=1.25$ to $s=21$ A^{-1}. The sector used for this experiment was a modified s^3 sector. The photometer curves of 7 single plates were studied. The usual corrections were made for the effect of the photographic emulsion, for the use of plane plates, and for the accurate form of the sector. The exact positions of the maxima and minima were determined using the approximation of parabolas to the regions around the extreme values. When these measured values were compared with theoretical data no phase shift effect of the order of magnitude reported by Karle was detected. The numerical values of the average deviation between experimental and theoretical values for the maxima and minima positions was found to be about 0.02 A^{-1}, and no systematic deviation was observed.

The r values from the observed maxima and minima were calculated using first the assumption of no phase shift and afterwards applying Karle's ϕ value of 0.3. The root-mean-square deviation of the r values was in the first case found to be 0.008 A and in the second case to be 0.040 A.

For a more complete analysis of the problem least-squares calculations[2] were carried out on each of the four single intensity curves of the 40.884 kv plates, to find the following parameters: (1) normalization factor; (2) I—I distance; (3) damping factor constant; and (4) phase shift. The zero-order approximation parameters were: $r_0=2.664$ A, $k_0=0.001513$ A^2, and $\phi_0=0$. The final average values for r and k were 2.671 A and 0.00182 A^2 ($u=0.060$ A). The average standard deviations were found to be 0.0046 A and 0.00027 A^2, respectively. The ϕ values found for the four curves were +0.079, +0.057, +0.055, and +0.066 with the corresponding standard deviations 0.044, 0.048, 0.051, and 0.053. The phase shift is thus about $\frac{1}{5}$ of that observed by Karle. The effect is found to be positive in all the four plates. However, the standard deviation is of the same order of magnitude as the phase shift, and the effect is accordingly within the error of the method equal to zero.

To check if the zero-order model is too far away from the final result it was started out with r and k values that deviate still more from the "true" values. The new zero-order parameters were $r_0=2.657$ A, $k_0=$

0.00121 A², and $\phi_0=0$, and the final values obtained were essentially the same as those found in the first calculation [$r=2.670$ A, $k=0.00188$ A² ($u=0.061$ A), and $\phi=0.054$ with corresponding standard deviations 0.0069 A, 0.00029 A, and 0.063].

This work was done in order to study the phase shift effect. The intention was not to carry out precision determinations of the I—I distance or the k value. In that case intensity curves from plates taken with shorter distances should have been included to obtain intensity data out to larger s values.

The authors wish to thank Norges tekniske høgskoles Fond for financial support without which the present work could not have been accomplished.

[1] I. L. Karle, J. Chem. Phys. **23**, 1739 (1955).
[2] Bastiansen, Hedberg, and Hedberg, J. Chem. Phys. **27**, 1311 (1957).

Remarks on the Electron Scattering by Iodine

I. L. KARLE

U. S. Naval Research Laboratory, Washington 25, D. C.

(Received November 27, 1959)

THE letter entitled "Electron scattering from iodine vapor" by Almenningen *et al.*[1] presents some interesting data on the scattering of iodine vapor by electrons at 38.70 and 40.88 kv. At these voltages they report an average phase shift $\phi=+0.064$. If one accepts their average value for the standard deviation of the measured shift per experiment, their observation appears to be significant. The stated standard deviation on each of their four experiments was 0.049, and hence the standard deviation for the experiment as a whole should be 0.025. It is seen that this observed phase shift of +0.064 is approximately two and one-half standard deviations. The chance of this occurring by accident is about once in eighty times.

The previous experiments on iodine[2] were performed precisely at 39.30 and 39.52 kv (regrettably, in my previous note these were referred to as 40 kv). A phase shift of +0.3 was found. The phase shift found in this earlier experiment appears to be real since similar scattering experiments were also performed on I_2 at 31.20 kv and on O_2 and Br_2 in the range 39.1–39.7 kv which yielded normal scattering curves. In each case, the values obtained for r_0 and $\langle l^2\rangle^{\frac{1}{2}}$ reproduced the spectroscopic values.

It seems possible from the results of Almenningen *et al.* and my experiment that the iodine molecule may exhibit some fairly sharp resonance effect depending upon the accelerating voltage of the electrons. It would therefore be desirable to perform additional experiments at closely spaced intervals in the vicinity of 39.5 kv.

[1] Almenningen, Bastiansen, Fernholt, Traetteberg, and J. Chem. Phys. **32**, 616 (1960), this issue.
[2] I. L. Karle, J. Chem. Phys. **23**, 1739 (1955).

Notes

Radiant Energy Emission from Excited Harmonic Oscillators*

S. S. PENNER

Daniel and Florence Guggenheim Jet Propulsion Center, California Institute of Technology, Pasadena, California

(Received October 14, 1959)

THE total radiant energy emitted by spontaneous transitions[1] is independent, to the harmonic oscillator approximation, of the initially excited vibrational level(s) for a fixed total energy input. The preceding statement may be verified readily by the following considerations.

Let $x_n(t)$ denote the number of vibrationally excited emitters in the nth quantum state at time t. Let n^* denote the vibrational quantum number of the energy level which is excited initially. Then

$$dx_{n^*}/dt=-A_{n^*,n^*-1}x_{n^*}=-A_{1,0}n^*x_{n^*} \qquad (1)$$

where we use the relation $A_{n,n-1}=nA_{1,0}$ between the Einstein coefficients for spontaneous emission, which is applicable to the harmonic oscillator approximation. It is apparent from Eq. (1) that $x_{n^*}=N\exp(-A_{1,0}n^*t)$ if $x_{n^*}(0)=N$. Similarly,

$$dx_{n^*-1}/dt=[n^*N\exp(-A_{1,0}n^*t)-(n^*-1)x_{n^*-1}]A_{1,0}$$

or

$$x_{n^*-1}(t)=n^*N\exp[-A_{1,0}(n^*-1)t][1-\exp(-A_{1,0}t)];$$

$$x_{n^*-m}(t)=(1/m!)[n^*!/(n^*-m)!]N \cdot\exp[-A_{1,0}(n^*-m)t][1-\exp(-A_{1,0}t)]^m,$$

$$m=0, 1, \cdots, n^*-1, n^*. \qquad (2)$$

The set of relations represented by Eq. (2) constitutes a general solution for the number of emitters in any energy level between the ground level ($m=n^*$, $n^*-m=0$) and the most highly excited level ($m=0$, $n^*-m=n^*$).

The total radiant energy transfer equals the product of the number of transitions per second and the energy

per transition. To the order of approximation used in the present analysis, $\nu_{n,n-1}=\nu=$constant. Hence the total radiant energy emitted in unit time is

$$d\epsilon/dt=A_{1,0}h\nu\sum_{m=n^*-1}^{0}(n^*-m)x_{n^*-m}(t)$$

or, using Eq. (2),

$$d\epsilon/dt=A_{1,0}h\nu n^*N\exp(-A_{1,0}t). \quad (3)$$

Reference to Eq. (3) shows immediately that the rate of radiant energy emission is independent of the value of n^* for the fixed energy input $n^*Nh\nu$.

The preceding result permits ready generalization to an arbitrary initial distribution in which $x_n(0)=N_n$. These distributions relax independently in such a way that the total rate of energy output becomes

$$d\epsilon_T/dt=A_{1,0}h\nu(\sum_{n=1}^{\infty}nN_n)\exp(-A_{1,0}t)$$

$$=A_{1,0}h\nu N_T\exp(-A_{1,0}t) \quad (4)$$

where

$$N_T=\sum_{n=1}^{\infty}nN_n$$

represents the total number of quanta of energy $h\nu$ distributed among the various vibrational energy states.

* Supported by the Office of Scientific Research, U.S. Air Force, under Contract AF 18(603)-2.

[1] For a general discussion of de-excitation of harmonic oscillators, see K. E. Shuler *et al.*, J. Chem. Phys. **26**, 454 (1957); J. Phys. Chem. **61**, 849 (1957); J. Chem. Phys. **28**, 4 (1958); **29**, 366 (1958).

Common Error Made in Treating Hyperfine Effects in Electron Paramagnetic Resonance Studies of Free Radicals

HENRY ZELDES, G. T. TRAMMELL, RALPH LIVINGSTON, AND R. W. HOLMBERG

Oak Ridge National Laboratory, Oak Ridge, Tennessee

(Received October 29, 1959)

THE proper interpretation and theoretical treatment of the hyperfine effect dates back to Fermi[1] in 1930. Since this time the theory has been applied to many special cases. One application of especial interest in paramagnetic resonance studies of chemical free radicals has frequently been presented incorrectly. We have in mind the simple case of a single electron (or hole) in a completely quenched orbital (isotropic g factor) which has an axis of symmetry. We present expressions for this case and for the more specialized case of a hybridized $s-p$ orbital, and show that the angular dependence of the hyperfine splitting in the absence of s contributions is $(3\cos^2\theta+1)^{\frac{1}{2}}$. This may be contrasted with the widely quoted angular dependence of $3\cos^2\theta-1$ for pure p orbitals.

The part of the Hamiltonian representing the interaction of the electron spin $\mathbf{S}$ and the nuclear spin $\mathbf{I}$ with each other and with the external field $\mathbf{H}$ is

$$\mathcal{H}=-g_e\beta_e\mathbf{S}\cdot\mathbf{H}-g_N\beta_N\mathbf{I}\cdot\mathbf{H}-g_e\beta_e\{(8\pi/3)\mathbf{S}\,|\,\Psi(0)\,|^2$$
$$-\langle(\mathbf{S}/r^3)-[(3\mathbf{S}\cdot\mathbf{rr})/r^5]\rangle\}g_N\beta_N\cdot\mathbf{I}, \quad (1)$$

where the angular bracket represents the expected value for the state involved. Expressions for the eigenvalues of $\mathcal{H}$ may be obtained in the conventional manner; however, simpler expressions result in the practically important case when the first term in $\mathcal{H}$ is large compared to the following ones (strong field case). $\mathbf{S}\cdot\mathbf{H}$ is then an (approximate) good quantum number and the energy levels of Eq. (1) will be those of

$$\mathcal{H}\doteq-g_e\beta_eMH-(\mathbf{H}+\mathbf{h})\cdot g_N\beta_N\mathbf{I}, \quad (1')$$

where $M(=\pm\frac{1}{2})$ is the component of the electron spin along $\mathbf{H}$. The magnetic field at the nucleus due to the electron is given by

$$\mathbf{h}=g_e\beta_eM\{(8\pi/3)\,|\,\Psi(0)\,|^2\tau_H+\tfrac{1}{2}\langle(3\mu^2-1)/r^3\rangle$$
$$\cdot[(3\cos^2\theta-1)\tau_H-3\cos\theta\sin\theta\tau_\perp]\}, \quad (2)$$

where τ_H is a unit vector in the direction of $\mathbf{H}$, and $\tau_\perp$ is a unit vector perpendicular to $\mathbf{H}$ in the $(\mathbf{H}, Z)$ plane, μ is the cosine of the angle between the electron radius vector and the symmetry (Z) axis, and θ is the angle between the applied field and the axis of symmetry. Usually $|\,\mathbf{h}\,|\gg H$ (if not there will be satellite hyperfine lines[2]), and when the electron flips its spin the nucleus will not. The separations between hyperfine lines are then $2\,|\,\mathbf{h}\,|\,g_N\beta_N$. From Eq. (2)

$$h=\tfrac{1}{2}g_e\beta_e\{[(8\pi/3)\,|\,\Psi(0)\,|^2+\tfrac{1}{2}\langle(3\mu^2-1)/r^3\rangle$$
$$\cdot(3\cos^2\theta-1)]^2+\tfrac{9}{4}\langle(3\mu^2-1)/r^3\rangle^2\cos^2\theta\sin^2\theta\}^{\frac{1}{2}}. \quad (3)$$

If the contact term $(\sim|\,\Psi(0)\,|^2)$ in Eqs. (2) or (3) is large compared to the remaining terms then the component of $\mathbf{h}$ in the direction of $\tau_\perp$ may be neglected and Eq. (3) becomes

$$h\doteq\tfrac{1}{2}g_e\beta_e[(8\pi/3)\,|\,\Psi(0)\,|^2+\tfrac{1}{2}\langle(3\mu^2-1)/r^3\rangle(3\cos^2\theta-1)] \quad (3')$$

On the other hand, if the contact term is absent (no s admixture), Eq. (3) becomes

$$h=\tfrac{1}{4}g_e\beta_e\langle(3\mu^2-1)/r^3\rangle[1+3\cos^2\theta]^{\frac{1}{2}}. \quad (3'')$$

The frequently quoted error has amounted to using Eq. (3′) when it is completely inapplicable; for example, the angular dependence for a pure p orbital has been given as $(3\cos^2\theta-1)$ when it should be [Eq. (3″)] $(3\cos^2\theta+1)^{\frac{1}{2}}$. As an application, for an $s-p$

hybrid Eq. (3) becomes

$$h=\tfrac{1}{2}g_e\beta_e\{[a_s^2(8\pi/3)\,|\,\Psi_s(0)\,|^2 + \tfrac{2}{5}a_p^2\langle 1/r^3\rangle_p(3\cos^2\theta-1)]^2 + \tfrac{36}{25}a_p^4\langle 1/r^3\rangle_p^2\cos^2\theta\sin^2\theta\}^{\frac{1}{2}}, \quad (4)$$

where a_s^2 and a_p^2 are the probabilities of having the electron on the atom in the s and p states, respectively, and where $\langle\mu^2\rangle_p=\frac{3}{5}$ has been used.

[1] E. Fermi, Z. Physik. **60**, 320 (1930).
[2] Trammell, Zeldes, and Livingston, Phys. Rev. **110**, 630 (1958).

Semiempirical Calculation on the Electronic Structure of the Nitrogen-Containing Heterocyclic Molecules. III. Lower Triplet Levels of Pyrazine

TOSINOBU ANNO, *Chemical Laboratory, General Education Department, Kyushu University, Ootsubo-machi, Fukuoka, Japan*

AND

AKIRA SADÔ, *Department of Chemistry, Faculty of Science, Kyushu University, Hakozaki, Fukuoka, Japan*

(Received July 16, 1959)

IN Part I[1] of this series a semiempirical theory for the calculation of the energy levels of the nitrogen heterocycles was proposed, taking the nonbonding electrons at the nitrogen atoms explicitly into account. Preliminary application to the singlet levels of the pyrazine molecule given in Part I was elaborated to include the doubly excited configurations into a CI calculation in Part II.[2] Recent work on the phosphorescence spectrum of pyrazine in EPA rigid solvent at 77°K and the $T\leftarrow S$ absorption spectrum at 293°K in isopentane solution by Goodman and Kasha[3] has prompted us to calculate the triplet levels of this molecule. The results will be briefly described in the following.

Integrals over AO's and the form of MO's are the same as those used in the calculation of the singlet levels.[1,2] Although doubly excited as well as singly excited configurations were considered in this calculation, some amount of labor to solve secular equations of higher degrees was avoided in the same manner as used in Part II.[2] The hybridization parameter λ of the nitrogen nonbonding AO[4] was assumed to be 0.339 (10.3% s character) which was determined so that the calculated value of the lowest $^1B_{1u}$, $^1B_{3g}\leftarrow{}^1A_g$ transition energies agree with the observed value. The calculated energy levels as well as the observed are given in Table I. In this table the singlet levels are also included.

Experimentally, a triplet level of this molecule has been located at 25 991 cm^{-1} (3.22 ev) by Goodman and Kasha[3] from the low-temperature emission spectrum. The experimental data for the other triplet levels are not available. From the observed blue shift upon conjugative substitution Goodman and Kasha have concluded that the 3.22-ev band corresponds to a $^3B_{1u}$ $(n-\pi)\rightarrow{}^1A_g$ intercombination transition.[5] The occurrence of the totally symmetrical angular distortion frequency as the dominant vibrational frequency in the spectrum is taken as an evidence supporting the assignment of this band to an $n-\pi$ transition by these authors. Mr. R. Shimada,[6] Faculty of Science of this University, has also studied the phosphorescence spectrum of this molecule and has confirmed that the transition is of an $n-\pi$ nature from the solvent effect. Since the emitting level is usually the lowest level of a given multiplicity,[7] the aforementioned facts suggest that the lowest triplet level of pyrazine is an $n-\pi$ level. As can be seen in Table I the theoretical calculation is consistent with this conclusion and predicts two triplet $n-\pi$ levels of accidental degeneracy as the lowest triplet levels, although the lowest triplet $\pi-\pi$ level is calculated to lie only a little above these levels. However, we believe that the exact value of the lowest triplet $\pi-\pi$ level is a little higher than 3.1 ev. As can be seen in Table I, the lowest singlet $\pi-\pi$ level ($^1B_{3u}$) which corresponds to the lowest triplet $\pi-\pi$ level ($^3B_{3u}$) is calculated to be 0.2 ev lower than the observed. This discrepancy is probably due to slightly inadequate values of the core integrals. The inadequateness of the core integrals affects the lowest singlet-triplet $\pi-\pi(^3B_{3u}\leftrightarrow{}^1A_g)$ transition energy in exactly the same manner as it affects the lowest singlet-singlet $\pi-\pi(^1B_{3u}\leftrightarrow{}^1A_g)$ transition energy, if we neglect CI. Singlet-triplet separation, on the other hand, is nearly insensitive (completely insensitive, if we neglect CI) to the core integral. Therefore, if we use the calculated

TABLE I. Calculated and observed energy levels of pyrazine.

	Type of transition from the ground state	Energy above the ground state (ev) Calc[a]	Obs
^1A_g	...	0.00	0.0
$^1B_{1u}$, $^1B_{3g}$	$n-\pi$	3.81	3.8[b]
$^1B_{3u}$	$\pi-\pi$	4.63	4.8[c]
$^1B_{2u}$	$\pi-\pi$	5.52	...
$^3B_{1u}$, $^3B_{3g}$	$n-\pi$	3.09$_{05}$[d]	3.22[e]
$^3B_{3u}$	$\pi-\pi$	3.09$_{49}$	...
$^3B_{2u}$	$\pi-\pi$	4.12	...

[a] Calculated values for singlet π-π levels listed in Table I of reference 2 under the heading "λ=0.339" are found to be slightly in error and are corrected here.
[b] Ito, Shimada, Kuraishi, and Mizushima, J. Chem. Phys. **26**, 1508 (1957).
[c] F. Halverson and R. C. Hirt, J. Chem. Phys. **17**, 1165 (1949).
[d] Calculated for species $^3B_{3g}$. Although the secular equation of CI calculation for $^3B_{1u}$ was not solved we can say that the lowest $^3B_{1u}$ and $^3B_{3g}$ levels are essentially in accidental degeneracy with each other, because values of corresponding configurational energies and interaction matrix elements are practically the same. The separation between the lowest $^3B_{1u}$ and $^3B_{3g}$ levels is calculated to be 0.0011 ev ($^3B_{3g}$ is higher than $^3B_{1u}$) if we neglect CI.
[e] See reference 3.

singlet-triplet separation of 1.5 ev (=4.6−3.1) and the observed energy of the lowest excited singlet $\pi-\pi$ level (4.8 ev) we can obtain 3.3 ev as the energy of the lowest $^3B_{3u}(\pi-\pi)$ level. As to the $^3B_{1u}$, $^3B_{3g}(n-\pi)$ energies they are not changed by the above treatment since the corresponding calculated singlet levels, $^1B_{1u}$ and $^1B_{3g}$, fit (rather, are fitted) to the observed value. Thus, we can conclude that the lowest triplet level is of an $n-\pi$ nature from the theoretical side also. Moreover, the calculated value of $T\rightarrow S$ transition energy is in close agreement with the observed as can be seen in Table I.

The authors express their sincere thanks to Professor S. Imanishi for his encouragement throughout this work. They are also indebted to Dr. Y. Kanda and Mr. R. Shimada for valuable discussion.

[1] T. Anno, J. Chem. Phys. **29**, 1161 (1958).
[2] T. Anno and A. Sadô, J. Chem. Phys. **29**, 1170 (1958).
[3] L. Goodman and M. Kasha, J. Mol. Spectroscopy **2**, 58 (1958).
[4] As to the definition of λ see Eq. (39) of reference 1.
[5] Symmetry notations are changed from those used by Goodman and Kasha in order to be consistent with those used in our previous papers. As to our notations see reference 1.
[6] R. Shimada (unpublished results).
[7] M. Kasha, Discussions Faraday Soc. **9**, 14 (1950).

Microwave Dielectric Measurements in a Liquid Crystal That Shows Polymesomorphism*

E. F. Carr
Physics Department, University of Maine, Orono, Maine

(Received October 8, 1959)

ETHYL anisal *p*-aminocinnamate is an example of a substance that exhibits more than one liquid crystal phase. Using optical methods Vorlander[1] observed the following scheme:

$$\text{liquid} \overset{139^\circ}{\rightleftarrows} \text{liq. cryst. I} \overset{118^\circ}{\rightleftarrows} \text{liq. cryst. II} \overset{91^\circ}{\rightleftarrows} \text{liq. cryst. III} \overset{83^\circ}{\rightleftarrows} \text{cryst.}$$

$$\text{cryst. II} \overset{108^\circ\text{C}}{\leftarrow}$$

Figure 1 shows the dielectric loss at a wavelength of 1.2 cm as a function of temperature with the sample in the presence of an external magnetic field of 4500 gauss parallel and perpendicular to the polarized microwave beam. The measurements for increasing temperature indicate a melting point in the neighborhood of 108°C which is consistent with Vorlander's observations. The alignment obtained in liquid crystal phase I for increasing temperature is comparable to that obtained for decreasing temperature which is consistent with results[2,3] on other liquid crystals of the nematic type. A 90-degree rotation of the external magnetic field in liquid crystal phase II which is a smectic type will produce a change in alignment in the direction of the field but it will be less than that obtained on cooling in the presence of a field. This is not consistent with the results[4] obtained for ethyl *p*-axoxybenzoate which is also a smectic type, or the results by Lippmann and Webber.[5]

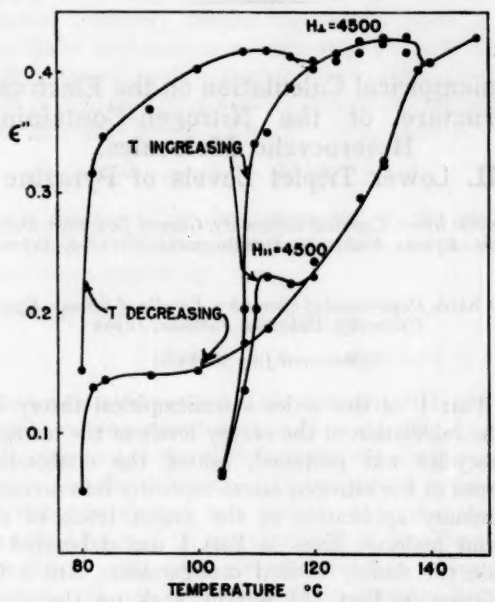

FIG. 1. The temperature-dependence of the dielectric loss at a wavelength of 1.2 cm and in the presence of an external magnetic field of 4500 gauss parallel and perpendicular to the microwave electric field for ethyl anisal *p*-aminocinnamate.

In order to obtain the curves shown in Fig. 1, it was necessary to melt the powdered sample in the cell, then cool it to its solid phase before proceeding. New samples that were melted from a powder were unaffected by the presence of a magnetic field until the temperature had fallen below 125°C. Similarly, used samples that were removed from the cell and powdered failed to respond to the field much above 125°C. If a sample, solidified in the cell and not repowdered, was heated to 180°C it would be unaffected by a magnetic field until the temperature had fallen a few degrees below 139°C. When heated to 200°C the field became effective at about 131°C. After the samples were solidified and reheated the field was effective up to about 139°C. This effect was observed by rotating the magnetic field and also by observing a decrease in absorption when the molecules in the cell started to align parallel to the applied field. A temperature range of only a few degrees is required

for an alignment to take place such that the absorption is comparable to that shown in Fig. 1. This seems to indicate that some sort of order exists throughout the liquid crystal range and into the normal liquid phase that can be partially broken up by heating to high temperatures or powdering the sample before melting. If this effect is due to the ordering of molecules in small groups the results indicate that the groups are anisotropic. The inability of the field to cause an alignment below 139°C has been observed a few times after melting a sample which had been solidified in the cell, but this was accompanied by an appreciable effect on the alignment due to the field below 108°C. This indicates that if an ordering does exist then it may be associated with some behavior in the crystal II phase.

Using optical techniques Bernal and Crowfoot[6] have suggested that liquid crystal phase I may have two different textures. What they have suggested may be responsible for the effects observed in this work. Some work[7] has been done on this compound using nuclear resonance techniques, and plans are now being made to continue this investigation.

There seems to be some indication that if a magnetic field is present when a sample is melted from a powder that the temperature at which it solidifies upon cooling will probably be lower than if it is first melted in the absence of a field, but this effect still needs further study before it can be established.

The author wishes to express his appreciation to Professor Jonathan Biscoe for his interest and encouragement during the course of this research and to the members of the Chemistry Department who have aided in the preparation of the samples.

* Supported in part by the Research Corporation and the Coe Fund, University of Maine.

[1] Vorlander, Trans. Faraday Soc. **29**, 913 (1933).
[2] Carr and Spence, J. Chem. Phys. **22**, 1481 (1954).
[3] Carr, J. Chem. Phys. **26**, 420 (1957).
[4] Carr, J. Chem. Phys. **30**, 600 (1959).
[5] H. Lippmann and K. H. Webber, Ann. Phys. **20**, 265 (1957).
[6] Bernal and Crowfoot, Trans. Faraday Soc. **29**, 1032 (1933).
[7] R. Ewing, thesis, Michigan State University (1954).

Visible Emission of Nickel-Activated CaS

M. AVINOR*

Philips Research Laboratories, N. V. Philips Gloeilampenfabrieken, Eindhoven, Netherlands

(Received September 21, 1959)

ADDITION of nickel to sulphide phosphors is known to shorten the phosphorescence duration

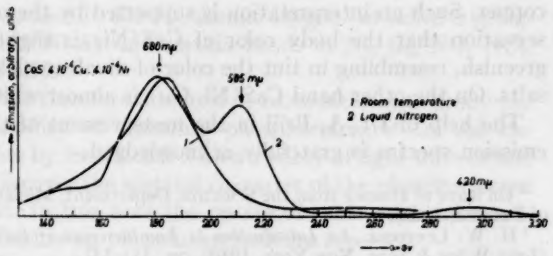

FIG. 1. Emission spectrum of CaS activated by copper and nickel.

at low concentrations and to quench it completely at higher concentrations.[1] However, there exists one claim in the literature to red visible emission due to nickel activation in CaS.[2] Because of its theoretical interest this work was repeated with improved technique. We found, however, that nickel-activated CaS (4.10^{-4} atom/mole) showed only a very weak greenish-yellow fluorescence and no phosphorescence or red emission. As there was always a possibility of unintentional contamination, especially in the earlier work, we tried to introduce simultaneously a second activator. Copper was the most likely suspect, and indeed we found that by activating CaS with nickel and copper together a red emission was observed at room temperature (Fig. 1). At first we thought that the red band was also due to copper and that the nickel served only to quench the well-known blue-green band of copper[3] selectively. This did not turn out to be the case. The emission of copper activated CaS (Fig. 2) is very weak in the red part of the spectrum. It is interesting to note that the red emission of CaS (Cu, Ni) shows medium duration phosphorescence comparable in its decay to CaS(Cu). The infrared emission claimed for nickel activated SrS[4] may also be due to double activation by nickel and copper.

The facts reported in the foregoing indicate that the luminescent centers of the red emission probably consist of associates of nickel and copper but further work is needed for conclusive proof. An alternative explanation might be that the red emission is due to trivalent nickel centers and that the incorporation of the nickel in the trivalent state is facilitated by the presence of

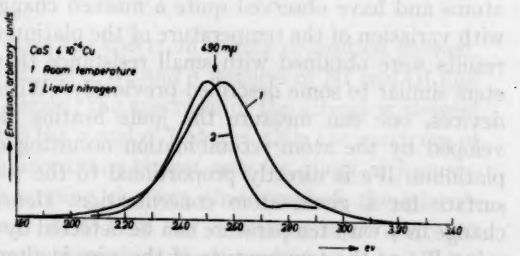

FIG. 2. Emission spectrum of CaS activated by copper.

copper. Such an interpretation is supported by the observation that the body color of CaS(Ni) is slightly greenish, resembling in tint the color of divalent nickel salts. On the other hand CaS(Ni, Gu) is almost white.

The help of Dr. A. Brill in the measurement of the emission spectra is gratefully acknowledged.

* On leave of absence from the Scientific Department, Ministry of Defense, Israel.

[1] H. W. Leverenz, *An Introduction to Luminescence of Solids* (John Wiley & Sons, New York, 1950), pp. 333–337.

[2] Lenard, Schmidt, and Tomaschek, *Handbuch der Experimental Physik* (Springer-Verlag, Leipzig, 1928), Vol. 23, p. 331.

[3] Reference 2, p. 332.

[4] Reference 2, p. 363.

Variation with Temperature of the Recombination of Oxygen Atoms on a Platinum Surface

GEORGE C. FRYBURG AND HELEN M. PETRUS

Lewis Research Center, National Aeronautics and Space Administration, Cleveland, Ohio

(Received October 29, 1959)

THE development of vehicles capable of flight at high Mach speeds and at extreme altitudes has restimulated interest in the "catalytic efficiency" of metals for recombination of atomic species of hydrogen, oxygen, and nitrogen. Most of the work to date has been of an exploratory nature, comparing the relative efficiencies of the different metals.

It is also of paramount importance to know whether the "catalytic efficiency," or more properly, the recombination coefficient γ varies with the temperature of the surface. It is usually tacitly assumed that γ is independent of temperature.[1,2] There is experimental support for this in the case of H atoms: Tollefson and LeRoy[2] have shown that γ for H atoms on Pt is constant between 125 and 450°C; more recently, Fox, Smith, and Smith[4] obtained a similar result for H atoms on Pt and W between 150 and 800°C, though they found a poisoning effect below 150°C.

We have had experience with platinum devices in O atoms and have observed quite a marked change in γ with variation of the temperature of the platinum. The results were obtained with small resistance thermometers similar to some described previously.[5] With these devices, one can measure the joule heating *Wo* developed by the atom recombination occurring on the platinum. *Wo* is directly proportional to the γ of the surface for a given atom concentration. Hence any change in γ with temperature can be detected by measuring *Wo* as the temperature of the wire is altered by electrical heating.

Our measurements indicate that there is a high- and a low-temperature region in which γ is constant, though different, separated by an unstable region. Some of our measurements in the high-temperature region were reported previously[5] and illustrate the consistency of *Wo* in this region. This region extends from 750°C upward. The lower region extends from about 500 down to 150°C. This region is characterized by sluggish behavior, dependence on past history, and poor reproducibility. The experimental values for *Wo* are scattered around a value 0.4 of that for the upper region which indicates that γ is roughly 0.4 of the γ for the upper region. The region between 500 and 750°C is an unstable region. If the platinum reaches a temperature of 500°C, it continues to increase in temperature more and more rapidly until it suddenly lights up well above 750°C. If the temperature is lowered below 750°C, the platinum decreases in temperature until it finally reaches some equilibrium value below 500°C. These results were independent of whether the oxygen was wet or dry.

The results are best explained by assuming that the higher value of γ is characteristic of a Pt surface and that the lower value is characteristic of an oxide surface. The evidence for this is indirect but convincing:

1. As evidence that a platinum surface is not covered with oxide at high temperature, we have shown that a platinum resistance thermometer heated at temperatures above 900°C in a stream of oxygen (pressure of 0.5 mm) remains clean and bright indefinitely while a visible oxide deposit accumulates on the wall of the enclosing tube.[5] Also, we have shown that the rate of oxidation in normal oxygen is directly proportional to the pressure of oxygen.[6] In addition, the literature[7] indicates that the dissociation temperature of both oxides of platinum, $PtO_{(s)}$ and $PtO_{2(s)}$, is 750°C. Under a pressure of 0.5 mm of oxygen, dissociation would be expected to occur at a much lower temperature. We have shown recently from the electron diffraction pattern that the oxide deposit, upon heating to 450°C in a high vacuum, dissociates leaving a residue of metallic platinum.

2. We have demonstrated previously[5] that platinum is oxidized more readily in "activated oxygen" than in normal oxygen, and that the enhanced oxidation occurs with little or no activation energy.[6] Consequently, it appears plausible that even for platinum, a very thin oxide layer can be formed on the metal at a fairly rapid rate (in an hour or less) at even moderate temperatures (150–500°C) in "activated oxygen."

3. As evidence that O atoms recombine on the oxide, we have observed that the oxide deposits that are formed by the O atoms are sensibly heated by the atoms indicating a fairly high γ. Also, we have shown that the oxide deposit causes a gradual decrease in the number of O atoms indicated by a platinum device even though the output of the discharge tube is constant.[5]

It is uncertain whether the low temperature region is characteristic of a PtO_2 or a PtO surface. It is fairly certain that PtO_2 is formed in normal oxygen.[6] We have some evidence that PtO is formed in "activated oxygen."[8] Also, we find that heating and cooling a platinum device in normal oxygen gives a surface that is very sluggish and unresponsive. However, heating and cooling in the presence of O atoms results in a responsive, active surface. This could be explained by assuming that the active surface characteristic of the low temperature region is a PtO surface and that PtO_2 acts as a poison for this.

Regardless of this, the important point is to emphasize the variability of the surface with temperature. If a Pt surface can oxidize in "activated oxygen," it seems reasonable to assume that other metals would be readily covered with a thin film of oxide. Grey and Darby[9] have found evidence for this with several metals, and Greaves and Linnett[10] explain their results on this assumption. As oxides are often subject to variable valences, phase changes, dissociation, volatilization, etc., upon heating, it would seem reasonable to predict that the recombination coefficient for O atoms on most metals would in general not be constant but would be temperature dependent.

[1] K. F. Bonhoeffer, Z. Physik. Chem. **113**, 199 (1924).
[2] Katz, Kistiakowsky, and Steiner, J. Am. Chem. Soc. **71**, 2258 (1949).
[3] E. L. Tollefson and D. J. LeRoy, J. Chem. Phys. **16**, 1057 (1948).
[4] Fox, Smith, and Smith, Proc. Phys. Soc. (London) **73**, 533 (1959).
[5] G. C. Fryburg, J. Chem. Phys. **24**, 175 (1956).
[6] To be published.
[7] L. Brewer, Chem. Revs. **52**, 1 (1953).
[8] Electron diffraction pattern is similar to that reported by Moore and Pauling (J. Am. Chem. Soc. **63**, 1392 (1941)) for PtO. However, this pattern has been questioned by Galloni and Busch [J. Chem. Phys. **20**, 198 (1952)].
[9] T. J. Gray and P. W. Darby, J. Phys. Chem. **70**, 209 (1956).
[10] J. C. Greaves and J. W. Linnett, Trans. Faraday Soc. **54**, 1323 (1958).

Phosphorescence of Nitrogen and Nitrogen-Argon Deposited Films at 4.2°K*

H. P. Broida and R. W. Nicholls†
National Bureau of Standards, Washington, D. C.

(Received September 15, 1959)

THE luminescence of nitrogen and nitrogen-argon films deposited from microwave discharges through the gases upon refrigerated surfaces at 1.3–20.6°K have been well investigated spectroscopically and otherwise.[1–5] The dominant spectral characteristics are lines of atomic nitrogen (so-called α group near 5230 A and δ group near 10 475 A), atomic oxygen (so-called β group near 5600 A) and certain bands of N_2, O_2, NO, NO_2, and NH.[1]

It is therefore a matter of some interest to study the possibility of inducing phosphorescence[6] in the deposits by irradiation with a variety of light sources and to discover the spectral character of the phosphorescent light. In this note the results of some exploratory experiments on phosphorescence are reported.

Four light sources: an intense medium pressure mercury arc lamp, a low-pressure mercury arc lamp, a 100-w projection lamp, and an iron arc were used separately and in conjunction with a number of filters (transmitting ir, ir and visible, and uv, respectively) in several experiments to irradiate nitrogen and nitrogen-argon films (0.1 to 1 mm thick) deposited upon a copper cone at 4.2°K. The familiar green deposition glow and afterglow were observed visually and allowed to decay. The light sources with and without filters were used separately to irradiate the films in the ultraviolet, visible, and infrared for periods from 1–60 sec. In all cases immediate enhancement of the green glow was observed, even at excitation wavelengths longer than 7500 A. Longer wavelengths were less effective in exciting the phosphorescence, and the low-pressure lamp with uv filter (mainly 2537 A irradiation) gave bright phosphorescence. It is therefore probable that the phosphorescence is not due to a direct heating of the film surface although an internal conversion of the absorbed energy into lattice vibrations cannot be ruled out. The phosphorescence generally appears to decay at about the same rate as the deposition afterglow.[2] However, in two out of about 100 times, the intensity remained nearly constant for about one minute. In many cases the phosphorescence appeared visually to be blue immediately after irradiation.

A series of spectroscopic observations were also made upon the phosphorescence produced in the films by 15- and 30-sec exposures to filtered and unfiltered Hg light. Spectra were also recorded of the deposition luminosity and during the afterglow, for comparison. A Perkin-Elmer $f/0.625$ grating instrument with Kodak 103a F(3) 16-mm film was used at dispersion of about 300 A/mm. Exposure times varied between 10 sec and 2 min. Exposures of longer than 30 sec were cumulatively built up in 30-sec intervals between each of which a re-illumination by mercury was made for 15 or 30 sec.

In all cases the spectrum during deposition showed, as expected, the α, α', and β features of NI and OI and of the B bands[1]; the spectrum of the afterglow showed as expected the α and α' features while the spectrum of the phosphorescence *showed only the α and α' features.* Although nothing else was photographed, the relative blackenings show that the α feature is at least 250 times more intense than any line which may be hidden in the emulsion grain.

Thus it would appear that the phosphorescence is a restimulation of the afterglow conditions under which N atoms emit α and α'. It is possible that the emission is a result of the recombination energy of two N atoms causing excitation of a third atom. Or it is possible that the radiation causes a long-lived ^2D atom to move into a radiating site.

In summary, therefore, light over the wavelength range 2000 A to greater than 10 000 A produces a phosphorescence in atomic nitrogen-molecular nitrogen and atomic nitrogen-argon deposits and there is spectroscopic evidence which shows that the phosphorescence is a restimulation of the familiar afterglow.

* This research was performed under the National Bureau of Standards Free Radicals Research Program, supported by the Department of the Army.

† On leave of absence from the University of Western Ontario, London, Canada.

[1] M. Peyron and H. Broida, J. Chem. Phys. **30**, 139 (1959).
[2] Peyron, Hörl, Brown, and Broida, J. Chem. Phys. **30**, 1304 (1959).
[3] Foner, Jen, Cochran, and Bowers, J. Chem. Phys. **28**, 351 (1958).
[4] B. Fontana, J. Appl. Phys. **29**, 1668 (1958).
[5] C. Herzfeld and H. Broida, Phys. Rev. **101**, 606 (1956).
[6] E. J. Bowen, *The Chemical Aspects of Light* (Oxford University Press, New York, 1949), second edition, Chap. 5.

Concentration Dependence of the Polarization and Relaxation Time of Al^{27} Nuclei in Ruby*

R. D. Spence and J. A. Cowen
Michigan State University, East Lansing, Michigan

(Received August 19, 1959)

RECENTLY the present authors[1] and others[2] have reported polarization of the Al^{27} nucleus in ruby containing 0.1% chromium. The method employed is that suggested by Abragam and Proctor[3] who consider a system containing weakly coupled nuclei and electrons in which the nuclear spin-lattice relaxation time is much greater than the electronic spin-lattice relaxation time. In such a system mutual spin flips may take place inducing either $\Delta M_I=+1$ or $\Delta M_I=-1$ transitions if the frequency of the microwave energy driving the paramagnetic resonance is the sum or difference of the electronic and nuclear resonance frequencies. If the transition $\Delta M_I=+1$ occurs the population of the nuclear levels changes so as to produce an enhanced absorption signal while if $\Delta M_I=-1$ an emission signal is observed.

In our original experiment we noted that the polarization built up and decayed with a rather long characteristic time. In the present note we discuss the dependence of the polarization time and enhancement on concentration.

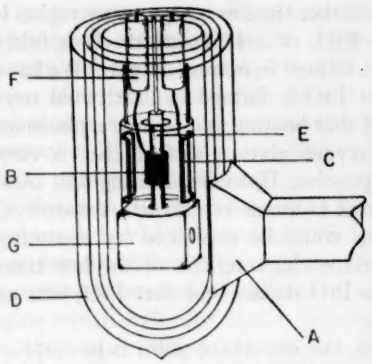

FIG. 1. The Experimental Apparatus: (A) microwave horn; (B) receiver coil; (C) transmitter coil; (D) Dewar; (E) ruby; (F) transmission lines; (G) microwave cavity.

The experiments were performed on well oriented ruby rods placed so that one end dips into a microwave cavity while the other is surrounded by the coil of a nuclear resonance spectrometer. The system is placed in an unsilvered glass helium Dewar with the temperature maintained at 4.2°K while the cavity is excited with microwaves from a horn placed outside the Dewar. (Fig. 1) The amount of polarization and the relaxation time are strongly angle dependent so that all of the data were taken with the c axis making an angle of 30° with the external magnetic field. This orientation gave maximum polarization and a large relaxation time. The return to equilibrium of the system after the microwaves were turned off occurred with the same time constant from the enhanced or the inverted state and the effect of the rf magnetic field was found to be slight.

The data were taken in samples containing 0.01%, 0.1%, and 0.25% chromium. In the 0.01% and 0.1% samples the enhancement was approximately 30 while in the 0.25% sample the enhancement was very slight. The relaxation time is 26 sec in the 0.01%, 2.6 sec in the 0.1%, and much less than one sec in the 0.25% sample.

An auxiliary experiment performed using the pulsed free induction apparatus in conjunction with the microwave system gave essentially the same enhancement and relaxation time as these steady state experiments using a modulated magnetic field; therefore it seems clear that the polarization does not depend on the incremental polarization achieved each time this system sweeps through resonance.

It should be noted that in addition to this relaxation time there exists another characteristic time for the nuclei in the ruby system which governs the redistribution of the population between adjacent levels. This may be measured by observing the return to equilibrium of a particular set of levels following a change in the rf power sampling this transition or following the excitation of a neighboring transition. This is much shorter than the relaxation time of the polarization.

We would like to thank Dr. C. Kikuchi and Dr. John Lambe of the University of Michigan Willow Run Laboratories for furnishing the samples.

* Supported by a grant from the National Science Foundation and by the Air Force Office of Scientific Research under Contract AF49(638)-613.

[1] Cowen, Schafer, and Spence, Phys. Rev. Letters 3, 13 (1959).
[2] Abraham, McCausland, and Robinson, Phys. Rev. Letters 2, 449 (1959).
[3] Abragam and Proctor, Compt. rend. 246, 2253 (1958).

On the Electron Spin Resonance Spectra of Hydrocarbon Radicals

PETER G. LYKOS

Solid State Science Division, Argonne National Laboratory, Lemont, Illinois, and Department of Chemistry,† Illinois Institute of Technology, Chicago, Illinois

(Received September 11, 1959)

RECENTLY, A. D. McLachlan[1] applied a crude form of valence-bond theory to the odd-electron model system consisting of a methyl group bonded to a carbon atom in an $sp^2\pi$ valence state. The odd electron was presumed to reside in the pi atomic orbital and the effect of its uncompensated spin on the other electrons was assessed by a perturbation-type treatment in which the exchange integrals arising from the mixing in of structures corresponding to the odd electron being on the methyl carbon and on the methyl protons were treated as perturbations. Thus, although the total spin density in each bond remains zero, a spin polarization of the bond is induced such that there is a finite spin density at the methyl protons of the same sign as that at the trivalent carbon. Extending McConnell's suggestion,[2] it was assumed that the hyperfine splitting constant for a methyl proton is directly proportional to the spin density at the trivalent carbon. The corresponding proportionality constant was then calculated using the hyperfine splitting due to the Fermi interaction for a free hydrogen atom and using bond energies to estimate the pertinent exchange integrals. It was also assumed in this treatment that the methyl group rotates about the carbon-to-carbon sigma bond with sufficient angular velocity that the effect of the three methyl protons is an average one.

Smaller and Matheson[3] of this laboratory obtained the electron spin resonance spectra at 77°K of a number of hydrocarbon samples irradiated at 77°K with Co^{60} γ rays. Among these were cyclohexane and cyclopentane where it is not unreasonable to expect to find cyclohexyl and cyclopentyl radicals, respectively. The result obtained with McLachlan's model is not applicable here, however, since the cyclic structure precludes the possibility of free rotation of the methylene protons about the carbon-to-carbon sigma bond.

We have extended McLachlan's treatment to the model system of two nonrotating methylene groups sigma-bonded to a carbon atom in a $sp^2\pi$ valence state. We included wave functions corresponding to the valence-bond structures depicted in Fig. 1 and otherwise paralleled McLachlan's approach even unto the same values for the basic integrals. However, where McLachlan finds an average value of $J(tp)$ as $\frac{1}{2}J_0$ we instead assume our model to have C_{2v} symmetry and equate $J(tp)$ to $\frac{3}{4}J_0$. Also, we find the expression for the expectation value of the spin density at a methylene proton for the ground state wave function for the perturbed system to be the same in form as for McLachlan's model,‡ namely, $\rho_H = A(1-\frac{1}{2}A)/\langle 0 \mid 0 \rangle$ where $A = \frac{1}{2}J(tp)/J(th)$. Substitution of the numerical values for the pertinent quantities yields $\rho_H = 0.052$ for McLachlan's model system and $\rho_H = 0.076$ for our model system. The corresponding hyperfine splitting constants become 26 and 38 gauss, respectively.

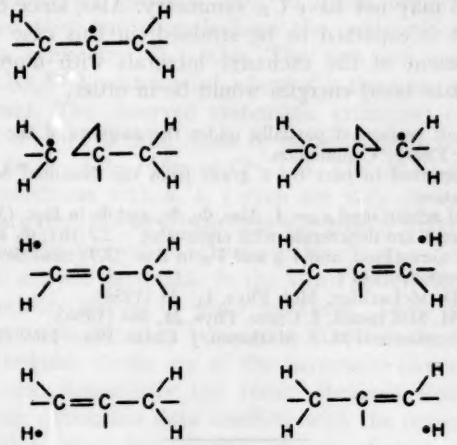

FIG. 1. Valence-bond structures included in the perturbation treatment.

If the bonds involving the odd carbon atom and the adjacent methylene groups in cyclopentyl and in cyclohexyl are not strained and otherwise correspond to our model system, then they should have the same spectrum. The four equivalent protons should split the electron spin resonance line into five components with spacing 38 gauss and relative intensities 1:4:6:4:1. The fifth proton which is bonded directly to the odd carbon atom should further split each of these five lines into a doublet with a spacing of about 25 gauss.[1]

For cyclohexyl only the six most intense lines are actually observed and two of these are only partially resolved.[3] Assuming the assignment given here is correct the corresponding hyperfine splitting constants inferred from the observed spectrum given by Smaller and Matheson are about 41 and 26 gauss, respectively,

in fairly good accord with the values suggested in the foregoing.

Eight of the expected ten lines appear very clearly in the observed spectrum for cyclopentyl.[3] Again assuming the foregoing assignment, the corresponding hyperfine splitting constants are found to be 45 and 24 gauss, respectively. The agreement here is not as good. Cyclopentyl may not have C_{2v} symmetry. Also, since cyclopentyl is expected to be strained, in this case a reassessment of the exchange integrals with more appropriate bond energies would be in order.

* Work performed partially under the auspices of the U. S. Atomic Energy Commission.

† Supported in part by a grant from the National Science Foundation.

‡ McLachlan used $\rho_H = A$. Also, Φ_2, Φ_3, and Φ_4 in Eqs. (3.7) in reference 1 are degenerate with eigenvalue $-2J$(th); Φ_2 and Φ_4 are not normalized, and V_{03} and V_{04} in Eqs. (3.9) need new constant coefficients of $\frac{1}{2}$.

[1] A. D. McLachlan, Mol. Phys. **1**, 33 (1958).
[2] H. M. McConnell, J. Chem. Phys. **24**, 764 (1956).
[3] B. Smaller and M. S. Matheson, J. Chem. Phys. 1169 (1958).

Dynamical Jahn-Teller Theorem*

WILLIAM L. CLINTON

Chemistry Department, Brookhaven National Laboratory, Upton, New York

(Received October 9, 1959)

RECENTLY the Jahn-Teller[1] theorem was reformulated[2] on the basis of the Hellmann-Feynman[3] theorem. In this electrostatic approach the electron density and its "shape" played a dominant role. The forces were only considered from a static point of view, however. It will be shown in the following that the authors' previous considerations can all be extended to the dynamical case if the nuclei are envisioned as moving classically and thus giving rise to time-dependent terms in the electronic Hamiltonian. The present treatment was inspired by the recent work of Kerner.[4]

Consider a system of three identical nuclei held fixed in an equilateral triangular configuration. We assume that the electronic state of this system is doubly degenerate, the wave function being, in general, $\psi = a_1\phi_1 + a_2\phi_2$. It is known that this state cannot be at equilibrium in the sense that all energy gradients $(\partial W/\partial q_K)_0$ vanish in the symmetrical configuration. Since the present example corresponds to D_{3h} spatial symmetry there will exist energy gradients with respect to the doubly degenerate displacement coordinate $q = b_1q_1 + b_2q_2$.

We now treat the nuclear displacement coordinates as time-dependent perturbations on the electronic state ψ. If these displacements are truly infinitesimal the time-dependent wave function can be expanded in the set (ϕ_1, ϕ_2)—i.e., $\psi(\mathbf{r}, t) = a_1(t)\phi_1(\mathbf{r}) + a_2(t)\phi_2(\mathbf{r})$ where $\mathbf{r}$ designates the whole electronic space. To further define the perturbation problem we expand the Hamiltonian as

$$\mathcal{H}(\mathbf{r}, t) = \mathcal{H}_0(\mathbf{r}) + \sum_i (\partial\mathcal{H}/\partial q_i)_0 q_i(t) + \cdots \quad (1)$$

and consider only linear terms designated by $V(\mathbf{r}, q)$. The initial conditions are as follows: at $t=0$, $|\psi(\mathbf{r}, 0)|^2 = |\phi_1(\mathbf{r})|^2$ so that $|a_1(0)|^2 = 1$ and $|a_2(0)|^2 = 0$. For times near zero, then, the differential equations for the expansion coefficients are

$$\dot{a}_1 = -(i/\hbar)V_{11}(\mathbf{r}, t); \qquad \dot{a}_2 = -(i/\hbar)V_{12}(\mathbf{r}, t), \quad (2)$$

where

$$V_{mn}(\mathbf{r}, t) = \sum_i q_i(t) \int \phi_m^* (\partial\mathcal{H}/\partial q_i)_0 \phi_n d\tau.$$

For D_{3h} symmetry ϕ_1 and ϕ_2 can be chosen such that under the group operations they transform in the same way as the y and x axes (see Fig. 1). Using these symmetry properties Eqs. (2) become

$$\dot{a}_1 = -(i/\hbar)q_1(t) \int \phi_1^* (\partial\mathcal{H}/\partial q_1)_0 \phi_1 d\tau \equiv -(i/\hbar)q_1(t)F_{11},$$

$$\dot{a}_2 = -(i/\hbar)q_2(t) \int \phi_1^* (\partial\mathcal{H}/\partial q_2)_0 \phi_2 d\tau \equiv -(i/\hbar)q_2(t)F_{12}.$$

In order to solve (3) we assume that the nuclear vibrations are harmonic about the true equilibrium position $q^{(0)}$, that is, $q_1 - q_1^{(0)} = A_1 \cos(\omega t + \delta_1)$ and $q_2 - q_2^{(0)} = A_2 \cos(\omega t + \delta_2)$. The expansion coefficients for $t \sim 0$ are then also harmonic.

We note now that $\psi(\mathbf{r}, t)$, as given by (3), acts just as a rotating vector in the xy plane of the molecule. The corresponding motion of the charge density is indicated in the figure for the simple case of a $2p$ hydrogen-like wave function.

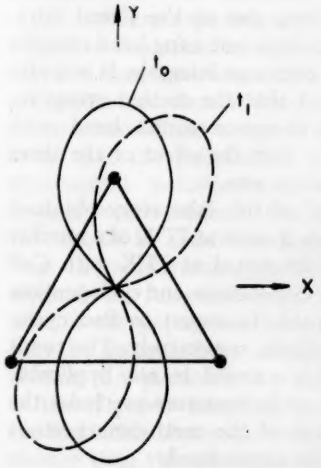

FIG. 1. Angular distribution of time-dependent density function using $2p$ hydrogen-like wave functions.

The preceding treatment lends itself well to the following physical interpretation of the dynamical JT effect. A degenerate electronic state can be interpreted in terms of the infinite number of ways in which the charge distribution can be oriented for the same energy. Although in atoms this has no physical significance, in molecules and crystals a built-in perturbation is present. That is, the moving nuclear framework serves as the perturbation necessary to define the orientation of the charge density (and also the spatial angular momentum). Further, since there is no energy difference between any two orientations of the unperturbed state, no activation energy is required to put the charge cloud into motion and hence only an infinitesimal perturbation is necessary to cause the aforementioned rotation of $\rho(\mathbf{r}, t)$.[5] This rotation in turn may be looked upon as if it were sweeping out the potential surface over which the nuclei move.

* Research performed under the auspices of the U. S. Atomic Energy Commission.

[1] H. A. Jahn and E. Teller, Proc. Roy. Soc. (London) **A161**, 220 (1937).

[2] W. L. Clinton and B. Rice, J. Chem. Phys. **30**, 542 (1959).

[3] H. Hellmann, *Binfuhring in die Quanten Chemie* (F. Deuticke, Leipzig, 1937), p. 285; R. P. Feynman, Phys. Rev. **56**, 340 (1939).

[4] E. H. Kerner, Phys. Rev. Letters **2**, 152 (1959). For a more rigorous treatment of the connection between quantum and classical vibratory motions see A. D. Liehr and H. L. Frisch, J. Chem. Phys. **28**, 1116 (1958).

[5] This simple form of motion is only true for $\omega t \sim 0, \pi/2, \pi, \cdots$. At intermediate times a more complicated motion is executed by both $\rho(r, t)$ and the nuclei. For a time-independent discussion of the sinusoidal behavior of Jahn-Teller wave functions see A. D. Liehr and C. J. Ballhausen, Ann. Phys. (N. Y.) **3**, 304 (1958).

Neutron Diffraction Study on Sodium Tungsten Bronzes Na_xWO_3 ($x=0.9\sim0.6$)*

MASAO ATOJI AND R. E. RUNDLE

Institute for Atomic Research and Department of Chemistry, Iowa State University, Ames, Iowa

(Received April 22, 1959)

NONSTOICHIOMETRIC sodium metatungstate Na_xWO_3, known as sodium tungsten bronze, has been the subject of a number of investigations.[1] X-ray diffraction has shown the cubic perovskite structure for Na_xWO_3 with $1>x>0.35$.[2] Recently, for $x>0.5$, Ingold and DeVries[3] found a temperature range over which a twinned structure exists, and optical behavior of the twinned phase which can be described in terms of a tetragonal cell with c/a slightly less than one. The present communication is a preliminary report on our neutron diffraction study of Na_xWO_3 with $0.86>x>0.56$. The crystals were prepared by the electrolytic reduction of a Na_2WO_4—WO_3 melt. The x value of each crystal was determined from x-ray lattice-constant measurements.[4] Neutron diffraction data of single crystals of Na_xWO_3 with $x=0.75$ and 0.64 and neutron powder data for $x=0.56$, 0.71, and 0.86 were obtained using the Argonne neutron diffractometer.

Single-crystal neutron data at room temperature showed that our crystals have the cubic reciprocal-lattice symmetry, O_h-m3m. The unit cell contains eight Na_xWO_3 with $a=2a'$, where a' is the x-ray lattice constant. The observed systematic extinction of hkl, when $h+k+l$ is odd, leads to possible space groups, O_h^9-Im3m, T_d^3-I43m or O^5-I43. The intensities of the reflections with h, k, l even are very strong and indicate that the structure does not greatly differ from the regular perovskite structure. However, reflections which are not detectable in the x-ray pattern are also appreciably strong in some instances. These results suggest the distorted perovskite structure in which the tungsten atoms are at the perovskite-like special positions. Apparently the result obtained from the neutron diffraction data conflicts with the optical observation, since our "single" crystals showed similar optical behavior to those reported by Ingold and DeVries. However, the dimensions of a single domain in the twinned phase were estimated to be smaller than 10 μ in linear average, while the dimensions of the single crystal used were approximately $0.3\times0.3\times1.5$ cm^3. Moreover, in our "single" crystals, a–a and a–c type twins[3] coexist without any preferred distribution. Furthermore, several crystals cut from a large crystal block gave a set of identical diffraction intensities regardless of the differences in distribution of the twinned domains. Consequently, it may be reasonably assumed that in our "single" crystals the a–a and a–c twinned domains are so distributed that the average structure over the crystal can be considered as isometric, although the structure of the single domain is optically birefringent.

Intensities obtained from neutron powder patterns agree well with those obtained from single crystals, except for systematic small discrepancies due to secondary extinction. Since preferred orientation of the twinned domain is greatly reduced in the powder sample, the foregoing result shows that the diffraction intensities from the different domains are well averaged in our single crystal data. The Patterson and difference Patterson functions and electron density projections were computed using the single-crystal data of Na_xWO_3 with $x=0.75$. Atomic parameters based on the best $Im3m$ model and refined by the least-squares method are summarized in Table I. For $x=0.75$, no sodium atom is found at (000) and $(\frac{1}{2}\frac{1}{2}\frac{1}{2})$. For $1>x>0.75$, these positions could be partly filled by sodium atoms. Tungsten atoms occupy regular perovskite positions, but oxygen atoms have a statistical distribution. Accordingly, the twin structure should have a close rela-

TABLE I. Atomic parameters of Na_xWO_3 ($x=0.75$).[a]

	$B(A^2)$[b]	x	y	z
6 Na in 6(b)	1.36	0.000	0.500	0.500
8 W in 8(c)	0.61	0.250	0.250	0.250
12 O_I in 48(k)	0.99	0.235	0.235	0.011
12 O_{II} in 48(k)	0.24	0.267	0.267	0.011

[a] The initial parameters in the least-squares treatment were set up at the general positions 96 (*l*) for all atoms. The *R* factor is 17% for the parameters listed in Table I.

[b] The coefficient in the isotropic temperature factor, $\exp[-B(\sin\theta/\lambda)^2]$. The displacements of the O_I atoms from the perovskite special positions are toward the vacant lattice points, (0 0 0) and ($\frac{1}{2}$ $\frac{1}{2}$ $\frac{1}{2}$), whereas the O_{II} atoms are displaced toward the filled lattice points, ($\frac{1}{2}$ $\frac{1}{2}$ 0). Therefore, the larger temperature factor for O_I than that for O_{II} may be expected as found in this table.

tion with the oxygen atoms. The sizes of the single domains vary to a large extent. In high magnification, we have found a multiply-twinned structure within an area which appears as a single domain in low magnification. Since the optical method was not capable of giving an unambiguous quantitative conclusion for the size distribution in the twinned phase, the trial-and-error method on the diffraction data seems the only way to find whether the scattered neutrons from the different domains are coherent to one another. This difficulty may be unavoidable, since it appears practically impossible to obtain a single-domain single crystal in large dimensions. The structure reported here is approximated as a disordered superposition of the various domain arrangements.

The calculated values of the interatomic distances in this statistical structure were reasonable. Several attempts to find a unique structure for a single domain with a tetragonal symmetry were made. Details will be published elsewhere.

Some neutron diffraction data were taken using single crystals at about -100°C where their optical properties show that the structure is untwinned and isotropic.[3] All diffraction symmetries remain the same as those at room temperatures. However, the intensities of the reflections with h, k, l all odd generally increase somewhat and others with h, k, l even decrease to some extent. These slight intensity changes are not indicative of an ordered low-temperature structure, but suggest a slight alteration of oxygen positions with temperature change.

The authors wish to thank G. C. Danielson for suggesting the problem, P. H. Sidles for growing the crystalline samples and S. Sidhu for making it possible for us to use the Argonne neutron spectrometer.

* Contribution No. 747. Work was performed in the Ames Laboratory of the U. S. Atomic Energy Commission.

[1] Rosen, Post, and Banks, Acta Cryst. **9**, 477 (1956).

[2] For general references on the x-ray study, see G. Hägg and A. Magneli, Revs. Pure and Applied Chem. Australia **4**, 235 (1954).

[3] J. H. Ingold and R. C. DeVries, General Electric Research Laboratory, Report No. 57-RL-1821 (1957).

[4] B. W. Brown and E. Banks, J. Am. Chem. Soc. **76**, 963 (1954).

Electrically Discharged CO_2 as a Source of Oxygen Atoms*

E. A. OGRYZLO AND H. I. SCHIFF

Department of Chemistry, McGill University, Montreal, Canada

(Received September 15, 1959)

WILDE, Zwolinski, and Parlin[1] have studied the production of CO from electrically discharged CO_2. Their results led them to conclude that the only significant reaction which occurs in the discharge is

$$CO_2 \rightarrow CO+O. \quad (1)$$

The reactions

$$CO+O+M \rightarrow CO_2+M, \quad (2)$$

$$O+O+M \rightarrow O_2+M \quad (3)$$

are thought to occur outside the discharge.

In connection with some atomic oxygen studies[2,3] it was desirable to have a source of large concentrations of atomic oxygen, free of molecular oxygen. CO_2 was therefore passed through an electrodeless discharge operating at 2450 Mc/sec. The percentage decomposition of CO_2 could be increased either by increasing the power input or by diluting the CO_2 with helium or argon. The unreacted CO_2 was recovered by condensation. The oxygen atom concentration was measured as a function of time in the interval between 10^{-2} and 10^{-1} sec after leaving the discharge, by the isothermal calorimeter technique[2] and by NO_2 titration.

The disappearance of O atoms was found to occur mainly by a first-order wall recombination at a very slow rate. It was therefore possible to estimate, by extrapolation, the atom concentration at the outlet from the discharge. Atom concentrations amounting to approximately 5% of the CO_2 flow rate were obtained. However, the quantity of CO_2 destroyed in the discharge was always found to be several times as great as the quantity of O atoms produced.

This observation was also confirmed by passing the discharged CO_2 directly over the leak of a mass spectrometer in a manner previously used in these laboratories to study discharged O_2.[4] Considerable decrease in the CO_2^+ peak was observed and large increases in the CO^+, O_2^+, and O^+ peaks.

These observations suggest that reactions of the type

$$CO_2+O \rightarrow CO+O_2 \quad (4)$$

must also occur in the discharge. Although reaction (4) is slow at room temperature, it could occur in the discharge if (a) the temperature in the discharged gas is high, (b) the O atom is in an excited state, or (c) either CO_2 or O is ionized.

Further support for the occurrence of reaction (4) in the discharge comes from the observation that the quantites of O atoms produced and of CO_2 decomposed

approached one another as the percentage decomposition of the CO_2 was increased.

* This work was supported in part by the Geophysics Research Directorate of the Air Force Cambridge Research Center under Contract AF 19-(604)4104, and in part by a grant-in-aid from the Defence Research Board of Canada.

[1] Wilde, Zwolinski, and Parlin, J. Am. Chem. Soc. **79**, 1323, (1957).

[2] Elias, Ogryzlo, and Schiff, Can. J. Chem. (to be published).

[3] E. A. Ogryzlo and H. I. Schiff, Can. J. Chem. (to be published).

[4] J. T. Herron and H. I. Schiff, Can. J. Chem. **36**, 1159 (1958).

Soundness of the Lattice of Zone-Refined Aluminum

M. E. Straumanis and T. Ejima

Department of Metallurgical Engineering, The University of Missouri School of Mines and Metallurgy, Rolla, Missouri

(Received August 26, 1959)

RECENT developments of the theory of dislocations have stimulated many experimental methods to check the validity of this theory. One of these may be the lattice constant and density method[1] especially if used to determine the actual number n' of molecules or atoms per unit cell[2]:

$$n' = dvN_0/A, \qquad (1)$$

d being the macroscopic density of the material, v the volume of the unit cell, N_0 Avogadro's number, and A the atomic weight of the homogeneous substance. If n is the theoretical number of atoms per unit cell, then the difference $n'-n$ gives the excess of defects (in atoms) per unit cell.

The validity of Eq. (1) actually follows from previous precision work.[1,3-5] However, a further check was made this time by directly determining n' for recrystallized zone-refined aluminum (99.9998% purity) which should have a sound or perfect lattice. The concentration of edge dislocations in this material is so small[6] that it does not affect the density or the lattice constant.

The density of the samples was determined by the modified suspension method[7] using small chips of the material, cut from the button, and recrystallized in vacuum at 250°C and 350°C (15 min). For the lattice constant measurements by the powder method with films in the asymmetric position, the necessary powder was obtained by scraping the zone-refined aluminum with a sharp edge of a silica glass piece. The powder was sifted through a 325-mesh screen, and one portion of the fine material was heated in vacuum at 250°C (15 min), the other at 350°C for 1 hr.

The density of the chips was the same regardless of the temperature of recrystallization: 2.69808 g cm^{-3} at 25° with a standard deviation of $s=\pm 0.00009$ (12 determinations were made). There is only one lower measurement, that obtained by Smakula *et al.*[3]: 2.69801 g cm^{-3}. The values for less pure aluminum are higher: e.g., Snoek[8] obtained $d_{25}=2.6993$ g cm^{-3} for 99.98% Al.

The lattice constant of the Al turned out to be $a_{25}=4.04958\pm 0.000025$ A (standard deviation) as an average of 4 determinations at 4 different temperatures, reduced to 25°, which is in perfect agreement with other values at 25°C: 4.04960,[3] 4.04963,[9] and 4.04961 A.[10]

The value of n' for this aluminum calculated from Eq. (1) using different combinations of values for N_0, A, and d are shown in Table I.

As it has been found that mass spectroscopic atomic weights fit much better than chemical weights for similar calculations (N from lattice constant and density data[3]), only the former are used in Table I. The table shows that the values of n' are completely within the limits of error ± 0.00044 atom/unit cell, calculated from error propagation,[7,2] and approach 4.0000, as expected for a sound lattice. DuMond and Cohen, in a least-squares evaluation of fundamental constants have suggested as a best value a smaller Avogadro number ($N_0=6.02336\times 10^{23}$, chem. scale),[12] which seemingly should give a smaller n'. However, it has to be remembered that in such a case the conversion factor Λ (changing kX into A) increases from 1.00202 to 1.002037 (Du Mond's best guess, 1959).[13] With these values for Λ and N_0, using v, d, and A_{sp} of Table I, $n'=4.000027$ is calculated which is in perfect agreement with the values of the table. This result is not surprising, because N_0 and Λ are connected by the relationship[1,14]:

$$N_0 = kN_s/\Lambda^3, \qquad (2)$$

where k is a correction factor ($=1.0002\pm 0.00003$) and N_s is Siegbahn's Avogadro number ($=6.0594\times 10^{23}$) used for the determination of x-ray wavelengths. Thus, this investigation confirms that Eq. (1) is well suited for calculation of n' at least in the case of very pure substances and that the lattice of zone-refined aluminum is sound.

Table I. Actual number of atoms n' per unit cell in zone-refined (99.9998%) Al.

Eq. (1)	n' atoms/u.cell	Defects $n'-n$ in + or − atoms/cm^3
dvN_0/A_{sp}	4.00026 ± 0.00044	$+(3.9\pm 6.6)\times 10^{16}$
dvN_0'/A_{sp}	4.00003	$+4.5\times 10^{17}$
$d'vN_0/A_{sp}$	3.99993	-1.1×10^{18}

$N_0=6.02403\times 10^{23}$; $N_0'=6.02368\times 10^{23}$ (chem scale)[a]

$d_{25}=2.69808$ g cm^{-3}; $d_{25}'=2.69801$ g cm^{-3} [b]

$A_{sp}=26.98256$[c]; $v=(4.04958)^3$ A^3

[a] See references 1 and 3.

[b] See reference 3.

[c] See reference 11.

We thank the National Science Foundation (Grant G 2585) for financial support, Dr. E. A. Bloch, Director of the Aluminum Research Institute AIAG (Switzerland) for the aluminum sample and Dr. W. J. James, professor of the Chemistry Department, for interest in this work.

[1] M. E. Straumanis, Phys. Rev. **92**, 1155 (1954); **95**, 566 (1954).
[2] M. E. Straumanis, Chimia **12**, 136 (1958).
[3] A. Smakula, J. Kalnajs, and V. Sils, Phys. Rev. **99**, 1747 (1955).
[4] M. E. Straumanis, Z. Physik **126**, 49 (1949).
[5] M. E. Straumanis and E. Z. Aka, J. Am. Chem. Soc. **73**, 5643 (1951); J. Appl. Phys. **23**, 330 (1952).
[6] P. B. Hirsch, Progr. Metal Phys. **6**, 236 (1956).
[7] M. E. Straumanis, Am. Mineralogist **38**, 662 (1953).
[8] J. L. Snoek, Phil. Mag. **41**, 1188 (1950).
[9] B. F. Figgins, G. O. Jones, and D. P. Riley, Phil. Mag. **1**, 747, 754 (1956).
[10] A. Ievins and M. Straumanis, Z. Phys. Chem. **B34**, 402 (1936).
[11] C. W. Li, Phys. Rev. **88**, 1038 (1952).
[12] J. W. M. Du Mond, Ann. Physics **7**, 365, (1959).
[13] J. W. M. Du Mond, Proc. Natl. Acad. Sci. U.S. **45**, 1052, (1959).
[14] M. E. Straumanis, Acta Cryst. **2**, 83 (1949); Z. Physik **126**, 65 (1949).

Heat Capacity of Terbium from 1.4 to 4.0° Kelvin*

R. M. Stanton, L. D. Jennings, and F. H. Spedding

Institute for Atomic Research and Department of Chemistry, Iowa State University of Science and Technology, Ames, Iowa

(Received July 22, 1959)

In order to obtain additional data useful in interpreting the heat capacity of the rare earth metals, we have undertaken a study of their heat capacity in the helium region. Using the calorimeter described by Griffel, Vest, and Smith[1] with a container designed to accommodate the terbium sample used in our high temperature investigation, we measured the heat capacity in the range 1.4 to 4.0°K.

The results are shown in Fig. 1. It is clear that one cannot obtain the electronic contribution or the Debye temperature from these data. We have started a program of investigation directed toward understanding the cause of the anomaly near 2.4°K but, as it will be some time before it is completed and in view of the work of Kurti and Safrata,[2] whose results are also shown in the figure, we felt it would be desirable to publish our curve at this time.

The anomaly contains less than 0.005 R units of entropy and cannot, therefore, be associated with a phenomenon arising from independent levels of terbium atoms. A possible explanation is that a nonmetallic impurity, presumably oxide, which in general forms a separate phase, has a magnetic ordering temperature at 2.4°K. Oxide is present to the order of 0.1% by weight in Ames Laboratory cast samples. On an atomic basis, this would be sufficient to yield the

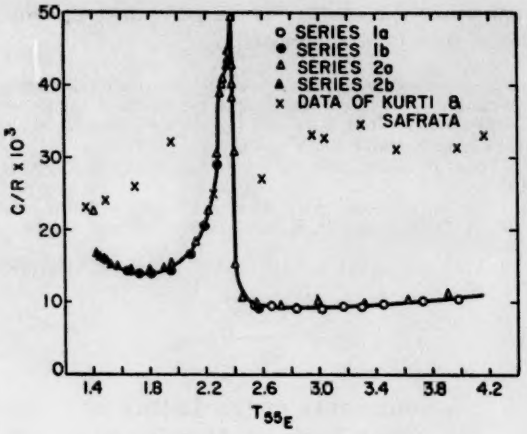

Fig. 1

above mentioned entropy, which is of the same order of magnitude as the entropy under the anomalies in Kurti and Safrata's data. This explanation could be investigated by using a sample of lower oxide content prepared by distillation of the metal. It would also be of interest to investigate the heat capacity of the oxides of terbium.

The rise below 1.5°K has been explained by Kurti and Safrata, whose data extend over a wider temperature range than do ours, as arising from hyperfine interactions. The generally higher values which they obtain above 1.5°K perhaps arise from the same cause as does the anomaly. Except for the anomaly, our data are not unreasonable as shown by the following considerations.

An estimate of the magnetic heat capacity may be made using the method outlined by Hofmann, Paskin, Tauer, and Weiss.[3] One calculates the effective value of the exchange integral from the total magnetic energy obtained from the higher temperature data and then calculates the heat capacity which spin wave theory predicts using this effective value of the exchange integral. This calculation does not require that the actual mechanism of magnetic coupling be simple exchange. The result is that $C/R=0.6\times10^{-3}T^{\frac{3}{2}}$ as compared with the value $2.5\times10^{-3}T^{\frac{3}{2}}$ which Kurti and Safrata obtain by fitting their data near 5°K.

The lattice heat capacity may be estimated from the value of the average Debye temperature (that value which gives the correct entropy near room temperature). Work on the nonmagnetic rare earths shows that the value of the Debye temperature near absolute zero is about 8% greater than the average value and thus would be about 170° for terbium.

If we use the values obtained previously for the hyperfine interaction and for the electronic term, we have

$$C/R\times10^{-3}=25/T^{2}+1.2T+0.6T^{\frac{3}{2}}+0.047T^{3}.$$

At 4°K this expression predicts a value of 14.2 which

is slightly greater than our value and less than that of Kurti and Safrata.

These results point up the necessity for understanding the causes for the low temperature anomalies in the rare earths so that one may obtain the electronic, the lattice, and the magnetic contributions to the heat capacity. Judging from the data so far available on the heavy rare earths, the latter rises more rapidly than T^3 at very low temperatures (of the order $T/T_c=1/10$) and much less rapidly near $T/T_c=1/4$, where T_c is the ordering temperature.

* Contribution No. 775. Work performed in the Ames Laboratory of the U. S. Atomic Energy Commission.

[1] Griffel, Vest, and Smith, J. Chem. Phys. **27**, 1267 (1957).
[2] N. Kurti and R. S. Safrata, Phil. Mag. **3**, 780 (1958).
[3] Hofmann, Paskin, Tauer, and Weiss, J. Phys. Chem. Solids **1**, 45 (1956).

Lower Excited Electronic States of Carbon Monoxide

P. MERRYMAN, C. M. MOSER,* AND R. K. NESBET†
RIAS, 7212 Bellona Avenue, Baltimore 12, Maryland

(Received August 13, 1959)

IT has recently been shown[1] that using the occupied and virtual orbitals calculated by the SCF–LCAO–MO method in its simplest form, the calculated order and spacing of the lower excited electronic energy levels of carbon monoxide agree reasonably well with experiment, at the ground state equilibrium internuclear distance (2.1319 au). The self-consistent molecular orbitals were expressed as linear combination of $1s$, $2s$, and $2p$ functions of exponential form, with best atom single exponents for both carbon and oxygen.[2] To see if the general qualitative behavior of these states near the equilibrium positions of the nuclei could be interpreted from such simple basis functions we have extended this calculation to cover a range of internuclear distances. Calculations were made for eleven equally spaced points between 1.5 and 4.0 au.

These are the first results obtained using digital computer programs written for the IBM 704 by one of the authors (R.K.N.) which include a program that obtains all required integrals by a uniform procedure. The integral program is designed to work with arbitrary values of parameters, such as the angular quantum numbers of the basic atomic orbitals. It uses methods developed by one of the authors (P.M.) from a method originally presented by Kotani[3] and later modified by Ruedenberg.[4] It is of interest to note that the entire programmed calculation, which included evaluation of all integrals, a matrix Hartree-Fock calculation, and transformation of molecular integrals to the self-consistent basis, required less than ten minutes for each internuclear distance.

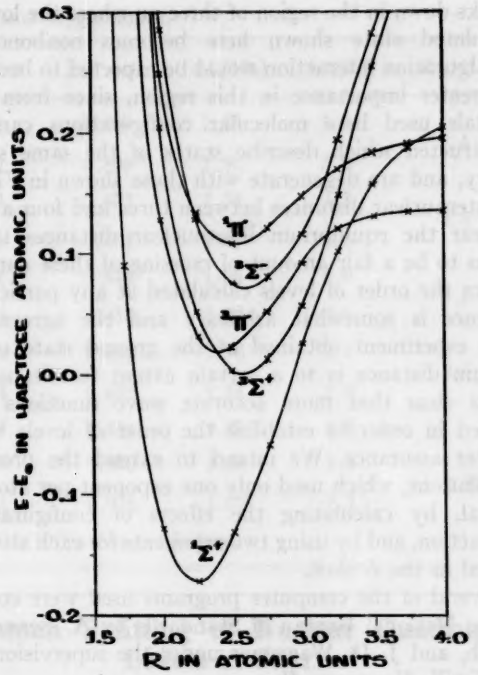

FIG. 1. Energy relative to free atoms as a function of internuclear distance R. Energies plotted are diagonal elements of the configuration interaction matrix. Free atom energies are calculated with the atomic basis orbitals used for the molecular calculations.

The results are given in Fig. 1. There are two important qualitative results. First the states $^3\Sigma^+$, $^3\Pi$, $^3\Sigma^-$, and $^1\Pi$ are all states with well-defined minima. Furthermore, these minima are found to be at internuclear distances larger than the equilibrium distance for the ground state, in agreement with experiment.[5] The behavior of these curves toward shorter interatomic distance seems reasonable. Towards larger interatomic distance this most simple approximation

TABLE I. Estimated position R_e of excited state potential minima and energies ΔE above ground state minimum.

State	R_e calc.		obs.[a]	ΔE calc.		obs.[a]
$^3\Sigma^+$	2.625 au	=1.39 A	1.359 A	0.175 au	=38 400 cm^{-1}	55 901 cm^{-1}
$^3\Pi$	2.375	1.26	1.2093	0.190	41 700	48 687.5
$^3\Sigma^-$	2.625	1.39	...	0.245	53 800	<64 802
$^1\Pi$	2.500	1.32	1.2351	0.280	61 500	65 074.8

[a] See reference 5.

breaks down in the region of three au where the lowest calculated state shown here becomes nonbonding. Configuration interaction would be expected to become of greater importance in this region, since from the orbitals used here molecular configurations can be constructed which describe states of the same symmetry, and are degenerate with those shown in Fig. 1 at internuclear distances between three and four au.

Near the equilibrium internuclear distances there seems to be a fair amount of crossing of these curves. Hence the order of levels calculated at any particular distance is somewhat arbitrary and the agreement with experiment obtained at the ground state equilibrium distance is to a certain extent fortuitous. It seems clear that more accurate wave functions are needed in order to establish the order of levels with greater assurance. We intend to extend the present calculations, which used only one exponent per atomic orbital, by calculating the effects of configuration interaction, and by using two exponents for each atomic orbital in the L shell.

Several of the computer programs used were coded at the National Bureau of Standards by A. Beam, P. Walsh, and J. D. Waggoner under the supervision of Dr. Emilie Haynesworth.

We are indebted to The Martin Company for the use of their IBM 704 computer for this project.

Part of this work, at Boston University, was supported by the National Science Foundation.

* Permanent address: Centre de Mécanique Ondulatoire Appliquée, 155, rue de Sèvres, Paris 15e, France.

† Permanent address: Department of Physics, Boston University, Boston 15, Massachusetts.

[1] H. Brion and C. M. Moser, J. Chem. Phys. (to be published).

[2] C. C. J. Roothaan, Technical Report, Laboratory of Molecular Structure and Spectra, University of Chicago, 1955, p. 24 (unpublished).

[3] Kotani, Amemiya, and Simose, Proc. Phys. Math. Soc. Japan **20,** Extra No. 1 (1938); **22,** Extra No. 1 (1940).

[4] K. Ruedenberg, J. Chem. Phys. **19,** 1459 (1951).

[5] G. Herzberg, *Molecular Spectra and Molecular Structure.* I. *Spectra of Diatomic Molecules* (D. Van Nostrand Company, Inc., Princeton, New Jersey, 1950).

Rate of Recombination of Oxygen Atoms*

ROBERT R. REEVES, GENE MANNELLA, AND PAUL HARTECK

Chemistry Department, Rensselaer Polytechnic Institute, Troy, New York

(Received October 12, 1959)

A PRECISE determination of the rate coefficient for the reaction

$$O(^3P)+O(^3P)+M\rightarrow O_2+M \qquad (1)$$

has not been made to date because of various experimental difficulties. These include the general problem of conveniently measuring oxygen atom concentrations, the interference of ozone formation at higher pressures and the wall effect at lower pressures. Considerable work has been done at high temperatures using shock tube techniques. Matthews[1] gives an extensive review of the literature and reports a value of $k_1=2.2\times10^{-33}$ (cc^2/molecules^2-sec) at 3500°K. The value reported herein of 2.7×10^{-33} at 300°K suggests that even taking into consideration the scatter in the high-temperature results, there is essentially no temperature dependence of the rate constant.

The rate constant reported here was obtained by producing O atoms in a discharge from O_2 argon mixtures, measuring the initial concentration by titration, and measuring the decrease in the afterglow intensity along a 4.2-cm i.d. tube. The equipment and technique were essentially the same as that used to determine the recombination of N atoms.[2] The basic reactions involved in the oxygen afterglow are given in another publication.[3] A small amount of N_2 impurity forms NO in the discharge which under our conditions consumes a negligible amount of O atoms.

Originally the efforts to titrate O atoms in the gas phase involved NO_2 alone. By adding NO_2 through a calibrated leak, the very fast reaction $NO_2+O\rightarrow NO+O_2$ (k approx. 10^{-12})[4] occurs, and will eventually extinguish the afterglow. At this point, the NO_2 equals the O atoms. However, it is very difficult to meter an NO_2 stream because of N_2O_4 formation and also because of the reactive nature of the gas. A two-step titration was developed which avoided this situation. This consists of adding NO_2 to the O atom stream and measuring the afterglow intensity with a photomultiplier. Since the intensity of the afterglow is proportional to the product of the NO- and O-atom concentration, a maximum light intensity occurs. At this point, the NO in the system equals $\frac{1}{2}$ the original O atoms (since each NO is formed by reaction of an O atom with NO_2). The second step of the titration is to add NO to the O-atom stream until this maximum intensity is again reached in the afterglow. The NO now equals $\frac{1}{2}$ the NO concentration in step one, since O atoms are now not consumed to form NO. From the foregoing analysis, it is seen that the NO added in step two equals $\frac{1}{4}$ the original O atoms. Hence, the atom concentration is obtained by determining the amount of NO added in step two and multiplying by 4.

The O-atom recombination rate is determined by measuring the relative intensity of the afterglow of the streaming gas at two points along the tube. The titration procedure requires that (1) the reaction between NO_2 and O is essentially instantaneous and (2) that the over-all reactions $2NO+O_2\rightarrow2NO_2$ ($k=2\times10^{-37}$)[5] $NO+O\rightarrow NO_2+h\nu$ ($k=10^{-17}$)[6], $NO+O+M\rightarrow NO_2+M$ ($k=7\times10^{-32}$)[3] are slow enough not to affect appreciably the O-atom concentration in the titrating zone; these conditions were fulfilled during these experiments.

TABLE I. Three-body recombination of oxygen atoms.

Run	$\%O_2$	Press. mm	$(O)_1\times10^{-15}$	$(O)_2\times10^{-15}$	$M\times10^{-16}$	ΔT sec	$(O)_{Av}/(O_2)$	$k_1\times10^{33}$	$K_{Av}\times10^{33}$
4	10	0.334	1.16	1.08	1.08	0.489	2.35	5.9	5.4
5	20	0.337	1.86	1.67	1.09	0.500	1.50	5.0	
1	5	0.460	0.79	0.77	1.48	0.475	2.33	2.5	3.5
2	20	0.454	2.22	1.92	1.46	0.463	1.13	4.5	
7	10	0.628	1.84	1.56	2.02	0.448	1.66	3.0	3.3
8	5	0.619	1.14	1.00	2.00	0.453	2.72	3.5	
9	5	0.954	1.51	1.24	3.06	0.698	1.98	2.7	2.7
10	10	0.945	2.44	1.78	3.04	0.695	1.34	2.9	
11	20	0.954	3.81	2.52	3.07	0.691	0.88	2.5	
14	5	1.33	1.90	1.26	4.28	0.970	1.58	2.8	2.75
15	10	1.34	2.98	1.63	4.31	0.976	1.07	2.7	

Av. value of last five runs: $k_1=2.7(\pm0.3)\times10^{-33}$ cc²/molecules²-sec.

The titration gives reproducibility of 1% with an estimated over-all error not exceeding 5%.

The results of the study are given in Table I. A pressure range of 0.334 to 1.34 mm Hg was investigated under such conditions that the consumption via $O+O_2+M\rightarrow O_3+M$ ($k=6\times10^{-34}$)[7,8] and $O_3+O\rightarrow2O_2$ ($k=2\times10^{-15}$)[8] was about 10–20% at the higher pressures. The correction for this effect is straightforward and the reported values have been correspondingly adjusted. At the lower end of the pressure range small errors in the measured O-atom concentration produce very large errors in the calculated rate constant because of the small amount of O atoms consumed. Even the small wall catalysis with an efficiency of about 10^{-6} contributes appreciably to the errors at low pressure and gives too high a rate constant. With increasing pressure, the accuracy improves significantly since the over-all rate of consumption is a strong function of the pressure. At the higher end of the pressure range, the value of k_1 levels off to 2.7×10^{-33} (cc²/molecules²-sec). The final result based on measurements at pressures of 0.95 to 1.34 mm Hg is probably valid within 10%.

* The research reported in this document has been sponsored by the Geophysics Research Directorate of the Air Force Cambridge Research Center, Air Research and Development Command under Contract No. AF19(604)-2205.

[1] D. L. Matthews, Phys. Fluids **2**, 170 (1959).
[2] Harteck, Reeves, and Mannella, J. Chem. Phys. **29**, 608 (1958).
[3] Harteck, Reeves, and Mannella, J. Chem. Phys. **29**, 1333 (1958).
[4] G. B. Kistiakowsky and G. G. Volpi, J. Chem. Phys. **27**, 1141 (1957).
[5] M. Bodenstein, Z. Elektrochem. **24**, 183 (1918); Z. physik. Chem. (Leipzig) **100**, 68 (1922).
[6] D. R. Bates, *The Earth as a Planet*, edited by G. P. Kuiper (University of Chicago Press, Chicago, 1954), Chap. 12.
[7] P. Harteck and R. R. Reeves, ASTIA Document AD 136421.
[8] S. W. Benson and A. E. Axworthy, Jr., J. Chem. Phys. **26**, 1718 (1957).

Zeeman Splitting of Nuclear Quadrupole Levels in Cuprite*

HENRY L. COX, JR., AND DUDLEY WILLIAMS
Department of Physics, The Ohio State University, Columbus, Ohio

(Received May 13, 1959)

EARLY[1] studies of powdered cuprous oxide revealed the presence of two relatively sharp absorption lines due to transitions between energy levels involving interactions between the crystalline electric field gradient and the electric quadrupole moments of Cu^{63} and Cu^{65}, both of which are characterized by a nuclear spin $I=\frac{3}{2}$. These lines occur in the vicinity of 26 Mc/s for Cu^{63} and 24 Mc/s for Cu^{65}. The present work involves a study of a single cuprite crystal and was undertaken with a view to comparing the spectrum of a single crystal with the spectrum predicted on the basis of the earlier work on powders, earlier nuclear magnetic resonance studies of solutions of copper salts, and the cuprite crystal structure as determined from x-ray data. Studies of single crystals provide the only method of determining the directions of principal electric field gradients and also permit precise determinations of field asymmetry parameters η.

In cuprite,[2] each copper atom lies midway between two oxygen atoms while each oxygen is surrounded by four copper atoms arranged in tetrahedral symmetry. The electric field at a copper nucleus is presumably due predominantly to the two neighboring oxygen atoms and the O—Cu—O bond axes would be expected to be an electric field symmetry axis. X-ray data would indicate that this electric symmetry is not destroyed by the six copper atoms nearest the O—Cu—O bond.

Thus, on the assumption that the time average *charge* distribution in the crystal is that determined by x-ray methods, an asymmetry parameter $\eta=0$ is to be expected.

Since there are four differently oriented O—Cu—O symmetry axes, there is a possibility of observing 16 absorption lines for each copper isotope when a cuprite crystal is placed in a magnetic field. This complicated 32-line spectrum makes it difficult to determine symmetry axis orientation from the observed spectrum alone. Fortunately, it was possible to obtain an initial clue as to the orientation of O—Cu—O bonds by observing external facets of the natural crystals employed; subsequent studies of the spectrum in a weak field of approximately 500 gauss then made it possible to verify that the O—Cu—O axes were indeed symmetry axes.

The first quantitative test involved a study of the splitting pattern for $\theta=0$ (O—Cu—O axes parallel to magnetic field) as a function of magnetic field H_0. The observed splitting led to the following values of pertinent parameters: $\mu^{63}=2.2261\pm0.007$ n.m.; $\mu^{65}=2.3765\pm0.007$ n.m.; $(eQq)^{63}=51.956\pm0.04$ Mc/s at 28°C; and $(eQq)^{65}=48.065\pm0.04$ Mc/s at 28°C. The agreement of these values with the more precise values of μ obtained in liquids and for eQq obtained with powders is regarded as satisfactory verification of the O—Cu—O axis as the electric symmetry axis. In making the comparison of eQq values with those of Meyer-Berkhout, it is necessary to make a temperature correction, since his observations were made at 16°C.

An experiment directed toward setting an upper limit on the asymmetry parameter was attempted. If a perfect crystal were mounted so that it could be rotated about an O—Cu—O symmetry axis aligned perpendicular to H_0, a line corresponding to the $\theta=90°$ orientation should have constant frequency if $\eta=0$. Orientation of the symmetry axis was accomplished as closely as possible by proper machining of the polystyrene rod used to support the crystal. The frequency of lines were measured for thirty-one different values of azimuthal angle ϕ. The measured line frequencies clustered closely about their average value; the *maximum* deviation corresponded to 24 kc in 30 538 kc for the magnetic field employed. A statistical treatment of the data leads to the conclusion that $\eta<0.0012$.

Additional experiments involved studies of line intensities for $\theta\neq0$. A comparison of "single-jump" lines at $H_0=500$ gauss and $H_0=3000$ gauss revealed that the lines at the higher field are generally weaker. This decrease in intensity is presumably accompanied by an increase in the intensity of the lines associated with "double-jump" transitions. This behavior is predicted from transition probability considerations.

The behavior of double-jump lines as a function of θ in a field of 2000 gauss was investigated. These lines disappeared in the noise as θ approached zero as expected, since $\Delta m=2$ transitions are strictly forbidden at $\theta=0$. This result indicates that possible local misalignments were not sufficiently great to cause an observable line at this orientation.

The spectrum observed in the vicinity of $\theta=90°$ had some rather interesting features. As θ approached 90° in a field of 2000 gauss, the single-jump and double-jump lines coalesced into a single line, any possible separation being less than the line width, approximately 15 kc. Another interesting feature was that the line intensities increased more rapidly than expected as θ approached 90°. This behavior is tentatively interpreted in terms of small local misalignments; as θ approaches 90°, the single-jump and double-jump lines gradually approach common limits so that the distribution of local θ values is less effective in smearing out the absorption lines, which therefore produce sharper lines on the derivative plot registered on the recorder chart.

In spite of possible minor imperfections in the natural crystals employed, it is believed that the present work definitely establishes the O—Cu—O bond as the axis of electric symmetry and establishes a definite upper limit on the value of the asymmetry parameter.

* Work supported in part by the Office of Scientific Research, Air Research and Development Command.

[1] H. Kruger and V. Meyer-Berkhout, Z. Physik **132**, 171 (1952).
[2] R. W. G. Wykoff, *The Structure of Crystals* (Chemical Catalogue Company, New York, 1924).

Emission of Diffuse Bands of Sodium behind Shock Fronts*

H. TAKEYAMA† AND A. GUTTMAN‡

Daniel and Florence Guggenheim Jet Propulsion Center, California Institute of Technology, Pasadena, California

(Received October 14, 1959)

WURM[1] has described a continuous emission band extending from 5490 A to the *D* lines and inferred the existence of van der Waals states of Na_2. Hamada[2] has classified sodium bands in the red and yellow regions into three groups, *viz.*, (1) red bands (λλ8150–5500), (2) cathode ray fluorescence band, and (3) the continuous band (λλ5470–7200). Recently, wide diffuse bands have been observed and discussed qualitatively for rubidium-rare gas mixtures.[3,4]

By utilizing the shock tube, we have observed the emission of a continuous band corresponding to Hamada's type (3) band. We used finely ground salts as a source of sodium in a one-inch diameter tube; the low-pressure section was 51 in. long and the high-pressure section had a length of 24 in. Mylar diaphragms

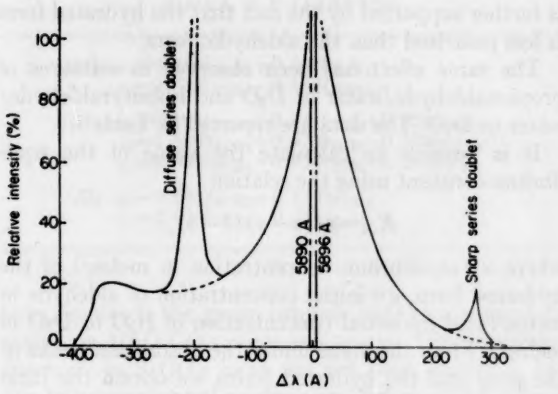

FIG. 1. Intensity distribution of band accompanying D lines; $p_1 = 50$ mm Hg, $p_4 = 395$ psi, $p_5 = 12$ atmos, $T_5 = 6300°K$, NaCl = 50 mg.

(0.003 and 0.005 in. thick) separated the two sections. Observations were made through a lucite block at the end of the low pressure section. Spectrograms were taken with a 1.5-m ARL spectrograph with a dispersion of 6.8 A/mm. Kodak Royal-X panchromatic sheet film and Kodak Tri-X panchromatic roll film were used. Intensity measurements were made with an ARL 2250 densitometer.

Measured quantities (from 5 to 300 mg) of finely ground sodium salts (e.g., NaCl, NaBr, and Na_2CO_3) were placed in the Lucite block and spread evenly. Argon, at pressures from 5 to 100 mm Hg, was admitted to the low-pressure section. The high-pressure section was filled with helium and a magnetic breaker used to burst the diaphragm.

We observed atomic lines of Na and a continuous band under various shock conditions. As the amount of sodium salt is increased at constant shock conditions, the D lines become stronger, wider and self-reversed; also the diffuse series lines (λλ5682, 5688) and sharp series lines (λλ6154, 6160) appear. When the quantity of sodium chloride exceeds about 10 mg, the diffuse band becomes superimposed on the atomic lines. Further increases in the amount of sodium chloride up to 300 mg did not change the general features of the spectrum. A typical intensity profile (Fig. 1) shows a continuous band starting at about 5490 A and extending beyond 6200 A. The quantities T_5 and p_5 were estimated by using ideal, one-dimensional shock theory.[5] An intermediate maximum occurs at about 5500 A; on the long-wavelength side the intensity decreases continuously without distinct cutoff.

There is little doubt that the continuous band λλ5490–6200 is identical with Hamada's (3) band and Wurm's band. The discrepancy in the long-wavelength extent of the band between Hamada's results and ours may be attributed to the extreme difference of excitation conditions. The principal support for the assertion that the band belongs to Na_2 molecular states comes from the observation that the emission spectrum is independent of the nature of the foreign gas. Wurm considered the structure in the long-wavelength region of the D lines to result from absorption of the red band of Na_2, the background being the broadening of the D lines. On the other hand, Hamada interpreted the entire continuum (both sides of the D lines) to constitute a single band caused by the same mechanism described by Wurm. Recently, Ch'en, Bennett, and Jefimenko[3] have presented potential curves that are consistent with both the red and violet bands. It appears reasonable to conclude that the continuous band results from a transition between a molecular state composed of ^2S and ^2P Na atoms and a similar molecule composed of two ground state Na atoms. It should be noted that Na_2 molecules should be formed behind shock fronts after interaction between the incident or reflected shocks and the rarefaction wave.

Further research of a more quantitative nature is now in progress and will be reported in the near future.

* Supported by the U. S. Air Force, Office for Advanced Studies, under Contract AF 18(603)–2. The authors are indebted to Dr. S. S. Penner for helpful discussions.

† Senior Research Fellow 1958–1960; permanent address: Department of Physics, Hiroshima University, Hiroshima, Japan.

‡ Guggenheim Fellow in Jet Propulsion, 1958–1959.

[1] K. Wurm, Z. Physik **79**, 736 (1932).
[2] H. Hamada, Phil. Mag. **15**, (7), 574 (1933).
[3] Ch'en, Bennett, and Jefimenko, J. Opt. Soc. Am. **46**, 182 (1956).
[4] O. Jefimenko and W. Curtis, J. Chem. Phys. **27**, 953 (1957).
[5] Ressler, Lin, and Kantrowitz, J. Appl. Phys. **23**, 1390 (1952).

NMR Study of Acetaldehyde-Water Mixtures*

E. LOMBARDI† AND P. B. SOGO‡

Lawrence Radiation Laboratory and Department of Chemistry, University of California, Berkeley, California

(Received August 3, 1959)

THE hydration of acetaldehyde and other carbonyl compounds has been extensively studied by using calorimetric and spectrophotometric methods.[1–3] We have applied the technique of high-resolution NMR to the study of acetaldehyde-water mixtures and our result is in agreement with the results obtained by the older methods.

We have calculated a value for the equilibrium constant between the two forms. The general expression of this equilibrium is

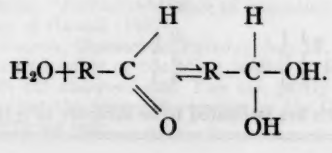

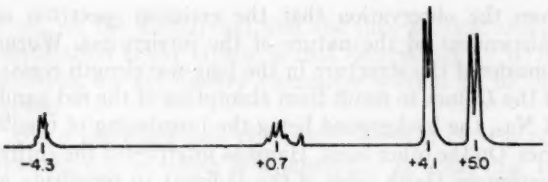

FIG. 1. NMR spectra of mixture containing 1 part acetaldehyde to 1 part D_2O.

We have used samples of acetaldehyde, propionaldehyde, and isobutyraldehyde which were purified by distillation. The purity of H_2O and D_2O was ascertained by NMR. All the spectra have been taken with a Varian Model V-4300 B spectrometer working at 40 Mc. The chemical shifts are expressed in ppm of the external magnetic field by the relation

$$\delta=(H-H_{ref})\times 10^6/H_{ref},$$

where H is the resonance field for the sample and H_{ref} is the resonance field of protons in water.

The spectrum of pure acetaldehyde consists of a quadruplet at $\delta=-4.3$ and a doublet at $\delta=+4.1$. The quadruplet represents absorption by the aldehydic proton which has been split by spin-spin interaction with the three protons of the methyl group, while the doublet represents absorption by the methyl group, split by the aldehydic proton.

When D_2O is added to pure acetaldehyde (Fig. 1) we observe the acetaldehyde spectrum consisting of a quadruplet at $\delta=-4.3$ and a doublet at $\delta=+4.1$. In addition, a quadruplet at $\delta=+0.7$ and a doublet at $\delta=+5.0$ appear. We have assigned these additional lines to the hydrated form of the acetaldehyde, with the quadruplet representing absorption by the proton of the acetal group, and the doublet representing absorption by the methyl group.

The intensities, but not the positions of the peaks assigned to the hydrated form, depend on the relative proportions of acetaldehyde and water. The assignment is further supported by the fact that the hydrated form is less polarized than the aldehydic form.

The same effect has been observed in mixtures of propionaldehyde/water or D_2O and isobutyraldehyde/water or D_2O. The data are reported in Table I.

TABLE I. Chemical shift of nonequivalent protons in aldehydes and their hydrated forms.

Acetaldehyde		Acetaldehyde+H_2O	Acetaldehyde+D_2O
−CHO	−4.3	0.6	0.7
$-CH_3$	4.1	5.0	5.0
Propionaldehyde		**Propionaldehyde +H_2O**	**Propionaldehyde +D_2O**
−CHO	−4.3	0.3	0.4
$-CH_2$	2.7	3.6	3.6
$-CH_3$	4.1	4.1	4.1
Isobutyraldehyde		**Isobutyraldehyde +H_2O**	**Isobutyraldehyde +D_2O**
−CHO	−4.1	0.6	0.6
CH	3.0	3.7	3.7
$-CH_3$	4.3	4.3	4.3

The shifts are estimated to be accurate to ±0.2 ppm.

It is possible to calculate the value of the equilibrium constant using the relation

$$K_{eq}=x/(a-x)(b-x),$$

where x=equilibrium concentration in moles/l of the hydrated form, a=initial concentration of aldehyde in moles/l and b=initial concentration of H_2O or D_2O in moles/l. From the areas under the absorption peaks of the pure and the hydrated forms we obtain the ratio $x/a-x$ from which we calculate x. The results of many experiments, using different amounts of acetaldehyde and water or D_2O gave for acetaldehyde at 25°C

$$K_{eq}=(2.7\pm 0.1)\ 10^{-2}/\text{moles/liter}$$

Bell and Clunie[2] obtain

$$\log-[CH_3CH(OH)_2]/[CH_3CHO]-=0.173$$

for a dilute aqueous solution of acetaldehyde at room temperature. Our value for the corresponding quantity is:

$$\log K_{eq}[H_2O]=0.176.$$

* The work described in this paper was sponsored by the U. S. Atomic Energy Commission.

† Present address: Instituto di Chimica Industriale del Politecnico, Piazza Leonardo da Vinci 32, Milano, Italy.

‡ Present address: Physics Department, San Diego State College, San Diego, California.

[1] R. P. Bell and M. H. Rand, Bull. Soc. Chim. France **1955**, 115.

[2] R. P. Bell and J. C. Clunie, Trans. Faraday Soc. **48**, 439 (1952).

[3] P. Rumpf and C. Bloch, Compt. rend. **233**, 1364 (1951).

Some Calculations Based on an LCGO-MO Treatment

JIRO HIGUCHI

Laboratory of Physical Chemistry, Tokyo Institute of Technology, Ookayama, Meguro-ku, Tokyo, Japan

(Received July 14, 1959)

IN the investigation of the electronic structures of molecules, the complete calculation becomes more difficult to carry out as the number of atoms in the molecules increases. Because of this, if the effect on the result is small, it is rather convenient to treat parts of the molecule as groups in order to reduce the labor of the procedure.[1] This is, for example, accomplished by the partial use of united atom orbital-molecular orbitals (UAO-MO's) for groups (i.e., radicals) in the molecule. As an example of this, the present note takes up the ionization potentials of some hydrocar-

TABLE I. SCF-LCGO-MOs

C_2H_6	$\varphi_1=0.6161\chi_{CH_3}+0.6161\chi_{CH_3}$
	$\varphi_2=0.8557\chi_{CH_3}-0.8557\chi_{CH_3}$
C_3H_6	$\varphi_1=0.1966\chi_{CH_2}+0.3281\chi_{CH}+0.8161\chi_{CH_3}$
	$\varphi_2=0.5880\chi_{CH_2}+0.5708\chi_{CH}-0.5846\chi_{CH_3}$
	$\varphi_3=0.8385\chi_{CH_2}-0.8509\chi_{CH}+0.2450\chi_{CH_3}$
C_3H_5	$\varphi_1=0.0923\chi_{CH_2}+0.9728\chi_{CH_3}$
	$\varphi_2=1.0290\chi_{CH_2}-0.3477\chi_{CH_3}$

bons, in which the group orbitals (GO's) are approximated as UAO-GO's with one center. Unfortunately, however, such GO's have not yet been obtained, but can be approximated as described below. For the ionization potential of hydrocarbons, in general, the orbitals in question are perpendicular to the molecular skeleton plane. In the LCAO-MO approximation, the MO's of the methyl and methylene group concerned can be expressed as $\alpha\mathbf{p}_C+\beta\mathrm{N}[\mathbf{h}_1+\mathbf{h}_2\exp(\pm 2\pi i/3)+\mathbf{h}_3\exp(\pm 4\pi i/3)]$ and $\alpha'\mathbf{p}_C+\beta'\mathrm{N}'(\mathbf{h}_1-\mathbf{h}_2)$, respectively. In this case, the corresponding coefficients of the normalized GO's, (α and α') or (β and β'), resemble each other and also those of the l_2 MO of the methane molecule (refer to the result of NH, NH_2, and NH_3 by the present author[2]). Accordingly, the methyl group can be treated as the methane molecule omitting the one hydrogen atom which lies in the bond direction (without its nucleus and its 1s AO). For the methylene or the other groups in the molecular skeleton plane, the GO concerned can well be approximated as the 2p AO of carbon or the other central atom, because of the slight contribution of the hydrogen in these groups to this GO. Accordingly, the LCAO-MO type calculation might be suitably called the LCGO-MO treatment.

In the present work, the calculation was carried out for the ethane molecule, the propylene molecule and the ethyl radical, by adopting the SCF-LCAO-MO method.[3,4] The C—C, C=C and C—H distances were taken as 1.55 *A*, 1.34 *A* and 1.09 *A*, respectively, and the bond angle of ∠CCC was assumed as 120°. The orbital exponent of the 2p-type GO of the methyl group was taken as 1.30 according to Bernal,[5] while for the carbon atom the usual value of 1.59 was used. The two-center one-electron integrals and the two-electron Coulomb integrals were calculated exactly and the other two-center integrals were evaluated by using Mulligan's approximation,[6] while the three-center integrals were obtained by Mulliken's approximation.[7] The core-field energies were evaluated by the Hartree-type approximation as in the usual π-electron calculation. By using these integrals and the observed ionization potentials of the carbon atom and of the methane molecule,[8] the SCF-LCGO-MO's of these molecules are obtained as given in Table I. In this table, one can recognize the fact that the large coefficient of the χ_{CH_3} in the lowest MO ϕ_1 is caused by the larger ionization energy of the methyl group[9] with reference to the carbon atom. On the other hand, the coefficients of the highest occupied orbital of the propylene ϕ_2 are almost the same in absolute value, but the electron population shows a large ethylenic character of about three times that of the methyl group, and the vacant orbital ϕ_3 is fairly similar to that of the ethylene molecule because of the small coefficient of the χ_{CH_3}. As the result of this, the excitation energies without CI (2.70 ev for **NT** and 9.43 ev for **NV**) are rather close to those of the ethylene molecule (1.78 ev for **NT** and 10.08 ev for **NT**) as in the experiment, although there is a little difference between them due to the influence of the methyl group. The ionization energies so obtained are 12.57 ev, 10.14 ev, and 11.42 ev, respectively, for the ethane molecule, the propylene molecule, and the ethyl radical, while the observed value are 11.63 ev,[10] 9.73 ev,[10] and 8.66 ev,[11] respectively. The calculated values are in general somewhat larger than the observed ones,[12] but the discrepancies between them may be unavoidable in such a calculation, since in the comparison with systems with the same number of carbon π-electrons, the differences from the observed values are about the same. This indicates the fact that the UAO-GO approximation used is fairly good on such calculations but a further improvement cannot be expected in so far as the so-called π-electron approximation is used.

In conclusion, it is important to consider further applications of the LCGO-MO's. Another fruitful example may be the electronic spectra of the complex salts, in which the orbitals of the ligands are treated by using the UAO-MO's, because the effect of the metal and that of the ligands have occasionally been discussed separately. On the other hand, however, it is impossible to apply this treatment to the molecular quadrupole moment, the internal rotation, and the other quantities which are strongly influenced by the charge distribution near the hydrogen nucleus. At any rate, the true validity of the present approximation will be clarified after the accomplishment of the calculation with the complete use of the UAO-GO's.

[1] From a similar viewpoint, some calculations were already carried out semiempirically, i.e., J. L. Franklin, J. Chem. Phys. **22**, 1304 (1954).

[2] J. Higuchi, J. Chem. Phys. **24**, 535 (1956).

[3] C. C. J. Roothaan, Revs. Modern Phys. **23**, 69 (1951).

[4] J. Higuchi, J. Chem. Phys. **26**, 151 (1957).

[5] M. J. M. Bernal, Proc. Phys. Soc. (London) **A66**, 514 (1953). For the 2*s*-type GO in the calculation of the core-field energy, the orbital exponent of 1.30 was also used, although exactly speaking the value of 1.75 should be used.

[6] J. F. Mulligan, J. Chem. Phys. **19**, 347 (1951).

[7] R. S. Mulliken, J. chim. phys. **46**, 497 (1949).

[8] W_{C2p} and $W_{CH4\,2s}$ were taken as −11.28 ev[7] and −12.99 ev[10], respectively.

[9] For the tetrahedral form of the methyl group, the ionization potential of 12.48 ev was obtained in the present calculation.

[10] K. Watanabe, "Preliminary table of ionization potentials in ev," University of Hawaii (1957).

[11] D. P. Stevenson, Discussions Faraday Soc. **10**, 35 (1951).

[12] The calculated value of the ethyl radical is fairly large as compared with the observed one. This can partly be explained from the fact that the energy depression by the CI is expected from the positive ion only.

Rational Approximations for the Debye Functions

HENRY C. THACHER, JR.*
Argonne National Laboratory, Lemont Illinois

(Received September 24, 1959)

FOR many purposes, and particularly for use with automatic computers, a function is more conveniently represented by an adequate rational approximation than by a table of values. It recently has been found that the Debye functions have the representations given below over the range $0 \leq x \leq 10$.

These approximations were calculated using a rotational interpolation logarithm[1] programmed for the Royal Precision LGP-30 computer. For the odd-numbered formulas, an iteration comparable to the Hastings technique was used so that the maximum errors were approximately equal. The more precise, even-numbered formulas are so accurate that round-off errors in the six-place table being fitted made the apparent errors fluctuate so much as to preclude careful adjustment of the maximum errors. A slight improvement in efficiency may therefore still be possible, although it is doubtful if the maximum error could be reduced by as much as 50%.

It must be emphasized that these approximations are valid only for the range $0 \leq x \leq 10$. Outside this range, the error may be expected to increase rapidly, and one of the asymptotic representations should be used. The success of these rational approximations suggests that rational interpolation may well be the method of choice for interpolation in tables of the Debye functions when high precision is desired.

* Performed under the auspices of the U. S. Atomic Energy Commission.

[1] J. Tukey and H. C. Thacher, Jr. (to be published).

$$(1) \qquad \frac{1}{x}\int_0^x \frac{t}{e^t-1}dt = \frac{24.155-0.2758x+0.08386x^2}{24.166+5.6522x+x^2}+\epsilon \quad |\epsilon|<0.00048.$$

$$(2) \qquad = \frac{3754.971-206.8950x+67.79818x^2-0.400109x^3+0.0421551x^4}{3754.969+731.8707x+146.41606x^2+15.897010x^3+x^4}+\epsilon \quad |\epsilon|<0.0000012.$$

$$(3) \qquad \frac{2}{x^2}\int_0^x \frac{t^2}{e^t-1}dt = \frac{21.973-2.5715x+0.11889x^2}{21.991+4.5815x+x^2}+\epsilon \quad |\epsilon|<0.00080.$$

$$(4) \qquad = \frac{2897.877-399.9480x+48.88118x^2-2.133801x^3+.0425266x^4}{2897.881+565.9609x+116.94965x^2+13.064515x^3+x^4}+\epsilon \quad |\epsilon|<0.0000016.$$

$$(5) \qquad \frac{3}{x^3}\int_0^x \frac{t^3}{e^t-1}dt = \frac{19.517-3.1264x+0.14979x^2}{19.539+3.9827x+x^2}+\epsilon \quad |\epsilon|<0.0012.$$

$$(6) \qquad = \frac{3953.632-800.6087x+85.07724x^2-4.432582x^3+0.0946173x^4}{3953.632+682.0012x+143.155337x^2+15.121491x^3+x^4}+\epsilon \quad |\epsilon|<0.0000021.$$

$$(7) \qquad \frac{4}{x^4}\int_0^x \frac{t^4}{e^t-1}dt = \frac{17.595-3.2071x+0.16157x^2}{17.619+3.15940x+x^2}+\epsilon \quad |\epsilon|<0.0014.$$

$$(8) \qquad = \frac{4044.481-955.8516x+103.00607x^2-5.49848x^3+0.1194766x^4}{4044.484+661.9293x+143.11660x^2+14.919715x^3+x^4}+\epsilon \quad |\epsilon|<0.0000035.$$